U.S.DEPARTMENT OF THE INTERIOR

U. S. GEOLOGICAL SURVEY

NATIONAL EARTHQUAKE HAZARDS REDUCTION PROGRAM, SUMMARIES OF TECHNICAL REPORTS VOLUME XXXIV

VOLUME I

Prepared by Participants in

NATIONAL EARTHQUAKE HAZARDS REDUCTION PROGRAM

December 1992

OPEN-FILE REPORT 93-195

Menlo Park, California

1993

DIRECTIONS FOR PREPARATION OF REPORTS

1. Use 8 1/2 x 11" paper for both text and figures.
2. Leave at least 1" margins at top, sides and bottom.
3. Type all text single-spaced.
4. Type only on one side of the paper.
5. Draft figures in black ink (color, weak or grey lines will not photo-reproduce) and make them simple and legibly lettered.
6. Type figure captions on the same page as the figure.
7. Please do not use staples.
8. Do not number pages.
9. Send original copies of text and figures. Do not send xerox copies as they do not photo-reproduce clearly. Do not send oversize photos. They should be able to be placed on regular sized paper and the caption must fit under it.
10. Do not type headings such as "Technical Report" or "Summary".
11. Do not use scotch tape. Use paste.
12. If you use photographs please send a glossy print of each.

U.S. DEPARTMENT OF THE INTERIOR
U.S. GEOLOGICAL SURVEY

NATIONAL EARTHQUAKE HAZARDS REDUCTION PROGRAM, SUMMARIES OF TECHNICAL REPORTS VOLUME XXXIII

Prepared by Participants in

NATIONAL EARTHQUAKE HAZARDS REDUCTION PROGRAM

Compiled by

Muriel L. Jacobson

The research results described in the following summaries were submitted by the investigators in September 1991 and cover the period from April 1991 through October 1, 1991. These reports include both work performed under contracts administered by the Geological Survey and work by members of the Geological Survey. The report summaries are grouped into the four major goals of the National Earthquake Hazards Reduction Program.

Open File Report No. 93-195

The data and interpretations in these progress reports may be reevaluated by the investigators upon completion of the research. Readers who wish to cite findings described herein should confirm their accuracy with the author.

EARTHQUAKE HAZARDS REDUCTION PROGRAM

CONTENTS - VOLUME I

Goal I - Understanding what happens at the earthquake source

Why and how does a segment of a geologic fault suddenly slip and produce an earthquake? What physical conditions within the Earth control where and when an earthquake occurs?

Goal II - Evaluating the potential of future earthquakes

Where are future earthquakes likely? How large will they be? How often will they occur? When will they occur? Where are future earthquakes unlikely?

EARTHQUAKE HAZARDS REDUCTION PROGRAM

CONTENTS - VOLUME II

Goal II - Evaluating the potential of future earthquakes

Where are future earthquakes likely? How large will they be? How often will they occur? When will the occur? Where are future earthquakes unlikely?

Goal III - <u>Predicting the effects of earthquakes</u>

During an earthquake of a certain magnitude, how severely and for how long will the ground shake? Where will hillsides slide, and flatlands fissure and crack? On what types of ground will earthquake damage be concentrated? Which faults will offset the Earth's surface? By how much? Which coastlines will be elevated or submerged? Where will destructive sea waves be generated? What losses to structures are expected?

Goal IV - <u>Using research results</u>

What new hazard reduction strategies become possible as understanding of earthquake phenomena advances? What scientific information is needed and can be furnished to practitioners in the engineering, land-use planning and emergency managements communities? How can such information be most effectively communicated to these practitioners?

Regional Seismic Monitoring Along The Wasatch Front Urban Corridor And Adjacent Intermountain Seismic Belt

1434-92-A-0966

W. J. Arabasz, R. B. Smith, J. C. Pechmann, and S. J. Nava
Department of Geology and Geophysics
University of Utah
Salt Lake City, Utah 84112
(801) 581-6274

Investigations

This cooperative agreement supports "network operations" associated with the University of Utah's 81-station regional seismic telemetry network. USGS support focuses on the seismically hazardous Wasatch Front urban corridor of north-central Utah, but also encompasses neighboring areas of the Intermountain Seismic Belt. Primary products for this USGS support are quarterly bulletins and biennial earthquake catalogs.

Results (October 1, 1991 - September 30, 1992)

General accomplishments. During the report period, significant efforts related to: (1) implementation of a distributed computer system (4 SUN Sparc 2 workstations with associated peripherals) for processing and analysis of network data and data from portable seismographs; (2) implementation of a Concurrent 7200 computer for online data acquisition (our prior data acquisition computer, a PDP 11/34, was phased out in September 1992); (3) experimental use of 5 REF TEK digital recorders for supplementing regional-network data collection; (4) continued upgrading of site hardware and electronics at field stations that have been operating since the mid-1970s; and (5) installation and operation of five temporary telemetered stations and one REF TEK digital recorder in and around the source area of an M_L 5.8 earthquake in southwestern Utah.

Network Seismicity. Figure 1 shows the epicenters of 1241 earthquakes ($M_L \leq 5.8$) located in part of the University of Utah study area designated the "Utah region" (lat. 36.75°-42.5°N, long. 108.75°-114.25°W) during the period October 1, 1991 to September 30, 1992. The seismicity sample includes 31 shocks of magnitude 3.0 or greater (earthquakes of M_L 4.0 and greater are labeled in Fig. 1) and 19 felt earthquakes.

The largest earthquake during the report period was a shock of M_L 5.8 on September 2, 1992 (10:26 UTC), located 8 km ESE of St. George, in southwestern Utah. This earthquake caused structural damage in at least three localities within about 50 km of the epicenter, produced liquefaction along the nearby Virgin River, and triggered a massive, destructive landslide 45 km to the ENE in the town of Springdale. No surface faulting was observed. This earthquake was followed by remarkably few aftershocks. Other notable earthquakes that occurred during the report period included: (1) an M_L 4.2 shock on March 16, 1992 (14:42 UTC), located under the western Traverse Mts., the southern boundary of the Salt Lake Valley; and (2) a swarm of 34 locatable earthquakes, occurring on June 28-29, 1992, 11 km NW of Cedar City ($0.5 \leq M \leq 4.1$). Approximately 25% of the seismicity detected during the report period was associated with an area of ongoing coal-mining related seismicity, located within a 60 km radius of Price in east-central Utah (311 shocks, $1.2 \leq M \leq 3.7$). For more details about some of the larger earthquakes, see our companion research summary in this volume (R.B. Smith and others).

Reports and Publications

Nava, S.J. (1991). Earthquake Activity in the Utah Region, January 1 - March 31, 1991, *Wasatch Front Forum (Utah Geological and Mineral Survey) 7*, no. 3, 2.

Nava, S.J. (1991). Earthquake Activity in the Utah Region, April 1 - June 30, 1991, *Survey Notes (Utah Geological and Mineral Survey) 25*, no. 1, 7; also published in *Wasatch Front Forum (Utah Geological and Mineral Survey) 7*, no. 4, 2.

Nava, S.J. (1992). Earthquake Activity in the Utah Region, July 1 - September 30, 1991, *Wasatch Front Forum (Utah Geological and Mineral Survey) 8*, no. 1, 2; also published in *Survey Notes (Utah Geological and Mineral Survey) 25*, no. 2, 11.

Nava, S.J. (1992). Earthquake Activity in the Utah Region, October 1 - December 31, 1991, *Wasatch Front Forum (Utah Geological and Mineral Survey) 8*, no. 2, 2.

Christenson, G.E. (Compiler) (1992). The March 16, 1992 M_L 4.2 Western Traverse Mountains earthquake, Salt Lake County, Utah, *Utah Geological Survey Open-file Report 255*, 18 pp.

Arabasz, W.J., Nava, S.J., and Pechmann, J.C. (1992). Earthquakes near Cedar City, Utah, June 28-29, 1992, *University of Utah Seismograph Stations Preliminary Earthquake Report*, 5 pp; also published in *Wasatch Front Forum (Utah Geological and Mineral Survey) 8*, no. 2, 4-7.

Arabasz, W.J., Pechmann, J.C., and Nava, S.J. (1992). The St. George (Washington County), Utah, earthquake of September 2, 1992, *University of Utah Seismograph Stations Preliminary Earthquake Report*, 6 pp.

Arabasz, W.J., Pechmann, J.C., Nava, S.J., and Wallace, T.C. (1992). EERI Special Earthquake Report, St. George, Utah, September 2, 1992, *EERI Newsletter 26*, no. 10, 6-7.

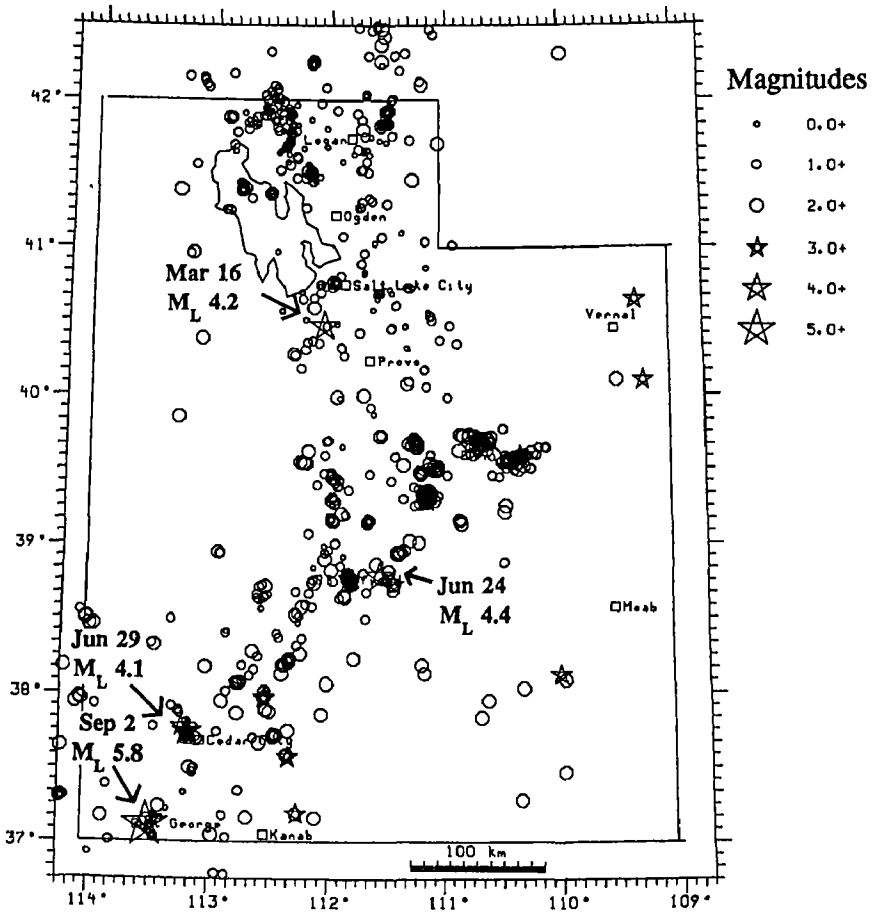

Figure 1. Earthquakes in the Utah region, October 1, 1991, through September 30, 1992. Shocks of magnitude 3.0 or greater are plotted as stars; those less than magnitude 3.0 as circles.

SPATIAL VARIATION OF STRESS DROPS OF LOMA PRIETA AFTERSHOCKS, DATED JANUARY 28, 1991

USGS 1434-92-G2204

Ralph J. Archuleta and Grant T. Lindley
Institute for Crustal Studies and Department of Geological Sciences
University of Calfiornia, Santa Barbara
Santa Barbara, CA 93106
(805) 893-4477 or x4893

Objective

The goal of this project is to measure source parameters of aftershocks of the October, 1989, Loma Prieta, California, earthquake and to study the variation of those source parameters with hypocentral location. In addition, the study has been broadened to examine the spatial variation of source parameters of aftershocks of the May, 1983, Coalinga, California, earthquake. The purpose is to study the spatial variation of source parameters of small earthquakes in order to better understand the nucleation and termination of large earthquakes. The ultimate goal is to be able to identify likely nucleation and termination zones of large earthquakes by analysis of small background earthquakes.

Results

Source parameters (stress drops and moments) have been determined for 392 aftershocks of the Loma Prieta earthquake and 108 aftershocks of the Coalinga earthquake. The data used in each case are digital recordings of aftershocks from portable instruments. The source parameters are determined from least-squares best fits to the Fourier amplitude spectrum of P- and S-waves. Parameters of the least-squares best fits to the Fourier spectra include the low-frequency spectral asymptote and the corner frequency. These parameters can be used to estimate the seismic moment and the stress drop of the aftershocks. Also included in the spectral fits is the parameter t* that determines the attenuation of the seismic waves. The parameter t* is the travel time divided by the quality factor of attenuation, Q. It is necessary to include attenuation in the spectral fits in order to accurately determine source parameters.

Cross sections showing stress drops of aftershocks of the Loma Prieta earthquake are shown in Figure 1. The darker areas show higher stress drop areas. A good correlation exists between the spatial variation of stress drop for P- and S-waves. The P- and S-wave spectral fits are independent of one another and the correspondence of the results is therefore important.

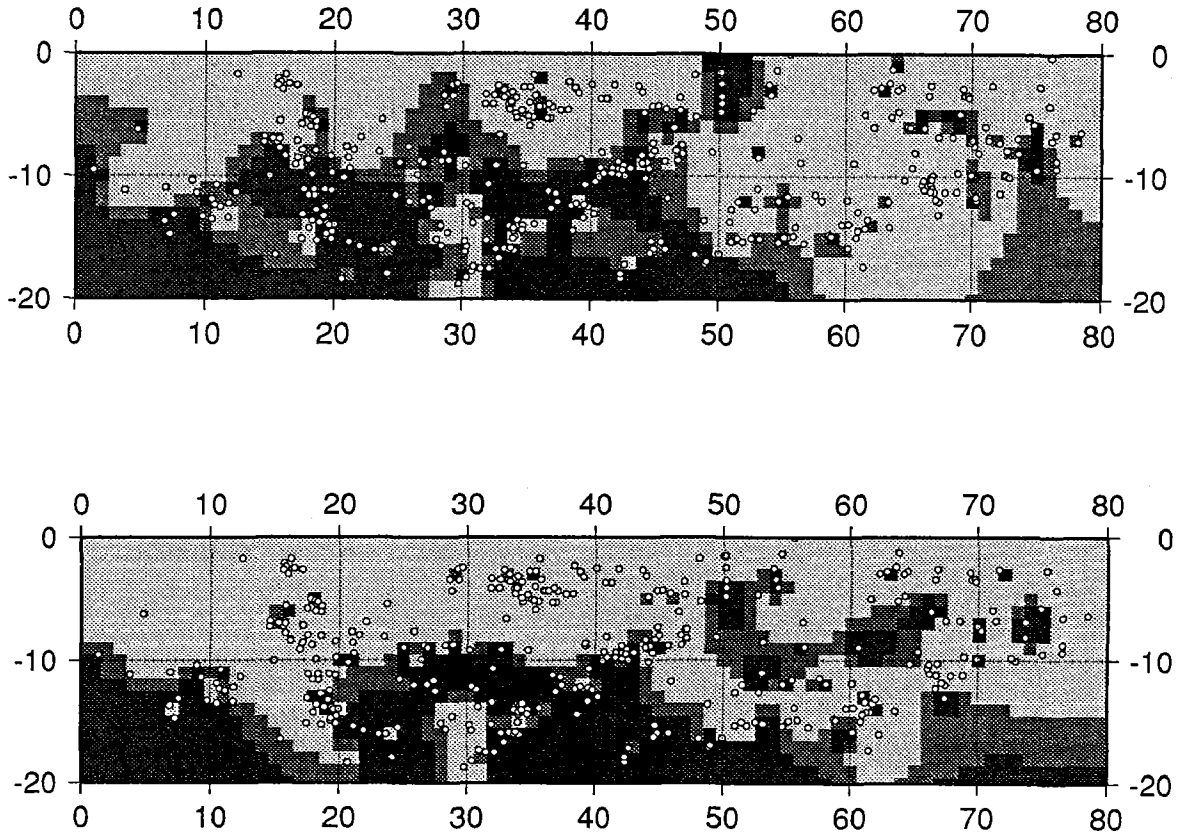

Figure 1. Cross sections along strike of the San Andreas Fault showing stress drops of Loma Prieta aftershocks: top) P-waves, bottom) S-waves. Higher stress drop areas are darker. Note the good correspondence of the P-wave and S-wave results.

Results at Coalinga indicate a high stress drop zone of aftershocks just above the main shock rupture zone (Figure 2). This high stress drop zone of aftershocks may indicate a high strength barrier that terminated the rupture of the main shock in the updip direction. The main shock hypocenter is located just below this zone of high stress drop aftershocks

and it is possible that the main shock nucleated at the edge of this high strength barrier. The cause for this high strength barrier is speculated to be the transition from a well-defined fault zone to intact rock. Also at Coalinga and Loma Prieta, there are several examples of high stress drop aftershocks that were followed by magnitude greater than five earthquakes located in nearly the same hypocentral locations. These results indicate that stress drops of small earthquakes may be useful in the identification of likely nucleation and termination zones of larger earthquakes.

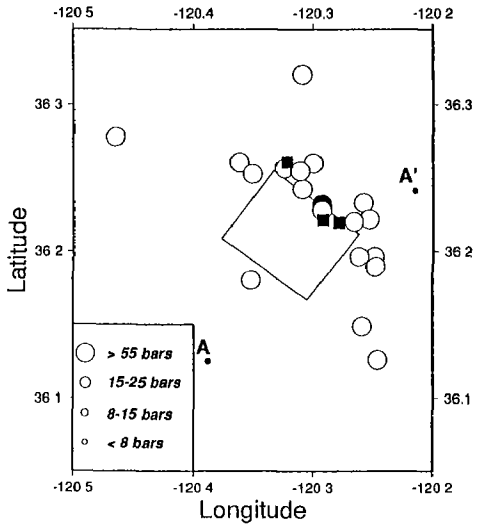

Figure 2. Map view shows twenty highest stress drop earthquakes. High stress drop earthquakes are concentrated to the north and east of the main shock rupture zone (rectangle) as identified by previous geodetic analysis. This zone is interpreted to be a high strength barrier that terminated the main shock rupture in the updip direction. Solid square shows the main shock hypocenter. Shaded circle and squares are magntiude >5 aftershocks.

Published Reports

Lindley, G. T. and R. J. Archuleta (1992). Earthquake source parameters and the frequency dependence of attenuation at Coalinga, Mammoth Lakes, and the Santa Cruz Mountains, California, *J. Geophys. Res.*, **97**, 14,137-14,154.

Lindley G. T. (1992). Spatial variation of aftershock source parameters and rupture process of the 1983, Coalinga, California, earthquake, submitted to *Bull. Seism. Soc. Am.*.

Lindley, G. T. and R. J. Archuleta (1991). Spectral analysis of Loma Prieta aftershocks to determine site and source effects (abstract), *Eos*, **72**, 338.

Seismic Source Analysis Using Empirical Green's Functions

9910-02676

John Boatwright and Leif Wennerberg
Branch of Engineering Seismology and Geology
U.S. Geological Survey, MS 977
Menlo Park, California 94025
(415) 329-5609, 329-5607

Investigations

(1) Seekins and Boatwright (1992) derived the relative site response as an function of frequency for a set of 11 accelerograph stations and 23 seismograph stations in the City of San Francisco. In general, the accelerographs recorded only the Loma Prieta main shock, while the seismographs recorded only aftershocks. The two data sets have been combined using recordings of aftershocks at four of the accelerograph sites. There is enough redundancy in the data set to make weak tests of the consistency of the strong and weak motion site response at these stations. We have grouped these 31 different sites according to the underlying rock-type: Franciscan sandstone, Franciscan serpentine, miscellaneous sand, and bay mud. Station MAS, sited in an ammunition bunker on Franciscan sandstone at Fort Mason, is used as the reference site. The relative site amplification for each rock-type appear to be remarkably consistent functions of frequency. The bay mud averages plotted in Figure 1 exhibit a peak at 1 Hz amplified by a factor of 5-6, a broad sidelobe at 2-3 Hz amplified by a factor of 3, and little relative amplification at 10 Hz. The sand averages have little relative amplification below 1 Hz, but are uniformly amplified by a factor of 2-3 at frequencies above 2 Hz. While these results are specific only to the limited range of rock-types and site conditions in San Francisco, this study is the first to demonstrate that site amplification can be regionally characterized using rock-specific functions of frequency.

(2) In FY91, Fletcher and Boatwright (1991) devised a spectral inversion technique to analyze the geometrical and anelastic attenuation using a line of stations sited along the axis of the San Francisco Pennisula from the Santa Cruz Mountains up to San Francisco. After fitting for source parameters and average attenuation parameters, the residuals are projected onto the set of stations and to a set of distances, resulting in a map of residual attenuation as a function of distance and frequency. These inversions are iterated until the misfit is minimized. This technique was applied to a set of vertical recordings of S-wave trains (that is, S, S_mS, S_n, and Lg) obtained from 1980 through 1990 on the Eastern Canadian Telemetered Network (ECTN). The 97 earthquakes analyzed range

in size from $3 < m_{bLg} < 6.5$; the epicentral distances range from 25 to 1000 km. The average S-wave attenuation for the data set is reasonably described by the function $R^{-\gamma}exp(\pi fT/Q)$ with $Q = 1997$ and $\gamma = 1$. The residual attenuation function is plotted in Figure 2. There is a single deep trough from 40 to 120 km which shallows with increasing frequency, then two ridges at 200 and 316 km which appear to represent energy that has been critically refracted from velocity discontinuities below the Moho. A broad region of relatively little variation extends from 200 to 800 km, indicating that recordings of the S-wave trains at this distance can be used to investigate source characteristics with minimal frequency-dependent effects.

Products

Boatwright, J., Regional propagation characteristics and source parameters of earthquakes in northeastern North America, submitted to *Bull. Seism. Soc. Am.*

Boatwright, J., L.C. Seekins, H-P. Liu, T.E. Fumal, and C.S. Mueller, Ground-Motion Amplification, in *The Loma Prieta, California, Earthquake of October 17, 1989 – Marina District, U.S. Geological Survey Professional Paper 1551-F*, Washington D.C., 1992.

Fletcher, J.B., and J. Boatwright, Source parameters of Loma Prieta aftershocks and wave propagation characteristics along the San Francisco peninsula from a joint inversion of digital seismograms, *Bull. Seism. Soc. Am.*, **81**, 1783-1812, 1991.

Seekins, L.C. and J. Boatwright, Ground-motion amplification, geology, and damage from the 1989 Loma Prieta earthquake in the City of San Francisco, submitted to *Bull. Seism. Soc. Am.*

Figure Captions

Figure 1. Average site amplifications for stations on bay mud (10 stations), sand (8), and Franciscan sandstone (8), plotted as a function of frequency. The shaded areas represent 68% confidence intervals. For reference, the range of fundamental frequencies for 2, 4, and 10-story buildings are shown at the bottom of the plot.

Figure 2. Residual attenuation of the S-wave trains, plotted as a function of hypocentral distance, as discerned from ECTN recorded at distances from 25 to 1000 km. The function is contoured in units of $\Delta \ln_e = 0.05$. The apparent high and low-frequency variations at the furthest distances are not statistically significant.

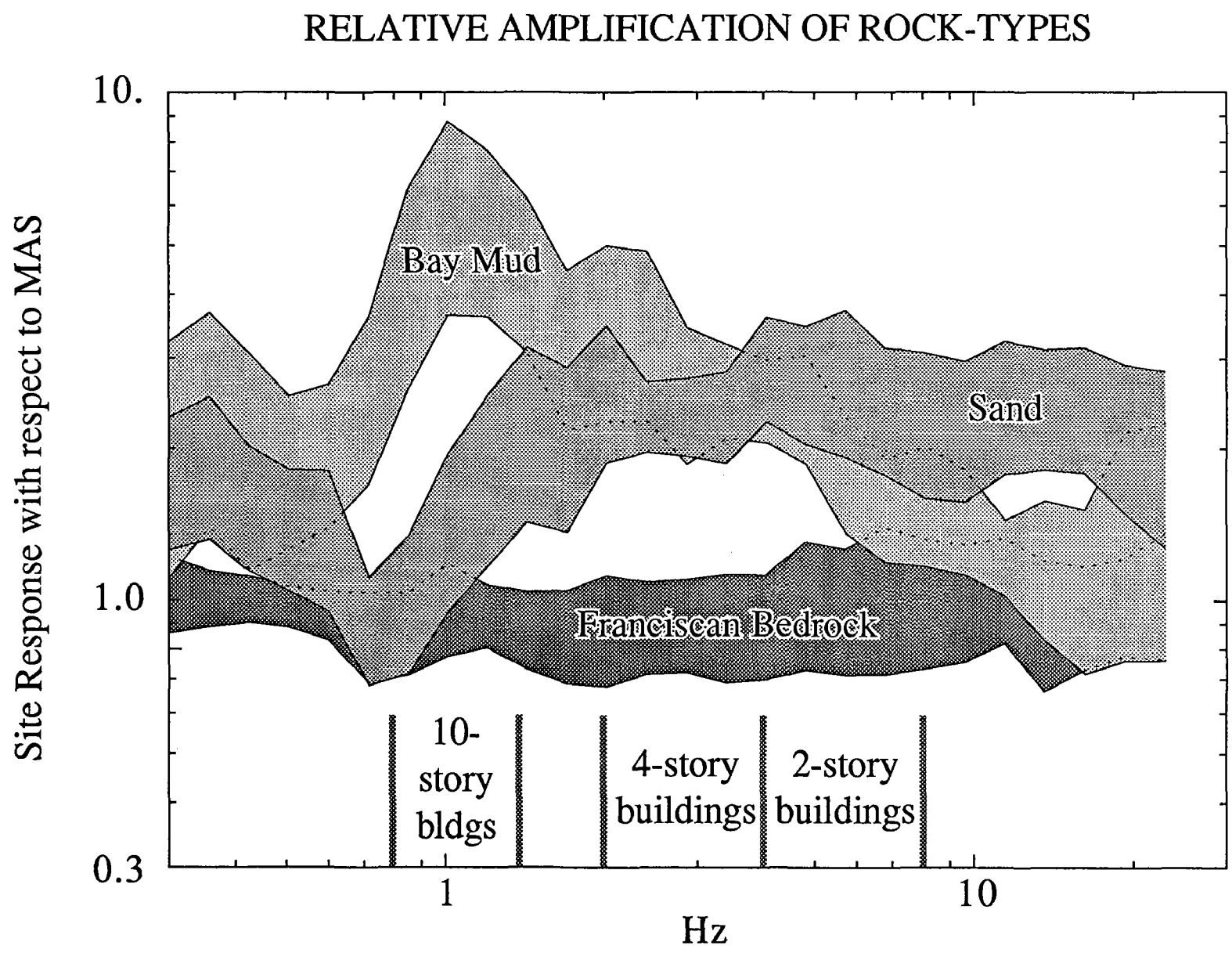
RELATIVE AMPLIFICATION OF ROCK-TYPES
10.
1.0
0.3
Site Response with respect to MAS
Bay Mud
Sand
Franciscan Bedrock
10-
story
bldgs
4-story
buildings
2-story
buildings
1
10
Hz

FIGURE 1

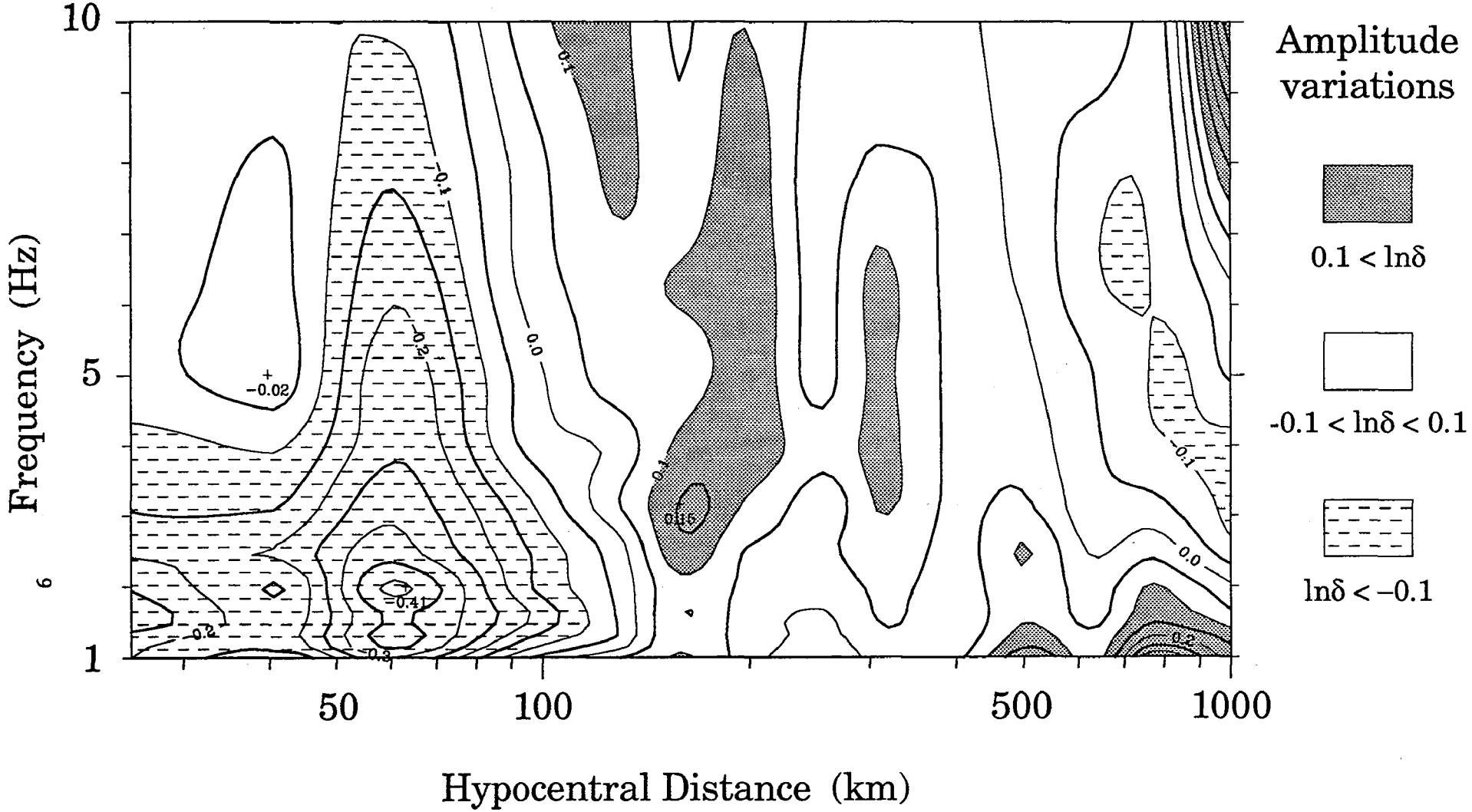
ECTN ATTENUATION
relative to Q = 1997 and R-1
10
5
1
Frequency (Hz)
50
100
500
1000
Hypocentral Distance (km)
Amplitude variations
0.1 < lnδ
-0.1 < lnδ < 0.1
lnδ < −0.1
+0.02
-0.41
0.15

FIGURE 2

SOUTHERN APPALACHIAN COOPERATIVE SEISMIC NETWORK

Award No. 1434-92-A-0971

G. A. Bollinger 703-231-9190
M. C. Chapman 703-231-5036
M. S. Sibol 703-231-4707
Seismological Observatory
Virginia Polytechnic Institute and State University
Blacksburg, Virginia 24061-0420

Objectives

This three-year cooperative project between Virginia Tech, Memphis State University, Tennessee Valley Authority and the University of North Carolina at Chapel Hill is designed to provide modern instrumental coverage of the Southern Appalachian Seismic Zone. The 32 stations of the Virginia Tech and Memphis State networks will be upgraded to three-component with high dynamic range by means of digital telemetry. Integration of the 19 station TVA network and the 5 station UNC network will result in the formation of a 56 station Southern Appalachian Cooperative Seismic Network (SACSN). There is to be common data formatting and access on computer networks to ensure near real-time waveform data sharing by the SACSN member institutions and accessibility to the general seismological community. This cooperative regional network is also scheduled to be fully integrated into the U.S. National Seismic Network.

Research objectives for the SACSN are focused on the Southern Appalachian Seismic Zone which is situated within a Paleozoic fold-and-thrust belt overlying a crystalline seismogenic basement weakened during Iapetan rifting. The research objectives include: earthquake detection and location and the study of seismogenic structures, earthquake source studies, wave propagation at local and regional distances, crustal velocity studies, temporal patterns of seismicity and seismic hazard assessment. Thus, the data and analyses from the SACSN are directed towards understanding the seismotectonics and assessing the seismic potential of the region.

The service objectives of the SACSN include the publication of an annual Seismicity Bulletin for the southeastern U.S. region, the development and maintenance of regional earthquake catalogs and general informational service to state/local governments and to the public.

Investigations

A high priority for this first year has been the development and implementation of a common data format and procedures for sharing seismic data in near real-time among the SACSN member institutions. Recognizing that there will never be total compatibility in acquisition packages due to differences in equipment, scale and logistics among the subnetworks, a more realistic goal is that member institutions have translation programs to convert from various data acquisition format(s) into a commonly agreed upon data format. Such "event" data, written in the agreed-upon format, is to be stored in accessible locations such as shared disk space or ftp-accessible partitions. Ideally, the data-exchange format will be the same as that used for analysis, and ultimately, we will want to ensure compatibility with other members of the USNSN.

As a first step, we have taken advantage of the fact that all of the SACSN member institutions have access to Sun Sparcstations with disk space which can be

dedicated to waveform data storage, and all have, or are in the process of installing, the LLNL Seismic Analysis Code (SAC) package. Accordingly, we have written translators for our two sources of digital data--a 32-channel short-period telemetered network and a three-component broadband GSE seismograph system at BLA--into both SAC data format and Center for Seismic Studies (CSS) data format. In addition, we have calibrated all channels and have the instrumental responses in both SAC-format pole-zero files and in frequency-amplitude-phase format. Data from recent events recorded with the Virginia Tech network have already been made available via our anonymous ftp directory on vtso.geol.vt.edu. For example, on August 21, a magnitude 4.1 shock occurred at 12:32 EDT northwest of Charleston, South Carolina. The NEIC released the location and size parameters for that event at 14:04 EDT. Our BLA broadband digital time series was available to SACSN in just over an hour after the USGS announcement and within three hours after the earthquake's origin-time.

Bulletin No. 26 of the *Seismicity of the Southeastern U.S.* for the calendar year 1991 was distributed this past June to over 230 institutions and individuals, including 40 foreign addresses. In addition to reporting the usual hypocentral parameters, magnitudes, etc. for the report period, the *Bulletin routinely presents a complete set of network catalog statistics for the 1977-1991 period* (see Tables 1 and 2 and Figures 1-5).

An investigation of the relationship between earthquake magnitude and the size of damage areas in the eastern and western United States has been concluded. To quantify damage area as a function of moment magnitude (**M**), 187 VI, VII, and VIII Modified Mercalli isoseismal areas for 112 earthquakes (76 in California and Nevada, 36 in the eastern United States and Canada) were measured. Regression of isoseismal areas versus **M** indicated that areas in the East were larger than in the West at all three intensity levels, by an average 4-5 times in the **M** 5 to 7 range. In terms of radii for circles of equivalent area, the results indicate that damaging ground motion from shocks of the same magnitude extend to twice the distance in the eastern United States compared to the West (see Figure 6).

To determine source and site parameters consistent with the above results, Response Spectral levels for eastern North America were stochastically simulated and compared to observed Response Spectral ordinates derived from recorded strong ground motion data in the western United States. Stress parameter values of 200 bars, combined with a surficial 2 km thick low velocity layer over rock basement, produced results that are compatible with the intensity observations, i.e., similar Response Spectral levels in the East at twice the western U.S. distance. These results suggest that ground motion modeling in eastern North America may need to incorporate source and site parameters different from those presently in general use. The results are also of importance to eastern U.S. hazard assessments as they require allowance for the larger damage areas in preparedness and mitigation programs. A paper presenting these results has been accepted by the **BSSA**, subject to revisions.

SEUSSN EARTHQUAKE CATALOG STATISTICS SECTION

TABLE 1

SEUSSN Report Period/Cumulative Earthquake Catalog Statistics

PERIOD: January through December 1991 (1 year)

	Tectonic	Reservoir
Number of Earthquakes with M ≥ 0.0	93	17
Number of Earthquakes with M ≥ 2.5	15	7
Number of Earthquakes with M ≥ 3.5	2	0
Number of Felt Earthquakes	11	10
Rate of Earthquakes with M ≥ 0.0 (per year)	93	17
Rate of Earthquakes with M ≥ 2.5 (per year)	15	7.0
Rate of Earthquakes with M ≥ 3.5 (per year)	2.0	0.0
Rate of Felt Earthquakes (per year)	11	10
Mean Earthquake Magnitude	1.8	2.2
Median Earthquake Magnitude	1.8	2.1
Number of Earthquakes with Known Dmin ≤ 5.0 km	7	12
Number of Earthquakes with Known Dmin ≤ 10.0 km	19	13
Number of Earthquakes with Known Dmin ≤ 25.0 km	51	13
Number of Earthquakes with Known ERH ≤ 5.0 km	81	14
Number of Earthquakes with Known ERZ ≤ 5.0 km	72	0
Number of Blasts or Questionable Events Reported	0	
Number of Events Outside the SEUSSN Area Reported	0	
Number of Seismograph Stations Operating	104	

Largest Earthquake: 15 March 1991; 06:54 - Sandy Hook, VA
mb(Lg)= 3.8, MDB= 3.3, MMI= V

PERIOD: July 1977 through December 1991 (14.5 years)

	Tectonic	Reservoir
Number of Earthquakes with M ≥ 0.0	1162	681
Number of Earthquakes with M ≥ 2.5	201	63
Number of Earthquakes with M ≥ 3.5	24	2
Number of Felt Earthquakes	136	20
Rate of Earthquakes with M ≥ 0.0 (per year)	80	47
Rate of Earthquakes with M ≥ 2.5 (per year)	14	4.3
Rate of Earthquakes with M ≥ 3.5 (per year)	1.7	0.1
Rate of Felt Earthquakes (per year)	9.4	1.4
Mean Earthquake Magnitude	1.6	1.4
Median Earthquake Magnitude	1.6	1.4
Number of Earthquakes with Known Dmin ≤ 5.0 km	85	75
Number of Earthquakes with Known Dmin ≤ 10.0 km	202	108
Number of Earthquakes with Known Dmin ≤ 25.0 km	628	140
Number of Earthquakes with Known ERH ≤ 5.0 km	1030	172
Number of Earthquakes with Known ERZ ≤ 5.0 km	861	116
Number of Blasts or Questionable Events Reported	182	
Number of Events Outside the SEUSSN Area Reported	12	

Largest Earthquake: 27 July 1980; 18:52 - Sharpsburg, KY
mb = 5.2, MMI = VII

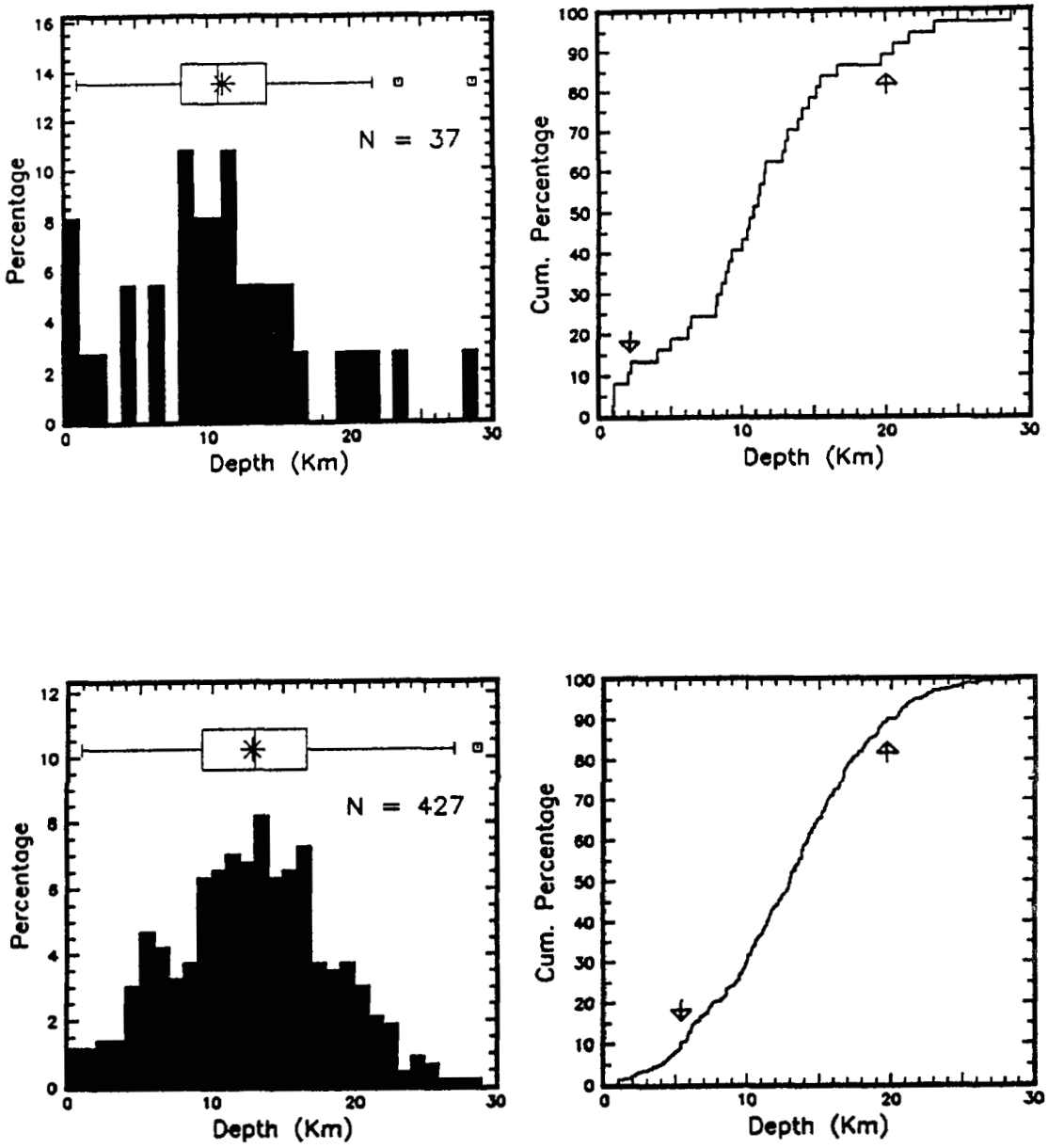

FIGURE 1. Focal Depth Distribution of Southeastern U.S. Earthquakes. The upper half of the figure shows the interval (left) and cumulative (right) depth distributions for the current report period while the lower half of the figure is a similar display for earthquakes reported during the period from July 1977 through this report period ($M \geq 0.0$, known ERZ ≤ 5.0 km, Dmin ≤ 20 km, and free depth determination). Displayed above both interval distributions is a box plot (Hoaglin and others, 1983, pp. 58-65). Indicated are the mean (star), the 25% and 75% quartile (box outline), the median (center bar), the upper and lower adjacent values (small vertical bars), and outliers (small squares). On the cumulative depth distributions arrows show the 10% and 90% depths.

COMPLETENESS ESTIMATES, MAGNITUDE DISTRIBUTIONS, AND RECURRENCE RELATIONS

TABLE 2

Completeness Estimates (Years) By Magnitude For The Southeastern U. S. And Subregions (Source: Bollinger and Others, 1989)

MAGNITUDE	2.25	2.75	3.25	3.75	4.25	4.75	5.25	5.75	6.25	6.75
Southeastern US	6	10	15	85	145	145	215	215	215	215
Valley & Ridge and Blue Ridge	9	10	20	75	110	215	215	215	215	215
Piedmont	10	10	115	215	215	215	215	215	215	215
Coastal Plain	10	10	60	145	145	215	215	215	215	215
Giles County, VA	10	15	15	30	30	215	215	215	215	215
Central Virginia	15	60	215	215	215	215	215	215	215	215
Eastern Tennessee	5	10	10	85	115	115	215	215	215	215
Charleston, SC	10	70	70	70	130	215	215	215	215	215

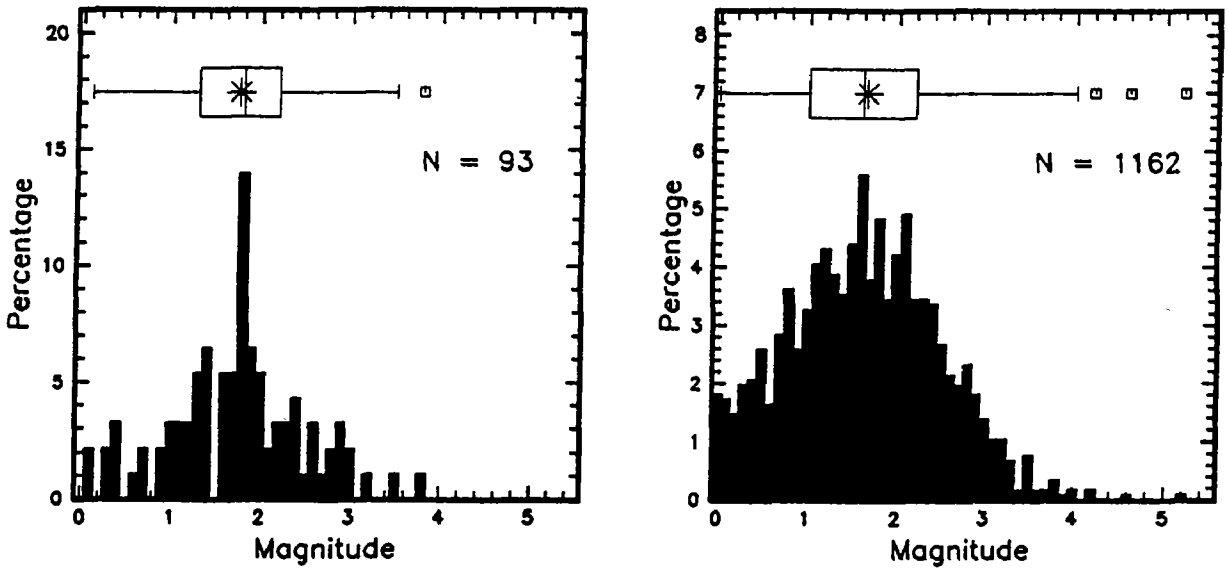

FIGURE 2. Magnitude Distributions of Southeastern U. S. Earthquakes. The left half of the figure shows the interval magnitude distribution for the report period while the right half of the figure shows a similar distribution for earthquakes from July 1977 through this report period. Displayed above both distributions is a box plot (Hoaglin and others, 1983, pp. 58-65). Indicated are the mean (star), the 25% and 75% quartile (box outline), the median (center bar), the upper and lower adjacent values (small vertical bars), and outliers (small squares).

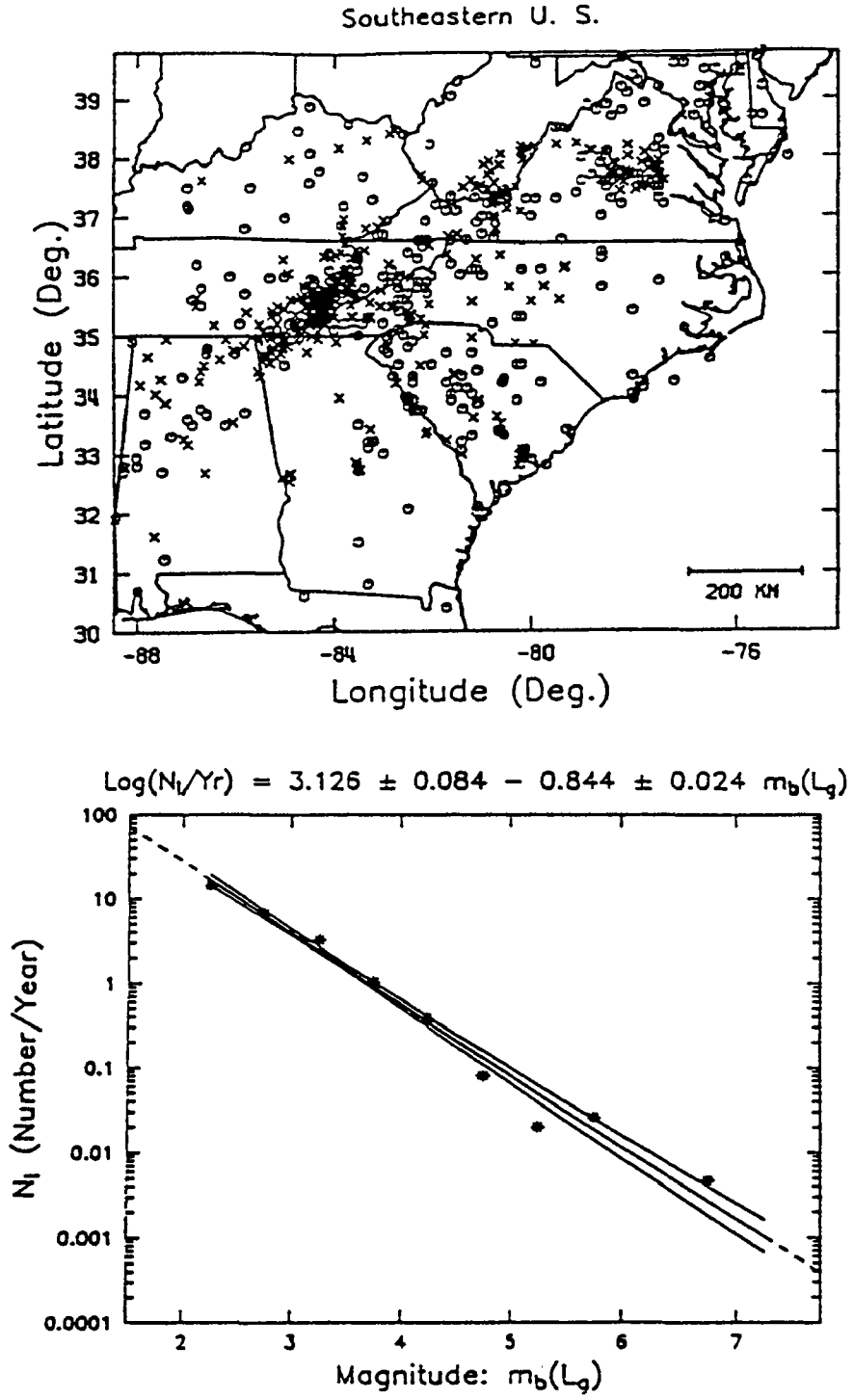

FIGURE 3. Magnitude Recurrence Relation For The Southeastern U. S. The upper half of the figure shows the seismicity map with historical (circles) and network (X's) epicenters for the time period 1772-1986. The lower half of the figure shows a plot of Log(NI) (interval number of earthquakes per year, m ± 0.25) versus mb(Lg) for the southeastern U.S. The maximum likelihood line includes 95% confidence intervals (Source: Bollinger and others, 1989).

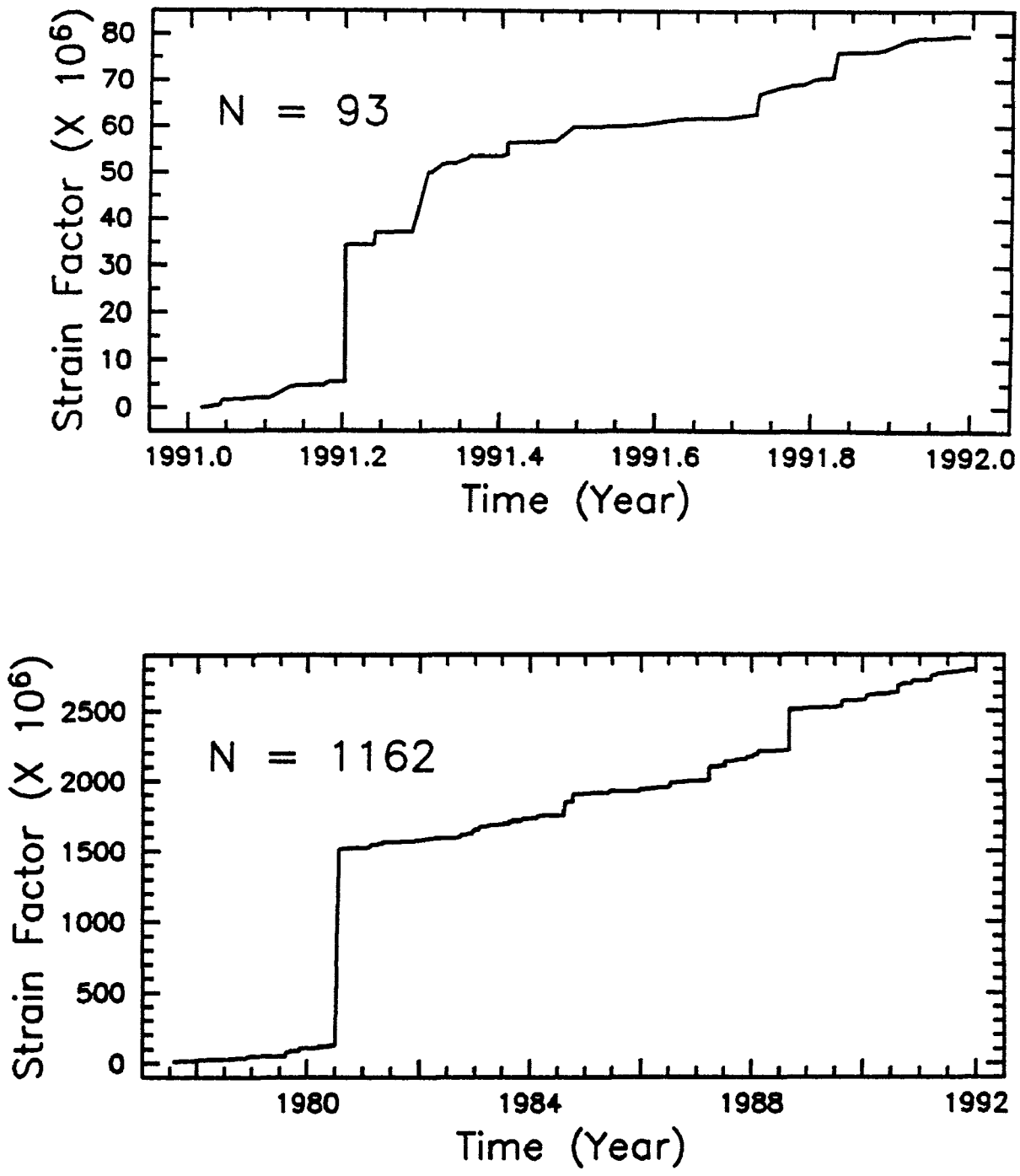

FIGURE 4. Cumulative Strain Factor History of Southeastern U.S. Earthquakes. The upper half of the figure shows the cumulative strain factor history for the report period, while the lower half of the figure shows a similar plot for earthquakes from July 1977 through this report period.

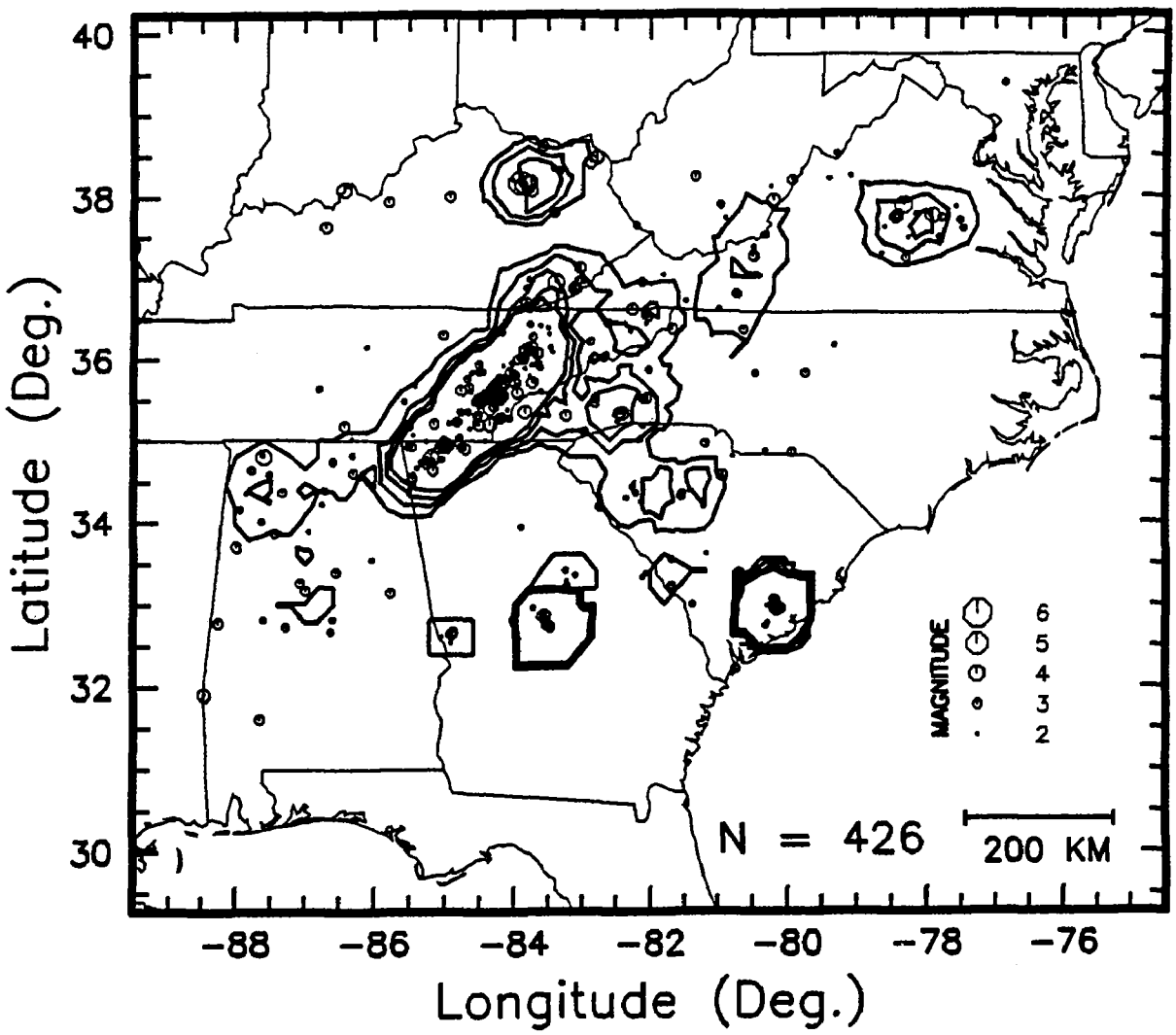

FIGURE 5. Epicenter Density Contour Map for Earthquakes (circles scaled to magnitude; M ≥ 2.0) in the Southeastern United States from July 1977 through this report period. Contours represent number of earthquakes within 50 km of a grid point scaled to number per 10,000 square km; grid spacing is 0.2 degrees. Lowest and highest contours are 5 and 20 events per 10,000 square km, respectively (contour interval is 5).

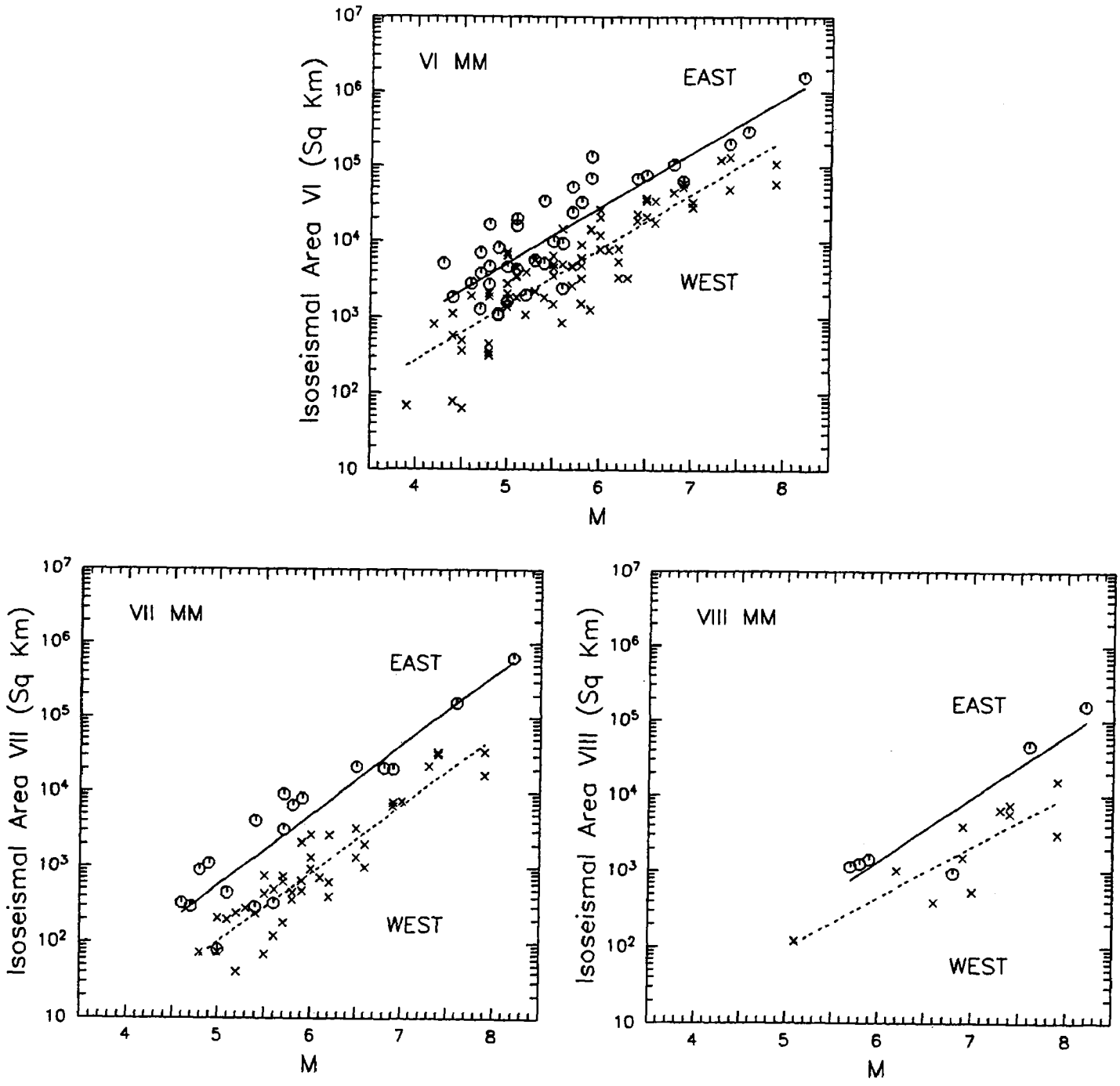

Figure 6. Isoseismal areas, at the MMI = VI, VII, VIII levels, versus moment magnitude for 112 VI areas, 58 VII areas and 17 VIII areas for 36 eastern North American earthquakes and 76 western U.S. earthquakes. ENA data = circles and WUS data = x's. The straight-line fits indicate that the ENA damage areas are about five times greater than those for the WUS.

Analysis of the 1957 Andreanof Islands Earthquake
14-08-0001-G1766

Thomas M. Boyd
Colorado School of Mines
Department of Geophysics
Golden, CO 80401
(303) 273-3522

Project Summary and Goals

Recent studies have indicated that the spatial distribution of moment release can be quite heterogeneous along any particular rupture zone. The most common explanation for this heterogeneity has been the rupture of strong patches, or asperities, along the fault plane [e.g., Ruff and Kanamori, 1983]. These strong patches could arise from spatial variations of the frictional characteristics along the fault or from geometrical barriers inherent to the fault's shape. Alternatively, the spatial distribution of moment release could have little to do with the physical characteristics of the fault's surface and may be related to the dynamics of slip and how regions of the fault interact with neighboring regions [e.g., Rundle and Kanamori, 1987; Horowitz and Ruina, 1989].

Distinctions between these two models can not be made from the analysis of single events [e.g., Thatcher, 1990]. Conclusive observations can only be drawn from a study of the moment-release distribution generated by several great earthquakes, all of which rupture the same fault segment. In this context, an excellent region of study is the central Aleutian Arc. In 1986, a magnitude 8.0 (M_W) earthquake occurred near the Andreanof Islands. Its slip distribution, aftershock, and preshock sequence have been described in detail in a number of recent studies. Prior to 1986, the central Aleutian Arc was ruptured by another great earthquake in 1957 ($M_W > 8.5$). The 1957 Andreanof Islands earthquake, however, remains poorly understood. Its seismic moment, slip distribution, and rupture area have not been well constrained.

The short time span between the 1957 and 1986 earthquakes provides us with a unique opportunity to study a complete seismic cycle bounded by two instrumentally recorded great earthquakes. In fact, it represents the only complete seismic cycle instrumentally observed along the Aleutian Arc. As briefly described in this summary, we are continuing our work on assembling and interpreting observations pertinent to the 1957 earthquake and the interseismic period between the 1957 and 1986 events. Progress can be summarized as;

1) We have constrained the rupture bounds of the 1957 earthquake using surface-wave directivity.

2) All seismicity occurring between 1957 and 1989 has been relocated.

3) A catalog of earthquake relocations is now available through anonymous FTP to the USGS in Golden or on the CD-ROM distributed as part of the Wadati Conference held in Fairbanks, Alaska in September, 1992.

Rupture Length Estimates

Accurate determinations of kinematic rupture parameters have been accomplished for some time using the so-called directivity function [e.g., Ben-Menahem, 1961; Ben-Menahem and Toksoz, 1962, 1963; Udias, 1971]. Unfortunately, because it is highly nonlinear, this function is difficult to invert. Using the simulated annealing method [Kirkpatrick et al., 1983], however, we have constructed an inversion process which is capable of extracting accurate estimates of kinematic rupture parameters and provides the probability distribution of their values.

A recent PhD. graduate who was supported by this project, David Lane, developed an ensemble approach in which several independent inversions are run simultaneously. The objective of each inversion is to maximize the joint probability distribution $P(\mathbf{M}=m|\mathbf{D}=d)$, where **M** represents the kinematic rupture parameters, and **D** represents the observed data. After several iterations the algorithm generates solutions distributed as $exp(-E/kT_j)$, where E represents the error between a possible solution and the observed data, and T_j is the control parameter of the *jth* inversion. We contend that the maximum likelihood estimate obtained during a single inversion is less important than the marginal distribution of rupture parameters. Since each of the inversions are independent we obtain the marginal distributions $P(M_i=n)$ by summing over the joint inversions. Figure 1 shows inversion results for the 1957 event using data recorded at Pietermaritzburg South Africa. As shown in Table 1., three solutions have been identified which match the observed directivity. These solutions rupture lengths of 874 km; 642 km to the east and 192 km to the west, 738 km; 550 km to the east and 188 km to the west; and 954 km, 601 km to the east and 354 km to the west. We are currently combining these results with those obtained by Satake under USGS grant 1434-92-G-2187 to obtain a final, consistent estimate of rupture length and moment-release distribution. Preliminary results from this portion of the project were presented at the 1990 Fall AGU meeting in San Francisco [Lane and Boyd, 1990] and recently at the 1992 Wadati Conference held in Fairbanks, Alaska [Boyd et al., 1992]. A paper by Lane in Boyd describing the results of this experiment is in preparation and will be submitted to BSSA within the next 3 months [Lane and Boyd, 1993].

Seismicity Relocations

We have relocated and cataloged seismicity recorded from 1957 through 1989 (March) with epicenters lying between 175°E and 160°W. Our relocations include epicenter-dependent, P-wave station corrections which account for near-source velocity structure. These corrections are calculated for 686 stations using a slab geometry detailed by a recent, teleseismic, travel-time study and the iasp91 travel-time model. Unless other information is available, source depths are constrained to 35 km. For events deeper than 50 km, station corrections are not applied and source depths are determined using both P and pP arrivals. Arrival times for earthquakes occurring between 1957 and 1963 are obtained by optically scanning of the ISS and BCIS bulletins. For this time period, magnitudes were available for only a small percentage of the relocated events. We calculated magnitudes for as many of these events as possible, using body- and surface-wave amplitudes recorded at Pasadena. For events recorded between 1964 and 1989,

arrival times and magnitudes are obtained from the ISC phase tapes.

The completed catalog consists of approximately 7300 earthquakes. Dividing the geographical distribution of observing stations into four azimuthal zones (Europe and the Arctic, North and South America, Asia, and the South Pacific), we classified earthquakes into one of four quality groups. Group A consists of events recorded by at least two stations in all four azimuthal zones. Group B consists of events recorded by at least two stations in three of the four azimuthal zones. Group C consists of events recorded by at least one station in three of the four azimuthal zones. Group D consists of all those events not meeting the requirements of groups A, B, or C. All events within groups A and B, 3200, have 90% error vectors of less than 25 km.

We determine the minimum magnitude of completeness for our catalog by plotting the number of events per magnitude increment. For this comparison, we have converted all of the observed magnitudes to Ms using a regression relationship derived from events for which both mb and Ms are available. Between 1964 and 1989, our catalog is complete above Ms=4.6. From 1957 through 1963, the minimum magnitude of completeness is 5.5. To uniformly sample the seismic record over the entire time period of our catalog, only events larger than or equal to 5.5 should be used. Also note that for each time period, earthquakes whose magnitudes are above the level of completeness are well located.

In Figure 2, we have plotted the epicenters of the shallow earthquakes listed in our catalog. Only events in groups A and B have been included. Notice that these events can be divided visually into two categories: 1) outer rise earthquakes (i.e., those events whose epicenters lie within or south of the trench), and 2) main thrust-zone earthquakes (i.e., those events whose epicenters lie between the trench and the arc massif). These two groups of earthquakes are separated by a clearly defined aseismic zone. The outer rise earthquakes are caused by deformation within the oceanic lithosphere whereas the main thrust-zone earthquakes are located at the coupled interface between the lithosphere and the overriding massif. Presumably, the aseismic region results from the presence of unconsolidated, overpressured sediments with strengths too low to support seismicity. Seismicity within the main thrust-zone, is bounded to the south and north by clearly defined seismic and aseismic fronts. In general, both the seismic and aseismic fronts are continuous, along-arc features. Five notable exceptions, however, can be observed. 1) The seismic front moves northward just south of Unalaska Island (166°W), and the level of activity within this region is lower than in surrounding regions. 2) Little seismicity has been detected over the past thirty years just east of the intersection point of the Amlia Fracture Zone with the trench at 173°W. We note, also, that the earthquakes within this region are large (Ms> 6.0), and occurred soon after the 1957 earthquake. 3) Near the Adak Canyon region (177°W), seismicity extends southward to the trench, while the aseismic front remains continuous. 4) Amchitka Pass (180°E) is aseismic. 5) The region near Murray Canyon (177°E) has generated very few earthquakes. Outer rise earthquakes occur along the entire arc, but cluster around a few specific regions: 178°E, 179°E, 177°W, 173°W, and 171°W. Most of the outer rise activity occurred soon after the large thrust faulting earthquakes of 1957 and 1965, with activity gradually decreasing from the time of the mainshock. Only one, well located, outer rise earthquake followed the 1986 event.

The space time distribution of main thrust-zone and outer rise earthquakes occurring within 30 days of the 1957 earthquake is shown in Figure 3. Except for the single event that occurred immediately after the mainshock near 165°W, earthquakes are initially

confined to a portion of the arc that lies between 167°W and 177°W. The initial aftershock area is consistent with the tsunami source area, and rupture length inferred from surface-wave directivity. Within a day after the mainshock, aftershock activity spread westward. Within three days, activity spread eastward. The final extent of the aftershock zone is some 1200 km. The larger events which extended the aftershock zone eastward all occurred within a small region east of Unalaska Island. Outer rise earthquakes are concentrated in three clusters; one each to the east and west of the intersection point of the Amlia Fracture Zone, and one south of Adak Canyon.

Figure 4 shows the epicentral locations of earthquakes occurring near Adak Island over three time periods; during the aftershock sequence of the 1957 earthquake, during the interseismic period between the 1957 and 1986 earthquakes, and during the aftershock sequence of the 1986 earthquake. Only shallow, well-located events larger than Ms=5.4 are included. The epicenters of the 1957 and and 1986 earthquakes are indicated by the largest filled circles in panels A and C.

The epicentral distribution of events is quite heterogeneous over time and space. During the aftershock sequence of the 1957 earthquake (Panel A, Figure 4), few events occurred along the main thrust-zone south of Amlia Island east of the epicenter of the mainshock. Many events occurred near Adak Canyon (177°W), southeast of Adak Island (176°W), and arcward of the intersection point of the Amlia Fracture Zone with the trench. Outer rise earthquakes cluster near the Amlia Fracture Zone and near the trenchward extension of Adak Canyon.

During the interseismic period (Panel B, Figure 4), many fewer outer rise events are detected, and those that did occur are clustered near the trenchward extension of Adak Canyon. As was observed for the 1957 aftershock sequence, few events are located along the main thrust-zone south of Amlia Island, while many events are observed arcward of the Amlia Fracture Zone, and southeast of Adak Island. Unlike the aftershock sequence, however, the region near Adak Canyon is seismically quiet during the interseismic period.

Aftershocks of the 1986 earthquake (Panel C, Figure 4) are concentrated near Adak Canyon, and south of Amlia Island. The section of the arc southeast of Adak Island that was seismically active during the 1957 sequence and during the interseismic period remains seismically inactive after the 1986 earthquake. Like the 1957 sequence, aftershocks of the 1986 event also cluster about the epicenter of the mainshock.

Studies of the moment distribution of the 1986 earthquake suggest that regions of high moment release generate few aftershocks. Seismic moment released during the 1986 event was concentrated in the regions just east of the mainshock's epicenter and along the western rupture extent, where few aftershocks occurred. Efforts are currently underway to constrain the seismic moment distribution of the 1957 earthquake independent of these speculations by modeling marigrams. Assuming an anti-correlation between aftershock locations and seismic moment release, we suggest that seismic moment was concentrated in an area bounded to the west by the mainshock's epicenter and to the east by the intersection with the Amlia Fracture Zone. Although a significant amount seismic moment may also have been released west of the mainshock to Adak Canyon, the concentration of the aftershocks southeast of Adak Island suggests this area did not generate significant slip during the 1957 earthquake.

Compared to the moment distribution of the 1986 earthquake, that which we have suggested for the 1957 earthquake different. If correct, regions of high seismic moment

release, asperities, may vary from earthquake to earthquake, suggesting that the moment distribution is not controlled by the strength distribution on the fault surface alone. Rather it is a consequence of the interaction of the fault's strength distribution with the dynamics by which rupture propagates.

Our relocation effort is complete, and a paper by Boyd, Engdahl, and Spence is in preparation. Preliminary results from this portion of the project were presented at the 1990 Fall AGU meeting [Boyd et al., 1990] and the 1992 Wadati Conference held in Fairbanks, Alaska [Boyd et al., 1992].

References

Ben-Menahem, A., and M. N. Toksoz, Source mechanism from spectra of long-period seismic surface waves, 1. The Mongolian earthquake of December 4, 1957. *J. Geophys. Res., 67,* 1943-1955, 1962.

Ben-Menahem, A., and M. N. Toksoz, Source mechanism form spectra of long-period surface waves, 2. The Kamchatka earthquake of November 4, 1952, *J. Geophys. Res., 68,* 5207-5222, 1963.

Boyd, T. M., E. R. Endgahl, and W. Spence, Aftershocks of the 1957 Aleutian Islands earthquake, *EOS, 71,* 1469, 1990.

Boyd, T. M., F. D. Lane, and E. R. Engdahl, Historical earthquakes: Rupture length estimates based on aftershock locations and surface wave observations, Abstract, *EOS, 72,* 189, 1991.

Boyd, T. M., E. R. Engdahl, and W. Spence, Analysis of seismicity associated with a complete seismic cycle along the Aleutian Arc: 1957 through 1989, Published in; Proceedings of the Wadati Conference on Great Subduction Earthquakes, University of Alaska, Fairbanks, AL, 43-51.

Boyd, T. M., E. R. Engdahl, and W. Spence, Analysis of seismicity associated with a complete seismic cycle along the Aleutian Arc: 1957 through 1989, to be submitted to, *J. Geophys. Res.*, 1993.

Dillinger, W. H., A. J. Pope, and S. T. Harding, The determination of focal mechanisms using *P-* and *S-wave* data, *NOAA Tech. Report NOS 44,* 56 pp., 1971.

Horowitz, F. G., and A Ruina, Slip patterns in a spatially homogeneous fault model, *J. Geophys. Res., 94,* 10,279-10,298, 1989.

Kirkpatrick, S., C. D. Gelatt, and M. P. Vecchi, Optimization by simulated annealing, *Science, 220,* 671-680, 1983.

Lane, F. D., and T. M. Boyd, A simulated annealing approach to the inversion of surface wave directivities: Application to the 1957 Aleutian Islands earthquake, *EOS, 71,* 1468, 1990.

Lane, F. D., and T. M. Boyd, Estimation of kinematic rupture parameters from historical seismograms, to be submitted to, *Bull. Seismol. Soc. Amer.*, 1993.

Ruff, L., and H. Kanamori, The rupture process and asperity distribution of three great earthquakes from long-period diffracted P-waves, *Phys. Earthq and Planet. Inter., 31,* 202-230, 1983.

Rundle, J. B., and H. Kanamori, Application of an inhomogeneous stress (patch) model to complex subduction zone earthquakes: A discrete interaction matrix approach, *J. Geophys. Res., 92,* 2606-2616, 1987.

Stauder, W., and A. Udias, S-wave studies of earthquake of the North Pacific, Part II: Aleutian Islands, *Bull. Seismol. Soc. Am., 53,* 59-77, 1963.

Thatcher, W., Order and diversity in the modes of Circum-Pacific earthquakerecurrence, *J. Geophys. Res., 95,* 2609-2624, 1990.

Udias, A., Source parameters of earthquakes from spectra of Rayleigh waves, *Geophys. J. R. Astr. Soc., 22,* 353-376, 1971.

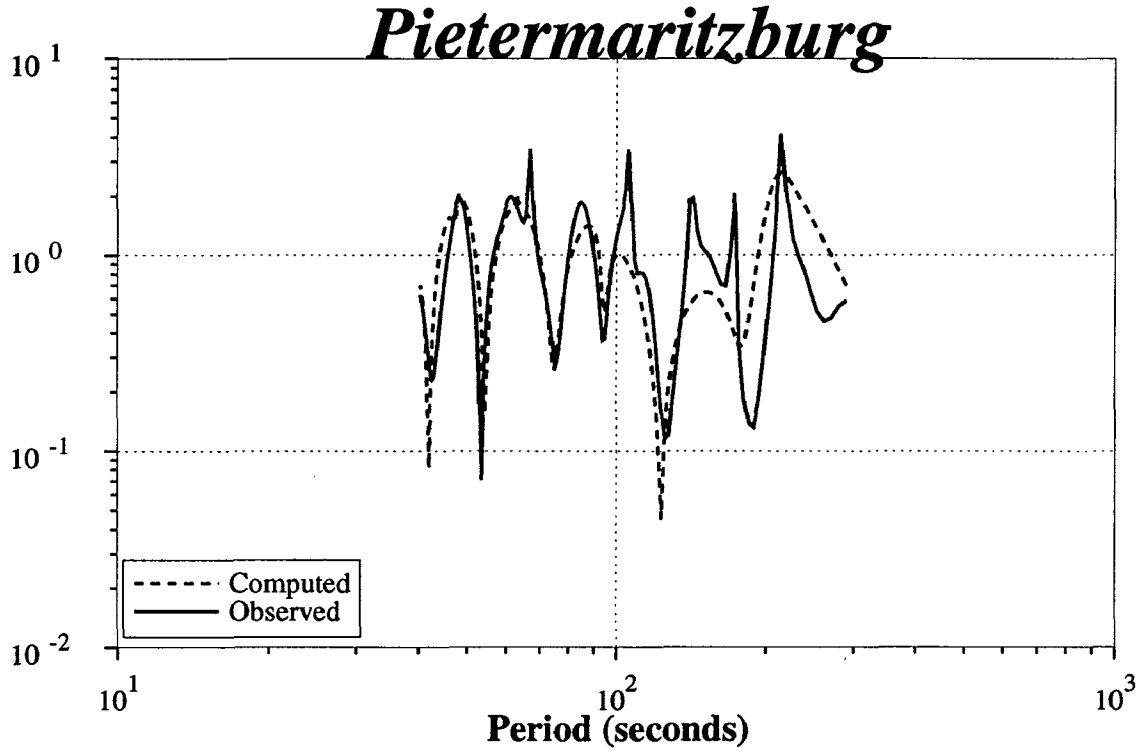

Figure 1: Computed, dashed line, and observed, solid line, directivity for the 1957 Andreanof Islands earthquake. Three different fault models were found that could produce the computed directivity shown above. The fault parameters for these three models are given in Table 1.

Table 1: Fault Parameter estimates

	Eastern Fault Length (km)	Western Fault Length (km)	Rupture Velocity (km/s)
Solution 1	682	192	2.2
Solution 2	550	188	1.9
Solution 3	601	354	2.1

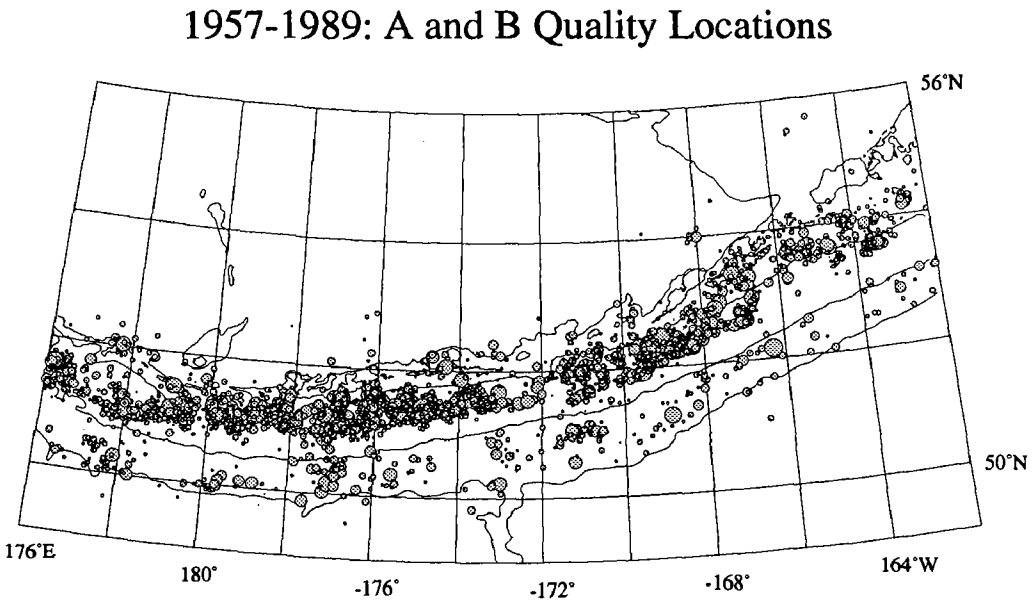

Figure 2: Epicentral locations of all earthquakes within groups *A* and *B* whose source depths are less than 50 km. Symbols are scaled by earthquake magnitude (M_S).

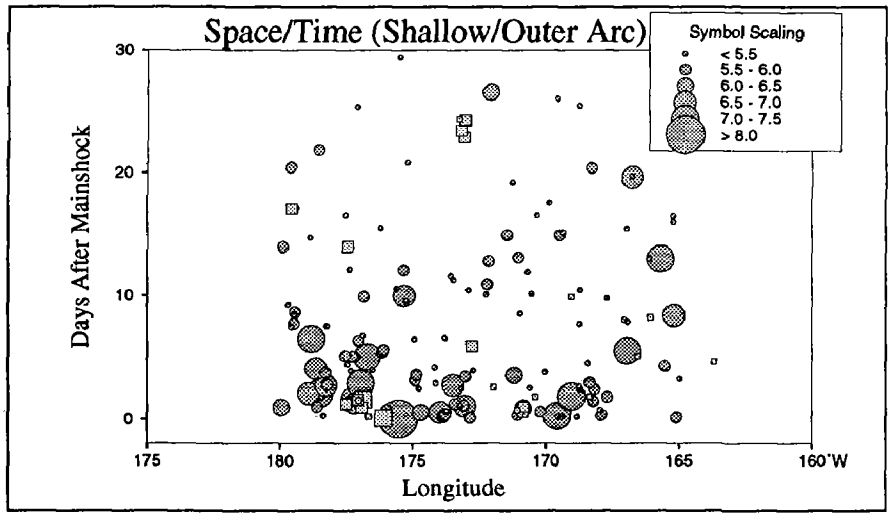

Figure 3: Space Time distribution of seismicity occurring within a month of the 1957 Aleutian Islands earthquake. Filled circles indicate earthquakes along the main thrust-zone, filled squares indicate outer rise earthquakes. The arrow indicates the rupture bounds of the 1957 event inferred from surface-wave directivity.

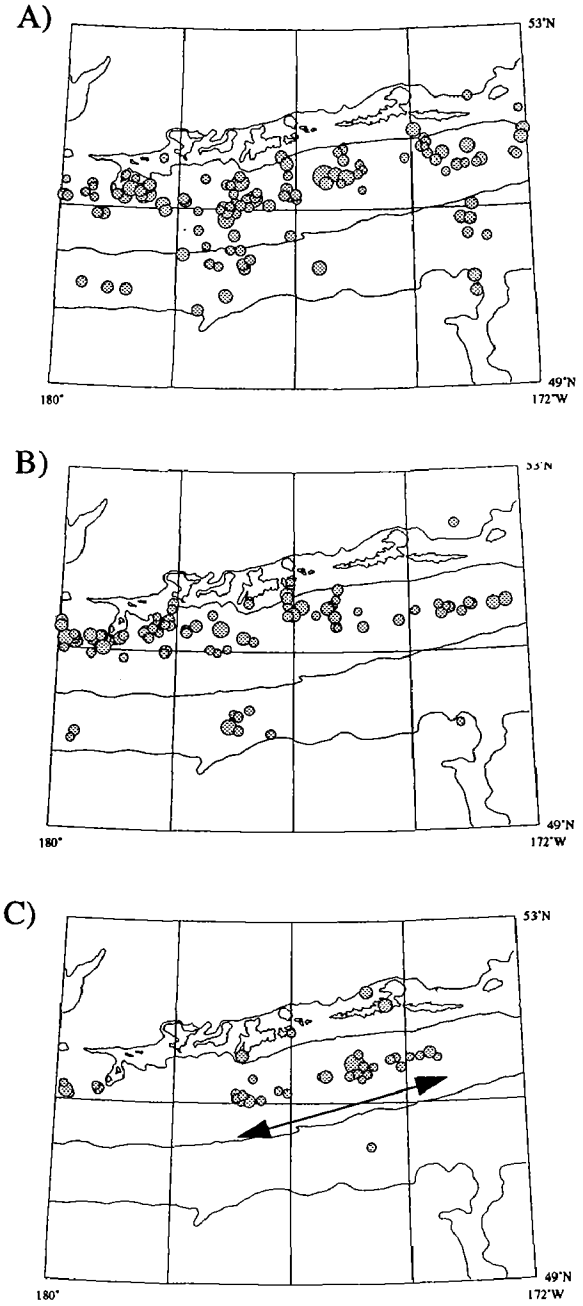

Figure 4: Well located earthquakes occurring around the rupture zone of the 1986 event with magnitudes above 5.4. Panel A shows events that occurred during the aftershock sequence of the 1957 earthquake (03/1957 - 05/1960). Panel B shows events occurring during the interseismic period (05/1960 - 05/1986). Panel C shows events occurring during the aftershocks sequence of the 1986 earthquake (05/1986 - 03/1989). Arrow indicates rupture bounds of the 1986 earthquake.

Characterization of Self-Similar Comminution and Slip Localization in Large-Displacement Faults for Application to Laboratory Fault Modelling

1434-92-G-2184

Frederick M. Chester

Department of Earth and Atmospheric Sciences, Saint Louis University
3507 Laclede Ave., St. Louis, MO 63103

James P. Evans

Department of Geology, Utah State University
Logan, UT 84322

Investigations

We are conducting a field geologic study of exhumed faults of the San Andreas system to infer the environmental conditions of faulting, the mechanisms of slip, and the physical and mechanical properties of fault zones at seismogenic depths. This type of research will help guide laboratory fault modelling efforts and ultimately will contribute to an understanding of the physics of the earthquake source. Up to this time we have focused our study to the North Branch San Gabriel fault because this fault segment is probably one of the most deeply exhumed and best exposed, large-displacement faults of the San Andreas system. To date we have conducted three related studies of the fault zone to characterize 1) mesoscopic scale subsidiary fault fabric, 2) mineralogic alteration and fluid/rock interaction, and 3) particle size distributions of the cataclastic fault rocks. The results of these studies have been integrated and used to develop a conceptual model for the internal structure and weakening mechanisms of the San Andreas fault and is presented by Chester et al. [1992]. The abstract of this paper is included below.

Our findings from the North Branch San Gabriel fault indicate localized but extensive evidence for fluid-rock interaction and mineralogic alteration contemporaneous with movement on the San Gabriel fault. This is in marked contrast with previous findings from petrologic study of several exposures of the San Gabriel fault west of our study localities [Anderson et al., *Tectonophysics*, *98*, 209-251, 1983]. Our most recent efforts have been directed toward trying to better characterize the differences in fault rock petrology along strike by expanding our study localities to include more western exposures of the San Gabriel fault in the Pacoima Canyon area. For several key localities of the San Gabriel fault we are investigating variations in bulk rock chemistry across and within the fault zone and surrounding host rock. Preliminary results indicate substantial mobility of some elements within the core of the faults and significant volume changes. We also have begun investigations of the San Andreas fault near Wrightwood so that we may better compare the characteristics of the San Andreas and San Gabriel faults.

Results

New observations of the internal structure of the San Gabriel fault (SGF) are combined with previous characterizations of the Punchbowl fault (PF) to evaluate possible explanations for the low frictional strength and seismic characteristics of the San Andreas fault (SAF). The SGF and PF are ancient, large-displacement faults of the SAF system exhumed to depths of 2 to 5 km. These fault zones are internally zoned; the majority of slip was confined to the cores of principal faults, which typically consist of a narrow layer (less than tens of centimeters) of ultracataclasite within a zone of foliated cataclasite several meters thick. Each fault core is bounded by a zone of damaged host rock of the order of 100 m thick. Orientations of subsidiary faults and other fabric elements imply that (1) the maximum principal stress was oriented at large angles to principal fault planes, (2) strain was partitioned between simple shear in the fault cores and nearly fault-normal contraction in the damaged zones and surrounding host rock, and (3) the principal faults were

weak. Microstructures and particle size distributions in the damaged zone of the SGF imply deformation was almost entirely cataclastic and can be modeled as constrained comminution. In contrast, cataclastic and fluid-assisted processes were significant in the cores of the faults as shown by pervasive syntectonic alteration of the host rock minerals to zeolites and clays and by folded, sheared, and attenuated cross-cutting veins of laumontite, albite, quartz, and calcite. Total volume of veins and neocrystallized material reaches 50% in the fault core, and vein structure implies episodic fracture and sealing with time-varying and anisotropic permeability in the fault zone. The structure of the ultracataclasite layer reflects extreme slip localization and probably repeated reworking by particulate flow at low effective stresses. The extreme slip localization reflects a mature internal fault structure resulting from a positive feedback between comminution and transformation weakening. The structural, mechanical, and hydrologic characteristics of the Punchbowl and San Gabriel faults support the model for a weak San Andreas based on inhomogeneous stress and elevated pore fluid pressures contained within the core of a seismogenic fault. Elevated fluid pressures could be repeatedly generated in the core of the fault by a combination of processes including coseismic dilatancy and creation of fracture permeability, fault-valve behavior to recharge the fault with fluid, post-seismic self-sealing of fracture networks to reduce permeability and trap fluids, and time-dependent compaction of the core to generate high pore pressure. The localized slip and fluid-saturated conditions are wholly compatible with additional dynamic weakening by thermal pressurization of fluids during large seismic slip events, which can help explain both the low average strength of the San Andreas and seismogenic characteristics such as large stress relief. In addition, such a dynamic weakening mechanism is expected only in mature fault zones and thus could help explain the apparent difference in strength of large-displacement faults from smaller-displacement, subsidiary seismogenic faults.

Reports

Chester, F.M., Subsidiary fault structure and paleostress of the San Gabriel fault zone, San Gabriel Mountains, California, Eos Trans. AGU, 72, 264, 1991.

Chester, F.M. , J.P. Evans, and R.L. Biegel, Internal structure and weakening mechanisms of large-displacement fault of the San Andreas system, Geol. Soc. Am. Abstr. w. Prog., 23, A103, 1991.

Evans, J.P., and F.M. Chester, Mechanisms of slip localization: No. Branch San Gabriel fault, CA, Eos Trans. AGU, 72, 435, 1991.

Chester, F.M., J.P. Evans, and R.L. Biegel, Internal Structure and Weakening Mechanisms of the San Andreas Fault, in press, J. Geophys. Res., 1992.

Friction Constitutive Behavior of Saturated Faults at Hypocentral Conditions

1434-92-G-2203

Frederick M. Chester

Department of Earth and Atmospheric Sciences, Saint Louis University
3507 Laclede Ave., St. Louis, MO 63103

Investigations

The goal of the project is to determine the friction constitutive behavior of water saturated faults at hypocentral conditions through laboratory experiments and constitutive modeling. I have focused my investigations on the temperature dependence of friction because this information is necessary to apply laboratory data to natural faulting and to identify the fundamental micromechanisms governing friction at hypocentral conditions. The results of this research should help to improve our understanding of earthquake faulting and provide the constitutive descriptions of fault zones that are necessary to formulate quantitative models of the earthquake source.

I completed the following tasks during the previous contract period: 1) formulation of a temperature-dependent constitutive relationship for friction in rock, 2) development of a multi-mechanism constitutive model that can describe frictional behavior at hydrothermal conditions, 3) experimentation with quartz gouge at hydrothermal conditions to determine constitutive behavior, and 4) experimentation with graphite to determine the rate- and temperature-depedent characteristics of the testing apparatus. The results of tasks (1) and (2) are reported by Chester and Higgs [1992]. Over the last year I have carried out a detailed analysis of the graphite experiments to quantify apparatus properties followed by an analysis of the quartz experiments to quantify constitutive behavior and to test the constitutive relationship that I formulated for temperature-dependent friction. Description of the experiments on quartz and graphite and the results of the analyses are summarized below and a manuscript is now in preparation [Chester, 1992].

Results

Thin layers of graphite powder and granular quartz were sheared in a gas confining medium, internally heated, triaxial apparatus using a standard triaxial shear configuration (Figure 1). The sample for both graphite and quartz experiments consisted of a cylinder of steel 32.8 mm in diameter cut in half along a plane inclined 35° from the cylinder axis. Either graphite or quartz was placed between the sample halves along the 35° inclined interface. The assemblies were sealed in metal sleeves and axially shortened at confining pressure. The metal sleeves consisted of copper foil (either 0.075 or 0.15 mm thick) centrally located within a lead foil totaling 2 mm thick. Confining pressure, pore fluid pressure, and axial shortening rate were servo-controlled during the experiments. Axial load was measured both inside and outside the pressure vessel. Axial shortening caused shear displacement of the sample halves and allowed measurement of the resistance of the graphite or quartz layers to shear.

Axial shortening of the assembly requires lateral motion of the sample halves. Lateral offset occurred along a single interface between steel spacers oriented perpendicular to the cylinder axis (Figure 1). In all experiments this spacer interface was ground smooth and separated by a layer of graphite approximately 0.2 mm thick. In addition to the lateral offset, shortening of the sample requires deformation of the metal sleeves used to seal the sample from the confining medium. Both the strength of the metal sleeves and the frictional resistance to slip along the spacer interface contribute to the total resistance to axial shortening of the sample. These two effects, though relatively small, were significant for the measurements of velocity and temperature dependencies of friction in the quartz layers. The metal sleeve, lateral slip surface, and the inclined interface are all coupled in the testing assembly and can not be isolated for characterization (Figure 1). However,

the behavior of each component can be determined by an appropriate parametric study because each has a different dependence on external parameters such as confining pressure, slip velocity, and temperature. The experiments on graphite were done primarily to characterize the two apparatus effects.

Axial displacement of the sample was measured with a displacement transducer located external to the pressure vessel. Displacement rate was specified with a 16 bit digital command signal generator and maintained by closed-loop servo control. The least significant bit of the command signal corresponded to 0.16 μm shear displacement, and I have verified through additional sensing transducers that the actuator achieved displacements at this level of precision. The displacement measurements over the course of an experiment were less accurate due to a number of factors including temperature-induced changes of the transducer outputs. Experiments were conducted by stepping shear velocity by a factor of ten between 4.0 and 0.04 μm s^{-1} in a standardized sequence. The step changes in velocity were essentially instantaneous.

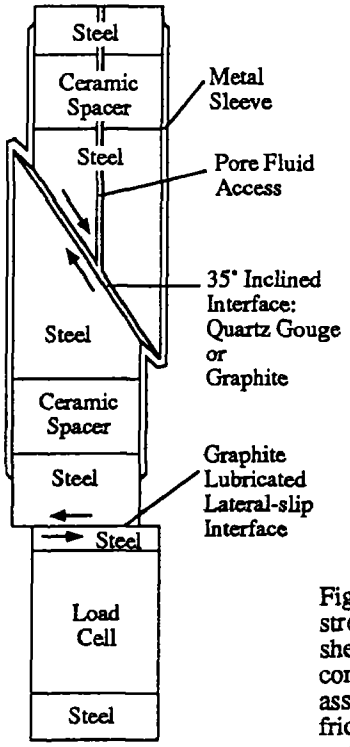

$$\mu_i = \frac{\tau_i}{\sigma_i} = \frac{\Delta\sigma_t(\cos\theta\sin\theta - \mu_{ls}\sin\theta) - \Delta\sigma_{ms}\cos\theta\sin\theta}{(P_c - P_p) + \Delta\sigma_t(\sin^2\theta + \mu_{ls}\cos\theta\sin\theta) - \Delta\sigma_{ms}\sin^2\theta}$$

μ_i = coefficient of friction of inclined interface

μ_{ls} = coefficient of friction of lateral-slip interface

$\Delta\sigma_t$ = total differential stress

$\Delta\sigma_{ms}$ = differential stress supported by metal sleeve

$(P_c - P_p)$ = effective confining pressure

$\theta = 35°$ = angle of inclined surface

Figure 1. Sample assembly for triaxial shear experiments. Shear strength of the inclined interface, strength of the metal sleeve, and shear strength of the graphite lubricated, lateral-slip spacer interface contribute to the total differential stress supported by the sample assembly and measured by the internal load cell. The coefficient of friction of the inclined interface is defined in terms of the other parameters by the equation above.

Elevated temperatures were achieved within the pressure vessel with a resistance furnace wrapped around the steel cylinder halves. The temperature of the furnace was controlled by a sensing thermocouple located at the furnace. The temperature of the specimen was monitored independently by a sensing thermocouple located at the gouge layer in the pore-fluid access hole. The temperature of the graphite lubricated, lateral slip surface also was monitored by a dedicated thermocouple. Temperatures in the center of the specimen were generally maintained to within 1°C. The cylinder halves were thermally insulated from the load column by Al_2O_3 ceramic spacers and from the confining medium and the pressure vessel walls by a ceramic fiber wrap. Insulation was not perfect, however, so other components of the load column such as the lateral-slip interface also experienced elevated temperatures. The furnace produced relatively small temperature gradients along the sliding surfaces and no restriction on the lateral motion of the sliding specimen halves. Temperature of the samples during tests were maintained constant at or stepped between room temperature (24° to 28°C), 57°C, and 82°C. By using steel cylinders with high thermal

conductivity and the proper sequence of variable power output by the furnace, an upward temperature step of 30°C to a new equilibrated temperature condition was achieved at the 35° inclined interface in approximately 100 s. Steps down in temperature from 82°C to 57°C took slightly longer, approximately 200 s. The lateral-slip interface took somewhat longer to reach equilibrium after temperature steps than the inclined interface. Temperature steps were conducted only during sliding at a constant velocity of 0.04 μm s^{-1}. Therefore, the shear displacement across the gouge layer during the temperature step was less than several μm. Based on the relatively rapid equilibration of pore fluid pressure in the samples, pore pressures were maintained constant during temperature steps.

Thermal expansion of the sample column during temperature changes was significant; expansion was approximately 1 μm axial lengthening per °C temperature change. The expansion was measured by the transducer used to generate the feedback signal for the displacement servo-control. Accordingly, the command signal was corrected to achieve a constant shear velocity of approximately 0.04 μm s^{-1} across the gouge layer during each temperature step. In practise, the average shear velocity during the temperature steps was maintained between 0.02 and 0.06 μm s^{-1}. Corrections to the command signal were based on separate calibrations conducted under load feedback that defined the thermal expansion of the sample column during temperature changes. To apply the proper correction to the command signal and achieve a constant shear velocity during the temperature steps, it was necessary to standardize the heating sequence during temperature steps. Due to slight variations in the furnace geometry between each sample assembly, it was necessary to calibrate the power requirements of the furnace and the heating sequence for each experiment. This calibration was done at confining and pore pressure and small differential load but prior to imposing shear displacement. The test assembly was permitted to equilibrate to the specified temperature of the experiment prior to initiating the shear displacement tests.

Analog and digital records of differential axial load, axial displacement, confining pressure, pore fluid pressure, pore volume changes, temperature along the 35° inclined interface, and temperature of the graphite lateral slip surface were collected for all experiments. Analog signals were digitized at 15 to 20 Hz with a 14 bit analog to digital converter. Digitized data was averaged and recorded by a computer every 3.0 μm of shear displacement during steady sliding and every 0.3 μm of shear displacement during friction transients associated with step changes in velocity, temperature, or pore-pressure. The least significant bit for digital records were 5.0 N axial load, 0.76 μm shear displacement, 10 kPa confining pressure, 0.24 kPa pore pressure, and 0.03 °C.

Graphite Experiments. In these tests the 35° inclined interface between sample halves and the thickness of the graphite along the interface was prepared the same as for the lateral-slip spacer interface. This simplifies the analysis of the experiments because the surfaces are described by the same constitutive relation. At the temperature and pressure conditions of the experiments, graphite lubricated interfaces are frictional in that they show a dependence of shear strength on pressure. In contrast, the strength of the metal sleeves is largely insensitive to pressure because they deform by intracrystalline plastic deformation mechanisms. Thus in these experiments the relative contributions of the graphite interfaces and the metal sleeves to the total strength of the sample assemblies varies with confining pressure. At high pressures the graphite surfaces support greater loads than the metal sleeves whereas at low pressures the opposite occurs. Accordingly, experiments were conducted at confining pressures ranging from 2 to 60 MPa. The dependence of the metal sleeve and of the graphite interfaces on temperature and velocity were defined by stepping velocity between 4, 0.4 and 0.04 μm/s and stepping temperature between 24 and 57 °C or 57 and 82 °C at a fixed confining pressure of 20 or 60 MPa. Samples with single- and double-thickness copper foil sleeves were used in both types of experiments.

By simultaneously modelling the results for all graphite experiments with single- and double-thickness metal sleeves at low and high confining pressure it is possible to define the relative contribution of the sleeves and the graphite to the temperature and velocity dependencies. I have found that the differential stress supported by the metal sleeves is insensitive to confining pressure and that the shear strength of the graphite lubricated interfaces is adequately described with a Coulomb relation ($\tau = C_0 + C_1\sigma$) over the range of normal stresses tested (Figure 2). Thus, the

coefficient of friction of graphite is a strong function of normal stress. Both graphite friction and metal sleeve strength are functions of displacement based on the results of fitting at three displacements. Steady-state graphite friction and metal sleeve strength increase with increased velocity (Figure 3) and decrease with increased temperature (Table 1). Although the dependence of

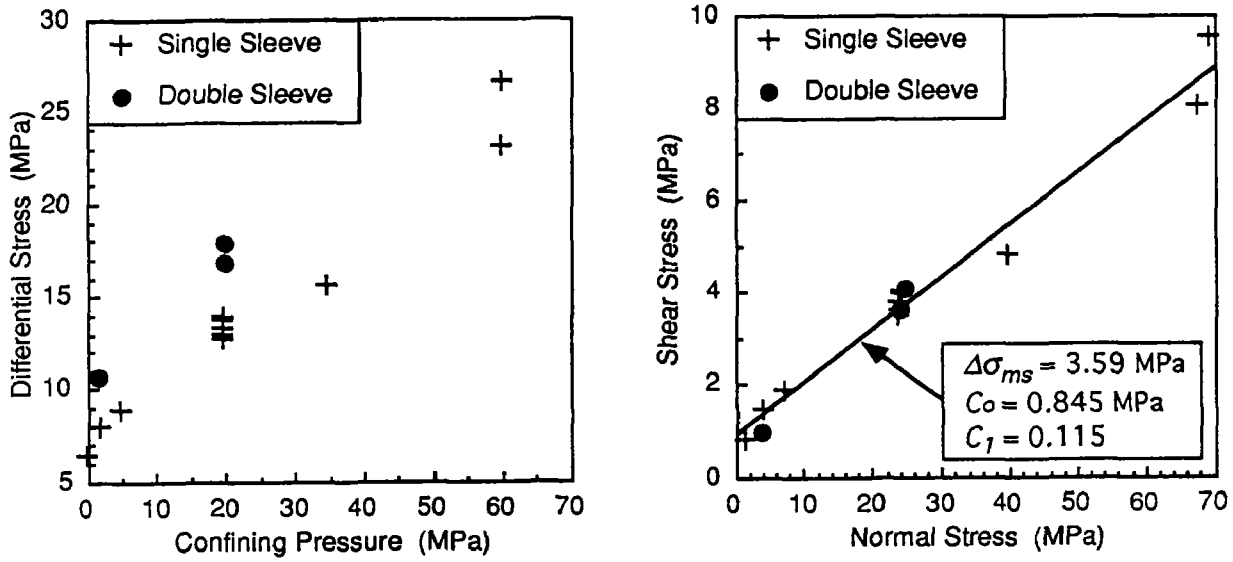

Figure 2. Results of graphite experiments conducted at slip velocity of 4 μm/s and room temperature. Plot on left shows total differential stress supported by the graphite assemblies at a shear displacement of 4.5 mm as a function of confining pressure and number of copper sleeves. Results clearly show that doubling the thickness of the sleeves increases assembly strength. Plot on right shows frictional strength of graphite on the inclined interface as a function of normal stress calculated from the same experimental data. Calculation of friction is based on equation shown in Figure 1 and assuming that the shear strength of graphite follows a Coulomb law and that the strength of the metal sleeve is a constant (see text). The best-fit values for sleeve strength and the Coulomb law are indicated.

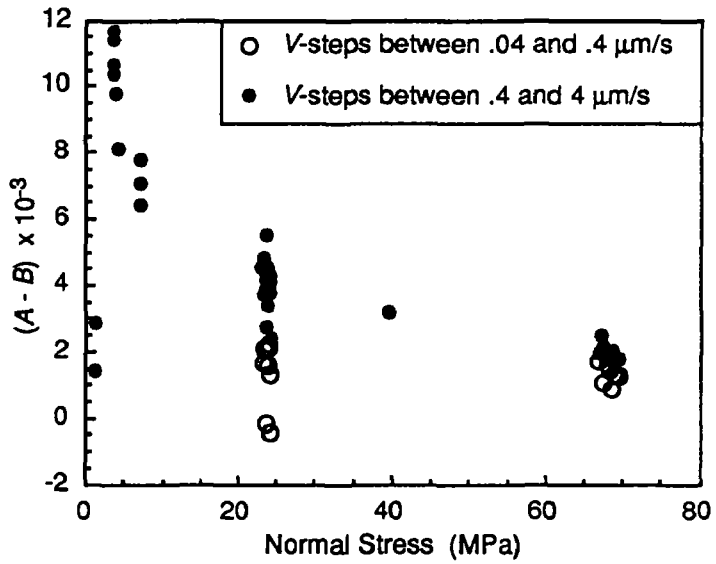

Figure 3. Steady-state velocity dependence of graphite friction at all temperatures and displacements as a function of normal stress. $(A - B)$ is equivalent to $d\mu^{ss}/d(\ln V)$. Although velocity dependence is a function of velocity, temperature and normal stress, it is fairly constant at normal stresses above 70 MPa. The normal stresses across the lateral-slip spacer interface in the quartz friction experiments is in the range of 80 to 100 MPa. Accordingly, steady-state velocity dependence of graphite friction can be assumed constant for purposes of calculating the coefficient of friction of quartz in the quartz gouge experiments (see text).

Table 1. Dependence of Graphite Friction on Temperature

Test #	P_c (MPa)	# Cu Sleeves	T-Step (°C)	Normal Stress (MPa)	$\frac{d\mu^{ss}}{d(1/T)}$
103	20	1	24 - 57	24	39.6
107	20	2	24 - 57	25	40.9
104	60	1	24 - 57	68	15.7
110	60	1	57 - 82 - 57	67	24.8

graphite friction on velocity changes with temperature and velocity at lower normal stresses, the velocity dependence is fairly constant at the high normal stresses appropriate for the apparatus corrections in the quartz experiments (Figure 3). The graphite experimental results indicate that the dependence of metal sleeve strength on velocity and temperature show little history effects, whereas the dependence of graphite friction on velocity and temperature shows significant history effects.

Quartz Experiments. For the quartz experiments, grooves with amplitude and periodicity of approximately 200 μm were ground into the 35° inclined interfaces. The grooves were oriented perpendicular to the cylinder axis and to the relative slip direction of the sample halves. These grooves caused the slip between sample halves to occur entirely within the 1.5 mm thick layers of fine-grained (< 100 μm diameter) granular quartz. For the tests without pore-water, the quartz was allowed to equilibrate at the laboratory conditions prior to testing. For the water-saturated tests, pore fluid access to the gouge layer was through a hole in the steel cylinder and pore pressure was maintained at a specified value by closed-loop servo-control. Pore pressure equilibration was sufficiently rapid within the gouge layers such that the pore pressure remained essentially constant over the range of velocity employed and during velocity and temperature steps. All quartz tests were conducted at an effective confining pressure of 20 MPa, and pore-fluid pressure was 5 MPa in the water-saturated tests. Each test involved a standardized sequence of velocity steps between 4, 0.4 and 0.04 μm/s and up to two temperature steps between 24 and 57 °C or 57 and 82 °C.

The coefficient of friction of quartz during each experiment was calculated from the differential stress versus displacement records using the formula shown in Figure 1. The calculations used the results of the graphite experiments to define the frictional properties of the graphite lubricated, lateral-slip interface and the strength of the metal sleeve. For the metal sleeve, the strength was calculated as a function of the displacement, velocity and temperature assuming a direct dependence on each parameter, i.e., the sleeve was always at steady-state. Coefficient of friction of the graphite lubricated lateral slip interface was defined by the displacement and the normal stress across the interface, and then modified to include the transient dependence of graphite friction on velocity and temperature, i.e., direct and history dependencies. Figure 4 shows a plot of the differential stress supported by a quartz gouge sample assembly in a typical velocity and temperature stepping experiment and the coefficient of friction calculated from that experiment as a function of displacement. Comparison of the two curves illustrate that corrections for apparatus effects is necessary to accurately determine the transient and steady-state frictional response of the quartz gouge to step changes in velocity and temperature.

In general, the water saturated quartz exhibits slightly lower coefficients of friction relative to the dry quartz at all displacements. All quartz experiments show a gradual increase in coefficient of friction with displacement superposed with the transient changes in friction associated with step changes in temperature and velocity. For purposes of analyzing the transient effects associated with velocity and temperature steps, the gradual slip hardening was modelled with a polynomial function and subtracted from the records. The polynomial was determined using the slope of the

friction record prior to the fourth and the sixth velocity steps. The polynomial and resulting detrended friction record for a representative experiment is shown in Figure 4.

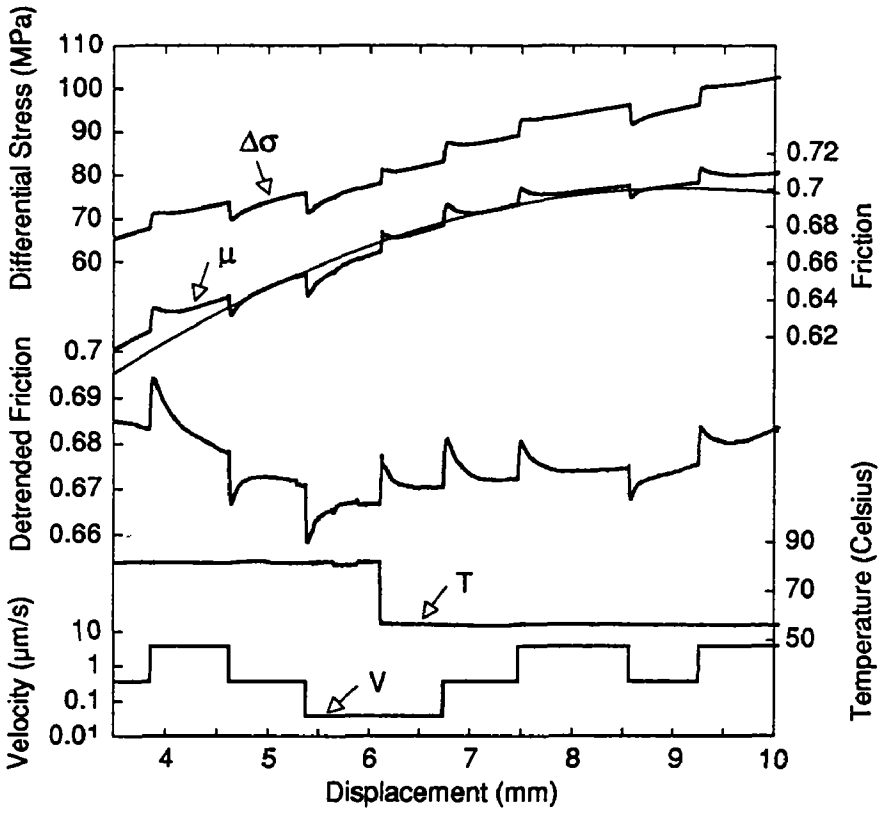

Figure 4. Representative results of an experiment on quartz gouge (hp106) at water saturated conditions. Velocity and temperature stepping sequence is shown. Total differential stress measured during the experiment and the coefficient of friction calculated are plotted as a function of shear displacement. The polynomial fit to the friction curve is shown by the thin line. The polynomial is used to remove the slip-hardening trend from the friction record to produce the detrended friction curve which is used for constitutive modelling.

Test of the Constitutive Model. I have proposed a temperature dependent friction constitutive relation based on the state variable friction constitutive relations developed by Dieterich [1979] and Ruina [1983]. Temperature dependence was added to the previous constitutive relations assuming velocity and temperature dependencies follow an Arrhenius relationship

$$\frac{d(\ln V)}{d(1/T)} = -\frac{Q}{R}$$

in which Q is the apparent activation energy for the rate limiting process [Chester, 1988, 1992; Chester and Higgs, 1992]. Following the notation of Dieterich and Linker [1992], the temperature and velocity dependent state variable friction relation is given by

$$\mu = \mu^* + A\left[\ln\left(\frac{V}{V^*}\right) + \frac{Q_a}{R}\left(\frac{1}{T} - \frac{1}{T^*}\right)\right] + B\Theta$$

$$\frac{d\Theta}{dt} = -\frac{V}{D_c}\left[\Theta + \ln\left(\frac{V}{V^*}\right) + \frac{Q_b}{R}\left(\frac{1}{T} - \frac{1}{T^*}\right)\right]$$

where $\Theta^{ss} = 0$ and $\mu^{ss} = \mu^*$ at $V = V^*$ and $T = T^*$. Previous versions of the temperature dependent friction relations presented by Chester [1988, 1992] and Chester and Higgs [1992] do not include the term with reference temperature T^*. All the relations are essentially the same except that $\Theta^{ss} = -Q_b/RT^*$ and $\mu^{ss} = \mu^* + (AQ_a - BQ_b)/RT^*$ at $V = V^*$ and $T = T^*$ in the previous versions. I prefer the version above because it adheres to original definitions of Θ^{ss} and μ^{ss} [e.g., Linker and Dieterich, 1992], and it is more consistent with the intent of the constitutive law to describe frictional behavior at or near steady-state conditions over a restricted range of velocity, temperature and normal stress conditions.

The proposed friction relation above predicts that 1) an abrupt increase in temperature induces a direct and transient change in friction similar to but in the opposite sense as that induced by a step increase in velocity, and 2) the characteristic distance for the transient response to evolve to a new steady-state coefficient of friction after step changes in temperature and velocity is the same. These two characteristics are evident from inspection of the friction versus displacement records of the quartz experiments (Figure 4).

I have modelled the frictional response of the quartz gouge experiments using the friction constitutive relations above in a simple spring slider system to quantify the friction parameters A, B, D_c, Q_a and Q_b. The modelling procedure is similar to that in previous studies [e.g., Marone et al., 1990; Chester and Higgs, 1992]. I compare forward models to the friction records during the velocity and temperature stepping sequence over the displacement range of 5 to 8 mm for each quartz experiment. The response to velocity steps was used to determine the parameters A and B, and the response to temperature steps to determine Q_a and Q_b. The response to all velocity and temperature steps was used to determine D_c. The results of the modelling are shown for two representative experiments (Figure 5).

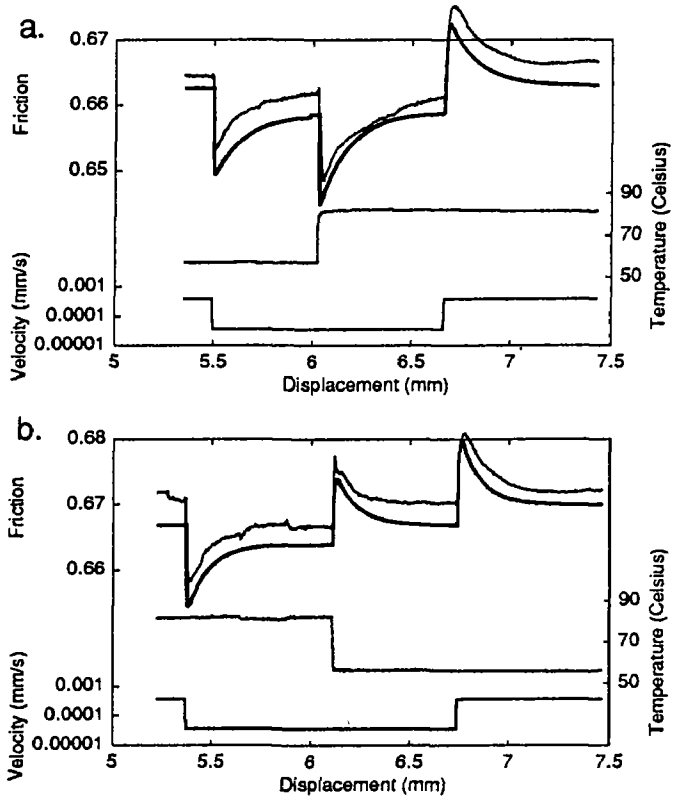

Figure 5. Example of model fits to friction data for velocity and temperature stepping experiments on water saturated quartz gouge. Velocity and temperature stepping sequence is shown. Thin lines at top of diagrams are the detrended friction records, and the thick lines are the model simulation. Model simulation is offset by .003 for ease of comparison. (a) experiment hp014. (b) experiment hp106.

Overall, the values of A, B and D_c are slightly larger and the values of Q_a and Q_b are slightly less for the water saturated tests relative to the dry tests as determined by modelling (Table 2). The variability in values for the apparent activation energies are sufficiently large that a difference in Q_a and Q_b can not be demonstrated. The magnitude of the average apparent activation energy in the water saturated tests (89 ± 23 kJ mol^{-1}) are similar to values determined for subcritical crack growth of quartz in hydrous environments [Atkinson, 1984] and for crack healing by diffusive mass transfer [Brantley et al., 1990]. The values are substantially larger than that determined by Chester and Higgs [1992] and Rutter and Mainprice [1978] for frictional slip at elevated temperatures and slow displacement rates where solution transfer processes are dominant. The activation energies in these experiments are significantly less than values typically determined for intracrystalline plasticity in quartz [e.g., Stesky, 1978]. Thus, the results of the quartz experiments are consistent with models of friction involving failure of contact junctions by sub-critical crack growth and time-dependent strengthening of contact junctions by either increasing the true area of contact through sub-critical cracking or by increasing the quality of contact junctions through healing.

Table 2. Model Parameters for Quartz Temperature and Velocity Stepping Experiments

Test #	T-Step (°C)	Q_a	Q_b	A	B	D_c (mm)
Dry						
hp011	24 - 57	87.1	139	.0035	.00246	.10
hp009	57 - 82	154	168	.0035	.00307	.11
hp105	82 - 57	60	43	.004	.00378	.10
Wet						
hp013	24 - 57	68.8	73.5	.0055	.00355	.13
hp014	57 - 82	101	143	.0062	.00446	.15
hp108u	57 - 82	89.2	113	.0062	.0042	.13
hp106	82 - 57	68.1	62.7	.006	.0047	.11
hp108d	82 - 57	85.7	82.2	.0062	.0042	.13

Average activation energies (Q_a and Q_b) for wet tests: 89 ± 23 kJ mol^{-1}

Conclusions:

1. A sudden change in temperature results in both a sudden and transient change in the frictional resistance to sliding, similar to but in the opposite sense as the change in friction produced by a sudden change in slip velocity.
2. The dependence of friction on temperature can be described adequately with state-variable friction constitutive relations previously used to describe velocity dependence and modified to incorporate temperature dependence based on the assumption that slip velocity and temperature follow an Arrhenius relationship.
3. For experimental shear displacement of water-saturated, granular quartz at 50 MPa normal stress, 0.004 to 4 μm/s slip velocity, and between 24 and 82 °C, the apparent activation energy for the sudden and transient changes in friction following a change in temperature or slip-velocity is 89 ± 23 kJ/mol. These activation energies are similar to values previously determined for sub-critical crack growth in quartz by stress corrosion and for healing of microcracks in quartz by diffusive mass transfer. Thus, experimental results are consistent with models of friction involving failure of contact junctions by sub-critical crack growth and time-dependent strengthening of contact junctions by either increasing the true area of contact through sub-critical cracking or by increasing the quality of contact junctions through healing.

References

Atkinson, B.K., Subcritical crack growth in geologic materials, *J. Geophys. Res.*, *89*, 4077-4114, 1984.

Brantley, S.L., B. Evans, S.H. Hickman, and D.A. Crerar, Healing of microcracks in quartz: implications for fluid flow, *Geology*, *18*, 136-139, 1990.

Chester, F. M., Temperature and rate dependence of friction for faults, *Eos Trans. AGU*, *69*, 471, 1988.

Chester, F. M., Temperature-time relationships for frictional strength of quartz gouge, *Eos Trans. AGU*, *71*, 1579, 1990.

Chester, F. M., Temperature-, rate- and state-dependent friction constitutive behavior of quartz gouge, in press, *Eos Trans. AGU*, 1992.

Chester, F.M. and N.G. Higgs, Multimechanism friction constitutive model for ultrafine quartz gouge at hypocentral conditions, *J. Geophys. Res.*, *97*, 1859-1870, 1992.

Dieterich, J.H., Modeling of rock friction, 1, experimental results and constitutive equations, *J. Geophys. Res.*, *84*, 2161-2168, 1979.

Linker, M.F. and J.H. Dieterich, Effects of variable normal stress on rock friction: Observations and constitutive equations, *J. Geophys. Res.*, *97*, 4923-4940, 1992.

Marone, C., C.B. Raleigh, and C.H. Scholz, Frictional behavior and constitutive modeling of simulated fault gouge, *J. Geophys. Res.*, *95*, 7007-7025, 1990.

Ruina, A.L., Slip instability and state variable friction laws, *J. Geophys. Res.*, *88*, 10359-10370, 1983.

Rutter,, E.H., and D.H. Mainprice, The effect of water on the stress relaxation of faulted and unfaulted sandstone, *Pure Appl. Geophys.*, *116*, 634-654, 1978.

Stesky, R.M., Mechanisms of high temperature frictional sliding in Westerly granite, *Can. J. Earth Sci.*, *15*, 361-375, 1978.

SEISMIC PROPERTIES OF ROCK FORMATIONS IN THE PUGET SOUND, WILLIAMETTE LOWLAND REGION

Agreement No. 1434-92-G-2189

Nikolas I. Christensen
Purdue University
Dept. of Earth & Atmospheric Sciences
1397 Civil Engineering Bldg.
West Lafayette, IN 47907-1397

(317) 494-1643

Investigations Undertaken

This project is part of a cooperative study with USGS scientists to obtain high-resolution seismic refraction/wide-angle reflection profiles in western Washington and Oregon, concentrating on areas of high population in the Puget Sound Basin and the Williamette Lowland. The field study has been successfully deployed and preliminary crustal and upper mantle models have been obtained based on qualitative analyses of the data. At present, the data is being analyzed using forward modeling and inversion techniques. The models obtained by these studies will aid in the accurate evaluation of crustal earthquake mechanisms and substantially improve our ability to locate and evaluate earthquakes in the region.

Physical property measurements of rock formations along the seismic transect are currently being studied in the Purdue Rock Physics laboratory. Compressional and shear wave velocities, densities, Poisson's ratios and attenuation measurements are providing important constraints on the nature and distribution of structures and lithologies to the base of the crust and into the upper mantle. By providing information critical for the extension of surface geology to depth, the laboratory studies will facilitate the integration of geological and geophysical data of the region.

Results Obtained

Over 40 samples, representing a variety of lithologies along the transect, were collected this past summer for physical property measurements. Many of these samples have been prepared for velocity and density measurements. To investigate anisotropy, a minimum of three cores have been taken from each sample. Measurements of velocities to pressures of 1000 MPa (equivalent to 35 km depth) are currently underway. Cores of selected samples have provided attenuation measurements (Figure 1) at elevated pressures using a pulse echo technique.

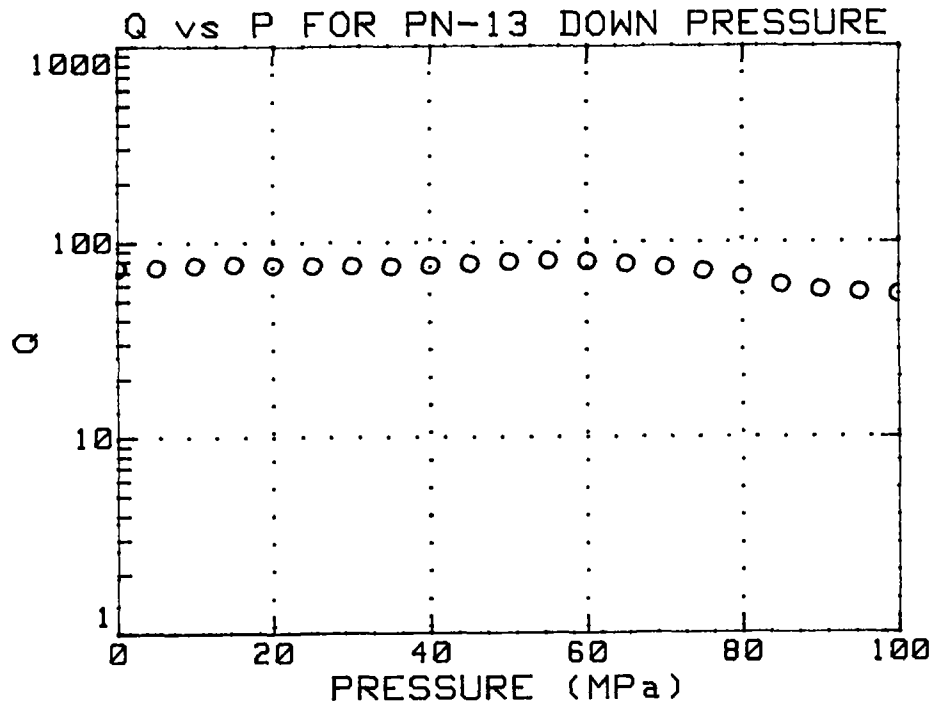

Figure 1. Q versus pressure for a western Washington basalt.

Publications

Luetgert, J., W.D. Mooney, E. Criley, A. Trehu, S.B. Smithson, C. Humphreys, N.I. Christensen, R. Clowes and I. Asudeh, Crustal velocity structure of the Pacific N.W.: The 1991 seismic refraction/wide-angle reflection experiment, Geol. Soc. Am., Cordilleran Section 1992 Abstracts with programs, 66, 1992.

Partial Support of Joint USGS-CALTECH Southern California Seismographic Network

#1434-92-A-0960

Robert W. Clayton
Egill Hauksson

Seismological Laboratory,
California Institute of Technology
Pasadena, CA 91125 (818-356-6954)

INVESTIGATIONS

This Cooperative Agreement provides partial support for the joint USGS-Caltech Southern California Seismographic Network. The purpose is to record and analyze data from more than 50,000 local earthquakes from October 1991 to September 1992 and generate a data base of phase data and digital seismograms. The primary product derived from the data base is a joint USGS-Caltech catalog of earthquakes in the southern California region. We also provide rapid response to media and public inquiries about earthquakes.

For more detailed information about data access, please contact:
Dr. Kate Hutton at (818)-356-6959;
or with E-mail: kate@bombay.gps.caltech.edu.

RESULTS

Network Operation

Southern California Seismographic Network. The SCSN has 230 remote sites (with 300 components) and gathers data from local, regional and teleseismic earthquakes. These data are used for earthquake hazards reduction as well as for basic scientific research. The earthquake hazards reduction effort has become more important as moderate-sized earthquakes continue to occur within densely populated areas in southern California. The largest damaging earthquake to occur was the (M_W=7.3) Landers earthquake of 28 June 1992, located in rural parts of San Bernardino County. It caused over $100 million in damage.

The average rate of 15 publications per year over the last 10 years using the network data illustrates the strength of the ongoing research activities that use the network data. Continued efforts to improve data quality and accessibility have created the arguably best regional earthquake data base in the world. The ongoing upgrading of the quality of the waveforms recorded by the short-period network and the addition of low-gain seismometers and accelerometers provide numerous new avenues of research. Most important of these is analysis of on-scale waveforms to determine source, path and site effects.

The USGS operates most of the remote stations in the SCSN. Caltech operates: 1) 24 short period telemetered stations; 2) 7 stations with local photographic recording of Wood-Anderson seismometers; and 3) 7 very broadband TERRAscope stations; in 1993 we plan to install 8 more TERRAscope stations. Caltech also maintains drum recorders and other equipment at the central site located in the Seismological Laboratory at Caltech.

The computer equipment at the central site has been upgraded and a switch-over to the new computers took place in January 1992. The SCSN data is recorded by two microVAX-III computers and the data processing is done on five VAX workstations using a VAX-4000 as a central server. The operation of this equipment is shared by Caltech and USGS personnel. To avoid duplication, software development is done in cooperation with the USGS in Menlo Park.

More than 50,000 earthquakes will be entered into the southern California earthquake catalog for this reporting period. Approximately 10.0-15.0 Mbytes of phase data and 100-150 Gbytes of seismograms will be archived. In addition to the data analysis we carry out software maintenance, hardware maintenance and other tasks necessary to complete the catalog. Caltech and USGS maintain a data base that includes: 1) earthquake catalog (1932-present); 2) phase data (1932-present); 3) photographic paper seismograms (1930-present); and 4) digital seismograms (1977-present). The earthquake catalog (1932-present) and phase data (1960-present) are available via dial-up and over INTERNET. Other data are available upon request. This data base is being made available to the DC/SCEC and will be the most voluminous part of the data stored in the DC/SCEC.

Near real-time reporting to USGS in Reston and the Governor's Office of Emergency Services and other response to any felt or damaging earthquake activity is provided by network personnel.

The Data Center of the Southern California Earthquake Center. This center has significantly increased the use of the data from SCSN for scientific research. The mass-store system, which became operational on 1 October 1991, provides on-line storage for more than 300 Gbytes of data. The availability of 60 years of catalog, 30 years of phase data, and 14 years of digital seismograms on both UNIX and VMS computers and on-line over INTERNET/NSFNET improves the access to the data.

Seismicity October 1991 - September 1992

The Southern California Seismographic Network (SCSN) recorded approximately 50,000 earthquakes during the 12 months from October 1990 through September 1991, an average of 4170 per month, making it the most active reporting period ever (Figure 1).

The (M_W6.2, 7.3, 6.3) 1992 Landers sequence that began on 23 April with the M_W6.2 1992 Joshua Tree preshock is the most substantial earthquake sequence to occur in the last 40 years in California. These earthquakes ruptured almost 100 km of both surficial and concealed faults and caused aftershocks over a 100 km wide and 180 km long area. The faulting was predominantly strike-slip and all three events had unilateral rupture to the north away from the San Andreas fault.

The M_W7.3 Landers mainshock occurred at 34°N13' and 116°W 26' at 11:58 GMT, June 28, 1992 with a seismic moment of $1x10^{27}$ dyne-cm (Figure 2). The distribution of more than 15,000 aftershocks, short period focal mechanisms, and onscale waveforms from TERRAscope illuminate a complex sequence of faulting (Hauksson et al., 1992). The aftershocks extend 65 km to the north of the mainshock epicenter along a system of at least five different surficial faults and 40 km to the south crossing the Pinto Mountain fault through the Joshua Tree aftershock zone, towards the San Andreas fault near Indio.

The aftershocks range in depth from near-surface down to 15-17 km depth. This is very different from the depth distribution observed in the 1979 Homestead Valley sequence indicating that the maximum depth of earthquake faulting is similar in this region as elsewhere in California.

A tight cluster of small foreshocks (M1.5-3.0) preceded the mainshock by 12 hours. The rupture initiated in the depth range of 5-10 km. The mainshock focal mechanism showed right-lateral strike-slip faulting with a strike of N8°W on an almost vertical fault. The rupture formed an arc-like zone defined by surficial faulting and aftershocks with more westerly faulting to the north. This change in strike is accomplished by jumping across dilational jogs connecting surficial faults with strikes rotated progressively to the west. The

most prominent off-fault aftershock cluster occurred 30 km to the west of the Landers mainshock.

The largest event within this cluster was the M_w6.3 Big Bear aftershock with a seismic moment of $3x10^{25}$ dyne-cm occurring at 34°N10' and 116°W49' at 15:05 GMT 28 June . It exhibited left-lateral strike slip faulting on a northeast striking and steeply dipping plane. The Big Bear aftershocks form a linear trend extending 20 km to the northeast with two lobes of aftershocks located within the dilational quadrants of the M_w6.3 rupture surface.

The faults that caused the Landers mainshock and the fault that caused the Big Bear aftershock are oriented 60° ap \rt, with the Camp Rock-Emerson fault at N10°W to N30°W and the fault for the Big Bear earthquake oriented at about N45°E. The Big Bear fault and the Camp Rock-Emerson fault form a conjugate set. The two faults form the legs of a triangle, the base of which is the Mission Creek strand of the San Andreas fault. The aftershock distributions of both faults touch the San Andreas at Yucaipa for the Big Bearfault and at Joshua Tree for the Landers fault. One earthquake, a M_L4.4 event on the first day, appears to have occurred on the San Andreas fault near Yucaipa with a N60°W fault orientation. The distance on the base of the triangle is approximately 70 km.

The M_w7.3 Landers mainshock occurred near the southernmost extent of the eastern Mojave shear zone, a 80 km wide and more than 400 km long zone of deformation. It extends into western Nevada and accommodates about 10-20% of the plate motion between the Pacific and North America Plates. The Joshua Tree preshock, its aftershocks, and Landers aftershocks form the previously missing link that connects the Mojave shear zone to the southern San Andreas fault.

PUBLICATIONS USING NETWORK DATA (ABSTRACTS EXCEPTED)

Biasi, G. P., and E. D. Humphreys, P-wave image of the upper mantle structure of central California and southern Nevada, *Geophys. Res. Lett., 19,* 1161-1164, 1992.

Hauksson, E., and L. M. Jones, The 1988 and 1990 Upland earthquakes: Left-lateral faulting adjacent to the Central Transverse Ranges, *J. Geophys. Res., 96,* 8143-8165, 1991.

Hull, A. G., and C. Nicholson, Seismotectonics of the northern Elsinore Fault zone, southern California, *Bull. Seismol. Soc. Amer., 82,* 800-818, 1992.

Magistrale, H., H. Kanamori, and C. Jones, Forward and inverse three-dimensional *P* wave velocity models of the southern California crust, *J. Geophys. Resl., 97,* 14,115-14,135, 1992.

Mori, J., Correlation of *P* wave amplitudes and travel time residuals for teleseisms recorded on the Southern California Seismic Network, *J. Geophys. Res., 97,* 6661-6674, 1992.

Nicholson, C., and J. M. Lees, Travel-time tomography in the northern Coachella Valley using aftershocks of the 1986 M_L 5.9 north Palm Springs earthquake, *Geophys. Res. Lett., 19,* 1-4, 1992.

Sung, L-Y., and Jackson, D. D., Crustal mantle structure under southern California, *Bull. Seismol. Soc. Amer., 82,* 934-961, 1992.

Vidal, A., and L. Munguia, Local magnitude and source parameters for earthquakes in the peninsular ranges of Baja California, Mexico, *Bull. Seismol. Soc. Amer., 81,* 2254-2267, 1991.

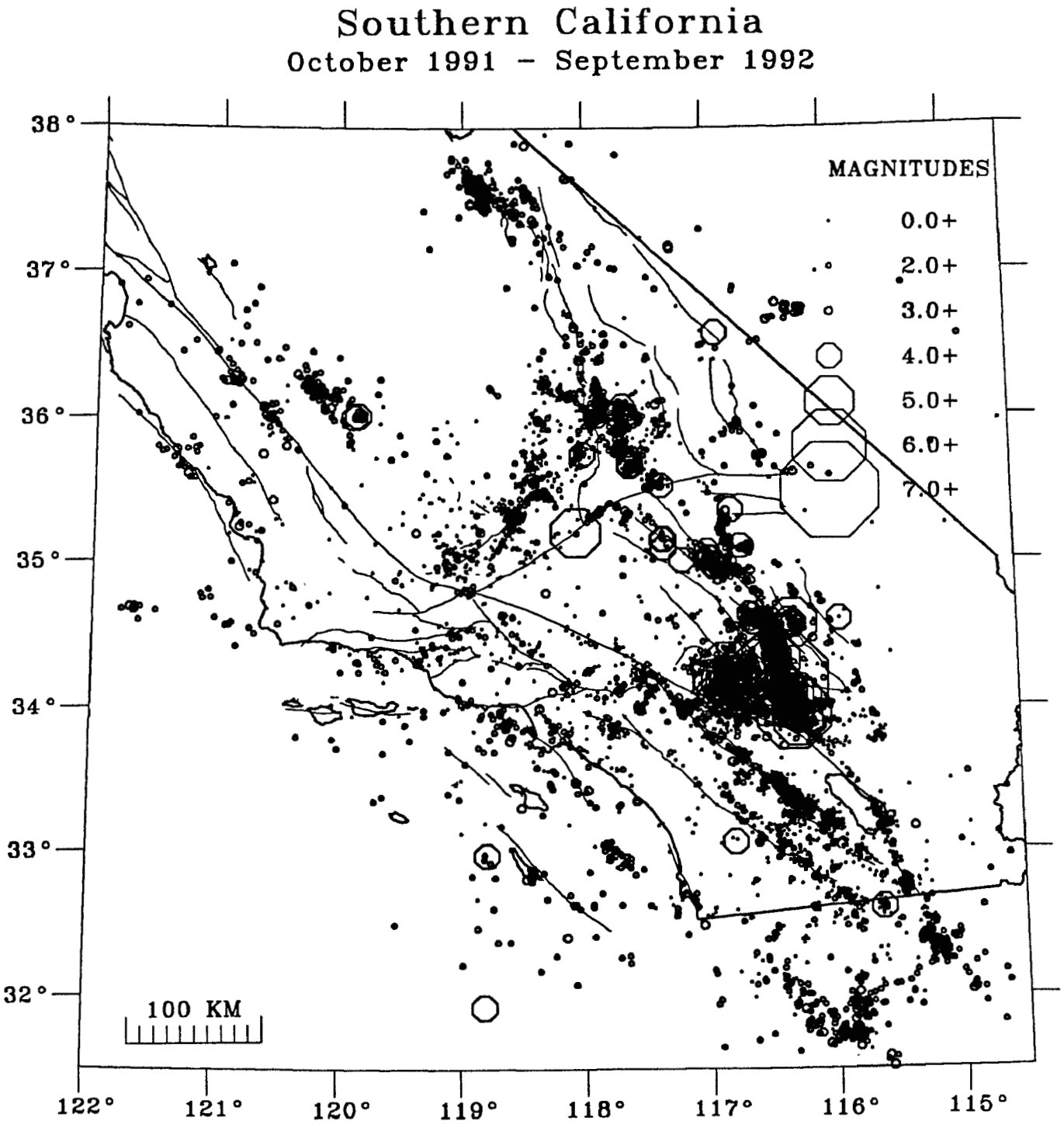

Figure 1. Map of epicenters of earthquakes in the southern California region, 1 October 1991 to 30 September 1992.

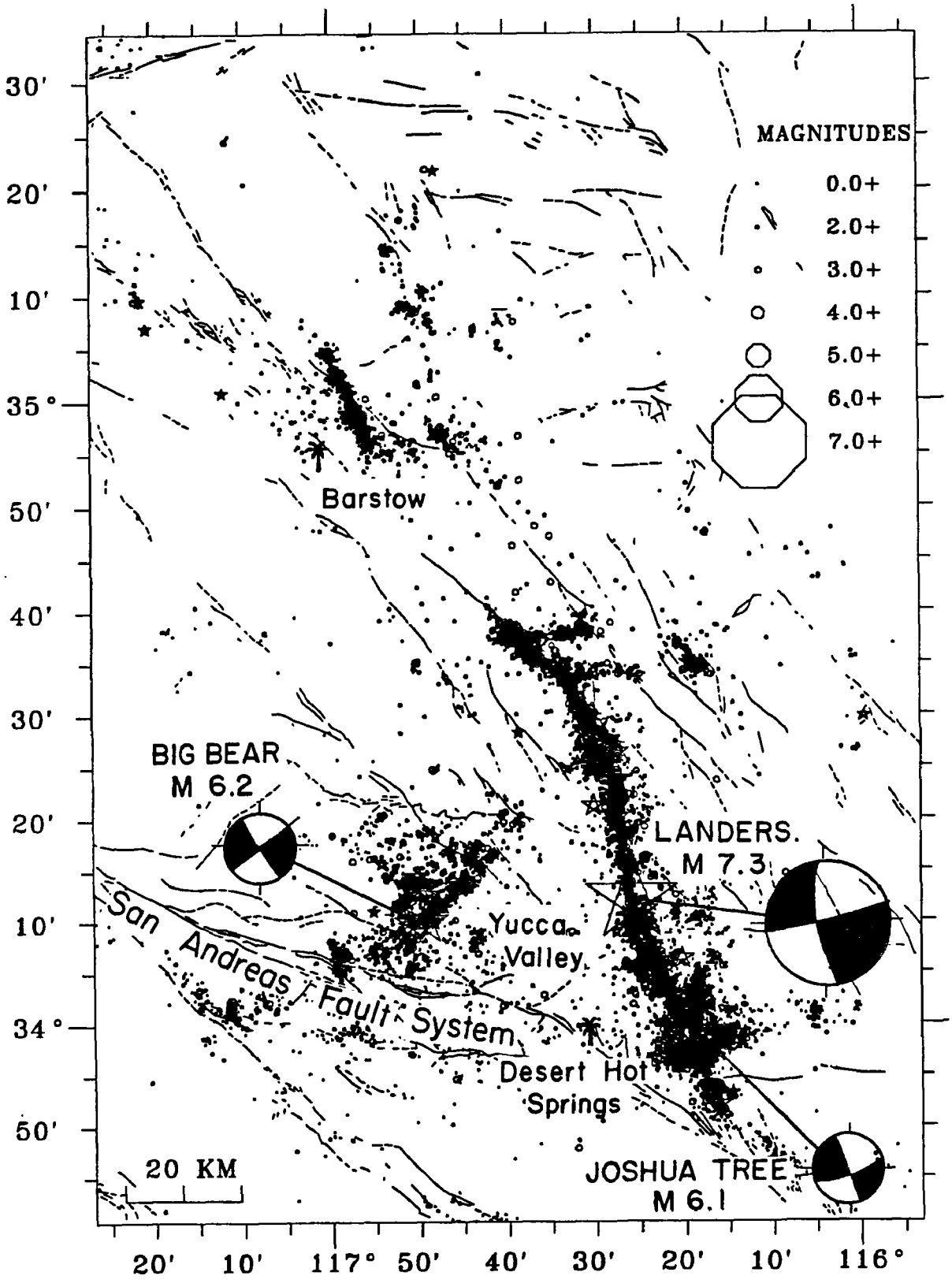

Figure 2. The 1992 Joshua Tree, Landers and Big Bear earthquakes and their aftershocks. The large spatial extent of this aftershock sequence is expected given the magnitude of the M_W7.3 mainshock. The strike-slip focal mechanisms of the M6.1 Joshua Tree, the M7.3 Landers mainshock and the M6.2 Big Bear aftershock are also included.

I

1. Regional Seismic Monitoring in Western Washington
1434-92-A-0964 R.S. Crosson, P.I.
and
2. Seismic Monitoring of Volcanic and Subduction Processes in Washington and Oregon
1434-92-A-0963 S.D. Malone and A.I. Qamar, P.I.s

R.S. Crosson, S.D. Malone, A.I. Qamar and R.S. Ludwin
Geophysics Program
University of Washington
Seattle, WA 98195
(206) 543-8020
Oct. 1, 1991 - Sept. 30, 1992

Investigations

Operation of the Washington Regional Seismograph Network (WRSN) and preliminary analysis of earthquakes in Washington and Northern Oregon continue under these contracts. Quarterly bulletins which provide operational details and descriptions of seismic activity in Washington and Northern Oregon are available from 1984 through the third quarter of 1991. Final published catalogs are available from 1970, when the network began operation, though 1986.

The University of Washington operates 81 stations west of 120°W under these agreements, 28 are supported under 1434-92-A-0964, 51 under 1434-92-A-0963, and 2 are operated jointly. This report includes a brief summary of significant seismic activity. Additional details are included in our Quarterly bulletins.

Network Operations and Outreach

Station WMO (Whale Mt.,OR) was replaced by BBO (Butler Butte, OR) and station APW (Alpha Peak, WA) was replaced by LCW (Lucas Creek, WA) during this contract period. We also installed a Guralp 3-component broad-band seismometer at Longmire, WA (funded under USGS contract #1434-92-G-2195) which is recorded on-site by a REFTEK digital data logger. Data of interest are retrieved from the data logger over telephone lines via modem.

Our processing scheme includes an automatic alarm for local events that initiates electronic mail or faxes to local emergency response agencies, operators of adjacent seismograph networks, and the National Earthquake Information Center in Colorado. When the event has been fully processed, the updated final information on it is also faxed or e-mailed. A taped message on our voice mail system (206) 543-7010 gives information on felt earthquakes in the last few days within our network, and a longer general message is available on earthquakes in the Pacific Northwest. In addition, locations of recent significant earthquakes can be obtained via modem by dialing (206)685-0889 and logging in as "quake" with password "quake", or via ethernet using the UNIX utility "finger quake@geophys.washington.edu".

We answer from 3-40 questions per day on Pacific Northwest seismicity and seismic hazards, and give about a half-dozen lab tours or presentations each month for a wide variety of age groups; students from elementary through post-graduate, retirees, science teachers, emergency educators, etc. Requests for information increased after the Landers and Big Bear earthquakes in southern California at the end of June.

Seismicity

The Washington Regional Seismograph Network processed 3,537 events between Oct. 1, 1991 and Sept. 30, 1992. Of these 2,613 were earthquakes or blasts within the network and the remaining events were either regional earthquakes (360) or teleseisms (564).

Figure 1 shows earthquakes (M_c ≥2.0) located in Washington and Oregon during this reporting period. Excluding blasts, probable blasts, and earthquakes outside the U. W. network, a total of 1,795 earthquakes west of 120.5°W were located between Oct. 1, 1991 and Sept 30, 1992. Of these, 631 were located near Mount St. Helens, which has not erupted since October of 1986. East of 120.5°W, 197 earthquakes were located.

During this reporting period there were 16 earthquakes reported as felt west of the Cascades, and 6 reported as felt to the east of the Cascades. No damage was reported. The largest earthquake within the area shown in Fig. 1 was a M_c 4.3 earthquake which occurred on November 28, 1991 at 01:08:59(UTC) at ~10 km depth. This earthquake was felt in the Walla-Walla, WA and Milton-Freewater, OR vicinity, and was followed by a few aftershocks. Other felt earthquakes in the same vicinity with similar mid-crustal depths also occurred on December 15, 1991 (M_c 3.3) and July 14 and Sept. 23, 1992 (M_c 4.1 and 2.8, respectively).

Reports and Articles

Benson, R., C.D. Lindholm, R.S. Ludwin, and A.I. Qamar, (in press), A Method for Identifying Explosions Contaminating Earthquake catalogs: Application to the Washington Regional Earthquake Catalog, Seis. Res. Lett.

Jonientz-Trisler, C. B. Myers, and J. Power, (in preparation), Seismic identification of gas-and-ash explosions at Mount St. Helens: capabilities, limitations, and regional application, in /flProceeding Volume, First International Symposium on Volcanic Ash and Aviation Safety,/fR USGS Bulletin 2047.

Ludwin, R.S., A.I. Qamar, S.D. Malone, C. Jonientz-Trisler, R.S. Crosson, R. Benson, and S. Moran (in preparation), Earthquake Hypocenters in Washington and Northern Oregon, 1987-1989, Washington State Dept. of Natural Resources.

Ludwin, R. S., S.D. Malone, R.S. Crosson, A.I. Qamar, (in press or submitted), Washington Earthquakes 1986, Washington Earthquakes 1987, Washington Earthquakes 1988, Washington Earthquakes 1989, in U.S. Earthquakes

Ludwin, R. S., C.S. Weaver, and R.S. Crosson, 1991, Seismicity of Washington and Oregon, Neotectonics of North America. Slemmons, D.B., E.R. Engdahl, D. Blackwell and D. Schwartz, editors; Decade of North American Geology Associated Volume CSMV-1;

Univ. of Wash. Geophysics Program, 1992, Quarterly Network Report 92-A on Seismicity of Washington and Northern Oregon

Univ. of Wash. Geophysics Program, 1992, Quarterly Network Report 92-B on Seismicity of Washington and Northern Oregon

Univ. of Wash. Geophysics Program, 1992, Quarterly Network Report 92-C on Seismicity of Washington and Northern Oregon

Abstracts

Qamar, A.I. and R.S. Ludwin, 1992, Stress directions in Washington and Northern Oregon inferred from earthquake focal mechanisms, Seis. Res. Lett., V. 63, No. 1, p. 28 (also in GSA 88th Annual Cordilleran Section, 1992 Abstracts with Programs, V. 24(5)).

Jonientz-Trisler, C. B. Myers, and J. Power, 1991, Seismic identification of gas-and-ash explosions at Mount St. Helens: capabilities, limitations, and regional application, in /fI First International Symposium on Volcanic Ash and Aviation Safety,/fR USGS Circular 1065, Program and Abstracts, Seattle WA, July 8 through 12, 1991.

Malone, S.D., (in press, Invited), Pacific Northwest earthquake hazards based on Historic seismicity, Report of the National Earthquake Prediction Evaluation Council, May 7-8, 1992.

Moran, S. C., S. D. Malone and S. E. Barker, 1991, Deep earthquakes at Mount St. Helens: evidence for a collapsing and dilating magma chamber (abstract), EOS, V. 72, p. 523.

Theses

Moran, S. C., 1992, Mount St. Helens, 1980-1992: The dynamics and evolution of an active magmatic system as inferred from earthquakes and focal mechanism, Master's thesis, Geophysics Program, Univ. of Wash., Seattle, WA.

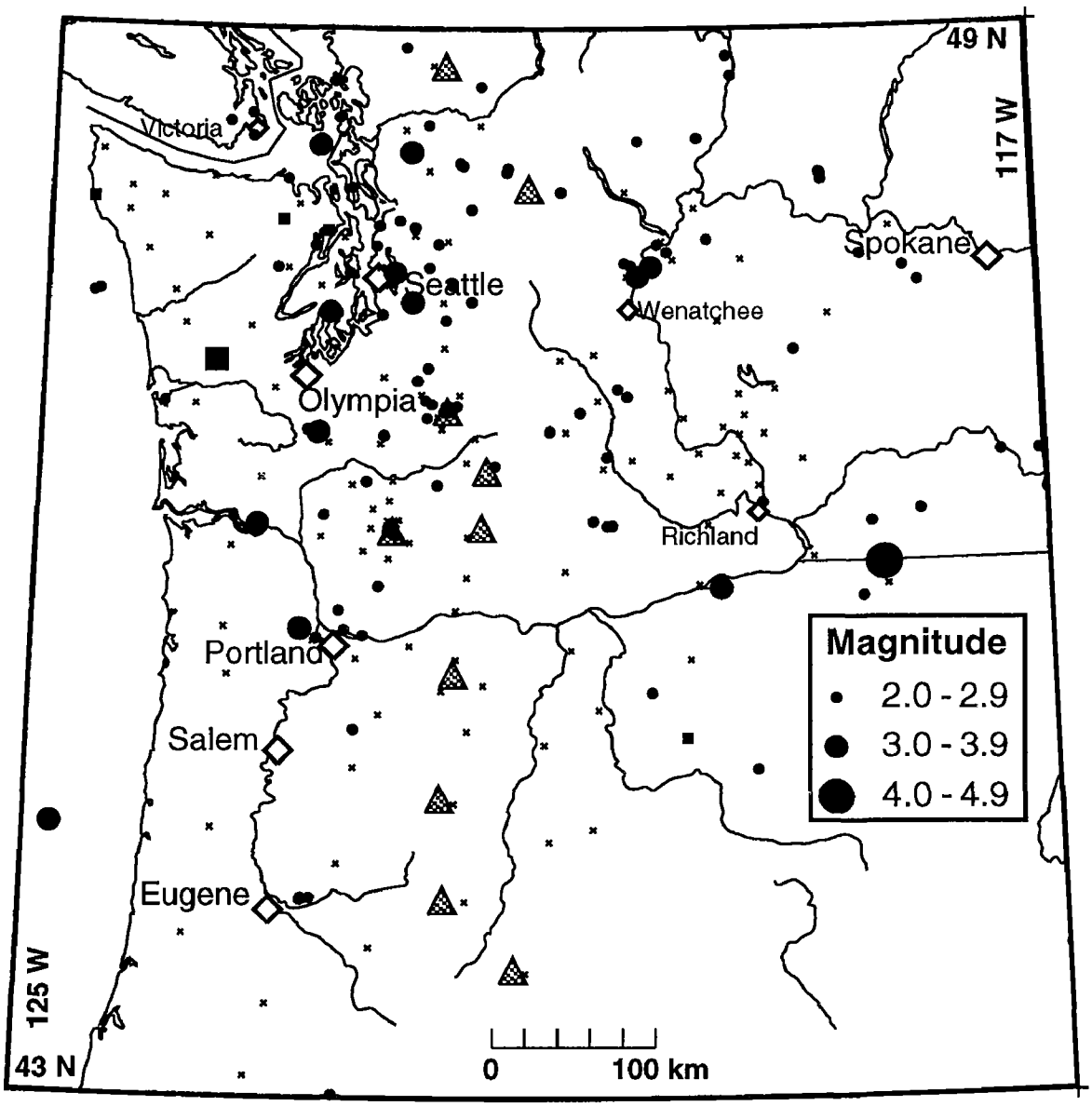

Figure 1. Earthquakes larger than magnitude 2.0 between October 1, 1991 and September 30, 1992. Locations of a few cities are shown as white-filled diamonds. Earthquakes are indicated by filled symbols, where the round symbols represent earthquakes at depths shallower than 30 km, and squares represent earthquakes at 30 km or deeper. Small "x" symbols indicate locations of seismometers operated by the WRSN at the end of September, 1992, and shaded triangles show the position of Cascade volcanos.

Stressing, Seismicity and Rupture of Slip-Deficient Fault Zones

14-08-0001-G1788

R. Dmowska and J. R. Rice (PI)
Division of Applied Sciences and Department of Earth and Planetary Sciences,
Harvard University, Cambridge, MA 02138
(617) 495-3452 and 3445

Investigations:

1.1 Stress transfers during the earthquake cycle in oblique subduction segments.

1.2 Modeling earthquake cycles in the Shumagins (Aleutians) subduction segment with seismic and geodetic constraints.

1.3 Physical modeling of earthquake cycles, asperity development, and characteristic earthquake response, considering lab-based friction, pore pressure and thermal structure.

1.4 Dynamics of rupture

Results:

2.1 Stress transfers during the earthquake cycle in oblique subduction segments have been studied. These transfers are between asperities along the interplate interface (zones of higher locking and high slip in large/great earthquakes) and outer-rise areas, adjacent to the rupture zones, as well as slab areas at intermediate depths, down-dip from the rupture zones. It has been shown previously in our work (Dmowska and Lovison, 1992) that locking of asperities during the cycle results in an uneven distribution of seismicity along strike, both in the outer-rise and at intermediate depth, with seismicity clustering next to asperities on the interplate interface. In subduction segments with direction of convergence approximately perpendicular to the trench (as, e. g., Alaska 1964, Valparaiso 1985) seismically active areas in the outer-rise and at intermediate depth are located next to asperities, along the direction of subduction. However, in study of oblique subduction segments in the western Aleutians (area of Rat Islands 1965 earthquake), we have found that the active areas of the outer-rise and of the slab at intermediate depth, associated with an asperity, locate next to asperities, but along directions somewhat between the convergence vector and the direction perpendicular to the trench. This is shown schematically in Figure 1, and is consistent with observations by Ekström and Engdahl (JGR,1989) that part of the trench-parallel component of subduction is accommodated in the thrust interface, and part in the strike-slip events in the back-arc region.

The position of the active areas seems to be independent of the time window during the cycle, even though the style of seismicity varies with time. E.g. the seismicity in the outer-rise would be tensional in the early part of the cycle and compressional (if at all present) in the later part; at intermediate depth, events after a great subduction earthquake could be compressional, but are tensional later in the cycle. We are planning 2D finite element modeling, somewhat analogous to that discussed next, to examine the magnitudes of cyclic stress transfers and to see what inferences about the stress state and failure process can be made from the seismicity locations.

The observations and computational results may provide better understanding of the mechanics of oblique subduction segments and outer-rise seismicity.

2.2 In continuation of recent work on assessing the seismic potential of the Shumagin Islands segment along the Aleutian subduction zone (Dmowska and Lovison-Golob, EOS, 72, 1991), we use a new 2D finite element model to analyze space- and time-dependent stress transfers in the area during the earthquake cycle. The model is a specific version of the one used by Rice and Stuart (EOS, 70, 1989), but tailored to the geometry of the Shumagins region as constrained by oceanic age and seismicity locations. It consists of an elastic oceanic plate dipping under an also elastic upper plate, into a viscoelastic mantle. The interplate interface undergoes periodically repeated slips and is otherwise locked. We are investigating different model possibilities, such as different geometries of the interplate interface as well as different locking depths (both, updip, between the trench and the upper part of the locked zone, and downdip), different viscosities of the mantle, thicknesses of oceanic and upper plates, etc.

We find that if approximately 15% of the convergence takes place seismically (consistent with $Mo = 1.7 \cdot 10^{20}$ Nm for the 1917 event, Estabrook and Boyd, 1992), if the thrust interface location is taken from seismicity data (Hauksson, BSSA, 1985) so as to dip at 30° beyond 30 km depth, after an initial approximately 10° dip, and is seismically coupled only between approximately 20 km and 50 km depth, but allowed to relax elsewhere (consistent with the finite-element mesh geometry of Figure 2), and if the mantle region relaxes on a time scale of order of 0.1 of the recurrence interval, then consistency with measured strain (Lisowski et al., JGR, 1988) and vertical displacement and tilt (Beavan, NEHRP Summary Reports, 1992) data is obtained, although the uplift and strain are slightly overpredicted. Figure 3 summarizes deformation predictions, with observational constraints shown as the short dashed-line segments. All deformation predictions are within observational ranges if, instead, just 10% of the convergence is assumed to take place seismically.

Our model simulations suggest that the Shumagins segment is capable of large earthquakes, and that the hypothesis of totally aseismic subduction is not consistent with current geodetic constraints.

2.3 A series of three-dimensional analyses have been completed (Rice, 1992a) of slip on a long vertical strike-slip fault between steadily driven elastic crustal blocks, based on depth-variable friction properties which are taken either as uniform along-strike at every depth or as perturbed modestly from uniformity . A rate- and state-dependent friction law governs motion on the fault; the law includes a characteristic slip distance L for evolution of surface state and slip-weakening. Because temperature and normal stress vary with depth, frictional constitutive properties (velocity weakening/ strengthening) do also, in a way constrained by data from Blanpied et al. (GRL, 1991) for granite under hydrothermal conditions. The governing equations of quasistatic elasticity and frictional slip are solved on a computational grid of cells as a discrete numerical system, and a viscous radiation damping term is included to approximately represent inertial control of slip rates during earthquake-like instabilities. The numerical results show richly complex slip, with a spectrum of event sizes, when solved for a grid with oversized cells, that is, with cell size h that is too large to validly represent the underlying continuous system of equations. However, in every case for which it has been feasible to do the computations (moderately large L only), that spatio-temporally complex slip disappears in favor of cycles of periodically repeated large earthquakes with reduction of cell size h. Further study will be necessary to determine whether a similar transition occurs when the elastodynamics of rupture propagation is treated more exactly. The transition from complex to ordered fault response occurs as h is reduced below a theoretically

derived nucleation size h* which scales with L but is $2 \cdot 10^4$ to 10^5 larger in cases considered. [It is given as $h^* = 2\, L\, \mu / \pi\, (B - A)_m$, where μ = shear rigidity and $(B - A)_m$ is the maximum value on the fault of the velocity weakening parameter $- V\, d\tau_{ss}(V)/dV$.] Cells larger than h* can fail independently of one another whereas those much smaller than h* cannot slip unstably alone, and can do so only as part of a cooperating group of cells. The results contradict an emergent view that spatio-temporal complexity is a generic feature of mechanical fault models. Such generic complexity does apparently result from models which are inherently discrete in the sense of having no well-defined continuum limit as h diminishes. Those models form a different class of dynamical systems from models like the present one that do have a continuum limit. Strongly oversized cells cause the model developed here to mimic an inherently discrete system. It is suggested that oversized cells, capable of failing independently of one another, may crudely represent geometrically disordered fault zones, with quasi-independent fault segments that join one another at kinks or jogs. Such geometric disorder, at scales larger than h*, may force a system with a well defined continuum limit to mimic an inherently discrete system and show spatio-temporally complex slip at those larger scales.

In continuing study of this type, a fault zone with highly variable properties along strike is being modeled. This variation has been induced in different studies either by varying the degree of pore pressurization along strike, or by assigning an amplitude factor to multiply some particular depth-variation and letting the amplitude factor vary along strike (this might crudely represent lithological variation). In the case studied most extensively so far, the latter method was used to simulate Parkfield-like conditions, thus producing a creeping zone that is bordered by moderate earthquake zones (like Parkfield and San Juan Bautista) which are, in turn, bordered by zones of infrequent great earthquakes (1857 and 1906 rupture zones). To induce this type of behavior, with characteristic earthquake behavior of different segments, it was necessary to have very strong property variations. E.g., the amplitude factor varied by a factor of 10 between the creep zone and moderate earthquake zones, and by a further factor of 5 between the moderate and great earthquake zones, in the case studied. This may be stronger variation than necessary, although trial runs with weaker variation often show a tendency for phase locking between different zones, which thus lose their characteristic behavior. Presumably, strong geometric barriers at zone ends could induce characteristic-like behavior with weaker variation from zone to zone. The Parkfield-like events, in versions of the model studied thus far, are found to have highly variable moment release and recurrence intervals. One sequence of five such events, in the time span between adjacent great earthquakes, has a ratio of sample standard deviation to mean of the recurrence intervals of about 0.59, higher than 0.33 for the Bakun and McEvily (JGR, '84) Parkfield catalog.

2.4 Crack dynamics studies of a type reported previously (Rice, Ben-Zion and Kim, 1991), in which a scalar wave approximation to elastodynamics is used, are being continued to study crack advance along a plane on which there is variable resistance to cracking. In that work the resistance to cracking is given entirely by a spatially variable critical fracture toughness, and zero stress is assumed on the rupture surface. We have also begun studies of the dynamics of slipping faults which satisfy rate- and state-dependent friction on their surfaces. The work is being done for the 2D anti-plane strain case at present, and uses a numerical algorithm of Madariaga and Cochard (manuscript, 1992) which we have adapted to the rate- and state-dependent context. The aims here are to see what type of stress heterogeneity is left on a fault

surface after a rupture has propagated spontaneously and undergone a wave-mediated arrest of slip after encountering an unbreakable region, and also to see under what conditions the rupture propagation has the form suggested by Heaton (PEPI, 1990), with all slip taking place just near the advancing front of the rupture and relocking behind that.

Reports:

R. Dmowska, "Stress transfers during the earthquake cycle in oblique subduction segments" (abstract), EOS, Trans. Am. Geophys. Un., vol.73, N.43, supplement, p.361, 1992

R. Dmowska, L. C. Lovison-Golob and J. J. Durek, "Partial breaking of a mature seismic gap: The 1987 earthquakes in New Britain", *Pure and Applied Geophysics*, **136**, 459-477, 1991.

R. Dmowska and L. C. Lovison, "Influence of asperities along subduction interfaces on the stressing and seismicity of adjacent areas", *Tectonophysics* , **211**, 23-43, 1992.

Dmowska R., G. Zheng, J.R.Rice and L.C.Lovison-Golob, "Stress transfer, seismic phenomena and seismic potential in the Shumagin seismic gap, Alaska" (abstract), Wadati Conference on Great Subduction Earthquakes, abstract book, 150-152, Fairbanks, Alaska, Sept.16-19, 1992.

H. Gao, J. R. Rice and J. Lee, "Penetration of a quasistatically slipping crack into a seismogenic zone of heterogeneous fracture resistance", *Journal of Geophysical Research*, **96**, 21535-21548, 1991

H. Gao, J. R. Rice and J. Lee, "Configurational stability of the uniform upward growth of a shear crack along a strike-slip fault zone" (abstract), AGU 1991 Fall Meeting Program and Abstracts (supplement to 29 Oct. 1991 EOS), S31C-6, p. 325, 1991

M. F. Linker and J. H. Dieterich ,"Stability of fault slip under conditions of variable normal stress", (abstract), EOS, Trans. Am. Geophys. Un., vol.73, N.43, supplement, p. 511, 1992

M. F. Linker and J. R. Rice, "The effective viscosity of the San Andreas fault beneath the seismogenic zone: Constraints from the response to the 1989 Loma Prieta earthquake" (abstract), ibid, S21C-9, pp. 310-311, 1991

M. F. Linker and J. R. Rice, "Models of postseismic deformation and stress transfer associated with the 1989 Loma Prieta earthquake", manuscript intended for inclusion in USGS Professional Paper on the Loma Prieta Earthquake, 1992

J. R. Rice, "Spatio-temporal complexity of slip on a fault", *Journal of Geophysical Research,* in press, 1992

J. R. Rice, "Fault stress states, pore pressure distributions, and the weakness of the San Andreas fault" in *Fault Mechanics and Transport Properties of Rocks,* ed. B. Evans and T.-F. Wong, Academic Press, pp. 475-503, 1992

J. R. Rice, "Variable earthquake recurrence intervals at Parkfield" (abstract), EOS, Trans. Am. Geophys. Un., vol.73, N.43, supplement, p.407, 1992

J. R. Rice, Y. Ben-Zion and K.-S. Kim, "A first order perturbation solution for a dynamic planar crack with a non-uniformly moving front" (abstract), AGU 1991 Fall Meeting Program and Abstracts (supplement to 29 Oct. 1991 EOS), S31C-7, p. 325, 1991

G. Zheng, R. Dmowska and J. R. Rice, "Modeling earthquake cycles in the Shumagins (Aleutians) subduction segment with seismic and geodetic constraints" (abstract), EOS, Trans. Am. Geophys. Un., vol.73, N.43, supplement, p.367, 1992

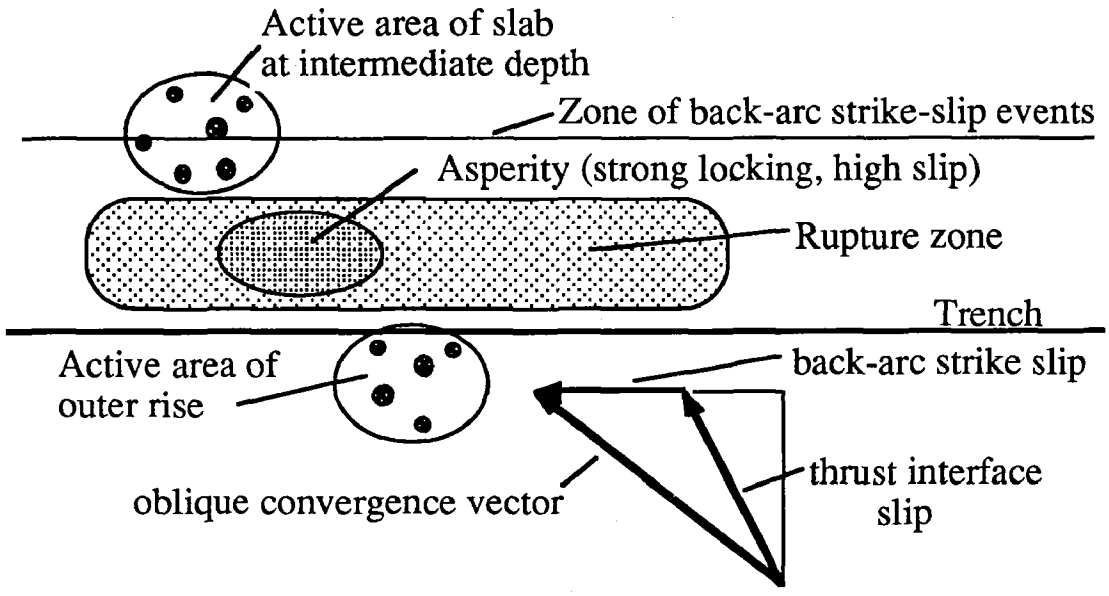

Figure 1: Oblique subduction and location of seismically active areas.

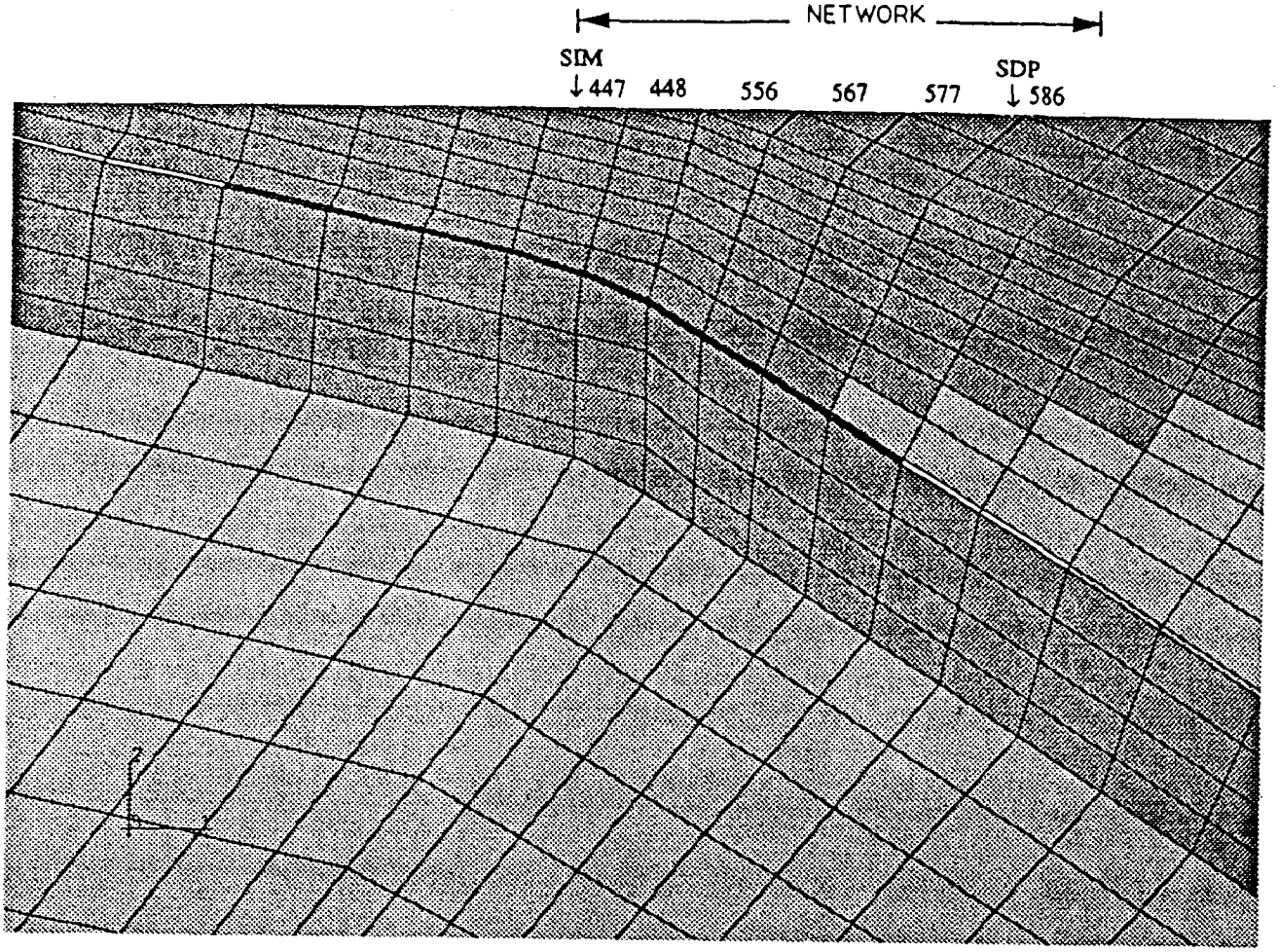

Figure 2: Finite-element mesh used for analysis of deformation at Shumagins subduction segment.

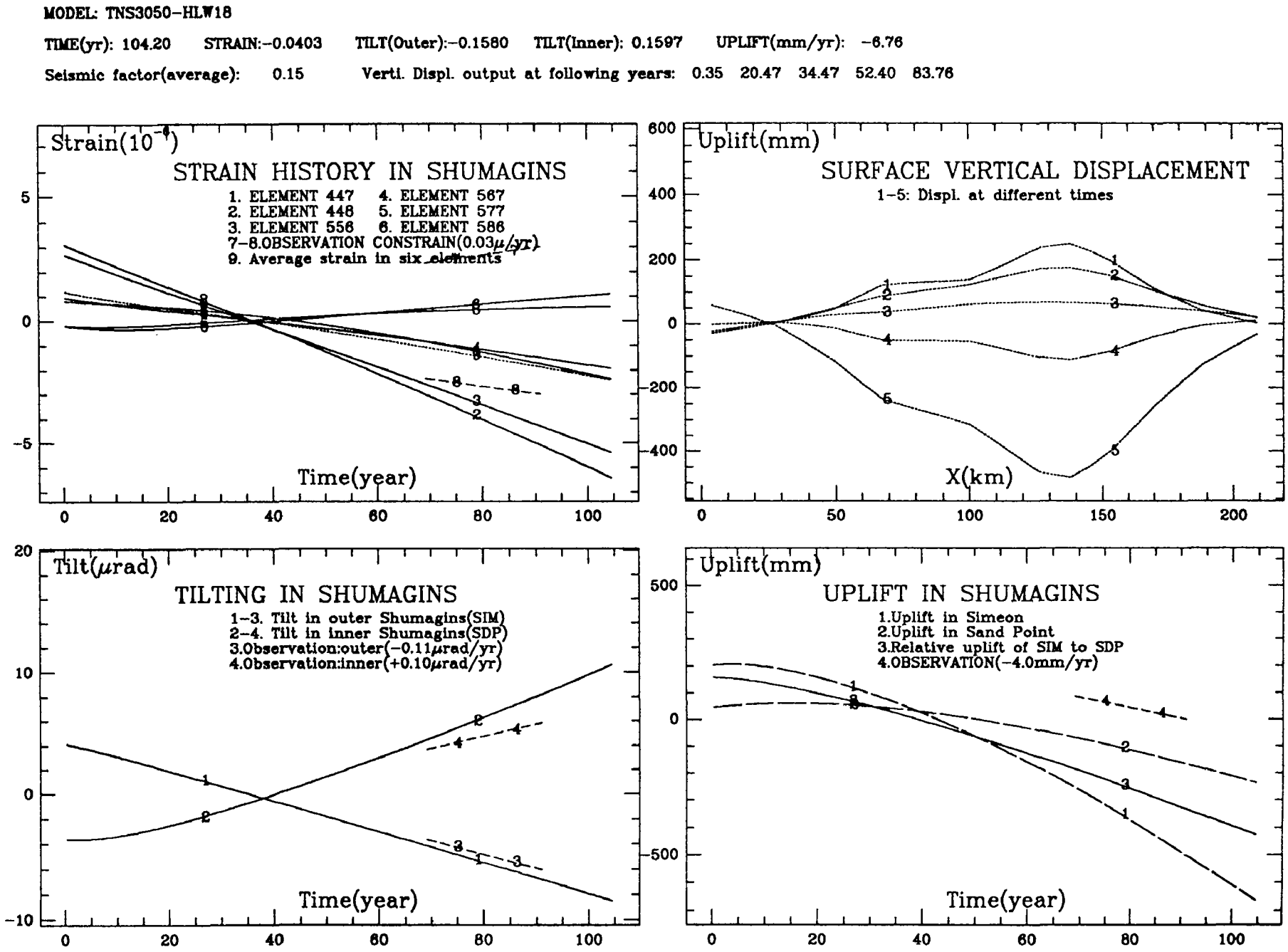

Figure 3: Deformation predictions in Shumagins area; preferred model with 15% seismic coupling.

The New England Seismic Network
Agreement No. 1434-92-A-0972

John E. Ebel
Weston Observatory
Department of Geology and Geophysics
Boston College
Weston, MA 02193
(617) 899-0950

Investigations

The operation of a regional seismic network to monitor earthquake activity in New England and vicinity is supported under this project. The purpose of this earthquake monitoring is to compile a complete database of earthquake activity in New England to as low a magnitude as possible in order to understand the causes of the earthquakes in the region, to assess the potential for future damaging earthquakes, and to better constrain the patterns of strong ground motions from earthquakes in the region. The New England Seismic Network (NESN) is cooperatively operated by Weston Observatory of Boston College and the Earth Resources Laboratory of the Massachusetts Institute of Technology (MIT).

Network Status

Weston Observatory presently has 30 seismic stations spread throughout New England, and in addition MIT is operating 9 seismic stations in New Hampshire and Massachusetts. At present, 26 of the Weston Observatory NESN remote seismic stations are single-component (vertical) stations (1 Hz velocity transducer geophones) linked via analog telephone telemetry to Weston Observatory where event triggering and recording is being done on a PC computer. The three other remote stations (at Moodus, CT, Gaza, NH and Milo, ME) are new PC-based stations, with digitizing and event triggering at the remote site and data telemetry via dial-up telephone connections. All three of these stations have three-component 1-Hz force-balanced sensors which are somewhat broader band than the standard velocity transducer. Weston Observatory and MIT are planning within the next year to install an additional 15 of these PC based stations throughout New England to replace the analog stations, all of which will lose their continuous telephone telemetry sometime during 1993.

Weston Observatory and MIT are presently archiving independently the waveform data for the seismic stations which they are presently operating. However, each institution now has the capability to convert these waveforms to SAC format for external distribution, and ftp accounts are being set up at each institution for easy external access to the waveforms as well as the event location data.

A satellite receiver to receive U.S. National Seismic Network (USNSN) waveforms has been installed atop Weston Observatory. Also, Weston Observatory is donating to the USGS a set of Streckheisen STS-1 seismometers for installation at its CBM site in northeastern Maine (at Caribou) as one of the new USNSN stations. When completely operational, there should be about 5 USNSN stations in New England in addition to the Weston Observatory/MIT regional network stations. Weston Observatory will act as a regional node with the capability of receiving and transmitting USNSN data.

Seismicity

Figure 1 shows the local and regional earthquakes recorded by Weston Observatory from October 1, 1991 to October 10, 1992. A total of 26 local earthquakes with magnitudes from 1.8 to 4.8 were detected and located by the network, five of which were felt. Also recorded on the new PC stations were several microearthquakes at Moodus, CT and at Milo, ME. Significant earthquakes during this time period included a $m_{Lg}(f)=3.4$ earthquake at Franklin, NH on October 6, 1992 which was felt throughout central New Hampshire. This was the latest and largest of several small shocks in that state during the past year. Also occurring was a $m_b=4.8$ earthquake centered on the continental slope south of Rhode Island and east of southern New Jersey. This earthquake was unusual in that it was very rich in low-frequency seismic energy and it was recorded teleseismically. Whether or not this earthquake represents a slump event on the continental slope, as has been proposed for the 1929 Grand Banks, Newfoundland earthquake, is being studied. Finally, a number of small earthquakes were recorded from central New Brunswick in the vicinity of the 1982 $m_b=5.7$ Miramichi aftershock zone. More than 10 years after the main shock, the seismic activity of this part of the northern Appalachians remains elevated above rates seen prior to 1982.

Publications

Doll, W.E., C.D. Rea, J.E. Ebel, S.J. Craven and J.J. Cipar, 1992. Analysis of shallow microearthquakes in the south Sebec seismic zone, Maine, 1989-1990, Seism. Res. Lett., 63, in press.

Zhu, H. and J.E. Ebel, 1992. Tomographic inversion for the seismic velocity structure beneath northern New England using seismic refraction data, submitted to J. Geophys. Res.

Abstracts

D'Annolfo, S.E. and A.L. Kafka, 1992. Lateral variation in the seismic velocity structure of the shallow crust beneath eastern Massachusetts and southern New Hampshire, Seism. Res. Lett., 63, in press.

Ebel, J.E., 1992. A revised Lg-wave magnitude scale for northeastern North America: Implications for seismic hazard assessment, Eos, Trans. Am. Geopyhys. U., 73, No. 14, 206.

Ebel, J.E., 1992. The $m_{Lg}(f)$ magnitude scale: A proposal for its use in northeastern North America, Seism. Res. Lett., 63, in press.

Jacobson-Carroll, M.R., and A.L. Kafka, 1992. Site effects on regional seismograms recorded in the vicintiy of Weston Observatory, Seism. Res. Lett., 63, in press.

Paulson, A.D. and J.E. Ebel, 1992. Analysis of the 1988 NYNEX seismic reflection/refraction data, Seism. Res. Lett., 63, in press.

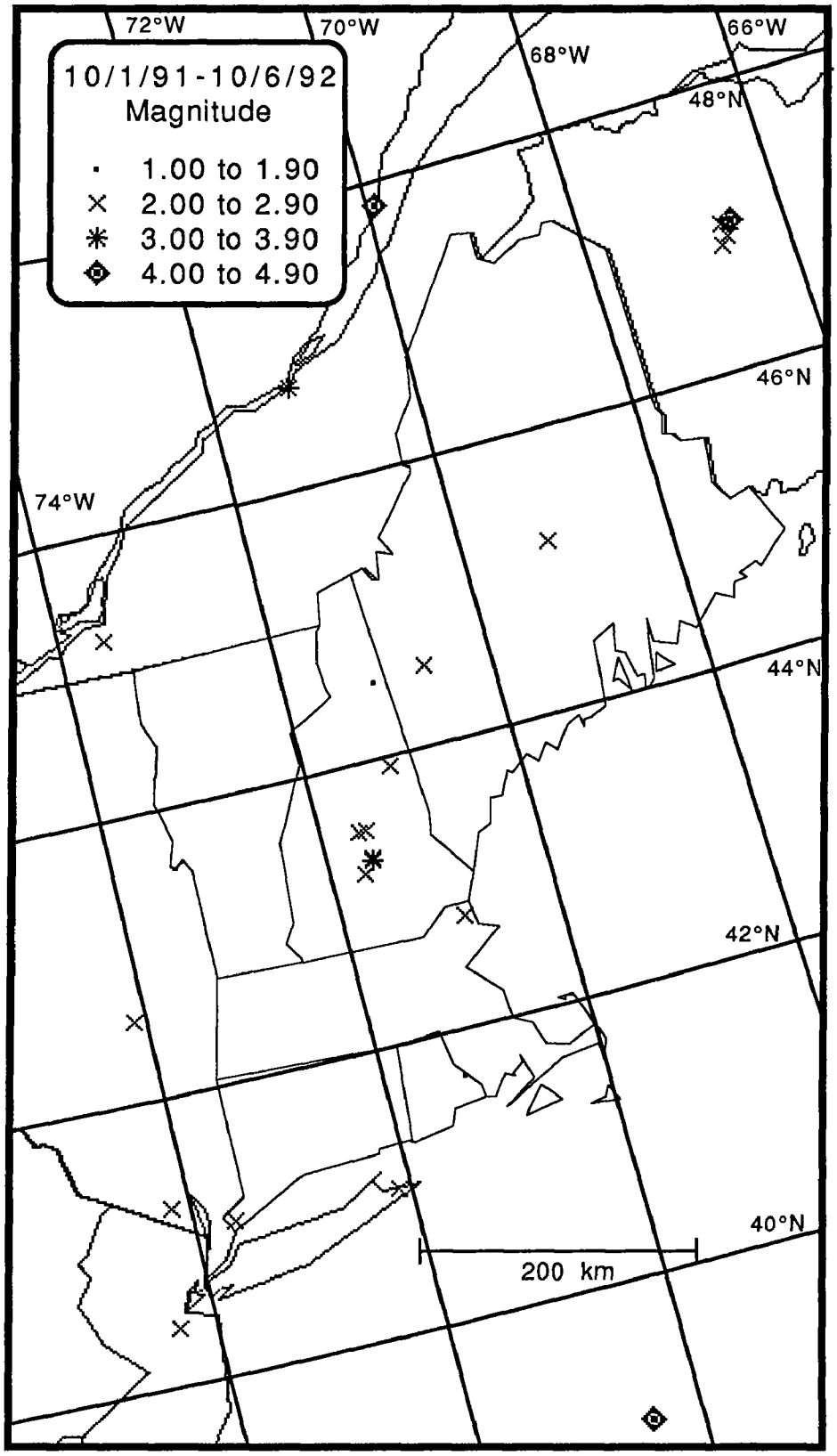

Figure 1. Seismicity recorded and located by the New England Seismic Network of Weston Observatory of Boston College from October 1, 1991 to October 10, 1992.

Central California Network Operations

9930-01891

Wes Hall
Branch of Seismology
U.S Geological Survey
275 Middlefield Road-Mail Stop 977
Menlo Park, California 94025
(415) 329-4730

Investigations

Maintenance and recording of 374 seismograph stations (474 components) located in Northern California, Central California and Oregon. Also recording 70 components from other agencies. The area covered is from the Oregon border south to Santa Maria.

Results

1. Site maintenance visits 550

2. Bench Maintenance Repair
   - A. seismic VCO units 310
   - B. summing amplifiers 38
   - C. seismic test units 13
   - D. VO2H/VO2L VCO units 63
   - E. dc-dc converters 30

3. Production/Fabrication
   - A. J512A VCO units 55
   - B. J512B VCO units 12
   - C. summing amplifier units 21
   - D. lithium battery packs 68
   - F. seismometer housing/cable 71

4. Rehabilitation:
   VCO enclosures 56

5. Computer site map plots
   - A. new 25
   - B. update 89

5. Discriminator repair and tuning (J120) 166

6. Revised and updated documentation on all wiring from telco input to disscriminator output. (cusp, RTP, Motorola, PC, helicorder, etc).

7. Ordered Parts for 175ea J512 VCO's and 100 ea J120 discriminators

8. Equipment Shipped:

   A. Cal Tech, Pasadena
      a. 60 ea. J601 DC-DC Convertors
      b. 1 J512B vco's
      c. 40 ea. J120 discriminators
      d. 1 ea. discriminator rack
      e. 6 ea. L4 seismometers
   B. University Washington

a. 15 ea. J512a vco's
b. 15 ea. J120 discriminators
c. 1 ea. discriminator rack

C. Hawaii Volcano Observatory
a. 20 ea. J512a vco's
b. 20 ea. J120 J120 discriminators
c. 1 ea. discriminator rack
f. 20 ea. summing amp PCB

D. University Utah
a. 25 ea. J120 discriminators

9. New installations

A.	CPI	(Pinole Ridge)
B.	JSB	(San Bruno Mountain)
C.	JCP	(Coyote Point)
D.	KSC	(Snow Mountain)
E.	KHB	Hayfork Bally)
F.	BPO	(Post Ranch Vertical)
	BPON	(Post Ranch North)
G.	OCR	(Cohasset Ridge)
H.	CGP	(Garin Park)
I.	CYB	(Yerba Buena Vertical)
	CYBN	(Yerba Buena North)
	CYBE	(Yerba Buena East)
	CYBZ	(yerba Buena Low Vertical)
J.	KTR	(Thompson Ridge)
K.	KCS	(Cold Spring)
L.	MBE	(Bear Mountain)
M.	MBU	(Bullion Mountain)

10. Stations discontinued.

A.	BPF	((Pfeiffer Point Vertial)
	BPFN	(Pfeiffer Point Horizontal)
B.	OCH	(Cohasset Ridge)
C.	CSC	(Silver Creek)
D.	HQR	(Quien Sabe)
E.	PRP	(Reason Peak)

THE USGS PARKFIELD DENSE SEISMOGRAPH ARRAY (UPSAR)

9910-03974

M. HELLWEG, L.M. BAKER, J.B. FLETCHER, P. SPUDICH, L.K. STECK
BRANCH OF ENGINEERING SEISMOLOGY AND GEOLOGY
345 MIDDLEFIELD ROAD, MS 977
MENLO PARK, CALIFORNIA 94025-3591
415/329-5654 FAX 415/329-5163

Investigations:

1. Temporal stability of coda Q at Parkfield, California.

2. Determination of transient dynamic stresses caused by the Landers, California, earthquake.

3. Investigations of scattering and multipathing of surface waves caused by large California earthquakes.

Results:

1. Since mid-1989, the USGS Parkfield Dense Seismograph Array, UPSAR, an array with 14 three-component seismographs located in a 1 km^2 area, has been recording seismicity in the Parkfield region. At present, it has recorded more than 600 local events. These earthquakes have occurred at all azimuths and at varying distances, and include spatial clusters as well as doublets. To test the temporal stability of the Qc measurement we used Haar's method (1989) to determine coda-Q of a cluster of 10 events that occurred between December 1989 and the present, all of which were located in a 1 km3 source volume. The use of events in a compact source volume minimized station-hypocenter variability in the coda-Q measurements. In the frequency bands 4-8 Hz and 8-16 Hz values of Qc did not vary from the mean values of 108 and 222, respectively by more than 10 per cent during this period. Qc differences between nearly simultaneous doublets was as large as the variation between temporally separate events. To improve the temporal coverage, we determined coda Q in the frequency bands, 2 4 Hz, 4-8 Hz, 8-16 Hz and 16-32 Hz, from a set of 68 events with epicentral distances of less than 60 km. Analysis of this set shows that there has been no significant variation in coda Q in the Parkfield region since December 1989.

2. The UPSAR accelerometers produced usable broadband records from many of the recent large California earthquakes, such as the Joshua Tree, Landers, Big Bear, Petrolia, and Ferndale events. In an attempt to understand the origins of the widespread earthquake triggering following the Landers earthquake, the UPSAR

acceleration records of the Landers event have been double-integrated to displacement and have been inverted to obtain the dynamic strains as a function of time produced at UPSAR (epicentral distance = 415 km) by this event. Preliminary inversion results yield peak shear strains of about 6 x 10^{-6}. Noise levels, inferred from displacement differences between the two closest stations of the array, are about 1 x 10^{-6}. The maximum strains occur during the surface wave train. To extrapolate surficial strains to seismogenic depths, we must account for the variation of the surface wave eigen functions with depth, which we are presently doing. A rough calculation shows that our observed strains correspond to transient dynamic stresses of about 1 bar at depth. This stress is about a factor of 50 larger than the stress changes induced by earth tides.

3. Records of the Landers event at UPSAR contain P_n, P_g, P_L, S_n, S_g, L_Q and L_R phases, as well as later-arriving scattered surface waves. On velocity seismograms, a number of distinct arrivals can be seen in both the P and S wave trains. Broad-Band Frequency-Wavenumber analysis shows that the first arriving P energy comes in at an azimuth of about 80 o s, whole the lower frequency S waves come in at 100 o s, closer to the expected value of 115 o 's. Fundamental mode Love and Rayleigh waves are observed to arrive from about 120 o 's. However, 200 s after the P-wave arrival, 10-20 s surface waves arrive from about 70 o 's azimuth. These waves are probably surface waves scattered from the Sierra Nevadas.

Reports:

Fletcher, J.B., Baker, L.M., Spudich, P., Goldstein, P., Sims, J.D., and Hellweg, M., 1992, The USGS Parkfield, California, dense seismograph array: UPSAR, Bull. Seismol. Soc. Am., v. 82, 1041-1070.

Hellweg, M. Fletcher, J.B., and Spudich, P., 1991, Coda coherence and Q from UPSAR, Parkfield, California, [abs.], EOS Trans. Am. Geophys. Un., v. 72, 483.

Hellweg, M. Spudich, P., and Fletcher, J.B., 1992, Coda Q in the region of Parkfield, California: a temporal and spatial investigation, [abs.], EOS Trans. Am. Geophys. Un., v. 73, 200.

Hellweg, M. Spudich, P., and Fletcher, J.B., 1992, Stability of Coda Q at Parkfield, California, [abs.], EOS Trans. Am. Geophys. Un., v. 73, 397.

Steck, L.K., Spudich, P., Hellweg, M., Baker, L., and Fletcher, J., 1992, Shear strain at Parkfield produced by the Landers earthquake, [abs]., EOS Trans. Am. Geophys. Un., v. 73, 374.

Source Characteristics of events along the Transverse Ranges

14-34-92-G2180

Donald V. Helmberger
Seismological Laboratory
California Institute of Technology
Pasadena, CA 91125

(818)356-6998

Investigations

A number of recent and historic earthquakes have occurred along the Transverse Ranges, causing significant damage to the greater Los Angeles region. Many of the historic events occurring in this region have been recorded (locally) by relatively low gain long period and short period torsion instruments operated by Caltech (1930 to 1960). Some of the larger events M>5 can be seen on the (Berkeley Galitzins) regionally while still larger events M>6 can be observed teleseismically, (De Bilt ,etc.).

To understand these seismograms or separate propagational distortions from source properties is relatively easy at teleseismic distances, but becomes more difficult at regional and local distances. Fortunately, the digital systems used in the TERRAscope array provides observations that greatly aid in establishing the nature of regional propagation. For example, the wide dynamic range allows motions from small events (aftershocks) to be compared with large events at the same site even though the motions can be different by several orders of magnitude. Signals at these distances have not suffered mantle attenuation and thus the broadband features of this system allow us to see obvious propagational effects (headwaves and critical reflections) and detailed source characteristics (near-field and source complexity).

Modeling attempts to date indicate that whole seismograms can be understood at ranges less than a few degrees with simple models. At larger ranges, the energy carried by direct S generally becomes scattered and difficult to model, presumably caused by shallow earth structure. Fortunately, at these larger ranges the mantle headwaves, Pn and Sn, become visible and we believe this beginning portion of records (excluding the surface waves) can be used in source estimation as demonstrated by our waveform inversion results.

Results

Several papers involving the Sierra Madre earthquake sequence have been published or "in press": (1) Source parameters of the Sierra Madre Earthquake from Regional and Local Bodywaves, Dreger and Helmberger (1991). (2) Strong motion and broadband Teleseismic Analysis of the 1991 Sierra Madre, California Earthquake, Wald (1992). (3) Impact of broadband seismology on Strong Motion Attenuation. Helmberger et al. (1992). (4) Broadband observations of rupture directivity for the 1991 Sierra Madre earthquake, Dreger and Helmberger (1992). In this summary we will emphasize the recent Landers earthquake and the complex faulting deduced from broadband modeling local, regional and teleseismic waveform observations, Wald et al. (1992).

We have determined a finite-fault source rupture model for the 1992 Landers earthquake consistent with both teleseismic and strong motion displacement data. The procedure followed is similar to previous efforts, see Wald et al. (1991). The fault model parameterization consists subfaults making up three separate fault planes, mimicking the mapped surface offset (Figures 1

and 2). Each subfault is 3 km across by 2.5 km down-dip, giving a total fault depth 15 km and a total of 186 subfaults. The hypocenter is assumed to be 9 km, as determined by the network location (star in Figure 2). The fault strikes of the Johnson Valley/Landers, Homestead Valley, and Emerson/Camprock Faults are 355°, 334° and 320°, respectively.

Currently our inversion employs a subset of 11 local strong motion records (including Amboy, Barstow, Big Bear, Lucerne Valley, Morongo Valley, and Joshua Tree) combined with near-regional TERRAscope data. We also use 11 teleseismic P waves and 10 SH waves. All data and synthetics were bandpassed between 20 seconds and 1.0 Hz. Shallow slip in our model is constrained to match that measured at the fault surface by assigning that slip value to the shallowest subfault elements. We have also performed a separated inversion of the teleseismic broadband data using the same fault parameterization.

Rupture models are consistent for both data sets: we found unilateral rupture with two main regions of slip, separated by about 35 km with a slip gap. This is in agreement with the measured surface offset. The effective rupture length is about 65 km and the seismic moment was computed to be about 0.8 - 0.85 x 10^{27} dyne-cm, with peak slips of nearly 7 meters. The seismic moments of slip for the three fault planes is about 0.20, 0.25 and 0.35 x 10^{27} dyne-cm. The rupture velocity is locally variable, but can be approximated with value of 2.5 km/sec, or about 75% of the local shear velocity.

We find the nucleation of the rupture to be a complex growth, perhaps stopping and restarting, as required by late teleseismic P wave arrivals as well as emergent local strong motion arrivals. This was accounted for in our modeling with the use of multiple time windows, i.e., allowing repeated rupture to occur on each subfault. The use of time windows also allows for the estimate of rupture duration. Local slip durations (rise time) are short, less than 2.0 sec on most of the fault, but may be up to 4.0 sec in region of maximum slip at depth.

References

Dreger, Douglas S. and D. V. Helmberger (1991). Source parameters of the Sierra Madre Earthquake from regional and local body waves, *Geophys. Res. Lett.*, **18**, 22015-2018.

Dreger, D. S. and D. V. Helmberger (1993). Broadband observations of rupture directivity for the 1991 Sierra Madre earthquake, *Bull. Seism. Soc. Am.* (in press).

Helmberger, D. V., D. Dreger, R. Stead, and H. Kanamori (1993). Impact of broadband seismology on strong motion attenuation, *Bull. Seism. Soc. Am.* (in press).

Wald, David J.(1991). Strong motion and broadband teleseismic analysis of the 1991 Sierra Madre, California, Earthquake, *Journal Geophys. Res.*, **97**, 11033-11,046.

Wald, D., D. Helmberger, and T. Heaton (1991). Rupture history of the 1989 Loma Prieta, California, earthquake, *Bull. Seism. Soc. Am.*, **81**, 1540-1572.

Wald, D. J. D. V. Helmberger and T. H. Heaton (1992). On developing a simgle rupture model for the 1992 Lander, California earthquake consistent with static, broadband teleseismic, regional and strong motions, *EOS*, American Geophysical Union (Fall Meeting).

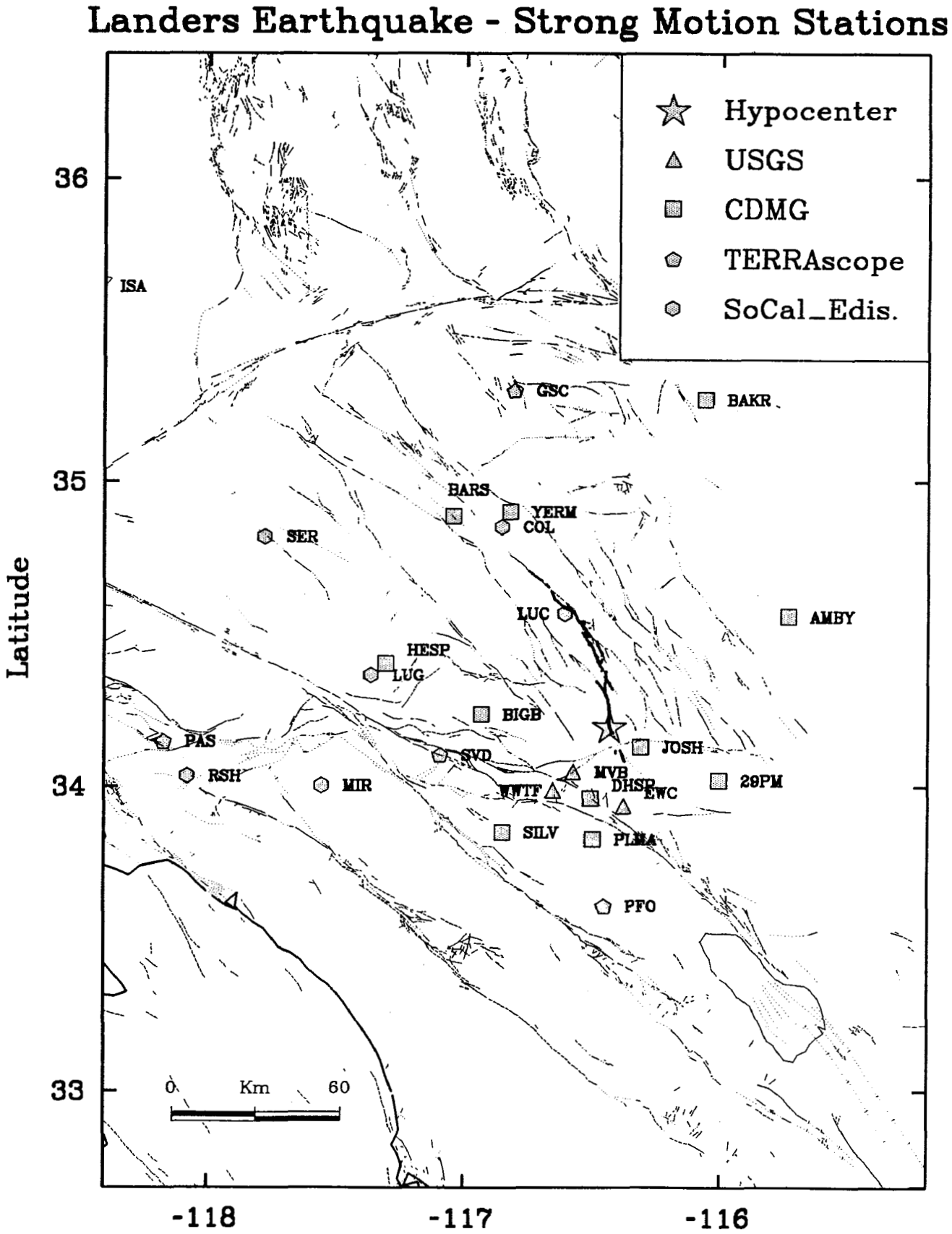

Fig. 1. Location map showing strong motion stations (solid symbols) for the Landers earthquake. Light lines are mapped faults and the thick line indicates surface offset from the Landers event (courtesy of K. Sieh, Caltech).

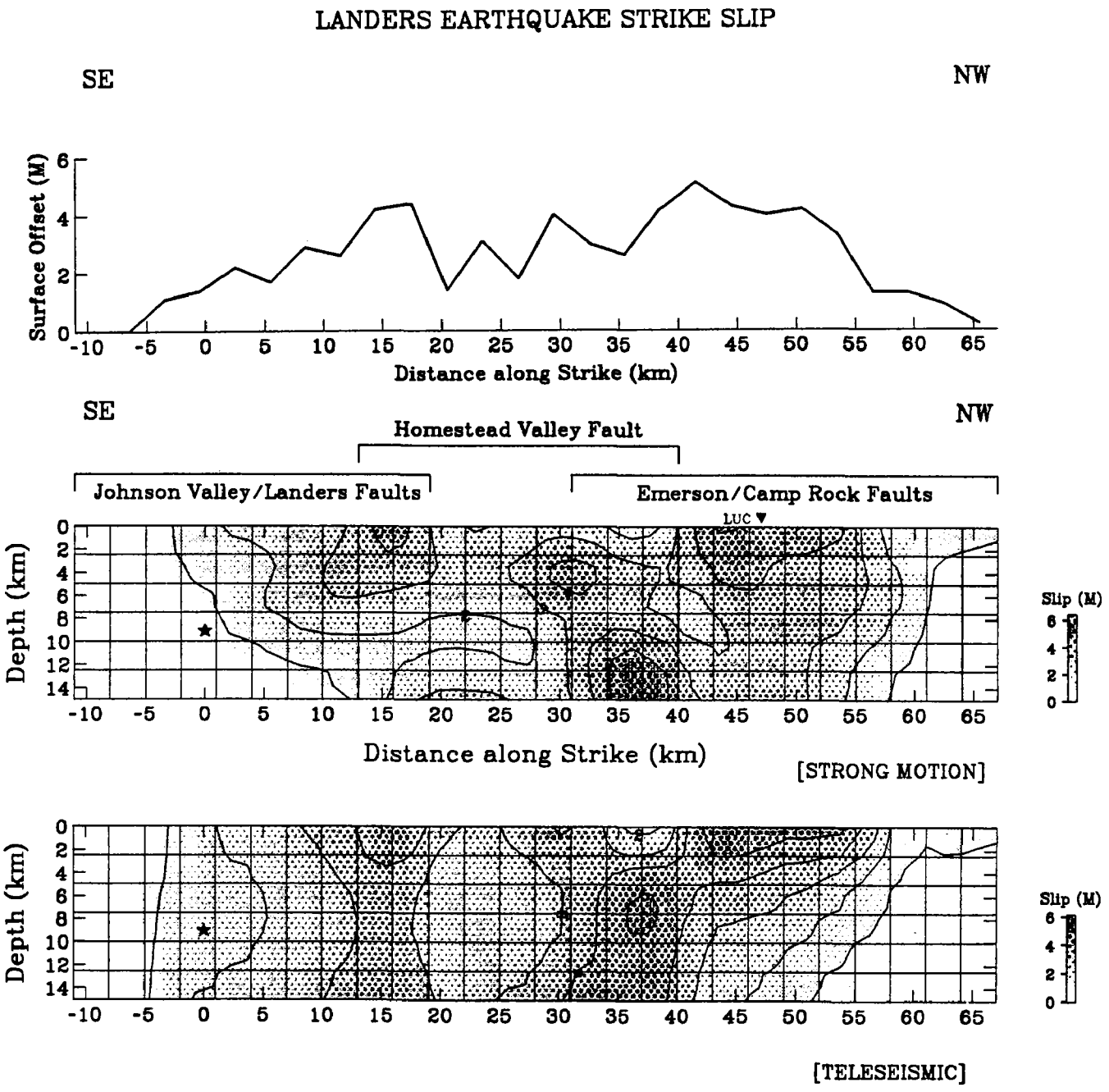

Fig. 2. Modeling results of the Landers earthquake showing strike-slip distribution. The three fault segments overlap as shown with braces and vertical dashed lines. Slip is given in meters with a contour interval of 1 meter. The observed surface slip, averaged over each 3 km horizontal subfault dimension is shown above (from K. Sieh).

Regional Microearthquake Network in the Central Mississippi Valley

14-08-0001-A0619

Cooperative New Madrid Seismic Network

14-34-92-A-0967

Robert B. Herrmann
Department of Earth and Atmospheric Sciences
Saint Louis University
3507 Laclede Ave.
St. Louis, MO 63103
314/658-3131, FAX 314/658-3117

Investigations

The purpose of the network is to monitor seismic activity in the Central Mississippi Valley Seismic zone, in which the large 1811-1812 New Madrid earthquakes occurred. The following section gives a summary of network observations during the last six months of 1991 and the first six months of 1992, as reported in Network Quarterly Bulletin Nos. 69 through 72.

Results

Event Location

From July 1, 1991 through June 30, 1992, 85 earthquakes, typically with magnitudes greater than 1.2, were located by the 40 station regional telemetered microearthquake network operated by Saint Louis University for the U.S. Geological Survey and the Nuclear Regulatory Commission. Figure 1 shows 77 earthquakes located within a 4° x 5° region centered on 36.5°N and 89.5°W. The magnitudes are indicated by the size of the open symbols. Figure 2 shows the locations and magnitudes of 68 earthquakes located within a 1.5° x 1.5° region centered at 36.25°N and 89.75°W.

During this time, 116 teleseisms were recorded by the PDP 11/34 microcomputer. Epicentral coordinates were determined by assuming a plane wave front propagating across the network and using travel-time curves to determine back azimuth and slowness, and by assuming a focal depth of 15 kilometers using spherical geometry. Arrival time information for teleseismic P and PKP phases has been published in the quarterly earthquake bulletin.

The significant earthquakes occurring from July 1, 1991 through June 30, 1992 include the following:

July 2, 1991 (0349 UTC). South-central Missouri. mbLg 3.3 <C.M.V.S.N.>.

July 7, 1991 (2124 UTC). Missouri-Arkansas Border Region. mbLg 4.0 (NEIS). 3.8 (TUL). Felt in Howell and Oregon Counties, Missouri. Also felt in northern Arkansas.

July 8, 1991 (2349 UTC). New Madrid, Missouri region. mbLg 2.9 <C.M.V.S.N.>.

October 3, 1991 (1146 UTC). New Madrid, Missouri region. mbLg 3.1 (GS). Felt (III) at Bladgett, Charleston and East Prairie. Felt (II) at New Madrid.

November 11, 1991 (0920 UTC). Southern Indiana. mbLg 3.8 (GS), 3.6 (TUL). Felt (III) at Bellmont, Birds, Claremont, Mt. Carmel, Newton, Noble, Parkersburg, Robinson, Sainte Marie, Sumner and West Liberty, Illinois. Also felt in the Lawrenceville, Illinois area.

November 13, 1991 (0943 UTC). Arkansas. <SLM-P>. MD 3.0 (SLM).

December 13, 1991 (1141 UTC). Arkansas. MD 2.8 (GS). Felt (IV) at Blytheville and (III) at Dell and Manila.

January 9, 1992 (0730 UTC). Felt in Tollesboro and Ribolt, Kentucky. MD 2.8 <K.D.S.N.>.

January 21, 1992 (1136 UTC). Central Missouri. Felt (IV) at Linn Creek. Felt (III) at Camdenton and Sunrise Beach. Also felt in the Osage Beach area. mbLg 3.2 <C.M.V.S.N.>.

March 3, 1992 (1230 UTC). New Madrid, Missouri region. Felt at Steele, Missouri. mbLg 2.6 <C.M.V.S.N.>.

March 27, 1992 (2157 UTC). Felt in Owingsville and Salt Lick, Kentucky. MD 2.4 <K.D.S.N.>.

April 3, 1992 (0306 UTC). Tennessee. <T.E.I.C.>. mbLg 3.5 (GS), 3.2 (TUL). Felt (IV) at Gates and Ripley. Felt (II) at Burlison. Felt in Dyer and Lauderdale Counties.

April 30, 1992 (0001 UTC). New Madrid, Missouri Region. mbLg 2.9 (TUL). Felt at Greenville, Piedmont, Poplar Bluff and Sikeston.

May 11, 1992 (0642 UTC). New Madrid, Missouri Region. mbLg 2.6. <C.M.V.S.N.>.

Data Acrhiving

As the seismic data acquisition has evolved from the PDP 11/34 to a PC based data acquisition and with the current upgrade to complete digital data acquisition, efforts have been made to ensure that all data digitally acquired since 1981 will be available for future reference and research.

This task involves many steps. First, all original time histories are reviewed, useless data are removed and all useful data are saved. The data are saved using the current formats, but a modern Center for Seismic Studies set of pointers into the binary data files is generated for the next generation of analysis software. The verified data set is then stored on optical disk with an exabyte backup. A master event list with pointers into the optical disk directories is also generated for rapid, automatic access of data.

During this report period, all teleseismic triggers have been stored on optical disk. This required reviewing about 1500 events and verifying their location parameters from the PDE. At the same time, system transfer functions have been documented to permit quantitative use of these data. This data set has already been used by a number of USGS investigators.

Future Plans

The archiving of digital recordings of all local and regional seismic events to optical disk will take place during the next year.

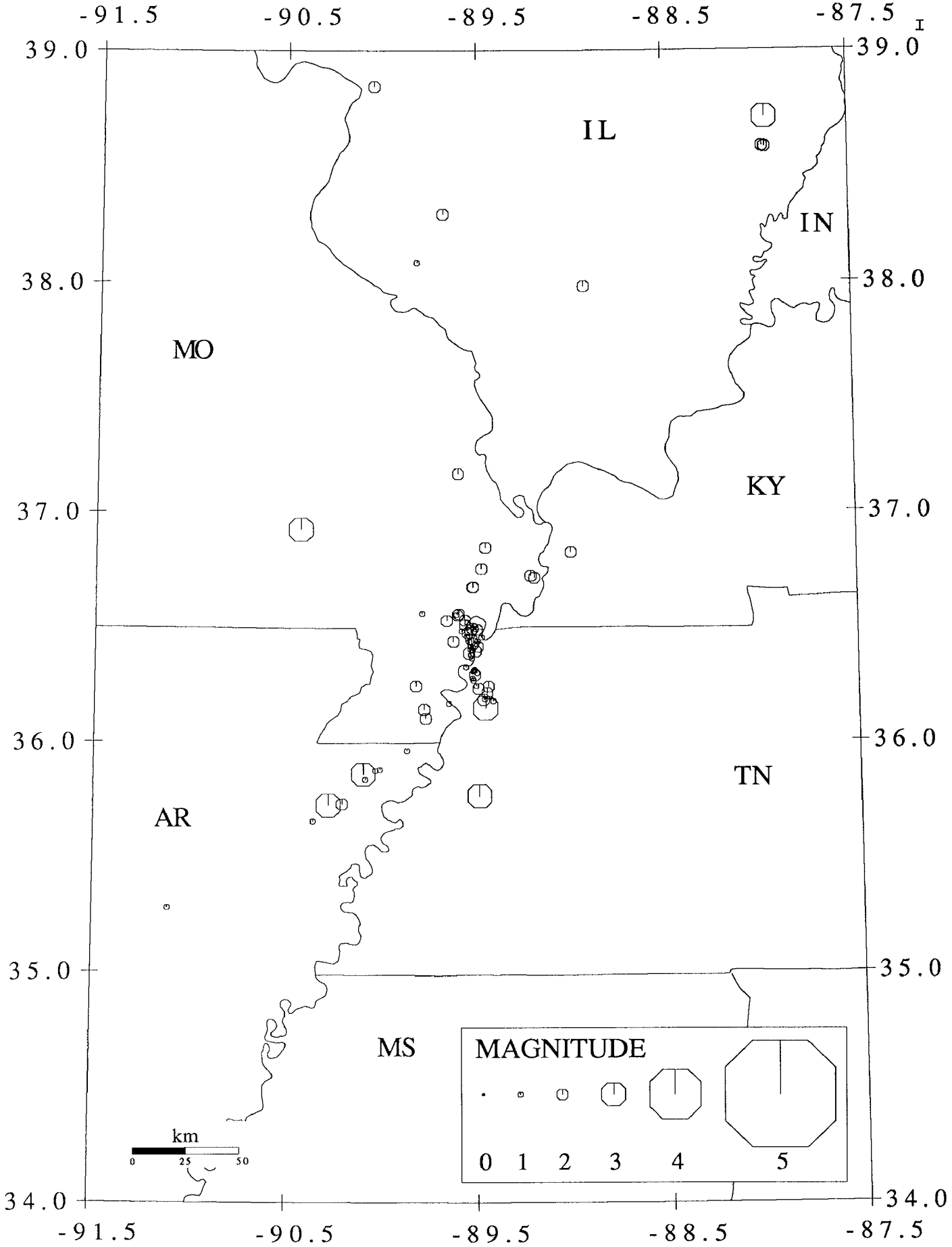

FIGURE 1

CUMULATIVE EVENTS 01 JUL 1991 TO 30 JUN 1992

LEGEND : △ STATION ⊙ EPICENTER

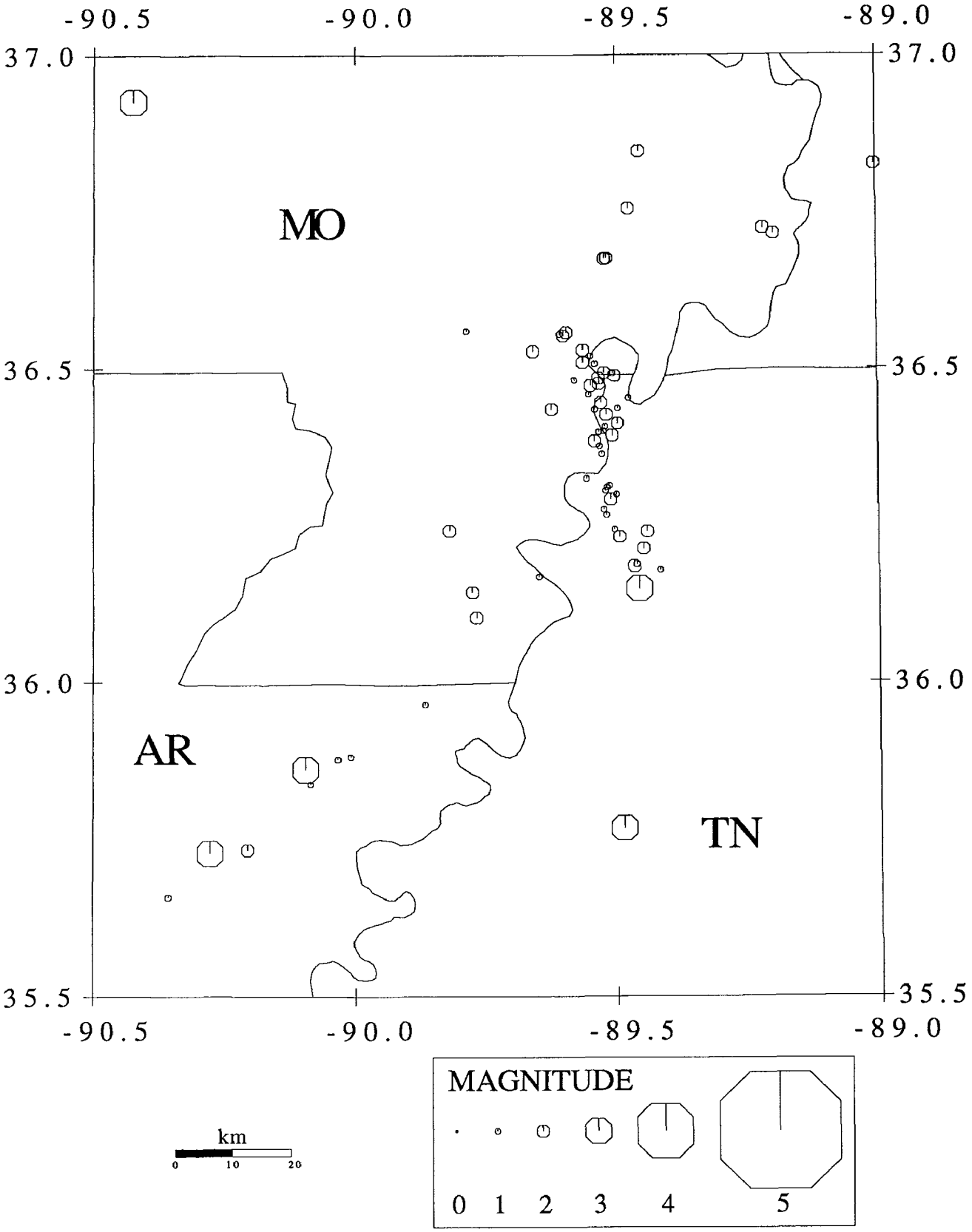

FIGURE 2

CUMULATIVE EVENTS 01 JUL 1991 TO 30 JUN 1992

LEGEND : △ STATION ⊙ EPICENTER

Cooperative New Madrid Seismic Network

14-08-0001-G1922
R. B. Herrmann
Department of Earth
and Atmospheric Sciences
Saint Louis University
3507 Laclede Avenue
St. Louis, MO 63103
(314) 658-3131

14-08-0001-G1923
A. C. Johnston, J. M. Chiu
Center for Earthquake
Research and Information
Memphis State University

Memphis, TN 38152
(901) 678-2007

Investigations

The object of this effort is to upgrade the regional seismic networks in the central Mississippi Valley to provide the data sets necessary for future research in the earthquake process and in earthquake generated ground motion.

In order to accomplish this, the satellite telemetry capability of the US National Seismic Network will be used to communicate between central data collection points at Memphis and St. Louis and the intelligent regional seismic network nodes to be placed at five sites in the region.

Major tasks involve the design and implementation of the data centers, the regional nodes at satellite uplink points, and the seismic sensors in the field. Data will be transmitted from the sensors to a node using all digital telemetry, 20 and 24 bit, to the extent possible with the present funding. The final network will consist of 5 nodes, each collecting data from a broadband sensor, an accelerometer and three-component seismometers.

Results

The previously reported PC based real time data acquisition for the current analog telemetry has proven very stable in over one year of service.

Current efforts are directed toward sending the seismic signals from a field unit using the USNSN packeting protocol.

Software development of the seismic data analysis system is underway. Given the expected data flow, data analysis will be performed without the use of a data base, using the computer file system as a simple flat file data base. All data acquired will be stored as created, and a Center for Seismic Studies *"wfdisc" pointers into the data file* will be used. The value of this is that data from a wide variety of sources can be analyzed by the same software, and also that all previously acquired network data can be so analyzed.

Discussions with local microwave networks and cable TV companies are underway for use of towers, network capacity, and grounds for satellite dishes.

Pressure Solution, Crack Healing and Crustal Stress

9960-04543

Stephen H. Hickman
U.S. Geological Survey
345 Middlefield Rd., MS 977
Menlo Park, CA 94025
(415) 329-4807

Investigations Undertaken

1. As part of a cooperative program between the USGS and the Russian deep scientific drilling organization, NEDRA, we are conducting an investigation of stress-induced borehole breakouts in a 4-km-deep well at Tyrnauz, Russia, in the Greater Caucasus Mountains. The Tyrnauz well is located within a granitic pluton in a region of active north-south crustal shortening associated with the collision of the Arabian and Eurasian plates. The goals of this study are to determine the nature of plate-interaction forces at a continent-continent collisional plate boundary and improve our understanding of the manner in which small- to intermediate-scale faults and topographic loads act to perturb the regional stress field. This work is being conducted in collaboration with Daniel Moos and Colleen Barton of Stanford University.

In a related investigation, we are collaborating with Carolyn Morrow and David Lockner of the USGS in Menlo Park in making measurements of permeability and resistivity on cores recovered from the 12-km-deep Kola well in Russia. Results from these measurements are discussed in the NEHRP Technical Summary by D. Lockner.

2. For many years, scientists affiliated with the USGS have performed a variety of experiments which involved making hydraulic fracturing stress measurements from drilling rigs deployed in tectonically active areas to constrain the mechanics of faulting and crustal deformation. To formulate a more viable and cost-effective in-situ stress program, beginning in Fiscal Year (FY) 1991 we have been building a wireline packer system that can be used without a drilling rig at depths of up to 1.5 km. The advantages of this wireline system over standard drill-pipe-deployed packer systems are threefold: (1) Because no drill rig is required during testing, the cost of making in-situ stress measurements is greatly reduced. (2) This wireline packer system is fully self-contained and therefore capable of making about twice as many measurements in a given amount of time as previously possible. (3) This wireline packer system measures both flow rate and fluid pressure downhole, improving the accuracy with which crucial test parameters such as shut-in and fracture-opening pressures (and, hence, in-situ stresses) can be determined.

3. We are conducting an experimental study of pressure solution and crack healing under load in simple quartz/water systems. These experiments employ single crystals in well-controlled model geometries inside a hydrothermal vessel equipped with an optical observation port. This port, in conjunction with a long-working distance microscope, allows the morphology and geometry of intergranular contacts and cracks to be continuously monitored. The goal of these experiments is to constrain the mechanisms and kinetics of solution-transport creep, asperity adhesion and crack healing and thereby provide fundamental constraints on processes controlling the spatial and temporal evolution of fault strength, permeability and other physical properties in the Earth.

Results Obtained

1. In the summer of 1991, we conducted a borehole televiewer log in the Tyrnauz well from a depth of 300 m to 3200 m. In FY 1992, we digitized this log to produce a continuous log of borehole radius and then analyzed this data to determine the orientations and widths of stress-induced borehole breakouts and natural fractures in this well.

Overall, the orientations of breakouts in the Tyrnauz well are extremely uniform, indicating that the direction of maximum horizontal compressive stress, S_{Hmax}, is N 13° E ± 10°, with an approximately 20° counterclockwise rotation in S_{Hmax} directions going down the well. This S_{Hmax} direction compares favorably with the NNW-NE range of P axis orientations determined from larger earthquakes in this region. Comparison to finite-element models of deformation in this region [*Oral et al.*, 1992] and relative plate motions [*Minster and Jordan*, 1978] shows that the orientation of S_{Hmax} at Tyrnauz is consistent with that expected if the source of the stress in the Greater Caucasus is the collisional force applied to the Eurasian plate by the northward-moving Arabian plate.

Applying the theory of *Moos and Zoback* [1990], in conjunction with laboratory measurements of uniaxial compressive strength on core obtained from this well, the observation that breakouts at Tyrnauz are nearly continuous below a depth of 400 m suggests that the horizontal stress magnitudes are very high and that the stress regime at this site is transitional from strike-slip to reverse faulting. This inference is in agreement with the occurrence of large- and intermediate-magnitude strike-slip and reverse-faulting earthquakes in the Greater Caucasus region.

At numerous depths in this well breakouts were observed to decrease in width or rotate near natural fractures or faults, suggesting localized perturbations to the regional stress field. In particular, theoretical modelling of a dramatic rotation in breakout azimuth observed above a fracture zone at about 3032 to 3045 m depth shows that this rotation can be accounted for by slip on faults observed to cut the well at this depth.

Most of the natural fractures observed in the televiewer log strike parallel to the S_{Hmax} direction at Tyrnauz and dip steeply (dips > 60°) to the west. These observations, together with the young age (2.5 Ma) of the granite in which this well is located, suggests that these fractures are tensile in origin and formed in response to the current tectonic stress field.

2. We completed construction of our wireline packer system in FY 92 and tested this system as part of two separate scientific studies: one in the Santa Cruz Mountains and the other in the Wawona area of Yosemite National Park.

Santa Cruz Mountains Experiment. Within minutes after the 1989 Loma Prieta earthquake, stream flows in the Santa Cruz Mountains immediately northwest of the epicenter began increasing by about a factor of 10 and ground-water levels in this area began to drop. One of the hypotheses advanced to explain these phenomena is that near-surface rocks in the Santa Cruz Mountains are under high ambient levels of deviatoric stress and that coseismic stress changes (dynamic and/or static) were sufficient to produce new fractures or reactivate pre-existing fractures, resulting in a dramatic increase in aquifer permeability (*Rojstaczer and Wolf*, 1992). In this experiment, which is conducted in collaboration with Stuart Rojstaczer of Duke University, we are using our wireline packer system and borehole televiewer to measure stress magnitudes and orientations, permeability and natural fracture orientations in shallow wells drilled in the Santa Cruz Mountains. We will then use these measurements, in conjunction with estimates of coseismic stress perturbations and simple rock failure criteria (both in shear and in tension), to test the Rojstaczer and Wolf (1992) model and determine the physical mechanisms responsible for these hydrologic changes. As part of this experiment, in July of 1992 we attempted to use our wireline packer system in two shallow wells located in highly fractured shales and sandstones near the top of the Santa Cruz Mountains, but problems with hole collapse and integrity of the surface casing in these wells prevented us from making any stress or permeability measurements. In February of 1993 we will attempt a similar suite of

experiments in shallow wells drilled in more competent and less fractured granitic rocks along the western flank of the Santa Cruz Mountains.

Wawona Experiment In this experiment we conducted hydraulic fracturing stress measurements and borehole televiewer logs in two shallow wells drilled by the National Park Service (NPS) in Yosemite National Park near the town of Wawona. This study, which is a multidisciplinary effort involving scientists from the USGS Water Resources and Geologic Divisions, private industry and the Lawrence Livermore and Los Alamos National Laboratories, is being conducted to ascertain if the ground water resources at Wawona are adequate to support relocation of NPS employees from the Yosemite Valley to the Wawona area. Our role in this study is to investigate the nature and origins of the shallow stress field and determine the extent to which these stresses control the orientations of permeable fractures and fault zones in the fractured granitic aquifer beneath Wawona.

Our field work at Wawona was quite successful and we obtained extremely high-quality hydraulic fracturing data from all 12 tests attempted. Although the field work was just completed in September of 1992, preliminary analysis of these data indicates that the shallow stresses at this site are transitional from a reverse faulting stress regime at depths of less than about 200 m to strike-slip faulting at depths of 200 to 300 m (the maximum depths of our tests). These data also indicate that the magnitudes of S_{Hmax} relative to the vertical stress at depths of 50 to 100 m are extremely high, being about twice as great as predicted using laboratory coefficients of friction and simple frictional faulting theory for reverse faulting. As Wawona is located in a topographically rugged area which has experienced rapid erosion, we attribute these high horizontal stresses to a combination of near-surface residual stresses and topographic effects. Based on borehole televiewer logs that we conducted in these wells, we hypothesize that high differential stresses can be maintained at Wawona because of the paucity of fractures in the shallow granite which are favorably oriented for reverse faulting. Our hydraulic fracturing tests indicate that the orientation of S_{Hmax} at Wawona is about N 55° W, an orientation that departs significantly from the roughly N-S to NNE regional trend and further suggests a local source for the stresses we measured in these wells.

Once in-situ permeability data collected at Wawona by scientists from the USGS Water Resources Division are analyzed, we will use these results to determine the relationship between permeability and the orientations and relative magnitudes of the in-situ stresses. In addition, our hydraulic fracturing tests were conducted while borehole seismometer and tiltmeter arrays were deployed in shallow boreholes at this site by scientists from the Los Alamos National Lab, the USGS and InfraSeismic Systems, Inc. The microseismic event locations and shallow tilts determined from these arrays will be used to delineate the geometry of some of our hydraulic fractures as they propagated away from the borehole, providing valuable constraints on the mechanics of hydraulic fracture propagation and an independent check on our determinations of stress orientations and relative magnitudes.

4. In FY 1992 we finished assembling and testing the pressure vessel, furnace and optical equipment to be used in the single-crystal pressure solution and crack-healing experiments. We are now adjusting the three-zone furnace while conducting temperature profiles of the pressure vessel at experimental conditions. Once this procedure is completed and the temperature gradients within the pressure vessel are minimized, we will begin conducting asperity adhesion and crack healing experiments in quartz.

References Cited

Minster, J. B., and T. H. Jordan, Present-day plate motions, *J. Geophys. Res., 83*, 5331-5354, 1978.

Moos, D., and M. Zoback, Utilization of observations of well bore failure to constrain the orientation and magnitude of crustal stresses: Application to continental, Deep Sea Drilling Project, and Ocean Drilling Program boreholes, *J. Geophys. Res., 95*, 9305-9325, 1990.

Oral, B. M., Reilinger, R. E., and Toksoz, M. N., Preliminary estimates of 1988 and 1990 GPS measurements in western Turkey and their tectonic implications, The Crustal Dynamics Project, Special Publications, AGU Monograph, 1992 (submitted).

Rojstaczer, S., and Wolf, S., Permeability changes associated with large earthquakes: An example from Loma Prieta, California, *Geology, 20*, 211-214, 1992.

Abstracts and Papers Published in FY 1992

Evans, B., and Hickman, S., Some experimental results on the effect of solution transfer processes on crack healing, cementation, and diagenesis, in *Proceedings 29th International Geol. Congress*, Kyoto, Japan, p. 456, 1992.

Hickman, S., and B. Evans, Growth of grain contacts in halite by solution transfer: Implications for diagenesis, lithification, and strength recovery, in *Fault Mechanics and Transport Properties of Rocks,* B. Evans and T.-F. Wong (eds.), Academic Press, pp. 253-280, 1991.

Hickman, S., D. Moos, C. Barton, and B. Khakaev, In-situ stress and borehole breakouts in the Tyrnauz Well, Caucasus Mountains, USSR, *EOS, American Geophysical Union Transactions*, *72*, p. 511, 1991.

Hickman, S., D. Moos, C. Barton, G. Katz, G. Budkov, and E. Kim, 1992, Borehole breakouts and in-situ stress in the Tyrnauz well, Caucasus Mountains, Russia, *Proceedings Sixth International Symposium on Observation of the Continental Crust Through Drilling, BRGM, Paris,* p. 135, 1992.

Morrow, C., Hickman, S., Lockner, D., and Khakaev, B., Permeability of granodiorite cores from the Kola Superdeep Well, USSR, *EOS, American Geophysical Union Transactions*, *72*, p. 475, 1991.

Morrow, C., Hickman, S., Lockner, D., and Khakhaev, B., Permeability of core samples from the Kola well, Russia, *Proceedings Sixth International Symposium on Observation of the Continental Crust Through Drilling,* BRGM, Paris, p. 189, 1992.

Zoback, M. D., and Hickman, S. H., Scientific rationale for drilling into the San Andreas fault zone, in *Proceedings 29th International Geol. Congress*, Kyoto, Japan, p. 31, 1992.

LATE QUATERNARY MOVEMENT ALONG THE HAT CREEK FAULT, NORTHEASTERN CALIFORNIA

9980-70338

Marie D. Jackson
Branch of Igneous and Geothermal Processes
U. S. Geological Survey
2255 North Gemini Drive
Flagstaff, Arizona, 86001
(602) 556-7186

Investigations

The Hat Creek fault, located about 30 km north of Lassen Peak, is composed of prominent NNW-trending escarpments that offset Quaternary and Pliocene volcanic rocks by more than 300 m. This fault, and the nearby McArthur, Pittville, and Mayfield faults (Wills, 1991) form an active system of normal faults, down-dropped to the west, that is the westernmost, and perhaps youngest, expression of Basin and Range normal faulting in northeastern California (Fig. 1). The Hat Creek escarpments, or rims, which are modified by erosion to a repose angle of about 35°, form the eastern side of an asymetric graben, along which the Hat Creek Basalt flowed during the Late Pleistocene or Early Holocene (Fig. 1) (Muffler *et al.*, submitted). The most recent slip along the fault forms a 20-km-long, left-stepping scarp as much as 30 m high cutting the Hat Creek Basalt (Fig. 2). Stream gravels, estimated to be no more than 15,000 years old (Muffler *et al.*, submitted), overlie the Hat Creek Basalt and were offset as much as 20 m by this youngest faulting. Monoclinal flexures with S-shaped axial planes link some of the left-stepping fault segments. The average Holocene vertical displacement along the fault has been about 2 mm per year, and the existence of this prominent young scarp in an area of low modern seismicity suggests that movement has been episodic with a periodicity of hundreds, or perhaps thousands of years (Muffler *et al.*, 1989).

This study uses field data and mechanical analysis to examine the structure of the Hat Creek fault and to evaluate its earthquake potential. In particular, this study investigates how a normal fault propagates and develops a surface rupture, and how its en echelon segments link to transfer predominantly dip-slip displacements. Field work undertaken includes 1:5000 mapping of the entire young Hat Creek scarp, detailed 1:1000 scale mapping of S-shaped monoclines at three large left-steps, and systematic measurement of structures resulting from fault-related flexure and fracture of the host basalt. Analytical work undertaken includes 1) mechanical analysis of the surface deformation over a growing normal fault and 2) analysis of interactions at left-steps using methods of fracture mechanics and plate bending theory.

Results

Geologic maps are the principal means of describing the structure of the young Hat Creek fault, and much progress has been made towards completion of these maps during the past year. Geologic field work is progressing well, following a productive three weeks of field work in May, 1992.

A preliminary map of the 20-km-long fault, compiled at 1:15,000 scale in winter and spring of FY'92 using a PG-2 stereoplotter, shows the overall structure of the young scarp. The young fault is composed of six left-

stepping segments (Fig. 2), 1.5- to 6.5-km-long, which offset the Hat Creek basalt. Some of these follow the older rim, and others extend past the older escarpments into the valley floor. Each of the long segments is composed of two or more 0.5- to 1-km-long, left-stepping segments which are, in turn, are made up of shorter, left-stepping segments, usually less than 100m in length. In this respect, the young scarp shows great similiarity to the recent Kaoiki earthquake ground ruptures on Mauna Loa Volcano in Hawaii (Jackson *et al.*, 1992).

S-shaped monoclines of warped and broken Hat Creek Basalt link all scales of the left-stepping segments. This year, the Flagstaff Photogrammetry group prepared detailed 1:1000 scale topographic maps of the three most prominent of these monoclines using an innovative method that does not require the use of surveyed control points. Geologic mapping of these monoclines in May 1992 shows that they are complex structures of flexed and faulted Hat Creek Basalt that have transferred both dip-slip and right-lateral displacements between adjacent left-stepping fault segments. The Photogrammetry Group has nearly completed a perspective digital image of one of the large monoclines, using digitized data from the topographic map and aerial photographs to show the three-dimensional structure of this area.

Along the fault segments, various left-stepping structures correlate with increased displacement. These include: 1) short, *en echelon* cracks that have small horizontal displacements, up to 0.5m, with components of both opening and right-lateral shear; 2) wider, longer, rubble-filled crack arrays with horizontal displacements of 0.5m to 2m; 3) low, 2- to 4-m-high scarps that are often expressed as gently faulted monoclines; 4) taller, scarp-parallel monoclines with steep limbs and larger wavelengths; and 5) high, long, near-vertical rubble-covered scarps.

Systematic measurements of the amplitude, wavelength and overall shape of the scarp-parallel monoclines, and detailed cross-sections across five of these, give important information about how these flexures developed and accomodated subsequent episodes of rupture. Large wavelength (>30m), high-amplitude (>10m) scarp-parallel monoclines may have formed during single large-magnitude seismic events. Subsequent faulting increased the vertical uplift of many monoclines. With continued seismic activity, however, some of the monoclines were strongly disrupted and collapsed into tall scarps covered with a rubble formed of broken columnar blocks of the host basalt.

To document the role of cracking and right-lateral shear in the propagation and transfer of slip along the ruptures, systematic field measurements of crack orientations, lengths and displacements were made in a manner similiar to that developed for the Kaoiki study (Jackson *et al.*, 1992). A 1:1000-scale map of a fascinating kilometer-long stretch of the Hat Creek fault gives a detailed picture of how the crack arrays coalesce to form short, left-stepping scarps and monoclines that are themselves linked by small S-shaped structures. These data form the basis of an interpretative map giving the lengths, vertical displacements and cross-cutting relationships of ruptures forming the young fault, and showing how motions along the scarp are related in time.

References cited

Jackson, M. D., E. T. Endo, P. T. Delaney, T. Arnadottir, and A. M. Rubin, 1992, Ground ruptures of the 1974 and 1983 Kaoiki earthquakes, Mauna Loa Volcano, Hawaii: Journal of Geophysical Research, v. 97, n. B6, p. 8775-8796.

Muffler, L. J. P., M. A. Clynne, and Holcomb, R. T., 1989, Late Quaternary faulting of the Hat Creek Basalt (Abs.): EOS (Transactions of the American Geophysical Union), v. 70, p. 1310.

Muffler, L. J. P., M. A. Clynne, and D. E. Champion, submitted, Late Quaternary faulting of the Hat Creek Basalt: Geol. Soc. Am. Bull..

Wills, C. J., 1991, Active faults north of Lassen Volcanic National Park, northern California: California Geology, p. 51-58.

Reports

Jackson, M. D., E. T. Endo, P. T. Delaney, T. Arnadottir, and A. M. Rubin, 1992, Ground ruptures of the 1974 and 1983 Kaoiki earthquakes, Mauna Loa Volcano, Hawaii: Journal of Geophysical Research, v. 97, n. B6, p. 8775-8796.

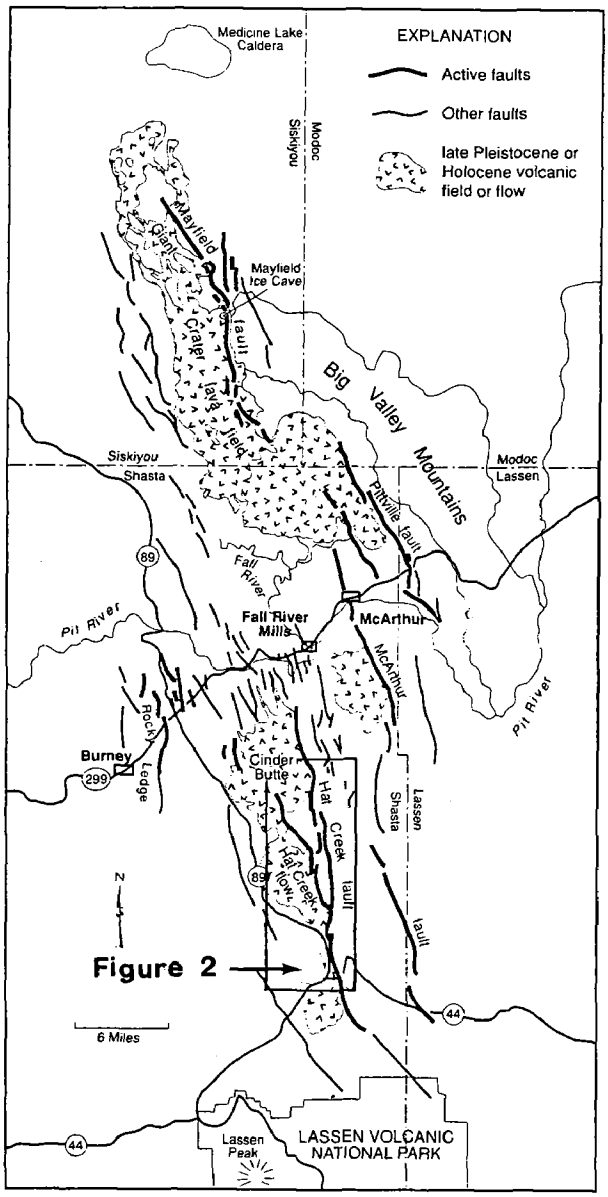

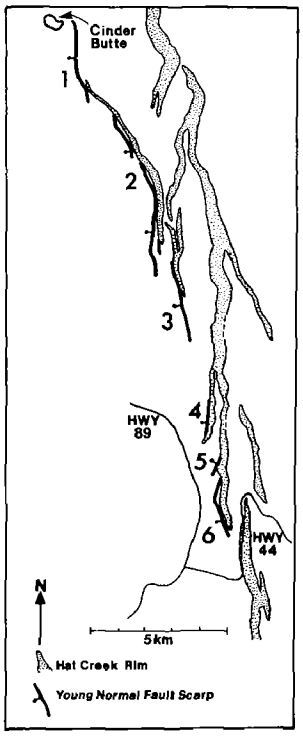

Figure 2. Sketch map of the Hat Creek Fault, showing the older escarpments and Late Quaternary ground rupture.

Figure 1. Simplified geologic map showing faults and young volcanic fields and flows between Lassen Peak and Medicine Lake volcano (after Wills, 1991).

State of Stress in the Rupture Zone of Large Earthquakes

Agreement No. 14-08-0001-G1773

Hiroo Kanamori
Seismological Laboratory
California Institute of Technology
Pasadena, California 91125

(818) 356-6914

Investigation

Investigation of the 1992 Landers, California, earthquake.

The 1992 Landers earthquake (M_S=7.5, M_W=7.3) was recorded at six TERRAscope stations in southern California. Peak accelerations ranged from 0.16 g at SVD (Δ=63 km) to 0.0092 g at ISA (245 km), decreasing with distance away from the fault zone. The peak velocity showed a different pattern reflecting the rupture directivity from south to north. The largest peak velocity, 19 cm/sec, was observed at GSC (Δ=125 km). Moment tensor inversion of long-period surface waves yielded a mechanism with M_0=1.1x10^{27} dyne-cm (M_W=7.3), dip=74°, rake=-176°, and strike=340°. Inversion of teleseismic *P* and *S* waves revealed two distinct sub-events of 6 and 8 sec duration and about 10 sec apart. The source parameters for the first and second events are: M_0=1.9x10^{26} dyne-cm, dip=83°, rake=179°, strike=359°; and M_0=6.1x10^{26} dyne-cm, dip=87°, rake=178°, strike=333°, respectively. The radiated wave energy, E_S, was estimated as 4.3x10^{23} ergs. The ratio E_S/M_0=3.9x10^{-4} corresponds to a stress drop of 280 bars, and suggests that the Landers earthquake belongs to the group of high stress drop earthquakes, and occurred on a fault with a long recurrence time. The rupture directivity can be seen clearly in the records from PFO (Δ=68 km) located to the south and GSC located to the north of the epicenter. The maximum displacement at PFO is only 13% of that at GSC despite the shorter epicentral distance to PFO than to GSC. The slip distribution determined with the empirical Green's function method indicates that the Landers earthquake consists of two distinct sub-events about 30 km apart, with the second sub-event to the north being about twice as large as the first one. This slip distribution is consistent with the teleseismic data and the surface offsets mapped in the field.

Publications

Hwang, L. J. and H. Kanamori, 1991, Rupture Processes of the 1987-88 Gulf of Alsaka Earthquake Sequence, J.G.R., in press.

Kanamori, H. and M. Kikuchi, The 1992 Nicaragua Earthquake -- Tsunami Earthquake?, Nature, submitted 1992.

Kanamori, H., Thio, H.-K., Dreger, D., Hauksson, E., Heaton, T., 1992, Initial Investigation of the Landers, California, Earthquake of 28 June 1992 Using TERRAscope, Geophys. Res. Lett., in press.

Kikuchi, M., H. Kanamori and K. Satake, Source complexity of the 1988 Armenian earthquake -- Evidence for a Slow After-Slip Event, Jour. Geophys. Res., submitted 1992.

Seismicity Patterns and the Stress State in Subduction-Type Seismogenic Zones

Grant Number 14-08-0001-G1810

Carl Kisslinger and Susanna Gross
Cooperative Institute for Research in Environmental Sciences
Campus Box 216, University of Colorado
Boulder, Colorado 80309-0216
(303) 492-6089

Research during the current grant year was directed to the following problems: (1) comparison of the seismicity rates and spatial patterns in the region monitored by the Central Aleutians Seismic Network (CASN) during 1988-1990 with those preceding the quiescence used a basis for the prediction of the May 7, 1986 great earthquake; (2) modeling the temporal behavior of aftershock sequences; (3) the effects of stress redistribution by moderate earthquakes on the spatial distribution of surrounding seismicity.

Comparison of Seismicity Rates in the Adak Region during 1988-1990 with those before and during the 1982-1986 Quiescence

A prediction of a major earthquake to occur near Adak Island, Alaska within six months of the end of October, 1985 was formulated and announced in 1985 (Kisslinger, et al. 1985, Kisslinger, 1986). The prediction was based on the observation, first noted in September, 1982, of strong and persistent quiescence in part of the seismic zone monitored by the CASN. On May 7, 1986, at the end of the time window specified in the prediction, a magnitude $M_S = 7.7, M_W = 8.0$ event did occur. Although the event that occurred differed in the details from the predicted parameters (magnitude was about 0.5 higher, rupture was in a section of the main thrust zone adjacent to that predicted), the preceding seismic quiescence observed with the local network was arguably related to this earthquake.

Questions have been raised about the validity of the prediction experiment, in particular whether the observed change in seismicity rate in parts of the seismic zone was natural or artificial. The principal concern has been that changes in instrumentation in mid-1982, designed to improve the detection capability of the network, may have inadvertently degraded the detection

threshold or introduced a shift in the magnitudes of events as determined in routine processing. The fact that the quiescence existed in all magnitude bands, the non-uniform distribution of the quiescence across the zone and the differences in the times of onset in different parts of the zone had been taken as evidence that the changes in rate were real. In an independent s-tudy, Wyss analyzed the reporting history of the CASN and concluded that the reported quiescence was most likely a natural phenomenon, but that this can not be proven beyond doubt.

It is impossible in principle to determine beyond doubt whether simultaneous changes occurred in both the real seismicity rate and in detection capability or analysis procedures, to produce an observed change in seismicity rate. However, under the hypothesis that a precursory quiescence ends with the occurrence of the strong earthquake. one test is a comparison of the seismicity rate several years after the mainshock with that prior to and during the interval of quiescence, with no changes in the instrumentation or data-processing procedures. The hypothesis is that a characteristic of the seismogenic cycle is that the seismicity rate should return to the pre-quiescence level after the aftershocks have ceased. It would be best to perform this test many years later, when there is confidence that the aftershocks have decayed to negligible numbers. However, the CASN has been terminated for financial reasons and the local data are available only through June, 1990. We, therefore, have compared the most recent documented seismicity with that prior to mid-1982, when the quiescence began, as well as during the interval of quiescence.

The data used cover the intervals 1977 through 1985 and September, 1988 through May, 1990. The year 1982 was eliminated because the strong quiescence began during that year at at time that is not easily fixed. The data were spatially grouped by the same geographic subregions used in the original analysis, Figure 1, and smoothed by counting events by quarters, from which mean monthly activity rates were calculated. Most of the work was done with a minimum duration magnitude of 2.3, the level determined earlier for catalog completeness. Tests were made in a number of magnitude bands, from 1.6 and above (known to yield an incomplete catalog) to 3.0 and above (complete catalog, but too few events for robust statistical confidence.)

The data since May 7, 1986 have been modeled to estimate the rate of aftershocks to be expected during the 1988-1990 interval. A newly developed program, in which the modified Omori relation is supplemented by adding

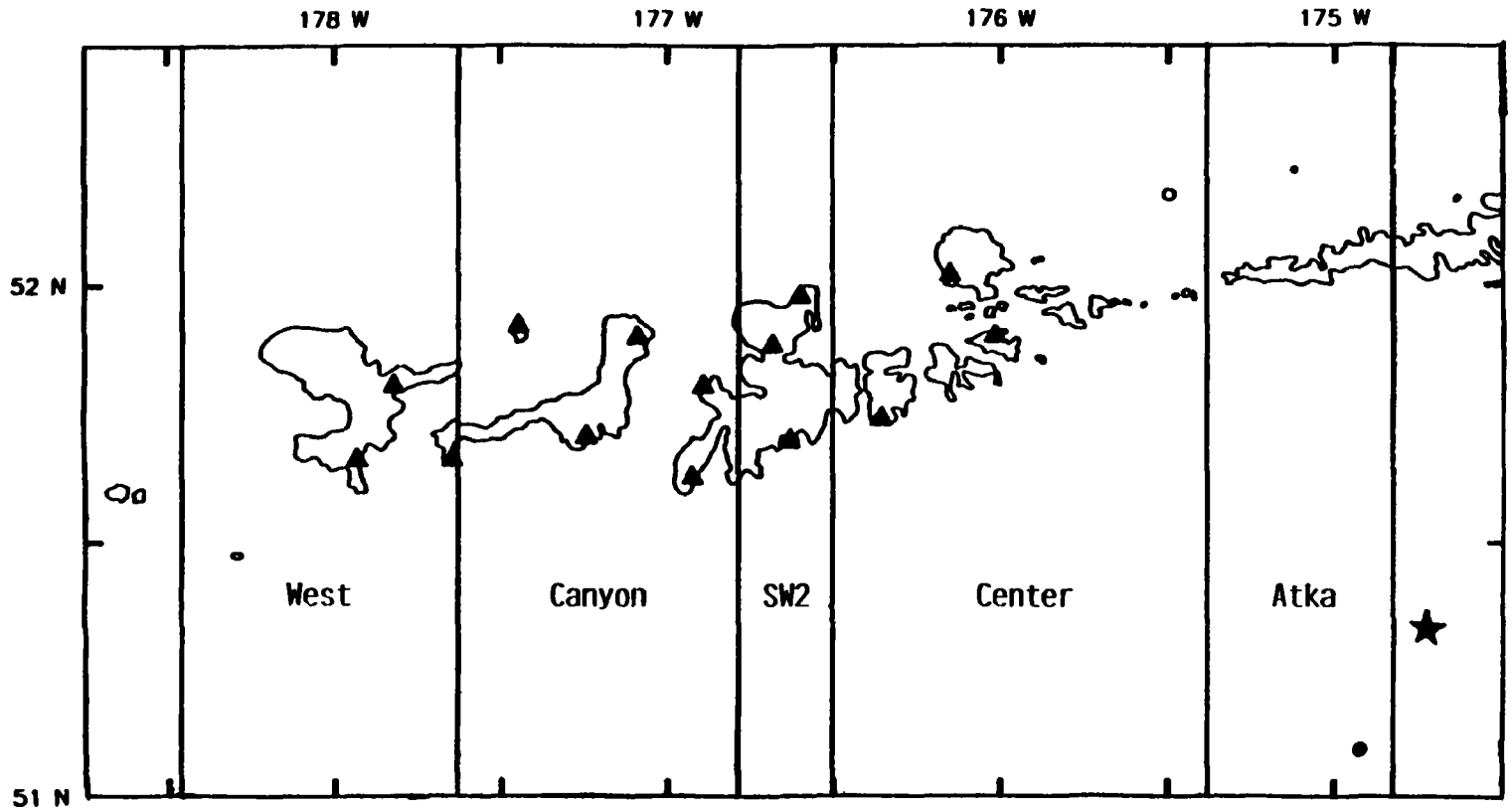

Figure 1. Map of the region monitored by the CASN. The network stations are marked by triangles. The star marks the epicenter of the May 7, 1986 $M_W = 8$ mainshock; the circle the epicenter of the March 12, 1990 $M_S = 6.2$ earthquake. The five subregions defined for the seismicity analysis are shown. The 1986 rupture terminated in SW2.

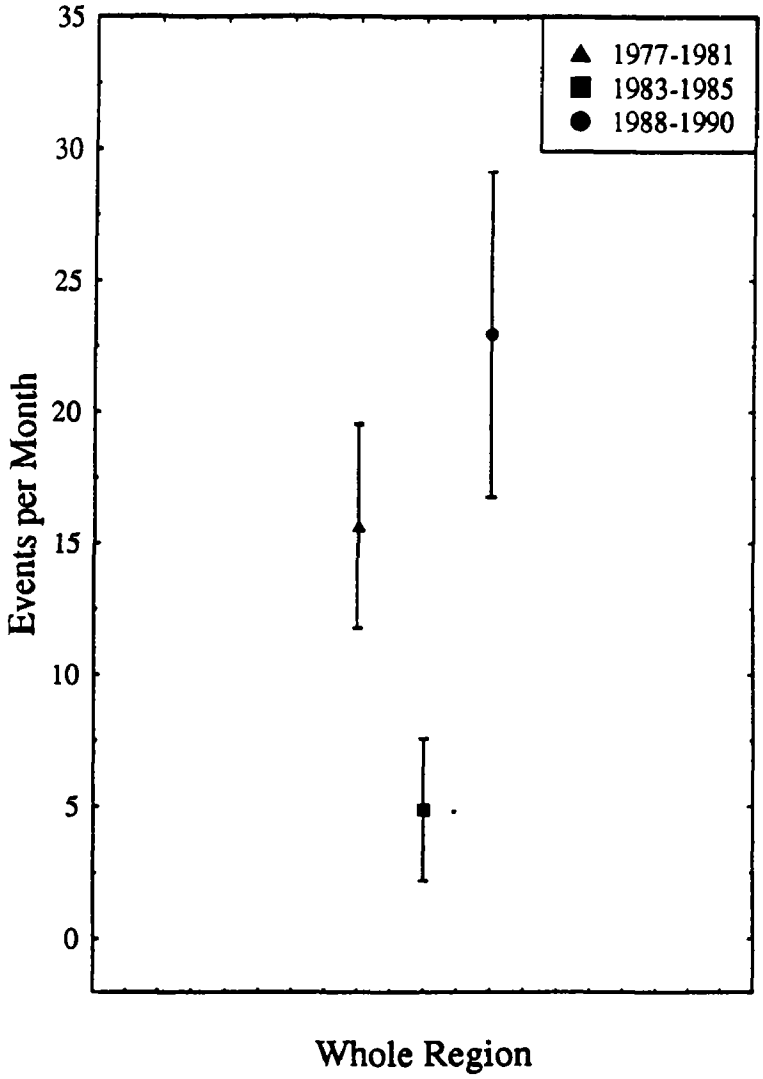

Figure 2: The mean monthly rates of activity for the entire region during the pre-quiescent interval, during the quiescence, and in the most recent interval for which CASN data are complete. The increased activity during 1988-90 (21 months) over 1977-81 agrees approximately with the rate of aftershocks of the May 7, 1986 event expected from a fit to the modified Omori relation.

a steady background rate of activity, was applied. We estimate that during the recent interval approximately 45aftershocks of 1986, superimposed on a steady rate close to that observed prior to 1982.

The principal result of this study is shown in Figure 2. Mean monthly rates for 1977-1981, 1983-1985, and September, 1988-May, 1990 for the whole Adak region are shown, with the standard deviation of the data. A more detailed breakdown will be given in the paper on this study now completed and to be submitted for publication. The pronounced quiescence on which the prediction was based is seen in the drop of mean rate from 15.65 per month to 4.89 per month. The recovery from the quiescence is shown by the recent rate of 22.24 events per month. The excess over the pre-quiescence interval, which is significant at the 98confidence level, is very close to the estimated fraction of aftershocks that were still in progress. The analysis also shows that the late aftershocks tend to be concentrated near the 1986 mainshock epicenter and near the western edge of the 1986 rupture zone.

The conclusion from this work is, if quiescence disappears after the mainshock and the previous rate is restored, the decrease in activity seen in 1982-1985 was a true quiescence and a precursor to the 1986 earthquake.

In an auxiliary study, two episodes of concentrated activity during 1989 and 1990 were examined. These occurred in the Atka subregion (Figure 1) and are interesting because the events filled a hole in the aftershocks of the 1986 earthquake, very near its hypocenter. The conclusion suggested by this observation is that the gap in aftershocks existed because the local strength was higher than the surrounding parts of the fault zone, so rupture was delayed.

Modeling Aftershock Sequences

The research on models of aftershock rate decay is completed. The work consisted of two parts: the investigation of the stretched exponential function as an alternative to the modified Omori relation, and the extension of both models to include a steady background rate of seismicity as an additional parameter in fitting the data. A paper on the first task is in press and scheduled for publication in the *Journal of Geophysical Research* in late 1992. A paper on the second task has been submitted to **JGR** and is in the review process. The results show that the widely-used modified Omori relation is a close approximation to the stretched exponential over the range of times usually used in aftershock studies. The stretched exponential is a general

relaxation law that has been found to describe relaxation processes in a variety of physical processes. The introduction of a steady background rate gives the best fit to the aftershock data in only some cases, principally those in regions of normally high seismicity. The techniques developed in this work are being applied to additional aftershock sequences and are applicable to foreshocks.

Influence of Earthquake-produced Stresses on Seismicity Distribution

This research involves models of stresses from a few dozen moderate magnitude (m_b about 4.7) earthquakes in the Central Aleutians and comparisons of the calculated stresses with the spatial distribution of seismicity observed by the Central Aleutians Seismic Network. The project represents both an attempt to find a deterministic element in the occurrence of earthquakes and an attempt to understand more about the physics of the earthquake process by selecting models with predictive power. The similarity between stresses and seismicity has been assessed through a quantitative measure of similarity based on a Student's t statistic.

The stress field has two elements, the background stress, and the stress due to the earthquake. The background stress is assumed to be homogeneous and appropriate for a dipping plate. The parameters defining it are the azimuth, plunge, and magnitude of the greatest principal stress.

$$\sigma_{\text{back}} = \begin{pmatrix} \sigma_1 & 0 & 0 \\ 0 & \frac{\sigma_1}{4} & 0 \\ 0 & 0 & 0 \end{pmatrix}$$

There are no free parameters in the earthquake stress, because the orientation of the double-couple which represents it is taken from the focal mechanism, and the magnitude provides an estimate of the moment.

$$\sigma_{xz} = \frac{\mu M_0}{4\pi\rho r^5}[(\frac{1}{\beta^2} - \frac{1}{\alpha^2})3(x^2 + z^2 - \frac{10x^2z^2}{r^2}) + \frac{1}{\alpha^2}(3y^2 - r^2)]$$

$$\sigma_{yz} = \frac{\mu M_0 3xy}{4\pi\rho r^5}[(\frac{1}{\beta^2} - \frac{1}{\alpha^2})(1 - \frac{10z^2}{r^2}) - \frac{1}{\alpha^2}]$$

$$\sigma_{zz} = \frac{\mu M_0 6xz}{4\pi\rho r^5}[(\frac{1}{\beta^2} - \frac{1}{\alpha^2})(2 - \frac{5z^2}{r^2}) - \frac{2}{\alpha^2}]$$

$$\sigma_{xx} = \frac{\mu M_0 6xz}{4\pi\rho r^5}[(\frac{1}{\beta^2} - \frac{1}{\alpha^2})(2 - \frac{5x^2}{r^2}) - \frac{2}{\alpha^2}]$$

$$\sigma_{xy} = -\frac{\mu M_0 3yz}{4\pi\rho r^5}[(\frac{1}{\beta^2} - \frac{1}{\alpha^2})\frac{10x^2}{r^2} + \frac{1}{\alpha^2}]$$

$$\sigma_{yy} = \frac{\mu M_0 6xz}{4\pi\rho r^5}[(\frac{1}{\beta^2} - \frac{1}{\alpha^2})(1 - \frac{5z^2}{r^2}) - \frac{1}{\alpha^2}]$$

The formula above applies to stresses induced by a double couple in an infinite elastic space. The coordinate system is centered on the double couple. The full model includes effects of the free surface by including an image source above the surface having opposite dip and rake. The model was checked by numerically computing the derivatives and computing the shear stress at the free surface. These two elements are rotated into geographic coordinates and added to give the total stress tensor.

In order to compare the resulting stress field with the seismicity, the tensor must be reduced to a scalar quantity which should influence the rate of occurrence of earthquakes. Physical models of fault geometry and properties provide many alternative approaches to how stresses could trigger earthquakes, and these fault and rupture models are the current focus of research in the project. Models explored so far include

- The magnitude of the greatest shear stress, independent of orientation, $\sigma_1 - \sigma_3$, which is thought to be appropriate for faults equally present in all orientations with substantial overburden pressure. This model has been quite successful.

- The magnitude of the shear stress on a particular weak plane. This model has the disadvantage of requiring two additional parameters to define the orientation of the plane. Its implications have just started to be explored.

- The magnitude of the pressure, or trace of the stress tensor $P = \sigma_{ii}/3$, which could act on faults through increases in the effective stress, $\sigma_{eff} - P$. This would be physically due to the contrast in bulk modulus between the rock and its pore fluids. The models incorporating this approach estimate the pore pressure field as a function of time by numerically convolving the Green's function for the diffusion equation (a gaussian) with the initial pressure field. These models show early

promise in predicting changes in the seismicity distribution. The fluid diffusivity enters as an extra parameter for these models.

- The rate of change of the pore pressure, dP/dt was postulated by Nur and Booker (1972) as a generator for aftershocks. In practical terms, this model is very close to those defined above, involving a different Green's function. The cases examined so far have not shown much resemblance to seismicity, but it merits more work.

It is postulated that the different fault and rupture models may be tested by comparing their ability to match the observed changes in spatial distribution of seismicity.

The actual comparison of stress models and seismicity is made using t-statistics. The quantities compared are changes in the triggering component of the stress evaluated at the hypocenters of surrounding earthquakes. The surrounding earthquakes are expected to occur more often in areas having high values of the triggering quantity and less often in areas with low values. The statistics are designed to compare sets of numbers and determine whether they are drawn from distributions having different means or not. The statistic used in this project does not assume that the standard deviations of the two sets, s_{before} and s_{after} are not equal:

$$t = \frac{\overline{\Delta\sigma_{\text{before}}} - \overline{\Delta\sigma_{\text{after}}}}{\sqrt{s^2_{\text{before}}/N_{\text{before}} + s^2_{\text{after}}/N_{\text{after}}}}$$

in which $\overline{\Delta\sigma}$ represents the average change in triggering component of stress at hypocenters of surrounding earthquakes. The statistics are calibrated by computing them for earthquakes that did not actually occur, so the clustering effects of real seismicity are included. Tests have shown that this approach is necessary, because clustering significantly changes the distribution of t-statistics.

The model also involves a temporal dimension which is just starting to be explored. The sets of surrounding earthquakes had formerly been defined in terms of numbers of events in the whole catalog. Typically the time window used for comparisons was 1000 events long, around 18 months. This definition has the advantage of reducing the effects of data gaps and magnitude shifts on the data, but the disadvantage of being unphysical. The model has been changed to allow temporal definitions of the before and after seismicity

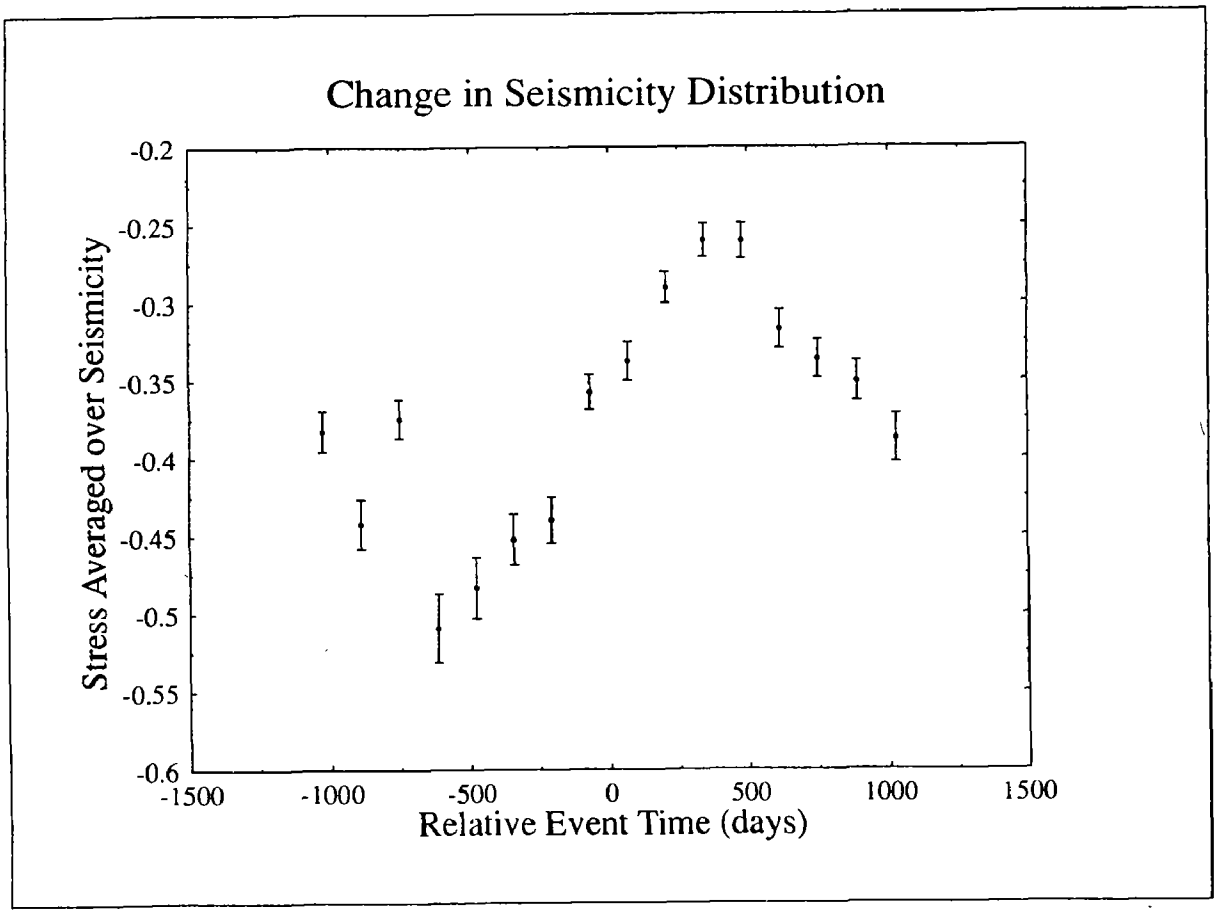

Figure 3: The average modeled change in shear stress at hypocenters of earthquakes surrounding 52 "target" events as a function of time relative to the target earthquake. The error bars apply to the standard deviation of the mean of the stress change, and may be slightly underestimated because the surrounding earthquakes are not independent of one another. The relatively lower values of stress before the earthquake imply that more of the seismicity is occurring in places which will experience larger decreases in maximum shear stress when the "target" earthquake occurs. After the target event, the seismicity moves to locations where the decrease in shear stress was less.

intervals. The most typical interval now used is 2 years. Longer intervals would probably be preferable, but limits in the catalog length would make statistics based on longer intervals harder to calibrate. The temporal signature of changes in the spatial distribution of seismicity which have been observed may be appreciated by examining Figure 3. This figure shows the average change in shear stress found at hypocenters of surrounding earthquakes as a function of time relative to the larger earthquake which caused the shear stress. All the data from the seismicity surrounding a set of 52 larger earthquakes has been combined on one plot. Changes in the average shear stress appear to be quite smooth, and vary most strongly around the time of the mainshock. The decrease in average shear stress before the event means that seismicity has become concentrated in those areas which will experience decreases in shear stress when the mainshock happens. The higher values afterwards mean that the seismicity has moved to occur in areas which have experienced shear stress increases.

Publications and Presentations based on the Research

Gross, S. and D. Schmerge, A Revised Duration Magnitude for the Central Aleutians Seismic Network (abs), *Seism. Res. Lett., 62*: 24, 1991.

Gross, S. J. and C. Kisslinger, A Subduction Stress Model Verified with Seismicity (abs), *Seism. Res. Lett., 63:* 66, 1992.

Gross, S. J., How Dependent are Earthquakes Upon One Another? Presented at the 1992 Seismological Society of America Eastern Section meeting.

Gross, S. J., A Test of the Fluid Diffusion Hypothesis of Aftershock Generation Using Changes in the Spatial Distribution of Seismicity (abs), *EOS, 73:* 389, 1992.

Gross, S. J. and C. Kisslinger, Tests of Models of Aftershock Rate Decay, *J. Geophys. Res.*, submitted, in review, 1993.

Huang, Z.X. and C. Kisslinger, Coda-Q before and after the 1986 Andreanof Islands Earthquake, *PAGEOPH, 138:* 1-16, 1992.

Kisslinger, C., The Stretched Exponential Function as an Alternative Model for Aftershock Decay Rate, *J. Geophys. Res., 97:* in press, 1992.

Kisslinger, C., Seismicity in Subduction Zones from Local and Regional Network Observations, *PAGEOPH,* accepted and in press, 1993.

Refinement of Pattern Recognition Procedures for Intermediate-Term Earthquake Prediction

1434-92-G-2214

L. Knopoff
Institute of Geophysics and Planetary Physics
University of California
Los Angeles, California 90024

(310)825-1885

Twenty-four of all of the 26 strong earthquakes in Southern and Central California and the Cape Mendocino area with magnitudes between 6 and 7.7 have been preceded by a significant increase in the rate of occurrence of intermediate magnitude earthquakes. The increased precursory activity takes place on an intermediate-term time scale that ranges from 2 to 10 years before the subsequent strong earthquake and scaled by the magnitude of the strong earthquake.

We began this study with an analysis of intermediate-magnitude earthquakes that precede strong earthquakes with $M_L \geq 6.4$, in Southern California, from the last half part of 1935 to the present. Seven out of 8 strong earthquakes in the magnitude range from 6.4 to 6.9 were preceded by a significant increase in the number of earthquakes with M_L in the range 4.8 to 6.3 in a window of 2 years duration; the peak persisted until 0 to 1 year before the strong earthquake (Fig. 1). We note particularly that the earthquakes that constitute the precursory spike are widespread over the entire extent of Southern California; in Fig. 2 we show the precursory seismicity of intermediate-magnitude events in the 10-year period before the Kern County earthquake. If the lower threshold for intermediate-sized earthquakes is lowered to 4.6 or raised to 5.0, the pattern persists. If we lower the threshold for definition of intermediate-magnitude earthquakes to 4.4, the correlation begins to vanish, and at a 4.0 threshold it has almost disappeared.

We hypothesize that an area of the seismogenic zone that is much larger than the dimensions of the future strong earthquake, has reached a critical threshold for fracture from 2 to 3 years before a strong earthquake, and hence that the precursory, intermediate-magnitude earthquakes are to be found over a broad region of elevated stress. We further hypothesize that the strong earthquake switches off the critical state over the larger region.

The correlation above failed to appear before the Landers earthquake at the threshold we had set for strong earthquakes in the M_L=6.3 to 6.9 range. We then made a hypothesis of self-similarity: the larger the future great earthquake, the larger all three parameters of the system would have to be, namely the size of the region in which precursory intermediate-sized shocks will occur, the time-window of anticipation, and the lower threshold for the definition of intermediate magnitude. With this redefinition, the Landers earthquake was also shown to be preceded by a spike in intermediate level seismicity.

However, the Landers earthquake was the only event of its size other than the Kern County earthquake (which was successfully fit by the original model), and to tailor a revision of the model to one event seemed unjustifiable. We therefore made the conjecture that the same change of scale in reverse, i.e., a reduced time window, a reduced area of interaction and a reduced magnitude

threshold for intermediate-magnitude events, would be appropriate for anticipation of strong earthquakes in the magnitude 6 to 6.3 range. In this application we were completely successful, except for one event with M_L=6.0 in 1940, that occurred within a few months of an earlier, stronger M_L=6.7 earthquake; in this case, the failure to fit the pattern was due to a feature of our model that resets the count of intermediate shocks to zero after a strong earthquake.

The model was then applied to earthquakes in the NEIS catalog (1965-1992) in Central California and the Pacific off Cape Mendocino, without change of parameters. NEIS magnitudes m_b were assigned equivalent M_L through a conversion derived from a comparison of (m_b, M_L) values for Southern California earthquakes. The Southern California pattern occurred in all cases in the other two regions without change of parameters; we summarize these results in Table 1. In the Table, we list the number of events in each region, followed by the number of times the anticipatory pattern described failed to appear.

Table 1

	Southern California	Central California	Mendocino
6.0 - 6.3	6/1*	2/0	1/0
6.4 - 6.9	8/1	1/0	3/0
7.0 - 7.3	0	1/0	2/0
7.4 - 8.0	2/0	0	0

* Failure to fit one event that was preceded by an earlier event within 7 months.

We comment on the case of the Loma Prieta earthquake. In this case there was sufficient precursory seismicity within 10 years and within 100 km of the epicenter of the strong shock that we would not have had to enlarge the space window as indicated; we could have continued to use the original Southern California space window without the modification to accommodate larger events.

The model has the following details: We remove aftershocks from the time series by the Gardner-Knopoff formula. (We have analyzed the complete catalogs, that is without removing aftershocks, and find that the model provides a fit that is almost as good as in the case in which aftershocks are removed.) For strong earthquakes in a range with M_o defined by its lower extreme (in Table 1 we have used M_o = 6.0, 6.4, 7.0, 7.4), we count the number of shocks in the relevant geographical area, with magnitudes between $(M_o - \mu, M_o - 0.1)$ in a τ year window sliding by 2 month increments. We construct a histogram of these values. We find that a spike threshold persists to less than 1 year before the strong event. A spike is considered to be a precursor if the count has a value greater than or equal to the nearest integer in the 10th to 25th percentile intervals of the histogram.

Details of the windows are given in Table 2. M_o is the lower cutoff magnitude for each strong magnitude band. The intermediate-magnitude earthquakes are defined in the interval from their lower bound listed in the second column to 0.1 magnitude units below M_o; the lower bounds for intermediate magnitudes can take on the broad range of values listed in column 2; our best fit is given in parentheses; μ is about 1.8. The widths of the sliding window are given in the third column. The range of distances in the fourth column is well-defined as the diameter of a circle in

the case of M_o=6.0; in the other cases, it is defined by the area covered by the catalog used. The number of strong shocks in each magnitude range in all three regions is given in the last column.

Table 2

M	$m \geq$	$\tau, years$	D,km	$Number$
6.0 - 6.3	4 - 4.4 (4.0)	2 - 5	200-300	9
6.4 - 6.9	4.6 - 5.0 (4.8)	2 - 5	500-600	12
7.0 - 7.3	5.0 - 5.4 (5.2)	5 -10	500-600+	3
7.4 - 8.0	5.4 - 5.8 (5.6)	5 -10	600-800	2

To summarize: The retrospective application of this model fit the occurrence of precursory seismicity before 14 out of 16 strong shocks (M=6.0) in Southern California between 1935-1992, and before all 10 such strong shocks in the Coast Range and Cape Mendocino areas between 1965-1992. The Landers, Loma Prieta and Kern County earthquakes are all successfully fit by the model. Of particular importance is our observation that the area of intensified activity in intermediate-magnitude events is much larger than the source dimensions of a subsequent strong earthquake and does not necessarily span it; this region is almost always distributed broadly in two-dimensions. If increased activity in the magnitude range (M_o - μ, M_o - 0.1) is spread out over even larger distances than D(M), it may be that the approach of an earthquake in a higher magnitude range is indicated.

The model is not a particularly strong prediction algorithm; the ratio of "alarm" times to total time is about 1:3 for earthquakes with magnitudes between 6.4 and 6.9. Measured in terms of the number of adjustable parameters, there are 5 degrees of freedom in this model; since this model is used to fit to 26 events, it is clear that we need additional data in the form of tests on additional seismically active regions of the world (in progress) or in the form of the future occurrence of clustering of seismic events in California, which is inevitable.

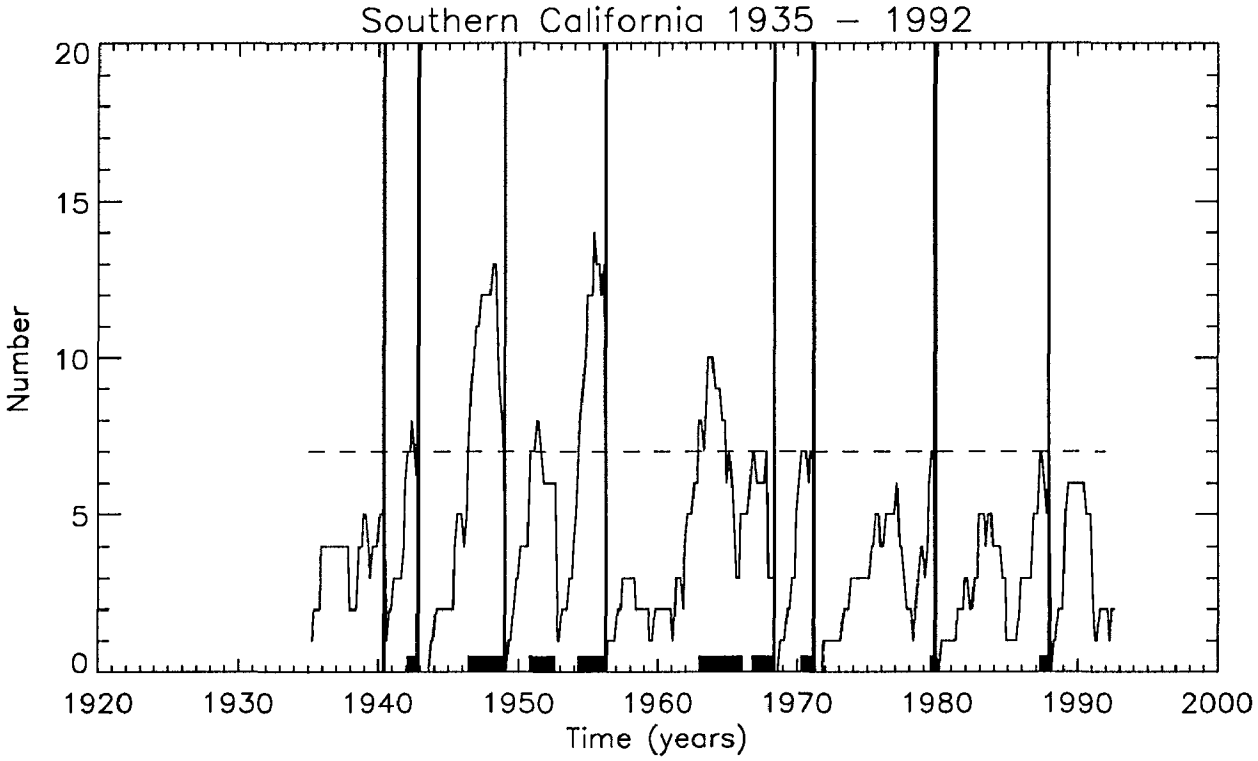

Number of intermediate magnitude events with $6.3 \geq M_L \geq 4.8$ in a 2 year sliding window. Dashed line is threshold. Vertical lines are times of strong earthquakes with $6.4 \leq M_L \leq 6.9$.

Fig.1

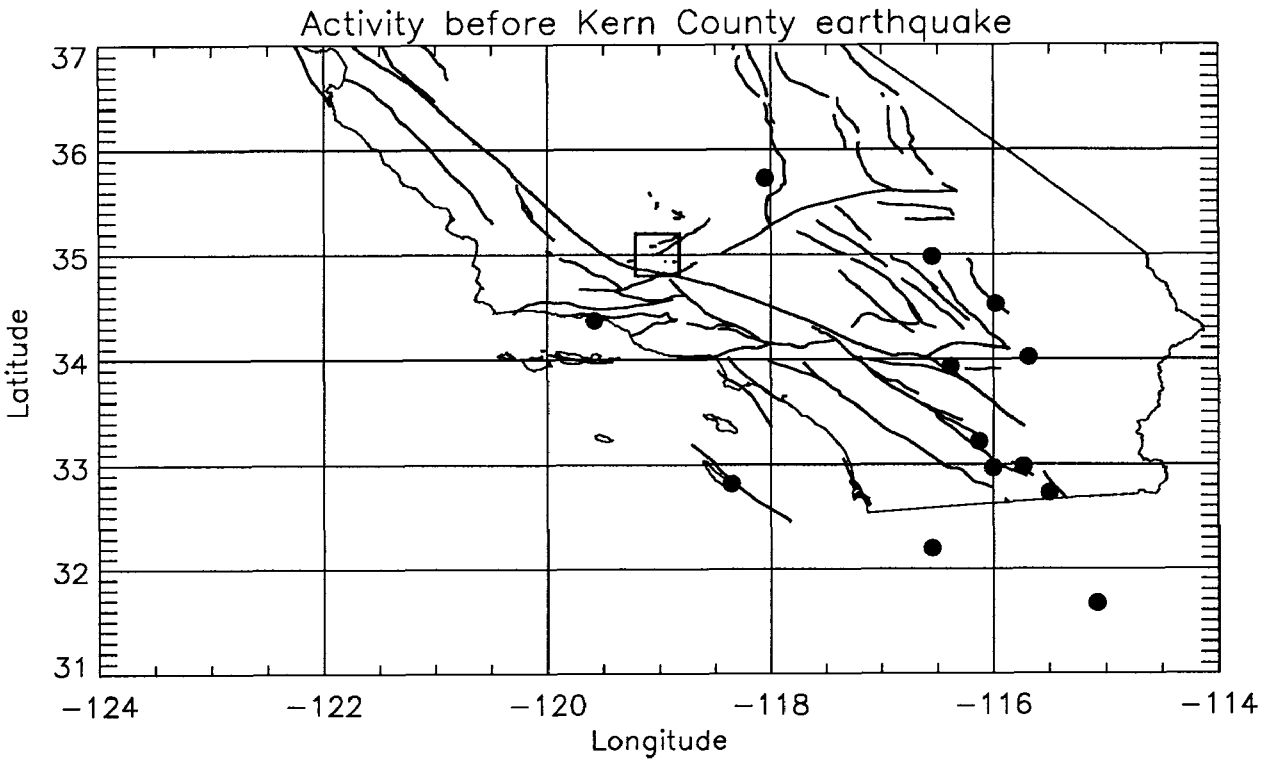

□ – Kern County earthquake (M =7.7);
• – intermediate magnitude events with magnitude M≧5.6 for ten years preceding August 21, 1952.

Fig.2

Stress and Anisotropy in Southern Hawaii

Contract No. 1434-92-G-2163

Clifford G. Munson and Clifford H. Thurber
Department of Geology and Geophysics
University of Wisconsin-Madison
Madison, WI 53706

608-262-6027

Investigations

From July to December 1990 four portable seismic arrays of 5-to-8 three-component PASSCAL instruments spaced approximately 1 to 2 km apart were deployed on the southeast flank of Mauna Loa (Figure 1). Seismic stations in the Bird Park array were located adjacent to the Mauna Loa Strip Road and Highway 11. The Ainapo seismic array was centered in the Keakapulu Flat area of the Kapapala Forest Reserve. The Waihaka and Punaluu Gulch arrays were located southeast of the Kau Forest Reserve in the Hilea region. Hundreds of microearthquakes were digitally recorded (100 sps and 60 s record) using 1 and 2 Hz seismometers. Two previous shear-wave anisotropy studies in southern Hawaii were done by Savage et al. [1989] (on Kilauea's south flank) and Booth et al. [1992] (in the Kaoiki area).

The Kaoiki seismic zone, situated between the volcanoes Kilauea and Mauna Loa, (Figure 1) has been subjected to frequent moderate to large earthquakes throughout this century. Crustal earthquakes in the Kaoiki seismic zone are a combination of shallow (< 9 km) strike-slip and deeper (9 to 12 km) low-angle seaward thrust events [Endo, 1985]. The neighboring Hilea seismic zone, to the southwest of Kaoiki along Mauna Loa's "exposed" southeast flank (Figure 1), is somewhat less active, but is thought to have been the locus of the great 1868 earthquake [Wood, 1914; Wyss, 1988]. The earthquakes in Hilea generally occur in the southern and eastern portion of the area between the southwest rift zones of Mauna Loa and Kilauea and are dip-slip events [Endo, 1985; Liang and Wyss, 1991]. The abundant seismicity indicates that significant levels of stress must be prevalent throughout the southeast flank of Mauna Loa.

Event locations provided by the Hawaiian Volcano Observatory (HVO) seismic network of the U.S. Geological Survey have allowed us to limit our analysis to arrivals from events within a 40° shear wave window (Figure 1). For obvious HVO network event mislocations, S - P times from our PASSCAL array data were used to relocate event hypocenters. The events analyzed ranged in depth from 1 to 14 km.

To estimate the shear wave polarization, we use a quantitative method based on a 3x3 particle motion covariance matrix decomposition [Jurkevics, 1988]. The polarization type and orientation of the particle motion is determined by computing a covariance matrix for the three components of motion in a selected time window. The orientation of the horizontal particle motion corresponds to the direction of the eigenvector for the largest eigenvalue of the covariance matrix projected onto the horizontal plane. Split shear wave arrivals are identified by their (1) rectilinear particle motion, (2) orthogonally polarized pulses, and (3) similar waveforms. Rectilinearity is measured by

$$1 - \frac{\lambda_2 + \lambda_3}{2\lambda_1}$$

where λ_1, λ_2, and λ_3 are the maximum, intermediate, and minimum eigenvalues [Jurkevics, 1988]. To estimate the time delay between the split shear wave arrivals (S_1 and S_2) we use the maximum value of the cross-correlation function derived from the two horizontal traces after rotation to the horizontal component of the S_1 polarization direction.

Results

Of the 381 arrivals that were examined, 311 had measurable leading shear wave polarization alignments and 106 showed clear evidence of shear wave splitting (i.e., a clear second shear wave arrival). Figure 2 shows the leading shear wave polarizations for each station among the four arrays. The measured S_1 polarizations for both of the arrays in the Kaoiki seismic zone show a high degree of alignment at each station as well as within the respective arrays (Bird Park N68°E ± 22° and Ainapo N99°E ± 11°). The measured S_1 polarizations for the Waihaka Gulch array are less aligned (N98°E ± 46°) both for the array as a whole and for individual stations. The number of observations at the Punaluu Gulch array is limited (24 arrivals), however the measured polarizations are strongly aligned (N172°E ± 20°). Table 1 shows the measured delay times for the four arrays. The delays vary from 100 msec to 270 ms, with a mean value of 187 ± 45 ms.

Focal mechanism studies in the Kaoiki and Hilea seismic zones [Wyss et al., 1992; Liang and Wyss, 1991] in addition to field measurement made in the vicinity of the 1974 and 1983 Kaoiki earthquakes [Jackson et al., 1992] lead us to conclude that the consistent leading shear wave polarizations for stations within the Bird Park, Ainapo, and Punaluu Gulch arrays are due to the presence of stress-aligned cracks. Wyss et. al [1992] determined the stress tensor orientation based on the inversion of 238 first motion fault plane solutions of earthquakes located in the 10-km radius Kaoiki crustal volume. The orientation of maximum principal stress, σ_1, for the southeast subarea of the Wyss et. al [1992] Kaoiki area is N83°E ± 7° and is near horizontal. This result agrees well with the leading shear wave polarizations for the Ainapo array (N99°E ± 11°) which was located in this subarea. Booth et al. [1992] also report a leading shear wave polarization of ENE-WSW for the three-component HVO station AIN which is near the Ainapo array. Field measurements of ground ruptures from the 1974 and 1983 Kaoiki earthquakes show that the mean strike of individual cracks is N91°E and N95°E respectively [Jackson et. al, 1992]. A focal mechanism study for the Bird Park array shows the orientation of σ_1 to be NE-SW and subhorizontal (P. Okubo, personal communication). The predominant S_1 polarization for events recorded by the Bird Park array is also NE-SW (N68°E ± 22°). Delaney et al. [1990] show that a reference baseline with a NW-SE orientation crossing the structural boundary between Mauna Loa and Kilauea (the Kaoiki fault zone) has been extending at a rate of 4.6 ± 0.5 cm per year since 1984, consistent with a NE-SW σ_1 orientation. Fault plane solutions for events near the Waihaka Gulch array (center subregion of Hilea) do not show a clear orientation for the maximum horizontal stress [Liang and Wyss, 1991]. Similarly, no predominant S_1 polarization is seen for events near the Waihaka Gulch array. For the center subregion of Hilea, Liang and Wyss (1991) report a maximum horizontal stress oriented approximately N144°E (with a dip angle of 7°) similar to the S_1 polarization for events near the Punaluu Gulch array (N172°E ± 20°).

For the 106 arrivals that show clear evidence of shear wave splitting, the average time between S_1 and S_2 is 187 ms with a standard deviation of 45 ms. For the 3-component HVO station AIN, Booth et al. [1992] were unable to measure a reliable delay between fast and slow shear wave arrivals due to interference by scattered or converted arrivals, although a few reliable arrivals indicate a time delay of approximately 190 ms. Savage et al. [1989] report delays ranging from 160 to 210 ms for the south flank of Kilauea. Thus our shear wave splitting observations are consistent with those of previous studies in southern Hawaii.

For the average event depth of 8 km, the time separation between split shear waves is 23 ms/km, the velocity anisotropy is about 7.5%, and the crack density is approximately 8% for the 8-km crustal section. However, a comparison of event depth vs. delay time shows that there is no increase in delay time with increasing event depth. This suggests that the observed delay times are caused by near-surface rather than pervasive anisotropy. Since shear wave splitting is observed for earthquakes as shallow as 3 to 4 km this indicates a transverse anisotropic velocity variation of about 14% and $e \approx 16\%$. For comparison, Leary et al. [1990] report a crack density range of 1 to 5% for most geolgical and tectonic regions and an extreme case of $e = 7\%$ for crystalline rock near an active normal fault in California. Thus our results indicate that the upper crust of the southeast flank of Mauna Loa is highly fractured.

TABLE 1. A Summary of Delay Times for the Four ALOHA Arrays

Array	Number	Delay Time (msec)
Bird Park	50	206 ± 37
Ainapo	36	166 ± 36
Waihaka Gulch	13	205 ± 47
Punaluu Gulch	7	123 ± 22

References

Booth, D. C., M. Wyss & D. Gillard, Shear-wave polarization alignments recorded above the Kaoiki fault zone, Hawaii, Geophys. Res Let. 19, 11, 1141-44, 1992.

Delaney, P.T., R. S. Fiske, A. Miklius, A. T. Okamura, & M. K. Sako, Deep magma body beneath the summit and rift zones of Kilauea volcano, Hawaii, Science 247, 1311-16, 1990.

Endo, E. T., Seismotectonic framework for the southeast flank of Mauna Loa, Hawaii, Ph. D. thesis, Univ. of Washington, Seattle, 349 pp., 1985.

Jackson, M. D., E. T. Endo, P. T. Delaney, T. Arnadottir, & A. M. Rubin, Ground ruptures of the 1974 and 1983 Kaoiki earthquakes, Mauna Loa volcano, Hawaii, J. Geophys. Res. 97, 8775-96, 1992.

Jurkevics, A., Polarization analysis of three-component array data, Bull. Seismol. Soc. Am. 78, 1725-43, 1988.

Leary, P. C., S. Crampin, & T. V. McEvilly, Seismic fracture anisotropy in the earth's crust: An Overview, J. Geophys. Res. 95, 11105-14, 1990.

Liang, B. and M. Wyss, Estimates of orientations of stress and strain tensors based on fault plane solutions in the epicentral area of the great Hawaiian earthquake of 1868, Bull. Seismol. Soc. Am. 81, 2320-34, 1991.

Savage, M. K., X. R. Shih, R. P. Meyer, & R. C. Aster, Shear-wave anisotropy of active tectonic regions via automated S-wave polarization analysis, Tectonophysics 165, 279-92, 1989.

Wood, H. O., On the earthquakes of 1868 in Hawaii, Bull. Seismol. Soc. Am. 4, 169-203, 1914.

Wyss, M., A proposed source model for the great Kau, Hawaii, Earthquake of 1868, Bull. Seismol. Soc. Am. 78, 1450-62, 1988.

Wyss, M., B. Liang, W. R. Tanigawa, & X. Wu, Comparison of orientations of stress and strain tensors based on fault plane solutions in Kaoiki, Hawaii, J. Geophys. Res. 97, 4769-90, 1992.

Contract Publications:

Munson, C. G., C. H. Thurber, & Y. Li, Seismic anisotropy in the Kaoiki and Hilea regions of southern Hawaii (abstract), Seismol. Res. Lett., 63, 59, 1992.

Munson, C. G., C. H. Thurber, and Y. Li, Observations of shear wave splitting on the southeast flank of Mauna Loa volcano, Hawaii, submitted to Geophys. Res. Lett., October 1992.

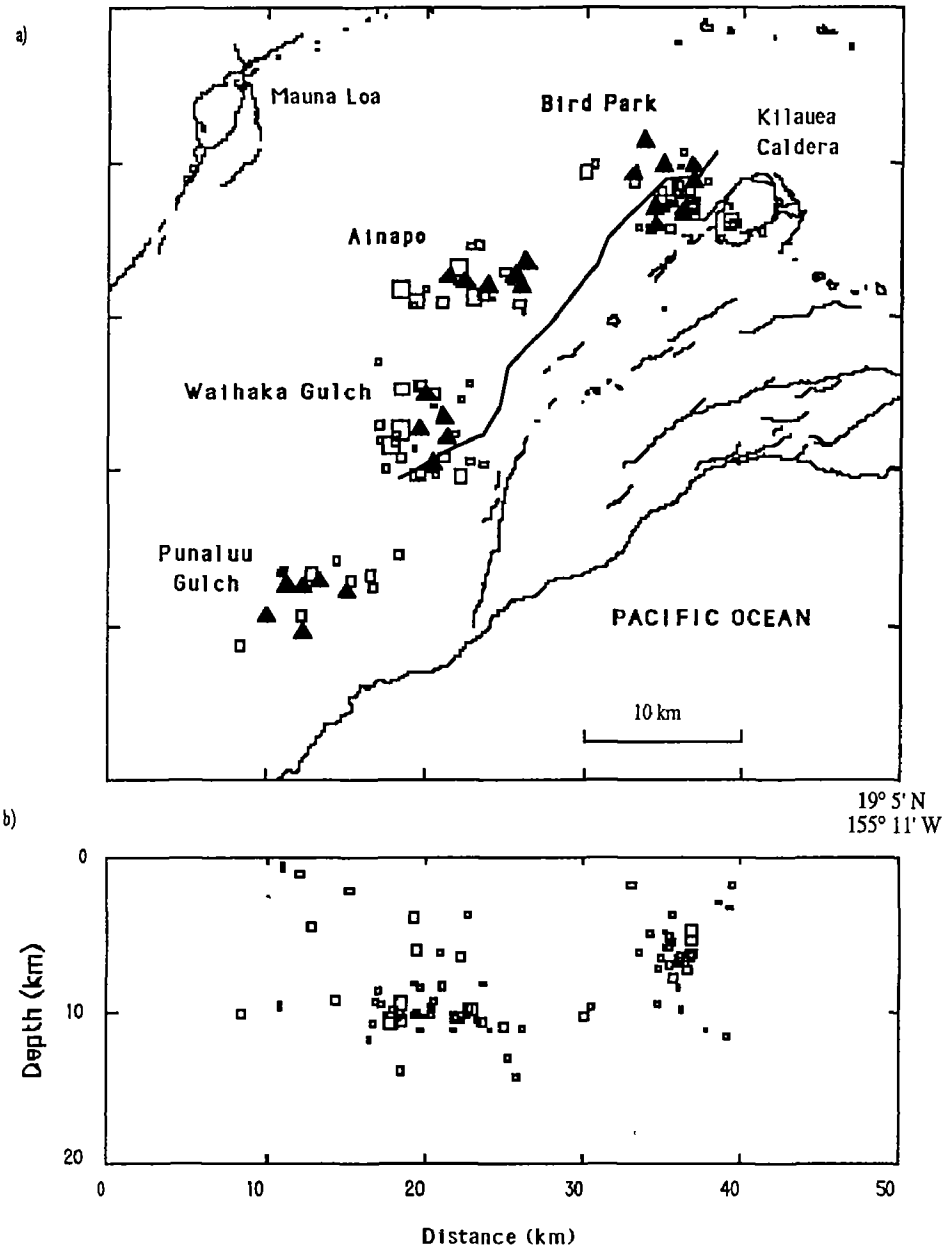

Figure 1. (a) A map of the Kaoiki and Hilea regions in Southern Hawaii, showing the locations of the PASSCAL stations (triangles) deployed from July to December 1990 and the events (boxes) that have been used in this study. The Bird Park and Ainapo arrays were located in the Kaoiki region and the Waihaka Gulch and Punaluu Gulch arrays were located in the Hilea region. The size of the boxes scale with magnitude; the smallest box represents a M = 0.5 earthquake, and the largest represents a M = 2.1 earthquake. (b) A cross section view of the 88 earthquakes showing the range of event depths.

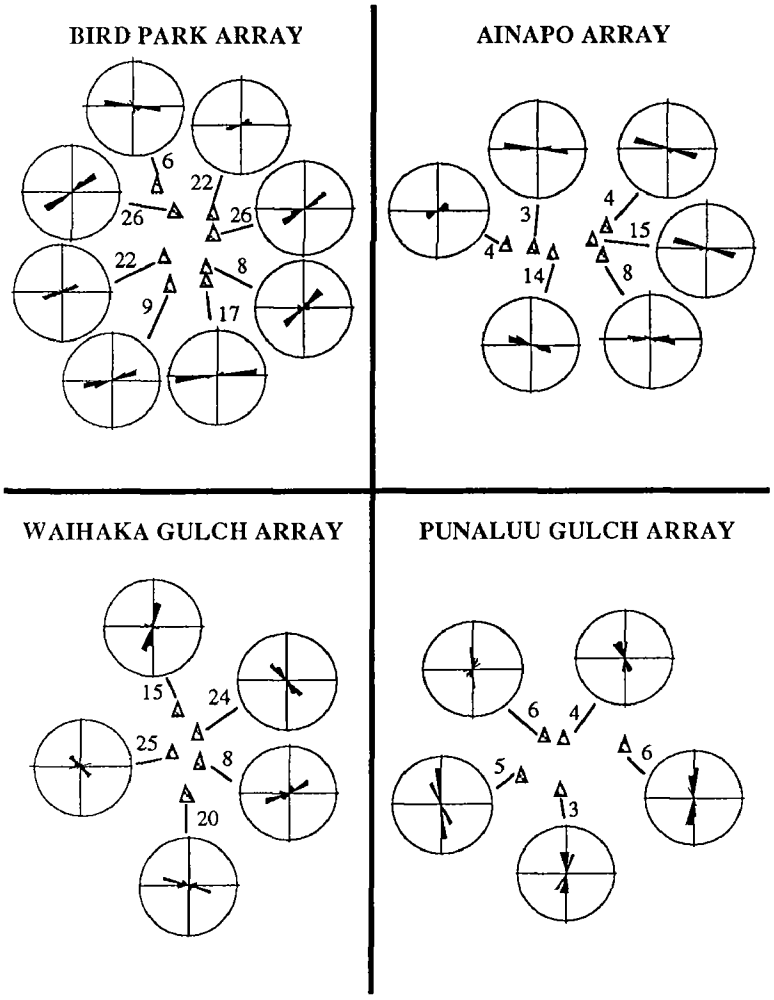

Figure 2. The measured polarization directions of the first-arriving shear wave from the four ALOHA arrays on Mauna Loa's southeast flank displayed as equal-area rose diagrams. The number of observations for each array ranges from 24 to 136.

I

Coupled Deformation-Diffusion Solutions for the Interpretation of Slip Induced Water Well Level Changes at Parkfield

Grant No. 1434-92-G-2164

J. W. Rudnicki
Department of Civil Engineering
Northwestern University
2145 Sheridan Road
Evanston, IL 60208-3109

(708)-491-3411

The purpose of this work is to develope more realistic coupled deformation-pore fluid diffusion solutions for fault slip and to use them to interpret observed water well level changes at Parkfield.

We have derived the coupled deformation diffusion solution for a plane strain slip that begins from rest, propagates a finite distance, and then stops. We intend to use this solution to explore the applicability of the previously used limiting cases of steady propagation [*Roeloffs and Rudnicki*, *PAGEOPH*, 1984/85] and simultaneous slip on a fault segment with a finite rise time [*Rudnicki and Hsu*, *JGR*, 1988]. The steady propagation solution idealizes cases in which the slip propagates primarily along strike. The simulataneous slip solution idealizes the case in which the slip propagates primarily from depth and reaches the surface essentially simultaneously at different positions along strike.

Earthquake Research in the Eastern Sierra Nevada Western Great Basin Region

Contract 14-08-0001-A0618

M. Savage, J. Anderson, J. Brune
Seismological Laboratory, MS 168
University of Nevada, Reno
Reno, NV 89557-0141
(702)784-4975

Investigations Undertaken

This contract supports continued research focussed on earthquakes in the eastern Sierra Nevada and western Great Basin region. We have investigated: 1) Quantitative determination of the probability that a moderate event will be a foreshock to a larger events; 2) Triggering of moderate earthquakes in Nevada following the M=7.5 June 28 1992 Landers, California earthquake; 3) The earthquake sequences of the M=5.6 June 29, 1992 Little Skull Mountain, Nevada, earthquake, and the M=5.0 October 24, 1990 Lee Vining, California, earthquake 4) The relation of precariously-balanced rocks in Nevada and California to past strong ground motion levels, with emphasis on using their presence to determine limits on past shaking 5) Microseismicity in the Mammoth Lakes, California and Yucca Mountain, Nevada region and the relation of microseismicity to the frequency of occurrence of larger events.

Results obtained

1) Foreshock Probabilities in the western Great-Basin eastern Sierra Nevada

We quantify foreshock occurrence probabilities in the eastern California/Western Nevada region by applying the empirical technique of Jones (1985) to the University of Nevada, Reno western Nevada-eastern California catalog from 1934 through 1991. We found it necessary to separate the Mammoth/Mono Lakes region from the rest of the catalog to determine the parameters that most effectively removed the aftershocks from the catalog. The probability that an $M \geq 3.0$ earthquake will be followed by an earthquake of larger magnitude within 5 days and 10 km is 10% in the Mammoth/Mono region and 6% in the Nevada region, and appears to be independent of the magnitude of the proposed foreshock. The probability that a mainshock at least one magnitude unit higher will occur decreases to about 2% in each region. These probabilities imply that the occurrence of an earthquake of $M \geq 4.0$ increases the possibility of a damaging earthquake of $M \geq 5.0$ by several orders of magnitude above the low background probability. Most mainshocks occur within a few hours after a possible foreshock, and the probability that a mainshock will still occur decreases logarithmically with time after the proposed foreshock. These properties are similar to those in southern California and in other parts of the world, with the exception that the Mammoth/Mono region, a volcanic area, exhibits more swarm-like behavior than does the southern California or Nevada region.

2) Earthquake Triggering from the Landers, California earthquake sequence

Within 24 hours after the Landers earthquake, there were 3 magnitude 3.4+ events in western Nevada and a general increase in the rate of small events. Based on the previous 25 year combined catalog for northern and southern Nevada, this level of widely scattered seismicity appeared quite unusual. Using a quantitative model that assumes statistical independence of these regions, the probability of this happening in a 24 hour period by random chance is less than once in 10^{10} years. Therefore, we conclude that there is a very high probability that these were triggered by the Landers event. The principal events that occurred were: Mina, 500 kilometers from Landers, M4.0, 36 minutes after Landers; Smith Valley, 590 kilometers from Landers, M3.4, 56 minutes after Landers; Little Skull Mountain, 280 kilometers from Landers, M5.6, 22.3 hours after Landers. These events are not associated with known volcanic activity or ongoing aftershock sequences. The evidence for triggering is particularly strong in the case of the Little Skull Mountain event, where an increased rate of microseismicity was evident as soon as small events could be identified in the coda of the Landers earthquake.

Earthquakes have been triggered in southern Nevada before, by nuclear testing and by filling of Lake Mead.

We speculate that these events are triggered by the dynamic low-frequency stress associated with surface waves propagating from the Landers earthquake. The distance dependence of static strain changes decrease as R^{-3} , which is much too rapid to cause a significant static strain change at the distances of the above events. Body wave amplitudes decrease more rapidly than surface waves with distance, so that the high-frequency strains associated with the body waves from the Landers earthquake would probably have been exceeded by other more local sources during the prior year. The above reasoning suggests that the cause of the distant triggering is the high amplitude, relatively longer period surface waves. Surface waves of a few seconds period have relatively high strains extending to a depth of more than 10 km. This mechanism for triggering satisfies the criterion of being a relatively rare phenomenon, since it is likely to occur only when a large surface wave is radiated into an area where strain has been building slowly toward the point where faults are unstable.

3a) The Little Skull Mountain, Nevada, earthquake sequence of June 29, 1992:

The Little Skull Mountain earthquake occurred about 20 km from the proposed high level nuclear repository at Yucca Mountain. The magnitude was 5.6, and the focal mechanism indicates normal faulting on a northeast trending structure. There is evidence that the earthquake was triggered by the magnitude 7.6 earthquake in Landers, California, which occurred less than 24 hours earlier. Preliminary locations of the hypocenter and several aftershocks define an "L" shaped pattern near the southern boundary of the Nevada Test Site. One arm trends to the northeast beneath Little Skull Mountain, and a shorter, more diffuse zone trends to the southeast. The aftershocks are mostly located at depths between 7 km and 11 km, and may suggest a southeast dipping plane. There is no clear correlation with previously mapped surface faulting. The strongest recorded acceleration is about 0.21 g at Lathrop Wells, Nevada, 15 km from the epicenter. An extensive network of aftershock recorders was installed by the Seismological Laboratory, University of Nevada, Reno, by the United States Geological Survey, Golden, Colorado, and by Lawrence Livermore Laboratory, Livermore, California. Aftershock experiments are ongoing as of November, 1992, and include experiments to improve location, depth, focal mechanism, and stress drop, study basin and ridge response near the epicenter and at Midway Valley, and study response of a tunnel at Little Skull Mountain. Analysis of this data, which includes thousands of aftershocks, has only begun.

3b) The October 24, 1990, Lee Vining, California Earthquake

On October 24, 1990, a magnitude 5.0 (Md) earthquake occurred near the town of Lee Vining, California. It was a strike-slip event with a hypocenter 5 km east and 11.5 km below the surface trace of the active (Holocene), vertically offset, Sierran frontal fault. A time domain deconvolution technique was used to obtain the source time function of this event using a small foreshock as an empirical Green's function. The resulting source time function indicates a simple rupture with a moderate stress drop of 31 bars. The distribution of aftershocks, duration of rupture, and lack of strong directivity observed in the first motion pulse widths, slightly favor bilateral rupture on a northwest striking vertical plane over unilateral rupture on a nearly vertical northeast striking plane. The Lee Vining main shock is the latest in a series of 27 magnitude 5.0 to 6.6 earthquakes to have occurred in the Walker Lane Belt since 1978. This is an area of diverse topography and numerous strike-slip faults which lies between the Sierra Nevada on the west and typical Basin and Range topography on the east. Between 86% and 91% of the cumulative moment released during these earthquakes was due to strike-slip motion (based on 20 available short-period focal mechanisms). Long-period mechanisms (centroid moment tensors) available for seven of the events also indicate a larger percentage of strike-slip than dip-slip motion. Slip ratios estimated for the two largest historic events in the Walker Lane Belt, the magnitude 7.7 Owens Valley earthquake and the magnitude 7.2 Cedar Mountains earthquake are consistent with these results. This indicates that the contemporary stress field has a significant component of horizontal shear.

4) Precarious Rocks

In several localized ares of California and Nevada there are large numbers of precariously balanced rocksrocks which could be knocked down by earthquake ground motion with peak accelerations of about 0.2g or less. In some cases geomorphic evidence indicates that these rocks have been in these precarious positions for thousands of years. In this study the locations of regions of precariously balanced rocks are compared with probability maps for strong ground motion, to help determine if the precarious rocks can be used as paleoindicators of peak acceleration. The following results are obtained:

1) No precarious rock zones are found within 15 km of known historic large earthquake rupture zones (e.g., Olinghouse, Fallon-Stillwater, Cedar Mountains, Nev.; Fort Tejon, Owens Valley, Borrego Mt., Tehachapi, Parkfield, Calif.)

2) Precarious rock zones have been found at the following sites: a) the region around Yucca Mountain, Nev., site of the proposed high level nuclear waste repository, b) the center of the Peninsular Ranges in southernmost Calif., c) 20 km north of San Gorgonio Pass, Calif., d) near Lida, Nev., 20 km southeast of the spectacular Holocene scarps in Fish Lake Valley, Calif., e) the West Walker River Canyon 15 km south of Walker, Calif., f) 25 km north of the ground rupture in the 1932 M=7.4 Cedar Mtn. earthquake.

3) In California these observations correlate well with published ground acceleration maps, but in Nevada there are significant discrepancies. The implications of these results for seismic hazard studies are discussed.

5) Microearthquakes

We set up four microearthquake stations near Mammoth Lakes, where we observed microearthquake rates of over 100 per day, most with S-P times of less than 3 sec. This confirms our previous expectations that in seismically active areas most events recorded on such instruments have S-P times of less than 3 sec. In a much less seismically active area, near Yucca Mountain, Nevada, there were many fewer events with short S-P times.

Publications

Refereed Journal Articles

Anderson, J. G., J. N. Brune, D. dePolo, J. Gomberg, S. C. Harmsen, M. K. Savage, A. F. Sheehan, K. D. Smith, Preliminary report: The Little Skull Mountain earthquake, June 29, 1992, *Proceedings of the ASCE Symposium on Dynamic Analysis and Design Considerations for High-Level Nuclear Waste Repositories, submitted.*

Brune, J.N., W. Nicks, and A. Aburto, Microearthquakes at Yucca Mountain, Nevada, *Bull. Seismol. Soc. Am.*, **82**, 164-174, 1992.

Horton, S., D. DePolo, and W. R. Walter, The October 24, 1990, Lee Vining, California earthquake and other recent moderate earthquakes in the western Basin and Range, *in revision, Bull. Seismol. Soc. Am.*, 1992.

Ozalaybey, S., and Savage, M.K. Inversion of double layers of anisotropy from waveforms of suites of seismograms, *to be submitted to Bull. Seismol. Soc. Am.*, 1992.

Savage, M.K. and P.G. Silver, Mantle deformation and tectonics: Constraints from seismic anisotropy in western United States, *Phys. Earth Planet. Int.*, in press, September 1992.

Savage, M.K., L. Li, J. Eaton, C. H. Jones, and J. N. Brune, Earthquake refraction profiles under the root of the Sierra Nevada, in preparation for submission to Geophysical Research Letters. (A draft is circulating among coworkers)

Savage, M.K., and D. DePolo, Foreshock probabilities in the eastern Sierra Nevada/Western Great Basin Region, *submitted to Bull. Seismol. Soc. Am.*, 1992.

Abstracts

Anderson, J., J. Louie, J. Brune, D. dePolo, M. Savage, and Y. Guang, Seismicity in Nevada apparently triggered by the Landers, California earthquake, June 28, 1992, *EOS, Trans. Am. Geophys. Union, 73,*, 393, 1992.

Brune, J.N. Distribution of precariously balanced rocks in Nevada and California: Correlation with probability maps for strong ground motion, *EOS, Trans. Am. Geophys. Union, 73,,* 351, 1992.

Brune, J. N. and J. W. Whitney, Precariously balanced rocks with rock varnish: Paleoindicators of maximum ground acceleration? *Seismol. Res. Lett., 63,,* 21

Horton, S.P., D. dePolo, and W. Walter, The October 24, 1990 Lee Vining, California earthquake and other recent moderate earthquakes in the western Basin and Range, *Seismol. Res. Lett., 63,,* 39

Li, L., M. K. Savage, J.N. Brune, J. Eaton, The Root of the Sierra Nevada: Evidence from Earthquake Refraction Profiles, *EOS, Trans. Am. Geophys. Union*73,, p. 369, 1992.

Ozalaybey, S. and M. Savage, Inversion of double layer anisotropy from SKS Phase, *EOS, Trans. Am. Geophys. Union, 73,,* 395, 1992.

Reasenberg, P.A., D. P. Hill, A. J. Michael, R. W. Simpson, W.L. Ellsworth, S. Walter, M. Johnston, R. Smith, S.J. Nava, W.J. Arabasz, J.C. Pechmann, J. Gomberg, J.N. Brune, D. DePolo, G. Beroza, S. D. Davis, J. Zollweg, Remote seismicity triggered by the M7.5 Landers, California earthquake of June 28, 1992, *EOS, Trans. Am. Geophys. Union, 73,,* 392, 1992.

Savage, M.K., and D. dePolo, Foreshock probabilities in the eastern Sierra Nevada/western Great Basin region, *Seismol. Res. Lett., 63,,* 21

Micromechanics of Rock Friction

Agreement No. USGS14-34-92 G2161

Christopher H. Scholz
Lamont-Doherty Geological Observatory
Columbia University
Palisades, New York 10964

(914) 359-2900

This is an experimental and theoretical study of rock friction in which the micromechanics of friction are studied by use of a model of the contact of random elastic surfaces.

In previous work the transition from partial to full sliding of the surfaces was studied. This takes place within the first 5-10 μm of sliding with the surfaces we study in the laboratory. Quantitative modeling show that this process can be well simulated with forward modeling based on measured topography of the experimental surfaces.

During the past year this has been extended through the stage of strong slip hardening until steady state friction is reached, in 0.1 to 1 mm of slip. To model this behavior we include the additional effects of oblique contacts (interlocking) and the evolution of surface topography during sliding (wear). This modeling successfully accounts for these later stages of friction and show that these processes account approximately equally to the additional friction that occurs after the onset of full sliding.

In order to facilitate the above study, an experimental study of the frictional wear of granite was also conducted. Modeling of the wear process allowed for the prediction of both transient and steady-state wear and the distinction to be made regarding the micromechanisms of 'riding up' and shearing through' to be distinguished for oblique contacts.

Work is continuing on scaling these processes to the geological scales, primarily through the scaling of the critical slip distance, D_c. Work is also continuing on the second order frictional effects, that of slip velocity and variable normal load.

Analysis of Seismic Anisotropy and Directional Site Resonance in the Loma Prieta Aftershock Zone

Agreement No. 14-08-0001 G2079

Susan Y. Schwartz
Institute of Tectonics, University of California, Santa Cruz, CA 95064
(408) 459-3133

Summary

The objectives of this research are twofold: to evaluate the existence, orientation and origin of crustal anisotropy in the aftershock zone of the 1989 Loma Prieta earthquake and to assess the influence of structural heterogeneities in the shallow crust on the seismic wavefield. To accomplish the first objective, we analyzed shear wave polarizations for evidence of seismic anisotropy using three-component digital recordings of Loma Prieta aftershocks recorded by PASSCAL instruments. Initial polarizations for over 60% of the records within the shear wave window (pre-critical arrivals) show clear evidence of shear wave splitting. Two fast directions of polarization parallel to the strike of the San Andreas Fault (290°-340°) and parallel to the direction of local maximum horizontal compressive stress (20°-45°) are observed. Stations located northeast of the San Andreas Fault predominantly show the fault parallel fast polarization direction which may result from mineral or fracture alignment caused by shearing along the plate boundary. Stations to the southwest of the San Andreas Fault show both fast directions of polarization. The direction perpendicular to the local axes of minimum horizontal compressive stress is consistent with the theory of extensive dilatancy.

Analysis of shear wave polarizations to investigate seismic anisotropy is often complicated by signal distortions produced by scattering and by the effects of shallow geology beneath the receiver. In order to understand these effects we investigate the site response and scattering properties of the shallow crust beneath one of our receivers. This investigation encompasses two experiments: the deployment of a 20-station small aperture array at station ZAYA to record five chemical explosions set off by the USGS in May of 1991, and a shallow refraction survey consisting of two orthogonal lines of geophones and both compressional and shear wave seismic sources. Analysis of three-component short-period recordings of the chemical explosions at our small array reveals: 1) smooth variations in shear wave polarization directions across the array, 2) a systematic bias of 30°-50° in the observed back azimuths of the P wave arrivals relative to known positions for the sources, and 3) a north-south preferred direction of arrival for P and S wave coda that is not consistent with the azimuth to the source. These results imply that the wavefield is strongly affected by regional velocity inhomogeneity beneath the receivers. To obtain more detailed information about the geology and seismic velocity layering beneath this array, we conducted a shallow refraction survey at ZAYA in August of 1992. This report describes the progress made in the first year of funding and the work we expect to accomplish during the second year.

Research Accomplished

1. Seismic Anisotropy in the Loma Prieta Rupture Zone

We have analyzed shear wave polarizations from three-component recordings of fifty-four aftershocks of the 1989 Loma Prieta earthquake for anisotropy induced shear wave splitting. Figure 1 shows the event-station geometry. Only events located at pre-critical distances from receivers (within the shear wave window) were analyzed to avoid distortions due to phase changes accompanying reflections and conversions from the free surface. We identify shear

wave splitting by: initial shear wave polarizations that abruptly change from linear to elliptical motion, consistent directions of initial linear polarization for many earthquakes with different focal mechanisms, and observations of the slow shear wave polarized in a direction orthogonal to the first arriving wave and delayed in time. To identify a transition from linear to elliptical particle motion at the onset of the shear wave, we plot the shear wave polarization vector as a function of time. Figures 2 shows horizontal component seismograms and polarization vectors plotted as a function of time, from two different earthquakes recorded at stations RADF and WVRD. Event 1 shows linear particle motion throughout the initial S arrival, as expected for propagation through isotropic material. S wave particle motion from event 2 is initially linear but abruptly changes to elliptical shortly after the S arrival. We interpret this behavior as evidence of anisotropy induced shear wave splitting, where arrival of the fast wave produces linear particle motion that changes to elliptical motion when the slow wave, polarized in the orthogonal direction, arrives.

For all events that show evidence of shear wave splitting, we determine the polarization direction of the fast wave directly from the polarization vector plot and compare it with directions determined by the aspect ratio (Shih *et al.*, 1989) and cross-correlation techniques. The aspect ratio method determines the initial polarization direction by searching through all azimuths for the maximum linear particle motion obtained from motions rotated onto a pair of orthogonal axes. The time separation between the fast and slow shear wave is estimated by advancing the slow wave by small time increments and searching for the time advance that yields the maximum linearity in particle motion. The direction indicated after this time shift represents the anisotropy corrected polarization direction, which we expect to be determined by the earthquake focal mechanism. The cross-correlation technique finds the azimuth and time delay that maximizes the waveform correlation between the fast and slow shear waves. For event 2 recorded at WVRD, the initial linear direction of polarization is 340° from the polarization vector plot (Figure 2), 330° from the aspect ratio technique (curve in Figure 3 marked with 0 delay time), and 335° from the cross-correlation method (Figure 4a). A delay time of 0.05 seconds between the fast and slow arriving waves results in the maximum aspect ratio (Figure 3) and a delay of 0.045 seconds produces the largest cross-correlation between the fast and slow waves. After correction for shear wave splitting of 0.05 seconds, the aspect ratio method indicates a direction of 285° (Figure 3). Before correction for shear wave splitting, linear particle motion persists for only .04 seconds from the onset of the shear wave (Figure 4b). After correcting for the .045 seconds indicated by the cross-correlation method, linear particle motion persist for over .2 seconds from the shear wave onset (Figure 4c). The direction after this correction is 290°. The shear wave polarization directions after correction for shear wave splitting indicated by cross-correlation and the aspect ratio technique are both consistent with the direction of 289° expected from the focal mechanism of this event.

For event 2, three methods of determing the initial polarization direction of the fast wave, and two methods to determine the time delay between the fast and slow wave are consistent providing confidence that the fast direction of polarization and the time delay until arrival of the slow wave are well determined. We are in the process of applying this methodology to 54 events recorded at 17 of the PASSCAL stations to look for evidence of anisotropy induced shear wave splitting and to evaluate the directions and time delays obtained. So far we have completed analysis at five stations which are indicated in Figure 1 using upward pointing triangles. Our results for four of the five stations are summarized in Figure 5 which shows the directions of initial polarization (solid lines) determined for many different earthquakes at each station. Polarization directions are plotted at the epicenter of the events for clarity. The range in delay time between the fast and slow shear waves observed at each station is indicated in milliseconds for each plot. At stations WVRD, WSWD and WAWA, all but one or two events show consistent directions of polarization that range between 140-160° at WVRD and WSWD and between 20-40° at WAWA. Results from station ZAYA are more mixed, with fast directions between 140-160° for only five of the nine events analyzed. Consistent directions of polarization at a particular station from events at different locations and with different focal mechanisms is diagnostic of anisotropy somewhere beneath the receiver. The observed directions of polarization are in most cases different from those originating at the source determined from P wave first

motion mechanisms of Oppenheimer (per. comm.). We are presently finishing our analysis on the remaining stations and looking for correlations between observed fast directions of polarization and known geologic information to isolate the origin of the seismic anisotropy. We are also correlating the delay times obtained with various parameters including focal depth, epicentral distance and azimuth. The different directions of fast polarization between stations WSWD and WAWA which are located very close to one another suggests that a component of the observed anisotropy occurs at very shallow depth. The mixed directions at ZAYA may result from strong velocity heterogeneity at shallow depth beneath this station that obscures any seismic anisotropy. The next sections of this report investigate the shallow velocity structure beneath the ZAYA station.

2. Dense Array Recording of Loma Prieta Rupture Zone Controlled Source Explosions

In an earlier study using data from the 6 element ZAYA sub-array of the 1989 Loma Prieta PASSCAL aftershock deployment (Figure 6), Bonamassa et al. (1991) found that in the frequency range between 1 and 20 Hz, different sites amplified ground motion in preferred directions that varied greatly between sub-array elements located only tens of meters apart. To further evaluate this phenomena, to investigate the relationship between the amplification and directionality of weak ground motions and microtremor at the same sites, and to study the scattering properties of the shallow crust, we deployed a dense array of 20 elements at the ZAYA site (Figure 6) and recorded five controlled source explosions located between 15 and 20 km from the array. Using several different array analysis techniques, we analyze the various signals from the explosions (including P wave arrivals and S wave coda) in the frequency band 2-26 Hz, to infer localized inhomogeneous velocity structure that may be associated with preferred polarization of ground motions.

Analysis of shear wave particle motions produced by the explosions showed that polarization directions changed smoothly across the 45 by 60 m array, and were more influenced by the site than by the location of the explosions. Lateral gradients in near-surface shear wave velocity are likely to cause these resonances. Changes in preferred polarization over short distances (<50 m) implies that the velocity heterogeneity responsible is located very near the receivers. Examination of explosion P wave arrivals also provide evidence of regional velocity inhomogeneity. We measured the arrival direction of the initial explosion P wave propagating across the array using three approaches: particle motion polarity, fitting a plane wavefront to relative arrival times, and frequency-wavenumber (f-k) analysis. Results of the three methods are consistent and reveal a systematic bias of 30-50° in the observed back azimuths of the P waves relative to known positions for the sources (Figure 7). It is unlikely that velocity structure far from the array is responsible for this strong deflection of the first arrival. Figure 8 shows a possible sub-array structure that may give rise to the observed bias. Quantitative modeling of potential structures is presently underway. We also analyzed the three-component signals throughout the P and S coda using f-k processing. We find a north-south preferred direction of coda arrival, which is not along the azimuth to the sources. We are using the three-component data to identify the polarization of these waves and to relate them to the preferred S wave polarizations.

3. Shallow Seismic Refraction Experiment

Our observations at ZAYA indicate that the seismic wavefield is strongly affected by local velocity inhomogeneity. In order to image the shallow velocity structure beneath ZAYA, we conducted a refraction experiment in August of 1992. Figure 6 shows the location of our two refraction lines relative to the dense array at ZAYA. The instrumentation consisted of a 64 channel, portable, PC-based recording system designed by W.H.K. Lee (Lee and Dodge, 1992), 23 Mark Products L-22, three-component geophones, an air-powered shear-wave generator designed by Liu et al. (1988) and a hammer P wave source. The source-receiver geometry is

shown in Figure 9 and consisted of two orthogonal rows of twelve sensors with 10 m spacings. Shear wave sources were detonated repeatedly at the ends of each line of geophones and at the center of the array (Figure 9). The sledge hammer source was used at each geophone location as well as at each of the shear wave source locations.

The air-powered, impulsive shear wave source and the hammer, produced clean, repeatable SH and P pulses. Multiple signals from each source location were stacked to improve the signal-to-noise ratio. Figure 10 shows profiles of stacked P and SH signals recorded on the north-south line with sources detonated at both the south end of the line (Figure 10a) and the north end of the line (Figure 10b). The reversed profiles reveal very different waveforms indicating a strongly varying velocity structure beneath the sensors. We will use this data to determine the shallow velocity structure beneath ZAYA and relate our results to the wavefield characteristics determined from the dense array.

References

Bonamassa, O., J.E. Vidale, H. Houston, and S.Y. Schwartz, 1991. Directional site resonances and the influence of near-surface geology on ground motion, *Geophys. Res. Lett, 18,* 901-904.

Lee, W.H.K., and D.A. Dodge, 1992. A course on: PC-based seismic Networks, U.S. Geol. Surv. Open-file Report 92-441, 535 pp.

Liu, H.P., R.E. Warrick, R.E., Westerlund, J.B.Fletcher, and G.L. Maxwell, 1988. An air-powered impulsive shear-wave source with repeatable signals, *Bull. Seismol. Soc. Am., 78,* 355-369.

Shih, X., R. Meyer, and J. Schneider, 1989. An automated, analytical method to determine shear-wave splitting, *Tectonophysics, 165,* 271-278.

Publications

Bonamassa, O., J.E. Vidale, W. Lee, and H. Liu, 1992. The Relation Between Ground Motions and Near-Surface Geology, Trans. Am. Geophys. Union, 73, 338.

Xu, Z., T. Lay, and S.Y. Schwartz, 1992. Seismic Wavefield Analysis Using a Very Small Dense Array, Trans. Am. Geophys. Union, 73, 367.

Zayante Seismic Experiment Team, 1992. Zayante Seismic Experiment: Data Report, U.S. Geological Survey Open-File Report, in press.

Zhang, Z. and S.Y. Schwartz, 1992. Seismic Anisotropy in the Crust of the Loma Prieta Rupure Zone, Trans. Am. Geophys. Union, 73, 402.

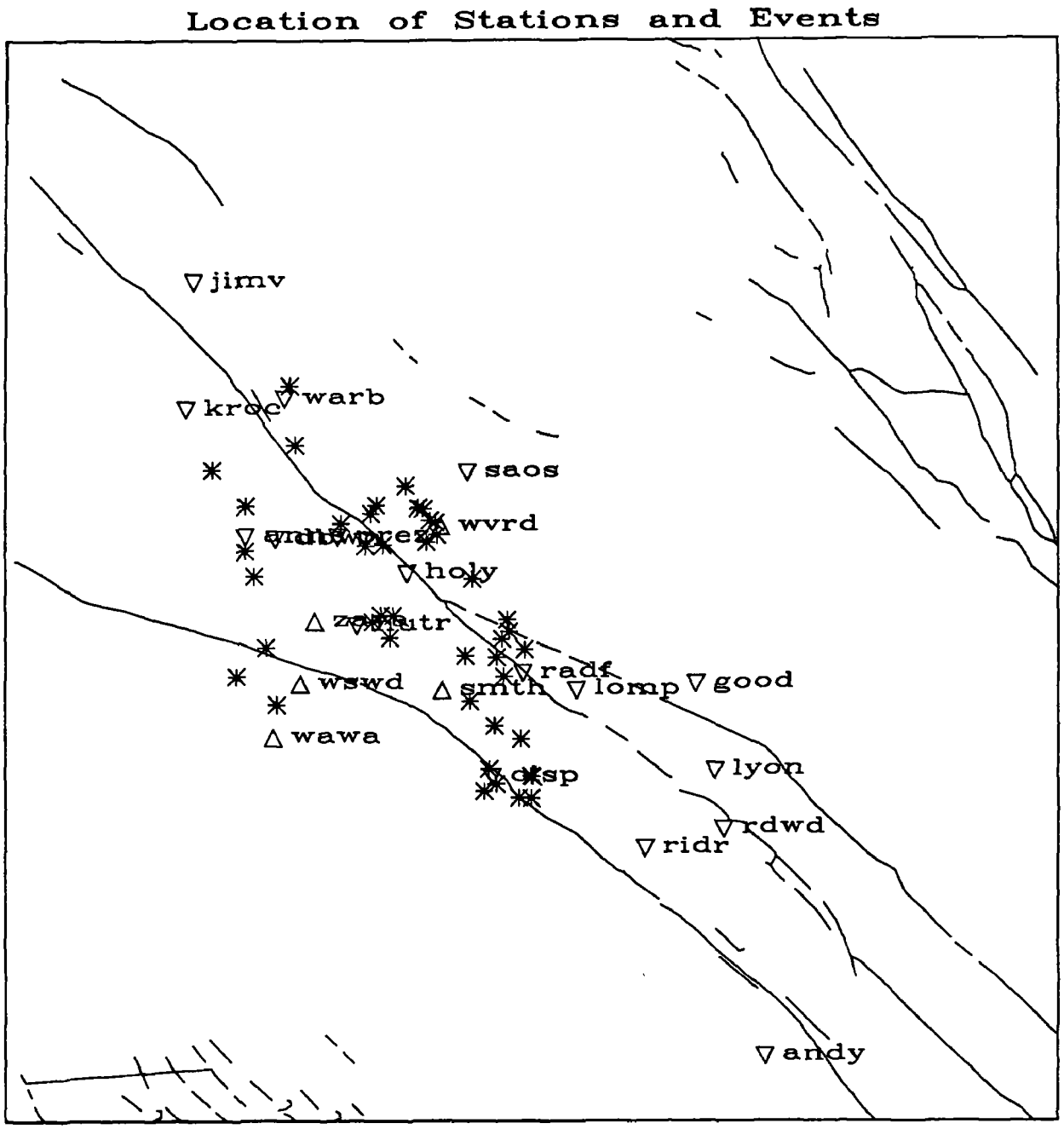

Fig. 1. Map showing location of Loma Prieta aftershocks (stars) and PASSCAL stations (triangles) used for the study of seismic anisotropy. Analysis on data from stations indicated with upward directed triangles has been completed and results are presented in this report.

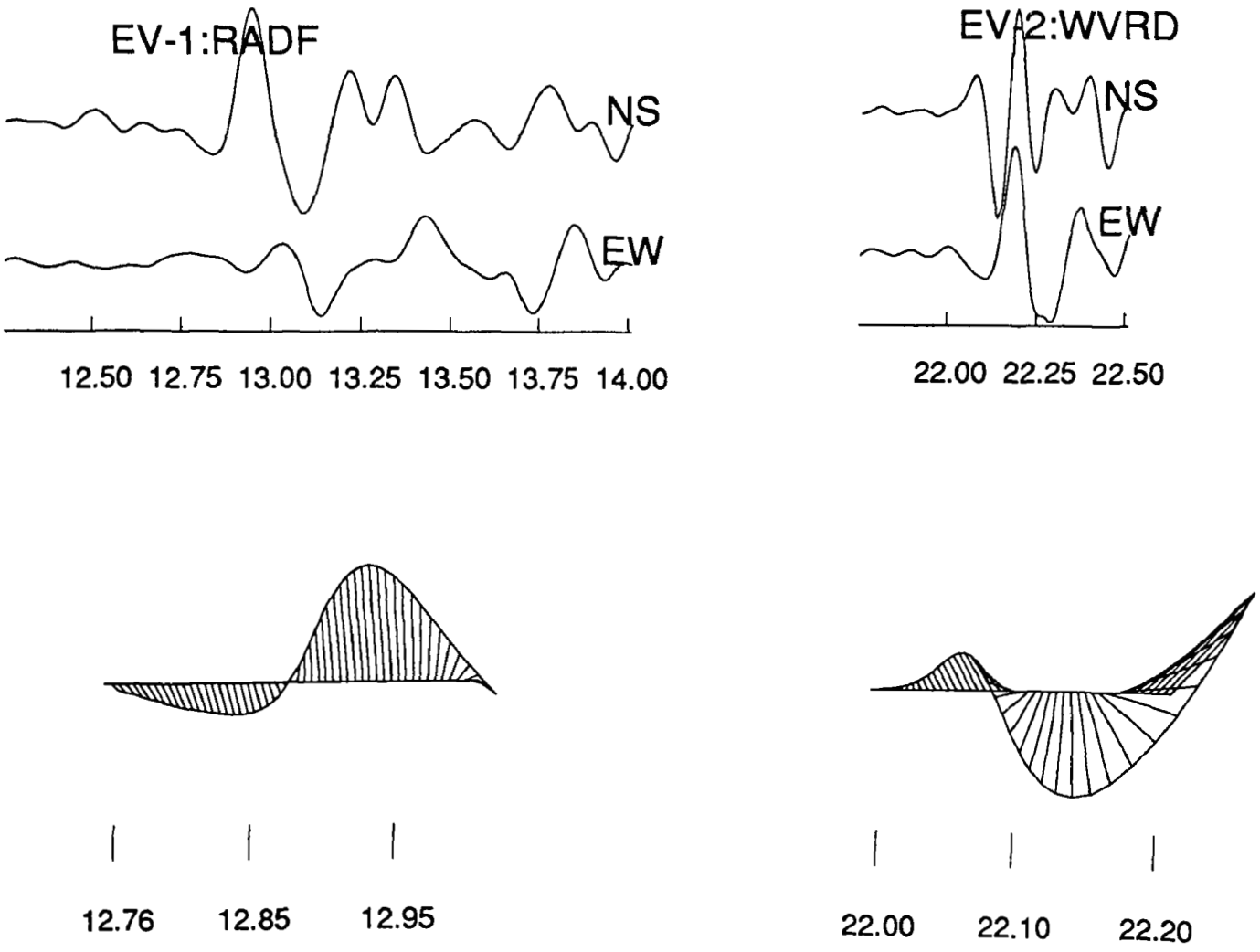

Fig. 2. Horizontal component S wave seismograms and polarization vector plots as a function of time for two earthquakes recorded at different stations. The polarization plot for event 1 indicates linear motion throughout the initial shear wave arrival. The polarization plot for event 2 indicates initial linear motion that abruptly changes to elliptical shortly after the onset of the shear wave. This behavior is suggestive of seismic anisotropy.

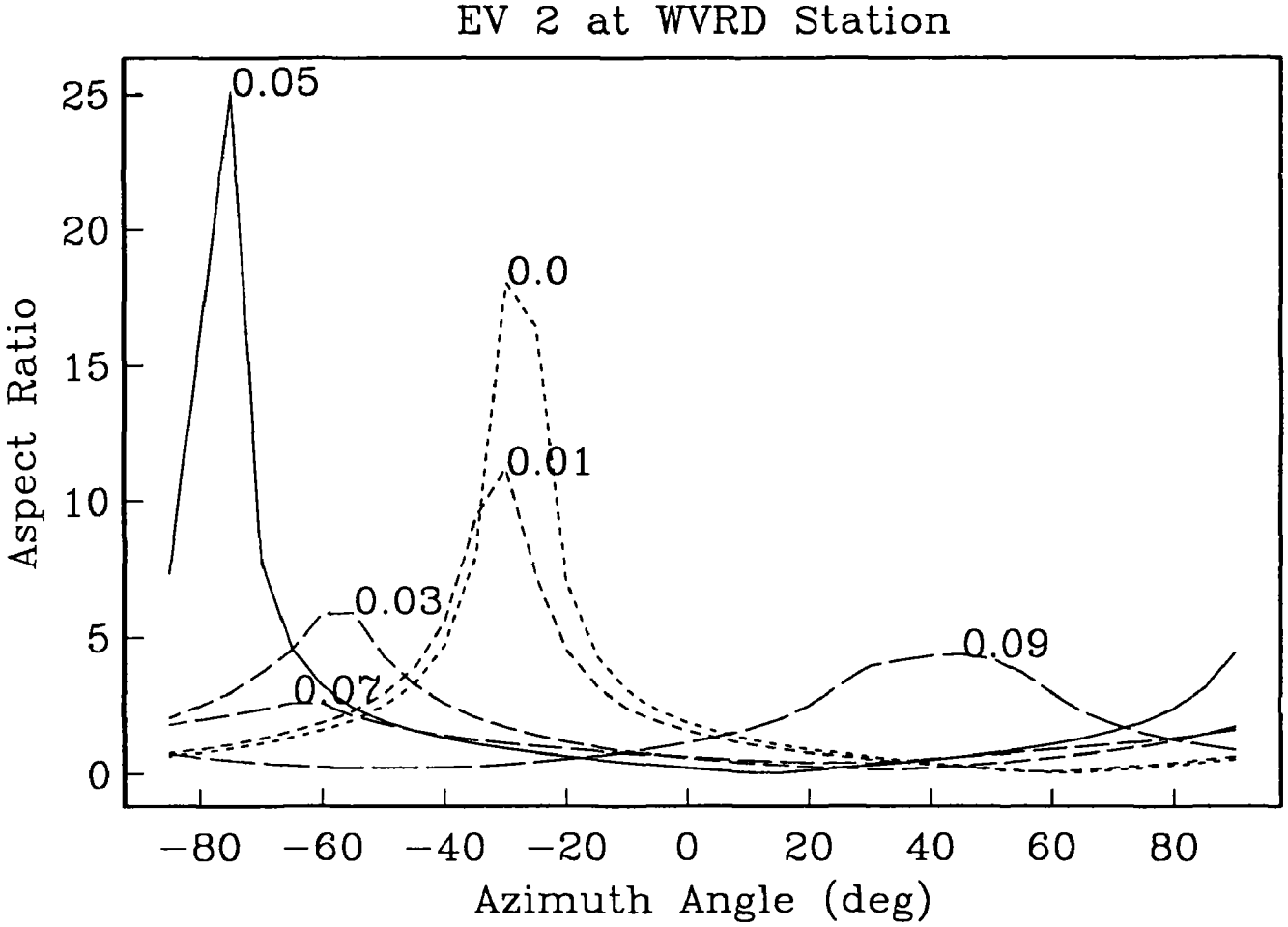

Fig. 3. Plot of aspect ratio versus polarization direction for initial shear wave as a function of different time delays of the fast wave. With no time delay, maximum linearity is obtained with a polarization direction of 330°. Maximum linearity is obtained when the fast wave is delayed by 0.05 s resulting in a polarization direction of 290°, consistent with the polarization at the source expected from the focal mechanism.

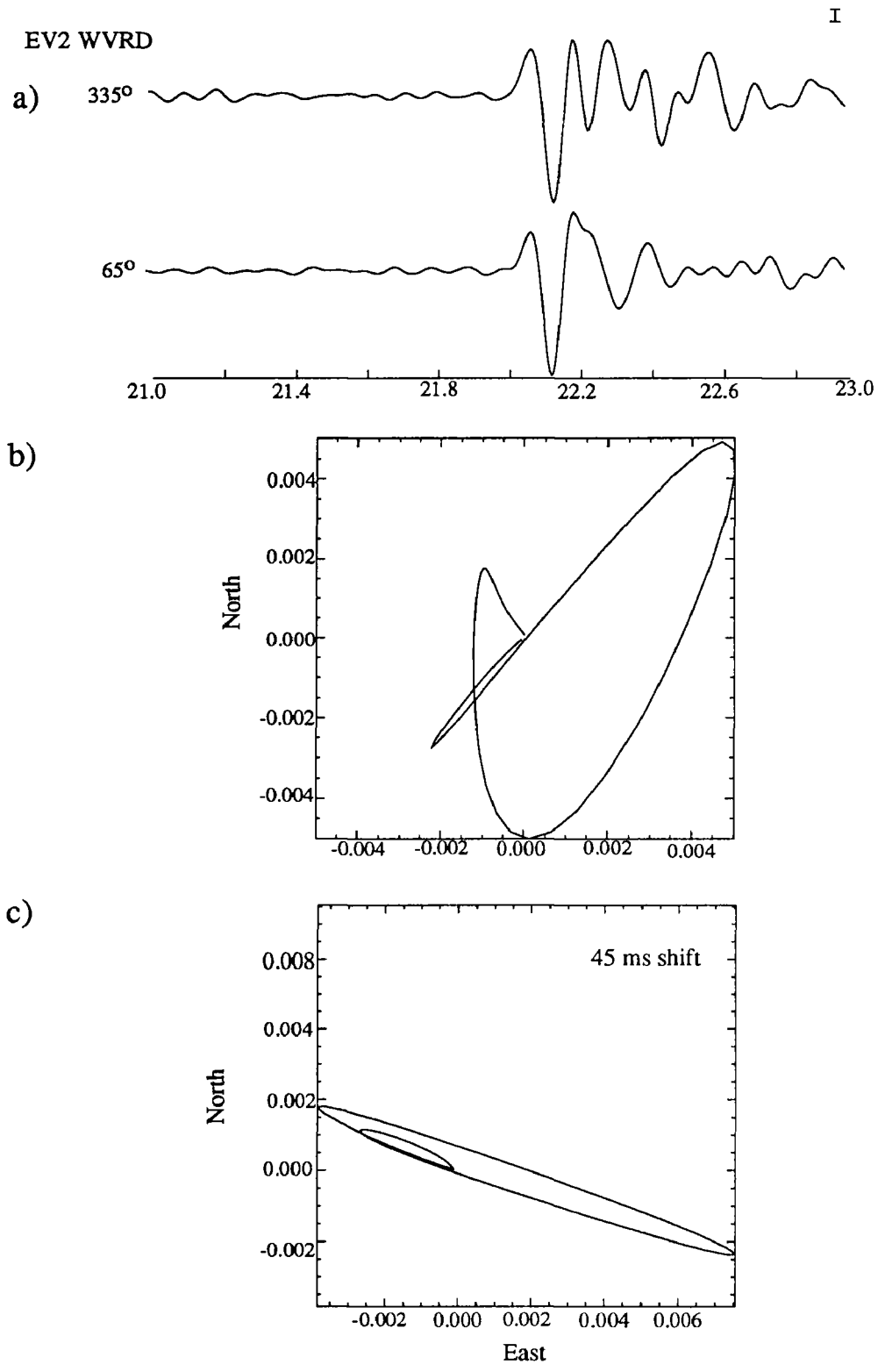

Fig. 4. a) A rotation of 335° and a delay time of 0.045 s yields the largest cross-correlation of horizontal component seismograms indicating this direction as the fast direction of polarization. b) Particle motion plot for the first 0.2 s of the shear wave before time shift shows an initial linear direction of 340°(first 0.04 s) that abruptly changes to elliptical motion after arrival of the slow wave. c) Particle motion for the same time window after delaying the fast wave by 0.045 s indicates linear motion with a direction of 290° as expected from the focal mechanism for this event.

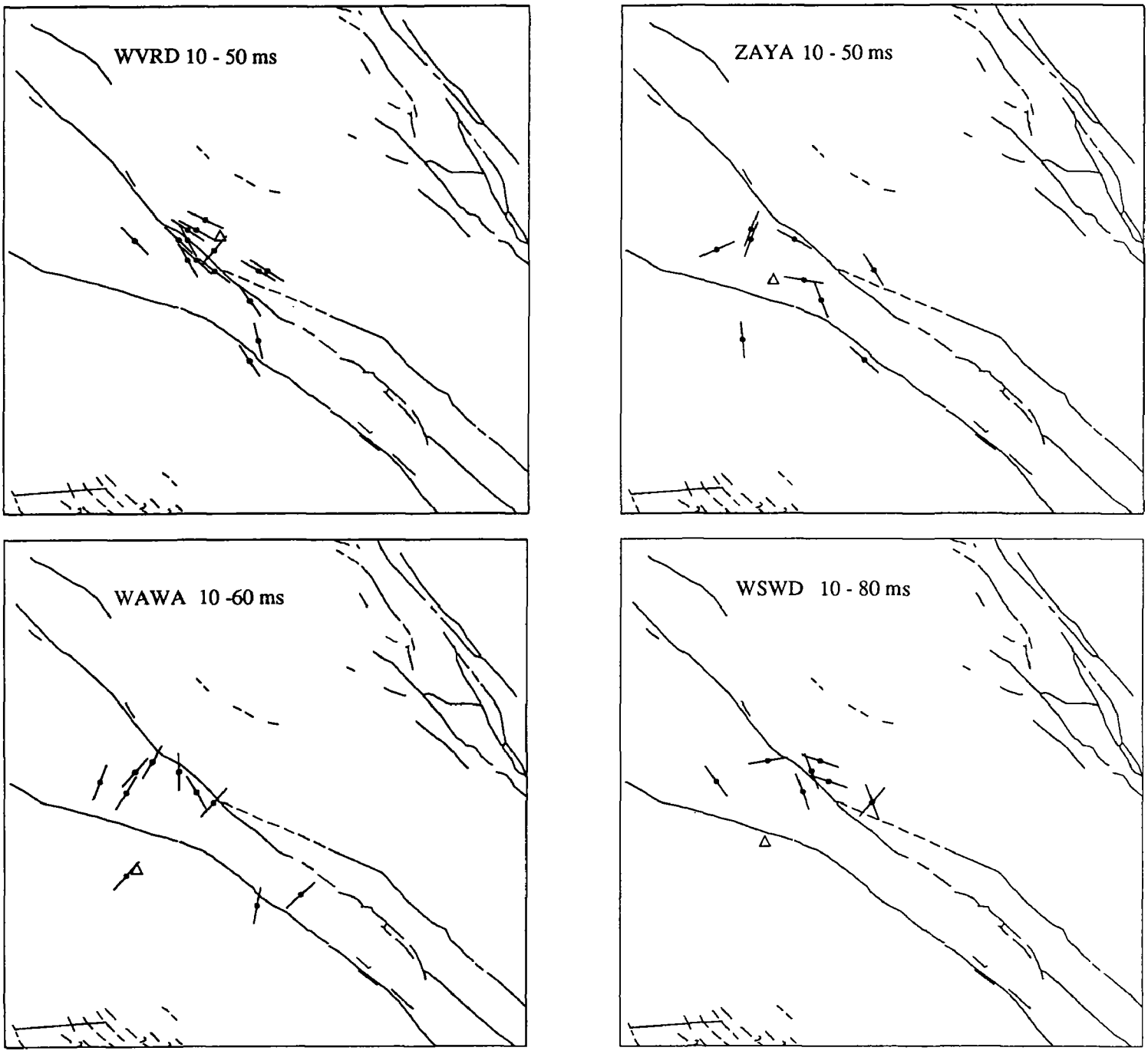

Fig. 5. Directions of initial polarization for many events determined at 4 stations. Polarization directions are plotted at the epicenter of each event for clarity. The range in delay time between the fast and slow wave at each station is indicated in milliseconds. Two dominant directions of polarization are observed, 140-160° and 20-40°.

Map of the 6-Station Array, Very Dense Array, and Shallow Refraction Seismology Lines in the Santa Cruz Mountains

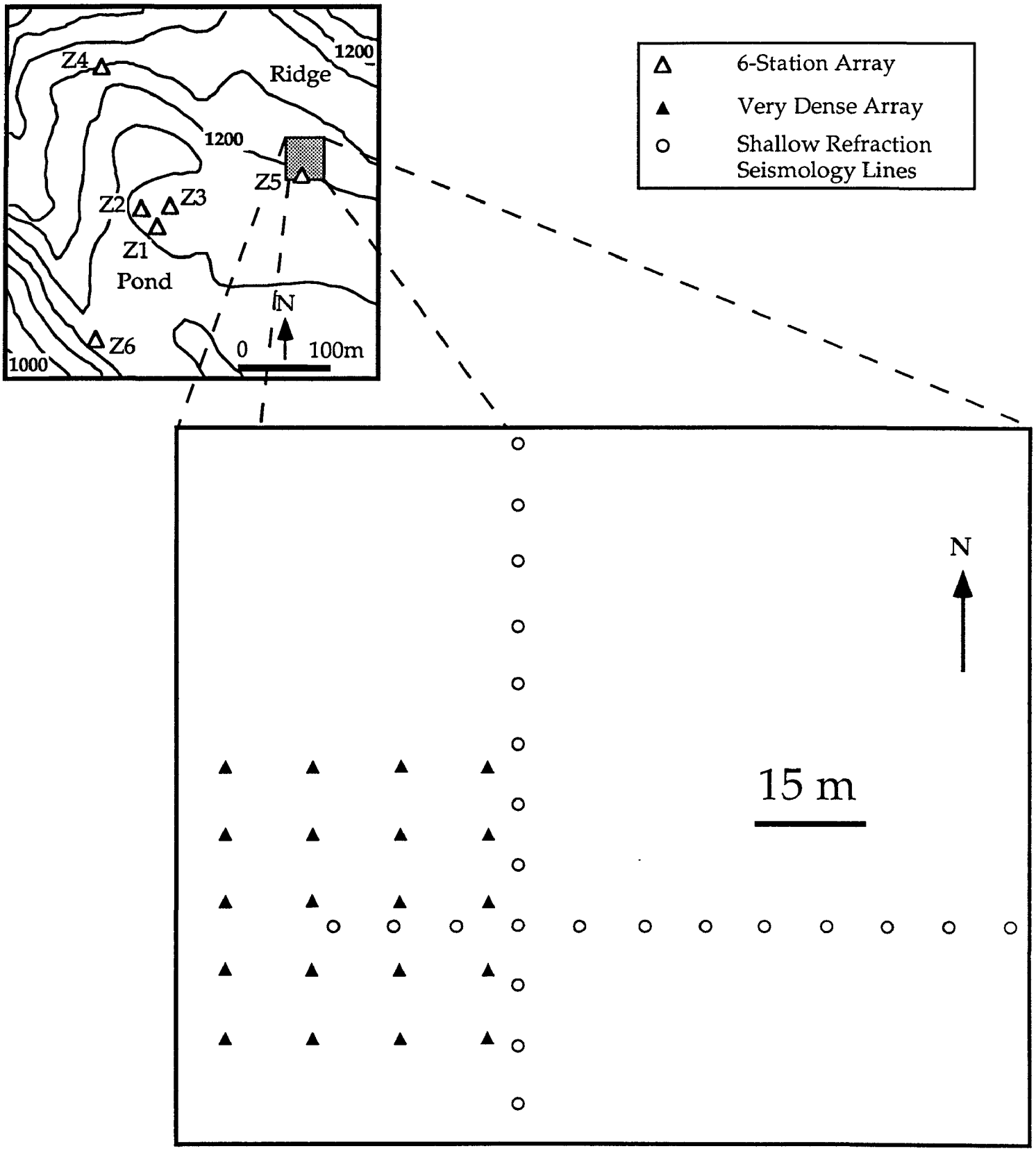

Fig.6 Map of the 6-station array, the very dense array, and the shallow refraction seismology lines deployed in the Santa Cruz Mountains.

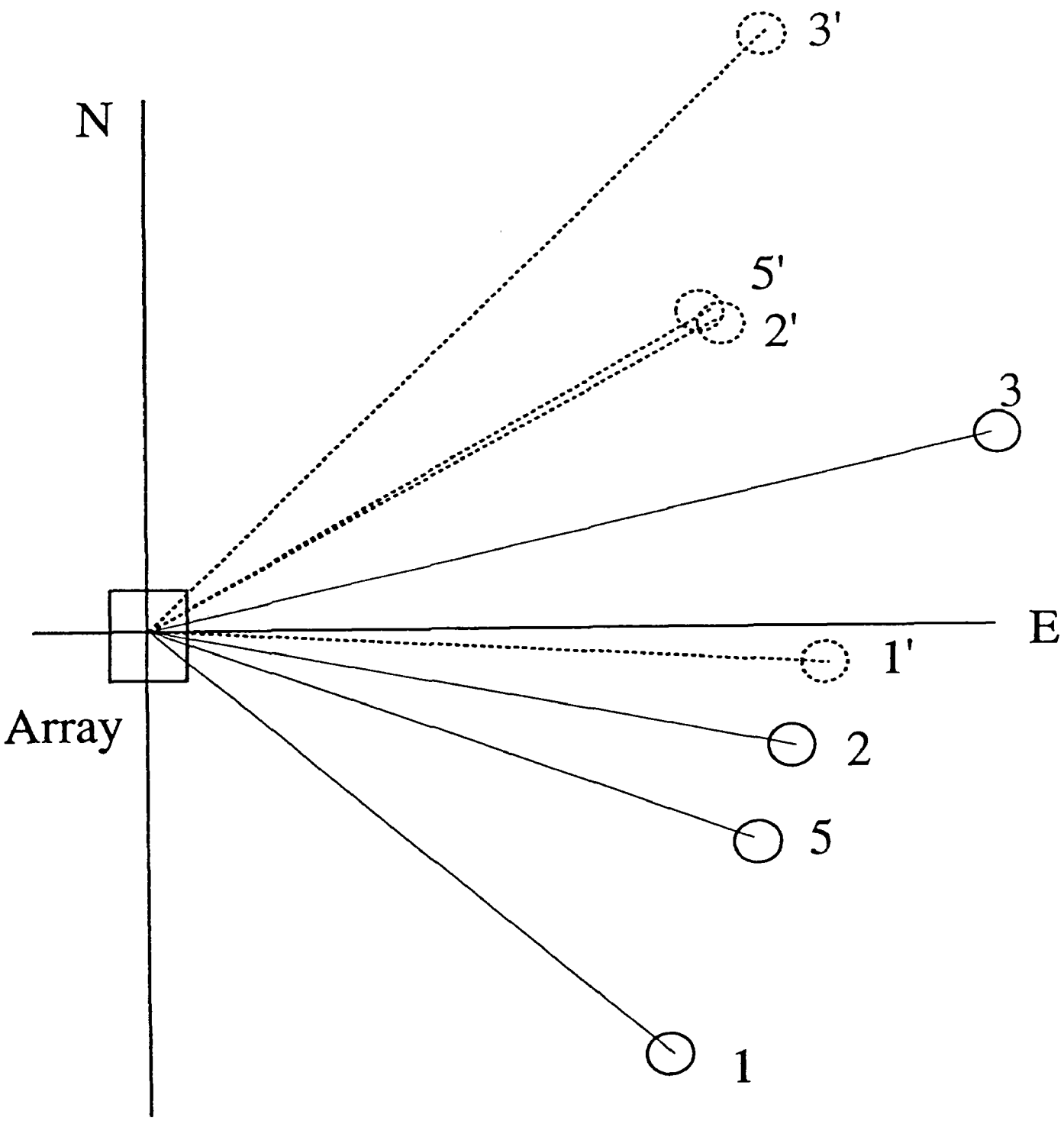

Fig. 7. Observed (dashed lines) and expected (solid lines) direction of back azimuth of the first P wave from 4 chemical explosions recorded at the dense ZAYA array. A systematic bias of 30-50° is observed for all 4 shots.

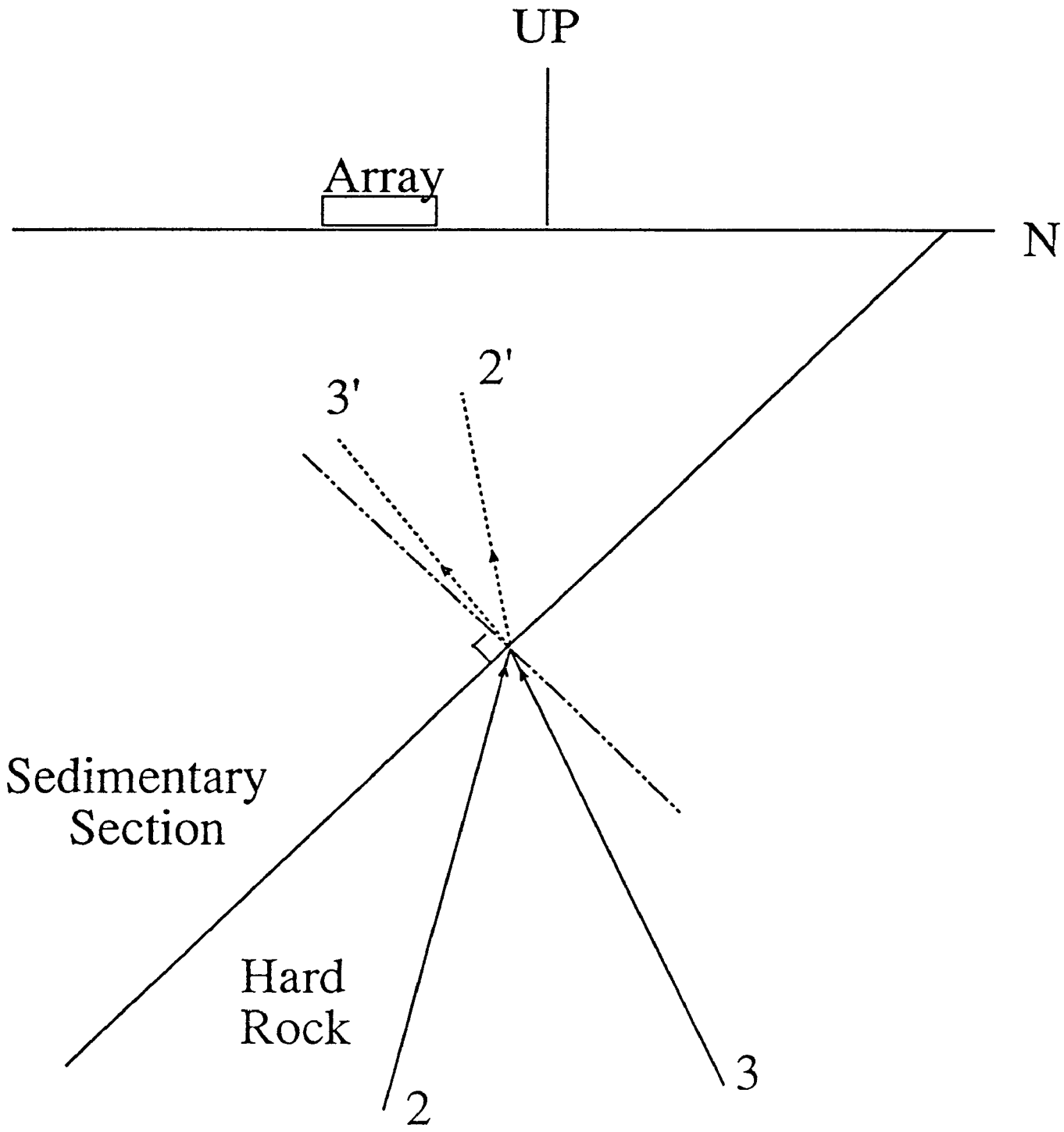

Fig. 8. Schematic cross-section of possible simple structure that may explain the systematic bias in back azimuth observations shown in Figure 7.

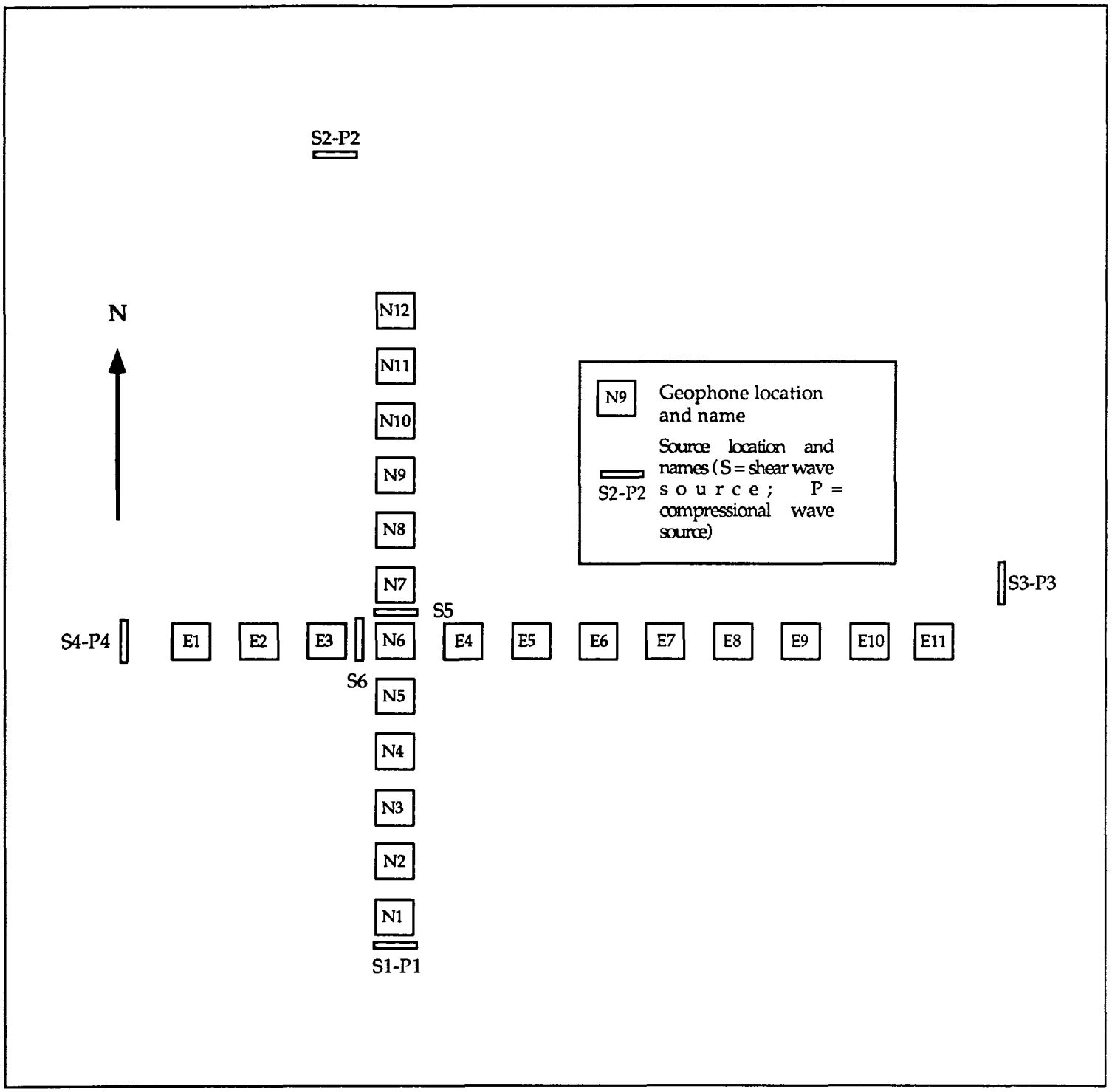

Fig. 9 Map of geophone and source geometries for refraction experiment. The map shows shear wave source locations and co-sited compressional wave sources. Compressional wave sources were also used at each geophone site (not shown).

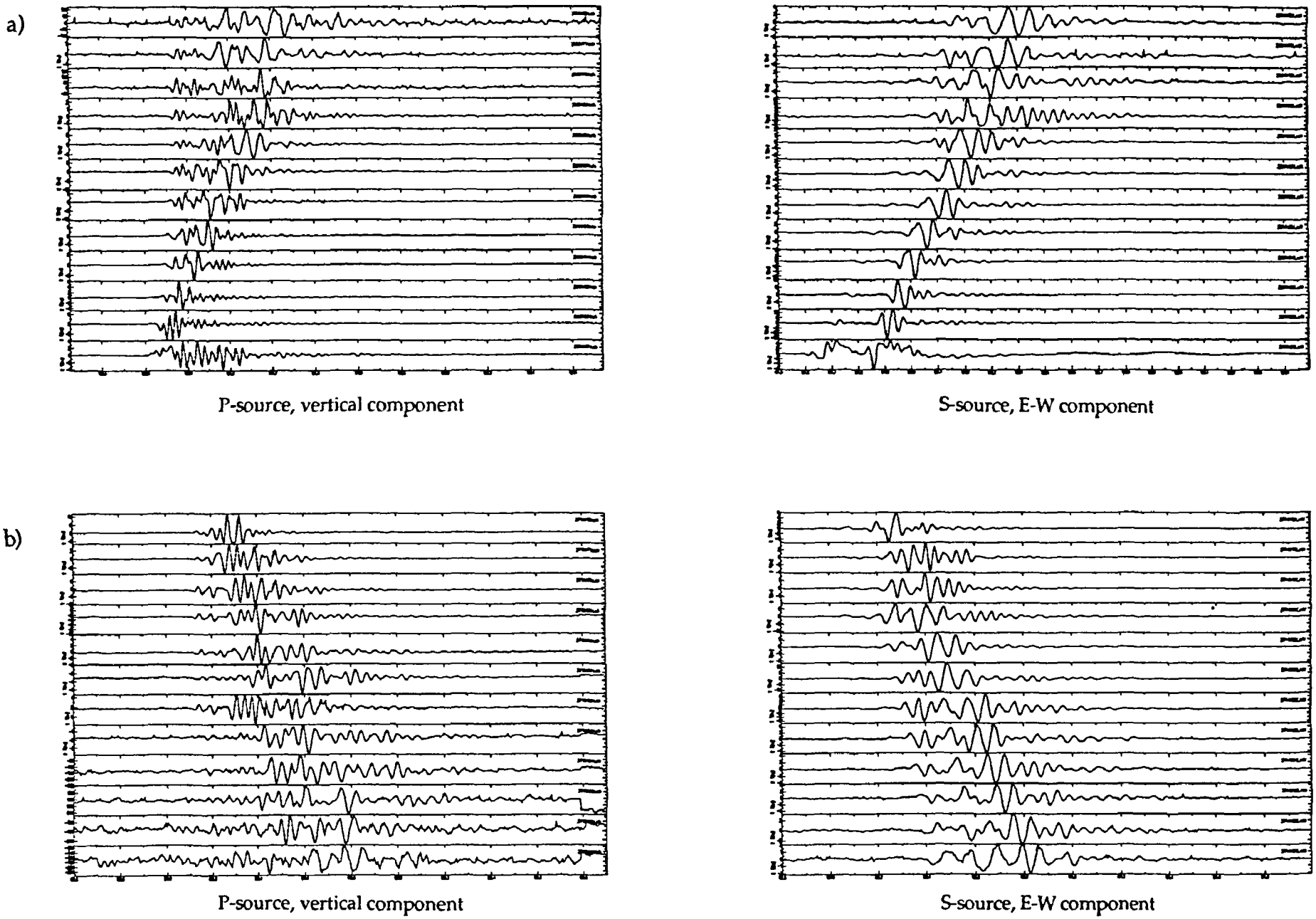

Fig. 10. Profile of normalized stacked signals recorded on the north-south line that lies along a topographic gradient. Sources are located at the south (a) and north (b) end of the line.

MECHANICS OF LITHOSPHERE PLATES

9960-03419

William D. Stuart and Ruth A. Harris
Branch of Tectonophysics
U. S. Geological Survey
Pasadena, California 91106
818 405-7816

Investigations

This project does theoretical analysis of earthquake faults. In FY92 we studied problems involving dynamic earthquake rupture across fault segments, static stress transfer to the San Andreas during the Landers earthquake sequence, interaction of large-scale tectonic plates, and precursory faulting at Parkfield.

2D and 3D Dynamic Rupture and Fault Segmentation

The magnitudes of most strike-slip earthquakes are controlled by their rupture lengths. Therefore if one could determine what controls the rupture length, one could determine the magnitude of a coming earthquake. The object of this study is to determine how fault geometry affects a propagating earthquake rupture. We specifically study 2D and 3D cases of parallel (non-collinear) strike-slip fault segments. The calculations simulate spontaneously propagating shear fractures. This work is with S. Day (SDSU).

Static Stress Changes from the June, 1992 Landers Earthquake Sequence

The goal of this study is to determine if coseismic slip of the Joshua Tree (M 6.1), Landers (M 7.5), and Big Bear (M 6.5) earthquakes loaded the nearby San Andreas fault closer to earthquake failure according to the Coulomb condition. The earth is represented by an elastic halfspace, and the appropriate stress components resolved on the San Andreas are calculated from static dislocation theory. This work is with R. Simpson.

Pacific-North America Plate Interaction

This work is an attempt to derive from mechanical principles the locations, slip rates, and lifetimes of major plate boundary faults in central and southern California since late Oligocene time. A special case is the present set of faults. The data most useful for testing the models for earlier times are measured offsets, rotations, and vertical motions of geologic units and crustal blocks. Results of this study may help explain average slip rates on modern seismically active faults, as well as apparent variations of brittle strength along strike.

Parkfield Precursors

A previously published model for earthquake instability at Parkfield has been modified to use the fault constitutive law developed by Dieterich, Kosloff, Liu, Ruina, Tse, and Rice. Instability models predict that precursory faulting occurs before the instability (mainshock). The anomalous fault slip causes ground deformation anomalies, which in some cases appear to be large enough to detect in field data before the mainshock. This work is with T. Tullis (Brown Univ.).

Results

2D and 3D Dynamic Rupture and Fault Segmentation

Two-dimensional finite-difference computer models were used to numerically simulate the interaction between an earthquake rupture and a geometrically segmented fault. Strike-slip earthquake ruptures are unlikely to jump across stepovers wider than 5 km. This conclusion assumes that the material in the stepover region is elastic, and that the faults do not merge at depth. When the effects of pore-pressure changes are included in the numerical simulations, changes in pore-pressure caused by a dynamically propagating earthquake rupture appear to inhibit an earthquake from jumping across dilational stepovers wider than 1 or 2 km. See Figure 1.

A 3D model for interaction between an earthquake rupture and a geometrically segmented fault was applied to the San Jacinto fault zone near Anza. Preliminary results for the Anza region suggest that if the dilational stepover at San Jacinto Valley is 4 km wide, and if the 1918 earthquake ruptured either the Claremont fault or the Casa Loma fault (both bound San Jacinto Valley), then the next Anza earthquake is unlikely to jump across San Jacinto Valley and rupture towards San Bernardino. The earthquake is unlikely to jump the step because the dynamic stress conditions will not be sufficient for failure.

Static Stress Changes from the June, 1992 Landers Earthquake Sequence

The Landers earthquake caused static normal stress changes of up to 10 bars on the San Bernardino segment of the San Andreas fault. These stress changes may have advanced the time of the next large earthquake on the San Bernardino segment of the San Andreas fault by 10–20 years. The location and mechanism of the Big Bear earthquake, which occurred 3 hours after Landers event, was consistent with loading by the coseismic Landers stress pulse.

Pacific-North America Plate Interaction

The plane–stress boundary value problem for several interacting plates has been posed and solved numerically. A plate may have any kind of boundary, i.e. transform, subduction, or ridge. Stresses are continuous across plate boundaries and satisfy a simple slip–rate dependent law. Displacement fields are continuous or discontinuous across plate boundaries, according to boundary type. Subducting plates have a fixed force representing slab pull. For the configuration of Pacific, North America, and Farallon plates in early to mid–Miocene time, and plausible assumptions of subduction pull, a southwest–northeast extensional stress field occurs in the part of the North America plate next to the Juan de

Fuca – Rivera transform boundary. This result could help explain the origin of eastern Mojave metamorphic core complexes.

A simplified version of the above model implies that the Garlock fault is caused, at least in part, by the stress concentration of the San Andreas bend near Gorman. Computed long term slip rate on the central Garlock is about 1/3 the San Andreas rate, in agreement with several reported field estimates.

Parkfield Precursors

Because the model simulates all stages of repeated earthquake cycles, one could in principle estimate values of model parameters (e.g. fault properties) using field data for a past stage and predict a future stage. At Parkfield we find that creep and trilateration data do not constrain model parameters well enough to predict the mainshock time with any useful precision. But if the next mainshock is assumed to have recurrence time and moment within the range of past values, predicted strain anomalies, as measured by extant borehole dilatometers and strainmeters, would be large enough to detect at least several weeks before the mainshock. Creep and trilateration precursors are too small to detect in this model, but were large enough to detect in a previous model based on a strain hardening and softening fault law. See Figure 2.

Reports

Banks, P. O., W. D. Stuart, and S. -W. Liu, Piezomagnetic fields of screw dislocation fault models, *Jour. Geophys. Res.*, *96*, 21,575–21,582, 1991.

Banks, P. O., W. D. Stuart, and Y. Sasai, Theoretical piezomagnetic field at Parkfield, (abstr.), *Eos Trans. AGU*, *73*, 397, 1992.

Eberhart–Philips, D., and W. D. Stuart, Material heterogeneity simplifies the picture: Loma Prieta, *Bull. Seismol. Soc. Am.*, *82*, 1964–1968, 1992.

Harris, R. A., Dynamic interaction of parallel strike-slip fault segment: some implications for the San Francisco Bay area, in Borchardt, G., et al., eds., *Proceedings of the Second East Bay Conference on Earthquake Hazards, CDMG Special Publication*, in press, 1992.

Harris, R. A., and S. M. Day, Dynamics of fault interaction: parallel strike–slip faults, *J. Geophys. Res.*, in press, 1992.

Harris, R. A., and R. W. Simpson, Static stress changes in southern California after the 1992 Landers earthquake (abstr.), *EOS Trans. AGU*, *73*, 373, 1992.

Harris, R. A., S. M. Day, and T. K. Rockwell, A 3-D dynamic rupture model of fault segmentation - with applications to the next Anza Gap earthquake (abstr.), *EOS Trans. AGU*, *73*, 389, 1992.

Harris, R. A., T. K. Rockwell, and S. M. Day, A 3-D dynamic rupture model for the next Anza Gap earthquake, (abstr.), *Seism. Res. Lett.*, *63*, 23, 1992.

Iyer, H. M., J. R. Evans, P. B. Dawson, and R. A. Harris, Seismic tomography of volcanic regions and individual volcanoes in western United States (abstr.), *Proceedings of the 29th International Geological Congress, Kyoto, Japan, 24 August - 3 September, 667*, 1992.

Roeloffs, E., and R. Harris, What will stop the next Parkfield earthquake? (abstr.), *EOS Trans. AGU*, *73*, 407, 1992.

Simpson, R. W., and R. A. Harris, Estimates of ongoing stress redistribution on southern California faults after the Landers earthquake (abstr.), *EOS Trans. AGU*, *73*, 373, 1992.

Stuart, W. D., Cause of the Garlock fault (abstr.), *GSA Abstracts with Programs*, *23(5)*, 198, 1991.

Stuart, W. D., Plate–induced Miocene extension in southern Calfornia (abstr.), *GSA Abstracts with Programs*, *24(7)*, 279, 1992.

Stuart, W. D., and T. E. Tullis, Instabilty model for repeated $M_W = 6$ earthquakes, (abstr.), *Eos Trans. AGU*, *73*, 406, 1992.

Tullis, T. E., and W. D. Stuart, Premonitory changes prior to a model Parkfield earthquake (abstr.), *Eos Trans. AGU*, *73*, 397, 1992.

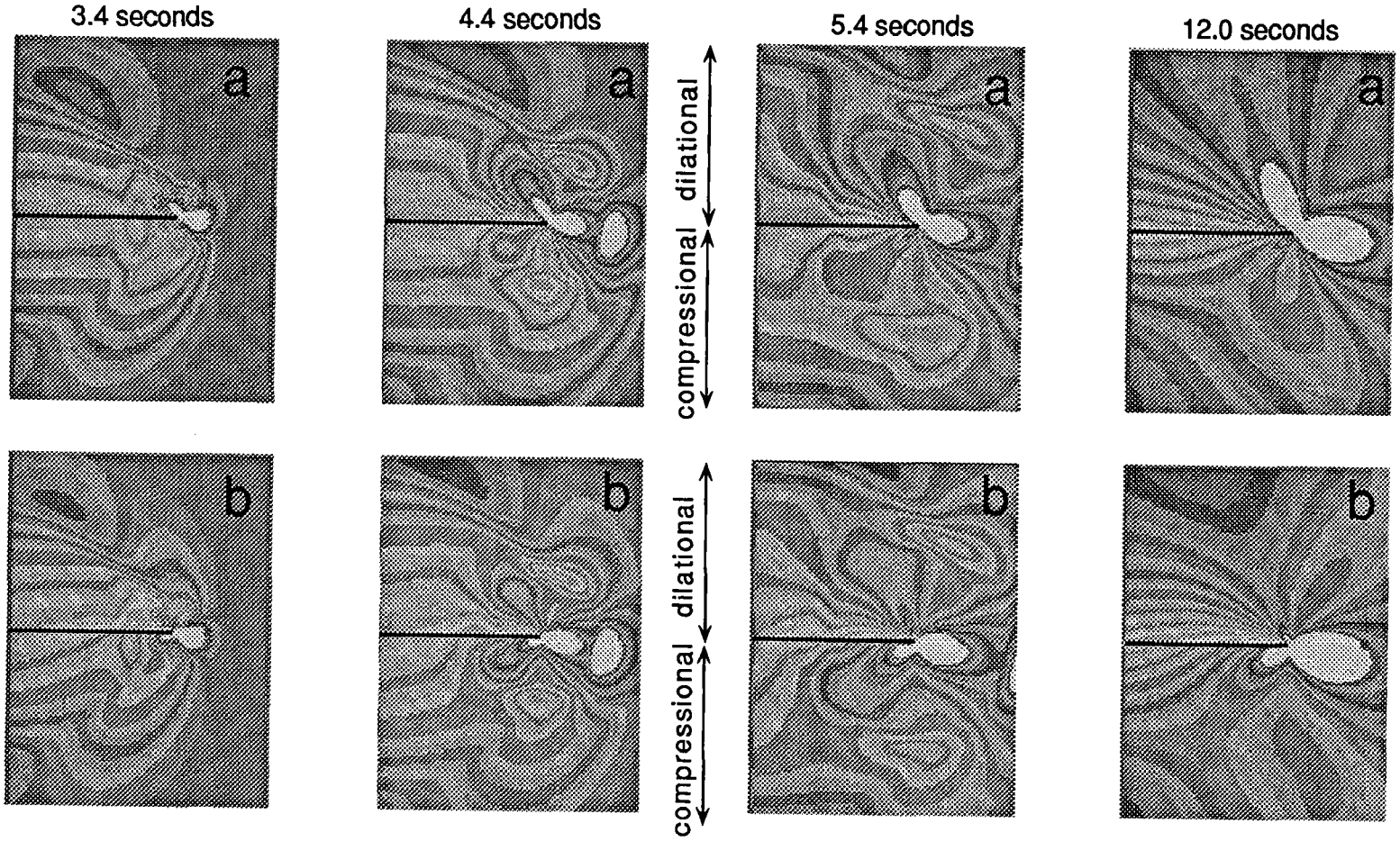

Figure 1. Two-dimensional failure stress for dynamically propagating ruptures [from *Harris and Day*, J. Geophys. Res., in press, 1992]. Case A assumes a 'dry' elastic medium and neglects the effects of changes in pore-fluid pressure, whereas case B includes the effects of pore fluid. For both cases, the dark line shows the location of the left-lateral strike-slip fault (shear crack), along which the rupture initially propagates. It takes the rupture 2.9 seconds to first reach the end of the fault. The light pattern shows where the rupture could jump to a second parallel fault segment, with regions above the dark line indicating locations of potential dilational stepovers, and regions below the dark line indicating locations of potential compressional stepovers. (a) This case assumes that the elastic medium between the two faults is 'dry', and ignores the effects of the dynamically propagating earthquake rupture on the pore fluids in the stepover region. The result is that wider dilational than compressional steps can be jumped, and that it takes longer to jump dilational steps than compressional steps (as can be observed by the time-dependent failure stress). (b) This case assumes that the elastic medium in the stepover region also contains 'undrained' pore fluids which are affected by the dynamically propagating rupture. The result is that the pore-pressure changes appear to inhibit jumps across dilational stepovers. The compressional stepovers appear to be relatively unaffected.

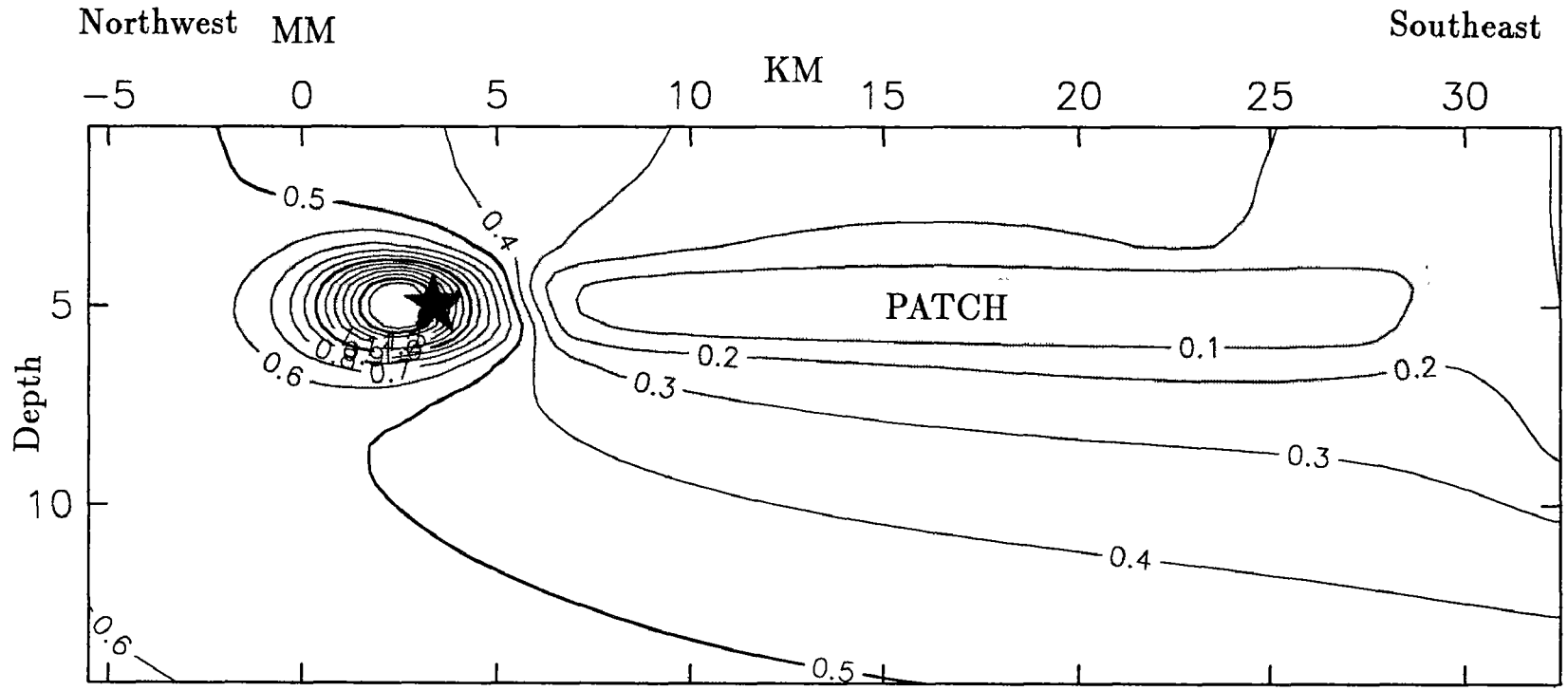

Figure 2. Accelerated preseismic slip on the San Andreas fault near Parkfield. Contours show fault slip velocity V scaled by plate slip rate $V_P = 35$ mm/yr at 0.1 yr before the model earthquake (instability). Anomalous slip rate $V/V_P > 0.5$ occurs near Middle Mt. (MM) and the theoretical focus (star). The anomalous slip rate increases with time and causes strain anomalies near the ground surface. The shaded area is a fault patch which fails before and during the mainshock.

INDUCED SEISMICITY AT BAD CREEK, SOUTH CAROLINA

1434-92-G-2199

Pradeep Talwani
Department of Geological Sciences
University of South Carolina
Columbia, South Carolina 29208
(803) 777-6449

INVESTIGATIONS:

(a) Field Studies: Monitoring of seismicity around Bad Creek Reservoir and Lakes Jocassee and Keowee was continued. Permanent stations were installed at JVW and CCK. Data from these and the Duke Power Company stations at BC, SMT, BG3 and MMC are collected at the Jocassee Dam (Fig. 1) and telemetered to USC, Columbia. These data are recorded digitally in an event triggered mode on a Puffin, and in an analog form on a tape recorder and on two Helicorders. The water levels at these lakes and Bad Creek Reservoir are monitored continuously as well as in the observation well OW3. OW3 is located about 1,000 feet (300m) from the reservoir and is open to a shear zone at a depth of 290 feet (88m) below the surface. The distance from the reservoir to the well along the shear zone is about 1,100 feet (335m).

(b) Modeling: (i) In view of the availability of detailed seismicity, groundwater, geological and in situ stress data at Monticello Reservoir, it was possible to study the role of elastic, undrained and drained responses in triggering earthquakes.

(ii) An analytical solution for the two-dimensional case of Biot's formulation for fluid infiltrated materials was developed. The model, similar to that of Roeloffs (1988) considers the changes produced in the environment of a reservoir due to a cyclic load. The mathematical solution was achieved by finding the eigenvalues and eigenvectors of the transformed system of equations expressed as function of stresses and pore pressure.

RESULTS:

The preliminary results of these investigations are summarized below.

(a) Groundwater Monitoring: Comparison of the water levels in OW3 and Bad Creek Reservoir (pool) following initial filling showed a systematic lag of about 80 hours. However, in 1992, there was a greater delay. Figure 2 shows a comparison of

pool and OW3 water levels for the period June 15 to August 29, 1992. The OW3 levels have been plotted on an enlarged scale to emphasize the similarity between the two curves. Cross correlation of the two time series showed that a lag of 98 hours fit the data well. In Figure 3 the pool levels have been shifted 98 hours. The two curves match rather well. These data imply a hydraulic diffusivity of about 3.2 x 10^3 cm^2/s. This value is towards the low end of diffusivity values found by Talwani and Acree (1984) for cases of reservoir induced seismicity.

The large fluctuations that were anticipated when the dam was built have not been realized so far. Compared to the largest drawdown possible (~100m) water level changes have not exceeded about 30m. The small change and the small volume of the reservoir are probable reasons why we have not observed an abrupt increase in seismicity.

(b) Seismicity Monitoring: Most of the events recorded near Bad Creek are small (magnitude <0.0). However, we are continuing to monitor both the lake levels and seismicity in anticipation of changed conditions.

(c) Modeling Studies: (i) The results of an analysis of seismicity that occurred following the impoundment of Monticello Reservoir were published recently (August, 1992 BSSA). They suggest that, during the filling period, the instability resulted from elastic, undrained, and possibly the onset of drained response. Subsequently, the seismicity showed a more consistent pattern associated with diffusion of pore pressure.

(ii) The 2D model was used to find the largest change in strength for different stress regimes. Variations in change in strength with different physical parameters (Skempton's constant, hydraulic diffusivity, Poisson's ratio and frequency of lake level change) affected not only the magnitude but also the spatial distribution of weakened regions. The largest changes were found to occur near the edge of the reservoir.

REPORTS PUBLISHED:

Kusala Rajendran and Pradeep Talwani, The role of elastic, undrained, and drained response in triggering earthquakes at Monticello Reservoir, South Carolina, **Bull. Seis. Soc. Am.**, 82, 1867-1888, 1992.

Roberto G. Ruiz, Mathematical modeling and monitoring of pore pressure in fractured crystalline-rock following reservoir filling. Masters Thesis, Department of Civil Engineering, University of South Carolina, Columbia, 108 & vi pp, 1992.

Pradeep Talwani, Kusala Rajendran, Roberto Ruiz and John Dickerson, On the mechanism of reservoir induced seismicity, presented at Workshop on Induced Seismicity, **33rd US Symposium on Rock Mechanics**, p 179, June 1992.

K. Rajendran, P. Talwani and E. Roeloffs, Do elastic models explain reservoir induced seismicity? (abstract), EOS Trans. AGU, 73(43), Fall Meeting Suppl., 405, 1992.

Pradeep Talwani, Roberto Ruiz, John Dickerson and K. Rajendran. Temporal pattern of reservoir induced seismicity. (abstract), EOS Trans. AGU, 73(43), Fall Meeting Suppl., 405, 1992.

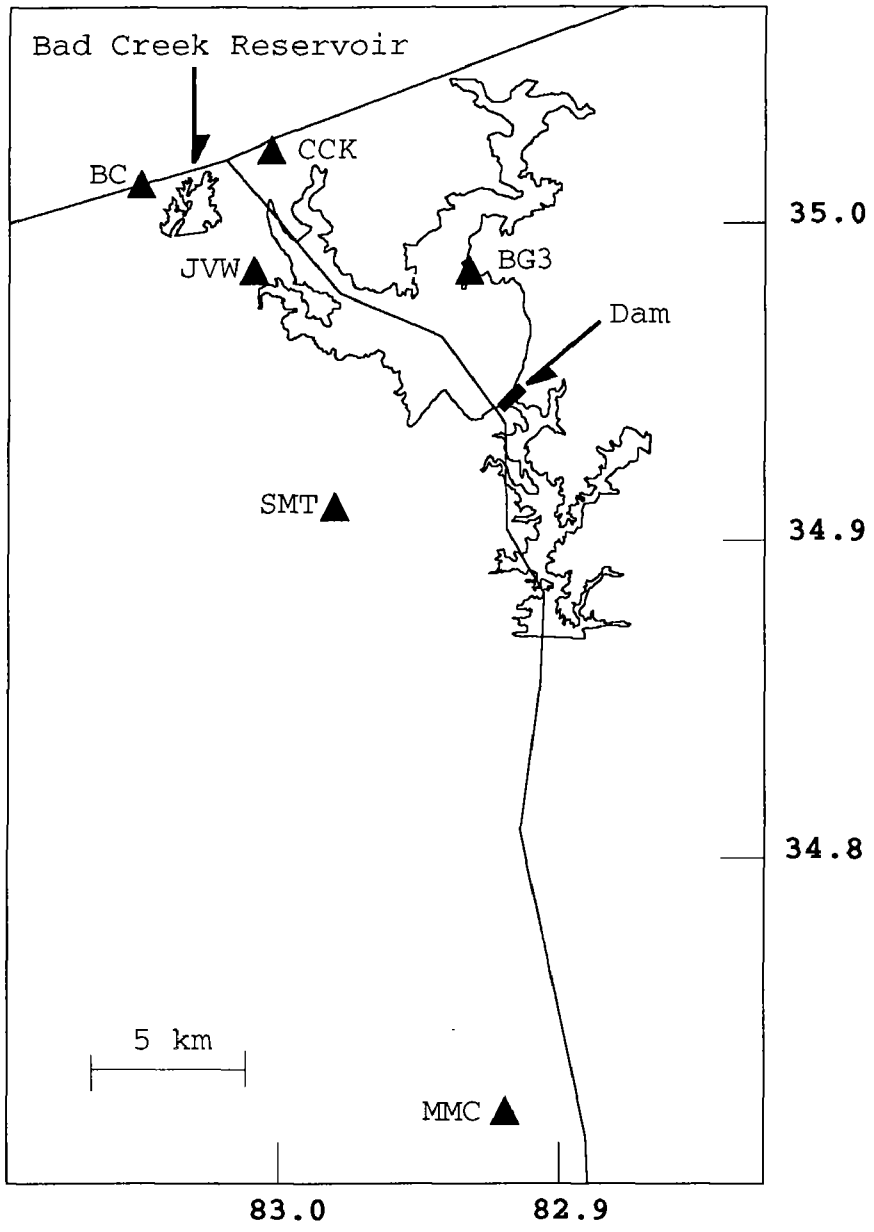

Fig.1 Locations of seismic stations near Bad Creek reservoir and Lake Jocassee. Data are collected at the Jocassee Hydro Dam and telemetered to USC.

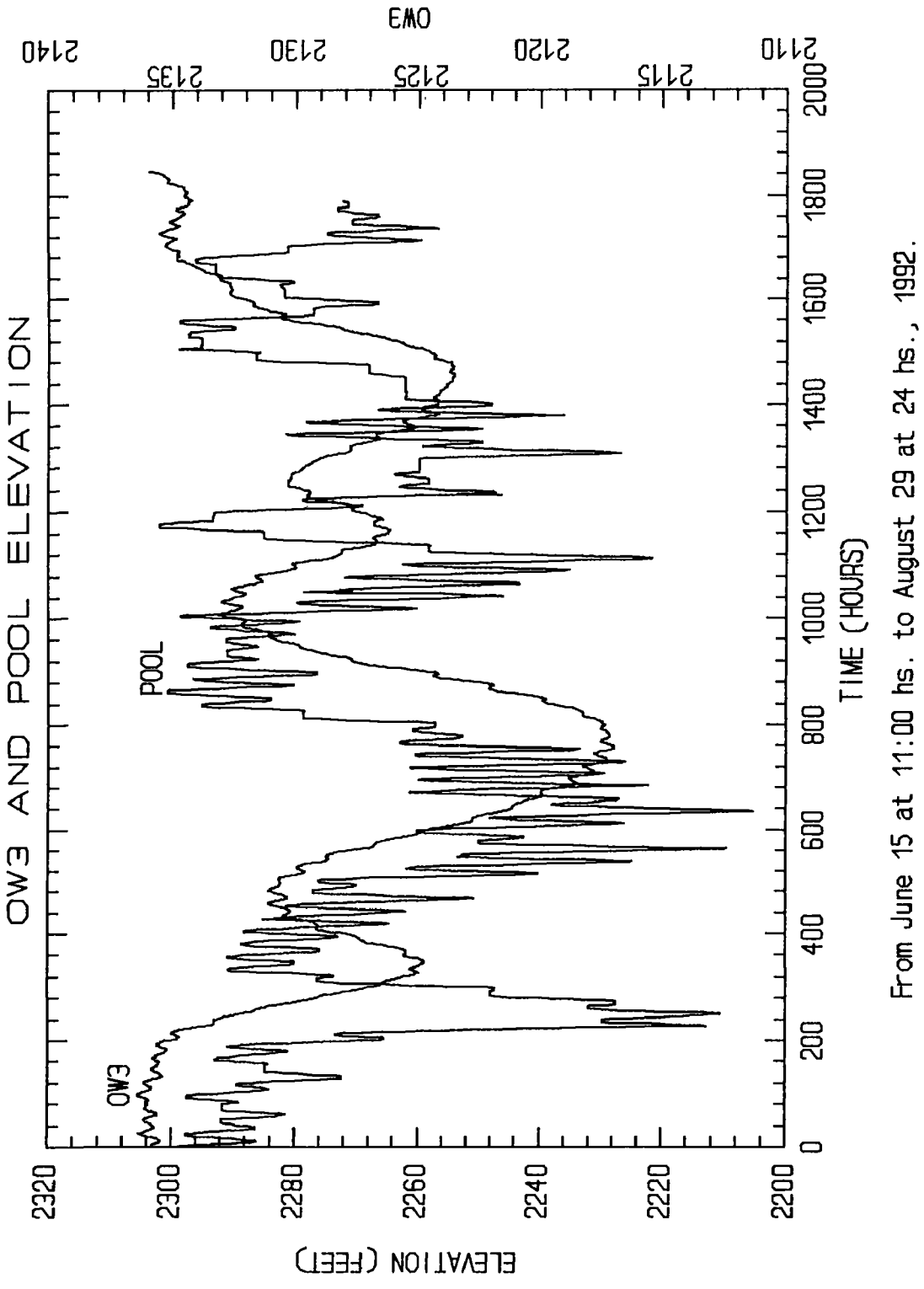

Figure 2. Water level in the pool and observation well OW3 for the period indicated. Note the difference in scale.

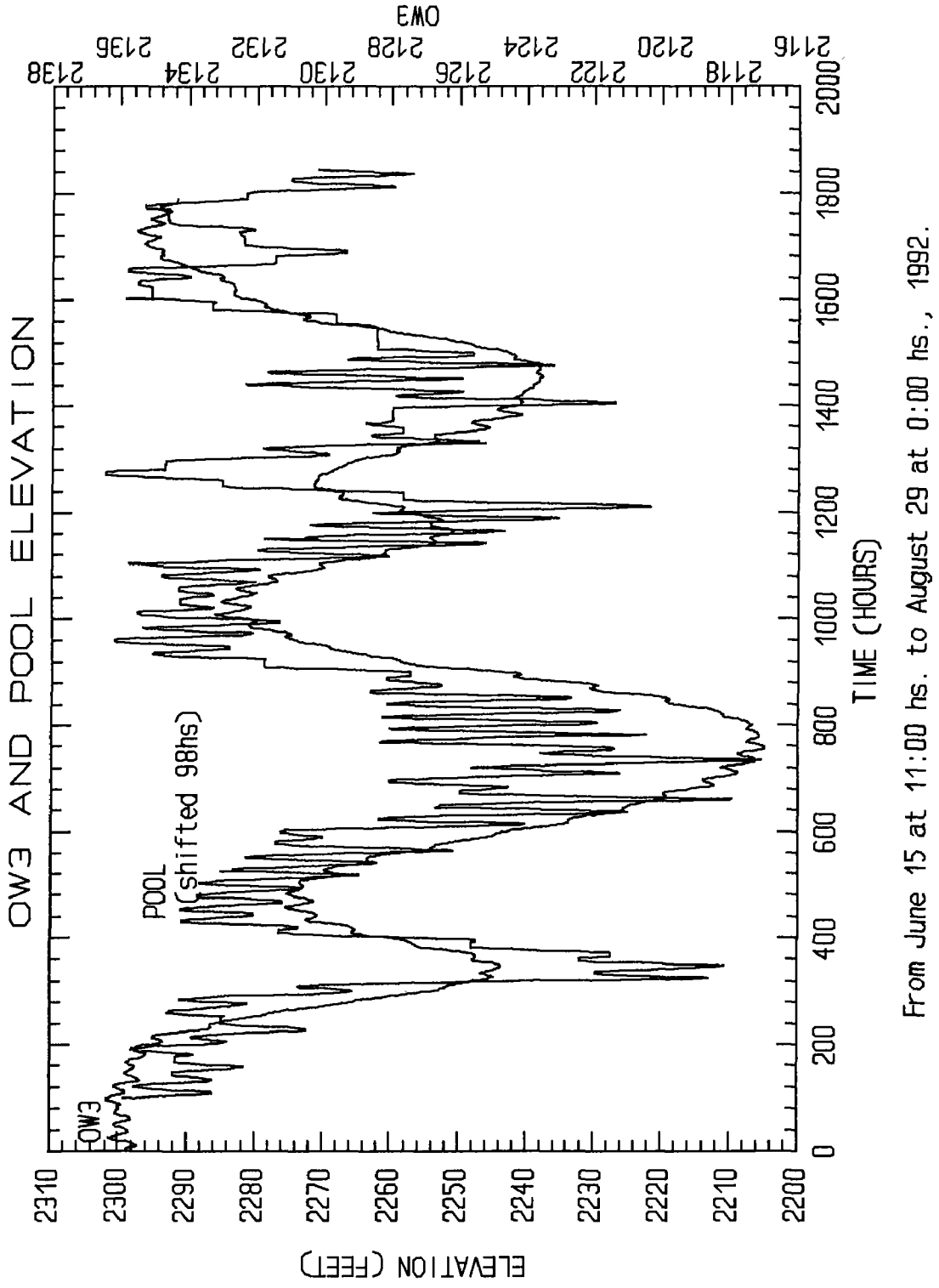

Figure 3. Same data as shown in Figure 2 with values for lake shifted 98 hours.

Earthquake Hazard Research in the Greater Los Angeles Basin and Its Offshore Area

Agreement # 14-08-0001-A0620

Ta-liang Teng and Thomas L. Henyey
Center of Earth Sciences
University of Southern California
Los Angeles, CA 90089-0740

BRIEF DESCRIPTION: This research is conducted in the Los Angeles metropolitan and offshore areas where urban centers of high population density coexists with high earthquake hazards. A special purpose seismic network has been established and has been in operation for the past 20 years. Against the noisy urban background, this network achieves its objective through deployment of both downhole and surface seismometers, through a diligent field instrument maintenance program, and through up-to-date data processing. Presently, the Los Angeles basin seismic network recording center at U.S.C. digitizes 70 channels of telemetered data from on land (surface and downhole) and offshore stations. This network is an important part of the research activity coordinated by the Southern California Earthquake Center (SCEC).

RESULTS OBTAINED: We have concentrated on advanced seismotectonic analysis based on data recorded by the network. This analysis goes beyond the conventional study of spatial and temporal distribution of seismic events. Shear-wave splitting and seismic waveform inversion are conducted using the network output for mapping of regional stress and source characteristics. A seismic database established for the Los Angeles basin is shown in Figure 1 (for the reporting year) and Figure 2 (for the period 1973 - 1992). Figure 3 shows the frequency of earthquake occurrence in the network coverage area. Clearly, 1991 is dominated by the occurrence of the mid-June M = 5.8 Sierra Madre earthquake and its aftershocks. Comprehensive studies have been continued on: S-wave splitting analysis; analysis of 3-D distribution of earthquakes along fault zones; seismotectonics of the Los Angeles basin; inversion analysis on the propagating fault rupture; site response and near-surface Q-values; and seismic response of a 2-D and 3-D sedimentary basin.

Recent improvements to the U.S.C. Los Angeles Basin Seismic Network (LABNET) consist of (1) operation of the PC-based backup recording system (16-bit 64-channel and expandable to 256 channels); (2) installation of the second generation of OTS (gain-ranging microprocessor-based telemetry) designed and constructed at USC to achieve an effective telemetry dynamic range of 120 dB; and (3) development and test the idea of neural network for intelligent event triggering in an urban environment and automation in seismic data processing.

Recent occurrences of the 1987 Whittier Narrows earthquake and the 1991 Sierra Madre earthquake present new views of the local seismotectonics. We have come to realize that:

1. Moderate-sized earthquakes do occur along faults previously deemed inactive, they do not necessarily occur along well-mapped universally recognized active fault strands.

2. These moderate-sized earthquakes have demonstrated that they are fully capable of producing higher than 0.5 g strong ground motion to the Los Angeles metropolitan area and can be very destructive.

3. These events are often located in the basement rocks beneath warps and uplifts in the overlying sedimentary section, which are common in the Los Angeles basin.

4. The Whittier Narrows earthquake occurred beneath a zone of uplifts stretching from Whittier, through downtown, to Malibu; these faults are collectively called the Elysian Park fault system. Other such zones may exist in the San Fernando Valley and South Bay area of Los Angeles

5. These kinds of earthquakes and their causal fault structures have not been adequately incorporated into earthquake hazards assessments for the Los Angeles area. For example, "design" earthquakes typically deal only with events on the San Andreas and the Newport-Inglewood faults.

RECENT RESESARCH FINDINGS:

Shear Wave Splitting and Stress Distribution in the Los Angeles Basin: On-scale short-period seismograms of numerous events of magnitudes between 2 - 4 from the portable RefTek recordings, from SCS array and from other field stations equipped with OTS telemetry are examined. Clear evidence of shear-wave splitting of 10-130 ms is found that implies a nearly NS regional compressional stress field. This finding is consistent with results from geological mapping and fault plane solutions. Furthermore, an inferred crack density of the crystalline basement is obtained. The quality of the on-scale seismic data from LABNET that makes this study possible(Figure 3).

Waveform Analysis: We are developing methodology that makes full use of waveform data from the LABNET with clear purpose of carrying out several significant scientific experiments. Short-period data is rich in information content and high in resolution when applied to the delineation of subsurface structures. However, the short-period waveforms can quickly lose their coherence in a complex medium where, beyond a certain frequency, a wavefield governed by a scattering process would then take over. The methodology we are working on spans a transition region between a deterministic approach where signals can be modeled as coherent propagating energy packets and a probabilistic approach where only the collective properties of the wavefield can be studied in a statistical sense.The frequency range of the transition region is probably covered by the band from 1 to 20 Hz -- a range that is mainly the operational band of current microearthquake networks. With large dynamic range and 3-component calibrated and matched seismic data provided by the OTS system, we plan to carry out a much more accurate study on coda waves. Moreover, we wish to explore the short-period limit on the applicability of waveform analysis and particle motion study that can only be performed over the coherent part of the signals. Available data from the LABNET are on-scale, matched 3-component, digital data from sources distributed throughout the Los Angeles basin and its offshore area. Different path combinations include paths through crystalline rocks, through basin sediments, and paths that traverse practically entirely inside a fault zone. The path differences are clearly manifested in the form of waveform differences.

REPORTS PUBLISHED

Li. Y.G., T.L. Teng, and T.L. Henyey, (1991) Shear-wave splitting observations and implications for the stress regime in the Los Angeles basin, Southern California, accepted with revision, Bull. Seism. Soc. Am.

Zeng, Y., K. Aki, and T.L. Teng, (1992) Mapping of high frequency source radiation for the Loma Prieta earthquake, California, Submitted to J. Geophys. Res.

Zeng, Y., K. Aki, and T.L. Teng, (1992) Source inversion of the 1989 Loma Prieta earthquake, California using isochron method, Submitted to Geophys. Res. Letters.

Zeng, Y., K. Aki, and T.L. Teng, (1992) Source inversion of the 1987 Whittier-Narrows earthquake, California using isochron method, Submitted to Bull. Seism. Soc. Am.

Chiu, H.C., Teng, T.L. , and Wong, H.L.(1991) Scattering effects on SH waves due to an irregular structure:A case at the SMART-1 Array site, Proceeding of the Geological Society of China, 34, 2, pp. 91-1110.

Su, F.,Aki, T., Teng, T.L., Zeng, Y., Koyonagi, S, and Mayeda, K. (1992) The Relation between site amplification factor and surficial geology in Central California, Bull. Seismol. Soc. Am., 82, No. 2, 580-602.

Wang, J. and T. L. Teng, (1992) Neural network-based detector for seismic triggering and P-picking, EOS, Trans. Am. Geophys. Union, 73

Teng, T.L., J. Qu, and J. Wang (1992) Propagation of surface waves in a 3-D basin, EOS, Trans. Am. Geophys. Union, 73

Qu, J. and T. L. Teng (1992) A constrained non-linear least squares method in the studies of seismic source, EOS, Trans. Am. Geophys. Union, 73

Li, Y.G. and T. L. Teng (1992) Seismic trapped waves along the San Jacinto fault at Anza, EOS, Trans. Am. Geophys. Union, 73

Li, Y.G., T.L. Teng and T.L. Henyey (1992) Shear-wave splitting in the Los Angeles basin, EOS, Trans. Am. Geophys. Union, 73

Henyey, T.L., Y.G. Li and T.L. Teng (1992) Observations of shear-wave splitting in source areas of 1992 Joshua Tree and Big Bear earthquakes, EOS, Trans. Am. Geophys. Union, 73

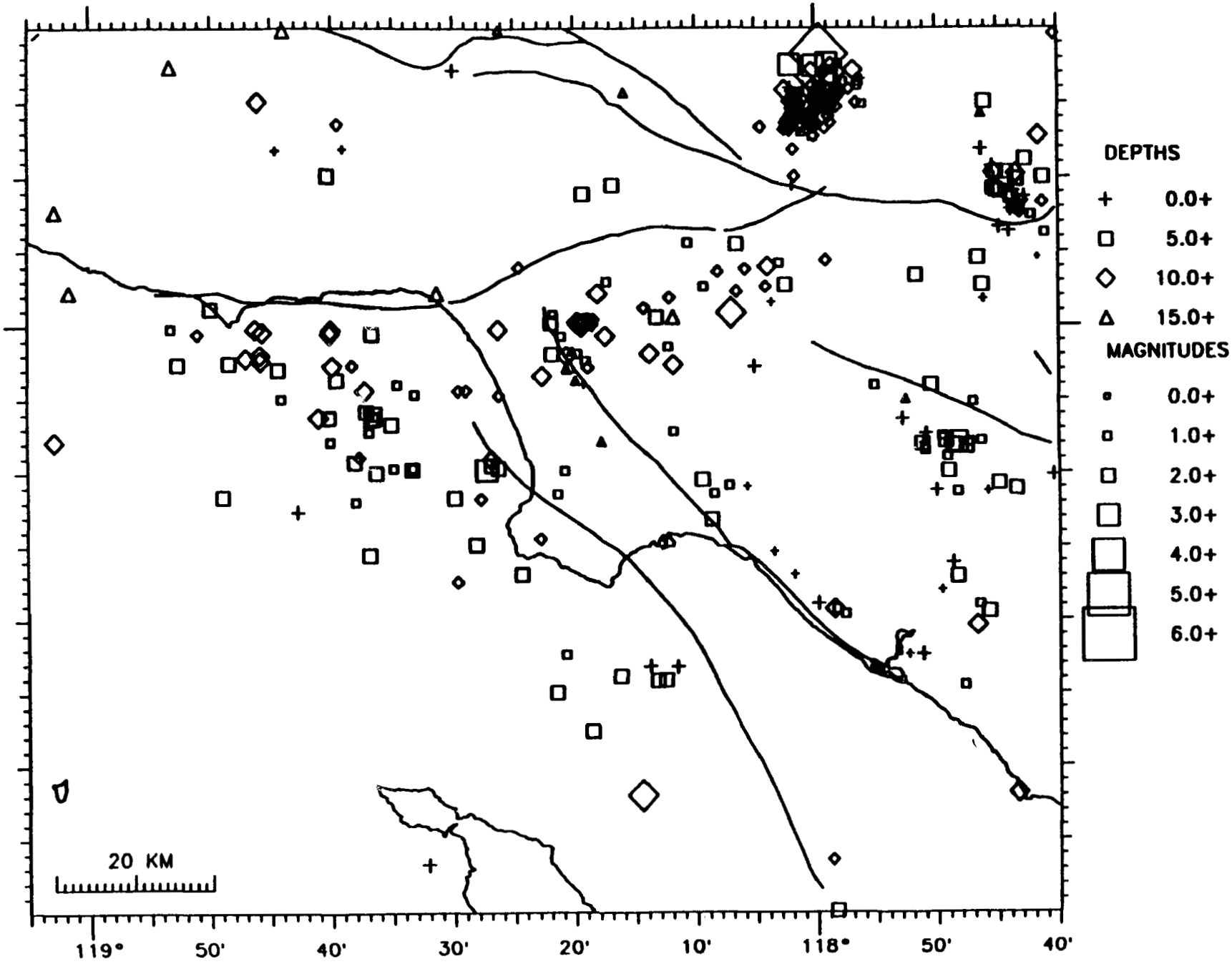
LOS ANGELES BASIN EARTHQUAKES
January – December 1991
DEPTHS
0.0+
5.0+
10.0+
15.0+
MAGNITUDES
0.0+
1.0+
2.0+
3.0+
4.0+
5.0+
6.0+
20 KM
10'
34°
50'
40'
30'
119°
50'
40'
30'
20'
10'
118°
50'
40'

Figure 1

Figure 2

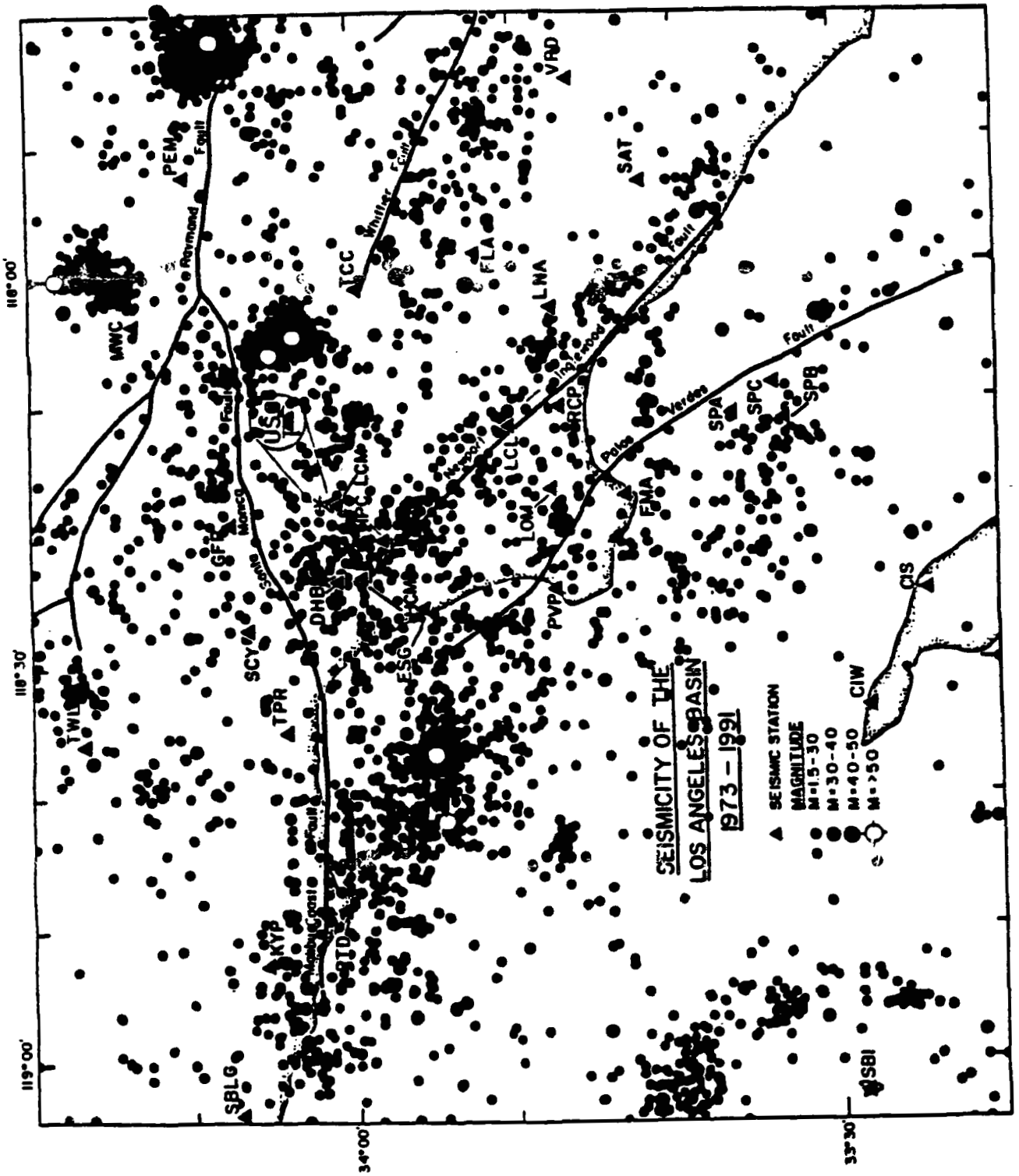
SEISMICITY OF THE
LOS ANGELES BASIN
1973 – 1991
SEISMIC STATION
MAGNITUDE
M 1.5-3.0
M 3.0-4.0
M 4.0-5.0
M > 5.0
PEM
MWC
ICC
VRD
SAT
FLA
LNA
TWI
SCY
GFT
DHB
LCM
ESG
LCL
LOW
PVP
RCP
FMA
SPA
SPC
SPB
CIW
CIS
TPR
KYB
SBLG
SBI
Raymond Fault
Whittier Fault
Newport-Inglewood Fault
Palos Verdes Fault
Santa Monica Fault
Hollywood Fault
Malibu Coast Fault
Sierra Madre Fault
Verdugo Fault
118°00'
118°30'
119°00'
34°00'
33°30'

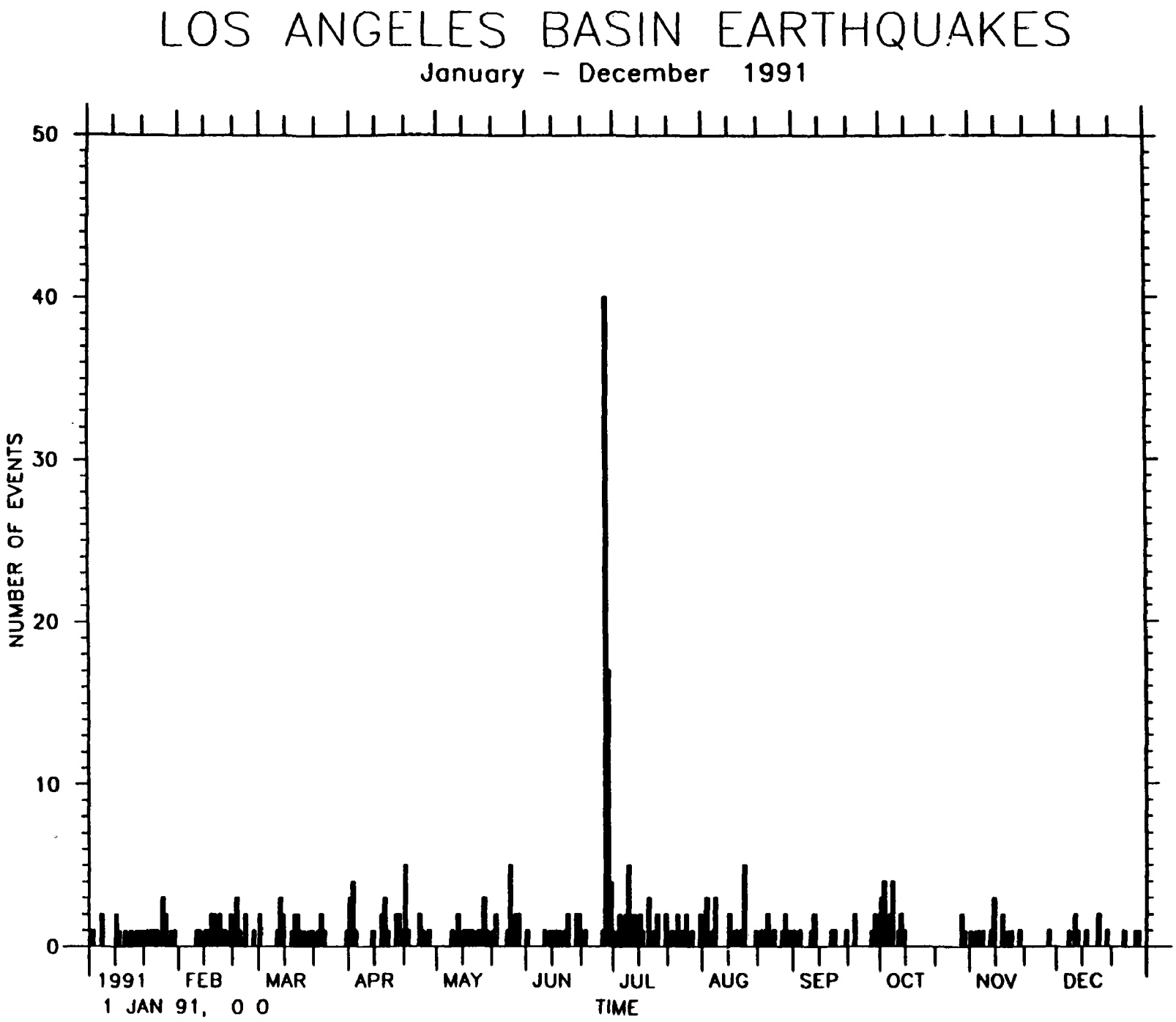
LOS ANGELES BASIN EARTHQUAKES
January – December 1991
NUMBER OF EVENTS
50
40
30
20
10
0
1991 FEB MAR APR MAY JUN JUL AUG SEP OCT NOV DEC
1 JAN 91, 0 0
TIME

137

Figure 3

The New England Seismic Network (Operated Collaboratively by M.I.T. and Boston College)

Contract no. 1434-92-A-0974

M. Nafi Toksöz
Massachusetts Institute of Technology
Earth Resources Laboratory
42 Carleton Street
Cambridge, Massachusetts 02142
(617)-253-7852

Investigations

The Earth Resources Lab at M.I.T. continues to maintain and operate the M.I.T. Seismic Network as part of the forty station New England Seismic Network under a collaborative arrangement with Weston Observatory of Boston College. The M.I.T. Seismic Network consists of nine digitally recorded short-period stations located in central and southern New Hampshire and eastern Massachusetts. Data from these stations are routinely analyzed to provide hypocentral, origin time and magnitude information for local earthquakes. Quarterly earthquake bulletins are published and available for the period October 1979 - March 1992. Figure 1 gives the station locations and seismicity for the reporting period January 1, 1992 - October 10, 1992. Two current research projects are focused on earthquake activity in central New Hampshire. One involves the relocation of earthquakes in that region, using a waveform correlation method, to search for significant changes in the spatial distribution of seismicity which might correlate with geologic structures. The second employs event pairs having similar hypocenters and focal mechanisms to estimate a source time function for the larger event. The source time function information can be used to study source parameters and the rupture process for the event.

Network Operations

The entire digital data archive (1980 to the present) is in the process of being converted to SAC binary format. The data will be archived on exabyte tape cartridges using the TAR tape facility to provide

convenient access for researchers at M.I.T. as well as other universities. In addition, an FTP anonymous account has been set up to provide on-line access to the most recent one year of digital waveforms and phase data files for local earthquakes. Details on accessing this account can be obtained by contacting Charles Doll at 617-253-7863 or doll@erl.mit.edu. The waveforms are in SAC binary format. These improvements will facilitate the transfer and analysis of seismic data between M.I.T. and Boston College using SAC, and will make the data available in a standard format used by many other institutions. To date, the procedure to download local earthquake data from our PC acquisition system to a Sun4 workstation and perform the basic analysis with SAC has been achieved, accelerating the process of locating earthquakes. Shortly, the same procedure will be implemented at Boston College, thus permitting new earthquake waveforms to be quickly exchanged between the two institutions and analyzed.

M.I.T. and Weston Observatory are conducting a joint project to upgrade and reconfigure the New England Seismic Network. Three-component wideband seismic systems will replace the present short-period, mostly vertical component only stations. On-site detection, digitization and recording will replace the present method of FM telemetry of analog signals and digitization at a central facility. Data transfer from the field unit to the central data collection node is accomplished through a modem-to-modem connection. These changes will improve the quality of data and greatly reduce the cost of data transmission. To date, three of these new units have been installed and are completely operational. With funds expected to be allocated by FEMA, M.I.T. and Boston College plan to begin deployment, during FY 1993, of an additional fifteen of these "new generation" seismic stations to replace the existing network.

Seismicity

Figure 1 shows the epicentral locations of local earthquakes within or adjacent to the M.I.T. Seismic Network for the period January 1 - October 10, 1992. Twelve earthquakes, with a magnitude range Mc 2.1 - 3.3, occurred during this period. No damage is known to have been caused by these events. Nine occurred in central New Hampshire, the area historically having the highest seismicity rate within the M.I.T. Seismic Network including two potentially damaging earthquakes in December 1940 (M_L=5.3 and 5.4; Ebel,

Somerville and McIver, 1986) and one in January 1982 (M=4.7) (Fig. 2). The recent nine and older events from this region (Fig. 2) suggest three linear trends of seismicity; A being ENE-WSW, B NNW-SSE, and C NE-SW. The purpose of relocating the seismicity is to test the validity of the proposed trends in Figure 2. Digitally recorded earthquakes along a trend are subdivided into clusters and relocated using a cross-correlation technique. This technique has been tested successfully with NORESS and New England explosion data. Figure 3 shows the raw data recorded at Station ONH for the three earthquakes making up the easternmost cluster of Trend A (Fig. 2). Figure 4 shows the correlation windows for P and S, the autocorrelation of these phases for event pair 1-1, and the cross-correlations of these phases for event pairs 1-2 and 1-3. Identical S-P times measured between the P and S peak correlation amplitudes for different event pairs indicates the same source to receiver distance for all three earthquakes. This procedure, repeated for different stations at nearly perpendicular axes, is used to constrain the event cluster to much closer relative locations. Preliminary results show closer clustering for some subgroups than previously determined by routine analysis using the Hypo inversion program. Further work is planned to relocate clusters for the other proposed trends, and then attempt to associate the spatial pattern of the relocated events with potential causative structures in that region. If these inferred linear trends of seismicity are related to faults, the comparable lengths of the trends imply the potential for future damaging earthquakes similar in size to the December 1940 or January 1982 events (Fig. 2). The M.I.T. Seismic Network detects more seismicity in central and southern New Hampshire than the Boston College network because of closer recording stations to the events.

Another technique employing event pairs relocated to similar hypocenters is being tested to estimate the source time function of the larger event of a pair. The smaller event (treated as an empirical Green's Function, EGF) is deconvolved from the larger one to obtain the estimate (e.g. Li and Thurber, 1988). On October 6, 1992, a magnitude 3.3 earthquake occurred and was followed by a magnitude 2.7 aftershock. The almost identical hypocenters and same first motion distributions for both events suggested a similar focal mechanism. This earthquake pair provided an excellent example where the source time function could be estimated quickly as part of the routine analysis. The result for this pair is shown in Figure 5. The source time function can be used to compute source

parameters and to study the rupture process. In the future, additional data for these events will be acquired for the Boston College stations to greatly expand the azimuthal coverage. The digital event locations in Figure 2 are divided into two periods corresponding to the approximate starting dates of digital recording at M.I.T. (1980) and Boston College (middle of 1985). Those events recorded beginning in 1986 will be used to expand the study discussed here. By computing estimates of the source time function using data recorded over a wide range of azimuths, we may be able to determine the rupture directivity for a given event. This information can help constrain which nodal plane of a fault plane solution is the probable fault, the result being correlated with the trends of mapped geologic faults in the source region, if present, or spatial patterns of the seismicity. The locations of the December 1940 and the January 1982 earthquakes along the trends proposed in Figure 2 illustrate the importance of collecting more data for these studies to thoroughly investigate the relationship between the spatial distribution and source parameters of the seismicity in central New Hampshire and potential causative structures. In the future, the EGF and relocation methods may be applied to other seismically active regions of New England, such as Moodus, Ct. and Milo, Me.

References

Ebel, J. E., P. G. Somerville, and J. D. McIver, 1986. A Study of the Source Parameters of Some Large Earthquakes of Northeastern North America. J. Geophys. Res. 91, 8231-8247.

Li, Yingping, and C. H. Thurber, 1988. Source Properties of Two Microearthquakes at Kilauea Volcano, Hawaii. Bull. Seis. Soc. Am. 78, 1123-1132.

M. I. T. Network Seismicity, January 1 — October 10, 1992

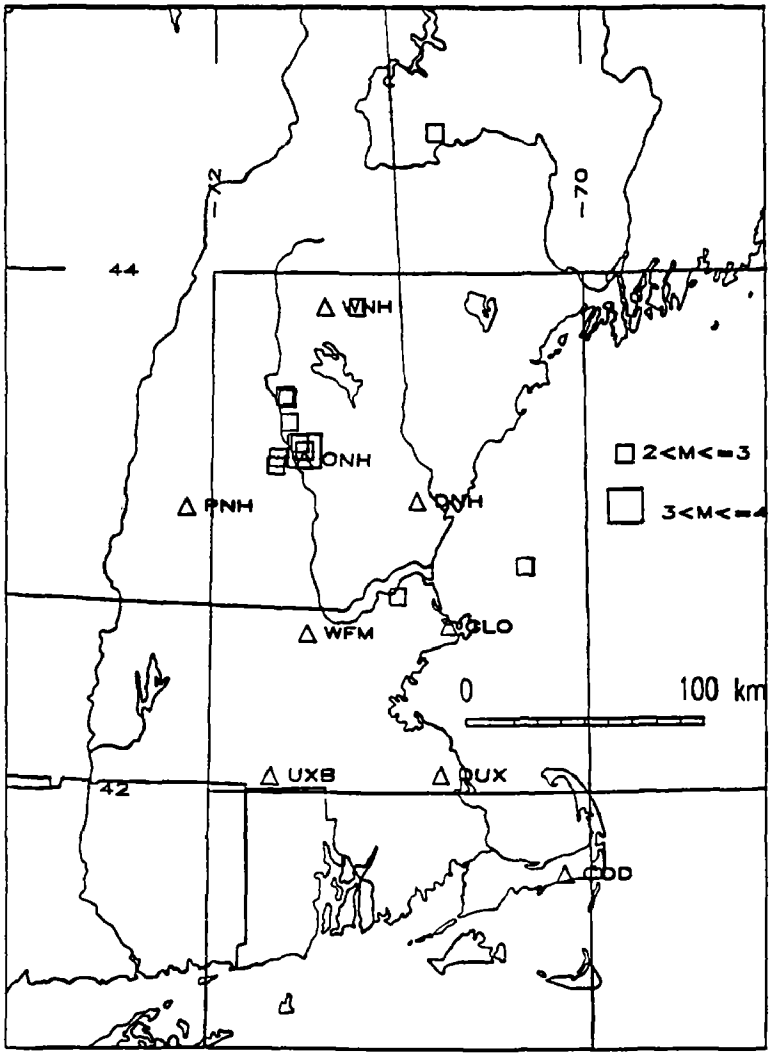

Fig. 1. Seismicity of New England recorded by the M.I.T. Seismic Network for the period January 1 - October 10, 1992. A majority of events is concentrated along a trend similar to that of the Merrimack River in central New Hampshire.

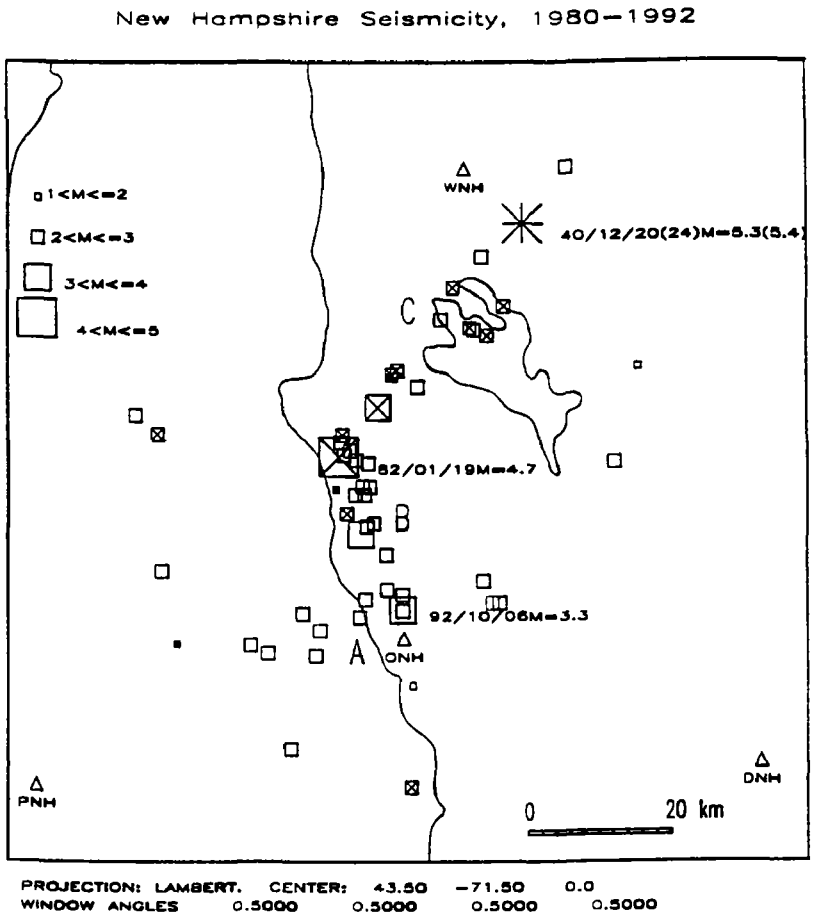

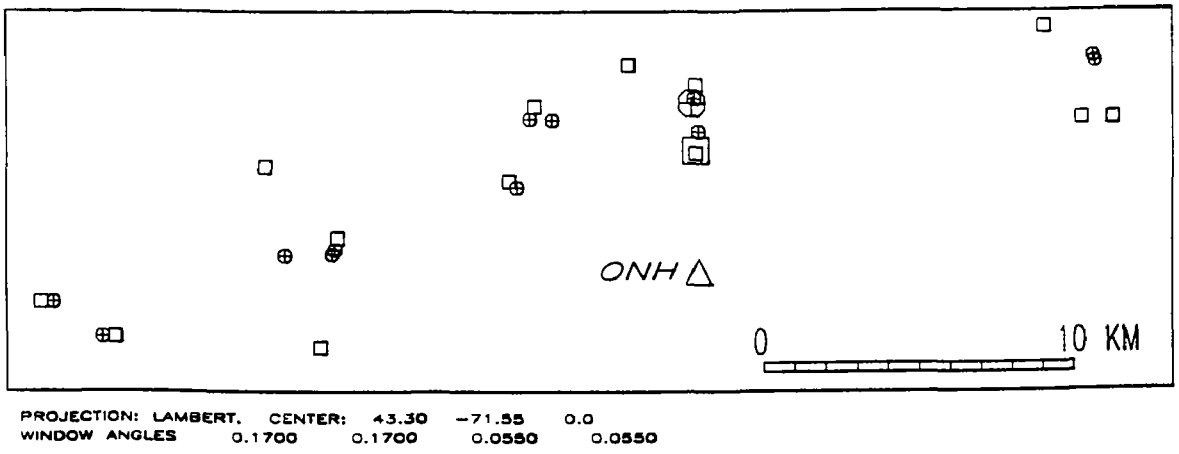

Fig. 2. Top figure is central New Hampshire seismicity recorded by the M.I.T. Seismic Network from 1980 - October 10, 1992. Three linear trends of seismicity are proposed. Trend A is ENE-WSW, B NNW-SSE, and C NE-SW. The boxes with an X and open boxes represent respectfully locations for digital events for 1980-1985 and 1986 to date. Bottom figure is original locations (boxes) and relative relocations (crosses) of clusters along trend A.

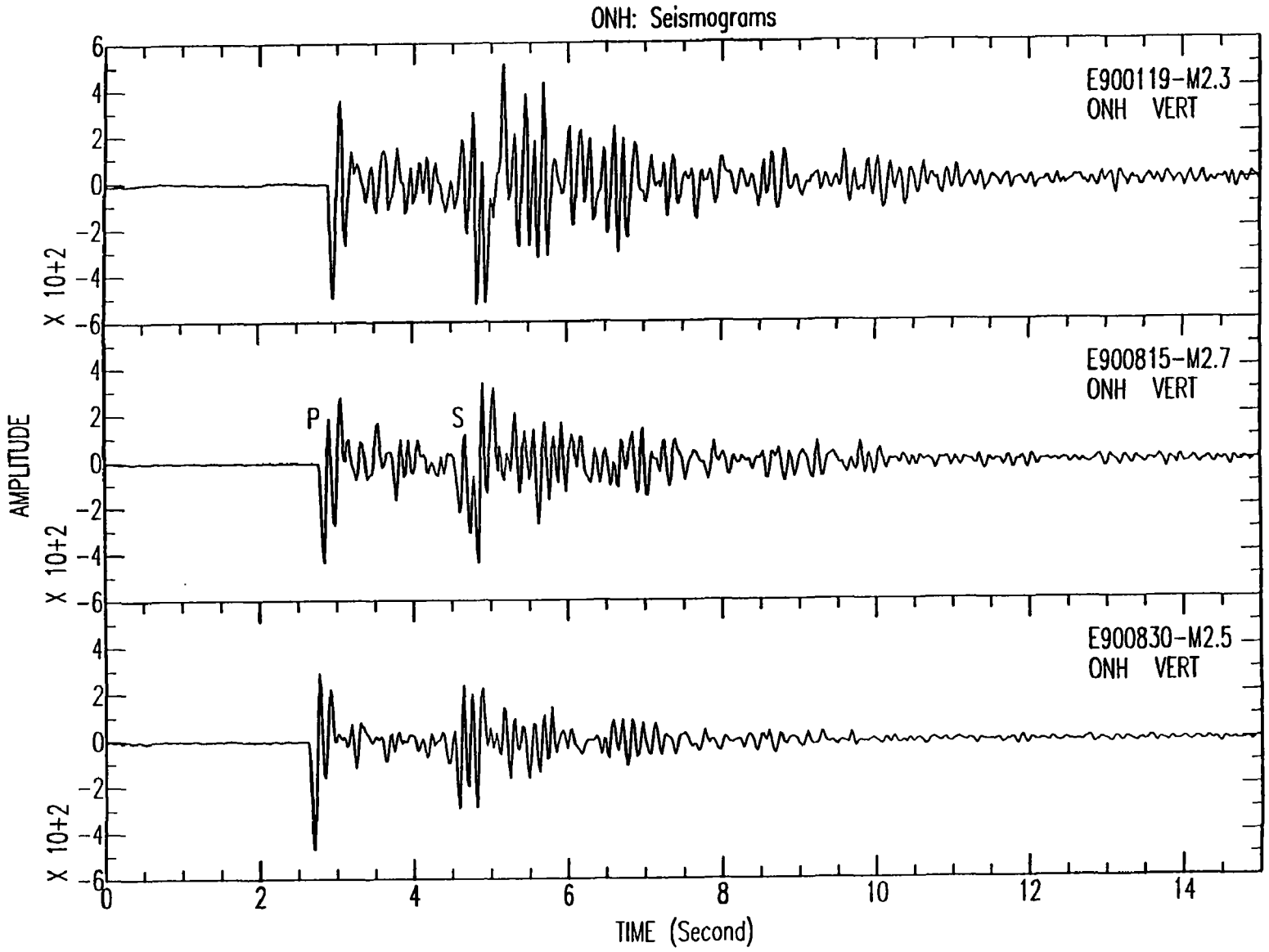

Fig. 3. Raw data recorded at station ONH for the easternmost cluster of three earthquakes of trend A in Fig. 2. The waveforms are similar.

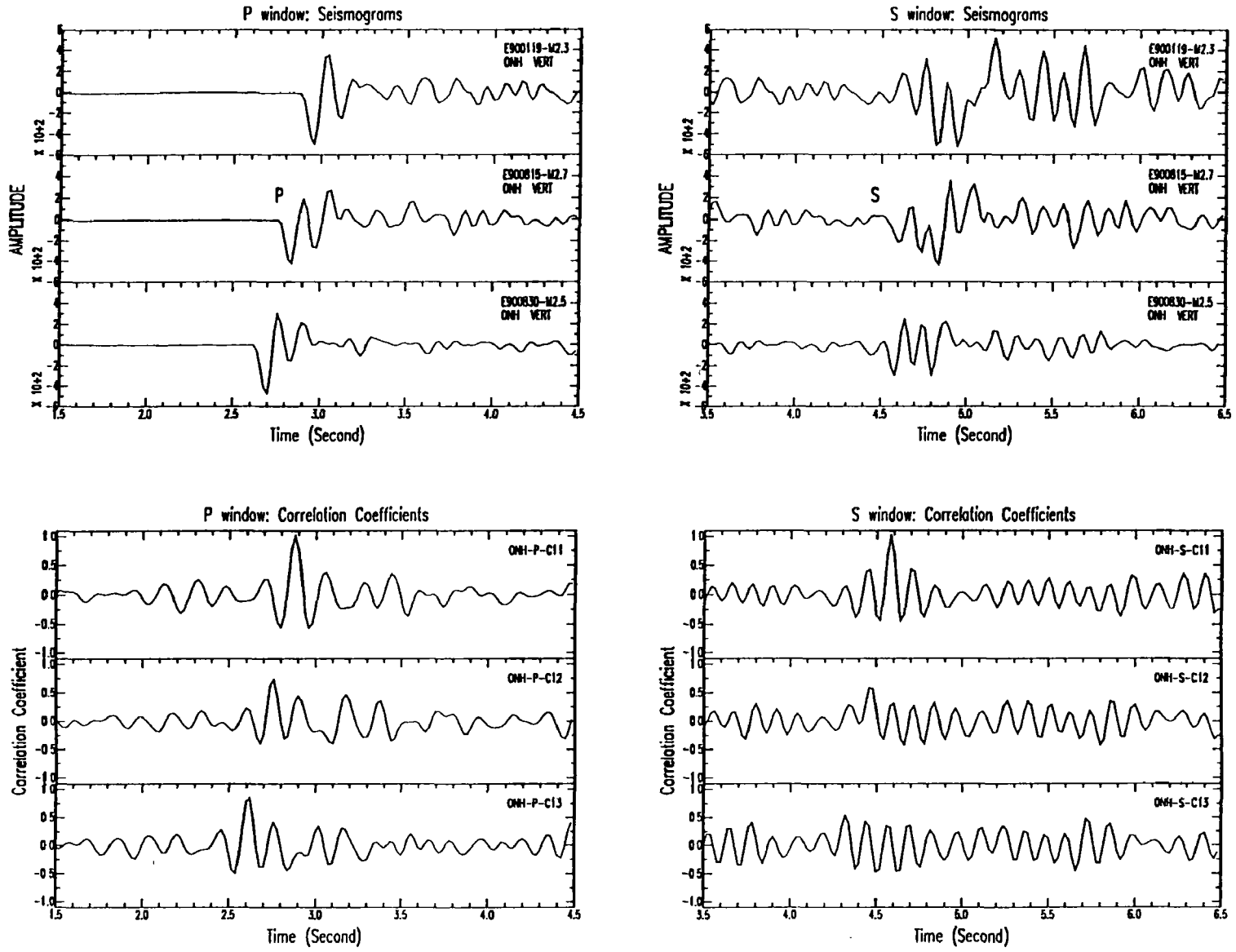

Fig. 4. Windowed P and S (top) and auto- and cross-correlations (bottom) of these phases for event correlation pairs C11, C12 and C13. Nearly identical time differences between S and P correlation peaks for these pairs suggest a similar location for the three events.

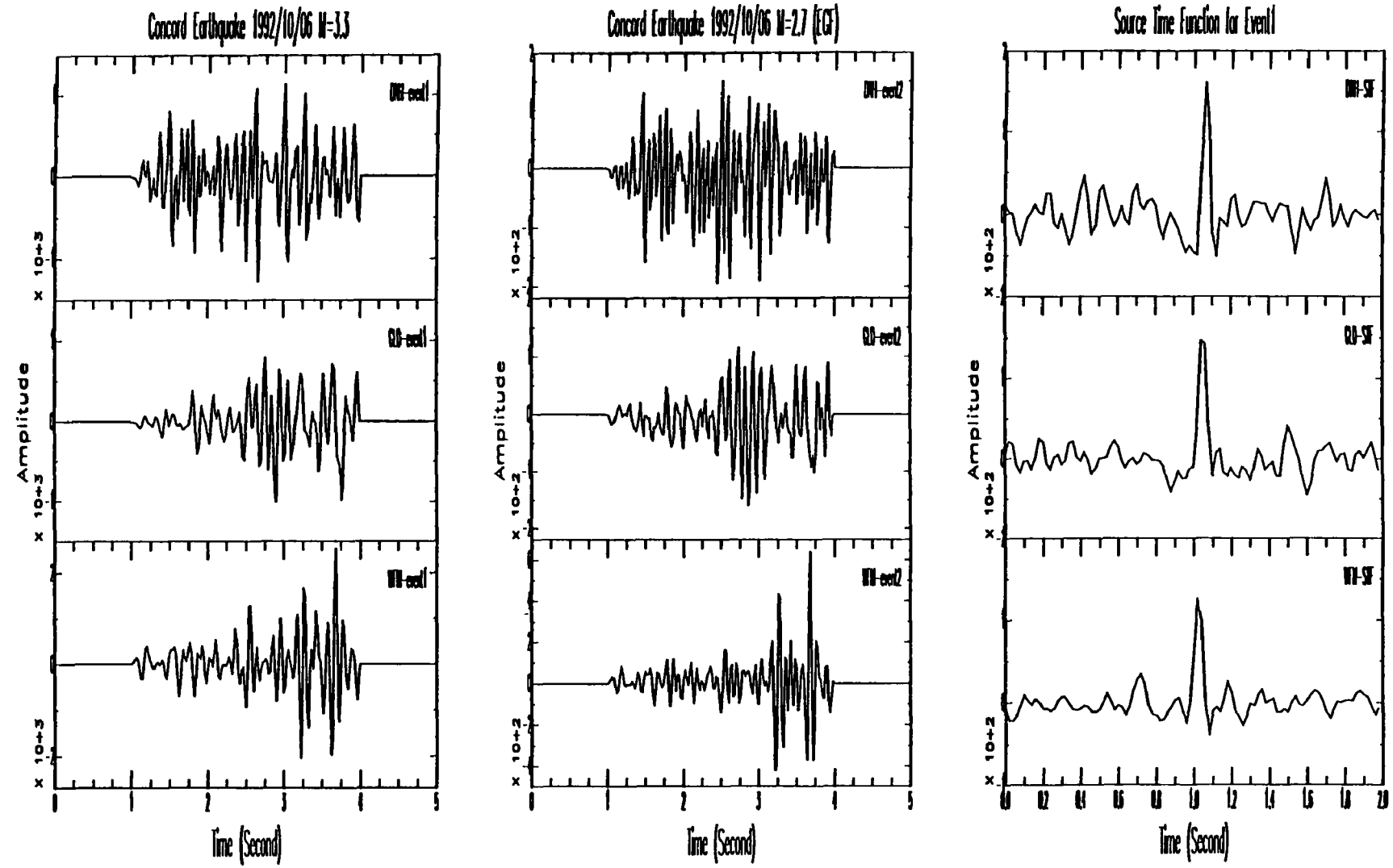

Fig. 5. Windowed P waves (for three stations) of a larger and a smaller event relocated to similar hypocenters. The smaller event (EGF = empirical Green's function) is deconvolved from the larger one to obtain the source time function estimate.

Earthquakes As Self-organized Critical Phenomena

Contract #1434-92-G-2165

Donald L. Turcotte
Department of Geological Sciences
Cornell University, Ithaca, New York 14853

(607) 255-7282

Investigations Undertaken

The objective of the research carried out is to understand whether earthquakes are an example of self-organized criticality. The approach is to develop analog models which are examples of self-organized criticality and which exhibit the important features of distributed seismicity. These models can then be examined for precursory behavior that can be predictive of major analog earthquakes. The results may provide the basis for new approaches to earthquake prediction.

The research is being undertaken in collaboration with Dr. Andrei Gabrielov who is on leave from the Institute for Theoretical Geophysics and Earthquake Prediction in Moscow and is spending the period of this grant at Cornell. Dr. Gabrielov was a leader in the development of the algorithems that successfully predicted the Armenian, Loma Prieta, and Landers earthquakes. One objective of our research is to test these algorithems on the analog SOC systems.

Results Obtained

It has been suggested that distributed seismicity is an example of self-organized criticality. If this is the case, the Earth's crust in an active tectonic zone is in a near-critical state and faults can interact over large distances. Observed seismicity and earthquake statistics are consequences of the dynamical interactions of seismic faulting over a wide range of scales. We address this problem by considering a two-dimensional array of slider blocks with static/dynamic friction. The two-dimensional system is treated as a cellular automaton such that only one slider block is allowed to slip at a given time and interacts only with its nearest neighbors through connecting springs. Because of this treatment, the amount of slip for each failed block can be obtained analytically, and the system is deterministic with no stochastic inputs or spatial heterogeneities. In many cases, the slip of one block induces the slip of adjacent blocks. The size of an event is specified by the number of blocks that participate in the event. The number of small events are close to a Poisson process, and gradually deviate towards periodicity for large events. The recurrence time statistics are generally insensitive to parameter variations. Large events may occur at stress levels considerably lower than the failure strength of an individual block, and the stress drops associated with large events are generally small. This may provide an explanation for observed low stress levels in tectonically active areas.

In the standard cellular-automata model for a fault an element of stress is randomly added to a grid of boxes until a box has four elements, these are then redistributed to the adjacent boxes on the grid. This redistribution may result in one or more of these boxes having four or more elements in which case further redistributions are required. On the average added elements are lost from the edges

of the grid. We have modified this model so that the boxes have a scale-invariant distribution of sizes. When a redistribution from a box occurs it is equivalent to a characteristic earthquake on the fault. A redistribution from a small (a foreshock) may trigger an instability in a large box (the main shock). A redistribution from a large box always triggers many instabilities in the smaller boxes (aftershocks). The frequency-size statistics for both main shocks and aftershocks satisfy the Gutenberg-Richter relation with $b = 0.835$ for main shocks and $b = 0.635$ for aftershocks. Model foreshocks occur 28% of the time.

Reports Published

1. B. Barriere and D.L. Turcotte, A scale-invariant cellular-automata model for distributed seismicity *Geophys. Res. Let.* **18**, 2011-2014 (1991)

2. G. Narkounskaia, J. Haung, and D.L. Turcotte, Chaotic and self-organized critical behavior of a generalized slider-block model *J. Stat. Phys.* **67**, 1151-1183 (1992)

3. G. Narkounskaia and D.L. Turcotte A cellular-automata, slider-block model for earthquakes. I. Demonstration of chaotic behavior for a low-order system, *Geophys. J. Int.*, in press (1992)

4. J. Huang, G. Narkounskaia, and D.L. Turcotte, A cellular-automata, slider-block model for earthquakes. 2. Demonstration of self-organized criticality for a two-dimensional system, *Geophys. J. Int.*, in press (1992)

QUATERNARY BLIND THRUSTING IN THE SOUTHWESTERN SACRAMENTO VALLEY, CALIFORNIA

Contract # 14-08-0001-G2059

Jeffrey R. Unruh (Lettis & Assoc., Oakland, CA; 510-832-3716)
Lewis P. Munk* (Dept. of Land, Air and Water Resources; 916-752-1406)
Bradley A. Loewen* (Dept. of Geology; 916-752-4950)
Eldridge M. Moores* (Dept. of Geology; 916-752-0352)
Randal J. Southard* (Dept. of Land, Air and Water Resources; 916-752-7041)

***all at*: University of California, Davis 95616**

OBJECTIVES

The goal of this investigation is to study Quaternary surface deformation related to movement on potentially seismogenic blind thrust faults in the Rumsey Hills/Dunnigan Hills region, southwestern Sacramento Valley, California. Our approach is to combine analysis of seismic reflection data with mapping of Quaternary tectonic-geomorphic features to infer the rate, timing and kinematics of late Cenozoic shortening. Additional studies have been undertaken to determine the origin of the blind thrust system beneath the southwestern Sacramento Valley, and to explore the relationship between anomalously high fluid pressures and active crustal shortening in western California.

INVESTIGATIONS UNDERTAKEN

Based on detailed surface mapping, analysis of seismic reflection profiles and drill hole data, we have developed a kinematically-restorable forward model for evolution of the blind thrust system in the Rumsey Hills/Dunnigan Hills region. The model is consistent with stratigraphic and structural relationships visible in deep seismic reflection profiles, and accounts for the development of angular unconformities in the section of Cretaceous-Tertiary forearc strata (Loewen and Unruh, 1992).

We conducted detailed field mapping and stratigraphic analysis of the late-Quaternary deposits and geomorphic surfaces in the Dunnigan Hills region to constrain the timing of the initiation of Quaternary deformation, and infer rates of tectonic uplift. Relative and absolute ages of the geomorphic surfaces and underlying sediments were determined via radiometric, (^{14}C, U/Th/Pa, K/Ar) magnetostratigraphic, geomorphic and tephrachronologic data. Soils underlying the geomorphic surfaces were described and sampled in 16 backhoe pits. Hundreds of additional obversations were made from natural exposures, auger holes and shallow pits. These data were used to develop soil morphological and chemical indices for the southwestern Sacramento Valley (Munk, 1992). Models for the development of the fluvial system of the Dunnigan and Rumsey Hills were developed based on field investigations and photo-interpretation.

We conducted field and aerial reconnaissance in order to map the locations of perennial saline springs emerging along thrust faults in the Rumsey Hills. The map data were combined with stable isotope analyses of the spring waters to relate spatial variations in fluid chemistry to distinct stratigraphic and structural horizons (Criss et al., 1992; Davisson et al., 1992).

RESULTS OBTAINED

Based on our structural studies, we conclude that the seismically-active blind thrust system beneath the southwestern Sacramento Valley initially evolved during progressive arcward-vergent contraction of the Mesozoic-Tertiary Great Valley forearc basin (Unruh et al., 1991). The youngest thrust fault in the study area is responsible for uplift and folding of the Rumsey Hills fault-propagation fold (Loewen, 1992). This young thrust roots in an older thrust fault, and folds

and deforms older structures. Displacement on this thrust has deformed the Plio-Pleistocene Tehama Formation (Loewen et al., 1992). Based on stratigraphic relationships in the Dunnigan Hills, we tentatively conclude that uplift, tilting and folding in this region began in middle Pleistocene and continued into the late Pleistocene (Munk, 1992).

Total late Quaternary displacement on the active thrust fault beneath the Rumsey Hills is estimated from the kinematic forward model and the structural relief on the deformed Tehama Formation. Based on a reasonable range of fault geometries and the age of the Tehama Formation, we calculate an average slip rate of 1-2 mm/yr. Using empirical relationships between fault area and earthquake magnitude, we estimate a maximum credible earthquake of Mw $6\frac{1}{4}$ for the blind thrust fault beneath the Rumsey Hills (Unruh and Loewen, 1992). Surface thrust or reverse faults in the Rumsey Hills that splay upward from the main thrust locally displace bedding contacts in the Tehama Formation approximately 0.5 m. These relationships yield a minimum estimate of cosesimic slip of 0.5 m. Assuming the slip rate calculated above, the recurrence interval for 0.5 m events is 250-500 yr. Paleoseismic investigations are neccessary to test these structurally-derived estimates.

Perennial saline springs emerge from thrust faults in the Rumsey Hills and are the surface expression of anomalously high fluid pressures generated by compressive forces and active shortening of Cretaceous marine sediments in the northern Coast Ranges (Unruh et al., 1992). The high fluid pressures may affect the mechanics of thrust displacement, and may also control the coseismic release of strain by blind thrusts (Ed Keller, personal communication, 1992). The perennial saline springs are aerially extensive and have been observed as far south as the northern Diablo Range (Criss et al., 1992). Discharge rates of individual saline springs in the Rumsey Hills are as high as 10 liters/minute and generally do not exhibit significant seasonal variations. Based on an estimated intergrated disharge rate throughout the Rumsey Hills, tectonic strain due to pore volume loss in this region may be locally as high as 10^{-7}/yr. The springs are rich in boron, and the high discharge rate suggests that the abnormally high boron concentrations in the potable groundwaters of the southwestern Sacramento Valley are probably due to contamination by fluids expelled from these saline springs.

REPORTS

Abstracts

Criss, R.E., Davisson, M.L., Loewen, B.A., Unruh, J.R., and Schaal, R.B., 1992, Occurrence of tectonically-driven, perennial saline springs in the eastern Coast Range, CA: Eos, Transactions, American Geophysical Union, Fall Meeting, V 73, #43.

Davisson, M.L., Presser, T.S., Criss, R.E., Unruh, J.R., and Loewen, B.A., 1992, Chemical and isotopic character of perennial saline springs in the eastern margin of the Coast Ranges thrust system, Rumsey Hills, California: Eos, Transactions, American Geophysical Union, Fall Meeting, V 73, #43.

Loewen, B.A., Unruh, J.R., Davisson, M.L., and Moores, E.M., 1992, Deformed Plio-Pleistocene fluvial deposits in the Rumsey Hills, California, and implications for late Cenozoic motion of an east-tapering underthrust wedge: Abstracts with programs, Cordilleran Section, Geological Society of America, p. 65.

Loewen, B.A., and Unruh, J.R., 1992, Kinematics and timing of progressive arcward-vergent contraction of the Mesozoic-Tertiary forearc basin, southwestern Sacramento Valley, California: Eos, Transactions, American Geophysical Union, Fall Meeting, V 73, #43.

Munk, L.P., and R.J. Southard. 1992. Soil stratigraphic relationships in a tectonically active landscape, Dunnigan HIlls, California. Abstracts. American Society of Agronomy, Annual Meetings, Minneapolis, MN, Nov. 1-6, 1992.

Unruh, J.R., Loewen, B.A., and Munk, L.P., 1992, Seismic hazard assessment of an active blind thrust fault beneath the Rumsey Hills, southwestern Sacramento Valley, California: Eos, Transactions, American Geophysical Union, Fall Meeting, V 73, #43.

Southard, R.J., and L.P. Munk. Quantitative clay mineralogy of a soil developmental sequence in a tectonic landscape.Abstracts. American Society of Agronomy, Annual Meetings, Minneapolis, MN, Nov. 1-6, 1992.

Theses and Dissertations

Loewen, B.A., 1992, Deformation of Lower Cretaceous through Tertiary strata in the Rumsey Hills-Capay Valley area: Implications for late Cenozoic motion of an east-tapering underthrust wedge: M.S. thesis, University of California, Davis, 84 p.

Munk, L.P., 1992, Stratigraphy, geomorphology, soils, and neotectonic interpretation of the Dunnigan Hills, California. Ph.D. dissertation, University of California, Davis.

Papers

Unruh, J.R., Ramirez, V.R., Phipps, S.P., and Moores, E.M., 1991, Tectonic wedging beneath forearc basins: ancient and modern examples from California and the Lesser Antilles: GSA Today, v. 1, p. 185-190.

Unruh, J.R., and Moores, E.M., 1992, Quaternary blind thrusting in the southwestern Sacramento Valley, California: Tectonics, v. 11, p. 192-203

Unruh, J.R., Davisson, M.L., Criss, R.E., and Moores, E.M., 1992, Implications of perennial saline springs for abnormally high fluid pressures and active thrusting in the southwestern Sacramento Valley, California: Geology, v. 20, p. 431-434.

Munk, L.P., and Southard, R.J., in press, Pedogenic and mineralogical implications of non-calcareous opaline pendants in some late-Pleistocene California Palexeralfs: SSSAJ, 57.

Unruh, J.R., Loewen, B.A., and Davis, D.L., in prep., Kinematics and timing of pregressive arcward-vergent contraction of the Mesozoic-Tertiary forearc basin, southwestern Sacramento Valley, California.

Unruh, J.R., Loewen, B.A., and Munk, L.P., in prep., Seismic hazard assessment of an active blind thrust fault beneath the Rumsey Hills, southwestern Sacramento Valley, California.

Phipps, S.P., and Unruh, J.R., in prep., Tectonic wedging beneath an imbricate roof thrust system, northern Coast Ranges, California.

Earthquake Prediction Experiments in the Anza-Coyote Canyon Seismic Gap

1434-92-A-0962

Frank Vernon
Institute of Geophysics and Planetary Physics
Scripps Institution of Oceanography
University of California, San Diego
La Jolla, California 92093
(619) 534-5537

Investigations: This report covers the progress of the research investigating the Anza-Coyote Canyon seismic slip gap for the period from January through November, 1992. The objectives of this research are: 1) To study the mechanisms and seismic characteristics of small and moderate earthquakes, and 2) To determine if there are premonitory changes in seismic observables preceding small and moderate earthquakes. This work is carried out in cooperation with Tom Hanks, Joe Fletcher and Larry Baker of the U. S. Geological Survey, Menlo Park.

Network status: During the period of this report, nine stations of the Anza Seismic Network were telemetering three component data. The network was set at a moderate gain so that a M=3.4 earthquake clipped the station directly over the hypocenter while the rest of the stations remained on scale. An STS-2 seismometer was installed at the PFO station to test the long term operational stability in preparation for the upgrade planned in 1993. The network has a front-end computer which allows the ANZA event data to be available over the INTERNET in near real time. No changes were made to the data logging software. Due to the abundance of aftershocks from the Joshua Tree -Landers - Big Bear earthquake sequence we now have a back log of P and S wave arrival picks and locations and focal mechanisms which need to be completed. The catalog is complete through April and we plan to be caught up by the end of December. The complete waveform data will also be loaded to the on-line optical disk storage system by the end of Decmeber.

Seismicity: Since the beginning of 1992, the ANZA network recorded 6270 events of which were large enough to locate and determine source parameters. This compares to 1437 from 1991. These events have magnitudes determined by of the Southern California Seismic Network from less than M=1.0 up to the Landers M=7.5 event. The seismicity pattern in the Anza region remained the same as in 1990. It is concentrated in two clusters located near the KNW and TRO stations respectively. These clusters have been active for the past 9 years while the ANZA network has been operational. The activity near TRO reached a maximum near the beginning of 1990 and is significantly higher than before 1989. The seismicity off the fault appears to be lower than the levels observed in the middle 1980s. It is also interesting that there is an apparent decrease in activity along the Anza segment of the San Jacinto fault after the Landers earthquake. We will investigate this further after completing our catalog for 1992.

A three-tiered investigation of seismicity and earthquake strains

Agreement No. 1434-92-6-2181

Steven N. Ward
Institute of Tectonics
University of California
Santa Cruz, CA 95064
404-459-2480

We have been attempting to revise the mean repeat time (T_{ave}) and coefficient of aperiodicity (ν) for segments of the San Andreas Fault by using models of synthetic seismicity. Primary inputs into the model are: 1) segment lengths and locations, 2) characteristic earthquake magnitudes, and 3) long-term slip rates. Of all the earthquake information available, these features are probably best constrained.

WGCEP (1990) has presented an eleven segment model for the San Andreas Fault. A slightly adjusted version containing 15 segments (Table 1) was employed to address the question: "Can the WGCEP segmentation reproduce observed SAF seismicity? If not, what needs to be done? If so, what can be said about T_{ave} and ν?" Figure 1 shows synthetic seismicity (*top*) and displacement (*bottom*) for a 1000 year piece of a 10,000 year run of the SAF model. Figure 2 (*stars*) overlays the synthetic seismicity with the observed annual rates (*boxes*) $N_>(M)$ and $N(M)$ of earthquakes within a 40 km wide band centered on the fault. The error bars show ±one standard deviation in the computed rates based upon 50, 200-year samples drawn from the 10,000 year history. We find that the synthetic seismicity model using the modified WGCEP segmentation is capable of generating the observed numbers of earthquakes over the magnitude range 4.5 to 8.0. Below we advance some recurrence statistics for the larger events.

Fault Averaged Results. Figure 3 plots cumulative probability of recurrence versus time for $M \geq M_o$ with M_o= 6.0 to 8.0. for the SAF model as a whole. Mean repeat time and spread parameter for a typical large event ($M \geq 7$) is 131 years and 1.1. It is important to recognize however, that both T_{ave} and ν are functions of magnitude; T_{ave} increases with M_o while ν decreases (bottom row, Table 2). Large earthquakes tend to be more periodic than small ones. Small ones tend to cluster early in the cycle. You can see this in the top panel of Figure 3, where the curves crowd to the left. The numerical value of ν bears directly on the concept of seismic gaps. If ν is less than 1.0, gaps behave normally in that the conditional probability of occurrence increases with gap time. If ν is greater than 1.0, the effect is reversed and conditional probability decreases as gap time increases. All of the models run so far show the same tendency; ν decreases from approximately 1.5 at M_o=6 to about 0.6 at M_o=7.75. The cross-over magnitude where gaps become a useful concept occurs around $M = 7$. Figure 4 visualizes this magnitude dependence of aperiodicity and clustering. In all instances the spread parameter that we find is much greater than the 0.21 value used by WGCEP.

Segment Specific Results. Earthquake aperiodicity, while on the average being a decreasing function of characteristic magnitude, is also dependent on the segment's relative location on the fault. Table 2 lists T_{ave} and ν for all of the SAF segments as a function of M_o. In scanning the columns, you can see that certain segments systematically behave more or less periodically than the fault as a whole. Generally, the more isolated a segment, the more periodic are its earthquakes. Note for instance, that the Parkfield segment tends to have a ν

less than the fault average. This segment borders the central creeping section to the north which provides a degree of isolation. Although very periodic failures of fault segments may exist, we find it difficult to make any segment conform to a spread value much less than 0.4. Given the information in Table 2 and the date of the last earthquake on a segment, the conditional probability of recurrence can be easily calculated. For the Parkfield segment [T_{ave}=27.6 and ν=1.12, 1966=previous quake], the conditional probability of recurrence of a $M \geq 6$ quake within the ten year Parkfield Prediction window beginning in 1983 is 29% (versus 95% estimated by Bakun and Lindh, 1985). Probability of recurrence in the 30 year WGCEP window starting in 1988 is 63% (versus > 90% estimated by WGCEP, 1988).

Verification. We have argued previously that unless the earthquake record contains at least ten recurrences, the estimated repeat time and aperiodicity coefficient will almost certainly be too low. Measured against this criteria, there are few data sets with which to compare (and correct) the model. Sieh (1989) reports nine recurrence intervals at Pallet Creek in the Mojave segment. Weibull function fits to these intervals give T_{ave} = 131.8 y and ν=0.84. Because it is not completely certain what magnitude earthquakes the paleoseismic data are detecting, we plot in Figure 5 (*dashed lines*) predictions for recurrence of M_o = 7, 7.25 and 7.5 quakes in the Mojave segment. The model reproduces both T_{ave} and ν quite well. Keep in mind that T_{ave} derives only from the segment length, characteristic magnitude, and slip rate. It is not an input parameter.

Weaknesses. Admittedly, products from synthetic seismicity models are easily attacked as nonunique or parameter dependent. We can't claim the contrary, but given the fact that there is almost a total lack of data on the recurrence statistics of SAF earthquakes, we believe that synthetic seismicity offers two unquestionable advantages over the real thing: 1) Synthetic seismicity can run as long as necessary to get a statistically significant sample. Individual products like "Segment X has a 50% chance of triggering Segment Y" may not agree with our limited historical sample, but at least there is a firm statistical basis for the statement. 2) Synthetic seismicity illuminates connections between physical parameters which otherwise would go unrecognized. Segment length, characteristic magnitude, mean repeat time and aperiodicity are linked; they can not be picked out of a hat. For instance, T_{ave} can not be arbitrarily decreased without cutting the characteristic magnitude or increasing slip rate. Likewise, the characteristic magnitude of a segment can not be reduced without (generally) increasing ν.

We believe that San Andreas earthquake recurrence statistics which derive from synthetic seismicity models such as these are as credible, if not more so, than any other method yet advanced.

Ward, S. N., 1992. An Application of Synthetic Seismicity in Earthquake Statistics: The Middle America Trench, *J. Geophys. Res.,97*, 6675-6682.

Segment	Length (km)	Characteristic Magnitude	Slip Rate (mm/y)
1. Medocino	100	7.0	15
2. North Coast	240	7.6	15
3. Mid Peninsula	41	7.0	18
4. N. Santa Cruz Mts.	20	6.5	15
5. S. Santa Cruz Mts.	39	6.9	15
6. Creeping Section	140	aseismic	30
7. Parkfield	30	6.3	36
8. Cholame	55	7.0	36
9. Carrizo	145	7.7	36
10. Mojave	100	7.4	30
11. San Bernardino	100	7.3	24
12. Coachella Valley	100	7.4	24
13. Brawley Seismic Zone	50	aseismic	30
14. N. Imperial Valley	30	6.5	30
15. S. Imperial Valley	30	6.6	30

Table 1. San Andreas Fault segmentation model. Slightly modified after WGCEP.

	$M \geq 6.0$		$M \geq 6.5$		$M \geq 7.0$		$M \geq 7.5$	
Segment	T_{ave} (y)	ν	T_{ave} (y)	ν	T_{ave} (y)	ν	T_{ave} (y)	ν
1. Medocino	86	1.4	90	1.4	122	1.1	278	0.5
2. North Coast	77	1.7	91	1.5	110	1.3	263	0.6
3. Mid Peninsula	74	1.4	78	1.4	137	1.0	476	0.4
4. N. Santa Cruz Mts.	43	1.4	60	1.2	117	1.0	530	0.5
5. S. Santa Crua Mts.	64	1.5	81	1.2	154	0.8	703	0.6
6. Creeping Section								
7. Parkfield	28	1.1	60	1.1	127	0.9	376	0.4
8. Cholame	52	1.4	63	1.2	124	1.0	362	0.4
9. Carrizo	158	1.5	175	1.3	188	1.2	326	0.5
10. Mojave	81	1.4	86	1.3	96	1.3	204	0.7
11. San Bernardino	60	1.5	69	1.3	86	1.1	203	0.7
12. Coachella Valley	91	1.5	107	1.3	134	1.0	273	0.4
13. Brawley Seismic Zone								
14. N. Imperial Valley	39	1.3	58	1.0	231	0.7		
15. S. Imperial Valley	44	1.2	55	1.0	231	0.7		
AVERAGE	57	1.5	75	1.3	131	1.1	315	0.6

Table 2. Predicted earthquake recurrence statistics for the San Andreas Fault segments for magnitudes greater than or equal to 6.0, 6.5, 7.0 and 7.5.

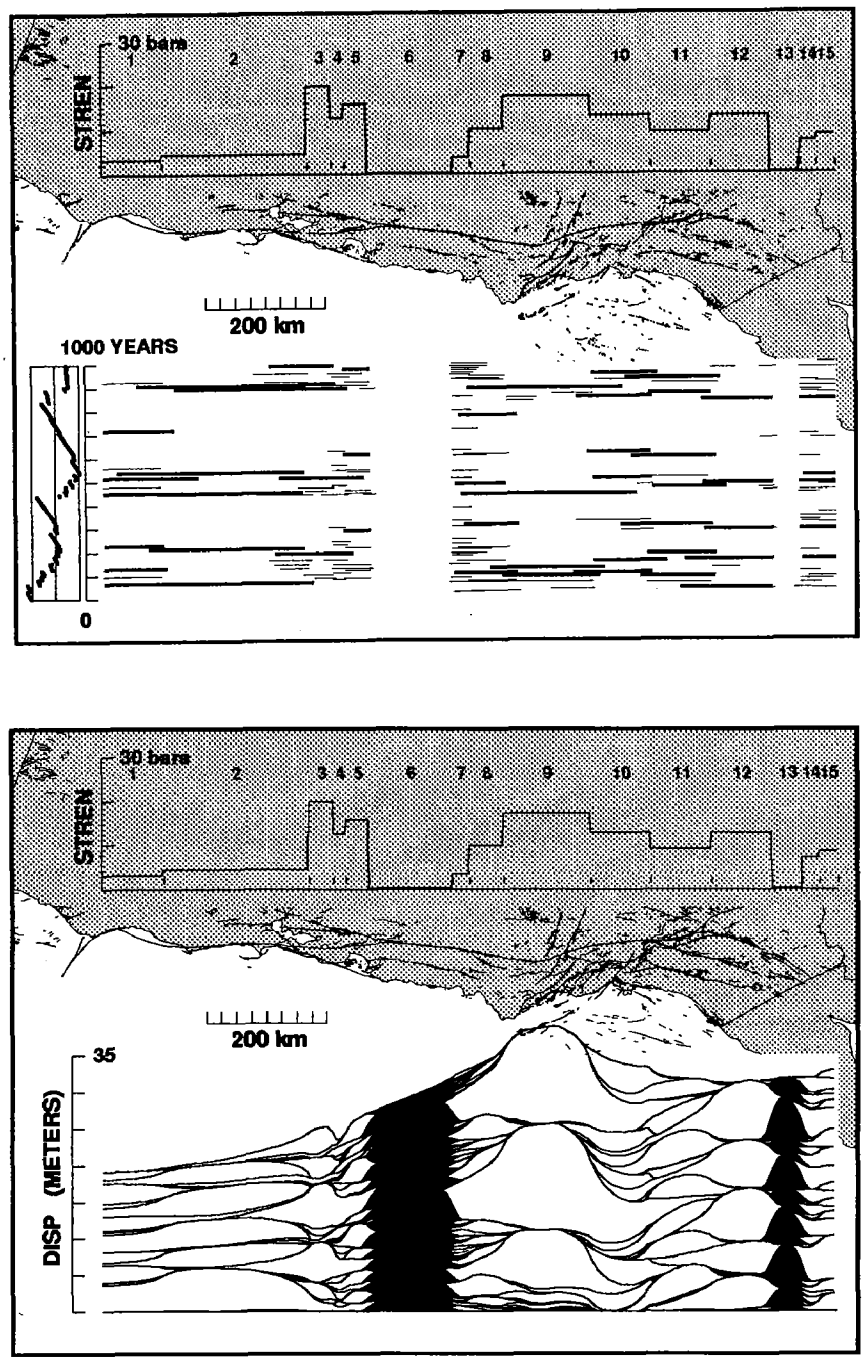

Figure 1. Synthetic seismicity (*top*) and displacement from the initial 1000 years of a 10,000 year run of a San Andreas Fault model based closely on the WGCEP segmentation. Length, position and strengths of the 15 segments are drawn along the top. Only events with $M \geq 6$ are shown. Bold line segments are $M \geq 7$ events. The blackened areas in the Central Creeping Section and Brawley Seismic Zone are aseismic slip. Note the mixture of characteristic and non-characteristic slip patterns in each segment.

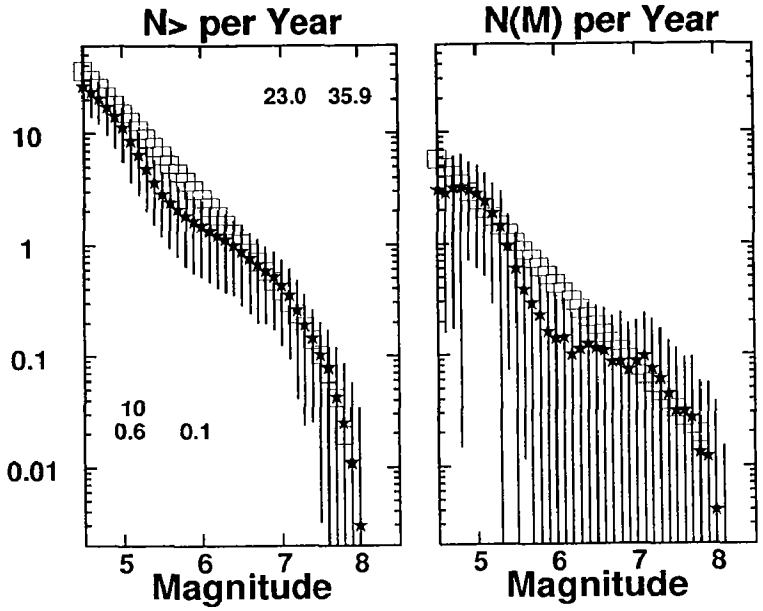

Figure 2. Observed seismicity (*boxes*) and synthetic seismicity (*stars*) from the model of Figure 1. The observed seismicity includes events within a 40 km wide band of the SAF. The modified WGCEP segmentation adequately represents observed seismicity.

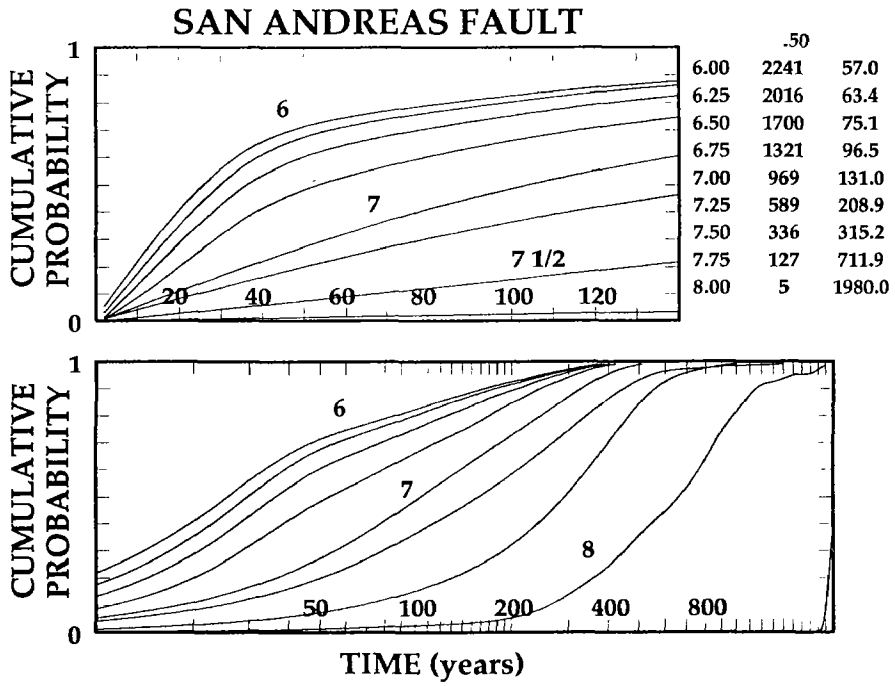

Figure 3. Cumulative probability for the recurrence of a $M \geq M_o$ earthquake within T years of a previous $M \geq M_o$ event. M_o covers the range M_o= 6.0 to 8.0 in 0.25 increments. Curves were tabulated from a 10,000 year run of synthetic seismicity for the SAF model. A segment is considered broken if more than 50% of its length slips during an earthquake. Numbers to the upper right give M_o, the number of segment recurrences, and the mean recurrence time. As can be seen in the steepening slopes of the curves, earthquakes tend to become more periodic with increasing magnitude. The concept of seismic gaps is useful for events of magnitude larger than about 7. For smaller quakes, increasing the gap time has little or diminishing effect on conditional probability of recurrence.

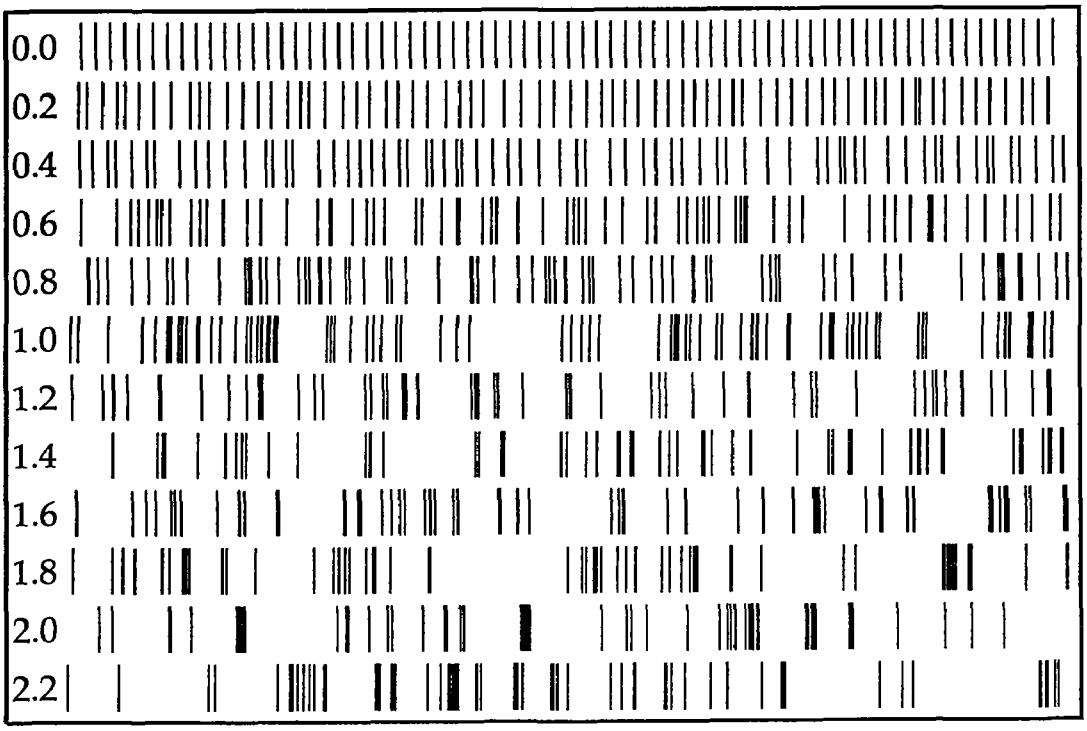

Figure 4. Visualization of the effect of the aperiodicity parameter ν on the recurrence of earthquakes. These 12 "bar code" lines show events drawn from a Weibull distribution of equal T_{ave} and ν increasing from 0.0 to 2.2. The trend toward temporal clustering of events as ν increases is obvious. Gap time is a useful concept only for time series with $\nu \leq 1$. We find: magnitude 6 events behave with $\nu \approx 1.5$; magnitude 6.5 events behave with $\nu \approx 1.3$; magnitude 7 events behave with $\nu \approx 1.1$; and magnitude 7.5 events behave with $\nu \approx 0.6$.

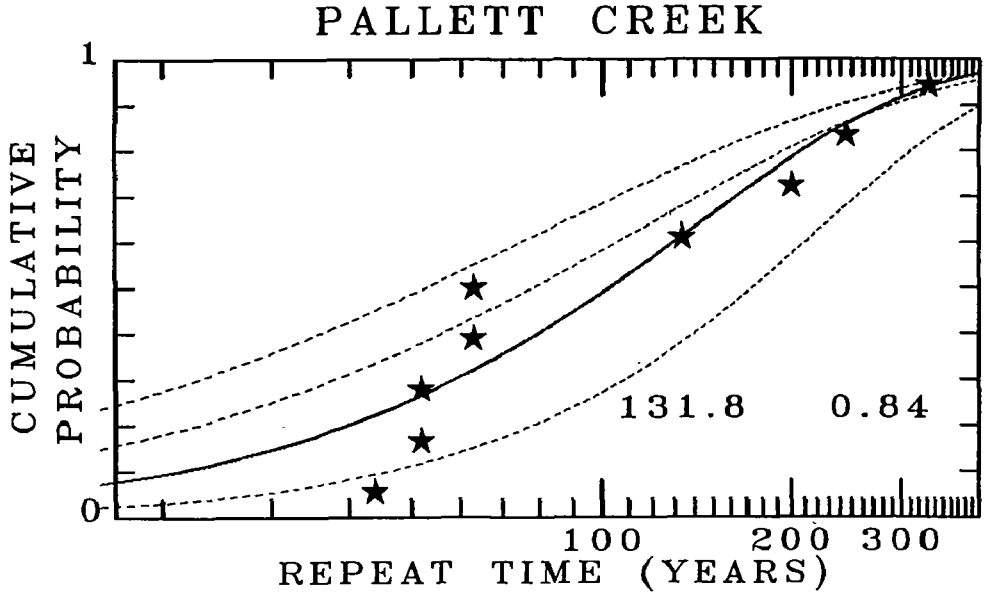

Figure 5. Cumulative probability Weibull fit (*solid line*) to the nine earthquake recurrence times given by Sieh (1989) for the Pallett Creek area of the Mojave segment. Left to right, the dashed lines are the predictions from the synthetic seismicity model for magnitudes greater than or equal to 7.0, 7.25 and 7.5. The predictions for events near 7.25 have no argument with the data.

Hayward Fault Recurrence Behavior: Trenching Studies, Fremont and Oakland California 14-08-0001-G2115

Patrick L. Williams and David L. Jones
Department of Geology and Geophysics
University of California
Berkeley, California 94720

Phone: (510) 486-7156
FAX: (510) 486-5686
e-mail: plw@geo.lbl.gov

Field work for the Tule Pond Paleosismic investigation is likely to finish in 1993. Substantial effort remains to establish age-control of offset strata. Our inventory of several hundred charcoal samples should allow us to accomplish this. Evidence remains good that at least seven paleoseismic events are recorded at Tule Pond.

FY1992 Accomplishments:

a) Logged two trenches at an additional paleoseismic site along the east flank of Tule Pond;
b) finished graphical representations of seven trenches;
c) collected and archived over 200 charcoal samples;
d) prepared over 40 charcoal samples for dating;
e) published Guidebook and Proceedings articles for the Second Conference on Earthquake Hazards in the Eastern San Francisco Bay Area;
f) presented case for dateable 1,100-foot offset of Strawberry Creek.

Recent Publications:

1991 Williams, P.L, Evidence of Late Holocene Ruptures, Southern Hayward Fault, California, *GSA Abstracts with Programs*, Spring 1991 SSA/GSA-Cordilleran meeting.

1992 Williams, P.L. and A.M. Hosokawa, Geomorphic features related to the Hayward fault at the University of California at Berkeley, in Taylor, C.L., Hall N.T. and Melody, M. eds., Field Trip Guidebook, Second Conference on Earthquake Hazards of the Eastern San Francisco Bay Area, 65-71.

1992 Williams, P.L., Earthquake recurrence studies at Tule Pond pull-apart, Fremont, California, in Taylor, C.L., Hall, N.T. and Melody, M. eds., Field Trip Guidebook, Second Conference on Earthquake Hazards of the Eastern San Francisco Bay Area, 179-189.

1992 Williams, P.L., Geological record of southern Hayward fault earthquakes, Proceedings, Second Conference on Earthquake Hazards of the Eastern San Francisco Bay Area, 1991-92, in press.

Acknowledgments

Preston Holland was co-leader of the 1992 investigations. Laurel Collins, Andrew Durham, Amy Hosokawa, and Laurie Schuur contributed to field and laboratory investigations.

CYCLIC STICK-SLIP INSTABILITY AS RELATED TO THE EARTHQUAKE CYCLE

USGS Grant #14-08-0001-G1807

Teng-fong Wong, Department of Earth and Space Sciences
State University of New York at Stony Brook
Stony Brook, NY 11794-2100
phone:(516) 632-8212; internet:tfwong@ccmail.sunysb.edu

Objectives

A physical understanding of the nonlinear dynamics of stick-slip instability as an analogue of earthquake rupture is of fundamental importance to earthquake mechanics. To this end, laboratory studies on rock friction can elucidate the friction constitutive relation, the micromechanics of frictional sliding and their relation to stick-slip instability behavior. In our previous study of cyclic stick-slip behavior of ultrafine quartz gouge [*Wong et al.*, 1992], we observed under high pressure a wide range of nonlinear oscillational and dynamic instability behavior which were in qualitative agreement with stability analyses and computer simulation of spring-slider system based on the Dieterich-Ruina type of friction law. The objective of the present study is to continue this line of research on simulated gouges of different mineralogy and particles size and to sliding surfaces of different roughness. Furthermore we proposed to pursue experiments in saturated samples under pore pressure, and to systematically investigate the deformation-induced microstructures.

Transition from stable sliding to cyclic stick-slip

The nonlinear dynamical behavior in the transition from stable sliding to cyclic stick-slip in two rock-gouge systems (sawcut Tennessee sandstone, and Tennessee sandstone with natural halite gouge) were investigated in a conventional triaxial configuration at confining pressures from 30 MPa to 110 MPa. The frictional sliding behavior was qualitatively similar to that of Westerly granite sandwiched with ultrafine quartz gouge. Induced by cumulative slip or load point velocity perturbation, the transition from stable sliding to cyclic stick-slip might involve several distinct sliding modes, including period doubling bifurcations and self-sustained periodic oscillations. The accumulation of slip may destabilize or stabilize the frictional sliding behavior, whereas an increase of load point velocity tends to stabilize the oscillational behavior. Apparently chaotic oscillations were also observed in the halite gouge. Details of the experimental observations were reported by *Gu and Wong* [1992a].

The experimental observations were interpreted using a spring-slider model with single degree of freedom. To reproduce the full range of sliding modes and their observed dependence on velocity perturbation, it was necessary to incorporate two state variables and high-speed cutoff of velocity dependence in the Dieterich-Ruina rate- and state-

dependent friction law. Analytic expression for the onset of Hopf bifurcation in such a system was derived. Stability boundaries dependent on stiffness, load point velocity, and friction constitutive parameters were established based on limit cycle oscillation modes observed in numerical simulations. Critical condition for the triggering of dynamic instability by sudden velocity perturbation was analyzed. The numerical simulation results were summarized by *Gu and Wong* [1993].

Development of Riedel shear localization in quartz gouge

Microstructures developed in ultrafine quartz gouge were compared with those in coarse quartz gouges. Several different country rocks (Westerly granite, Sioux quartzite, Frederick diabase and Blair dolomite) were considered. In the ultrafine quartz gouge, Riedel shear developed very early during frictional sliding, with density increasing with the cumulative slip and number of cyclic stick-slip events. In contrast, the Riedel shears were less developed in the coarser quartz gouge which underwent stable sliding, implying that comminution and compaction stablized the frictional sliding behavior. The detailed results will be presented by *Gu and Wong* [1992b].

Ongoing experimental studies

Ultrafine gouges of feldspar and crushed Westerly granite have been prepared. Frictional sliding experiments at confining pressures up to 400 MPa and at loading velocities between 0.1 to 10 μm/s are being conducted on sawcut Westerly granite samples sandwiched with the ultrafine gouges using our servo-controlled triaxial apparatus. Preliminary experiments have also been conducted on ultrafine quartz gouge under saturated conditions at pore pressures ranging up to 200 MPa. The drained and undrained behavior will be compared. In parallel, the permeability of the gouge will be determined as a function of normal stress and cumulative slip. The development of Riedel shear localization and comminution in the gouge layer will be characterized quantitatively.

References

Gu, J. and T.-f. Wong, The transition from stable sliding to cyclic stick-slip: effect of cumulative slip and load point velocity on the nonlinear dynamical behavior in three rock-gouge systems, in *Rock Mechanics Proceedings of the 33rd U. S. Symposium*, ed. J. R. Tillerson and W. R. Wawersik, A. A. Balkema, Rotterdam, 151-158, 1992a.

Gu, J. and T.-f. Wong, Development of shear localization in ultrafine and coarse grained quartz gouge, *EOS, Trans. Am. Geophys. Union*, **73**, No. 43 supplement, 516, 1992b.

Gu, J. and T.-f. Wong, Nonlinear dynamics of the transition from stable sliding to cyclic stick-slip in rock, submitted to "*Nonlinear Dynamics and Predictability of Critical Geophysical Phenomena*", ed. A. Gabrielov and W. Newman, Am. Geophys. Union Monograph, 1993.

Wong, T.-f., Y. Gu, T. Yanagidani and Y. Zhao, Stabilization of faulting by cumulative slip, in "*Fault Mechanics and Transport Properties of Rocks*", ed. B. Evans and T.-f. Wong, Academic Press, 119-143, 1992.

Collaborative Research (Tennessee Division of Geology and Vanderbilt University): Gravity Survey in the New Madrid Seismic Zone

USGS Grant Award No. 1434-92-G-2233

Ronald P. Zurawski
Tennessee Department of Environment and Conservation
Division of Geology
13th Floor, L & C Tower
401 Church Street
Nashville, TN 37243-0445
615-532-1504

Richard G. Stearns
Geology Department
Vanderbilt University
Box 1615, Station B
Nashville, TN 37235
615-322-2420

Investigations

We are performing a gravity survey of all of five and parts of three 7.5-minute quadrangles near the Mississippi river, north of Latitude 35.5 degrees and west of Longitude 88.5 degrees in Lauderdale and Tipton counties, Tennessee. We also propose to fill gaps in present coverage north of Latitude 35.75 degrees near the Mississippi River. Present coverage includes all of the area of the Mississippi Valley Graben (MVG) north of Latitude 35.75 degrees (over fifty 7.5- minute quadrangles); some of this work is published and some is in preparation.

This project will result in coverage of all of the area of the MVG in Tennessee. The 1.5 km station spacing will be about the same as the one mile spacing between flight lines in existing aeromagnetic maps. The eight quadrangle area of new coverage includes the edge of the MVG where it crosses the Mississippi River, the Chickasaw Bluffs lineament (a likely fault parallel to and close to the edge of the MVG) and other lineaments relating to that feature, and the magnetic high marking the Covington pluton, one of several plutons believed to be related to the edge of the MVG.

The gaps in present coverage are in areas that are difficult to approach, because they are in large farms, swampy areas, or isolated by such river-related features as sloughs or chutes. Reelfoot Lake (tectonically sunk during the 1811 earthquake) is mostly a large swamp accessible only by boat, and many of the areas near the Mississippi river can be best (or only) approached by boat. Gaps are important because they tend to be in areas of land subsidence (such as Reelfoot Lake) , or are near suspected faults (such as straight reaches of rivers).

The completed survey will consist of about 400 new stations, plus an estimated 100 reoccupations of old stations. There are already about 20 stations in each quadrangle (for which we have full original records). We also customarily reoccupy one or more old stations during each loop to check for bad loops. For fill-in surveys more reoccupations will be needed.

There are four base stations in or near the project survey areas. Gravity stations are occupied using loops and data will be reduced in the usual manner. Based on reoccupation statistics for surveys we have made so far, observed gravity will be better than 0.3 mgal standard deviation. Relatively low relief makes it likely that standard deviation of Bouguer anomaly will be near the same low value.

Results

Background

Gravity surveys have been made in the project area by Vanderbilt University since 1967 (Smith, 1967). This survey was incorporated into the regional survey of West Tennessee supported by USGS. Station spacing for this survey was about two miles (15-20 stations in each 7.5-minute quadrangle). Vanderbilt surveyed the area of West Tennessee west of 89 degrees Longitude and University of Kentucky (G. R. Keller, now at the University of Texas-El Paso) surveyed West Tennessee from 88-89 degrees Longitude. A regional map (Hildebrand and others, 1977) published by USGS and a map of West Tennessee (Stearns, Keller, and Templeton, 1980) published by the Tennessee Division of Geology resulted from this survey.

Soon after (1979-1982) more detailed surveys were made in the area working outward from the area of Reelfoot Lake in the northwest corner of Tennessee. A detailed gravity map was published by the Tennessee Division of Geology of the area close to Reelfoot Lake (Stearns, 1980). Surveys supported by the US Nuclear Regulatory Commission were published in NUREG documents (Keller, 1980; Stearns, 1986 and 1987).

These surveys used a variety of bases, and had sufficient data problems that Stearns judged that a thorough editing and possible recalculation was warranted. This task was carried on along with limited field work, including surveys of several quadrangles to square up the survey area. Once the editing job was completed, a project to make maps of the large area began with G. R. Keller at the University of Texas-El Paso, who had surveyed the area east of 89 degrees Longitude in 1978.

The entire area of the MVG now lacks only the data that will be acquired during this project.

Recent Work

During the first quarter of the project period we made 276 station occupations in eighteen 7.5-minute quadrangles. There were 34 loops; 4 to 15 stations in each loop. Every loop included at least one reoccupied old station (average of 2, range 1 to 10). There are 202 new stations and 74 reoccupations.

Stations were taken to fill gaps in earlier surveys, most in places hard to access because they are in the Mississippi River floodway, wetlands, or in large farms with few or no roads. Specific areas include:

Mississippi bank and floodway from Madrid Bend in Kentucky to the Cottonwood Point Quadrangle near 36 degrees Latitude.
Reelfoot Lake shore and wetland accessible by four-wheel drive vehicle.
Obion River bottoms upstream to the Rives and Rutherford quadrangles.
Part of the Forked Deer River bottom north of 36 degrees upstream to the Tatumville Quadrangle.

Future Work

Our plan is to continue the survey when weather and ground conditions improve. Our priorities are:

1- Survey of quadrangles south of 36 degrees in the bottoms, wetlands and floodway of the Mississippi and Hatchie rivers,
2- Finish some remaining gaps in the bottoms and wetlands of the Obion and forked Deer rivers, and
3- Reach some so-far inaccessible places by boat.

References Cited

Hildebrand, T. C., Stearns, R. G., and others, 1977, Bouguer gravity map of the Northern Mississippi Embayment, parts of Missouri, Arkansas, Tennessee, Kentucky and Illinois, U. S. Geological Survey Open File, Map No. 77-228.

Keller, G. R. and others, 1980, Bouguer gravity anomaly map of the east-central Midcontinent of the United States, U.S. Nuclear Regulatory Commission, NUREG/CR-1663, 12 p. with map, scale 1:1,000,000.

Smith, J. R., 1967, The Covington Pluton, unpublished Master's Thesis, Vanderbilt University, Nashville, Tennessee.

Stearns, R. G. and others, 1980, Gravity anomaly maps of Tennessee, West sheet, Tennessee Division of Geology, scale 1:250,000.

Stearns, R. G., 1980, Gravity anomaly map of the Reelfoot Lake Area, Tennessee (including a portion of southwest Missouri), Tennessee Division of Geology, scale 1:62,500.

Stearns, R. G., 1986, Post-Eocene fault near east edge of Reelfoot Rift in Lauderdale County, Tennessee, (with S. L. Wilson and S. J. Naval), U. S. Nuclear Regulatory Commission, NUREG/CR-4702, 36 p.

Stearns, R. G., 1986, One-dimensional gravity calculation and paleozoic structure and plutons at Reelfoot Scarp, (with S. L. Wilson), U. S. Nuclear Regulatory Commission, NUREG/CR-4703, 43 p.

Stearns, R. G., 1987, An integrated geological, geophysical and geochemical investigation of the major fractures on the east side of the New Madrid Earthquake Zone, (with A. L. Reesman), U. S. Nuclear Regulatory Commission, NUREG/CR-4936, 27 p., May.

Reports Published

None this reporting period.

Determination of earthquake source parameters from regional waveforms: Analysis of sparse network data in the Aleutians

1434-92-G-2200

Geoffrey Abers, Won-Young Kim
Lamont-Doherty Geological Observatory of Columbia University
Palisades, New York 10964
(914) 359-2900, 365-8828

Investigations Undertaken

We study wave propagation effects and develop appropriate procedures for calculating regional waveforms and determining source parameters in a subduction environment. We study amplitudes and phases observed in broadband and intermediate period seismograms recorded at stations in the east Aleutians, in particular the seismographic station at Sand Point, Alaska, for east Aleutian earthquakes. These waveforms and full waveform modeling methods are used to better understand propagation effects for these paths, and the sensitivity of these waveforms to earthquake source parameters. The goal of these studies is to characterize Aleutian propagation effects sufficiently to invert regional subduction zone seismograms for earthquake source parameters, and to develop appropriate inversions. In the future, such inversions may provide most of the information available for Aleutian earthquakes that are too small to study from teleseismic data, if monitoring in the Aleutians is based upon a sparse distribution of broadband stations.

Results Obtained

Work thus far has concentrated on assessing wave propagation properties to the station SAN in Sand Point, Alaska, where broad-band and intermediate-period digital waveforms have been recorded since 1982 (funding cuts forced the termination of digital data collection in the summer of 1992). The first part of this work has been to compile focal mechanisms from local network data, recently made possible by the determination of 3D velocity structure and accurate ray tracing through the model [Abers, 1992]. The most promising events are those that show interplate thrusting and events within the downgoing plate next to the interplate thrust events (Figure 1). The interplate thrust events are the most numerous and pose the most significant seismic hazard, so their evaluation is a high priority. The events below the thrust zone have different focal mechanisms and are 5-15 km deeper with similar epicenters; they are similar in depth and mechanism to events at the top of the downgoing plate in subduction zones where interplate thrust events are absent, such as Cascadia or the post-1964 Gulf of Alaska. Because paths are similar for these two sets of events but depths and mechanisms vary, they make a useful data set to test the ability of waveforms to recover source parameters.

Record sections have been constructed for interplate thrust events to station SAN, using broadband and intermediate period waveforms (Figure 2). These figures compare vertical and transverse seismograms, and show differences in arriving *P* and *SH* energy. These events are 25-40 km deep. Several types of complexity are apparent in these record sections:

- Waveforms make the transition at ~150 km range from impulsive seismograms, with most energy in the initial P/S cycle, to emergent records with energy dispersed over many cycles at longer ranges. The more distant class of seismograms will be much more difficult to model by direct waveform matching.
- Significant energy is observed on the transverse component soon after the initial *P* onset, in some cases (~90 km range) within a fraction of a second. Some of this energy has the form of discrete phases, and suggests specific scatterers. These arrivals will be impossible to model using a plane-layered propagation structure, and can be used to estimate the signal-generated noise level that will limit quality of seismogram fit.

• Distinct phases are seen to arrive on vertical component seismograms in the interval between *P* and *S*, the largest arriving 2-4 s before the transverse-component *S* arrival. These are probably *S*-to-*P* conversions, either at the free surface (e.g., Figure 3) or at other interfaces directly below the receiver (more likely for a phase 2-4 s before direct *S*). A successful Green's function must include the generation of these phases, because their amplitude is comparable to direct phases and ignoring them could lead to potentially large errors.

Several sensitivity tests have been conducted of seismogram matching. In one example, a complex plane-layered structure was used to generate seismograms at a series of depths (Figure 3). A prominent phase ~5 s after direct *P* is modeled as a *S*-to-*P* conversion at the free surface; timing of this phase is relatively independent of structure. Large amplitude variations are seen in synthetic seismograms in the first 5-10 s after direct S, due to crustal reverberation (labelled S1S). The amplitude variations of S1S can be equally well modelled by changes in depths to mid-crustal interfaces, comparable to direct *S* amplitudes, suggesting that the early S coda will hard to model without very good estimates of path structure. Another example demonstrates sensitivity to focal mechanism orientation, and shows that even a single seismogram may provide useful constraints on fault orientation (Figure 4).

Publications

Abers, G.A., and W.-Y. Kim, Potential of broad-band regional seismographs in the Aleutians, in Christensen et al., eds.,*Wadati Conference on Great Subduction Earthquakes*, U. Alaska Fairbanks, p. 154-155, 1992.

Abers, G.A., Plate configuration and seismogenic deformation of the Shumagin region, in Christensen et al., eds.,*Wadati Conference on Great Subduction Earthquakes*, U. Alaska Fairbanks, p. 147-149, 1992.

Abers, G.A., Relationship between shallow- and intermediate-depth seismicity in the eastern Aleutian subduction zone, *Geophys. Res. Lett.*, **19**, 2019-2022, 1992.

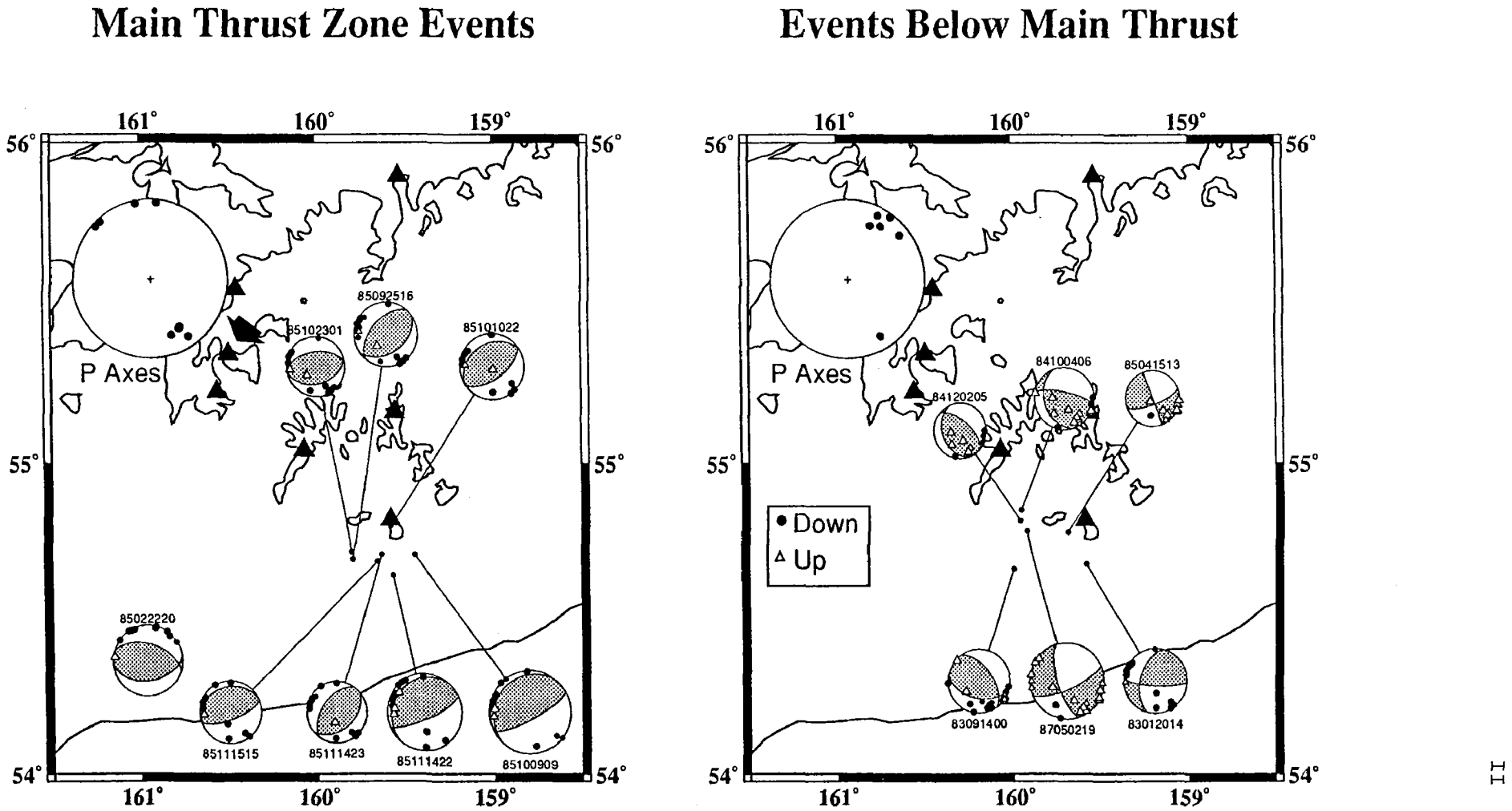

Fig. 1. First motion fault-plane solutions for events on and near the interplate thrust zone in the Shumagin Islands region. Open triangles are dilatations, circles are compressions. Events are relocated in 3D velocity model and rays are determined by exact ray tracing through the model. Events >5 km below main thrust zone show different mechanisms with rotated P axes. Solid triangles show network stations; SAN is indicated by large arrow. All results here are well-constrained by short-period arrival times and first motions; these events can be used to assess inversions of intermediate-period and broadband waveforms.

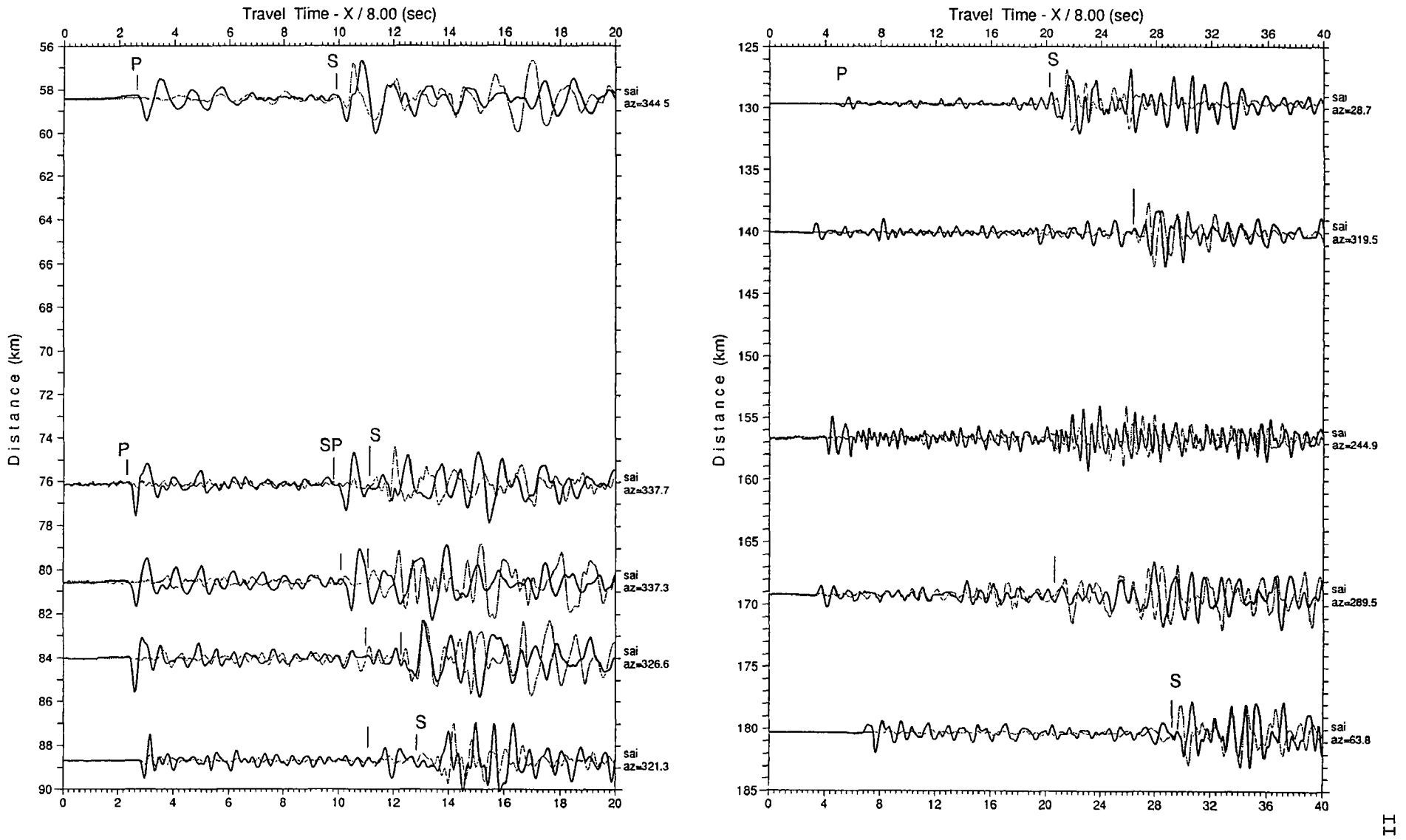

Figure 2. Record sections to station Sand Point (SAI) from interplate thrust zone earthquakes for distance range 56 to 90 km (**left panel**) and for distance range 125 to 185 km (**right panel**). For each event, vertical (*solid*) and transverse (*dotted*) components of intermediate-period records are plotted together for comparison. Records at 156.6 km are broadband. Major phases between P and S are probable converted phases and the most prominent phases (SP) arrive 1-2 sec before S with similar amplitude as S. Timing is modeled by S-P conversion ~10 km below station. Phase arrives too late for Sp free-surface critical refraction. These phases are large and are necessary to understand in modeling waveforms.

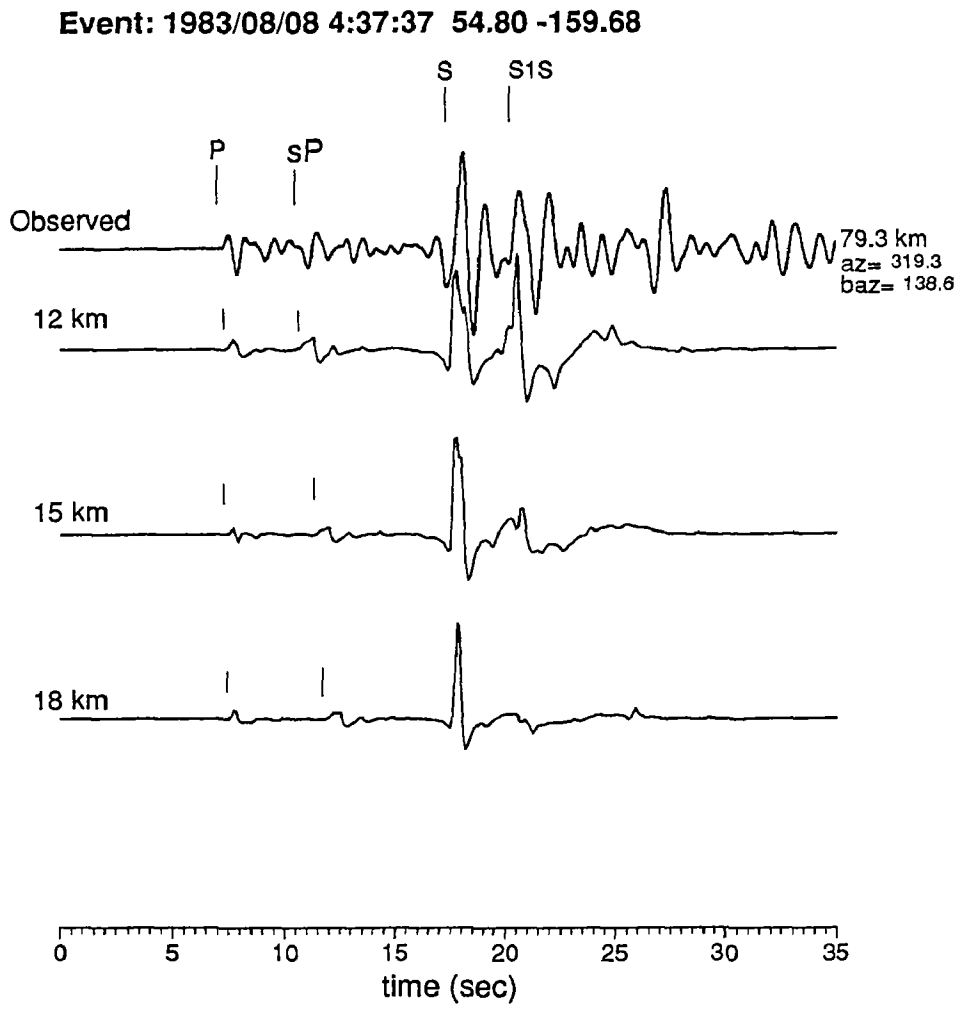

Figure 3. Observed and calculated vertical-component intermediate-period seismogram for event an upper-plate event 79 km from station at Sand Point, Alaska (event depth ~15 km from S-P times at station directly over event). Calculated seismograms are generated for mechanism consistent with first-motions, for depths of 12, 15, and 18 km. Calculation is a full-waveform seismogram using reflectivity and wavenumber integration, assuming a plane-layered structure similar to one determined from arrival-time inversion. The sP is the phase modelled as a S-to-P converted phase reflected off of the free-surface. Note relatively constant S-P times and 1 s change in sP-P times. Relative amplitudes of S to crustal reverberation S1S vary significantly with depth, because distance to nearest layer boundary changes (layer boundaries are at 10, 20, 30, 40, 75 km depth). Similar amplitude changes can be generated by moving interface with depth fixed, so if depth is known (from sP-P) then structure can be constrained.

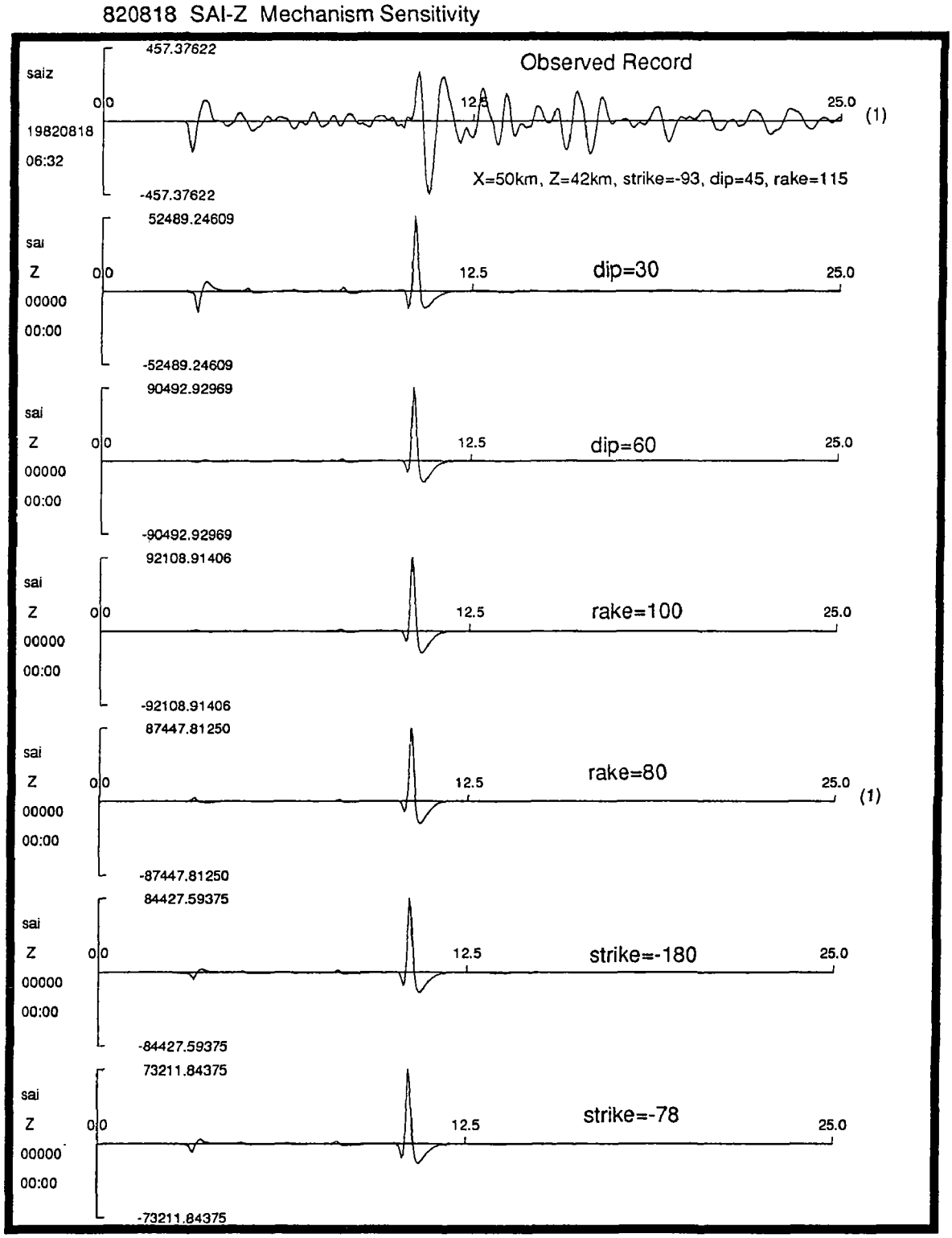

Figure 4. Vertical-component IP seismogram for event 820818 (42 km deep, 50 km distance) compared with seismograms calculated for varying mechanism. Mechanism determined from network first-motion polarities is oblique-reverse slip; parameters given at top. Observed seismogram is on top, followed by seismograms where each of strike, dip, slip is perturbed by 15 degrees. All seismograms are scaled by maximum amplitude. Velocity structure resembles that determined from inversion of arrival-times. Increase in rake or dip gives P arrivals that are too small.

Studies on Intrinsic Q^{-1} and Scattering Q^{-1} in Earthquake Source Regions

1434-92-G-2179
Keiiti Aki and Anshu Jin
Department of Geological Sciences, University of Southern California
Los Angeles, CA 90089-0740

INVESTIGATION

Introduction and objective

Attenuation of S-waves measured by Q^{-1} consists of contributions from scattering and absorption, namely, $Q^{-1} = Q_s^{-1} + Q_i^{-1}$, $Q_s^{-1}=k^{-1}\eta_s$ and $Q_i^{-1}=k^{-1}\eta_i$, where k is the wavenumber and η_s and η_i are the scattering and intrinsic attenuation coefficients, respectively. Hoshiba et al., (1991) have developed a method, called " multiple lapse time analysis", in which they consider energy for three consecutive time windows as a function of hypocentral distance to estimate the seismic albedo, $B_0=\eta_s/(\eta_s+\eta_i)$, and the total attenuation coefficient L_e^{-1}. Where $L_e=1/(\eta_s+\eta_i)$ is the extinction distance over which the primary S-wave energy is decreased by e^{-1}. Figure 1 shows how the energy determined for the three time windows varies as a function of source-receiver distance. They are calculated by Monte-Carlo simulations using homogeneously distributed scatterers in a full-space with uniform intrinsic attenuation under the assumption of isotropic multiple scattering for various B_0 and L_e (Hoshiba et al., 1991).

The objective of this study is to determine the intrinsic Q^{-1} and scattering Q^{-1} separately by applying the method of Hoshiba et al.(1991) to the broad-band high dynamic range seismograms of the TERRAscope network in southern California .

Data

Figure 2 shows the locations of the 6 TERRAscope seismic stations and the earthquakes used in this study. To obtain both the scattering and intrinsic Q^{-1} as a function of frequency, we selected earthquakes within 70 km for each station. Then we calculated, for each seismogram, the squared amplitude spectrum, $|F(\omega)|^2$ for the following three time windows: 0 to 15 seconds , 15 to 30 seconds, and 30 to 45 seconds measured from the onset of the S-wave arrival. We eliminated the effect of ambient noise by taking a noise sample of length 25 s prior to the P-wave arrival and subtracting the noise power spectra from the signal power spectra in each time window assuming that signal and noise are statistically independent. Data with signal power less than twice the noise was discarded. To normalize the observed energy for different magnitude earthquakes we chose a coda sample at a reference lapse time of 45 ± 2.5 seconds and calculated the squared amplitude spectrum, $|F^{ref}_{coda}(\omega)|^2$. The spectra for each lapse time window and the coda spectra at the reference lapse time (45 s) are averaged over three components and the normalized energy, $\frac{|F(\omega)|^2}{|F_{coda}(\omega)|^2}$, is calculated for each station - earthquake pair.

RESULTS

(1), No significant differences, neither in B_0 nor L_e^{-1}, have been found between the stations located on or near the San Andreas fault (such as station SVD, PFO, and PAS) and the stations far away from the fault (such as station ISA and GSC).

(2), Figure 3 shows the normalized energy, corrected for geometrical spreading by $4\pi r^2$ as a fuction of hypocentral distance for all stations at frequencies 0.75, 1.5, 3.0, and 6.0 Hz. The preliminary estimates of B_0 and L_e^{-1} for the whole of southern California, and corresponding scattering, intrinsic and total attenuation values, Q_s^{-1}, Q_i^{-1} and Q_t^{-1}, are listed in Table 1. Scattering dominates intrinsic absorption at low frequencies and vice versa at high frequencies. This is a universal observation for the frequency range 1 to 10 Hz.

Table 1

frequency (Hz)	Bo	δBo	L_e^{-1}	δL_e^{-1}	Q_s^{-1}	Q_i^{-1}	Q_t^{-1}
0.75	0.70	0.20	0.050	0.020	0.0223	0.0095	0.0318
1.5	0.50	0.12	0.075	0.025	0.0119	0.0119	0.0238
3.0	0.35	0.10	0.048	0.018	0.0027	0.0050	0.0077
6.0	0.30	0.07	0.048	0.018	0.0011	0.0027	0.0038

$B_0 = \eta_s L_e$, $L_e^{-1} = \eta_e = (\eta_i + \eta_s)$, where η_s, η_i, and η_e are the scattering, intrinsic and total attenuation coefficients, respectively. Attenuation was determined by: $Q_s^{-1} = \eta_s k^{-1}$, $Q_i^{-1} = \eta_i k^{-1}$, and $Q_t^{-1} = \eta_e k^{-1}$, where $k = 2\pi f/\beta$ and $\beta = 3.0$ km/s. δB_0 and δL_e^{-1} is the standard error of B_0 and L_e^{-1}, respectively.

Reference

Hoshiba, M, H. Sato, and M. Fehler, Numerical basis of the Separation of scattering and intrinsic absorption from full seismogram envelope, --a Monte-Carlo simulation of multiple isotropic scattering, Meteorology and Geophysics, 42, 65-91,1991.

Figure captions

Figure 1. Energy for the three time windows (0-15s, 15-30s,and 30-45s) plotted as a function of hypocentral distance r (km) for different pairs of L_e and B_0 predicted by Monte-Carlo simulations. Here the scatterers are statistically uniformly distributed in a full-space with uniform absorption coefficient. The scattering is assumed to be isotropic. (Following Hoshiba et al., 1991.)

Figure 2. Locations of the 6 TERRAscope seismic stations (the triangles) and the earthquakes used in theis study (the solid dots).

Figure 3. Plots of normalized energy corrected for geometrical spreading, $4\pi r^2$, as a function of hypocentral distance r (km), for frequencies 0.75, 1.5, 3.0, and 6.0 Hz (from the top to the bottom), measured at station SVD (right) which is located on the San Andreas fault, and ISA (left) which is located at a distance from the fault. E_1, E_2, and E_3 represent energy measurements for time windows of 0-15, 15-30, and 30-45 second, respectively.

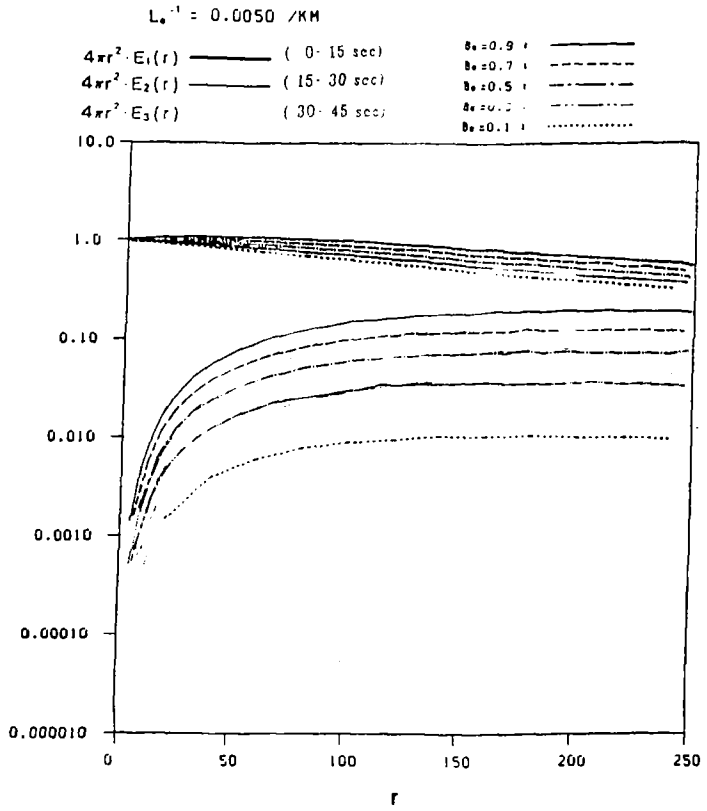
L_e^{-1} = 0.0050 /KM
$4\pi r^2 \cdot E_1(r)$ (0- 15 sec)
$4\pi r^2 \cdot E_2(r)$ (15- 30 sec)
$4\pi r^2 \cdot E_3(r)$ (30- 45 sec)
B_e=0.9
B_e=0.7
B_e=0.5
B_e=0.3
B_e=0.1
10.0
1.0
0.10
0.010
0.0010
0.00010
0.000010
0
50
100
150
200
250
r

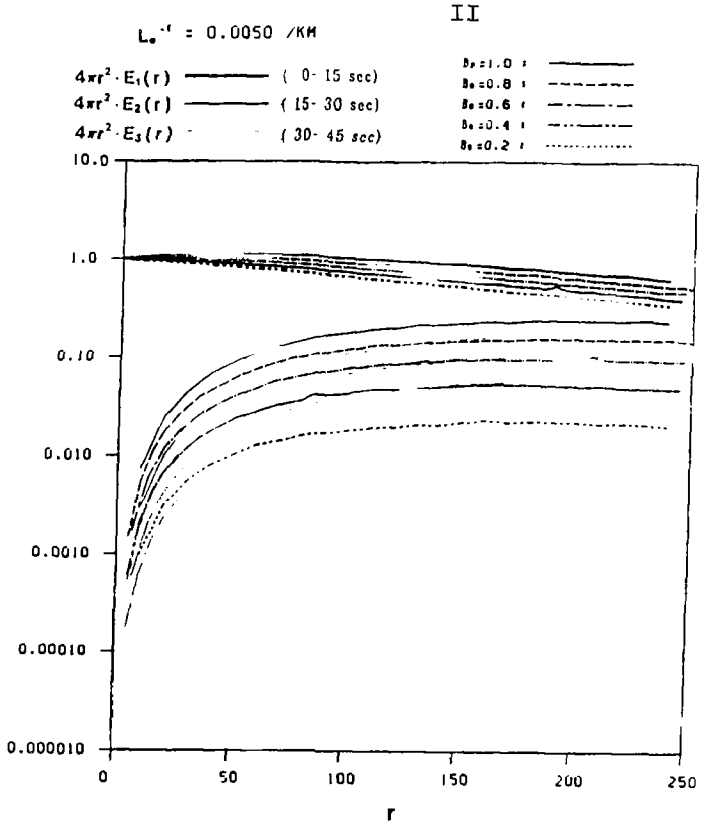
L_e^{-1} = 0.0050 /KM
$4\pi r^2 \cdot E_1(r)$ (0- 15 sec)
$4\pi r^2 \cdot E_2(r)$ (15- 30 sec)
$4\pi r^2 \cdot E_3(r)$ (30- 45 sec)
B_e=1.0
B_e=0.8
B_e=0.6
B_e=0.4
B_e=0.2
10.0
1.0
0.10
0.010
0.0010
0.00010
0.000010
0
50
100
150
200
250
r

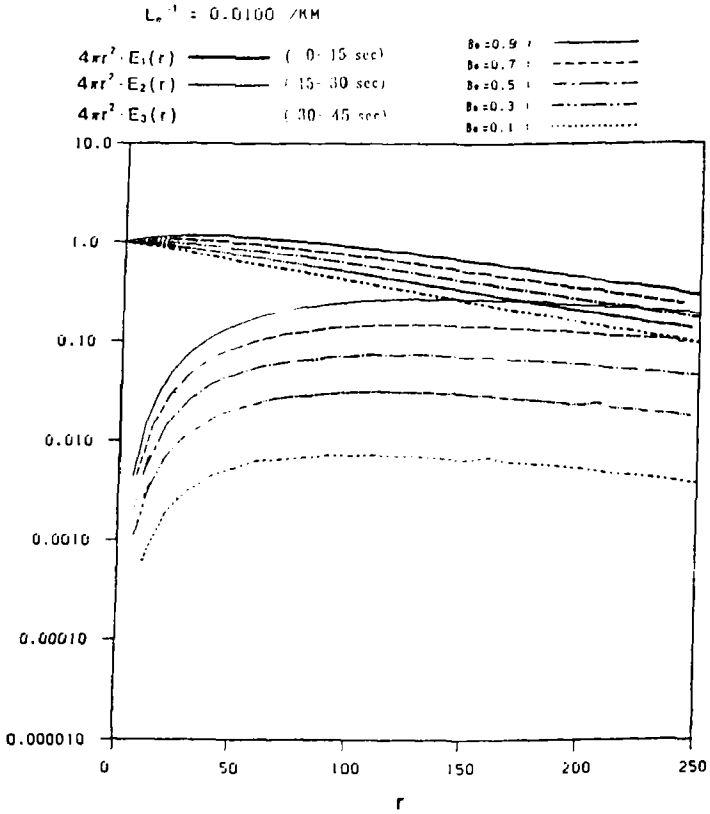
L_e^{-1} = 0.0100 /KM
$4\pi r^2 \cdot E_1(r)$ (0- 15 sec)
$4\pi r^2 \cdot E_2(r)$ (15- 30 sec)
$4\pi r^2 \cdot E_3(r)$ (30- 45 sec)
B_e=0.9
B_e=0.7
B_e=0.5
B_e=0.3
B_e=0.1
10.0
1.0
0.10
0.010
0.0010
0.00010
0.000010
0
50
100
150
200
250
r

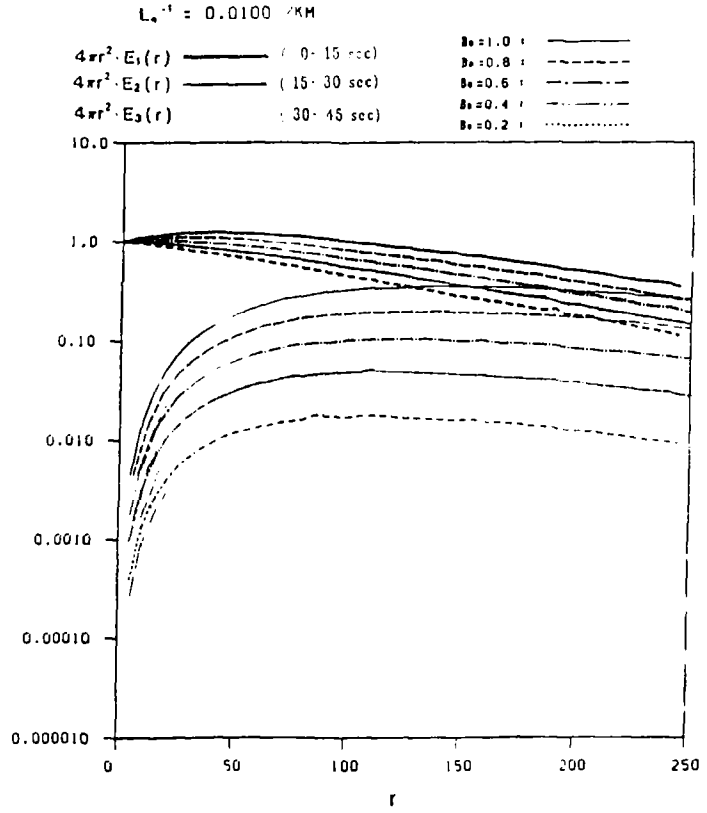
L_e^{-1} = 0.0100 /KM
$4\pi r^2 \cdot E_1(r)$ (0- 15 sec)
$4\pi r^2 \cdot E_2(r)$ (15- 30 sec)
$4\pi r^2 \cdot E_3(r)$ (30- 45 sec)
B_e=1.0
B_e=0.8
B_e=0.6
B_e=0.4
B_e=0.2
10.0
1.0
0.10
0.010
0.0010
0.00010
0.000010
0
50
100
150
200
250
r

Figure 1

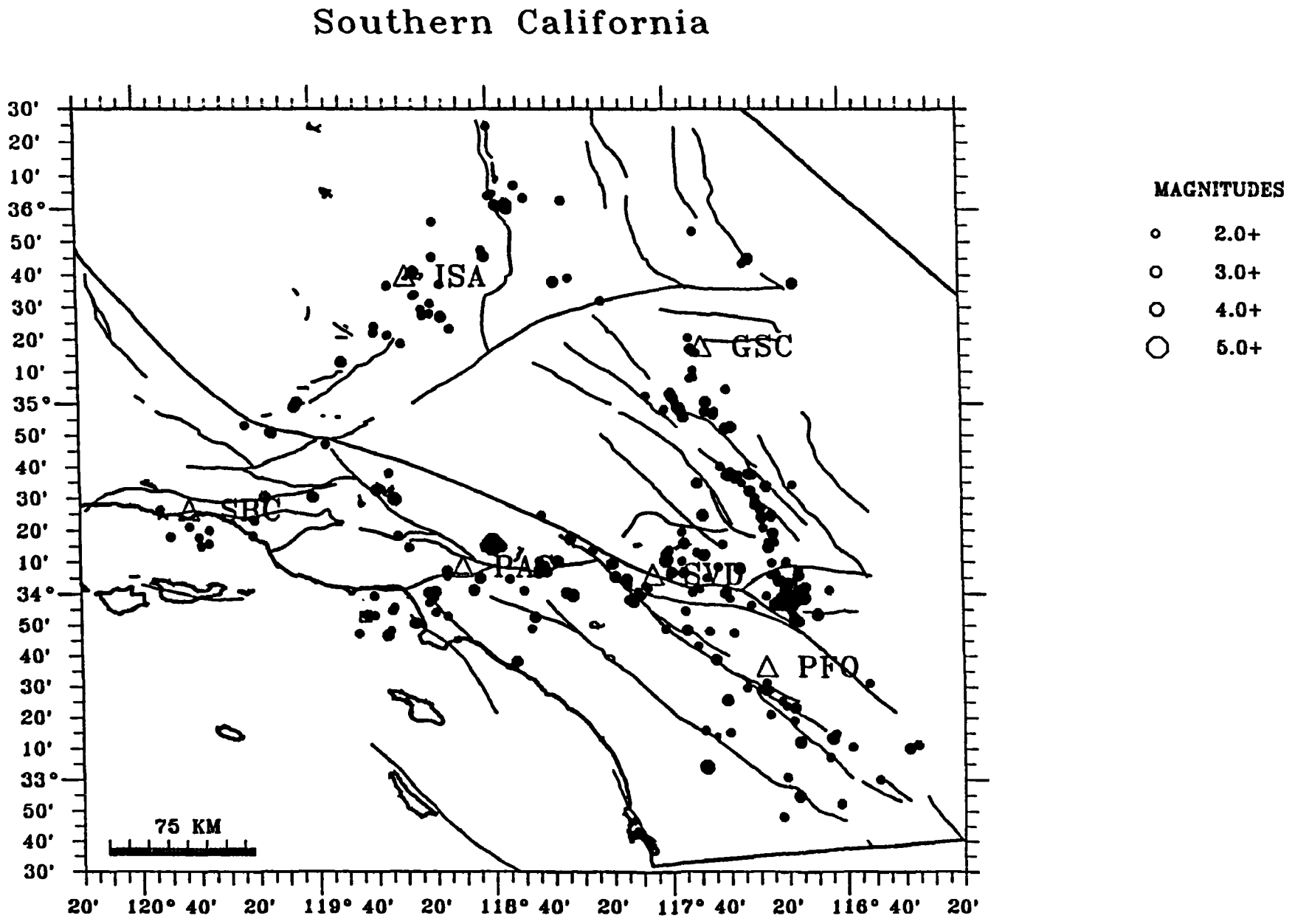
Southern California
MAGNITUDES
2.0+
3.0+
4.0+
5.0+
ISA
GSC
SBC
PAS
SVD
PFO
75 KM
30'
20'
10'
36°
50'
40'
30'
20'
10'
35°
50'
40'
30'
20'
10'
34°
50'
40'
30'
20'
10'
33°
50'
40'
30'
20'
120° 40'
20'
119° 40'
20'
118° 40'
20'
117° 40'
20'
116° 40'
20'

Figure 2

REGIONAL AND LOCAL HAZARDS MAPPING IN THE EASTERN GREAT BASIN

9950-01738

R. Ernest Anderson
Branch of Geologic Risk Assessment
U.S. Geological Survey
Box 20546, MS 966, Denver Federal Center
Denver, Colorado 80225
(303) 273-8578

INVESTIGATIONS

1. Studied the interrelations between Neogene strain and its bearing on horizontal extension and horizontal and vertical contraction at the eastern margin of the extensional orogen, Mormon Mountains area, Nevada and Utah.

2. Studied the interrelations between Neogene strain and its bearing on horizontal extension, and horizontal and vertical contraction at the transition zone of the Colorado Plateau and Basin and Range in the tricorner area of the Virgin River depression, Utah, Nevada, and Arizona.

RESULTS

1. Analysis of the distribution, geometry, and kinematics of structures of known or suspected Neogene age ranging in size from mountain blocks to outcrop scale between the southern Mormon Mountains and the Colorado Plateau shows that extensional deformation was accompanied by major vertical structural uplift and associated structural thinning (attenuation) and by extension-normal horizontal contraction. The vertical attenuation developed mainly by normal-sense displacements on steeply dipping to horizontal faults and appears to be most intense on the flanks of and above severely uplifted and tilted footwall blocks, several of which are major structural culminations that expose Precambrian crystalline basement rocks. Tilts of strata in these footwall culminations commonly exceed those in the hanging wall, suggesting convex-upward fault geometry. The faults either have curved traces concave upward toward the culmination or consist of two segments whose obtuse intersection angle faces the culmination. Stratigraphic throw either decreases abruptly away from the culmination axis or is fed abruptly into major transverse accommodation zones that possibly represent long-lived structural flaws. Typically, the culminations have strike lengths only two to three times their maximum throw, suggesting extreme lateral strain heterogeneity. Most are too small and have flanks that dip too steeply for isostatic uplift following tectonic denudation to be a cause of their formation. Also, in plan view, they tend to be arranged en echelon such that strain is not cumulative from one to the other along sections paralleling their kinematic axes. A major effect of hanging-wall structural attenuation adjacent to and above the culminations is to subdue the potential surface relief associated with uplift and tilting of the footwall.

2. The Virgin River depression and surrounding mountains in the Utah, Nevada, and Arizona tricorner area are Neogene features that are partly contiguous with the little-strained rocks of the structural transition to the Colorado Plateau province. This contiguity makes the area ideally suited for evaluating the sense, magnitude, and kinematics of Neogene deformation. Analysis along the strain boundary shows that, compared to the adjacent little-strained area, large-magnitude vertical deformation (both uplift and depression, locally exceeding 10 km) greatly exceeds extensional deformation and that there are tectonically significant amounts of lateral displacement approximately parallel tot he province

boundary. Extensional kinematics, the directions of lateral displacements, and the positioning and orientation of uplifts and one major depression are such that isostatic rebound following tectonic denudation is an unlikely direct cause of the strong vertical structural relief adjacent to the strain boundary. Instead, the observed structures are first-order features that define a three-dimensional strain field that formed in response to approximately east-west extension, vertical structural attenuation, and extension-normal shortening.

REPORTS

Anderson, R.E., and Barnhard, T.P., 1991, Relationship between Miocene plutonism, uplift, and extension Lake Mead area, northernmost Arizona and adjacent Nevada: Geological Society of America Abstracts with Programs, v. 23, p. A245.

____1992, Neotectonic framework of the central Sevier Valley area, Utah, and its relationship to seismicity: U.S. Geological Survey Professional Paper 1500-F, p. F1-F48.

____1992, Heterogeneous Neogene strain and its bearing on horizontal extension and horizontal and vertical contraction at the margin of the extensional orogen, Mormon Mountains area, Nevada and Utah: U.S. Geological Survey Bulletin B-2011, 113 p.

____(in press), Aspects of three-dimensional strain at the margin of the extensional orogen, Virgin Depression area, Nevada, Utah, and Arizona: Geological Society of America.

Anderson, R.E., and Hintze, L.F., 1991, Geologic map of the Dodge Spring quadrangle, Washington County Utah, and Lincoln County, Nevada: U.S. Geological Survey Open-File Report OF-360, scale 1:24,000

____1992, Geologic map of the Dodge Spring quadrangle, Washington County, Utah, and Lincoln County, Nevada: U.S. Geological Survey Quadrangle Map GQ-1721, scale 1:24,000.

Barnhard, T.P., and Anderson, R.E., 1991, Tectonic significance of dike orientations int he Lake Mead area of Nevada and Arizona: Geological Society of America Abstracts with Programs, v. 23, p. A233.

Analysis of Similar Earthquakes in Seismic Gaps

Award number 1434-92-G-2202

Richard C. Aster (P.I.)
Joseph A. Henton (Graduate Student)
Department of Geoscience/Geophysical Research Center
New Mexico Institute of Mining and Technology
Socorro, NM 87801
(505) 835-5924

Introduction

We utilize nearly identical microearthquake pairs recorded by the Anza, Parkfield, and Southern California seismic networks as quasi-repeating broadband sources at depth to probe seismic gaps in California for possible temporal variations in the seismic Green function. Significant progress has been made over the past year on the three principal goals of this project:
(1) Comprehensive identification of similar earthquake pairs and clusters in large microearthquake data sets.
(2) Development and evaluation of techniques for relative waveform analysis.
(3) Analysis of similar microearthquake seismograms to identify or establish limits on temporal variability in seismic Green's functions, specifically concentrating on seismic velocity, coda decay, and shear-wave anisotropy.

Progress

Comprehensive identification of similar earthquakes in large microearthquake data sets.

The first step in the project, now nearly completed, is to identify all earthquake pairs and clusters most suitable for similar earthquake analysis. One may, in principle, evaluate the complete upper-triangular matrix characterizing the waveform similarity of all of the earthquake pairs. For large data sets such as those considered here, however, this process may become prohibitively time consuming, as the amount of work required is proportional to $N(N-1)$. It is thus worthwhile to consider reasonable precomparison criteria which allow one to dismiss *a priori* those earthquake pairs which are highly unlikely to have similar seismograms.

Studies of waveform coherence from earthquake sources (e.g., Geller and Mueller, 1980; Thorbjarnardottir and Pechmann, 1987) suggest that a search for similar events would not need to consider earthquake pairs with interhypocenter separations of much more than a few times $\lambda_{max}/4$, where λ_{max} is the longest wavelength of interest. More recent work (Hutchings and Wu, 1990; Harris, 1991; Vernon, 1992; Scott, 1992) indicates that the $\lambda_{max}/4$ guideline is too restrictive in some cases, and that appreciable coherence can exist for interhypocenter separations of up to a few times λ. Thus, if one only examines seismograms from earthquake pairs with interhypocenter separations of $\Delta \leq \Delta_{max}$, where Δ_{max} is taken to be both several times the maximum dimension of a typical hypocenter error ellipse and several times λ_{max}, then essentially all highly similar earthquake pairs will be identified, despite a large reduction in computer time.

For the Anza network (Berger et al., 1984; Vernon, 1989) catalogue typical hypocenter errors are approximately 1 km (Scott, 1992; Scott et al., 1992), however, it is possible for an event to be mislocated by much more than this if one or more of the picks has an anomalously large picking error due to a phase misinterpretation. As a result of this problem, standard cluster studies based on nearly identical hypocenters may miss some nearly-identical pairs. Our algorithm can overcome this difficulty when a fairly generous value for Δ_{max} is chosen.

For the Anza data set, Δ_{max} was taken to be 10 km. To further reduce the work required to characterize waveform similarity, we eliminated from the analysis waveforms which were identified in the Anza data base as being unreadable. These precomparison criteria reduced the number of three-component seismogram pairs which needed to be cross-correlated by over an order of magnitude, from approximately 9×10^7 to approximately 5×10^6.

In general, any commutative measure may be chosen to quantify waveform similarity. For Anza network recordings which satisfied the above precomparison criteria, the three-component shear-wave seismogram cross-correlation peak between pairs of events (Aster et al., 1990) observed across the network was taken as the similarity measure. The median was chosen after trying several other operators. The minimum or mean cross-correlation was found to be unduly sensitive to low cross-correlation outliers which occasionally occurred when the S-wave arrival times used for the initial alignment of the two events exceeded the window length used in the cross-correlation at one or more stations. The maximum cross-correlation operator, on the other hand, tended to unduly emphasize the contribution of seismograms recorded at stations which were band-limited due to high near-surface attenuation (e.g., stations WMC and LVA; Hough and Anderson, 1988; Hough et al., 1988; Vernon, 1989).

The similarity measure for events j and k is thus $S_{jk} = \text{median}_i\{C_{ijk}\}$, where i is a station index and C_{ijk} is the three-component cross-correlation maximum. The time window used was 0.512 s ($M = 128$ samples) of the shear wave, beginning 0.128 s (32 samples) before the S arrival time pick. The S_{jk} were estimated for 1,121,332 earthquake pairs, requiring approximately 3 weeks of CPU time on a SUN sparc2 workstation. A plot of the S_{jk} versus estimated interhypocenter separation is shown in Figure 1.

The S_{jk} are quantitative measures of the degree of similarity between wavefield pairs, as spatially sampled by stations in the network. It is often the case that many mutually similar earthquakes will be generated in a small region, (e.g., Ishida and Kanamori, 1978; James and Savage, 1990). An equivalence class (EC) algorithm (e.g., Knuth, 1968; Press et al., 1986) was used to organize the pair similarity information into similar earthquake clusters. The EC procedure organizes the pair similarity catalogue into nonintersecting sets of events, the elements of which satisfy a commutative "sameness". In this application, the resulting event trees are open in that if earthquake pairs (A, B) and (B, C) both satisfy the sameness condition, then A, B, and C will be grouped into the same equivalence class, regardless of the similarity measure between A and C.

The sameness condition for the Anza network data was taken to be $S_{jk} \geq \beta$, where β is a value between 0 and 1. If β is close to 1, then the EC algorithm will identify a small number of tiny clusters consisting of earthquakes with extremely similar seismograms. As the β cutoff is reduced, new pairs become eligible for consideration, and are either incorporated into existing clusters or are assigned to new clusters. Additionally, two or more formerly separate clusters may coalesce into a single cluster. As β becomes close to the cross-correlation noise value, coalescence will eventually dominate, resulting in a small number of huge clusters containing almost all of the earthquakes. Because of the competing processes of new cluster formation and cluster coalescence, some value of β will produce a maximum number of clusters (there may be multiple maxima for some data sets).

To find a near-optimal β value for organizing events pairs into clusters, the number of event pairs, the number of equivalence classes, and the number of individual events were counted for $\beta = \{0.975, 0.950, 0.925, ..., 0.400\}$ (Figure 2). In the Anza data set, clustering was maximized ($N_{Equiv} = 290$) for $\beta \approx 0.725$ (1255 events; 1720 pairs). Figure 3 shows the locations of events in clusters with ten or more members, the largest of which occur along the Buck Ridge fault near Toro peak (number 276; 202 events) and in the Cahuilla Swarm zone, west of the seismic gap (number 212; 118 events). Both of these clusters have been sporadically active throughout the operational period of the Anza network (with pronounced peaks in activity during 1990 for the Buck Ridge cluster and during 1983 for the Cahuilla Swarm) and have produced similar earthquakes pairs with large temporal separations.

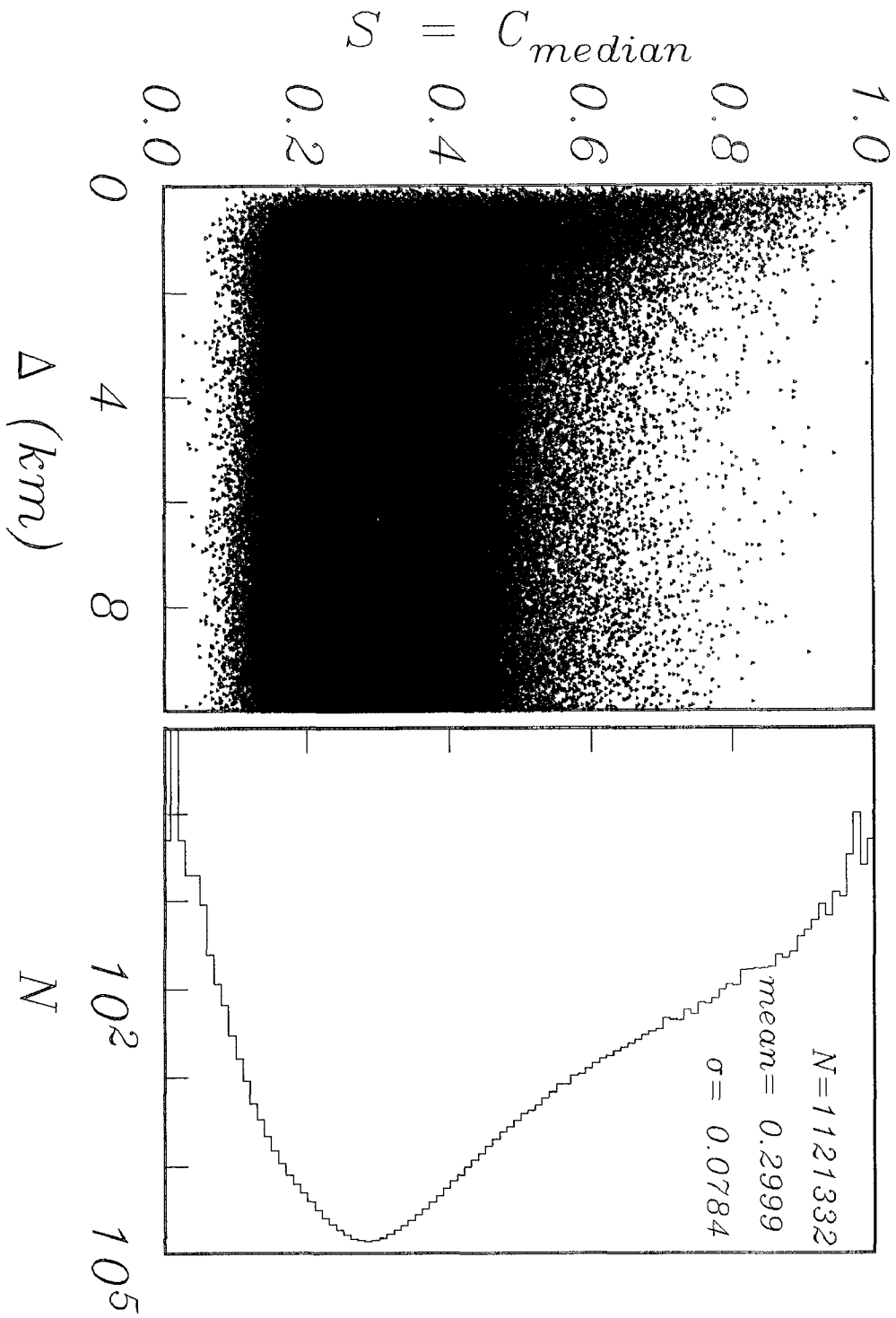

Figure 1. Median values of the shear-wave cross-correlation maximum, S, versus interhypocenter distance, $\Delta \leq 10$ km, for 1,121,332 Anza seismogram pairs satisfying the precomparison criteria (see text). The earthquakes were recorded between October, 1982 and April, 1992. A histogram of S values is shown at *right*. The wide range of S at small values of Δ indicates that small interhypocenter separations from network locations alone are insufficient to identify events with highly similar waveforms. The falloff of S values to background levels by about $\Delta = 3$ km indicates that $\Delta_{max} = 10$ km was sufficiently large for this data set to encompass almost all highly similar earthquake pairs.

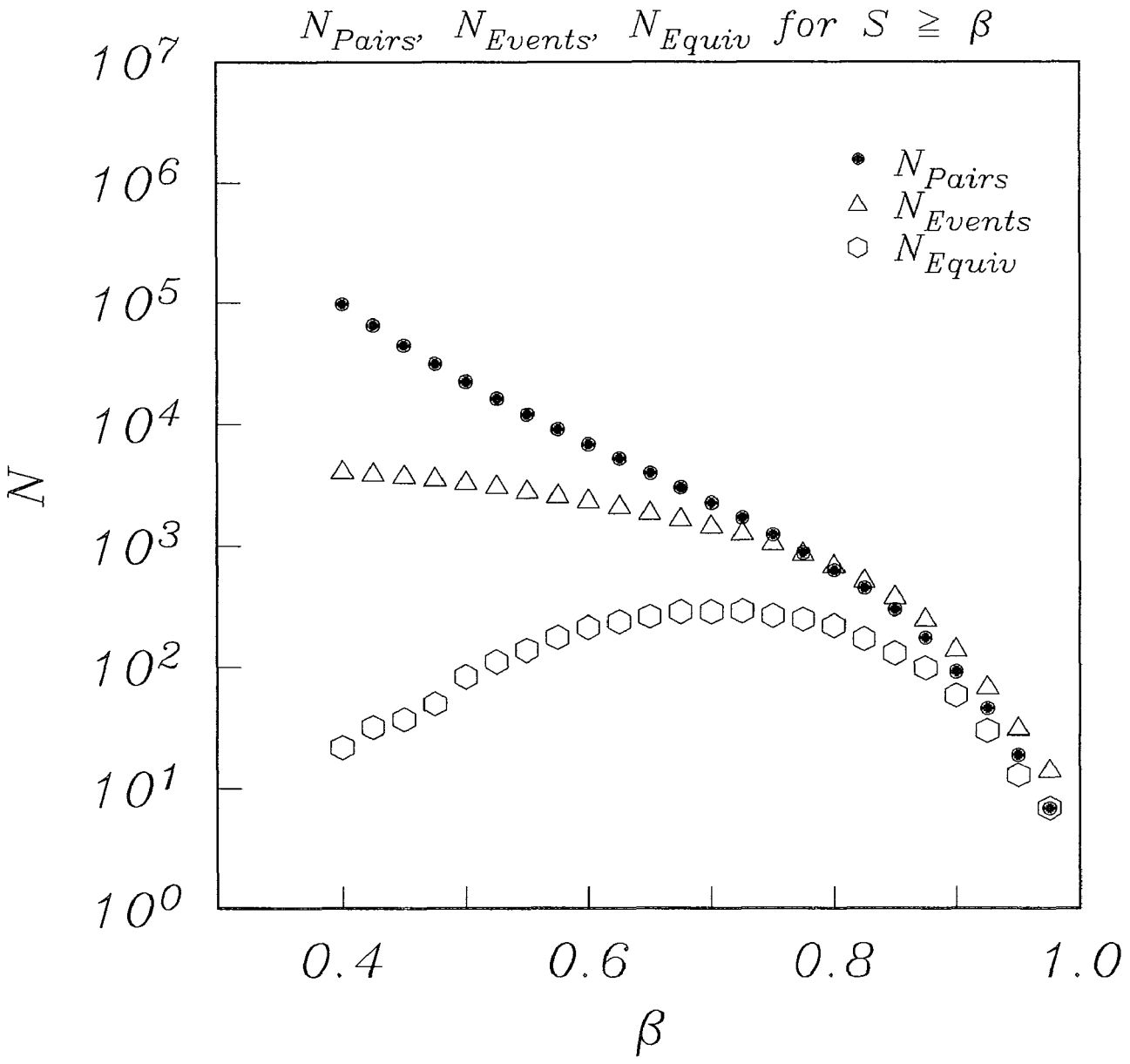

Figure 2. Number of earthquake pairs, events, and equivalence classes as a function of β, the minimum value of the median shear-wave crosscorrelation value (Figure 1). The number of clusters is maximized near β = 0.725).

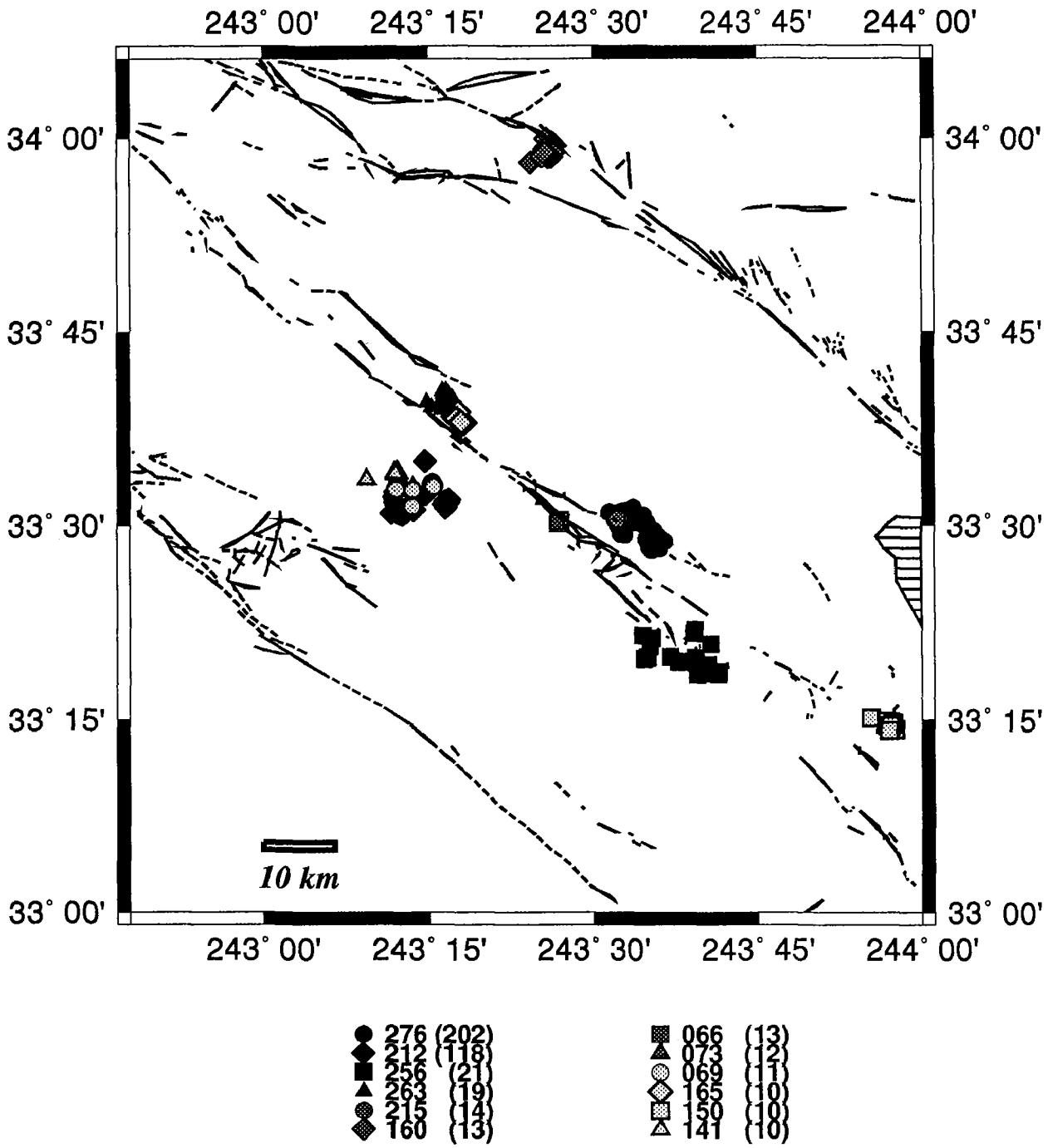

Figure 3. Network epicenters of the twelve largest ($N_{Equiv} \geq 10$) similar earthquake clusters identified at Anza for $\beta = 0.725$ (Figure 2). The legend denotes each cluster number and population.

This similar event identification algorithm is also currently being applied to obtain a comprehensive similar event catalog for Parkfield HRSN data by Bob Nadeau and Mike Antolik at U.C. Berkeley (Nadeau et al., 1991). This counterpart catalogue will ultimately enable direct comparisons between similar seismogram analyses at Anza and Parkfield.

Development and evaluation of techniques for relative waveform analysis.

The signal processing aspects of similar earthquake analysis generally involve two overlapping concerns. 1) Temporal alignment (or equivalently, lag estimation), either in moving windows or for entire seismograms. This type of measurement is especially appropriate for analyzing possible velocity variations in direct body phases and possibly for secondary phases buried in the coda (e.g., Verwoerd et al., 1992, Ellsworth et al., 1992). 2) Estimation of moving-window spectral ratios. This technique is most appropriate for coda or attenuation analysis, where one is testing for smooth variations in the Green function frequency response, such as might be induced by temporal variations in the degree of lithospheric microcracking.

When seeking to positively identify what may be very small variations in the response of the Earth to seismic waves, it may be essential to use the most robust and high-resolution techniques available on a large number of microearthquake pairs. We have progressed this year on developing the best possible techniques currently available for estimating relative lag times by testing both coherence-weighted phase slope methods (e.g., Poupinet et al., 1985) and Fourier interpolation methods (e.g., Aster and Shearer, 1992). We have also written and implemented multitaper spectral methods for estimating relative spectral amplitudes and coherence, as developed by Thomson (1982) and subsequently adapted for seismological applications by Park et al. (1987) and by Vernon (1989; 1992). Preliminary indications using a limited range of synthetic seismogram pairs suggest the the most robust estimates of relative times may be obtainable using Fourier interpolation and that the most robust spectral estimates are obtainable using multitaper Fourier analysis techniques.

Analysis of similar microearthquake seismograms to identify or establish limits on temporal variability in seismic Green's functions.

Our present emphases in relative seismogram analysis to assess any variability in seismic coda (Aster et al., 1992) and/or seismic velocities (Scott et al., 1992) using Anza network data from 1982 to present.

Temporal changes in seismic velocity. If temporal changes in seismic velocity exist due to stress-induced changes in or near the fault zone, they may be detectable in the variation of travel time residuals for rays which sample the same region at different times (Poupinet et al., 1984; 1985). Signals from nearly identical earthquakes in the Anza similar event catalogue are ideal for this type of analysis as differences due to path and source differences will be minimized. Scott et al. (1992) analyzed a highly similar pair of events with a 945 day time separation recorded at 8 stations. and found that relative travel-times of direct phases could be fit to less than 3 ms for P and less than 5 ms for S with an interhypocenter separation of 50 m. Preliminary indications are that temporal velocity changes for those ray paths sampled are less than about 0.1% for both P and S. Future work will also be extended to secondary phases in the coda

Temporal changes in seismic coda. Coda Q offers perhaps the brightest hope for finding definitively identifying temporal changes in Earth response. Besides having the advantage of sampling a large volume, coda analysis is especially intriguing because numerous reports (although none yet checked by using similar earthquakes) exist in the literature of reported temporal variations, some of which were precursory to large earthquakes (see Sato, 1988; Wyss et al., 1991). Regions with reported temporal changes include the Anza area; Haar (1989) analyzed 37 earthquakes recorded by the Anza network between June, 1984 and December, 1987 and reported an intriguing increase (at a confidence level of greater than 0.99) in the coda decay rate observed Anza network station KNW. This study noted an anomalously high attenuation, for earthquakes occurring in the 18 months before the North Palm Springs earthquake. A similar conclusion was reached by Su and Aki (1990) examining SCSN data. Our methodology for searching for temporal changes in seismic coda, assumes a single-scattering envelope decay function of the form (e.g., Aki and Chouet, 1975)

$$A(f,t) \propto S(f)\, t^{-m}\, e^{-\pi f t/Q} \tag{1}$$

where t is the time elapsed since the earthquake origin time and $S(f)$ is the source amplitude spectrum. A change in Q between two otherwise identical earthquake signals would thus appear as a change in time-varying exponential filtering. Specifically, an estimate of the change in Q^{-1} between similar earthquake seismograms observed at a given station can be obtained by aligning the two waveforms to sub-sample accuracy and examining moving-window estimates of the log of the spectral ratio as a function of time (e.g., Got et al., 1991; Got and Fréchet, 1992)

$$C(f,t) = \ln\left[\frac{A_1(f,t)}{A_2(f,t)}\right] = \pi\Delta Q^{-1} f t + \ln\left[\frac{S_1(f)}{S_2(f)}\right] = R(f,t) + W(f) \tag{2}$$

where $R(f,t)$ is an exclusively earth-dependent term and $W(f)$ is an exclusively source-dependent term.

We have recently implemented an algorithm which uses multiaper techniques to estimate $C(f,t)$, around N frequency points and M time points. Standard errors are obtained from bootstrap estimates (Efron and Tibshirani, 1986). Early indications are that the behavior of this estimate is remarkably similarly for different stations from the same event pair, which is suggestive of site-invariance, and is also similar across the three seismogram components, which suggests that the coda decay function is fairly independent of particle motion direction. An example of the output from the moving-window spectral ratio procedure is shown in Figure 4.

Differential measurements of changes in reciprocal Q and in the source spectral ratio term, $W(f)$, with error bars and significance levels can be estimated in the context of a discrete linear over-determined least-squares problem by fitting (2) to the estimated sonogram. The system to be solved is (unweighted for clarity):

$$\begin{bmatrix} C(f_1,t_1) \\ C(f_2,t_1) \\ \vdots \\ C(f_N,t_1) \\ C(f_1,t_2) \\ \vdots \\ C(f_N,t_M) \end{bmatrix} = \begin{bmatrix} \pi f_1 t_1 & 1 & 0 & 0 & \cdots & 0 \\ \pi f_2 t_1 & 0 & 1 & 0 & \cdots & 0 \\ & & & \vdots & & \\ \pi f_N t_1 & 0 & 0 & 0 & \cdots & 1 \\ \pi f_1 t_2 & 1 & 0 & 0 & \cdots & 0 \\ & & & \vdots & & \\ \pi f_N t_M & 0 & 0 & 0 & \cdots & 1 \end{bmatrix} \begin{bmatrix} \Delta Q^{-1} \\ W(f_1) \\ W(f_2) \\ \vdots \\ W(f_N) \end{bmatrix} \tag{3}$$

For Anza data, signals from each of the component seismometers will be averaged by fitting the parameter vector to mean spectral ratio values from all three components.

Once relative estimates of ΔQ^{-1} are obtained for all pairs of events in a similar event cluster at a given station, a subsequent linear inverse problem can be cast to obtain the best set of absolute Q^{-1} values (with an arbitrary mean value), e.g. for a cluster of four earthquakes consistent with the available ΔQ^{-1} estimates from (3). For example, for a cluster consisting of four earthquakes the system to be solved is (again, unweighted for clarity):

$$\begin{bmatrix} \Delta Q_{21}^{-1} \\ \Delta Q_{31}^{-1} \\ \Delta Q_{41}^{-1} \\ \Delta Q_{32}^{-1} \\ \Delta Q_{42}^{-1} \\ \Delta Q_{43}^{-1} \end{bmatrix} = \begin{bmatrix} -1 & 1 & 0 & 0 \\ -1 & 0 & 1 & 0 \\ -1 & 0 & 0 & 1 \\ 0 & -1 & 1 & 0 \\ 0 & -1 & 0 & 1 \\ 0 & 0 & -1 & 1 \end{bmatrix} \begin{bmatrix} Q_1^{-1} \\ Q_2^{-1} \\ Q_3^{-1} \\ Q_4^{-1} \end{bmatrix} \tag{4}$$

A statistical test for detectable variability in Q^{-1} is thus whether or not a linear regression applied to the solution of (4) differs significantly from a zero-slope line.

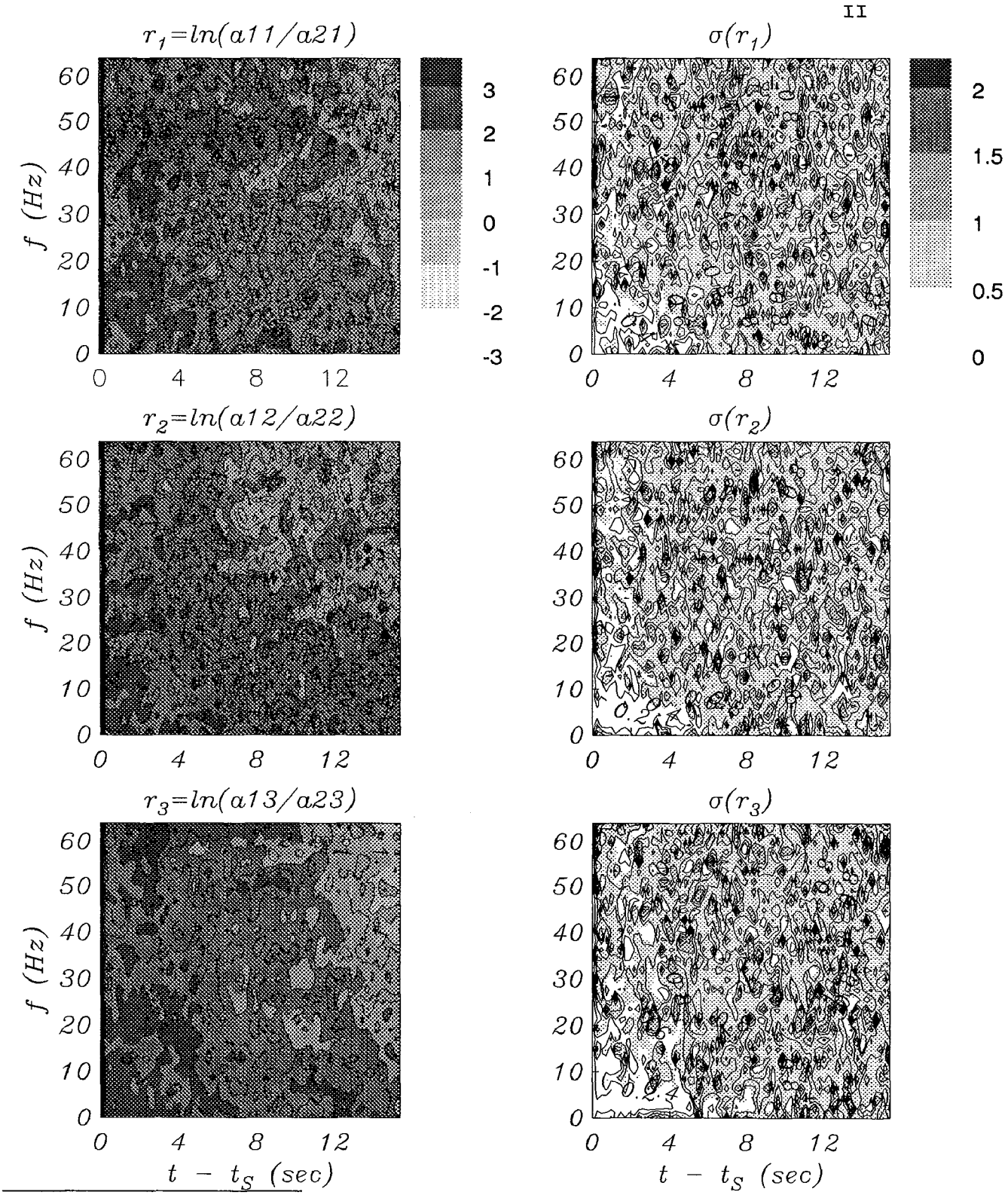

Figure 4. Shaded contour plot of the moving window log spectral ratio $C(f, t)$ and its standard deviation estimated for three components recorded at station WMC (vertical at top, NW-SE in the middle and NE-SW at bottom) for a similar earthquake pair from cluster 135 (5^{th} on the list shown in Table 1). Time is given relative to the S-wave arrival time. Multitaper spectral estimates using 8 prolate spheroidal taper functions were evaluated for 0.512 s 50% overlapping windows with a spectral averaging bandwidth of 8 Hz. Standard deviations were estimated using a statistical bootstrap with N=200 realizations.

Anza Similar Events ($\Delta t \geq 100$ days; $S \geq 0.86$; $N_{sta} \geq 3$)

Cluster	$event_1$	$event_2$	Δt *(days)*	Δh *(km)*	N_{sta}	S
276	aza001/82290101308	aza013/90057033115	2688.7	0.22	4	0.89
276	aza001/82290101308	aza013/90050151458	2682.2	0.53	5	0.90
174	aza002/84139101553	aza020/91094095001	2512.0	1.07	9	0.89
220	aza006/87307221107	aza024/91274052047	1427.3	0.54	5	0.89
135	aza005/86287100614	aza015/90105071049	1278.9	1.64	7	0.87
067	aza002/84175093325	aza006/87024033152	944.7	0.25	6	0.95
212	aza003/84306203243	aza005/86287175236	711.9	0.36	6	0.96
080	aza004/86182224033	aza008/88143113117	690.5	0.46	9	0.87
263	aza008/88292030028	aza018/90233080037	672.2	0.98	5	0.90
276	aza014/90095070015	aza025/91362100105	632.1	1.97	7	0.86
276	aza008/88206005916	aza013/90050055248	575.2	0.37	6	0.89
276	aza018/90239134028	aza025/91362100105	487.8	1.60	4	0.90
158	aza010/89307114605	aza018/90344061520	401.8	3.18	7	0.89
276	aza018/90334065756	aza025/91351083517	382.1	2.22	4	0.86
276	aza013/90052060711	aza019/91017103908	330.2	1.30	4	0.87
276	aza010/89279194452	aza018/90238224549	324.1	0.66	7	0.87
133	aza005/86240150620	aza006/87197222209	322.3	1.70	4	0.90
212	aza002/84191151716	aza003/85134220533	309.3	1.02	4	0.93
276	aza009/89108235416	aza013/90050105751	306.5	0.90	3	0.88
276	aza009/89108235416	aza013/90050055248	306.2	0.40	3	0.87
212	aza003/84207221148	aza003/85134220533	293.0	0.96	4	0.92
073	aza005/86200192301	aza006/87128153540	292.8	0.60	5	0.89
276	aza018/90334065756	aza023/91242203241	273.6	0.12	3	0.90
276	aza013/90050111412	aza018/90303163508	253.2	0.27	5	0.90
276	aza013/90050151458	aza018/90303042613	252.6	0.70	5	0.86
276	aza013/90050091713	aza018/90302141145	252.2	0.64	3	0.88
276	aza013/90050111412	aza018/90302141145	252.1	0.36	3	0.89
276	aza013/90051051508	aza018/90303042613	252.0	0.39	5	0.90
276	aza013/90051051508	aza018/90302141145	251.4	0.44	3	0.90
276	aza013/90052132750	aza018/90302141145	250.0	0.54	3	0.88
276	aza013/90057033115	aza018/90303163508	246.5	0.33	4	0.89
276	aza013/90057033115	aza018/90303042613	246.0	0.07	4	0.88
276	aza013/90057033115	aza018/90302141145	245.4	0.40	3	0.87
276	aza013/90059032744	aza018/90303042613	244.0	0.32	5	0.91
276	aza013/90059032744	aza018/90302141145	243.4	0.19	3	0.88
276	aza014/90092182003	aza018/90304031218	211.4	0.22	3	0.90
276	aza014/90092182003	aza018/90303042613	210.4	0.18	4	0.86
276	aza014/90095070015	aza018/90304031218	208.8	0.82	3	0.88
276	aza014/90095070015	aza018/90303042613	207.9	0.69	4	0.86
276	aza013/90050151458	aza018/90239134028	188.9	0.48	4	0.87
276	aza018/90304031218	aza021/91127062056	188.1	8.93	3	0.91
276	aza015/90115032939	aza018/90302141145	187.4	6.86	4	0.88
127	aza010/89230221814	aza013/90050234422	185.1	0.80	5	0.91
276	aza019/91062061528	aza022/91216110027	154.2	0.80	7	0.88
238	aza022/91212114921	aza025/91338212420	126.4	2.39	4	0.91
276	aza018/90239134028	aza018/90346211245	107.3	0.52	3	0.89
111	aza010/89260193523	aza011/89361113901	100.7	1.11	6	0.88

Table 1

Summary.

We have completed the compilation of a similar event catalogue for Anza network data from October 24, 1982 through April 15, 1992 and have programs in place for updating this catalogue as more recent seismograms and locations become available from UCSD (currently backlogged by the enormous number of events associated with the Landers/Big Bear earthquakes). We also have access to SCSN network seismograms through the Southern California Earthquake Center for these events which will be used to extend the geographic range of the study. A comparable organizational effort is also well underway at U.C. Berkeley for the Parkfield data set. A list of the "best" events from the Anza catalogue is shown in Table 1, where δh is the estimated hypocenter separation from network locations, N_{sta} is the number of Anza stations in common, and S is the median shear-wave crosscorrelation of 0.512 s of the aligned 3-component shear wave signal.

Work is presently proceeding on exploiting this catalogue to test waveform data for evidence of temporal variability in seismic velocities and seismic coda. An analysis of variation or stability in shear-wave splitting will also be performed using comparative techniques developed by Aster et al. (1990). Although the stable results of that study were negative with respect to one proposed precursor at a single station, the present state of data and programming organization now enables us to perform a far more comprehensive survey with relatively little additional effort.

We thus anticipate rapid progress during the next year on addressing the issue of Green function stability or variability at Anza and Parkfield. A future priority will be identifying and analyzing similar event pairs from the Anza and SCSN networks which sample the vicinity of the the Landers and Big Bear earthquakes of June 28, 1992.

Reports, Papers and Presentations Associated with this Project.

Aster, R., Scott, J., Comprehensive Identification of Similar Earthquakes in Microearthquake Data Sets, 1992. *Bull. Seism. Soc. Am.*, accepted for publication.

Aster, R., Scott, J., Shearer, P., Vernon, F.L., Analysis of near-repeating earthquake wavefields in the San Jacinto fault zone, southern California, 1991. *EOS trans. AGU*, **72**, no 44, p. 352.

Aster, R., Scott, J., Shearer, P., Vernon, F.L., Similar earthquakes in the Anza Seismic Gap, 1992. *Seism. Res. Lett.*, **63**, p. 63.

Aster, R., Henton, J., Scott, J., Shearer, P., Vernon, F.L., Comparative coda analysis of similar earthquakes with large temporal separations near the Anza seismic gap, southern California, 1992. *EOS trans. AGU*, **73**, no 43, p. 361.

Nadeau, R., Aster, R.C., McEvilly, T.V., Analysis of P and S wave polarizations at the Parkfield high-resolution seismic network (HRSN), 1991. *EOS trans. AGU*, **72**, no 44, p. 483.

Scott, J., Shearer, P., Aster, R., Constraints on temporal variations in velocity near Anza, California, from analysis of similar event pairs, 1992. *EOS trans. AGU*, **73**, no 43, p. 360.

Additional References

Aster, R., Shearer, P., and J. Berger (1990). Quantitative measurements of shear-wave polarizations at the Anza seismic network, southern California — implications for shear-wave splitting and earthquake prediction, *J. Geophys. Res.* **95**, 12,449-12,474.

Berger, J., L.N. Baker, J.N. Brune, J.B. Fletcher, T.C. Hanks, and F.L. Vernon (1984). The Anza array: a high-dynamic-range, broadband, digitally radiotelemetered seismic array, *Bull. Seism. Soc. Am.*, **74**, 1469-1481.

Efron, B., Tibshirani, R. (1986). Bootstrap methods for standard errors, confidence intervals, and other measures of statistical accuracy, *Statistical Science*, **1**, 54-77.

Ellsworth, W., Beroza, G., Verwoerd, M. (1992). Changes in crustal wave velocity associated with the 1989 Loma Prieta, California earthquake, *EOS trans. AGU*, **73**, no 43, p. 360.

Geller, R., and C. Mueller (1980). Four similar earthquakes in central California, *Geophys Res. Lett.*

7, 821-824.

Got, J.-L., Poupinet, G., and M.-J. Fréchet (1990). Changes in source and site effects compared to coda Q^{-1} temporal variations using microearthquake doublets in California, *PAGEOPH* **134**, 195-228.

Got, J.-L., Fréchet, J., 1992. Origins of amplitude variations in seismic doublets: Source or attenuation process?, *submitted for publication.*

Haar, R., 1989. *Spectra and Time Decay of Coda*, Ph.D. Thesis, Stanford University.

Harris, D. (1991). A waveform correlation method for identifying quarry explosions, *Bull. Seism. Soc. Am.* **81**, 2395-2418.

Hough, S., Anderson, J. (1988). High frequency spectra observed at Anza, California: Implications for Q structure, *Bull. Seism. Soc. Am.* **78**, 692-707.

Hough, S., J. Anderson, J. Brune, F. Vernon, J. Berger, J. Fletcher, L. Haar, T. Hanks, Baker, L. (1988). Attenuation at Anza, California, *Bull. Seism. Soc. Am.* **78**, 676-691.

Hutchings, L., and F. Wu (1990). Empirical Green's functions from small earthquakes: A waveform study of locally recorded aftershocks of the 1971 San Fernando earthquake, *J. Geophys. Res.* **95**, 1187-1214.

Ishida, M., and H. Kanamori (1978). The foreshock activity of the 1971 San Fernando earthquake, California, *Bull. Seism. Soc. Am.* **68**, 1265-1279.

James, D., and M. Savage (1990). A search for seismic reflections from the top of the oceanic crust beneath Hawaii, *Bull. Seism. Soc. Am.* **80**, 675-701.

Knuth, D. (1968). *Fundamental Algorithms, The Art of Computer Programming*, Addison-Wesley, Reading, Massachusetts.

Park, J., C. Lindberg, and F. Vernon (1987). Multiper spectral analysis of high-frequency seismograms. *J. Geophys. Res.* **92**, 12,675-12,684.

Poupinet, G., Ellsworth, W., and M.-J. Fréchet (1984). Monitoring velocity variations in the crust using earthquake doublets: An application to the Calaveras fault, California, *J. Geophys. Res.* **89**, 5719-5731.

Poupinet, G., Fréchet, M.-J., Ellsworth, W., Frémont, M.-J., and F. Glangeaud (1985). Doublet analysis: Improved accuracy for earthquake prediction studies, *Earthquake Predict. Res.* **3**, 147-159.

Press, W., Flannery, B., Teukolsky, S., and W. Vetterling (1986). *Numerical Recipes*, Cambridge University Press, Cambridge, U.K..

Scott, J. (1992). *Microearthquake studies in the Anza seismic gap*, Ph.D. thesis, Scripps Instit. Oceanogr., Univ. of Calif., La Jolla, California.

Scott, J., Masters, T.G., and Vernon, F. (1992). *Three-dimensional velocity structure of the San Jacinto fault zone near Anza, California, Part I: P waves submitted to Geoph. J. Int.*

Su, F., Aki, K. (1990). Spatial and temporal variation in coda Q^{-1} associated with the North Palm Springs earthquake of 1986, *Pure Appl. Geophys.*, **133**, 23-52.

Thorbjarnardottir, B., and J. Pechmann (1987). Constraints on relative earthquake locations from cross-correlation of waveforms, *Bull. Seism. Soc. Am.* **77**, 1626-1634.

Thomson, D., Spectrum estimation and harmonic analysis, *IEEE Proc.*, **70**, 1055-1096.

Vernon, F.L. (1989). *Analysis of Data Recorded on the Anza Seismic Network*, Ph.D. thesis, Scripps Instit. Oceanogr., Univ. of Calif., San Diego, La Jolla.

Vernon, F.L. (1992). Coherence vs. distance (abstract), *Seism. Res. Lett.*, **63**, 40.

Verwoerd, M., Ellsworth, W., Cole, A., Beroza, G. (1992). Changes in crustal wave propagation properties associated with the 1989 Loma Prieta, California earthquake: Implications for coda-Q as an earthquake precursor and for the mechanism of stress-induced velocity changes. (abstract), *Seism. Res. Lett.*, **63**, 71.

Holocene Paleoseismology in Western Washington

9540-10180
Brian F. Atwater
U.S. Geological Survey at University of Washington AJ-20
Seattle, Washington 98195
(206) 553-2927

Investigations:

My research in 1992 was focussed on four questions about great earthquakes that have been inferred for the Cascadia subduction zone:

1. **Did the ground really shake?** Great Cascadia earthquakes have been inferred primarily from coastal deposits that indicate abrupt subsidence, but evidence for shaking during this subsidence has proven elusive. In particular, few prehistoric liquefaction features of Holocene age have been found at the Cascadia subduction zone. In 1992, I looked for liquefaction features in a large excavation in Seattle, and I visited sites along the lower Columbia River at which Stephen Obermeier discovered liquefaction features of late Holocene age.

2. **What were the magnitudes?** (a) Work continued on maximizing the resolution of radiocarbon dating to test the coevality of subsidence along the Cascadia coast (B.F. Atwater, M. Stuiver, and D.K. Yamaguchi, *Nature*, v. 353, p. 156, 1991). The main goal in 1992 was a comparison of high precision radiocarbon ages on spruce stumps, southern Washington versus northern California (with Minze Stuiver, Gary Carver). (b) Work also continued on the death and survival of spruce trees near Portage, Alaska, that subsided into the intertidal zone during the 1964 Alaska earthquake (with David Yamaguchi, Eileen Hemphill-Haley). (c) Work began with the use of tree rings to put limiting minimum ages on the most recent great earthquake inferred for coastal Washington. This work consisted of coring live tidal-swamp spruce in parts of coastal Washington where spruce were killed by salt and (or) submergence from the most recent abrupt subsidence sometime between AD 1695 and 1710 (with Boyd Benson, David Yamaguchi).

3. **What were the recurrence intervals?** This also entails high-precision dating, for which sampling and dating continued in 1993 (with Minze Stuiver).

4. **What, if any, is their relationship to crustal earthquakes at Puget Sound?** This question has become important in light of recent findings, by Robert Bucknam and others, about prehistoric seismicity on structures in the North America plate near Seattle. I looked for tsunami deposits at Puget Sound to learn whether uplift near Seattle happened during an earthquake, as inferrred by Bucknam. I also sampled such deposits for plant fossils to obtain high-precision radiocarbon ages (with Minze Stuiver) and tree-ring correlations (with Gordon Jacoby).

Results:

1. **Shaking**--Atwater found gravel and sand intrusions less than 2000 years old in sewer excavation in Seattle (see 4, below). Independently, Obermeier found liquefaction features about 300 years old along the lower Columbia River.

2. **Magnitude**--(a) Stuiver supplied high-precision ages for spruce killed by the youngest abrupt subsidence event at Humboldt Bay, California. These ages are not statistically different from ages 600 km to the north, in southern Washington. The dating leaves intact the hypothesis of magnitude-9 earthquakes on the Cascadia subduction zone. The Washington ages were published in the *Nature* paper cited above; a manuscript on the California ages is in preparation. (b) Yamaguchi found that some of the spruce near Portage survived several months beyond the 1964 earthquake, as shown by partial 1964 growth rings. Implication for Cascadia: the season of tree death cannot be used with confidence to test coevality of subsidence. (c) At least a dozen Sitka spruce of modern tidal swamps in southern Washington contain more then 300 annual rings and thus should have survived any earthquake close to A.D. 1700. There is a chance that such trees would reveal the year and season of the most recent great earthquake in coastal southern Washington.

3. **Recurrence**--Samples for high-precision dating of earlier earthquakes were collected in July and August, 1992.

4. **Puget Sound seismicity**--A Puget Sound tsunami coincided, to the year, with abrupt tectonic subsidence in northern Seattle and with landslides into Lake Washington about 1000 years ago.

Reports

Atwater, B.F., 1992, A Seattle tsunami 1100 years ago [abstract]: *Geological Society of America Abstracts with Programs*, v. 24, no. 5, p. 4.

Atwater, B.F., 1992, Prehistoric earthquakes in western Washington [abstract]: *Geological Society of America Abstracts with Programs*, v. 24, no. 5, p. 4.

Atwater, B.F., and Moore, A.L., 1992, A tsunami 1000 years ago in Puget Sound, Washington: *Science* (in press).

Benson, B.E., Amidon, L., Yamaguchi, D.K., and Atwater, B.F., 1992, Limiting tree-ring ages for plate-boundary seismicity in southern coastal Washington [abstract]: Eos (in press).

Carver, G.A., Stuiver, M., and Atwater, B.F., 1992, Radiocarbon ages of earthquake-killed trees at Humboldt Bay, California [abstract]: Eos (in press).

SYNTHESIS OF DATA AND EXPLORATORY TRENCHING ALONG THE NORTHERN SIERRA NEVADA FAULT ZONE

1434-92-G-2217

John W. Bell, Alan R. Ramelli, Craig M. dePolo

Nevada Bureau of Mines and Geology
University of Nevada
Reno, Nevada 89557
(702) 784-6691

Objectives

1. Compile and synthesize existing data related to distribution and age of late Quaternary faulting along the northern Sierra Nevada fault zone (NSNFZ).

2. Conduct exploratory trenching of the southern portion of the NSNFZ (Genoa fault).

3. Estimate short- (Holocene) and long-term (late Quaternary) slip rates along the NSNFZ.

Results

Synthesis of fault data

Late Quaternary faulting within the Washoe City, Mt. Rose NE, Genoa, and Minden 7½-minute quadrangles was evaluated through analysis of aerial photography and existing geologic mapping. Definitive late Quaternary fault traces (primarily scarps) along the frontal fault zone in Washoe Valley to the northern edge of the Mt. Rose fan complex have been compiled and digitized using Generic CADD.

While the spatial distribution of active fault traces within the Washoe City and Mt. Rose NE quadrangles is fairly well represented on published maps, the age relations as shown are in some cases misleading or erroneous. For example, nearly continuous fault traces are assigned differing ages where they offset different-age deposits. Some scarps show greater offset of older surfaces suggesting recurrent faulting; however, displacement varies rapidly along strike of many traces, complicating such interpretations. Many of the scarps shown as "Donner Lake age" (~200 ka) on published maps in fact influence Holocene and active drainage patterns, indicating much more recent activity.

Late Quaternary faulting of the Mt. Rose outwash-fan complex forms a series of subparallel grabens traversing the outwash-fan, rather than being an antithetic (west-facing) system as described in previous work. These grabens generally trend north-south and are commonly sigmoidal-shaped. Northwest- to north-northwest-trending faults cutting the Mt. Rose outwash-fan commonly are linear and have a strong left-stepping en echelon pattern, suggesting right lateral movement. One northwest-trending fault cutting across the Mt. Rose fan appears to separate differentially deforming areas to the north and south. To the north, there are at least five subparallel grabens evenly spaced across the Mt. Rose fan, whereas to a south, faulting is mostly confined to the single complex graben lying between Steamboat Hills and Mt. Rose.

Exploratory Trenching

Three exploratory track-hoe trenches were excavated across portions of the Genoa fault in July, 1992 (Fig. 1), and the logging of the trenches has been completed by the Principal Investigators. The structural-stratigraphic relations exposed in all three trenches confirm that the Genoa fault is the most youthful segment of the NSNFZ and is currently believed to have the highest seismogenic potential of any fault in the Reno-Carson City urban corridor.

The most recent faulting event is displayed in the Jacks Valley and Sturgis trenches, respectively located near the northern and southern ends of the most recent surface rupture, where latest Holocene alluvial-fan deposits exhibit 4-4¼ m of total, single-event, stratigraphic throw. Topographic profiles across these respective fault scarps indicate that geomorphic surfaces also display about 4¼ m of vertical throw. Net dip-slip surface displacement is estimated to be about 5 m for this most recent event. Two events are exposed in the Walleys trench: the most recent event as well as an older event of comparable magnitude. A total of 7.6 m vertical throw of late Holocene deposits is recorded at the Walleys site, equivalent to about 9 m of dip-slip displacement.

Geomorphic and soils relations suggest that the faulted deposits at the three sites are late Holocene age. The complete lack of any significant soil horizonation in the most recently faulted deposits strongly suggests a numerical age for the youngest deposits of less than about 1,000 years. This is expected to be confirmed by radiocarbon dating of samples collected from all three trenches. The Jacks Valley and Sturgis trenches expose extensive sequences of faulted and unfaulted charcoal-rich horizons derived from repeated and alternating episodes of forest fires and debris- and flood-flow alluviation. A total of 49 charcoal samples has been collected from the Jacks Valley and Sturgis trenches, which will probably allow the precise bracketing of the age of the most recent 5 m displacement. A maximum age for the earlier event exposed in the Walleys trench will be estimated from dating two charcoal lenses preserved in the down-faulted block of alluvial-fan deposits. The presence of an incipient cambic (Bw) horizon in the faulted fan surface suggests that both events are less than a few thousand years in age.

Slip rates

Radiocarbon dating of samples (in progress) from the three trenches will allow estimation of mid- to late Holocene slip rates for the Genoa fault. Preliminary results based on ages inferred from soil and geomorphic evidence suggest that as much as 10 m of displacement associated with two major events has occurred during the mid- to late Holocene. This suggests that Holocene slip rates may be on the order of 1-2 mm yr^{-1}. Preliminary data also suggest that this rate may be greater than the longer-term (late Quaternary) average. At the Walleys trench site, alluvial-fan deposits estimated to be 100-200 ka on the basis of soil morphology are offset by a 20-m high scarp. Although this offset is a minimum value because of the likelihood of burial of the downthrown block, this offset suggests that the late Quaternary average slip rate for the Genoa fault is less than the Holocene rate, perhaps by as much as an order of magnitude.

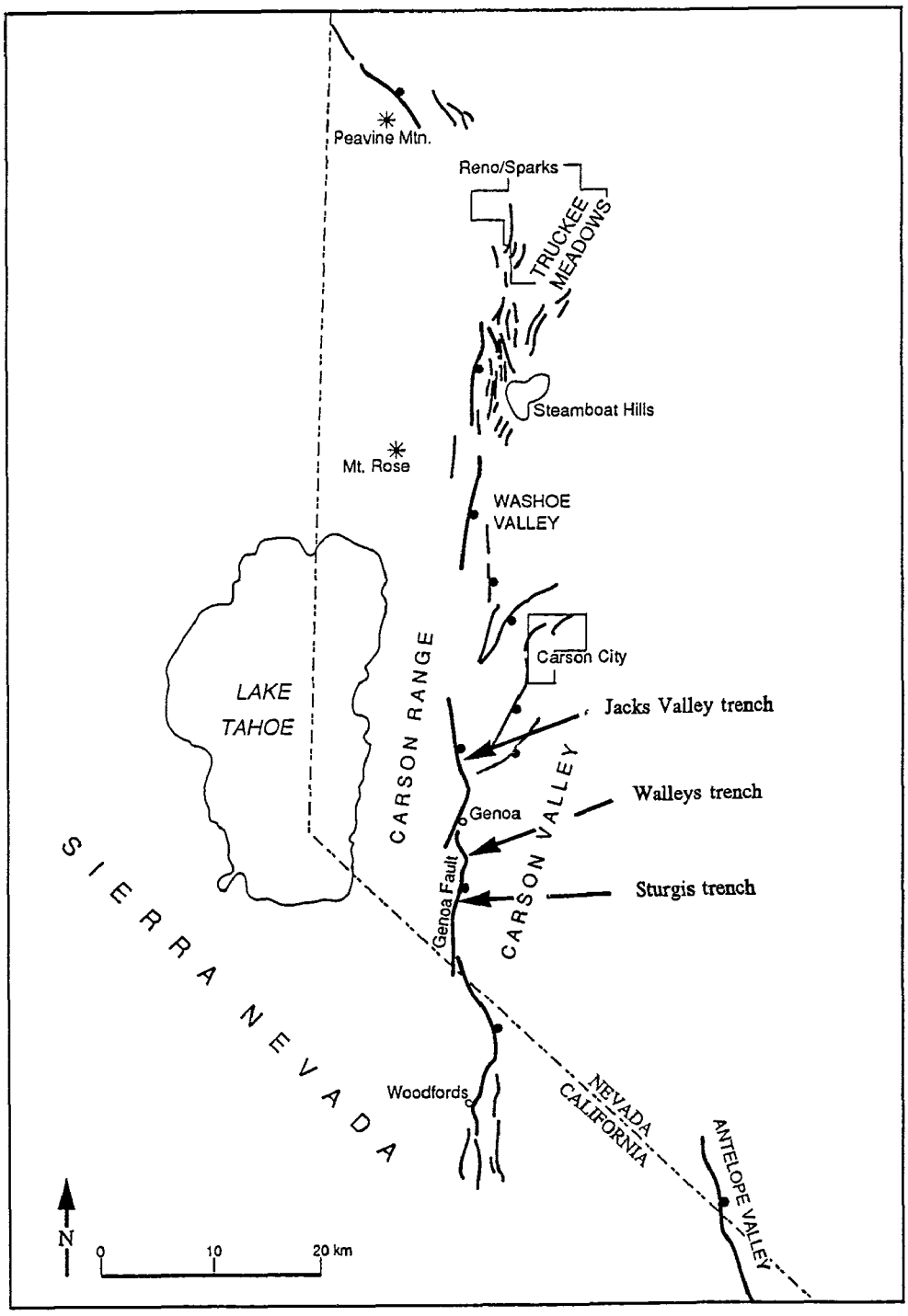

Figure 1. Generalized late Quaternary fault map of the northern Sierra Nevada fault zone showing the location of exploratory trenches across the Genoa fault. North-trending, east-facing faults form the main frontal fault zone of the Basin and Range-Sierra Nevada boundary at this latitude.

Detailed and Reconnaissance Finite Element Models of Four Fault Systems in the United States

Agreement No. 14-08-0001-G-1947

Peter Bird
Department of Earth and Space Sciences
University of California
Los Angeles, CA 90045

(310) 825-1126

Recent improvements in the technique of modeling fault networks with thin-plate finite elements yield fully-convergenced velocity/strain-rate/stress solutions, without any compromise in the representation of the frictional rheology of the upper crust or the transition to dislocation creep in the lower crust. Such models yield quantitative constraints on the rheologies of faults and crustal blocks, as well as specific predictions concerning long-term seismic risk.

Investigations Undertaken:

1. California: (The initial stages of this project were described in last year's report.) We applied these techniques to model the California region, incorporating all faults with estimated slip rate over 1 mm/yr, as well as variations in elevation, heat flow, and crustal thickness. Velocity boundary conditions on the model sides were based on the NUVEL-1 plate model and an approximation of deformation in the Great Basin. The frictional and dislocation-creep rheologic constants of the crust were calibrated to reproduce the observed variations in the maximum depth of seismicity, which occurs at model temperatures of 350-410 C. This left two free parameters: the coefficient of friction on faults, and the apparent activation energy for creep in the lower crust.
These parameters were systematically varied in three sets of 10, 81, and 64 experiments, respectively. The predictions of each model were tested against three published datasets: a set of 79 geologic limits on average slip-rate on faults, a set of 221 principal stress directions, and a set of 841 secular rates of geodetic baselines (both trilateration and VLBI).

2. New finite element code: The program referred to above, named FAULTS, includes only the crust in its model domain. This is appropriate where the crust is only weakly attached to the mantle lithosphere, as in California. However, it is not a good way to model regions of very thin crust (e.g., ocean basins) in which the crust is firmly bonded to the mantle lithosphere. Therefore, program FAULTS was modified to create the new program PLATES, in which the domain in the entire lithosphere. The approximations and assumptions are the same, except that the strength and density structure of the mantle lithosphere are included in all vertical integrals. This program was then used in the modeling of Alaska (below), where it was necessary to include the region of the Bering Sea.

3. Models of the Alaskan syntaxis: By modeling the region of the Alaskan syntaxis it may be possible to determine: (a) whether the extreme weakness of faults previously found in California is a general property of the Pacific margin; (b) how great is the seismic hazard to inland regions from faults within the North American plate; (c) whether terranes are continuing to flow around the syntaxis into the Aleutian forearc as they once did; and (d) what causes the observed radiation of principal stresses away from the syntaxis.

To reduce artificial edge effects, the models extend from Vancouver Island north to the Nansen Ridge, and west along the Aleutians to Kamchatka. The grid of 1500 nodes, 600 continuum elements, and 130 fault elements incorporates all mapped faults identified as active by Geist *et al.* (1988), Page *et al.* (1991), or Cooper *et al.* (1992). Topography is taken from the ETOPO5 digital dataset, and heat-flow from the GSA/DNAG map of Blackwell and Steele (1992). Crustal thickness is computed to achieve isostasy (outside the forearc), and mantle lithosphere thickness is derived from the heat-flow. Side boundary conditions are from NUVEL-1, and include an Okhotsk plate after Cook *et al.* (1986). The rheology is friction above the brittle ductile transition(s) (located separately in crust and mantle lithosphere) and dislocation creep below. The crustal creep parameters are taken from the study of California described above.

4. New Madrid seismic zone: In preparation for modeling the midcontinent (Mississippi Valley) seismic zone, references and maps have been collected from the literature.

Results Obtained:

1. California: The patterns of model scores indicate that the friction coefficient of major faults is only 0.17-0.25, or only 20-30% of the value (0.85) that is assumed for the friction in the intervening blocks. (The laser trilateration data taken alone would indicate a preference for a high-stress model, but this model is one with very little fault slip and seismicity, which can be rejected on other grounds.) In the final 3-parameter set of 64 models, we tested whether the anomalous weakness of faults is uniform or proportional to net slip. With slip-dependent weakening, there was a general reduction in prediction errors which supports the hypothesis. The geologic data and geodetic data agree in implying that fault weakness (e.g., friction of 0.17) is general, with an additional 30% slip-dependent weakening of the San Andreas (to friction of 0.12, or 14% of normal). However, the stress data is fit best if all weakness is slip-dependent (effectively, only the San Andreas is weak). Thus, the hypothesis that all weakening is slip-dependent should not be rejected.

The best models predict all available data with RMS mismatch of as little as 3 mm/yr (6% of the relative plate velocity), so their predictions may be useful for seismic hazard estimation, at least along faults where no data are available.

This study extends the finding of very low friction from subduction zones, where it was previously documented, to a dominantly strike-slip system in which underthrusting of wet sediment is not widespread. Return of previously subducted water from the mantle, and its chemical or physical binding in fine-grained gouge are possible explanations for the very low friction.

Results of these models may be useful for improving estimates of long-term seismic hazard, by contributing new limits on the long-term-average slip rate of each fault. Of course, it is necessary to give priority to actual geodetic and geologic data, and to only use computer models where data are absent or ambiguous. Also, it is necessary to consider the full range of rates displayed in a set of models (all those with reasonably good scores) in order to avoid giving a misleading impression of precision.

Following this philosophy, we have constructed Table 1, in which all available data are summarized and tentative conclusions offered. Space does not permit the listing of references in this table. Geologic slip rates are either from Bird and Rosenstock (1984) or manuscript #3 below. Where multiple studies gave overlapping rate windows, the common central segment is quoted. However, where multiple studies disagreed, the quoted range covers both opinions. Geodetic rates are all derived from laser geodimeter trilateration data of Lisowski et al. (1991) or Savage et al. (1990). (However, the assignments of equivalent slip rates to individual faults are our own subjective estimates.) The column "Good Models" gives the range of rates

found among the 30 models from group III which had global prediction errors of 4 mm/year or less. In combining the different kinds of limits, the highest weight is given to geodetic data, the geologic data are ranked second, and the models are considered the weakest.

Given these conservative rules, it is not surprising that these models add little to our knowledge of the intensively-studied San Andreas system. What we can add is some limits for minor branches: the Carneros fault of northern California probably does not exceed 6.6 mm/year, and the San Juan-Whiterock-Morales system of the southern Coast Ranges probably moves no more then 9 mm/year.

These models are most useful in suggesting estimates for offshore and coastal faults which are difficult to access, for thrust faults which typically 'bury their evidence', and for faults in less populous areas which have been given low priority in funding of studies. For example, these models address the controversy over the Hosgri fault, where Hamilton and Willingham (1977) inferred only 2-4 mm/year from geologic evidence, while Hall (1978) argued for 16-19. We never find rates over 3 mm/year on the San Gregorio-Carmel Canyon-Hosgri system in our models, so the lower rate is probably appropriate for seismic hazard evaluation (regardless of which is the correct mean rate for Pliocene-Quaternary time). In the southern California borderland, we confirm that the shoreline-cutting Newport-Inglewood-Rose Canyon-Vallecitos and Palos-Verdes-Coronado Bank systems are moving at no more than a few millimeters per year. One surprising result here is that we have good models in which the slip on the outer Santa Barbara Island-San Diego Trough-Agua Blanca system increases northwestward, from about 2 mm/year in Baja California to as much as 19 mm/year at the intersection with the Santa Barbara Channel structures. However, this result is not unique, as we have other good models where this system moves very slowly. Perhaps GPS observations at Santa Barbara and San Clemente islands can be used to resolve this.

It is important to estimate the slip rates of the thrust faults along the southern margin of the Transverse Ranges because of the high population densities there. Geodetic data are still inconclusive, and geologic rates must usually be treated as lower limits because of the tendency of thrusts to splay over a broad zone. Thus, it was ominous when Bird and Rosenstock (1984) used rigid-block kinematics to infer slip rates of 7-15 mm/year along this zone. Weldon and Humphreys (1986) showed an alternative kinematic model with slower thrusting, but did not resolve the new problems that this would create in the borderland. In this study, we find rates that are about half as great as Bird and Rosenstock's, but still indicative of real hazard. The Cucamonga fault slips at about 7 mm/year and the Sierra Madre fault rate is 3-6 mm/year. Along the southwest branch of this system (Santa Monica and Malibu Coast faults) the model rates are scattered, from under 1 to over 18 mm/year; however, since there is a geologic constraint showing slow motion (<1.1 mm/year) on the Santa Monica fault, this probably applies to the whole branch. On the northwest branch (Sierra Madre-San Fernando-Santa Susanna-San Cayetano-Red Mountain-Santa Barbara Channel faults) the models suggest an upper limit of 7 mm/year for the San Fernando fault and an upper limit of 3 mm/year for the Santa Barbara Channel fault. The fact that the fastest-slipping models just match the lower geologic rate limit (9 mm/year) on the central Red Mountain-San Cayetano fault segment suggests that these models may be the ones closest to reality.

All of these computations were completed before the two San Bernardino Mountains earthquakes of June 1992, so the new fault segments which they revealed are not included in our finite element grid. However, the grid does include the Pipes Canyon fault, which is parallel and close to the rupture of the larger event at Landers. Thus, the range of model slip rates that we found for the Pipes Canyon fault (0.2-2.1 mm/year) may be of interest to help place these events in context. Apparently, major events on these faults should have long recurrence times, and the fact that these

segments now appear to be more active than the adjacent San Andreas fault is only an artifact of the short instrumental record.

2. The new program PLATES passed all the validation tests previously applied to program FAULTS (which models the only the crust).

3. Models of the Alaskan syntaxis: In the first set of Alaskan experiments, the friction coefficient of faults was varied, while the friction within crustal blocks remained at 0.85. While the models have yet to be objectively scored against geologic, geodetic, and stress data, it is already apparent that:
A. The subduction traction on the base of the Aleutian forearc cannot exceed 10 MPa (or else the forearc bonds to the Pacific plate, and the effective plate boundary jumps to the volcanic arc).
B. Faults of the Alaskan interior (e.g., Denali, Tintina) would not be active at all if they did not have low friction.
If their friction coefficient is similar to that of strike-slip faults in California (0.17), then their time-averaged slip rates are approximately 5-10 mm/year. Thrusting at similar rates occurs on the Duke River fault, the Pamplona zone, and on the south branch of the Denali fault, beneath Mt. McKinley.
C. Trench-parallel compression develops in the forearc region of the syntaxis. This would tend to force crust westward along the forearc, but movement is blocked because the accomodating Castle Mt. and Bruin Bay faults are not mapped as continuous with arc-parallel faults further west.
D. All models confirm the rapid arc-parallel transport of the western Aleutian forearc that has been inferred from seismic slip vectors (Ekstrom and Engdahl, 1989).

4. New Madid seismic zone: We are prepared to create the finite elements grids for this region. Obviously, it is important to incorporate all major faults (or at least one fault from each family of subparallel strands) in order to give the model as many degrees of freedom as the real Earth. However, it remains unclear whether the Mississippi Valley fault system merely terminates in Illinois and Tennessee, or whether this cryptic sub-plate boundary continues in another direction. We currently plan to conduct two sets of model experiments. In the first, only mapped faults will be gridded, so that displacements will tend to go to zero at the northeastern end of the system. In the second grid, however, we will investigate the possibility that slip is transformed northwestward along a dextral strike-slip zone through central Missouri and into Kansas, to connect to the inactive(?) mid-continent rift marked by the well-known midcontinent gravity high.

Reports Published:

1. Bird, P., and X. Kong (1991) First accurate thin-plate models with faults (abstract), Eos (Trans. Am. Geophys. U.), 72, 121.
2. Bird, P. (1992) Computer simulations of neotectonics around the Alaskan syntaxis, Eos, 73, 504.
3. Bird, P., and X. Kong., Computer simulations of Calfornia tectonics confirm very low strength of major faults, submitted to Geol. Soc. Am. Bull., 8/92.

TABLE 1.

Final Slip-Rate Estimates for California Faults

(all figures in mm/year;
* marks conclusions which depend on computer models)

Fault	Geologic Rate	Geodetic Rate	Good Models	Best Model	Our Conclusion
Agua Blanca	2.4-5	---	0.2-1.3	0.7	~2.4
Anticline Ridge-Kettleman Hills	1.2-1.9	---	0.1-0.2	0.2	1.2-1.9
Avawatz Mountains	---	---	0-3.7	0.2	<3.7*
Banning	>1.7	---	0-0.3	0.2	~1.7
Black Mountain (Death Valley)	4.1-6.3	---	0.5-2.4	0.8	4.1-6.3
Brawley seismic zone	---	---	4.5-54	14.6	4.5*-54*
Calaveras (Gilroy)	---	12-22	0.1-26	18.0	12-22
Calaveras (Pleasanton)	~3	---	0-6.4	4.0	<6.4*
Carmel Canyon	---	---	0-2.7	0.6	<2.7*
Carneros	---	---	0.1-6.6	3.9	0.1*-6.6*
Cerro Prieta	---	---	22-42	31.9	22*-42*
Channel Islands (Santa Cruz I.)	>3	---	0.4-4.5	3.1	3-4.5*
Chino	0.1-0.4	---	0.4-5.3	1.5	~0.4
Cleghorn	0.9-2	---	0.1-3.1	2.9	0.9-2
Coronado Bank	---	---	0.1-1.9	1.1	0.1*-1.9*
Crystal Creek (N.San Bern.Mts.)	0.2-0.3	---	0.0-0.7	0.6	0.2-0.3
Cucamonga	>6.6	---	0.5-6.9	4.1	~6.6
Elk Hills	---	---	0-0.3	0.1	<0.3*
Elsinore	0.8-9	8-16	0.4-18	7.5	8-9
Furnace Creek	<0.7	---	0-1.1	0.2	<0.7
Garlock (Antelope Valley)	---	---	0.2-11	4.0	0.2*-11*
Garlock (Mojave)	---	---	0.3-9.9	2.8	0.3*-9.9*
Garlock (Searles Lake)	5.4-13	---	0.1-7.9	3.1	5.4-7.9*
Hayward	7-10	---	0.1-22	14.7	7-10
Hilton Creek	---	---	0.1-0.7	0.6	0.1*-0.7*
Honey Lake	---	---	0.1-10	2.2	0.1*-10*
Hosgri	2-19	---	0.2-3.1	2.1	0.2-3.1*
King City-Monterey Bay	---	---	0.1-1.7	1.4	0.1*-1.7*
Laguna Salada	---	0-4	0.5-21	10.4	0.5*-4
Lake Almanor-Mohawk Valley	---	---	0-0.1	0.0	<0.1*
Ludlow	---	---	0.6-2.8	1.9	0.6*-2.8*
Malibu Coast	---	---	0.7-8.6	6.1	0.7*-8.6*
central Mojave group (sum)	6-12	5.4-10	0.1-3.4	2.8	6-10
Montezuma-Birds Landing	---	---	0-0.1	0.0	<0.1*
Morales	---	---	0-9.0	5.3	<9*
Morongo Valley	---	---	0.1-6.2	3.5	0.1*-6.2*
Newport-Inglewood	0.4-0.8	---	0-0.2	0.0	~0.4
Ortigalita	---	---	0.1-0.9	0.8	0.1*-0.9*
Palos Verdes	0.7-1.4	---	0.3-2.4	1.9	0.7-1.4
Panamint Valley	1.6-6.1	---	0.3-2.5	1.5	1.6-2.5*
Pinto Mountain	>5.3	---	0.1-2.1	2.1	~5.3
Pipes Canyon	---	---	0.3-2.1	1.6	0.3*-2.1*
Pleito	---	---	2.4-17	16.1	2.4*-17*

Raymond	0.3-0.6	---	0.2-6.8	2.7	0.3-0.6
Red Mountain-San Cayetano	9.6-13.6	---	0.8-9.1	4.5	~9.6
Rinconada	3.5-12	---	0.1-10	8.6	3.5-10*
Rodgers Creek	>2.1	---	0-24	14.4	2.1-24*
Rose Canyon	1-2.2	---	0.1-1.2	0.6	1-1.2*
San Andreas (Mecca)	21-35	18-22	3.5-38	14.1	21-22
San Andreas (San Gorgonio)	13-28	12-20	0.4-36	4.4	13-20
San Andreas (San Bernardino)	<29	---	5.6-39	11.1	5.6*-29
San Andreas (Pearblossom)	35-60	18-30	16-33	22.0	18-30
San Andreas (Elkhorn Hills)	31-37	25-30	15-36	22.9	25-30
San Andreas (Parkfield)	32-59	16-40	24-38	29.2	32-38*
San Andreas (San Francisco)	10-38	16-24	8.3-46	18.1	16-24
San Andreas (Tomales Bay)	<25	---	5.2-38	15.1	5.2*-25
San Clemente Island	---	---	0.1-2.2	1.0	0.1*-2.2*
San Diego Trough	---	---	0.1-7.9	3.3	0.1*-7.9*
San Fernando	---	---	0.7-7.2	3.0	0.7*-7.2*
San Gregorio (sensu stricto)	---	---	0.1-3.5	2.1	0.1*-3.5*
San Jacinto	13.3-14	11-15	0.2-30	16.2	13.3-14
San Juan-Whiterock	---	---	0.1-5.3	3.5	0.1*-5.3*
San Pedro Martir	---	---	0.2-6.1	1.7	0.2*-6.1*
Santa Barbara Channel (N. side)	---	---	0.1-2.7	1.8	0.1*-2.7*
Santa Barbara Island	---	---	0.2-19	9.2	0.2*-19*
Santa Monica	0.8-1.1	---	0.3-18	10.8	0.8-1.1
Sierra Madre	2.8-7.1	---	0.1-5.7	1.6	2.8-5.7*
Sierra Nevada	0.3-1.5	---	0.1-6.9	0.9	0.3-1.5
Vallecitos	---	---	0.4-2.7	2.0	0.4*-2.7*
White Mountains	~0.9	---	0.6-9.1	3.1	~0.9
White Wolf	7.1-20	---	0.2-9.6	8.2	7.1-9.6*
Whittier	1-1.5	---	0.2-16	10.0	1-1.5

A Strategy for Obtaining High Temporal and Spatial Resolution of Crustal Deformation using GPS

USGS 1434-92-G2196

Yehuda Bock
Institute of Geophysics and Planetary Physics
Scripps Institution of Oceanography
La Jolla, CA 92093
(619) 534-5292
E-Mail: bock@bull.ucsd.edu

Objectives

GPS surveying has the potential to provide crustal deformation precursors for the prediction of large earthquakes and, in particular, to allow *frequent and dense* monitoring of coseismic and postseismic strain transients which would add to our fundamental understanding of the physics of the earthquake process. The goal of this research is to develop and evaluate the capability of surveying *spatially dense, local to regional scale, three-dimensional geodetic networks, in near real-time with several millimeter-level accuracy* using GPS in a continuously operating and kinematic-type modes.

Investigations Undertaken and Data Collected

Southern California Permanent GPS Geodetic Array

The Permanent GPS Geodetic Array (PGGA) has been operated in southern California since the spring of 1990 by SIO and JPL with assistance from Caltech, MIT and UCLA (Figure 1). Funding for the maintenance of the network is provided by NASA, NSF and USGS. The goals of the PGGA are to monitor crustal deformation related to the earthquake cycle in California, continuously, in near real-time and with millimeter accuracy, using a fully automated and economically viable system. The roles of the PGGA also include providing reference sites and precise GPS orbital and earth rotation information to support detailed GPS geophysical surveys in California. We have collected and analyzed an uninterrupted time series of data since 14 August, 1991. The Landers earthquake sequence generated the first real geophysical signals detected by PGGA. Data collected around the period of the Landers and Big Bear earthquakes have been studied extensively for coseismic and postseismic deformation. PGGA data has been a very important asset for our investigations of the spatial and temporal resolution of GPS under this award.

We have developed an automated system to collect, analyze and archive data from the PGGA sites at JPL, Piñon Flat Observatory (PFO), SIO, Goldstone and Vandenberg Air Force Base, and from a globally distributed set of about 30 GPS tracking stations (Figure 2). We monitor data at a 30 second sampling rate to all visible satellites, 24 hours a day, 7 days a week. All raw data in the SIO archive are translated into the Receiver Independent Exchange (RINEX) format for GPS data. These are archived on an optical storage device, the Epoch-1 Infinite Storage Server. All raw data collected to data are on-line and accessible via anonymous ftp.

Parkfield to Cholame Surveys

We have surveyed with GPS since 1990 several small networks along the San Andreas Fault between Parkfield and Cholame These surveys include measurements of (1) the

USGS GPS quadrilateral near Parkfield, (2) a 12-station fault crossing transsect through Parkfield, (3) the 10-station Kennedy Ranch Alinement Array [Genrich and Bock, 1992], and (4) a 12-station fault transsect along Highway 46 near Cholame. In October, 1992 we responded (at the request of USGS) to the level A alert at Parkfield by resurveying these four arrays [Genrich et al., 1992].

Japanese Permanent GPS Geodetic Array

We have analyzed 17 months of continuously monitored GPS observations collected at a ten station network in the Kanto-Tokai district in Japan by the National Research Center for Disaster Prevention. This is the first such network established in the world. Experience with these data have been invaluable in developing data analysis, handling and archiving algorithms for use in the California PGGA.

Results Obtained

Results from the Southern California Permanent GPS Geodetic Array

We have been estimating the position of the PGGA stations daily since August 1991. We perform, at twenty-four hour intervals, a simultaneous weighted least squares adjustment of the station positions and improved satellites ephemerides. During this period, we have also been generating precise satellite ephemerides and improved earth orientation parameters (polar motion) in support of GPS surveys in southern California. These products are available via anonymous ftp over Internet within 5-7 days of collection. We evaluate the precision of our satellite parameters based on overlapping orbital arcs and baseline repeatability. Our orbital ephemerides are sufficiently precise to support any crustal deformation GPS survey in California, thereby eliminating the time consuming and costly need for each investigator and/or analysis center to compute their own orbit improvements.

The time series of length determinations of the PGGA stations with respect to the DRAO site in Penticton, British Columbia more than 1700 km away is shown in Figure 3, indicating clearly interseismic deformation, and coseismic and postseismic signatures related to the Landers (M_S 7.5) and Big Bear (M_S 6.5) earthquakes on 28 June, 1992. The largest deformation was detected at PFO, which is situated about 80-90 km from the rupture zone, with respect to a reference frame defined by a globally distributed station of orbit tracking stations (Figure 4). We are able to detect significant "absolute" coseismic deformation of 1-5 cm with respect to the global frame (Figure 5), and postseismic deformation of nearly 1 mm/day at Goldstone for the two week period following the earthquakes (Figure 6). The details of our Landers analysis can be found in Bock et al. (1993).

As part of our PGGA efforts, we have made significant improvements to the GAMIT GPS software package in collaboration with investigators at MIT [King and Bock, 1992].

Results from the Japanese Permanent GPS Geodetic Array

Results from this extensive study are reported in Shimada and Bock [1992]. Although we obtained significant crustal deformation measurements in the region of central Japan, the primary thrust of our research related to this award was to demonstrate convincingly the power of regionally based, continuously monitoring GPS networks for obtaining temporally dense measurements of small horizontal and vertical crustal movements across plate boundary zones. This research has been invaluable for our work with the southern California PGGA.

Reports published (1992)

Journal articles

Genrich, J.F. and Y. Bock (1992), Rapid resolution of crustal motion with short-range GPS, *J. Geophys. Res.*,**97**, 3261-3269.

Shimada, S. and Y. Bock (1992), Crustal deformation measurements in central Japan determined by a GPS fixed-point network, *J. Geophys. Res.*, **97**, 12,437-12,455.

Bock, Y., D.C. Agnew, P. Feng, J.F. Genrich, B.H. Hager, T.A. Herring, K.W. Hudnut, R.W. King, S. Larsen, J.-B. Minster, K. Stark, S. Wdowinski and F.K. Wyatt (1993), Detection of crustal deformation from the Landers earthquake sequence using continuous geodetic measurements, *Nature*, in press.

Doctoral dissertations

Genrich, J.F., 1992: Geophysical applications of GPS kinematic techniques, Scripps Institution of Oceanography, Univ. of California San Diego.

Monographs and Conference Proceedings

Bock, Y., J. Zhang, P. Fang, J.F. Genrich, K. Stark and S. Wdowinski (1992), One year of daily satellite orbit and polar motion estimation for near real time crustal deformation monitoring, Proc. IAU Symposium No. 156, Developments in Astrometry and their Impacts on Astophysics and Geodynamics, Springer Verlag, in press.

King, R.W. and Y. Bock, 1992: "Documentation of the GAMIT GPS analysis software," Mass. Inst. of Technology and Scripps Inst. of Oceanography, September, 1992.

Abstracts

Bock, Y., J. Zhang, P. Fang, J. Genrich, J.B. Minster, K. Stark and S. Wdowinski (1992), Nine months of precise satellite ephemerides and high-frequency polar motion determined with an operational GPS global analysis system, *Eos, Trans. Amer. Geophys. Union, 73,* 85.

Genrich J., J.B. Minster, and Y. Bock (1992), Rigid body kinematics from multiple unit GPS pseudo range and phase measurements with applications to marine geophysical surveys, *Eos, Trans. Amer. Geophys. Union, 73,* 86.

Bock. Y. (1992), Towards a real-time crustal deformation monitoring system as a tool for earthquake hazards mitigation, *Eos, Trans. Amer. Geophys. Union, 73,* Vol. 43, 69.

Fang, P., Y. Bock, J.F. Genrich, V. Otero, K. Stark, S. Wdowinski, J. Zhang, T.A. Herring and R.W. King (1992), Determination of precise satellite ephemerides, high-frequency earth rotation, and crustal deformation before and during the IGS campaign, *Eos, Trans. Amer. Geophys. Union, 73,* Vol. 43, 134.

Hudnut, K.W., S. Larsen, M. Lisowski, K. Gross, J. Svarc, D. Jackson, Z. Shen, Y. Bock, and P. Fang (1992), Coseismic displacements in the Landers sequence: constraints from near-field geodetic data, *Eos, Trans. Amer. Geophys. Union, 73,* Vol. 43, 365.

Genrich, J.F., Y. Bock, S.S.O. Puntodewo, S. Wdowinski, and K. Hudnut (1992), GPS-determined slip rates across the San Andreas Fault near Parkfield, poster presented at AGU Fall Meeting, San Francisco.

Wdowinski, S., Y. Bock, P. Fang, J.F. Genrich, D.C. Agnew and F.K. Wyatt (1992), The 1992 Landers earthquake sequence: Detection of coseismic and postseismic surface displacement, *Eos, Trans. Amer. Geophys. Union, 73,* Vol. 43, 364.

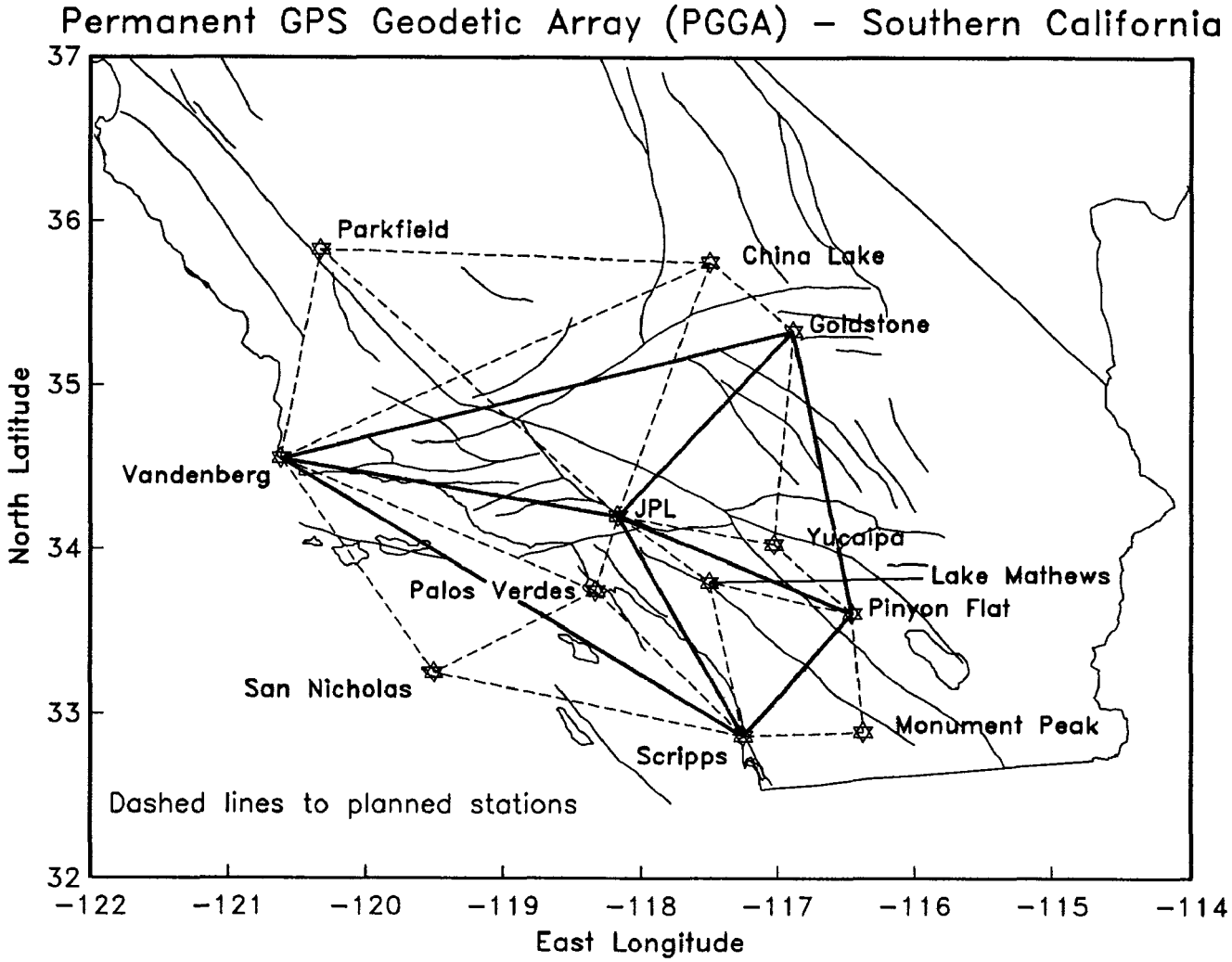

Figure 1: Operational and planned sites of the Southern California Permanent GPS Geodetic Array (PGGA) as of December 1992.

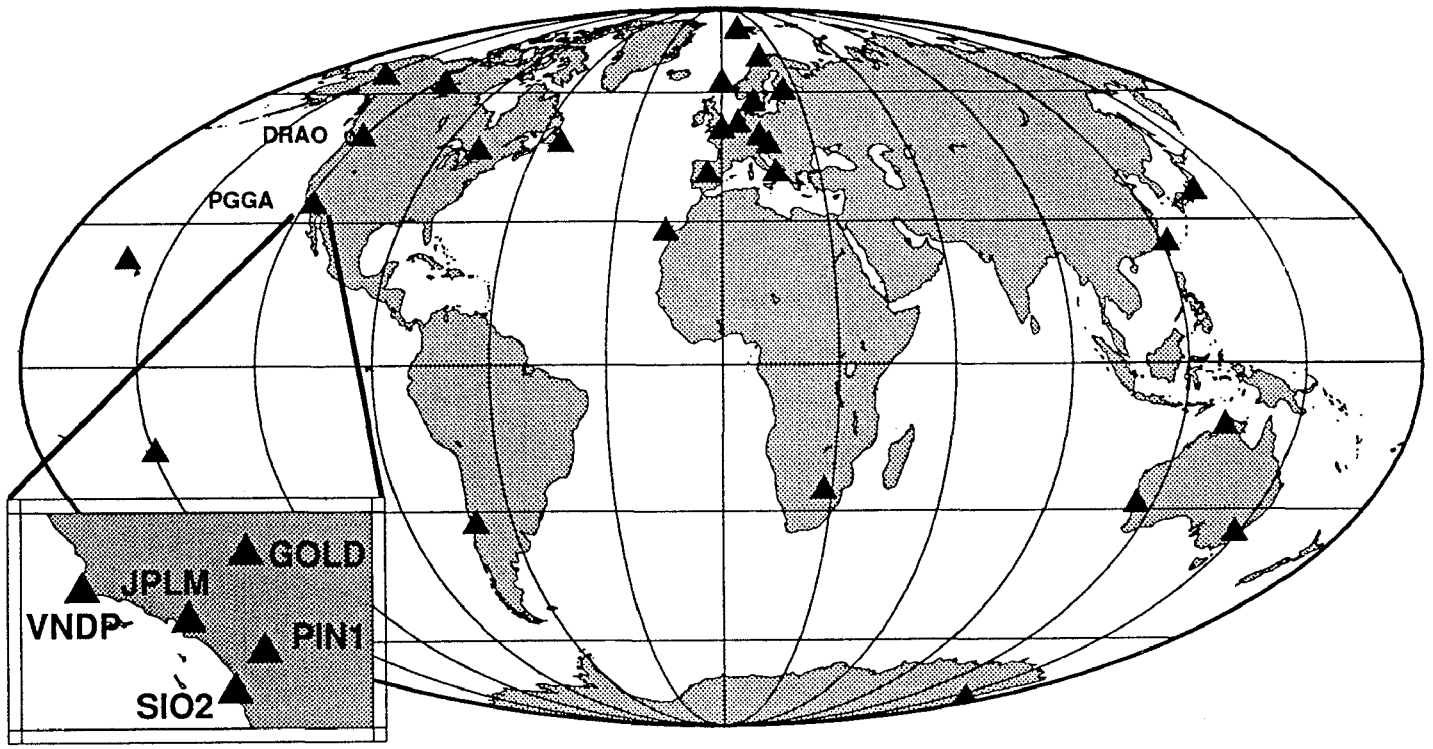

Figure 2: The current distribution of global GPS permanent tracking stations and the PGGA sites in southern California. The global tracking network is usually described by the acronyms CIGNET and FLINN for Cooperative International GPS Network and Fiducial Laboratories for an International Natural science Network, and more recently by the International GPS Service (IGS).

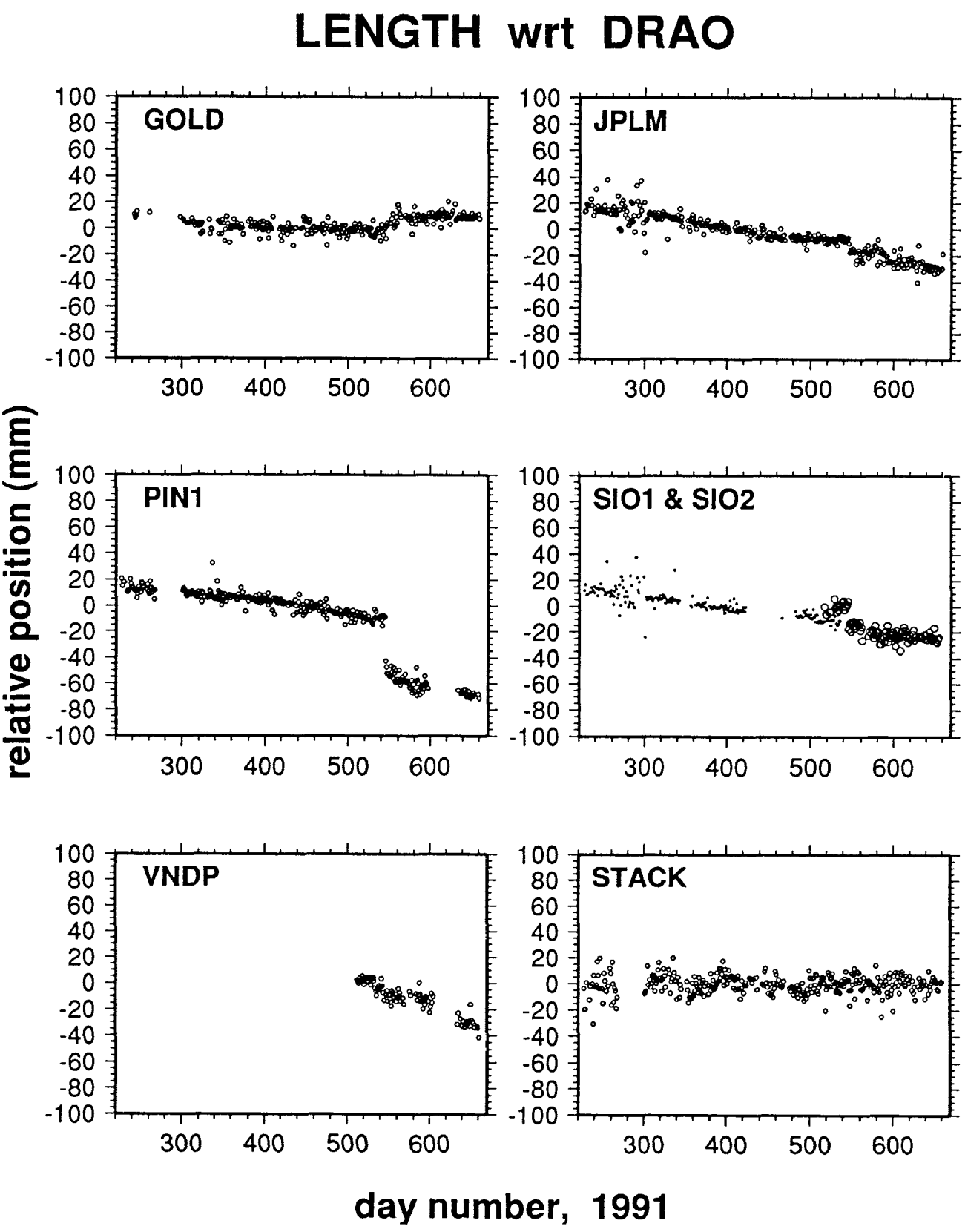

Figure 3: Time series of daily length determinations of the PGGA stations with respect to the DRAO site in Penticton, British Columbia from the time period August 1991 to October 1992. The baseline length is greater than 1700 km. From Wdowinski et al. [1992].

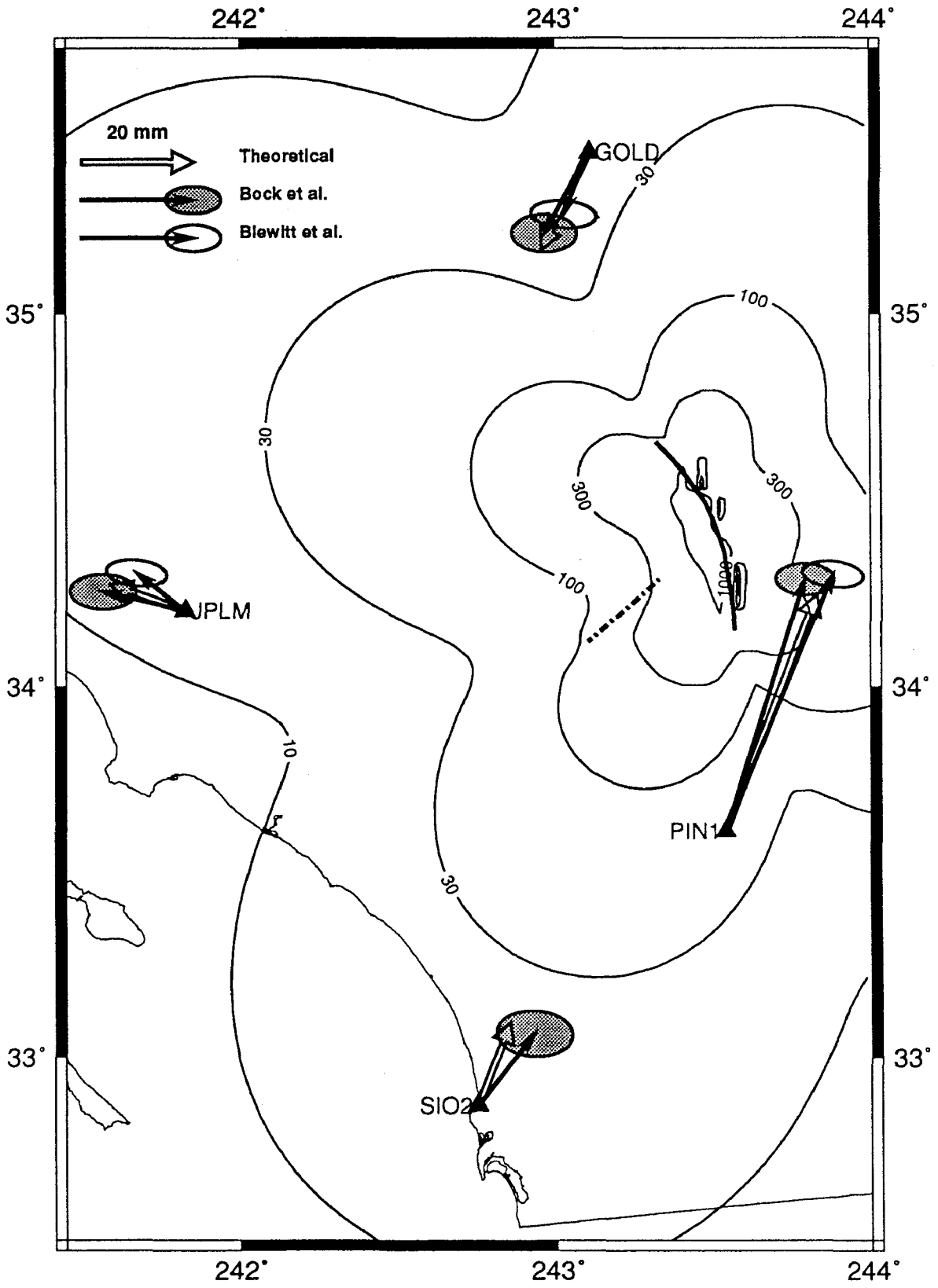

Figure 4: Plot showing the observed (solid arrows) and computed (open arrows) displacements at the PGGA stations, and a comparison of our results with Blewitt et al. at JPL. The contours (displacement magnitude), and the computed displacements are for an elastic halfspace (all units mm). The Landers earthquake break is indicated by a solid line and the Big Bear earthquake by a dotted line. Adapted from Bock et al. [1993].

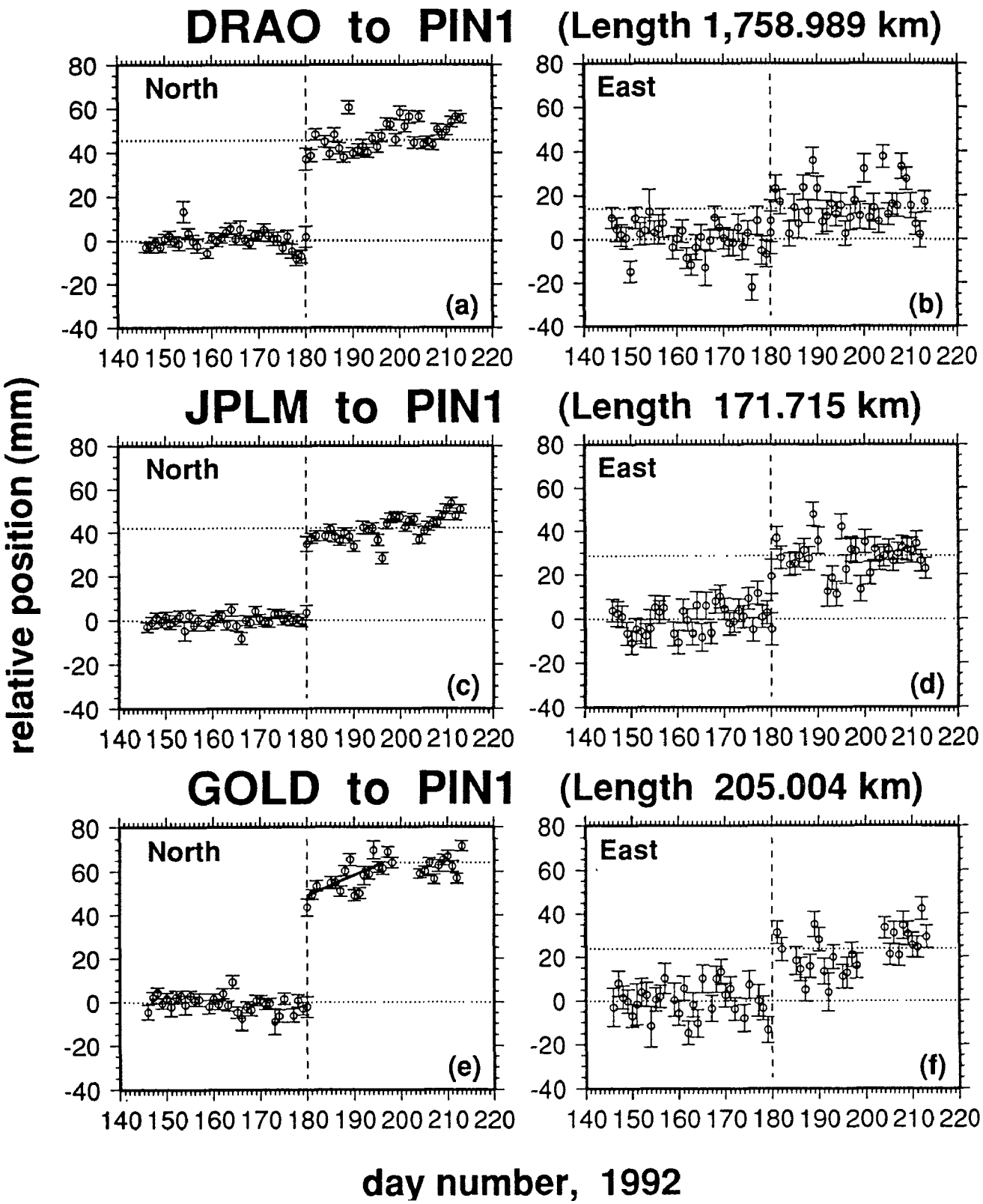

Figure 5: Time series of daily horizontal relative positions over a ten week period centered on the day of the earthquakes (day 180, 28 June 1992) for the DRAO to PIN1, JPLM to PIN1, and DRAO to GOLD baselines. The dotted horizontal lines are determined from the weighted means of the data points for the five week period before and after the earthquakes, and indicate the coseismic signature The error bars are one-sigma standard deviations. The apparent postseismic displacement between GOLD and PIN1 is fit by a solid line in the lower frame. Adapted from Bock et al. [1993].

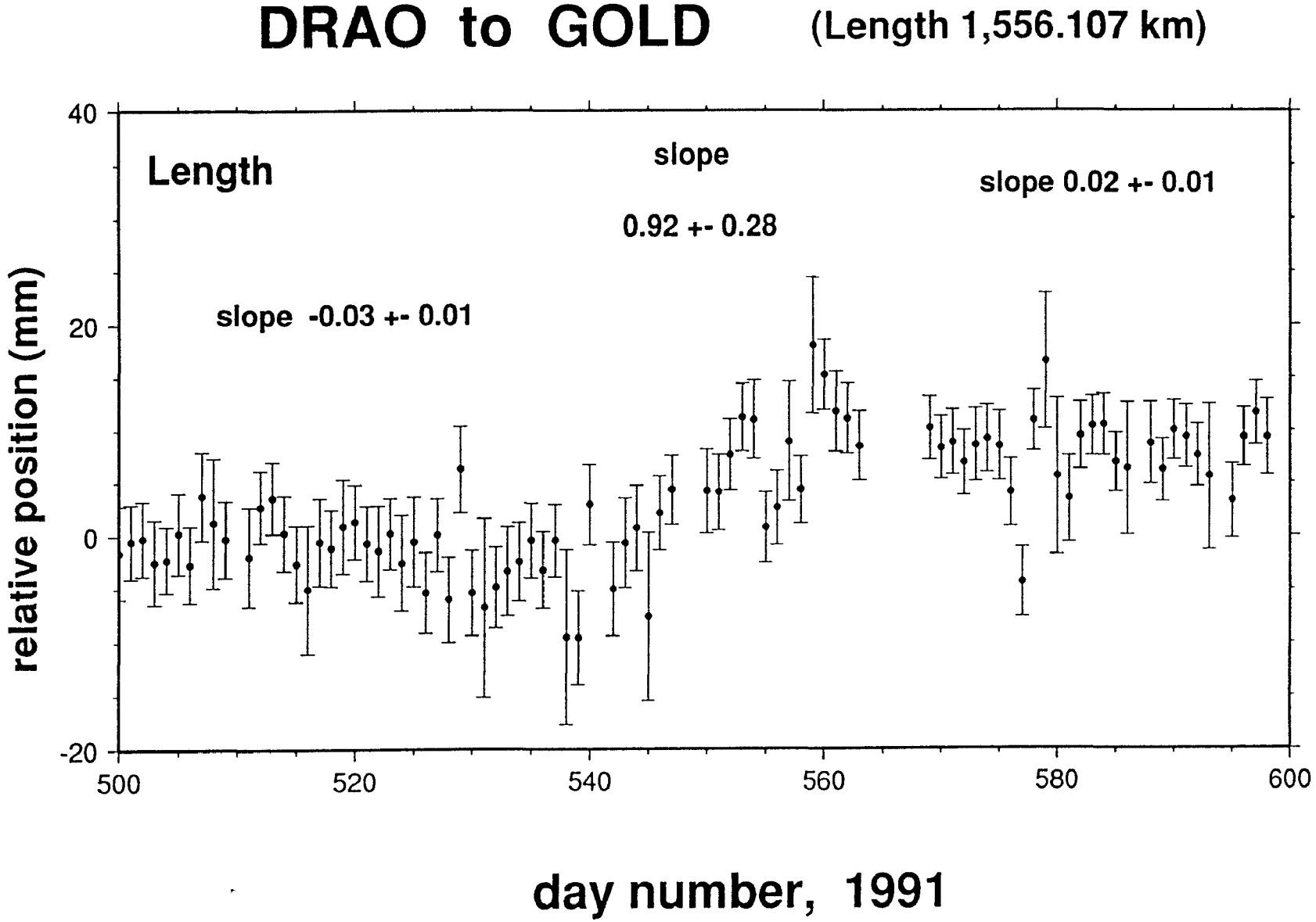

Figure 6: Apparent postseismic displacement at Goldstone with respect to DRAO for the two week period following the Landers earthquake [Wdowinski et al., 1992].

Surface Faulting Studies

9910-02677

M.G.Bonilla
Branch of Engineering Seismology and Geology
U.S. Geological Survey
345 Middlefield Road, MS 977
Menlo Park, CA 94025
(415) 329-5615

Investigations

Compilation and analysis of geologic information that can be used to evaluate and mitigate hazards from faulting and associated earthquakes on part of the San Andreas fault system. The focus is on the San Francisco South quadrangle, which contains the San Andreas and related faults, many landslides, and formations of widely different response to shaking, including Franciscan bedrock, Tertiary sediments, Bay mud, and artificial fills. A 1971 MF geologic map and a 1964 Open-File map showing contours on the bedrock surface are being revised. The revised maps are being compiled in GIS (ARC/ALACARTE) format and prepared for publication on a modern base. Emphasis is being placed on late Quaternary deformation, thickness and nature of unconsolidated deposits, and earthquake-related ground failure.

Results

Reviewed published and unpublished post-1971 reports and 1952-1964 field notes on geology of the quadrangle; searched for new artificial exposures of surficial materials and bedrock using 1989 aerial photos; made field reconnaissance of Serra thrust fault; selected site for augering to confirm probable Holocene displacement on Serra fault; looked for field evidence of possible Quaternary displacement on north part of the Hillside fault (none found to date); compiled information on and collected samples from a tunnel that is under construction near Lake Merced to use in interpreting late Quaternary geologic relations there; revised surficial/bedrock contact at northwest end of San Bruno Mountain; began compilation of new borings and geophysical data; began revision of map showing contours on the bedrock surface using GIS (ARC/ALACARTE) technology.

Revised paper on Marina District and technically reviewed several papers for the USGS Professional Paper on the Marina District.

Reports

Bonilla, M. G., 1992, Geologic and historical factors affecting earthquake damage, in O'Rourke, T.D., ed., The Loma Prieta, California, earthquake of October 17, 1989—Marina District: U.S. Geological Survey Professional Paper 1551-F, p. F7-F34.

11/92

Holocene Slip Rate of the Hayward Fault, Union City, California

Agreement No. 14-08-0001-G2078

Glenn Borchardt
Soil Tectonics
P.O. Box 5335
Berkeley, California 94705-0335

(510)654-1619

Objectives

This project was a cooperative effort with Jim Lienkaemper of the USGS to complete the Union City project. At Union City a stream cuts through the uplifted northeastern side of the fault near Masonic Home and debouches onto an alluvial fan on the southwest side of the fault. Excavations across the fan and parallel the fault uncovered an extremely complicated series of channel fills and interleaved soils. We had initially expected a simple record of successively older buried channel deposits laid down as the debouchment point moved to the northwest. Instead, the record shows a complex of buried alluvial fans having projected apexes of increasing age and offset. The relatively stable points of debouchment apparently were established in conjunction with several right-lateral offsets in the stream.

The preliminary slip rate for fan offset about 67 m was between 7 and 9 mm/yr for the last 8.3 ka. The preliminary slip rate for a fan offset about 43 m was between 6 and 10 mm/yr for the last 4.7 or 6.6 ka. To increase the precision and accuracy of these measurements, we needed to improve our knowledge of the sequence of events that would yield the precise time when each of the stream offsets was initiated.

Fortunately, the site had much datable charcoal and six major paleosols which will help in unraveling the depositional sequence. The paleosols formed on the stable portions of former fan surfaces at the same time as the channels were cutting still other portions of the same fans. Paleosols can be used as stratigraphic markers that constrain the ages of the channel fills that we use as piercing points. Many of these fills are by no means easy to recognize from trench-to-trench. When the size, morphology, and contents of a fill do not suffice, its relationship to the paleosol of the same age becomes the deciding factor in its identification.

Results

We obtained 115 soil samples and performed 55 particle size distribution analyses on 11 vertical sections taken in a 130-m trench. During the project period we completed the soil de-

scriptions and interpretations of the soil data in the context of the channel-fill sequence and 35 C-14 dates on disseminated charcoal (Fig. 1). The soil stratigraphic work supports the following conclusions:

1. The six major paleosols have the following pedochronology (Borchardt, 1992a):

	P1	P2	P3	P4	P5	P6
t_o, ka*	4.7	7.1	8.3	10.7	17.1	~23
t_b, ka	0.5	4.7	7.1	8.3	10.7	17.1
t_d, ky	4.2	2.4	0.8	2.4	6.4	~ 6

*t_o = age when soil formation or aggradation began, t_b = age when soil or strata was buried, and t_d = duration of soil development or aggradation.

2. The primary datum is the P3/P4 paleosol sequence formed during an extremely dry climatic period between 10 ka and 7 ka. These paleosols are easily distinguished by their unique Bk horizons, which contain nodular calcite.

3. Holocene soils at the site are gray brown and associated with varying fluvial conditions, while the Pleistocene soils are yellow brown and associated with relative landscape stability.

4. The youngest age in the G fan was 5.2 ka and the oldest age in the E fan was 5.1 ka. The E fan therefore was established at 5.15 ka. The 43-m offset yields a rate of 8.3 $\pm$1.0 mm/yr.

5. The youngest age in the I fan was 8.5 ka and the oldest age in the G fan was 8.3. The G fan therefore was established at 8.4 ka. The 67-m offset yields a rate of 8.0 $\pm$ 0.6 mm/yr.

6. The oldest age so far determined in fan I was 11 ky B.P. U/Th-corrected to 12.9 ka. The approximate 98-m offset yields a preliminary rate of 7.6 $\pm$ 0.4 mm/yr.

7. The average of the first two determinations yields a slip rate of 8.2 $\pm$0.8 mm/yr for the last 8 ka.

8. There has been no detectable change in the slip rate on the Hayward fault throughout the Holocene.

Reports Published in FY92

Borchardt, Glenn, 1992a, Pedochronology along the Hayward fault, in Galehouse, J.S., ed., Program and Abstracts: Second Conference on Earthquake Hazards in the Eastern San Francisco Bay Area, March 25-29, 1992, California State University, Hayward, p. 9.

Borchardt, Glenn, 1992b, Field trip contributions concerning the Hayward fault at Point Pinole Regional Park, Richmond, Contra Costa College and El Portal School, San Pablo, Hillside School and the University of California, Berkeley, Lake Temescal, Oakland, and Fremont Central Park, Fremont, in Taylor, C.L., Hall, N.T, and Melody, Moya, eds., Field Trip Guidebook, Second Conference, Earthquake Hazards in the Eastern San Francisco Bay Area, March 28-29, 1992: California State University, Hayward, California, p. 13-21, 23-24, 59, 61-63, 77-81, 191-197.

Borchardt, Glenn, Hirschfeld, S.E., Lienkaemper, J.J., McClellan, Patrick, Williams, P.L., and Wong, I.G., editors, 1992 (in press), Proceedings of the Second Conference on Earthquake Hazards in the Eastern San Francisco Bay Area: California Division of Mines and Geology Special Publication 113.

Borchardt, Glenn, and McClellan, Patrick, 1992, Highlights of the Second Conference on Earthquake Hazards in the Eastern San Francisco Bay Area: California Geology, v. 43, no. 4, p. 124.

Borchardt, Glenn, Lienkaemper, J.J., and Budding, K.E., 1992, Holocene slip rate of the Hayward fault at Fremont, in Galehouse, J.S., ed., Program and Abstracts: Second Conference on Earthquake Hazards in the Eastern San Francisco Bay Area, March 25-29, 1992, California State University, Hayward, p. 10.

Borchardt, Glenn, and Mace, Neal, 1992, Clastic dike as evidence for a major earthquake along the northern Hayward fault in Berkeley, in Galehouse, J.S., ed., Program and Abstracts: Second Conference on Earthquake Hazards in the Eastern San Francisco Bay Area, March 25-29, 1992, California State University, Hayward, p. 11.

Lienkaemper, J.J., and Borchardt, Glenn, 1992a, Hayward fault: Large earthquakes versus surface creep, in Galehouse, J.S., ed., Program and Abstracts: Second Conference on Earthquake Hazards in the Eastern San Francisco Bay Area, March 25-29, 1992, California State University, Hayward, p. 41.

Lienkaemper, J.J., and Borchardt, Glenn, 1992b, Holocene slip rate of the Hayward fault at Union City, California, in Galehouse, J.S., ed., Program and Abstracts: Second Conference on Earthquake Hazards in the Eastern San Francisco Bay Area, March 25-29, 1992, California State University, Hayward, p. 42.

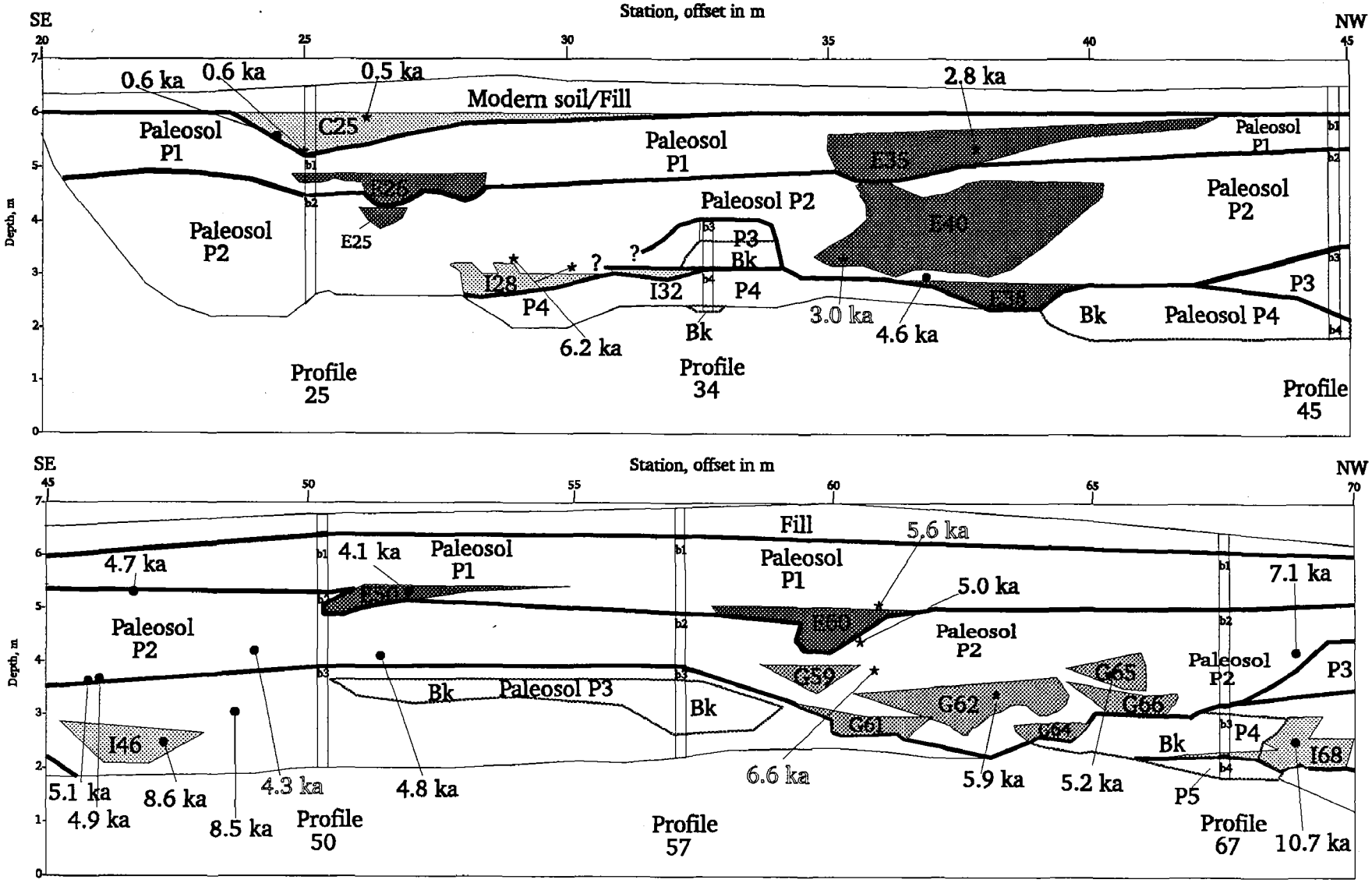

Figure 1. Simplified, reversed, and reduced-scale log of the soil and alluvial relationships parallel and southwest of the Hayward fault at Union City. 1989 trench used as the base. Only the most important channel fills and paleosols are shown. Abbreviations: G74 = channel fill from apex G at station 74; b1 = surface of buried soil; P3 = third youngest paleosol; ka = C-14 date corrected to thousands of calendar years; Bk = soil horizon containing calcite; * = charcoal from this exposure; o = charcoal from another exposure; open letters indicate discordant ages.

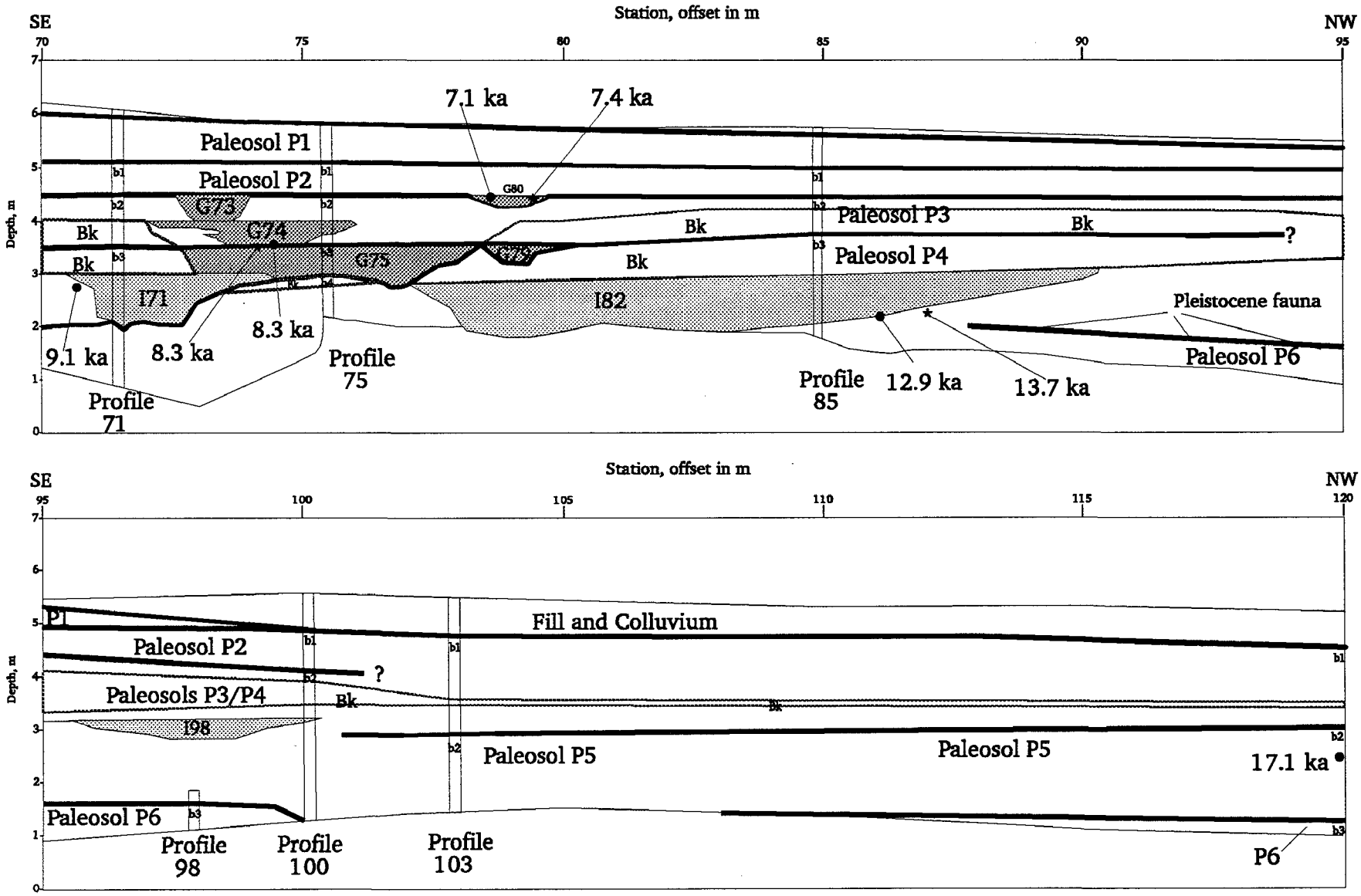

Figure 1. (continued)

ACCELERATION, VELOCITY, AND VOLUMETRIC STRAIN FROM PARKFIELD GEOS NETWORK

9910-02089

ROGER D. BORCHERDT, MALCOLM J. JOHNSTON,
C. DIETEL, G. GLASSMOYER, AND ALLAN LINDH
BRANCH OF ENGINEERING SEISMOLOGY AND GEOLOGY
U.S. GEOLOGICAL SURVEY
345 MIDDLEFIELD ROAD, MS 977
MENLO PARK, CALIFORNIA 94025
415/329-5619

Investigations

* Maintain GEOS array near Parkfield, CA, to serve as a strong-motion array to provide broad-band, high-resolution measurements of the mainshock as well as an array to provide measurements of pre-, co-, and post-seismic strain and displacement field perturbations for purposes of earthquake prediction.

* Maintain up-to-date archive of all events recorded in anticipated rupture zone.

* Develop theoretical basis and models to interpret collocated measurements of volumetric strain and seismic displacement fields.

Results

* An array of 13 stations is being maintained at 95% or greater reliability near Parkfield, CA. Array maintenance is being provided by C. Dietel. He is also maintaining an up-to-date digital data archive and providing summaries for monthly internal USGS reports. (See previous reports for detailed description of the array.) Events recorded along Parkfield segment of study zone during time interval indicated are summarized according to magnitude and depth (Table 1, Figure 1). Stations that triggered on the events are shown in Table 2.

* An example of magnitude 4.7 event recorded at all stations is shown in Figures 2, 3 4, and 5. Measurements of volumetric strain at the six dilatometer sites are arranged in record section format (Figure 2). Three-component measurements of ground acceleration velocity are shown in Figures 3, 4, and 5.

Reports

(see projects Borcherdt et al., [9910-02689 and 9901-03009] and Johnston for related reports.

TABLE 1

HYPO-71 LISTING: PARKFIELD EARTHQUAKES RECORDED ON ONE OR MORE GEOS STATIONS FROM OCTOBER 1, 1991 OCTOBER 20, 1992.

9110 3	547	10.42	35	55.70	120	28.46	4.78	0.83	11	147	3.1	0.03	0.4	0.7	
9110 9	1648	19.75	35	44.76	120	17.76	6.11	0.96	12	90	4.5	0.05	0.4	0.9	
911018	959	5.54	35	55.27	120	28.09	5.69	3.53	42	75	3.7	0.12	0.2	0.2	
911027	610	6.89	36	1.14	120	34.60	5.78	2.93	42	88	4.4	0.09	0.2	0.3	S
911029	628	34.05	35	59.12	120	33.77	9.73	0.94	11	116	3.5	0.11	0.6	0.7	S
911101	1909	36.48	36	1.08	120	34.56	5.63	3.0	28	131	4.	0.08	0.3	0.3	B
911102	0635	17.18	35	59.98	120	33.23	4.91	3.2	17	133	5.	0.04	0.3	0.5	B
911102	0652	16.33	35	59.75	120	33.82	5.56	2.3	21	94	4.	0.09	0.3	0.4	B
911108	0300	48.46	36	4.75	120	38.04	7.16	4.8	45	58	8.	0.12	0.2	0.4	B
911108	0301	25.16	36	4.77	120	37.93	7.46	3.3	20	133	9.	0.08	0.3	0.6	B
911116	1802	18.10	36	2.11	120	35.52	6.65	2.7	30	130	6.	0.08	0.2	0.4	B
911201	0012	30.35	35	57.88	120	30.62	7.40	1.4	15	161	1.	0.04	0.5	0.3	B
911201	0025	43.21	35	57.88	120	30.65	7.27	1.6	20	135	2.	0.05	0.3	0.3	B
911201	0140	12.99	35	57.98	120	30.46	7.40	1.9	24	137	1.	0.07	0.3	0.3	B
911217	0356	17.22	36	4.80	120	38.24	3.22	3.0	32	123	8.	0.08	0.2	0.8	B
911218	1442	19.58	35	57.90	120	31.08	11.57	3.0	37	132	2.	0.11	0.2	0.3	B
920104	1035	03.70	35	55.79	120	28.50	4.93	1.8	17	148	3.	0.04	0.4	0.4	B
920126	1712	51.31	35	59.47	120	33.89	4.92	1.8	24	91	3.	0.07	0.2	0.3	B
920206	0321	16.19	36	1.25	120	34.58	5.71	2.5	31	89	5.	0.07	0.2	0.3	A
920222	1410	50.12	35	48.17	120	21.35	9.04	2.2	27	72	5.	0.08	0.2	0.5	A
920224	1724	01.62	35	47.71	120	21.11	10.10	3.0	32	54	6.	0.12	0.3	0.7	A
920311	2051	35.70	35	52.95	120	25.67	5.95	2.0	26	128	2.	0.06	0.2	0.2	B
920317	1228	53.13	35	55.75	120	28.38	5.01	1.9	22	133	3.	0.05	0.3	0.3	B
920404	0311	16.64	35	58.47	120	31.13	7.55	1.5	20	137	3.	0.03	0.4	0.3	B
920404	0311	48.70	35	58.40	120	31.20	7.61	1.3	16	135	3.	0.02	0.5	0.4	B
920404	0830	17.74	35	55.73	120	28.42	5.02	1.0	17	148	3.	0.03	0.3	0.4	B
920408	1533	03.38	36	1.68	120	35.23	4.58	2.4	30	130	5.	0.11	0.3	0.5	B
920416	0633	54.03	35	58.87	120	31.73	8.03	3.1	14	175	4.	0.03	0.6	0.4	B
920529	1703	01.75	35	49.70	120	22.78	7.68	3.8	37	46	2.	0.13	0.2	0.3	A
920618	1154	35.04	36	3.40	120	36.19	5.54	2.1	29	130	8.	0.06	0.2	0.3	B
920618	1439	17.48	35	59.43	120	33.83	5.09	1.3	12	90	3.	0.07	0.3	0.7	A
920619	1118	55.03	35	47.63	120	20.86	9.15	1.5	21	65	7.	0.06	0.3	0.6	A
920703	0154	58.22	36	3.25	120	36.26	8.41	1.9	24	129	8.	0.07	0.3	0.4	B
920707	1335	53.71	36	1.75	120	35.70	8.25	2.6	31	150	5.	0.11	0.2	0.2	B
920711	0046	57.35	35	51.48	120	24.14	5.19	2.6	27	87	2.	0.07	0.1	0.2	A
920711	0158	15.39	35	51.47	120	24.07	5.25	2.7	29	89	2.	0.07	0.2	0.2	A
920724	1208	28.48	35	58.26	120	32.47	4.08	1.1	9	106	4.	0.09	0.4	1.6	B
920813	0757	08.20	36	.66	120	33.76	5.45	1.7	15	176	5.	0.05	0.4	0.3	B
920818	0703	53.10	35	48.53	120	21.39	5.06	2.1	26	77	5.	0.07	0.2	0.4	A
920819	2221	30.25	35	59.10	120	33.58	5.54	1.5	13	115	4.	0.07	0.3	0.6	B
920911	1351	41.64	36	2.77	120	36.51	10.46	2.8	33	91	7.	0.07	0.2	0.4	B
920914	1301	38.43	35	58.97	120	33.14	5.79	1.7	11	120	4.	0.08	0.4	0.5	B
920916	0525	13.52	35	52.91	120	25.62	5.94	3.4	37	133	5.	0.08	0.2	0.2	B
921001	0611	35.99	35	56.70	120	29.07	10.42	2.0	22	159	2.	0.07	0.3	0.4	B
921004	1816	57.32	35	55.65	120	28.18	9.79	4.0	39	76	3.	0.08	0.2	0.3	A
921005	0401	25.61	35	55.76	120	28.12	9.90	1.5	22	155	4.	0.05	0.4	0.3	B
921005	1859	32.18	35	55.73	120	28.22	9.76	3.3	35	82	3.	0.07	0.2	0.3	A
921007	1304	28.31	35	58.36	120	31.50	5.25	3.4	37	161	3.	0.09	0.3	0.2	B
921020	0528	08.91	35	55.69	120	28.26	9.91	4.7	46	70	3.	0.09	0.2	0.3	A
921020	0541	53.23	35	55.87	120	28.12	10.32	1.7	24	157	4.	0.06	0.3	0.3	B
921020	0548	04.11	35	55.67	120	28.36	9.99	2.7	27	146	3.	0.09	0.3	0.4	BO
921020	0555	54.39	35	55.75	120	28.07	10.21	1.9	26	156	4.	0.06	0.3	0.3	B
921020	0620	55.64	35	56.03	120	28.32	10.47	1.8	25	158	3.	0.06	0.3	0.3	B

TABLE 2

"WHERE" LIST OF TRIGGERED GEOS STATIONS FOR PARKFIELD EARTHQUAKES DURING THE TIME PERIOD OCTOBER 1, 1991 THROUGH OCTOBER 20, 1992.

	M	J	D	V	F	E	G	K	R	P	S	W	C	I
2760547	*													
2831648													*	
2910959	*	*	*	*	*	*	*	*		*		*		*
3000610	*		*		*	*								
3020628			*											
3051909	*		*		*	*		*		*				
3060635	*		*	*	*	*		*		*		*	*	
3060652	*		*							*				
3120300	*	*	*	*	*	*		*	*	*			*	
3120301					*									
3201802	*		*		*									
3350012			*		*									
3350025		*	*		*									
3350140		*	*		*									
3510356			*							*				
3521442		*	*	*	*	*		*		*			*	
0041035		*	*		*					*				
0261712			*											
0370321			*		*					*				
0531410		*			*	*		*					*	
0551724		*			*	*		*	*				*	
0712051		*			*	*		*						
0771228	*	*			*									
095031117	*		*		*									
095031148			*		*									
0950830	*	*	*											
0991533			*		*									
1070633			*		*									
1501702(3)	*		*	*	*	*	*	*		*			*	*
1701154											*			
1701439											*			
1711118								*						
1850154											*			
1891335	*	*	*		*					*	*			
1930046(7)		*	*		*	*	*	*		*				
1930158		*	*		*	*	*	*		*				
2061208											*			
2260757										*				
2310703							*	*						
2322221										*				
2551351			*		*					*	*			
2581301										*				
2600525	*	*	*	*	*	*	*	*		*				*
2750611		*	*		*									
2781816	*	*	*	*	*	*	*	*	*		*			*
2790401			*											
2791859	*	*	*	*	*	*		*			*			*
2811304	*	*	*	*	*	*		*			*			
2940528	*	*	*	*	*	*	*	*	*		*			*
2940541			*					*						
2940548	*	*	*	*	*	*	*	*			*			*
2940555			*		*			*			*			
2940620			*					*						
	M	J	D	V	F	E	G	K	R	P	S	W	C	I

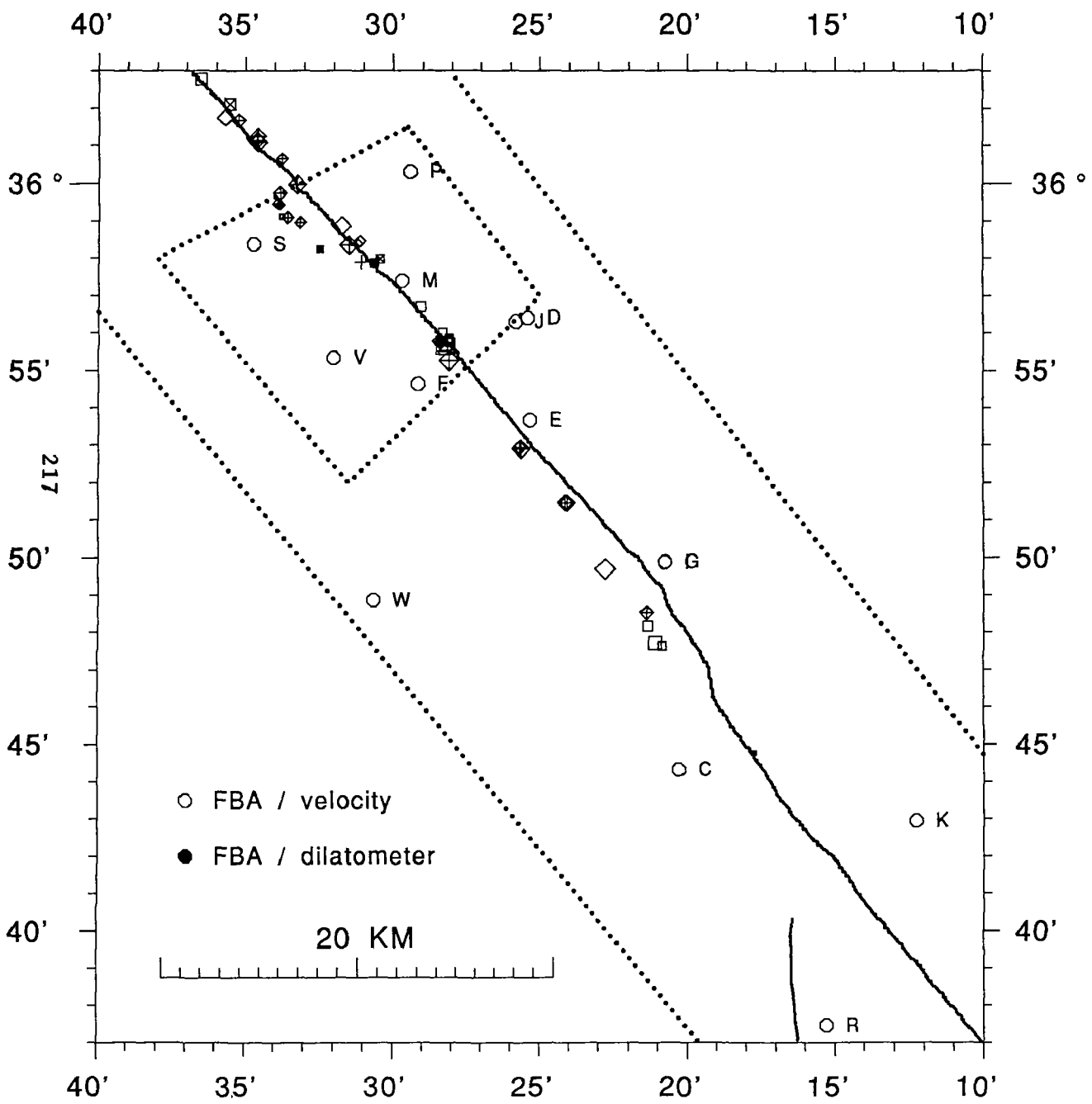

DEPTHS

- 0.0+
- 1.5+
- 3.0+
- 4.5+
- 6.0+
- 7.5+
- 9.0+
- 10.5+
- 12.0+
- 13.5+

MAGNITUDES

- 0.0+
- 0.5+
- 1.0+
- 1.5+
- 2.0+
- 2.5+
- 3.0+
- 3.5+
- 4.0+
- 4.5+

Figure 1

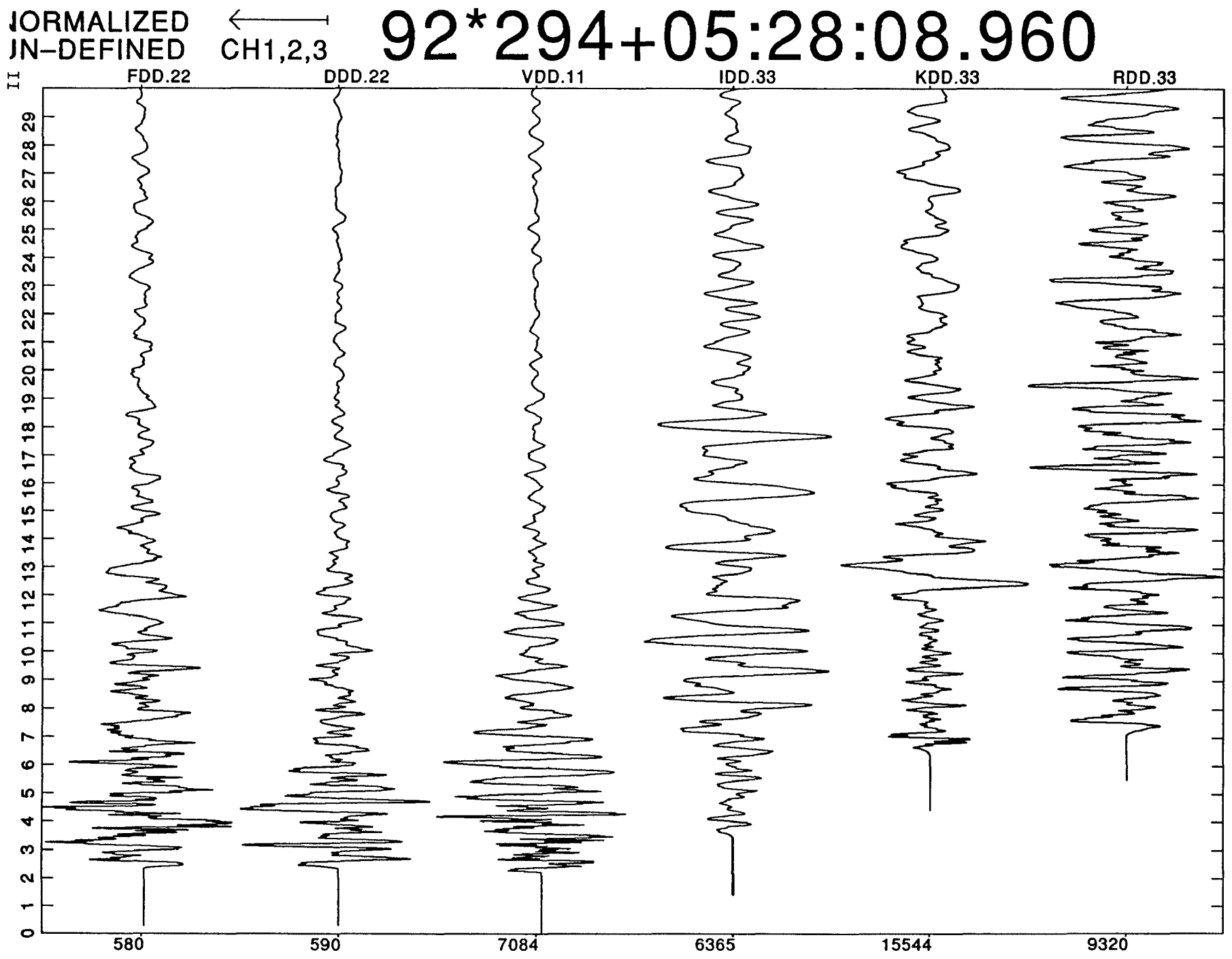
NORMALIZED
UN-DEFINED
CH1,2,3
92*294+05:28:08.960
FDD.22
DDD.22
VDD.11
IDD.33
KDD.33
RDD.33
0 1 2 3 4 5 6 7 8 9 10 11 12 13 14 15 16 17 18 19 20 21 22 23 24 25 26 27 28 29
580
590
7084
6365
15544
9320

Figure 2

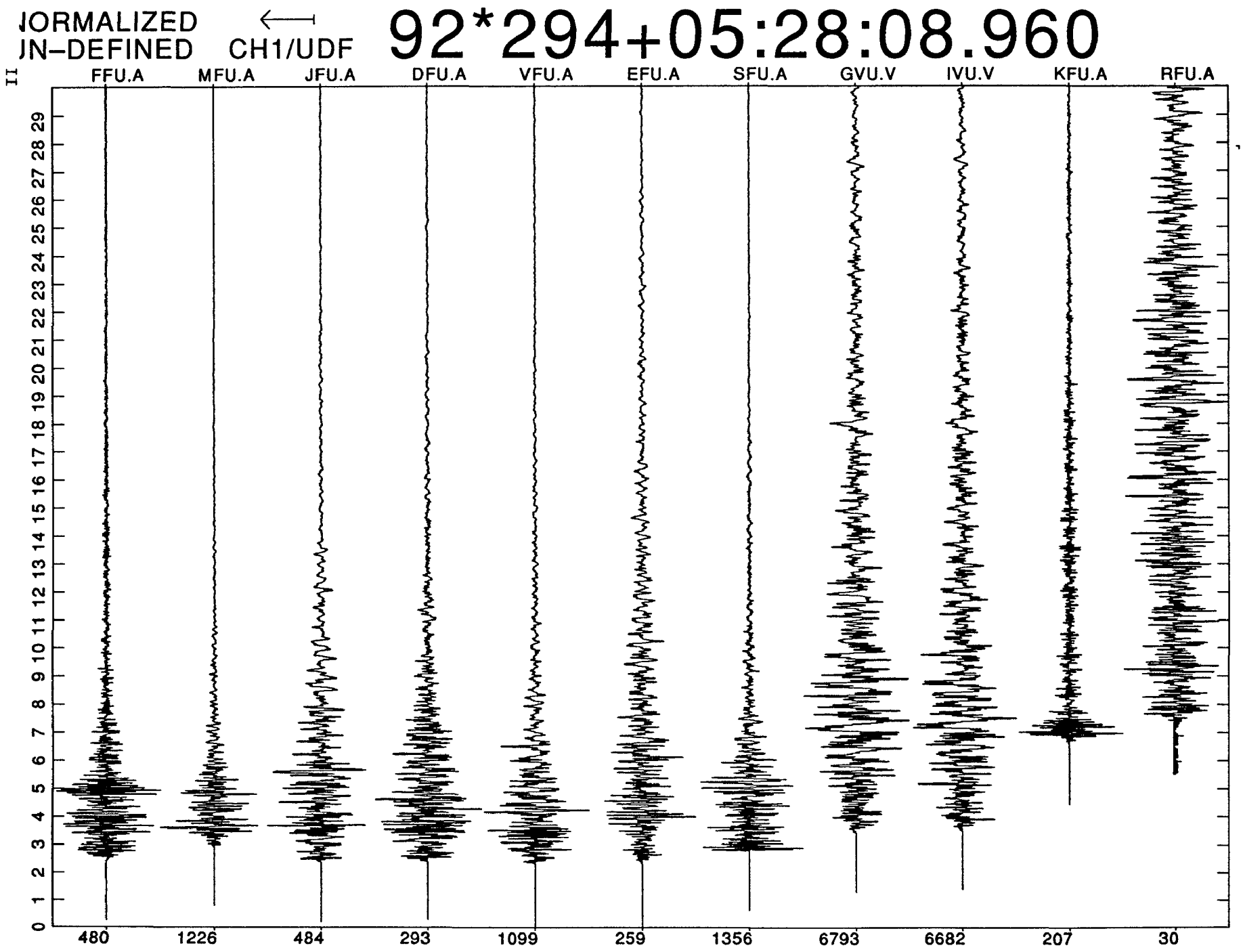
JORMALIZED
JN-DEFINED
CH1/UDF
92*294+05:28:08.960
II
FFU.A
MFU.A
JFU.A
DFU.A
VFU.A
EFU.A
SFU.A
GVU.V
IVU.V
KFU.A
RFU.A
0 1 2 3 4 5 6 7 8 9 10 11 12 13 14 15 16 17 18 19 20 21 22 23 24 25 26 27 28 29
480
1226
484
293
1099
259
1356
6793
6682
207
30

Figure 3

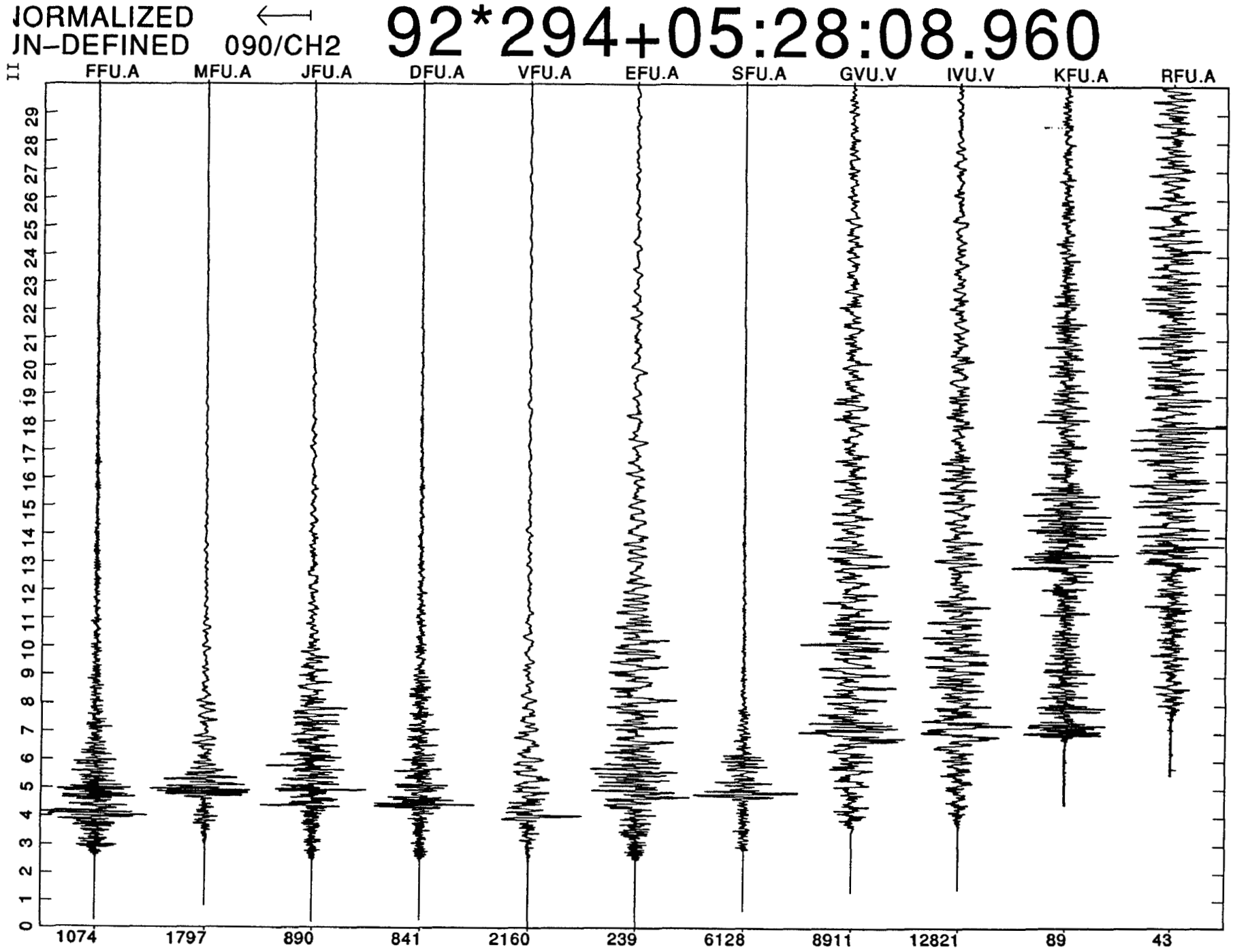
NORMALIZED
UN-DEFINED
090/CH2
92*294+05:28:08.960
FFU.A
MFU.A
JFU.A
DFU.A
VFU.A
EFU.A
SFU.A
GVU.V
IVU.V
KFU.A
RFU.A
0 1 2 3 4 5 6 7 8 9 10 11 12 13 14 15 16 17 18 19 20 21 22 23 24 25 26 27 28 29
1074
1797
890
841
2160
239
6128
8911
12821
89
43

Figure 4

220

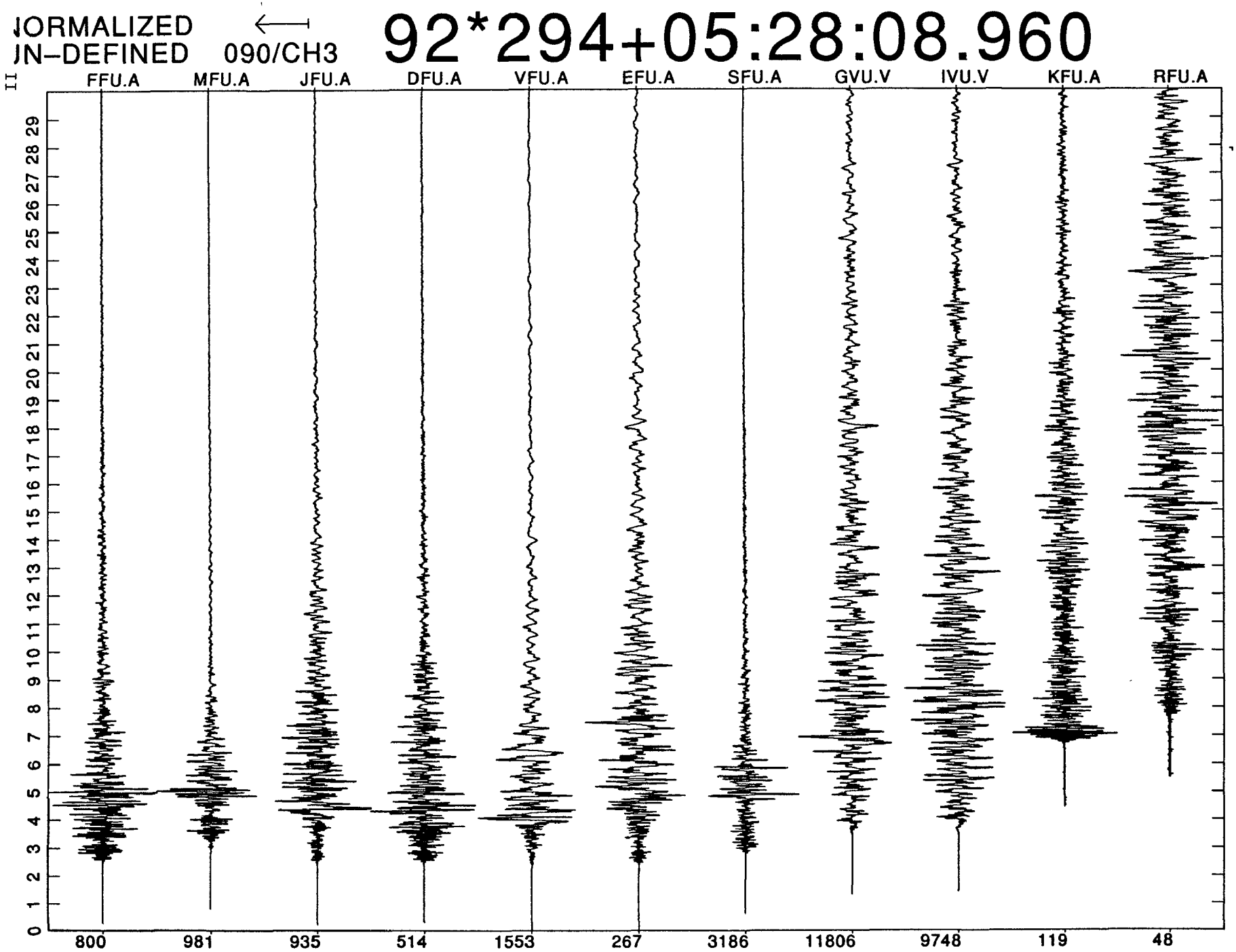
NORMALIZED
UN-DEFINED
090/CH3
92*294+05:28:08.960
FFU.A
MFU.A
JFU.A
DFU.A
VFU.A
EFU.A
SFU.A
GVU.V
IVU.V
KFU.A
RFU.A
0 1 2 3 4 5 6 7 8 9 10 11 12 13 14 15 16 17 18 19 20 21 22 23 24 25 26 27 28 29
800
981
935
514
1553
267
3186
11806
9748
119
48

Figure 5

ANALYSIS OF WIDE-ANGLE REFLECTION/REFRACTION RECORDINGS FROM THE BAY AREA SEISMIC IMAGING EXPERIMENT (BASIX[1])

Seismic Reflection Crustal Studies Project: Project No. 9930-70253 (formerly 04323)

T. Brocher
OEVE, Branch of Seismology
U. S. Geological Survey
345 Middlefield Road, MS/977
Menlo Park, California 94025
Telephone: (415) 329-4737
brocher@andreas.wr.usgs.gov

INVESTIGATIONS UNDERTAKEN

The primary goal of the Bay Area Seismic Imaging eXperiment (BASIX) was to image the subsurface geometry of the crust in the vicinity of the major earthquake producing faults in the San Francisco Bay Area. In September, 1991, BASIX obtained seismic reflection lines designed to provide a picture of the crust down to the base of the crust using a large airgun source and receivers moored to buoys in the water. At the same time, temporary seismic recorders were deployed throughout the Bay Area (see Figure 1) to record these airgun signals at large distances (wide-angles).

We have reduced and begun to analyze the high-quality wide-angle seismic data recorded using five-day recorders during the BASIX experiment. The analysis of these records has consisted of identifying and correlating arrivals recorded at each receiver, digitizing the travel times of these arrivals, and forward modeling and inversion of travel times. A primary goal of this research is to relate the velocity structure to seismic reflections observed in the BASIX multichannel seismic reflection profile. Copies of the five-day recorder data have been distributed to BASIX participants, including Kevin Furlong of Pennsylvania State University, Steve Holbrook of Woods Hole Oceanographic Institution, and Uri ten Brink of the USGS/Woods Hole.

Processing of the wide-angle data as near-vertical incidence reflection profiles represents a high priority for ongoing data processing and analysis. The 5 to 10 km spacing of 5-day and CALNET recorders along these lines, and the proximity of these recorders to the seismic lines, has permited us to generate a single fold seismic reflection line along these transects for comparison to the stacked marine multichannel reflection data acquired using the moored hydrophones. Plots of the wide-angle data as reflection gathers provide exciting images of the middle and lower crust in the Bay Area.

In addition, we have completed an similar wide-angle investigation conducted in the vicinity of Loma Prieta (Brocher et al., in review; Page and Brocher, in review).

---

[1]The BASIX Working Group includes: R. Anima, J. Childs, P. Hart, and M. Marlow of the Branch of Pacific Marine Geology; R. Clymer, D. Jones, E. Karageorgi, T. McEvilly, and P. Williams of UC Berkeley; T. Brocher, M. Moses and A. Michael of the Branch of Seismology; U. ten Brink of the Branch of Atlantic Marine Geology; S. Holbrook of Woods Hole Oceanographic Institution; S. Klemperer and G. Thompson of Stanford University; and K. Furlong of Pennsylvania State University.

RESULTS

Work to date has provided preliminary velocity and structural models for the Bay Area in the following areas: 1) the crustal block beneath SF Bay between the San Andreas and Hayward faults, 2) the crust beneath the East Bay faults between the San Andreas fault and the Great Valley, and 3) the San Andreas fault and continental shelf and slope offshore San Francisco. Similarly, velocity and structural models have been developed for the vicinity of the Loma Prieta earthquake.

San Francisco and San Pablo Bays

The block bounded by the San Andreas and Hayward faults is structurally high, having only a thin 100-200 m sediment cover, and has velocities less than 6 km/s to about 10 km, as one would expect for the Franciscan assemblage. The Hayward and Rodgers Creek faults bounded a 1.5 km deep basin filled with low velocity (2 km/s) sedimentary rocks. Franciscan rocks are thought to extend to a depth of about 16-18 km based on the analysis of the travel-time moveout of wide-angle reflections (Figure 2).

At a depth of about 16-18 km, San Pablo Bay and the northern end of San Francisco Bay are underlain by a prominent mid-crustal reflector (Figure 3), which in turn is thought to be underlain by a high-velocity (velocity about 7 km/s) mafic layer (Figure 2). This reflection can be identified on several recorders located in this portion of the Bay Area . The identity of the mafic layer is uncertain; it could represent a slab of subducted oceanic crust or a magmatically underplated unit.

The crustal thickness underneath this region is currently uncertain. Near-vertical reflections from both 9 and 11 s two-way travel time suggest that the crust may be either about 27 to 33 km thick. Additional wide-angle data acquired during BASIX must be analyzed to address this issue.

East Bay Faults and Crust

The Green Valley fault is also associated with a vertical offset of about 600 m, with the sense of motion being down to the east. From west to east between the Hayward to the Antioch faults, the top of the Franciscan plunges eastwards beneath younger sedimentary rocks to about 3 km depth (Figure 4). Velocities of the rocks to a depth of about 10 km are constrained by reversed Pg arrivals.

Unreversed Pn arrivals recorded by stations located in the Sierran foothills and eastern Great Valley suggest that the crust thins in the vicinity of the Antioch fault to about 24 km (Figure 4). Alternatively, these data, as well as compilations of previous refraction/reflection experiments by Fuis and Mooney (1990), suggest that the crust thickens towards the Coast Range and towards the Sierras. The crustal thinning occurs in the vicinity of deep seismicity near Antioch, and the depth to the base of seismicity can be traced to nearly the Moho near Antioch.

The San Andreas fault and Continental Shelf and Slope

Velocities in the shallow crust east of the San Andreas are lower than 6 km/s and are consistent with Franciscan rocks. The five-day data provide evidence for a low-velocity zone in the upper crust seaward of the San Andreas fault similar to that observed near Año Nuevo by

Brocher et al. (in review). The five-day recorder data obtained along Line OBS2 will be used by BASIX participants Holbrook and ten Brink to refine velocity models obtained from Ocean Bottom Seismometer recordings of this line.

Velocity Model near the Loma Prieta Epicenter

Wide-angle seismic reflection/refraction data obtained in the vicinity of the epicenter of the 1989 Loma Prieta earthquake provide evidence for a slab of oceanic crust extending from the deep sea floor to the San Andreas fault. During marine seismic reflection profiling of the north-central California margin in May 1990, two onshore recording arrays were deployed transverse to and straddling the San Andreas fault in the Santa Cruz Mountains and Diablo Range (Figure 5). Wide-angle reflections recorded by these arrays define the top and bottom of the oceanic crust as far east as the San Andreas fault. The wide-angle refraction data obtained by the arrays provide evidence that the oceanic crust, apparently connected to and inferred to represent Pacific plate, is overlain by a seaward tapering wedge of rocks having velocities between 6.0 and 6.6 $\pm$ 0.1 km/s (Figure 6). We interpret this wedge as being composed of slivers of San Simeon and Salinian (and perhaps other) rocks. The wide-angle data are consistent with a landward dip on the oceanic crust of between 8^{o} and 11^{o}. The velocity model inferred from these data suggests that the hypocenter of the magnitude 7.1 1989 Loma Prieta earthquake was located near the base of the interpreted wedge of Salinian rocks beneath the continental margin, but above the oceanic crust. On the basis of this geometry we infer that the top of the oceanic crust represents a detachment surface accommodating oceanward movement of North America. This oceanward movement mirrors the east-directed tectonic wedging observed beneath the Diablo Range and western Great Valley. An observed concave-upward geometry of the Moho in the vicinity of the San Andreas fault should strongly focus wide-angle reflections from the Moho which travel along the fault from earthquake sources on or near the fault.

Wide-angle seismic reflection and refraction data, mapped geologic structures, and marine magnetic anomalies provide evidence that oceanic crust underlies the coastal margin of California from Morro Bay northward beyond San Francisco. Page and Brocher (in review) interpret the presence of this oceanic slab to be the result of pseudo-subduction, i.e., underthrusting/ overthrusting of the Pacific and North America plates, during Pliocene-Quaternary time, well after the cessation of true subduction at this margin. Likely causes of this thrusting are the change in plate motions at about 3.5 Ma and extension in the Basin-and-Range Province.

Reports

Brocher, T.M., M. J. Moses, W.S. Holbrook, U.S. ten Brink, and S.L. Klemperer, Wide-angle seismic recordings of BASIX, EOS Trans. AGU, 73, 401, 1992.

Brocher, T. M., M. J. Moses, and S. D. Lewis, Wide-angle seismic recordings obtained during seismic reflection profiling by the S.P. Lee offshore the Loma Prieta epicenter, U. S. Geological Survey Open-file Report 92-245, 63 pp., 40 figs., 1992.

Brocher, T. M., M. J. Moses, and S. D. Lewis, Evidence for oceanic crust beneath the continental margin west of the San Andreas fault based on onshore-offshore wide-angle seismic recordings, U. S. Geological Survey Professional Paper on Loma Prieta, Vol. 1., in review.

Brocher, T.M., M. J. Moses, and J. McCarthy, Onshore-offshore wide-angle seismic recordings of BASIX, U. S. Geological Survey Open-file Report, in preparation.

Holbrook, W. Steven, U. S. ten Brink, and T. M. Brocher, Crustal structure beneath San Francisco Bay from BASIX wide-angle seismic data, EOS Trans. AGU, 73, 404, 1992.
Moses, M. J, and T.M. Brocher, Wide-angle seismic recordings of BASIX: Five-day recorder profiles, EOS Trans. AGU, 73, 404, 1992.
Page, B. M., and Brocher, T. M., Evidence for Pliocene-Quaternary pseudo-subduction, Coastal California, Geology, submitted to the journal for review.

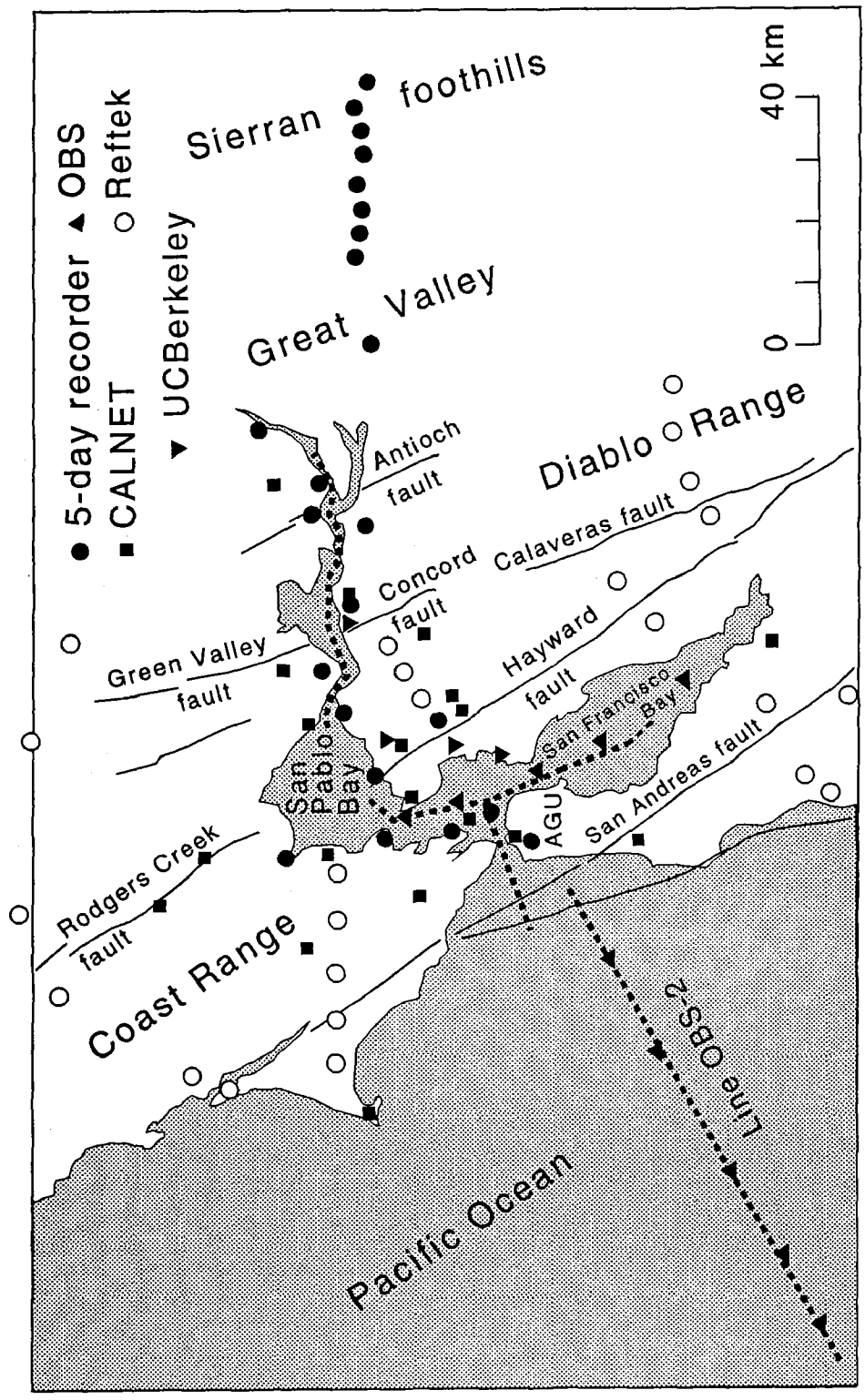

Figure 1. BASIX Seismic Reflection Lines and Wide-angle Recorders.

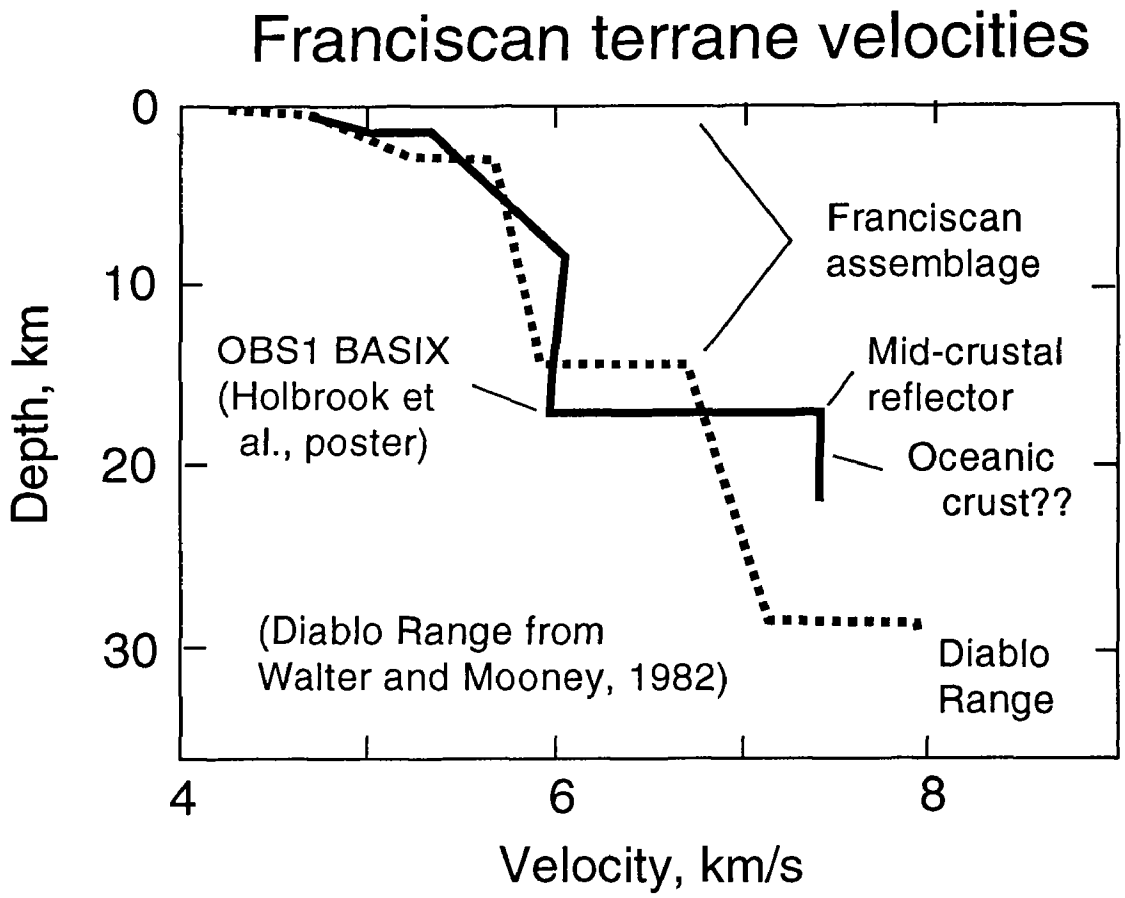

Figure 2. One-dimensional velocity model obtained for N-S line in San Francisco and San Pablo Bays compared to that from a previous strike-line in the Diablo Range (Walter and Mooney, 1982). Note the presence of a high velocity (7 km/s) layer beneath the prominent mid-crustal reflection at 6 s twtt (depth about 16-18 km).

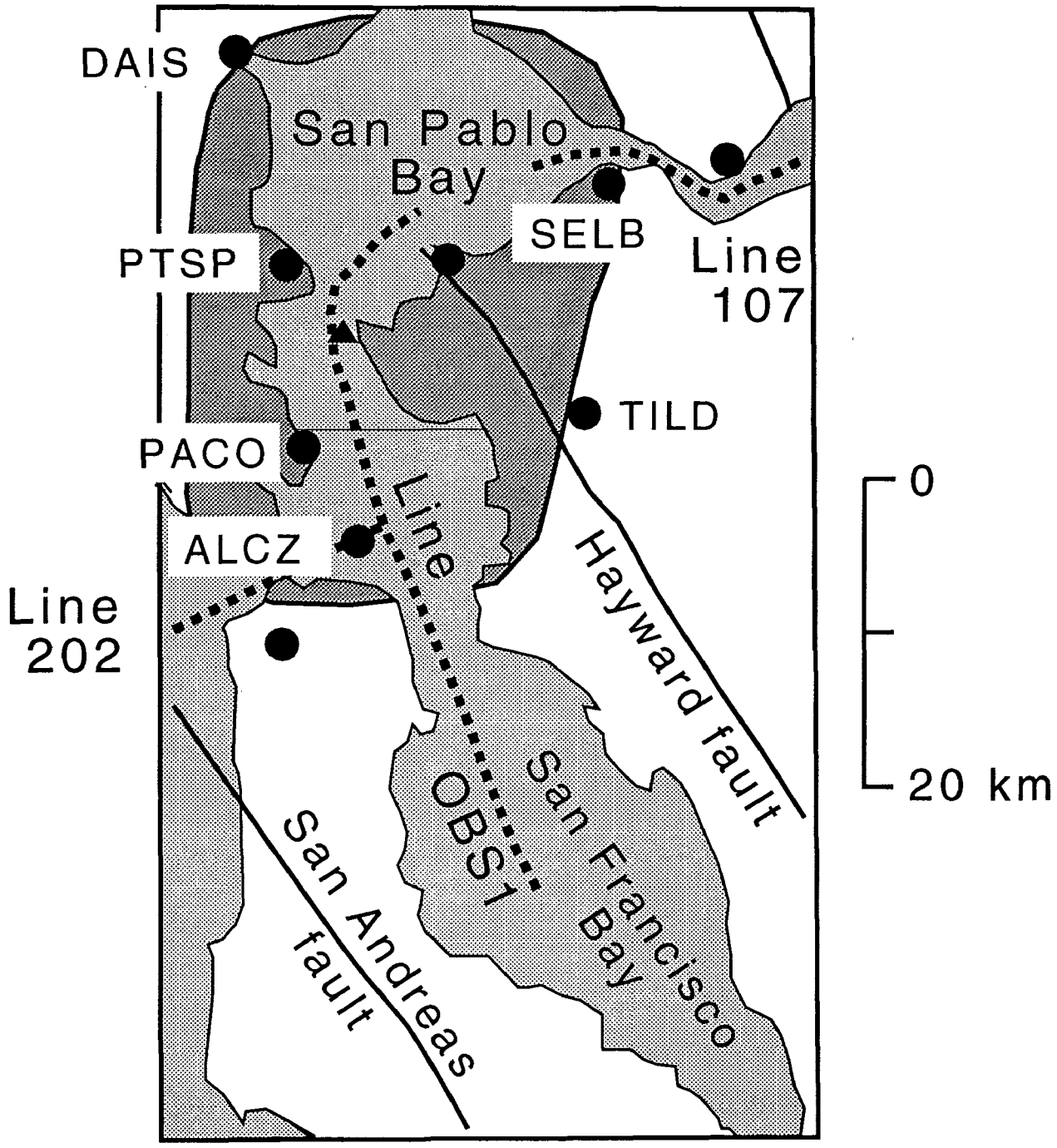

Figure 3. Extent of Mid-crustal Reflector.

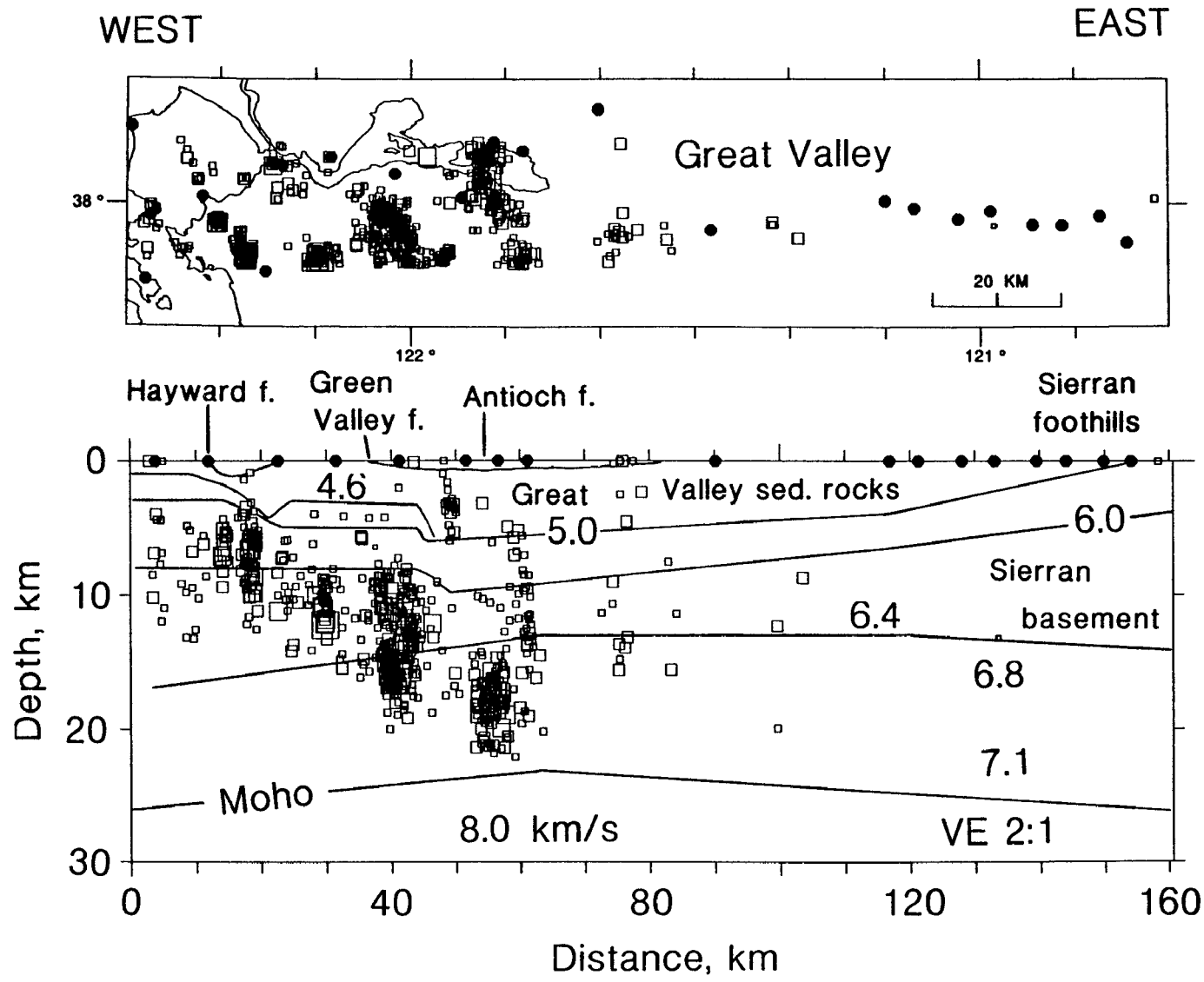
WEST
EAST
Great Valley
38°
20 KM
122°
121°
Hayward f.
Green Valley f.
Antioch f.
Sierran foothills
0
4.6
Great Valley sed. rocks
5.0
6.0
Sierran basement
10
6.4
6.8
20
7.1
Moho
8.0 km/s
VE 2:1
30
Depth, km
0
40
80
120
160
Distance, km

Figure 4.

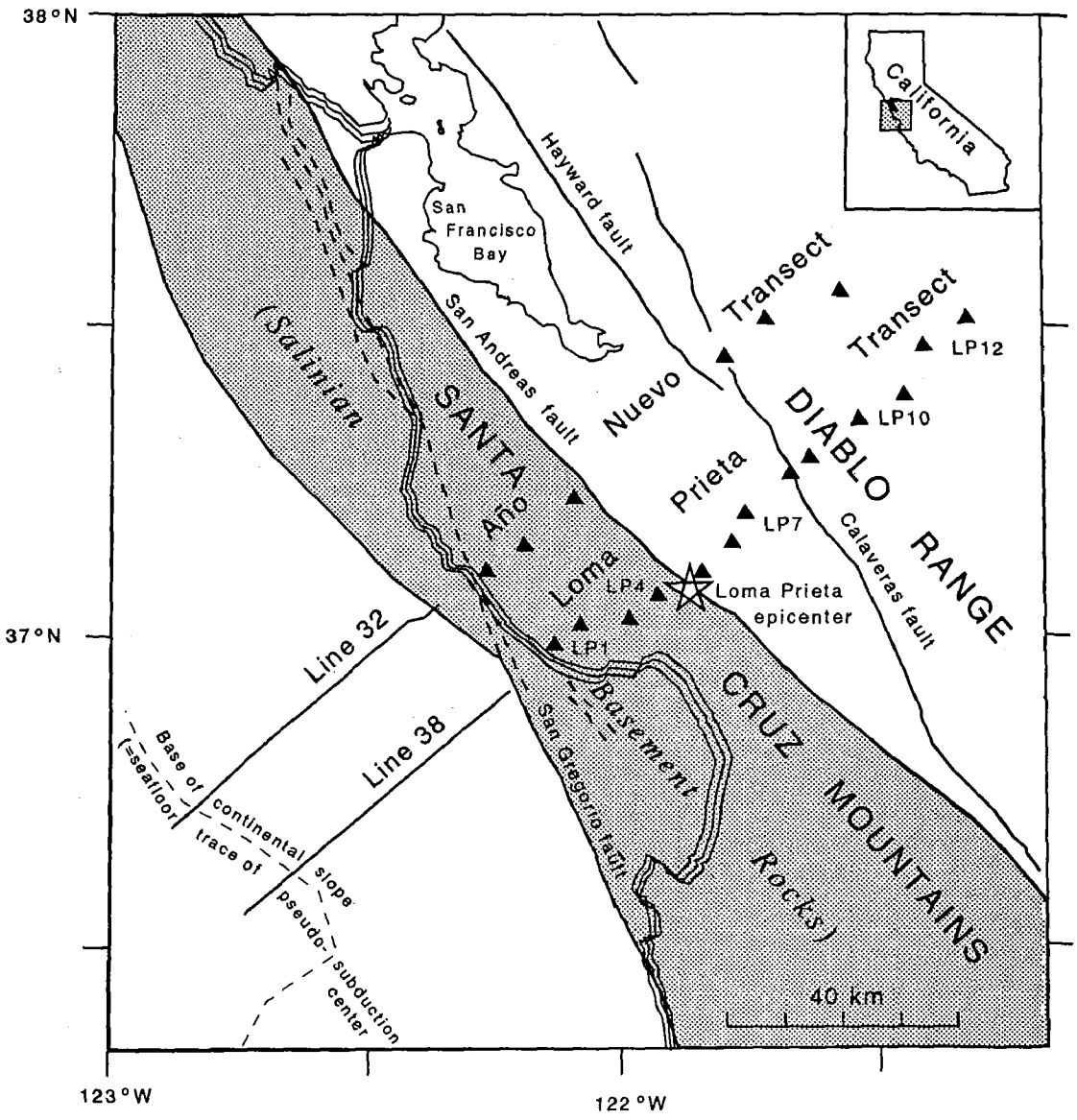

Figure 5. Location map showing seismic lines and recorder locations used for onshore-offshore wide-angle seismic experiment near the epicenter of the Loma Prieta earthquake.

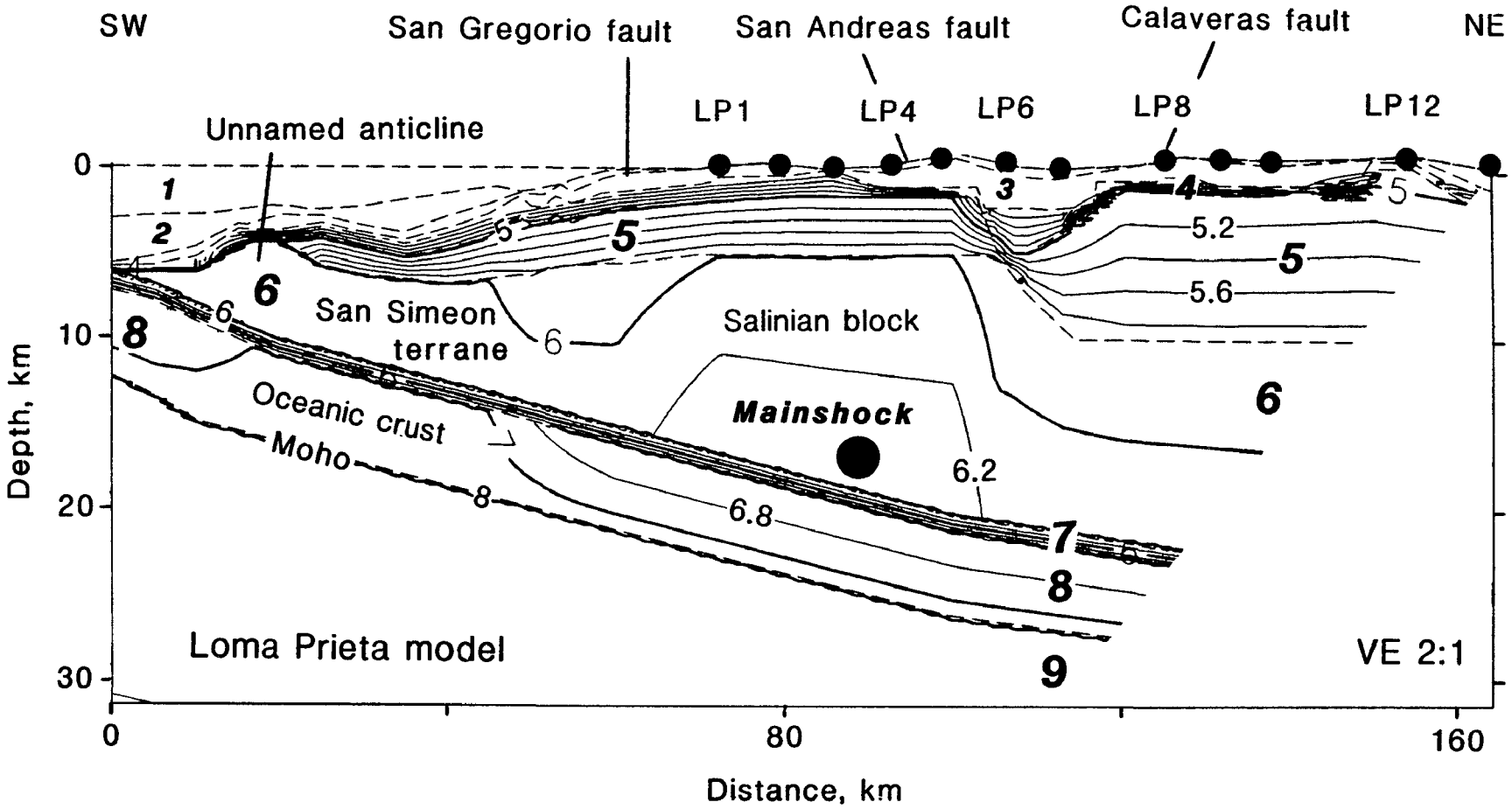
SW
San Gregorio fault
San Andreas fault
Calaveras fault
NE
LP1
LP4
LP6
LP8
LP12
Unnamed anticline
San Simeon terrane
Salinian block
Mainshock
Oceanic crust
Moho
Loma Prieta model
VE 2:1
Depth, km
Distance, km
0
10
20
30
80
160
5.2
5.6
6.2
6.8

Figure 6.

Northern San Andreas Fault System

9910-03831

Robert D. Brown
Branch of Engineering Seismology and Geology
U.S. Geological Survey
345 Middlefield Road, MS 977
Menlo Park, California 94025
(415) 329-5620

Investigations

1. Synthesis studies of the geology, seismology, and tectonics of the San Andreas fault system, especially in northern California.

2. Advisory activities for Bay Area Regional Earthquake Preparedness Project (BAREPP) and San Francisco Bay Conservation and Development Commission (BCDC), both of which are state agencies.

3. Research on applications of earth science-information, reviews of applications work by others, and interpretation of geologic and geophysical results for non-technical audiences.

Results

1. Revised paper, with D. Hill and R. Wallace, on the San Andreas fault system. Originally planned for book publication, the paper has been revised for publication in an issue of Annales Tectonicae that describes the geological character of active fault zones.

2. Late Holocene slope failures adjacent to the San Andreas fault in the Lakes district of Point Reyes National Seashore appear to document systematic tilting--up to the southeast--on a thrust fault that converges with the San Andreas fault north of Bolinas. Landslide blocks and other rocks above the fault plane exhibit structural complexities and compressed northwest-striking folds that contrast with relatively uniform, low, northwest dips beneath the fault. Relict ledges and patches of cemented iron-stained gravel that are attached to both bedrock and slide deposits at about 1 m above the present shoreline angle also suggest recent

uplift. G. K. Gilbert recorded evidence of vertical deformation near Bolinas and reactivation of some Lake district tension fractures immediately after the 1906 earthquake, but he observed no major reactivation of the landslides. The landforms and shoreline deposits predate the 1906 earthquake; one landslide is dated at about 3300 yr B. P. (Roger Byrne, personal communication, 4 March, 1992) and most of the other slides appear to be at least as recent. Evidence of coastal uplift along the San Andreas fault also occurs to the south along the San Francisco Peninsula and, of course, near the Loma Prieta earthquake of 1989. Thus, some earthquakes in this region may depart from the simple strike-slip model that is generally assumed. Any substantial component of vertical slip on this or other bay region faults introduces new and significant hazards during large earthquakes.

3. Continued to participate in activities of BAREPP and BCDC, but meetings of BCDC's Engineering Review Board were curtailed early in the year because of budgetary and staff shortages. Testified regarding USGS findings regarding Diablo Canyon Long Term Seismic Program at California State Senate hearings on nuclear power plants. Served as associate editor for Earthquakes and Volcanoes.

Reports

1. Brown, Robert D., 1991, Testimony *at* Hearing by California Senate Committee on Energy and Public Utilities regarding: California's Nuclear Power Plants: Their Safety, Environmental Impacts and Economic Costs, p. 75-81 and appendix.

11/92

PUGET SOUND PALEOSEISMICITY

9950-10175

Robert C. Bucknam
U.S. Geological Survey
M.S. 966, Box 25046
Denver, Colorado 80225
(303)273-8566

INVESTIGATIONS:

The primary objective of this project is to document and characterize Holocene deformation in the Puget Sound, Washington, region and develop an understanding of its structural and tectonic origins.

Work during the reporting period focused on an area of late Holocene uplift in central and southwest Puget Sound that has been inferred to have been the site of a large earthquake about 1000 years ago (Fig. 1). Paleontological analyses of diatoms from a core at Winslow collected in August 1991 were done by Eileen Hemphill-Haley, U.S. Geological Survey, Menlo Park, California. Analyses of plant macrofossils from the core were done by Estella Leopold and Daniel Ekblaw at the University of Washington. About 5 m of core was collected from another raised marsh at Restoration Point on Bainbridge Island, west of Seattle, in August 1992 for detailed paleoecological and radiocarbon age studies. Previous studies have shown that the section, which includes Mazama ash, was deposited during about the past 8,000 years. The long record offers an opportunity to study the history of relative sea level at the site and thus provides a means of determining if other large uplift events have occurred at the site in the past few thousand years.

Fieldwork at uplift sites in southwest Puget Sound in 1992 has provided additional constraints on the amount of uplift in that area.

RESULTS:

1. *Paleoecology of the Winslow marsh*

Two continuous 7.5 cm-diameter, 3-meter-long cores were collected in plastic pipe from a small coastal salt marsh near Winslow in August 1991. Previous work had shown that the marsh was present when about 7 meters of uplift occurred at Restoration Point, 5 km to the south, probably 1000 to 1100 years ago. Because of its proximity to the uplift area and to an inferred fault that crosses Puget Sound at Seattle, the site is a key to interpreting possible fault slip. Preliminary analysis of the core this year shows that organic mud at the Winslow marsh was deposited 1600 to 2100 years ago and contains diatoms characteristic of freshwater ponds. Gyttja overlying the mud was deposited 1400 to 1700 years ago and contains diatoms characteristic of fresh or slightly brackish water as well as seeds and fragments of freshwater plants. Several lenses of sand within the gyttja contain abundant foraminifera, including a high salt marsh species, suggesting that the site was at or near the level of high tide but probably isolated from Puget Sound by a storm bar. Peat deposited 700 to 900 years ago, after the uplift at Restoration Point, contains leaf bases and rhizomes of salt marsh plants showing that relative sea level rose at the Winslow marsh, probably as a result of subsidence during the time period of the nearby uplift at Restoration Point. The change from gyttja to overlying peat is marked by an abrupt contact. Additional detailed study of the section is underway to further characterize the timing and amount of possible subsidence at the Winslow marsh.

2. *Amount of uplift in southwest Puget Sound*

Relief on the surface of an uplifted tidal flat at Lynch Cove (Fig. 1) and the vertical range of shells that lived on the tidal flat shows that uplift there 1,000 to 1,500 years ago was greater than 2 m and less than 4 m. The former tidal flat surface slopes gently toward the central part of the cove. Plant fossils in freshwater peat that overlies the former tidal flat shows that before uplift, the highest point on the former tidal flat was below high tide, and after uplift the lowest point on that surface was above high tide. The relief between these two points, 2 m, is a minimum measure of the amount of uplift at the site. A shell-rich layer in the mud that underlies the former tidal flat contains abundant articulated remains of the Olympic oyster (Ostrea lurida). They commonly live between mean tide and low tide and are uncommon subtidally. The vertical range of their shells in the raised tidal flat mud at Lynch Cove limits the maximum amount of uplift to 4 m.

REPORTS PUBLISHED:

Bucknam, R.C., Hemphill-Haley, E., and Leopold, E.B., 1992, Abrupt uplift within the past 1700 years at southern Puget Sound, Washington: *Science*, in press.

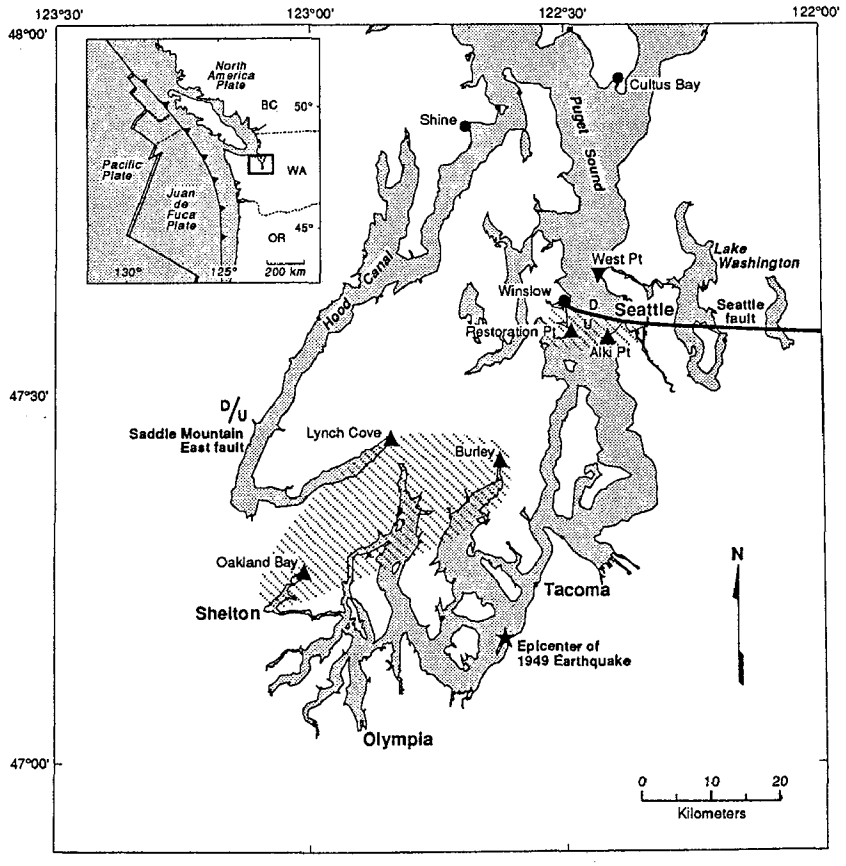

Figure 1. Diagonal ruling shows approximate minimum extent of late Holocene uplift in central and southwest Puget Sound. Sites with stratigraphic or geomorphic evidence of uplift shown by upward pointing triangles. Site with evidence of subsidence of 1 m or more shown by downward pointing triangle (After Atwater and Moore, *Science*, 1992). Stable sites (Cultus Bay; Atwater and Moore, Science, 1992; Shine; Eronen and others, Quaternary Research, v. 27) or sites with less than about 1 m subsidence shown by solid circles.

Global Seismograph Network

9920-10162

Howell M. Butler
Branch of Global Seismology and Geomagnetism
U.S. Geological Survey
Building 10002, Kirtland AFB-East
Albuquerque, New Mexico 87115-5000
(505) 846-5646

Investigations

The Global Seismograph Network (GSN) presently consists of the Global Digital Seismic Network (GDSN) 10 stations; the China Digital Seismic Network (CDSN) 10 stations; the Incorporated Research Institutions for Seismology Network (IRIS/GSN) 21 stations and the Worldwide Standardized Seismograph Network (WWSSN) 66 stations. Support is furnished at a level needed to keep the GSN at the highest percentage of operational time in order to provide the improved geographical coverage with analog and digital data from highly sensitive short-period and very broadband seismic sensor seismograph systems. This support includes provision of operational supplies, replacement parts, repair services, modifications, on-site system installation, maintenance, training and system calibration.

Results

The GSN continues with a combined total of 107 WWSSN/SRO/ASRO/DWWSSN/ CDSN/IRIS-1/IRIS-2 stations. Global seismic data coverage is provided to the National Earthquake Information Center (NEIC) and to other data centers and research organizations throughout the world.

IRIS-2 seismograph systems were installed at eight location: Narrogin, Australia (NWAO); South Pole, Antarctica (SPA); Rarotonga, Cook Islands (RAR); South Karori, New Zealand (SNZO); Yuzhno Sakhalinsk, Russia (YSS); Chiang Mai, Thailand (CHTO); Taipei, Taiwan (TATO); and Ankara, Turkey (ANTO).

On-site maintenance visits were required at the following locations: Albuquerque, New Mexico (ANMO); Guam, Mariana Islands (GUMO); College, Alaska (COL); Garni, Armenia (GNI); Toledo, Spain (TOL); and Grafenberg, Germany (GRFO).

Site surveys were performed at the following locations: Caico, Brazil (CAI); New Delhi, India (NDI); Kodaikonal, India (KOD); Magadan, Russia (MAG); Yakutsk, Russia (YAK); and Petropavlovsk, Komchalskiy (PET).

Aseismic Creep and Crustal Deformation of Large Normal Faults: Implications from the Teton Fault

USGS Grant #14-08-0001-G1970

John O.D. Byrd and
Robert B. Smith, Principal Investigator
Department of Geology and Geophysics
University of Utah
Salt Lake City, Utah 84112
gg-rbs@mines.utah.edu
(801) 581-7129

Investigations Undertaken: October 1, 1991-September 31, 1992

1. Analysis and boundary element modeling of 1st order leveling-line reobservations across the central portion of the Teton fault, collected in 1988, 1989, and 1991 (in a cooperative project with Dr. Arthur Sylvester of the University of California, Santa Barbara)

2. Reduction and two-dimensional modeling of detailed gravity profiles, in conjunction with construction and inversion of two-dimensional ray-tracing models of seismic refraction data across the hanging wall of the Teton fault to assess subsurface fault and hanging wall basin geometry.

Introduction

This study focuses on the mechanics of large normal faults and their seismogenic behavior as manifested by the Teton fault, Wyoming. The Teton fault is characterized by a generally continuous 55 km long series of Quaternary scarps, 3 m to 52 m in height, that offset post-glacial (~14,000 year) and younger deposits at base of the precipitous east side of the Teton Range (Figure 1). The Teton region is surrounded by zones of active seismicity including the historic scarp-forming 1959 M_S =7.5 Hebgen Lake, Montana, earthquake, and other zones of extensive Quaternary faulting. On the basis of fault segment lengths the Teton fault is considered a major seismogenic structure that has been assigned a maximum credible earthquake of M_S = 7.5. In addition, Quaternary deformation of the Teton fault

hanging-wall associated with prehistoric earthquakes on the fault appears to be expressed as asymmetric stratal tilt of the surface topography and Quaternary volcanic layers. We also note that the Teton fault coincides with one of the longest continuous zones of seismic quiescence within the Intermountain Seismic Belt. Information from our age-dating of the southern segment of the Teton fault suggests that it is overdue or "on schedule" for a major scarp-forming earthquake.

Results Obtained

Leveling Results:

The results of the three tectonic 1st-order surveys (Figure 1) in 1988, 1989, and 1991 have been discussed by Sylvester elsewhere in this volume and are only briefly summarized here. Arbitrarily fixing the west end, GT42, of the level line, the observed height changes (corrected for refraction errors by the National Geodetic Survey) between the 1988 and 1989 surveys indicate an anomalous 8 ± 0.7 mm of hanging wall uplift relative to the footwall block of the Teton normal fault (Sylvester and others, 1991). Comparison of the 1991 and 1988 surveys indicates this anomalous uplift persisted during the 1989-1991 two year interval, however, the maximum amplitude of the uplift decreased to 4 ± 0.7 mm (Figure 1a). The three surveys were conducted during a period of seismic quiesence at the M 3+ level, on the Teton fault, implying the observed deformation profiles are the result of aseismic or nontectonic mechanisms.

Comparison of the 1989 and 1991 survey results (Figure 1b) suggest subsidence of the hanging wall (the valley of Jackson Hole) was hinged at the Teton fault. The composite short wavelength-high amplitude, 5 km and 8 mm, component of the deformation signal centered around the Teton fault trace may be the result of near surface fault creep, or possibly differential subsidence of the hanging wall strata adjacent to the fault. However, the relatively long wavelength, 10 km, subsidence pattern of the hanging wall suggests large-scale aseismic creep may have occurred on the fault at depths up to 12 km.

Modeling Procedure:

In order to evaluate the nature of the observed 1989 to 1991 deformation profile, we have constructed a series of boundary element models followed the modeling procedure of King and others (1988) and King and Ellis (1991). The models invoke a stress-free elastic layer,

brittle layer, overrlying an inviscid fluid, plastic layer, where the elastic layer, region 1, is defined by two horizontal surfaces corresponding to a horizontal datum at the earth's surface, x_1=0 km, and a discrete lower boundary, x_1=12,15,18, or 20 km, representing the brittle-plastic transition. This elastic-layer is 'tethered' in the manner following King and Ellis (1991) where the horizontal displacement, u_3, and shear stress, σ_{13}, are set to zero along the vertical interface at x_3 = -60 km. Across the vertical boundary at x_3 = 48 km the shear and normal stresses, σ_{13} and σ_{33}, are set to zero. The block length is such that the boundary conditions at these boundaries do not affect the deformation imposed by faulting in the central portion of the block in the area of x_3 = 0 km.

A series of fault geometries, 30° to 75° E dips, and depths, 12 to 20 km, to the brittle-plastic transition were tested in the context of a simplified model of the footwall and hanging wall blocks determined from the ray-tracing and gravity modeling of the Teton fault and Jackson Hole. In each model run the fault -"ground surface" intersection, and hanging wall geometry were fixed. Variations in the fault dip and depth to the brittle-plastic transition resulted in changes in the vertical and horizontal stresses and displacement across the plane of the model. The variations in stress were discretized by dividing the hanging wall portion of the block model into a series of five vertical geometrically defined zones based on the hanging wall cut-off of the Tertiary strata at the fault, and the relationship of the deepest portion of the basin to the fault plane brittle-plastic transition intersection.

Modeling Results

The boundary element modeling results suggest the observed 1989 to 1991 height changes may be due to a combination of 3.5 cm and 5.0 cm of creep across a 60° E dipping planar normal fault zone at depths of 0.5 to 2 km, and 10 to 12 km, respectively (Figure 2a). The narrow wavelength and relatively large amplitude of the hanging wall subsidence adjacent to the fault restricts shallow slip to the upper 2 km. However, the average 4 mm subsidence of the hanging wall block at distances 10 km from the fault trace suggest this portion of the deformation signal is contributed by deep seated slip on the fault. Unfortunately, the short length of the level line relative to the wavelength of deformation associated with creep at depth on the fault it is very difficult to evaluate the possible contribution, or existence of this deeper seated signal.

Papers and Reports Published

Byrd, J.O.D. and R.B. Smith, 1991, Paleoseismicity, near-surface fault geometry, and segmentation of the Teton fault, Wyoming, (abs), Eos Trans. Amer. Geophys. Union, 72, 316.

Byrd, J. O. D., 1991, Paleoseismicity of the Southern Section of the Teton Fault, Wyoming, 1991 Abs. with Prog., 1991 Annual Meeting, Geol.Soc.Amer., 23, 5.

Meertens, C. M. and R. B. Smith, 1991, Crustal deformation of the Yellowstone caldera from first GPS measurements: 1987-1989, Geophys.. Res. Lett., 18, 1763-1766.

Sylvester, A.G., J.O.D. Byrd and R.B. Smith, 1991, Geodetic evidence for aseismic reverse creep across the Teton fault, Teton Range, Wyoming, Geop. Res.Lett, 18, 6, 1083-1086.

Smith, R. B. and W. J. Arabasz, 1991, Seismicity of the Intermountain Seismic Belt, in Seismicity of North America, editor E.R. Engdahl, Decade of North American Geology, Bull. Geol. Soc.Am. (in press).

Smith, R.B., J.O.D. Byrd, and D.D. Susong, 1993, Quaternary History, Neotectonics, and Earthquake Hazards of the Teton Fault, Wyoming, submitted to "The Geology of Wyoming", A. Snoke and J. Steidtmann *eds*, published by Wyoming Geological Association, in press.

Smith, R.B., K.L. Pierce, and R. J. Wold, 1993, Seismic Surveys and Quaternary History of Jackson Lake, Wyoming, submitted to "The Geology of Wyoming", A. Snoke and J. Steidtmann *eds*, published by Wyoming Geological Association, in press.

Figure 1A.

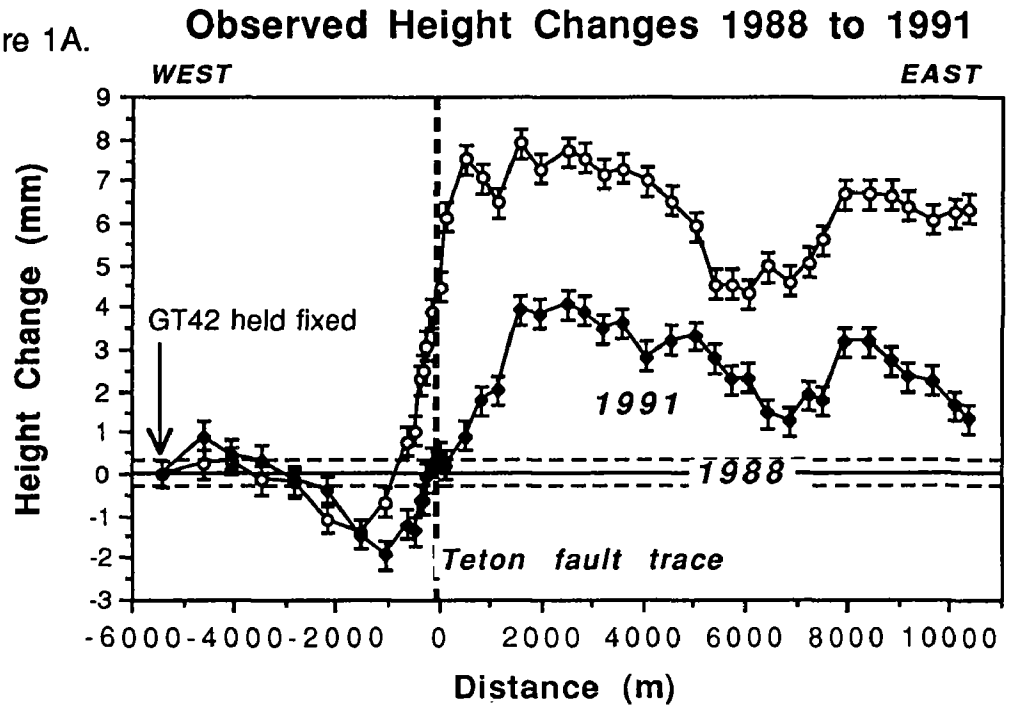

Figure 1B

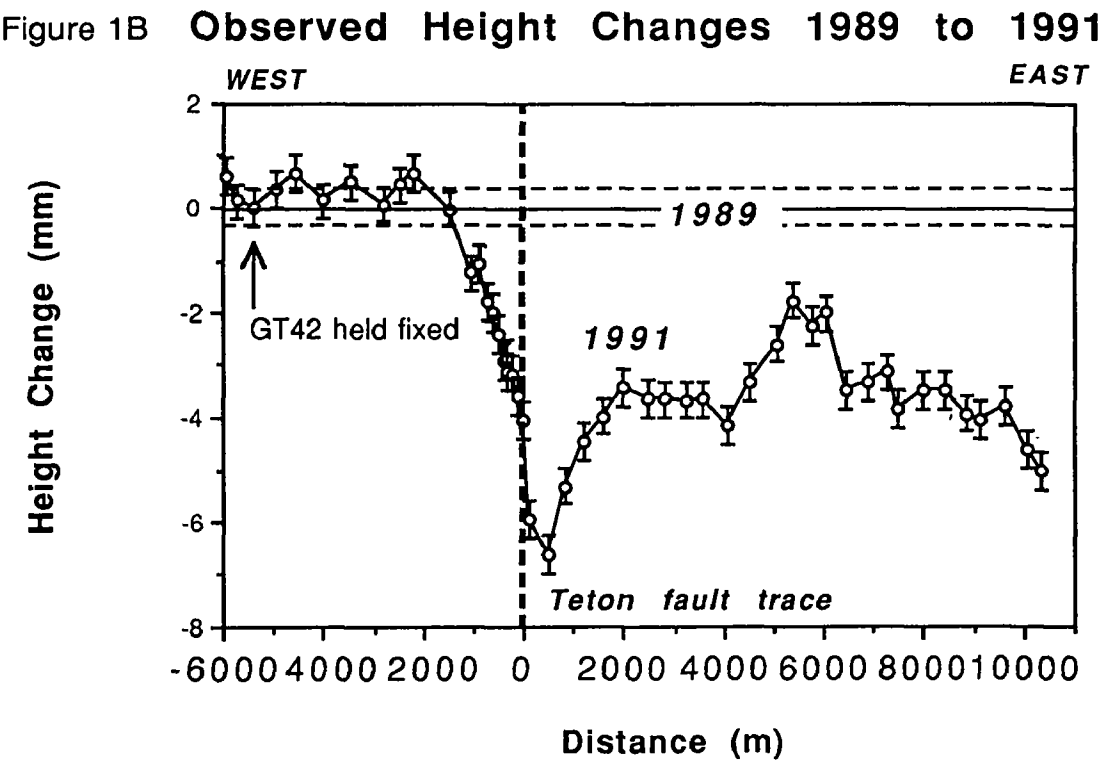

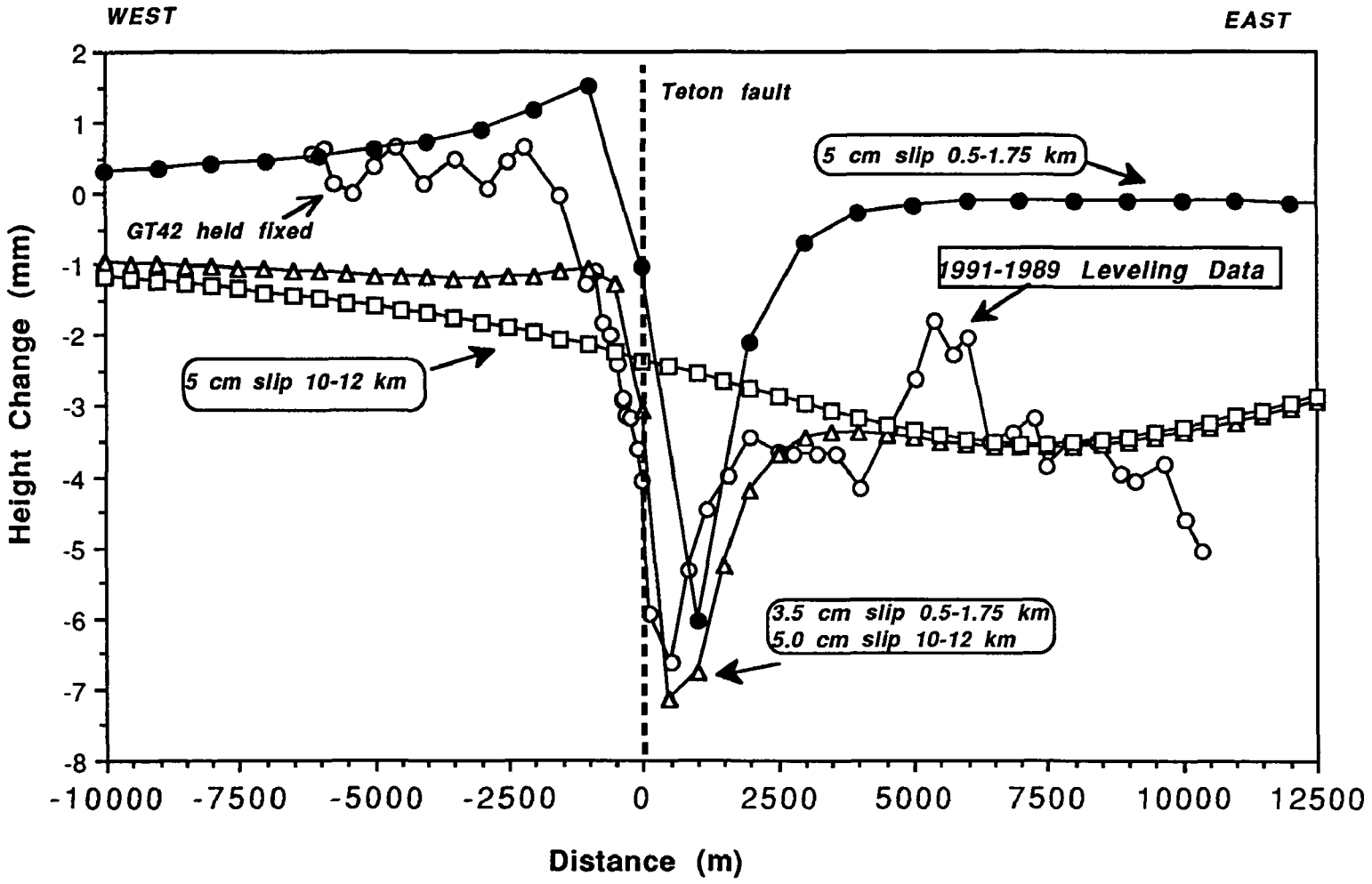
Surface Displacement 60° dip and 12 km bp
WEST
EAST
Teton fault
5 cm slip 0.5-1.75 km
GT42 held fixed
1991-1989 Leveling Data
5 cm slip 10-12 km
3.5 cm slip 0.5-1.75 km
5.0 cm slip 10-12 km
Height Change (mm)
Distance (m)
2
1
0
-1
-2
-3
-4
-5
-6
-7
-8
-10000
-7500
-5000
-2500
0
2500
5000
7500
10000
12500

Figure 2

SEISMIC REFRACTION/REFLECTION INVESTIGATIONS IN THE S. F. BAY AREA AND THE CENTRAL U. S.

Project Number: *1-9930-02102*
Investigator: *R. D. Catchings*
Institution: *U.S. Geological Survey, OEVE*
345 Middlefield Rd., MS 977
Menlo Park, CA 94025
FTS 459-4749; (415) 329-4749

Investigations Undertaken

In October and November of 1991, we acquired a 400-km-long seismic line between the cities of Memphis and St. Louis in order to look at long-range attenuation and strong ground motion in the Central U. S. These data are still being analyzed and are being compared with similar data from the Loma Prieta, CA area in order to estimate the effects of a M. 7.1 earthquake in the New Madrid region.

Investigations of strong ground motion and crustal structure of the San Francisco Bay area, as shown by active seismic experiments in May, 1991, continues . Specifically, we are examining the effect of crustal structure in influencing strong ground motion and attenuation during large earthquakes. In addition to the Loma Prieta earthquake, several other earthquakes are being examined, including the 1985 Mexico City earthquake.

Results Obtained

Data from the October/November 1991 Central U. S. experiment have been processed and plotted into seismic record sections. We have begun velocity analysis to determine the gross structure of the crust and the configuration of the Moho between Memphis and St. Louis. We have also calculated the ground motion from the shots to examine areas with unusually high amplitude variations. Those data have been directly compared with the type of data from the Loma Prieta area. We find that the ground motion resulting from a shot located near New Madrid, Missouri produces very strong amplitude seismic waves near the cities of Memphis and St. Louis. These amplitudes are significantly higher than those observed for shots in the Loma Prieta area. Thus, our data suggest that the cities of Memphis and St. Louis should should expect much more severe shaking from a M 7.1 New Madrid earthquake than San Francisco experienced during the 1989 Loma Prieta earthquake.

From the May 1991 San Francisco Bay area experiment, we have found very strong evidence that much of the damage from the 1989 Loma Prieta earthquake resulted from reflected energy from crustal interfaces and the Moho. The correlation between the geographical areas with high amplitudes from our seismic survey and those areas that experienced significant damage during the 1989 earthquake is striking. We have also correlated the wave propagation paths from the 1985 Mexico City earthquake and found strong evidence that reflected seismic energy was a major factor in the loss of 8000

lives and 4 billion dollars damage. A similar crustal configuration exists in the Pacific Northwest U. S., with implications for the safety of a large complex of Nuclear facilities.

Reports Published

(1) Catchings, R. D. and W. M. Kohler, (in press), Reflected Seismic Waves Damage Far from Earthquake Epicenters: An Example from the 1989 Loma Prieta Earthquake (in review, submitted to Science)

(2) W. M. Kohler, R. D. Catchings, and G. S. Fuis, (in press), Crustal Structure of the San Francisco Peninsula, (in review, submitted to*Bull. Seis. Soc. Am.*

(3) R. D. Catchings and W. D. Mooney, New Madrid and Central California Apparent Q from Seismic Refraction Data, *Seis. Res. Lett.*, **63**, 49 (1992)

(4) R. D. Catchings, W. M. Kohler, and G. S. Fuis, Influence of Crustal Structure on the 1989 Loma Prieta Earthquake and Associated Destruction, EOS Trans AGU, 1991

(5-7) Three abstracts in the 1992 AGU EOS. Several Abstracts to Eastern Meetings.

INSTRUMENTATION OF STRUCTURES

9910-04099

MEHMET ÇELEBI
BRANCH OF ENGINEERING SEISMOLOGY AND GEOLOGY
U.S. GEOLOGICAL SURVEY
345 MIDDLEFIELD ROAD, MS 977
MENLO PARK, CALIFORNIA 94025
415/329-5623

Investigations

1. The process of selection of structures to recommended for strong-motion instrumentation has continued in Hawaii, Puget Sound (Seattle), Reno (Nevada), and Puerto Rico.

2. The Veterans Hospital in Palo Alto, California, has been instrumented as a joint effort between VA and USGS.

3. Instrumentation at 575 Market Street, in San Francisco, California, has also been upgraded.

4. Agreements have been made with UCLA to convert the wind-monitoring system in the Theme Building in Los Angeles (previously financed by NSF) into a strong-motion monitoring system. Plans are being made to implement the conversion, whenever funds are available.

5. Studies of records obtained from instrumented structures are carried out. In particular, the records obtained during the October 21, 1987 Whittier Narrows earthquake from 1100 Wilshire Finance Building (Los Angeles), the Bechtel Building (Norwalk), and the Santa Ana River Bridge (base-isolated) are being investigated.

6. Studies of records obtained from instrumented structures during the October 17, 1989, Loma Prieta earthquake are carried out. In particular, Transamerica Building in San Francisco and Pacific Park Plaza in Emeryville have been investigated. Data from Embarcadero Building (San Francisco) has been studied. Papers are prepared.

7. Cooperative project with NIST on low-level amplitude tests of instrumented structures carried out and report and papers are prepared.

8. The instrumentation of building in Seattle completed.

9. Cooperative instrumentation of building in Olympia, Washington, in progress.

Results

1. The Hawaii Committee on strong-motion instrumentation of structures has completed its deliberations and a draft report is being prepared.

2. As final report of the Puget Sound (Seattle) advisory committee for strong-motion instrumentation has been completed.

3. Papers resulting from study of records obtained from structures are prepared.

4. Invited talks given at conferences and/or other gatherings.

Reports

Çelebi, M., and Şafak, E., 1991, Recorded seismic response of Pacific Park Plaza—Part I: Data and preliminary analysis: ASCE, July 1992.

Şafak, E., and Çelebi, M., 1991, Recorded seismic response of Pacific park Plaza—Part II: System identification: ASCE, June 1992.

Çelebi, M., Phan, L.T., and Marshall, R.D., 1992 Dynamic characteristics of five buildings determined from their response to the 10/17/1989 Loma Prieta (California) earthquake and low-level amplitude tests: in review, ASCE, 1992.

Çelebi, M., 1992, Coherency of free-field motions near a structure—a case study: (invited paper) ASCE Structures Congress, San Antonio, Texas, April, 1992.

Marshall, R.D., Phan, L.T., and Çelebi, M., 1990, Measurement of structural response characteristics of full-scale buildings: comparison of results from strong-motion and ambient vibration records: USGS Open-File Report 90-667 (also NISTIR 4884).

Çelebi, M., Lysmer, J., and Luco, E., 1992, Recommendations for a soil-structure interaction experiment: USGS Open-File Report 92-295, April 1992.

Çelebi, M., 1992, Earthquake response of an eccentrically braced tall building: Accepted by ASCE, Journal of Structural Division.

A Collaborative Research: Analysis of PANDA Data and Continuation of PANDA Experiment in the Central New Madrid Seismic Zone

#14-08-0001-G2143

Jer-Ming Chiu and Arch C. Johnston
Memphis State University
Center for Earthquake Research and Information
Memphis, TN 38152
901-678-2007

Robert B. Herrmann
Department of Earth and Atmospheric Sciences
Saint Louis University
3507 Laclede
St. Louis, MO 63103
314-658-3131

Investigations

Field work of the PANDA experiment in the central New Madrid seismic zone has been completed by the end of August 1992. More than 850 earthquakes with magnitude ranging from -2.0 to 4.6 were on-scale recorded by PANDA during the three years of field work. Prelminary analyses of portions of three-component high-resolution PANDA data have already produced significant new results that are impossible from any previous experiment in the region.

Results

Principal results obtained from preliminary analysis of PANDA data during field work period include:

(a) the identification of P to S and S to P converted waves from the bottom of the sedimentary basin from all three-component seismograms which enable a reliable imaging of 3-dimensional geometry of the sedimentary basin in the upper Mississippi basin.

(b) results of layered crustal structure inversion support a low velocity zone with Vp=4.83 km/sec at depth 2.5 to 5 km. Vp/Vs ratio inside this low velocity zone as determined from independent Vp and Vs inversion is 1.51 which may be due to the presence of fluid- or vapor-filled cracks and/or pores, probably under elevated pore fluid pressures. A large amplitude downward motion arrivals can be identified from the USGS explosions which provide a direct evidence of the existence of a low velocity zone at this depth.

(c) well-determined crustal velocity model for both P and S waves and unambiguous identifications of both P and S arrivals from all PANDA three-component seismograms allow reliable determination of earthquake hypocenters. The new data provides, for the first time, a clear 3-dimensional image of the active fault zones in the NMSZ (Figure 1). Our preliminary results corroborate the vertical (strike-slip) faulting of the southwest (axial), north-northeast, and western arms of the NMSZ and define two new dipping planes in the central NMSZ. The seismicity of the left-step zone between the NE-trending vertical segments is concentrated about a plane that dips at $\sim 31°$ SW; a separate zone to the SE of the axial zone defines a plane that dips at $\sim 48°$ SW. When these dipping planes are projected up dip, they intersect the surface along the eastern boundary of the Lake County Uplift (LCU) and the western portion of Reelfoot Lake. If these SW-dipping planes are thrust faults, then the LCU would be on the upthrown hanging wall and Reelfoot on the downthrown footwall.

(d) spectrum differences between the direct S and the converted P waves from the bottom of the sedimentary basin allow the determination of attenuation characteristics of seismic waves inside the sedimentary basin. These parameters (Vp, Vs, Qp, and Qs) will allow a reliable estimation of seismic response of the basin and what maximum

ground motion should be expected on the surface from active fault zones of known geometry beneath the sediments.

Papers Published and/or in Press

Imaging the active faults of the central New Madrid seismic zone using PANDA array data, in press (December 1992 issue), *Seismol. Res. Lett.*, J.M. Chiu, A.C. Johnston, and Y.T. Yang.

Papers in Review

Shear-wave splitting from microearthquakes in the New Madrid seismic zone, in press to be published in a special issue of Crustal Anisotropy, *Can. J. Expl. Geophys.*, H. Rowlands, D.C. Booth, and J.M. Chiu.

Crustal velocity structure studies in the New Madrid seismic zone from USGS explosion data recorded by the PANDA seismic array, submitted December 1992 to *Seismol. Res. Lett.*, Z.S. Liaw, J.M. Chiu, and A.C. Johnston.

Crustal velocity structures in the central New Madrid seismic zone using velocity inversion method and data collected by the PANDA array, submitted December 1992 to *Seismol. Res. Lett.*, Y.T. Yang, J.M. Chiu, and A.C. Johnston.

3-dimensional configuration of the sedimentary basin in the upper Mississippi embayment using S-to-P conversions, submitted December 1992 to *Bull. Seismol. Soc. AM.*, K.C. Chen, J.M. Chiu and A.C. Johnston.

$Q_p - Q_s$ relations in the sedimentary basin of the upper Mississippi embayment from the spectra ratio between the direct and the converted waves, submitted December 1992 to *Bull. Seismol. Soc. Am.*, K.C. Chen, J.M. Chiu, and A.C. Johnston.

3-dimensional color graphics presentation of the active fault zones in the New Madrid seismic zone, submitted December 1992 to *Nature*, J.M. Chiu, Y.T. Yang, and A.C. Johnston.

Abstracts

A high resolution PANDA experiment in the central New Madrid seismic zone, presented in the annual meeting of ESSA, Oct. 1990, J.M. Chiu, K.C. Chen, Y.T. Yang, S.C. Chiu, A.C. Johnston, and the PANDA Group.

The PANDA II - a PC-based seismic array, presented in the annual meeting of ESSA, Oct. 1990, J.M. Chiu, G.C. Steiner, R. Smalley, A.C. Johnston, and the PANDA Group.

The Cape Giradeau earthquake and its aftershock, presented in the annual meeting of ESSA, Oct. 1990, J.M. Chiu, A.C. Johnston, and the PANDA Group.

The CERI seismic networks in the New Madrid and the southern Appalachians, presented in the annual meeting of ESSA, Oct. 1990, A.C. Johnston, and J.M. Chiu.

A high resolution PANDA experiment in the central New Madrid seismic zone, presented in the annual meeting of GSA, Oct. 1990, J.M. Chiu, K.C. Chen, Y.T. Yang, S.C. Chiu, A.C. Johnston, and the PANDA Group.

A high resolution PANDA experiment in the central New Madrid seismic zone, *EOS*, Vol. 71, No. 43, 1435, presented in the Fall AGU, Dec. 1990, J.M. Chiu, K.C. Chen, Y.T. Yang, S.C. Chiu, A.C. Johnston, and the PANDA Group.

A gain-ranging and PC-based seismic array: PANDA II, presented in the annual SSA meeting, March 1991, *Seismol. Res. Let.*, 62(1), p. 22, J.M. Chiu, G.C. Steiner, R. Smalley, A.C. Johnston, and the PANDA Group.

The cooperative New Madrid seismic network - implementation of regional network nodes, presented in the annual SSA meeting, March 1991, *Seismol. Res. Let.*, 62(1), p. 33, E.J. Haug, R.B. Herrmann, and J.M. Chiu.

Fault zone geometry and crustal velocity structures in the central New Madrid seismic zone using the PANDA data, presented in the Spring AGU, May 1991, *EOS*, 72(17), p. 264, Y.T. Yang, J.M. Chiu, Z.S. Liaw, K.C. Chen, S.C. Chiu, A.C. Johnston, and the PANDA group.

Three-dimensional geometry of the sedimentary basin and its tectonic implications in the upper Mississippi embayment: results from the PANDA experiment, presented in the Spring AGU, May 1991, *EOS*, 72(17), p. 264, K.C. Chen, J.M. Chiu, Y.T. Yang, S.C. Chiu, A.C. Johnston, and the PANDA group.

3-dimensional fault zone geometry and sedimentary basin basin configuration in the central New Madrid seismic zone: determined from PANDA array data, presented in the annual ESSA meeting, Oct. 1991, J.M. Chiu, Y.T. Yang, K.C. Chen, Z.S. Liaw, S.C. Chiu, A.C. Johnston, and the PANDA group.

Determination of Q_p-Q_s relations in the sedimentary basin in the upper Mississippi embayment using converted phases, presented in the annual ESSA meeting, Oct. 1991, K.C. Chen, J.M. Chiu, Y.T. Yang, S.C. Chiu, A.C. Johnston, and the PANDA group.

Progress in implementing the cooperative New Madrid seismic network, presented in the annual ESSA meeting, Oct. 1991, R.B. Herrmann, E.J. Haug, A.C. Johnston, and J.M. Chiu.

The Risco, Missouri earthquake, May 4, 1991, presented in the annual ESSA meeting, Oct. 1991, S.C. Chiu, H. Hwang, J.M. Chiu, and A.C. Johnston.

3-Dimensional fault zone geometry and sedimentary basin configuration in the central New Madrid seismic zone determined from PANDA data, presented in the Fall AGU, Dec. 1991, *EOS*, 72(44), p. 429, J.M. Chiu, Y.T. Yang, K.C. Chen, Z.S. Liaw, S.C. Chiu, A.C. Johnston, and the PANDA group.

Seismological studies in the New Madrid seismic zone using the PANDA seismic array, presented in the Annual SSA meeting, April 1992, *Seismol. Res. Lett.*, 63(1), 49, J.M. Chiu, A.C. Johnston, Y.T. Yang, K.C. Chen, Z.S. Liaw, S.C. Chiu, J. Bollwerk, D. Reinbold, R.B. Herrmann, and the PANDA group.

3-D sedimentary basin configuration and seismic wave attenuation inside the sedimentary basin in the New Madrid seismic zone, presented in the Western Pacific Geophysical Meeting, August, 1992, *EOS*, 73(25), 50, K.C. Chen, J.M. Chiu, Y.T. Yang, S.C. Chiu, A.C. Johnston, and the PANDA group.

PANDA II and PANDA III seismic arrays and their applications in modern seismological observations, presented in the Western Pacific Geophysical Meeting, August, 1992, *EOS*, 73(25), 57, J.M. Chiu, G. Steiner, D. Xu, and D. Smith.

Imaging of fault zone geometry in the central New Madrid seismic zone using PANDA data, presented in the annual Eastern Seismological Society Meeting, Richmond, October, 1992, Y.T. Yang, J.M. Chiu, and A.C. Johnston

Crustal velocity studies in the New Madrid seismic zone from USGS explosions recorded by the PANDA seismic array, presented in the annual Eastern Seismological Society Meeting, Richmond, October, 1992, Z.S. Liaw, J.M. Chiu, and A.C. Johnston.

Three-dimensional color graphics presentation of the active fault zones in the New Madrid seismic zone, presented in the annual Eastern Seismological Society Meeting, Richmond, October, 1992, J.M. Chiu, A.C. Johnston, and Y.T. Yang.

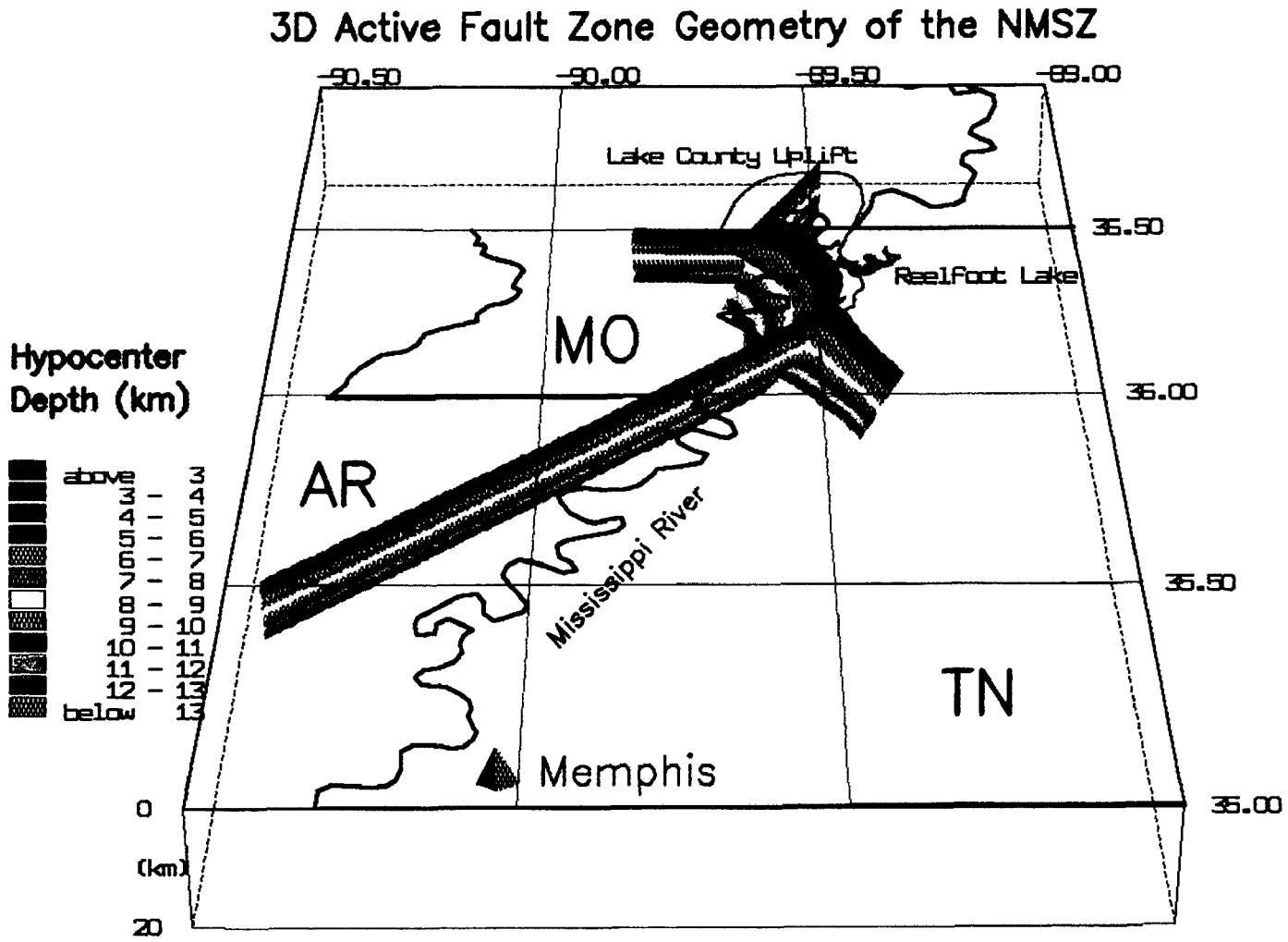

Figure 1. 3-dimensional configurations of the active fault zones in the New Madrid seismic zone showing the vertically dipping SW, NE, and NW segments and the gently southwest dipping central segment. Up-dip projection of the southwest dipping central segment will intersect with the surface between the Lake County Uplift and Reelfoot Lake. Relationships between these surface features and the underneath active zones are discussed in Chiu et al., (1992).

LATE QUATERNARY SLIP RATES ON ACTIVE FAULTS OF CALIFORNIA

9910-03554

MALCOLM M. CLARK
BRANCH OF ENGINEERING SEISMOLOGY AND GEOLOGY
345 MIDDLEFIELD ROAD, MS 977
MENLO PARK, CALIFORNIA 94025-3591
415/329-5624 FAX 415/329-5163

Investigations

1. Recently active traces of the Calaveras fault zone at Tres Pinos and San Felipe Creeks, California (K.J.Kendrick, J.W. Harden, M.M. Clark).

2. Recently active traces of Owens Valley fault zone, California (Sarah Beanland (NZGS), Clark).

3. Degradation of fluvial terrace risers along Lone Pine Creek, San Bernardino County (Kendrick, in conjunction with J.B.J. Harrison, L.D. McFadden (UNM), and R.J. Weldon (University of Oregon)).

4. Revision of slip-rate table and map of late Quaternary faults of California (Clark, Kendrick, J.J. Lienkaemper, K.R. Lajoie, C.S. Prentice, M.J. Rymer, D.P. Schwartz, R.V. Sharp, J.D. Sims, J.C. Tinsley, R.J. Weldon).

5. Late Quaternary evolution of the San Timoteo Badlands region, southern California (Kendrick, in conjunction with D.M. Morton and L.D. McFadden).

6. Post-earthquake investigations:
   a. Mono basin earthquake of 23 Oct 90 (Clark)
   b. Landers earthquake of 28 Jun 92 (Clark and Kendrick)

Results

2. Owens Valley fault zone. See v. 33, p. 202-3 of this publication for results summarized from our report, USGS Bulletin 1982, *in press,* listed below. This Bulletin features a 1 :24,000-scale strip map of the Owens Valley fault zone, a table of characteristics and measurements of active traces at 40 sites along the fault zone from Owens Lake to north of Big Pine, and text.

5. The degree of soil development associated with geomorphic surfaces in San Timoteo and Reche Canyons near the San Jacinto fault in the San Timoteo Badlands is comparable to that of nearby, dated soils and allows correlation of the surfaces. Twenty soil profiles have been described and sampled, including four surface soils and two buried soils associated with surfaces in San Timoteo Canyon (Q1-Q4), and

to surface soil associated with two surfaces in Reche Canyon (Q2, Q3). Soil development indices, based on field descriptions as well as laboratory analysis, provide a basis for comparison of these soils to each other and to dated soil chronosequences at Cajon Pass, Merced, and Anza.

The soils in the San Timoteo Badlands region record a complex tectonic and climatic history. Evidence includes buried soils, tilting and warping of both buried and surface soils, calcium carbonate coatings on manganese oxide and clay films, and the presence of silica cementation of soils in Reche Canyon, but not in the adjacent San Timoteo Canyon. The San Timoteo Badlands include preserved surfaces intermediate in soil development to those at Cajon Pass, and do not preserve a record of the major late Pleistocene to early Holocene aggradational event observed elsewhere in the region. In spite of the variability of the surfaces in this study area, soil development is similar to that of soils at other sites. With time the profiles develop progressively thicker argillic horizons, and increase in soil rubification, total mass of clay and crystalline iron oxides, and content and thicknesses of clay films.

The composition and content of iron species in soils of the San Timoteo study area is similar as in nearby sites, including the Cajon Pass chronosequence, Little Tujunga Canyon, Arroyo Seco Canyon, San Gabriel River, Day Canyon, Duncan Canyon, and the San Gorgonio Wash. With increasing soil age, there is an increase in the ratio of dithionite-extractable iron to total iron, a decrease in the ratio of ferrous to ferric iron, and a decrease in the ratio of oxalate- to dithionite-extractable iron, though all these trends are more subdued in the San Timoteo study area than elsewhere in the region. These patterns suggest that the slightly higher temperature and lower precipitation of the San Timoteo Badlands region may be responsible for both a slower rate of transformation of ferrihydrate to hematite and a shift in the maximum content of oxalate-extractable iron towards older soils.

Weighted means of soil development indices and rubification index values are used to compare the soils of this study to those at Cajon Pass, Merced, and Anza. Wide-range age estimates are determined using the maximum limits of these values, and result in 27.5-305 ka for Q1, 67-570 ka for Q2, and 305-700 ka for Q3 and Q4. Best estimates of age are determined by directly correlating soils with the same degree of soil development between this study and the closest chronosequence, Cajon Pass. This method constrains the time of formation of the Q1 surface to between 27.5-67 ka and the Q2 surface to 43-67 ka, and does not change the age estimates of the older surfaces.

Distinctive clast assemblages, identified by Morton and Matti (in press) are present along a limited section of the NE side of the San Jacinto fault, and are preserved on two surfaces within Reche Canyon, on the SW side of the fault. Subsequent displacement along the fault has resulted in offsets of approximately 1 and 4 km (Morton and Matti, in press). Age estimates based on comparisons of soil development allow us to better constrain these offsets, with resulting slip rates of 7-13 mm/yr since the formation of Q3, and 13-26 mm/yr since the formation of Q2.

6a. Mono Basin earthquake of 23 Oct 90. See K.R. Lajoie's results in v. 33, p. 381-2 of this publication.

6b. Landers earthquake of 28 Jun 92. We helped organize the post-earthquake geologic investigation and obtain existing and new aerial photos, and we contributed to the early mapping of surface ruptures.

Reports

Beanland, Sarah, and Clark, M.M., The Owens Valley fault zone, eastern California, and surface rupture associated with the 1872 earthquake: U.S. Geological Survey Bulletin 1982, *in press.*

Harrison, J.B.J., Kendrick, K.J., Weldon, R.J., and McFadden, L.D., 1992, Spatial and temporal variation in terrace scarp catinas in the Transverse Ranges, southern California: Catina, *in press.*

Kendrick, K.J., Harrison, J.B.J., McFadden, L.D., and Weldon, R.J., 1992, An evaluation of a non-linear diffusion equation as a model for determining the rate of scarp degradation in Cajon Pass, southern California (abs.); in Mörner, N.A., Owen, L.A., Stewart, I., and Vita-Finzi, C., eds., Neotectonics—recent advances: Abstracts vol., Quaternary Research Association, Cambridge.

Lajoie, K.R., Clark M.M., Hill, D.P., Lindh, A.G., Oppenheimer, D.H., and Yount, J.C., 1991, Mono Basin earthquake of October 23, 1990: U.S. Geological Survey administrative report.

Staff, USGS and CDMG, 1992, Pattern of surface ruptures associated with the June 28, 1992, Landers earthquake (abs.): EOS Trans. AGU, v. 73, no. 43, Fall Meeting Suppl., page 357-8.

INVESTIGATION OF PEAT STRATIGRAPHY IN ESTUARINE FLATS NEAR ANCHORAGE, ALASKA, AS A MEANS OF DETERMINING RECURRENCE INTERVALS OF MAJOR EARTHQUAKES

14-08-0001-G1949

Rodney A. Combellick and Richard D. Reger
Alaska Division of Geological & Geophysical Surveys
794 University Ave., Suite 200
Fairbanks, Alaska 99709
(907) 474-7147

Investigations

The goal of this project is to investigate the subsurface stratigraphy and sedimentology of estuarine deposits along the eastern shore of Cook Inlet (fig. 1) to obtain a record of subsidence events associated with major earthquakes. The results of this study, together with results of similar studies in the Prince William Sound, Copper River delta, and Middleton Island areas, are helping to develop estimates of the recurrence frequency of coseismic vertical tectonic displacements during the late Holocene.

Borehole drilling along Turnagain and Knik Arms in upper Cook Inlet during 1985-1989 revealed multiple submerged peat layers, possibly associated with six to eight coseismic subsidence events during the past 4,700 calendar years (Combellick, 1991b). In the current program, we have extended regional data coverage by drilling additional boreholes and examining tidal-channel exposures in estuaries of Fox River (Kachemak Bay), Kasilof River, Kenai River, and Chickaloon Bay. We also reexamined exposures at Girdwood and Goose Bay that have become more visible because of tidal erosion.

During 1991, we drilled nine hollow-stem boreholes and eight hand-auger holes at Fox River flats, four boreholes at Kenai River flats, and two boreholes at Kasilof River flats. Additionally, we examined extensive river-bank exposures at Kenai and Kasilof River Flats and tidal-bank exposures at Girdwood. We prepared and submitted 54 peat, wood, and organic silt samples for radiocarbon dating, and completed grain-size analyses of 83 samples to assist in interpreting depositional environment. During 1992, we examined tidal-channel exposures at Chickaloon Bay, Girdwood, and Goose Bay, and submitted an additional 17 organic samples for radiocarbon dating.

Results

A borehole at Portage, near the area of maximum 1964 subsidence, revealed the largest number of buried peat layers among all boreholes and exposures observed in this study. If all six peat layers at this site were buried as a result of pre-1964 coseismic subsidence, they imply an average recurrence interval of about 800 yr during the late Holocene. This value may underestimate the recurrence interval if some peats were

buried as a result of nonseismic processes and may overestimate the interval if some large subduction earthquakes did not result in peat burial at this site.

A buried peat layer indicating regional submergence between about 700 and 900 yr ago is present at Girdwood, Portage, Palmer Hay Flats, Goose Bay, and Chickaloon Bay. At Girdwood, this layer includes rooted stumps of trees that were probably killed by salt-water influx in the same manner as modern trees at Girdwood and Portage were killed as a result of the 1964 great earthquake. Evidence for coseismic uplift during the same period is present at Copper River Delta and at Cape Suckling. Although we cannot prove that submergence at all of these sites was coeval, the data strongly suggest that the most recent great earthquake prior to 1964 was about 700-900 yr ago.

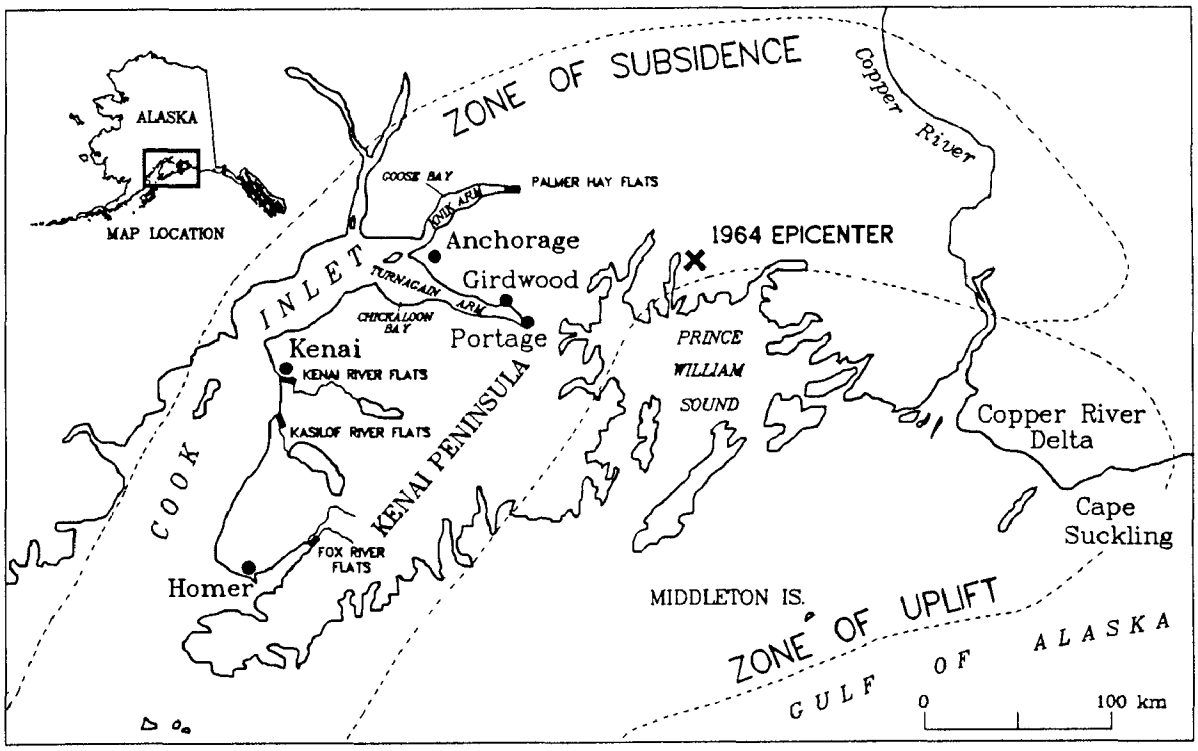

Figure 1. Study region in southcentral Alaska, showing zones of uplift and subsidence during the 1964 great earthquake.

Other than the postulated 700-900-yr event, the regional radiocarbon data set does not provide precise ages of all paleoseismic events. Uncertainty in age correlations among sites results from large standard deviations, some stratigraphic discordances and lateral inconsistencies, and the possibility that some ages may represent nonseismic events or local earthquakes (Combellick, 1991b; Bartsch-Winkler and Schmoll, 1992). However, if the data set is reduced to calibrated radiocarbon ages that appear coeval in two or more marshes, they cluster roughly into six to eight age groups during the past 5,000 yr, implying an average recurrence interval of about 600-800 yr (Combellick, 1992b).

A freshly eroded tidal-bank exposure near Girdwood corroborates previous radiocarbon data and reveals an extensive but formerly unrecognized peat layer with a radiocarbon age of 1,380±60 yr B.P. This layer may represent coseismic submergence that

is coeval with uplift dated at 1,350±200 yr B.P. at Middleton Island (Plafker and Rubin, 1967). Tidal-bank exposures at Goose Bay and Chickaloon Bay show as many as three submerged peat layers that pre-date the 1964 event, including the most recent regional event 700-900 yr ago. At Goose Bay and Palmer Hay Flats, there is evidence of a possible local event about 400-600 yr ago, perhaps an earthquake on the Castle Mountain fault, about 20 km north.

At Fox River flats, 17 boreholes and several shallow exposed sections failed to reveal any buried peat layers like those observed in upper Cook Inlet. The estuarine sediments are sandier, indicating that deposition may be dominated by the fluvial system of Fox River and Sheep Creek and that their deltas may be prograding over and reworking the tidal flat. The ages of some organic-rich horizons agree with ages of buried peats elsewhere, but we are reluctant to conclude that they are related to coseismic subsidence. Other ages are anomalously old (5-7 ka) for their shallow depth (less than 2 m) and we suspect that they may be contaminated by detrital coal, which is abundant in exposures of Tertiary rocks in the drainage basin.

At Kenai and Kasilof River flats, which are near the arcward limit of 1964 deformation, a thick (2 m), near-surface peat sequence spanning the late Holocene from about 1,000 to 7,000 yr B.P. is largely devoid of interseismic mud layers, indicating minimal coseismic subsidence in this area. Radiocarbon ages of several samples at the interface between the top of this thick peat and overlying intertidal mud indicate probable submergence about 1,300 yr B.P. (uncalibrated), which may correspond to similarly dated submergence at Girdwood and uplift at Middleton Island. The 700-900-yr-B.P. event is not represented by a buried peat layer in intertidal sections that we observed at Kenai or Kasilof. Vertical variations in vegetation type within the thick peat include alternations between forest and brackish marsh that may reflect responses to small coseismic vertical changes, but these cannot be accurately dated. The long-term relative stability of the Kenai-Kasilof area (near the zero isobase of 1964 subsidence) and repeated large subsidence at Portage (near the area of maximum 1964 subsidence) imply that coseismic deformation during late-Holocene events was generally similar to deformation during the 1964 earthquake (Combellick, 1992b).

Project Reports

Combellick, R.A., 1986, Chronology of late-Holocene earthquakes in southcentral Alaska: Evidence from buried organic soils in upper Turnagain Arm [abs.]: Geological Society of America Abstract with Programs, V. 18, no. 6, p. 569.

Combellick, R.A., 1990, Evidence for episodic late-holocene subsidence in estuarine deposits near Anchorage, Alaska: Basis for determining recurrence intervals of major earthquakes: Alaska Division of Geological & Geophysical Surveys Public-Data File 90-29, 67 p.

Combellick, R.A., 1991a, Paleoseismicity of the upper Cook Inlet region, Alaska, as recorded by peat stratigraphy in nine tidal-flat boreholes [abs.]: Geological Society of America Abstracts with Programs, v. 23, no. 2, p. 15.

Combellick, R.A., 1991b, Paleoseismicity of the upper Cook Inlet region, Alaska: Evidence from peat stratigraphy in Turnagain and Knik Arms: Alaska Division of Geological & Geophysical Surveys Professional Report 112, 52 p.

Combellick, R.A., in press, The penultimate great earthquake in southcentral Alaska: Evidence from a buried forest near Girdwood, *in* Solie, D.N., ed., Short Notes on Alaskan Geology, 1992: Alaska Division of Geological & Geophysical Surveys Professional Report.

Combellick, R.A., 1992a, Paleoseismicity of the upper Cook Inlet region, Alaska [abs.]: Geologic Reason--A Basis for Decisions Affecting Society, Symposium and Annual Meeting, Lake Tahoe, NV, Sept. 27-30, 1992, American Institute of Professional Geologists, p.18.

Combellick, R.A., 1992b, Coseismic and long-term tectonic subsidence in the Cook Inlet region, Alaska [abs.]: EOS, in press (abstracts of the December 1992 annual meeting).

Other Reference Cited

Bartsch-Winkler, Susan, and Schmoll, H.R., 1992, Utility of radiocarbon-dated stratigraphy in determining late Holocene earthquake recurrence intervals, upper Cook Inlet region, Alaska: Geological Society of America Bulletin, v. 104, no. 6, p. 684-694.

Plafker, George, and Rubin, Meyer, 1967, Vertical tectonic displacements in south-central Alaska during and prior to the great 1964 earthquake: Journal of Geosciences, Osaka City University, v. 10, no. 3, p. 53-66.

TECTONICS OF SEISMIC SOURCE ZONES, CENTRAL INTERIOR OF THE UNITED STATES

9950-04542

ANTHONY J. CRONE
Branch of Geologic Risk Assessment
U.S. Geological Survey
Box 25046, MS 966,
Denver, Colorado 80225
(303) 236-1595

PURPOSE OF PROJECT

This multidisciplinary project involves studies that provide basic geologic and geophysical information on the distribution, characteristics, and frequency of large earthquakes in the central interior of the United States and contribute to a better understanding of the structural features that might produce large, potentially damaging intraplate earthquakes. Individuals that contributed to this report include Donley S. Collins, Anthony J. Crone, Richard L. Dart, Sharon F. Diehl, William L. Ellis, Meridee Jones-Cecil, Donald T. Rodbell, and Henri S. Swolfs.

INVESTIGATIONS

Subsurface Stratigraphy and Structure—New Madrid Seismic Zone (NMSZ)

D.S. Collins completed an analysis of the insoluble residues from cuttings of the Strake Petroleum #1 Russell drill hole and the lithologies in the Killan #1 Pattinson drill hole, both in Pemiscot Co. Mo. These studies helps define the stratigraphy, depositional history, and tectonic framework of the Lower Paleozoic rocks in southeastern Missouri. This stratigraphic information combined with similar data from other deep drill holes in the New Madrid region aids in clarifying structural relations by improving correlations of Lower Paleozoic rocks in the Reelfoot rift. A report describing these relations is nearly complete.

A.J. Crone completed his initial analyses of about 135 km of industry Vibroseis seismic-reflection data across the Crittenden County fault zone in northeastern Arkansas and finalized a manuscript describing the results of this study for publication in *Seismological Research Letters*. (See also related investigations listed below.)

R.L. Dart has completed a series of subsurface structure-contour, isopach, and geologic subcrop maps and companion stratigraphic cross sections of the upper Mississippi embayment region. This work will be published as a Miscellaneous Field Studies Map. The process of updating the subsurface geologic database from which these maps and cross section were generated has been completed and a revised version of the drill-hole catalog has been prepared for publication as a USGS Open-File Report. The database has been converted to a GIS ARC/INFO data format, which provides the opportunity to merge and plot these data with other GIS databases.

Dart also made inquiries to the National Geodetic Survey (NGS) regarding the location and availability of recent geodetic data in the New Madrid region. He also requested information about the necessity and methods of applying various standard corrections to older leveling data.

S.F. Diehl continued her analyses of authigenic minerals and microstructural fabric of rocks in the Reelfoot rift and adjacent terrains. These studies revealed petrographic evidence of deformational and fluid-migration events in the rift that help characterize the rift's complex structural history. Specific investigations include petrographic studies of drill-hole samples from the USGS-New Madrid Test well in Pemiscot Co., Mo., and the Dow Chemical #1 Garrigan drill hole in Mississippi Co., Ark., and of lamprophyres from the Dow Chemical #1 Wilson drill hole in Mississippi Co., Ark.

In collaboration with C.K. Throckmorton, (Br. Central Regional Geology), and C.W. Clendenin (private consultant and former quarry employee), S.F. Diehl mapped the English Hill fault that is exposed in the Grays Point Quarry, near Scott City, southeastern Mo., and sampled the fractured Paleozoic rocks adjacent to the fault. The mapping determined the attitude of bedrock fractures and the relation of the fractures to the fault. These studies are part of an effort to clarify the relations between diagenetic events and periods of tectonic movement.

Diehl also completed revisions of two manuscripts. One report, which is coauthored with F.A. McKeown, discusses the spatial coincidence of high fluid pore pressure and contemporary seismicity in the New Madrid seismic zone. The second report, which is coauthored with M.B. Goldhaber (Br. of Geochemistry), documents the flow of acidic fluids out of the Reelfoot rift and into adjacent areas by mapping the regional extent of dissolved authigenic potassium feldspar.

H.S. Swolfs completed his analysis of structural features in the Dow Chemical #1 Garrigan drill hole to clarify the origin, evolution, and extent of deep-seated seismogenic structures that underlie and are perhaps associated with structurally high features in the Reelfoot rift. This drill hole is on the southeastern flank of the Blytheville arch, a major structural feature that coincides with the narrow, 120-km-long, southwest-trending zone of seismicity of between Caruthersville, Mo., and Marked Tree, Ark. The results of this study are being published in a special issue of the *Seismological Research Letters*.

Quaternary Deformation and Paleoseismicity—NMSZ

D.T. Rodbell completed two investigations: a) the distribution, age, and downvalley gradient of the alluvial terraces along the Obion River in northwestern Tennessee, and b) the distribution of probable 1811-12 liquefaction features that are present on these terraces and the number of seismic events recorded by these features. Reports describing these studies are in press.

Distribution of Stress—NMSZ

W.L. Ellis revised a manuscript titled "Summary and discussion of crustal stress data in the region of the New Madrid seismic zone," which will be submitted for publication as a chapter in the forthcoming USGS Professional Paper on current research in the New Madrid region.

Investigations of the Meers Fault, Southwestern Oklahoma

M. Jones-Cecil finalized her analysis of the magnetic field in the area of the Meers fault, southwestern Oklahoma, to examine subsurface structural relations and how they may affect the fault's seismic potential. Jones-Cecil finalized models of eight ground-magnetic profiles across the fault and three regional profiles across the entire Frontal Wichita fault system (FWFS) using aeromagnetic data. The FWFS separates the Anadarko basin to the northeast from the Wichita uplift to the southwest. The models incorporate *in situ* and laboratory magnetic susceptibility measurements, paleomagnetic data from drill core of holes adjacent to the Meers fault (on loan from Ken Luza of the Oklahoma Geological Survey), and petrologic information from the core (see below).

D.S. Collins examined the petrography of 28 thin sections and hand samples from the core of three aligned drill holes across the Meers fault. The petrographic data on the lithologies and mineral alterations of igneous rocks adjacent to the fault zone provide important constraints on the models of magnetic data near the fault. The net result is to refine the models and help clarify the structural relations of rocks across the fault zone.

Related Investigations

Although not directly funded by NEHRP, M. N. Machette (Br. Geologic Risk Assessment) and Crone, in conjunction with J.R. Bowman, completed two comprehensive USGS Bulletins that present their detailed field data and describe the results of their G.K. Gilbert Fellowship studies on the paleoseismicity of the 1986 Marryat Creek and 1988 Tennant Creek, Australia intraplate earthquakes. These Bulletins contain lithologic/structural maps of six trenches, detailed site maps,

scarp profiles, and the results of thermoluminescence and electron-spin resonance dating of Quaternary deposits in the two areas. The Bulletins document the long recurrence time between successive earthquakes on these faults and discuss the implications of these long recurrence times on seismic hazards in stable continental tectonic settings. Machette and Crone also presented the results of these studies at the 1991 Geological Society of America annual meeting (10/91) and at a workshop on "Cratonic Seismicity and Strain" sponsored by the USGS, the Nuclear Regulatory Commission, and the Electric Power Research Institute (7/92).

RESULTS

Subsurface Stratigraphy and Structure—NMSZ

(Collins) Analyses of the insoluble heavy minerals from the Strake Petroleum #1 Russell drill hole reveal that igneous rocks were exposed in the source area during deposition of Cambrian pre-Bonneterre rocks and the lower part of the Upper Cambrian Bonneterre Formation. In contrast, both igneous and high-grade, metamorphic rocks provided sediment during deposition of the upper part of the Bonneterre Formation and the overlying Lower Ordovician Eminence or Potosi Formations. The heavy minerals that indicate metamorphic rocks in the source area include kyanite, sillimanite, zoisite, and staurolite; the minerals that indicate an igneous source area include brookite, anatase, augite, ilmenite, magnetite, chromite, phlogopite/biotite, apatite, hornblende, wolframite, scheelite, garnet, zircon, and tourmaline. It is significant that the heavy mineral suites from neither the Dow Chemical Co. #1 Garrigan drill hole, which is about 90 km south of the Strake drill hole, nor the Killam #1 Pattinson drill hole, which is about 5 km southeast of the Strake drill hole contained evidence of metamorphic rocks in the sediment source areas. This suggests the presence of isolated depocenters that had different source terrains in the Reelfoot rift during the Early Paleozoic. The closest known major source of metamorphic rocks is the central Missouri high, which is about 240 km west of the Strake drill hole. The Precambrian igneous rocks that are exposed on the west side of the St. Francois Mountains may have been the main source of igneous detritus for Early Paleozoic rocks in the Strake, Killam, and Garrigan drill holes. These studies show that insoluble residues cannot be used to correlate the Early Paleozoic rocks on the carbonate platform along the northwestern flank of the Reelfoot rift with the dominantly siliciclastic rocks in the interior of the rift.

(Dart) R.L. Dart has completed revising his series of 14 subsurface maps and 11 stratigraphic cross sections that were derived from his database of subsurface information in the New Madrid region. These maps and cross sections will be published as a three-part series of USGS Miscellaneous Field Studies maps. Part 1 will contain three maps showing a variety of geologic and geophysical information about the subsurface geology of Paleozoic and Precambrian rocks. Part 2 will be a series of 10 structure contour, isopach, and subcrop maps of individual systems within the Paleozoic stratigraphic section. The third part will contain 11 northwest-southeast and northeast-southwest stratigraphic cross sections of the area.

Dart's inquiries to the NGS concerning new leveling data from the Mississippi embayment revealed that, in recent years, several new leveling lines have been completed along previously leveled routes. His inquiries concerning the need to apply corrections revealed that the necessary routine corrections have been applied to all data that is in the NGS vertical-control database. Upon request, the NGS can generate level profiles for any releveling route within the Mississippi embayment from their vertical-control computer database. Level profiles are fundamental tools for the recognition of recent vertical crustal deformation using geodetic data. The NGS's ability to produce level profiles and apply corrections to all old leveling data supersedes Dart's study of these data that was done in the early 1980's. However, Dart's earlier compilation and profiles of the leveling data from the Mississippi embayment can be used to make a preliminary identification of areas of possible crustal deformation.

(Dart & Swolfs) The principal objective of this research is to collectively interpret all of the available geological and geophysical subsurface data in the area of abundant seismicity to identify fault-related features and to evaluate the tectonic significance of these features. The comprehensive subsurface database and the resultant subsurface maps and cross sections permit preliminary structural interpretations that will lead to working hypotheses about the geological setting of seismically active fault zones. A three-dimensional image of the Precambrian bedrock surface shows previously unrecognized large-scale topography on the floor of the Reelfoot rift. The image shows a northwest-trending trough in northeastern Arkansas that is flanked on the northeast by a 2-km-high ridge. These major features are oriented normal to the northeast-trending rift axis and correlate well with similar structures expressed on a recently compiled depth-to-magnetic-basement map (Hildenbrand and Hendricks, USGS Professional Paper). The upward projection of the gently southwest-dipping boundary between the trough and ridge may be expressed in the subcrop maps of the Cambrian and Ordovician surfaces as mapped by Dart (in prep.) and Schwalb (1971), respectively. Along this boundary, key stratigraphic horizons are all displaced down to the southwest. The nature and tectonic significance of this boundary remains to be resolved, but in Precambrian basement rocks, it coincides with the southwestern terminus of the NMSZ and the end of the Blytheville arch near Marked Tree, Ark. During the past few decades, some of the largest earthquakes in the NMSZ have occurred in this area. This intra-rift basement structure may concentrate stress and/or act as a structural barrier that limits the seismicity at the southwestern end of the axial fault zone.

(Diehl) Paleozoic carbonate rocks from the USGS-New Madrid Test well, which is near the crest of the Pascola arch, are brecciated and enriched with sulfide and rare-earth minerals (Crone, 1981; Goldhaber and others, 1993). Petrographic analysis of samples from the drill hole shows that the sulfide mineralization is concentrated along intersecting fractures and stylolites. Scanning-electron-microscope mapping of the sulfides using the IPP program, which can selectively map as many as 8 different elements, shows an alignment of epigenetic minerals along fractures and demonstrates that fluid flow in the rock was controlled by internal structures.

The direct evidence of alkaline igneous activity in the Reelfoot rift has been limited to the presence of lamprophyric dikes and syenite penetrated in a few deep drill holes, but new petrographic studies of the sedimentary rocks in the region provide indirect evidence of alkaline magmatism and related metasomatism. These studies show that fluorite and elevated fluorine concentrations are present in several drill holes in the rift. Furthermore, the presence of fluorapatite, inclusion-rich potassium feldspar cement, monazite, and other rare-earth minerals suggests that metasomatism by alkaline magmatic fluids has occurred in these rocks.

Mapping along the segment of the English Hill fault that is exposed in the Grays Point quarry revealed evidence of fault movement during the Middle-Late Ordovician, which is earlier than the Devonian age of fault movements that is commonly interpreted throughout southeastern Missouri (Harrison and Schultz, 1992). In the quarry, the fault offsets the Ordovician Plattin, Decorah, and Kimmswick Formations, but the Ordovician Maquoketa Shale and undeformed Thebes Sandstone fill a synform along the fault. The fault is not mineralized by carbonate-rich fluids, but adjacent carbonate-filled fractures contain evidence of three periods of movement: (1) formation of fractures that were sealed by authigenic cement, (2) renewed deformation and partial recrystallization of subrounded breccia clasts, and (3) another episode of brecciation that produced angular clasts and allowed carbonate-rich fluids to precipitate minerals in fractures and vugs. Each successive fluid-flow event produced coarser authigenic mineral cement than the preceding event.

(Swolfs) The study of the cores from the Garrigan well was initiated to improve our understanding of the origin and extent of deep-seated seismogenic faults that underlie and are perhaps associated with the Blytheville arch in the Reelfoot rift (Swolfs, 1992). Two additional manuscripts are in various stages of preparation and contain, respectively, a detailed descriptive lithologic log of the oriented core (90% complete), and a summary of the methods used to obtain and record directional data in the oriented core (60% complete). A compendium of published and unpublished geologic information on the sub-Cretaceous rocks in the Reelfoot rift, obtained from studies of about twenty drill holes in this region, is ready for branch review. The subsurface data

compiled in this progress report includes information ranging from biostratigraphy to drill-stem test results, and its intended purpose is to complement the catalog of drill-hole data prepared by R.L. Dart (in prep.).

(Crone) The preliminary interpretation of recently purchased industry seismic-reflection data in the vicinity of the Crittenden County fault zone in northeastern Arkansas documented the structural relations that exist across the rift-bounding fault zones. Several profiles in this data set contain groups of prominent moderate to strong reflectors in the upper crust at depths that are below the top of crystalline basement. Many of the reflections are still visible at the base of the industry-processed record sections (5.0 sec two-way travel time), which corresponds to depths of approximately 15 km. These groups of strong reflectors, which are continuous for distances of several kilometers, typically have gentle dips. These data are being reprocessed (in collaboration with T. Pratt, Br. Geologic Risk Assessment) to yield 12-sec-long record sections; initial reprocessing shows that groups of strong reflectors are present in the crust to depths of about 20 km.

Quaternary Deformation and Paleoseismicity—NMSZ

(Rodbell) The terrace study, the results of which have been submitted for publication as a U.S. Geological Survey Bulletin, has led to the recognition of three terrace levels along the Obion River, thus corroborating the findings of Saucier (1987). In addition to elevation above the modern stream, these terraces can be differentiated by the number of loess units that mantle their surfaces and by how extensively they are dissected by tributary streams. These parameters permit correlation of the terraces and thus provide a method to test Saucier's (1987) two hypotheses concerning possible Quaternary deformation in the eastern uplands adjacent to the Mississippi River. Several cores, which were retrieved from these terraces using a hydraulically powered drill rig, contained radiocarbon datable materials from the base of the loess mantle. The youngest terrace is named the Finley terrace, and is mantled by Peoria loess. A radiocarbon date of 21.6 ka from the terrace alluvium beneath the loess indicates that the Finley terraces formed during the late Wisconsin rather than during the early Wisconsin as previously postulated (Saucier, 1987). The next older terrace is the Hatchie terrace, which is mantled by the Peoria and Roxana loesses. The presence of these two loesses indicates that these terraces are early Wisconsinan in age. The oldest terrace is the Humboldt terrace. A single core from this terrace near the edge of the bluffs penetrated more than 8 m of Peoria and Roxana loess and did not penetrate the underlying alluvium. Based on its extensive geomorphic modification, the Humboldt terrace believed to be pre-Wisconsinan in age.

Results of the liquefaction study are reported in a USGS Miscellaneous Field Studies Map (Rodbell and Bradley, in press) and in a note in the *Bulletin of the Seismological Society of America* (Rodbell and Schweig, in press). In this study, we excavated three trenches across sand blows that formed in sandy alluvial deposits underlying the Finley terrace in western Tennessee. The deposits are susceptible to liquefaction and have been in a geomorphic setting that is favorable for liquefaction for at least the past 21.6 ka. The lack of significant soil development on numerous sand-blow deposits exposed in three exploratory trenches indicates that the sand blows probably formed during the multiple episodes of strong ground shaking from the 1811-12 earthquakes. We found no convincing evidence of prehistoric liquefaction in our trenches. These results imply that shaking strong enough to cause liquefaction has not occurred at this site in at least the past 10,000 years. This result is consistent with the results of similar studies elsewhere in the NMSZ (Wesnousky and Leffler, 1992).

Investigations of the Meers Fault, Southwestern Oklahoma

(Jones-Cecil) The Meers fault is one of the few examples of an exposed, recently reactivated fault in the central and eastern U.S. Hence, understanding its structural role within the Frontal Wichita fault system (FWFS) and the Southern Oklahoma aulacogen, its orientation relative to the current regional stress field, and the degree of deformation and alteration within the fault zone may reveal reasons for the late Holocene reactivation of the fault. The possible causes of reactivation help to

characterize other potentially seismogenic faults in the vicinity of the Southern Oklahoma aulacogen, and, in turn, advances our understanding of intraplate seismicity.

The objective of the geophysical study of the fault was to examine its geometry and its relationship to other faults within the FWFS and to the present-day regional stress field. This study clearly demonstrates the importance of preexisting structures in controlling the location of the reactivated part of the fault. The last major episode of movement on the fault occurred in Late Paleozoic time. The northwestern limit of the Holocene rupture appears to have been controlled by splaying of the older Meers fault that occurred at a left step in the primary fault. At least two scarps of secondary reactivated faults coincide with minor faults that were modeled from the magnetic data. This result exemplifies of the extent to which preexisting structures apparently controlled the reactivation of even small-scale faults. The Meers fault's linear surface trace, trenching studies, and shallow seismic-reflection data all show that the fault has a near-vertical dip in the shallow subsurface. Models of the magnetic data also constrain the dip to be near-vertical to about 0.5 km depth. The up-to-the-north movement during Holocene faulting is qualitatively more compatible with a near-vertical dip at depth in the present-day regional stress field than with reactivation on a moderate southwest-dipping fault that was interpreted from COCORP reflection data (Brewer and others, 1983). If this qualitative assessment is true, then there are few faults with similar strikes and steep dips in the FWFS and within the area of the Southern Oklahoma aulacogen, and therefore few that are favorably oriented to be reactivated in the current regional stress field.

A dikelike body immediately south of the fault has been interpreted from magnetic data (Purucker, 1986) to extend along almost half the length of the Quaternary scarp. The Oklahoma Geological Survey (OGS) drill holes across the fault cored diorite/gabbro that has high magnetic susceptibility and is at the appropriate depth and location to be the probable source of the magnetic anomaly. Rock in the core is highly altered and sheared and has a high clay content. Preliminary detailed gravity profiles show a 1 mGal high associated with the dikelike body, implying that the alteration is limited to the near-surface. The presence of the dikelike body along the fault may localize stresses along the fault.

(Collins) Core samples from three OGS drill holes contain igneous rock of intermediate(?) composition probably from the Roosevelt Group, diorite and gabbro from the Roosevelt Group, and rhyolite from the Carlton Rhyolite Group. These rocks could not be correlated between the drill holes because of pervasive alteration and/or because each of the core holes penetrated different bodies of igneous rock. Differences in the amount of intragranular fracturing and degree of alteration between the drill holes suggest that the block of igneous rock sampled by the core holes is bounded on the north by the Meers fault and on the south by a subsurface fault that has no surface expression. Four types of fractures common in the core samples are from oldest to youngest: 1) breccia-filled fractures, 2) clay-filled fractures, 3) iron-oxide filled fractures, and 4) open (unfilled) fractures. Crosscutting relations of the fractures suggest that an early faulting event(s) was followed by at least three later extensional events.

Related Investigations

Results of Machette's and Crone's Gilbert Fellowship research on the Marryat Creek and Tennant Creek scarps in central Australia (Crone and others, 1992; Machette and others, in press) show that these historical earthquakes reactivated ancient faults and that the recurrence time of major earthquakes these faults is measured in time scales of many tens of thousands to hundreds of thousands of years, or possibly longer. Six trenches across the historical ruptures revealed no clear evidence of prehistoric scarp-derived colluvial deposits. Furthermore, we did not find compelling geomorphic evidence ancient scarps along the ruptures. These field studies and our brief examination of a trench across the 1968 Meckering (Western Australia) scarp suggest that surface ruptures on Australian intraplate faults have very long repeat times. If this is true for most faults in the stable interior of continents, then the concept of recurrence intervals may not be appropriate in characterizing the behavior of these faults. A more realistic model for earthquake-hazard assessment of continental interiors might be based on infrequent but moderate- to large-

magnitude earthquakes that can occur on any suitably oriented fault, rather than basing the assessments on only those faults that have Quaternary movement.

REFERENCES CITED

Brewer, J. A., Good, R., Oliver, J. E., Brown, L. D., and Kaufman, S., 1983, COCORP profiling across the southern Oklahoma aulacogen--Overthrusting of the Wichita Mountains and compression within the Anadarko basin: Geology, v. 11, p. 109-114.

Crone, A.J., 1981, Sample description and stratigraphic correlation of the New Madrid Test Well-1-X, New Madrid County, Missouri: U.S. Geological Survey Open-File Report 81-426, 26 p.

Harrison, R.W., and Schultz, A.P., 1992, Faulting at Thebes Gap, MO.-ILL.—Implications for New Madrid tectonism: Geological Society of America Abstracts with Program, v. 24, no. 7, p. A191.

Hildenbrand, T.G., and Hendricks, J.D., Geophysical setting of the Reelfoot rift and relations between rift structures and the New Madrid seismic zone: U.S. Geological Survey Professional Paper.

Purucker, Michael, 1986, Interpretation of an aeromagnetic survey along the Wichita Frontal fault zone *in* Gilbert, M.C., ed., Petrology of the Cambrian Wichita Mountains igneous suite: Oklahoma Geological Survey Guidebook 23, p. 129-136.

Saucier, R. T., 1987, Geomorphological interpretations of late Quaternary terraces in western Tennessee and their regional tectonic implications: U. S. Geological Survey Professional Paper 1336-A, 19 p.

Schwalb, Howard, 1971, The northern Mississippi embayment—A latent Paleozoic oil province, *in* Proceedings of symposium on future petroleum potential on NPC region 9 (Illinois basin, Cincinnati arch, and northern part of Mississippi embayment): Illinois State Geological Survey, Urbana, IL, Illinois Petroleum 95, p. 44-56.

Wesnousky, S.G., and Leffler, L.M., 1992, The repeat time of the 1811 and 1812 New Madrid earthquakes—A geological perspective: Bulletin of the Seismological Society of America, v. 82, p. 1756-1785.

REPORTS

Collins, D.S., 1992, A petrographic study of igneous rock from three drill holes near the Meers fault, Oklahoma: U.S. Geological Survey Open-File Report 92-411, 25 p.

Collins, D.S., Taylor, M.E., Repetski, J.E., and Palmer, A.R., 1992, New sedimentological data for the Dow Chemical #1 B.L. Garrigan drill hole, Mississippi County, Arkansas: U.S. Geological Survey Open-File Report 92-6, 38 p.

Crone, A.J., 1992, Structural relations and earthquake hazards of the Crittenden County fault zone, northeastern Arkansas: Seismological Research Letters, v. 63, no. 3, [in press].

Crone, A.J., Machette, M.N., and Bowman, J.R., 1992, Geologic investigations of the 1988 Tennant Creek, Australia, earthquakes--Implications for paleoseismicity in stable continental regions: U.S. Geological Survey Bulletin 2023-A, 52 p.

Dart, R.L., Drill-hole data catalog of Paleozoic subsurface geology in the upper Mississippi embayment - A revision of Open-File Report 90-260: U.S. Geological Survey Open-File Report, [in press].

Dart, R.L., Maps of the Paleozoic and Precambrian rocks of the Mississippi embayment from drill-hole and seismic reflection data: U.S. Geological Survey Miscellaneous Field Studies Map, [in press].

Diehl, S.F., Throckmorton, C.K., and Clendenin, C.W., 1993, Significance of recurrent fault movement at Grays Point, Missouri (abs): Geological Society of America Abstracts with Programs, North-Central Section, March 29-30, 1993, [submitted].

Diehl, S.F., and Goldhaber, M.B., Feldspar diagenesis in Cambrian clastic rocks of the southern Ozarks and Reelfoot rift, southeast Missouri and northeast Arkansas--Implications for Mississippi Valley-type ore genesis, *in* Day, Warren, and Lane, Diane, eds., Strategic and critical minerals of the midcontinent, U.S.A.: U.S. Geological Survey Bulletin 1989, [in press].

Goldhaber, M.B., Diehl, S.F., Flohr, Marta, and Sutley, S., 1993, Evidence for alkaline igneous activity and associated metasomatism in the Reelfoot rift: Geological Society of America Abstracts with Programs, North-Central Section, March 29-30, 1993, [submitted].

Jones-Cecil, Meridee, Total-field aeromagnetic and derivative maps of the Lawton area, southwestern Oklahoma: U.S. Geological Survey GP-998-A, 2 sheets, scale 1:100,000, [in press].

Jones-Cecil, Meridee, Donovan, R. N., and Bradley, L.-A., Structural framework of the Meers fault and Slick Hills area, southwestern Oklahoma, based on magnetic data, *in* Johnson, K.S, Structural styles of the southern mid-continent--a symposium: Oklahoma Geological Survey Circular, [Director's approval 7/92].

Jones-Cecil, Meridee, and Robbins, S.L., Bouguer and isostatic residual gravity anomaly and derivative maps of the Lawton area, southwestern Oklahoma: U.S. Geological Survey GP-998-B, 3 sheets, scale 1:100,000, [in press].

Machette, M.N., Crone, A.J., and Bowman, J.R., Geologic investigations of the 1986 Marryat Creek, Australia, earthquake--Implications for paleoseismicity in stable continental regions: U.S. Geological Survey Bulletin 2032-B, [in press].

Repetski, J.E., Taylor, M.E., Collins, D.S., Palmer, A.R., and Wood, G.E., 1992, Cambrian and Ordovician paleontological studies in the Reelfoot basin, southern Midcontinent, U.S.A. [abs.]: Fifth North American Paleontological Convention, Field Museum of Natural History, Chicago. (unpaginated).

Rodbell, D.T., and Bradley, L.A., Logs of exploratory trenches through liquefaction features on late Quaternary terraces in the Obion River Valley, northwestern Tennessee: U.S. Geological Survey Miscellaneous Field Studies Map, [in press].

Rodbell, D.T., and Schweig, E.S., III, The record of seismically-induced liquefaction on late Quaternary terraces in northwestern Tennessee: Bulletin of the Seismological Society of America, [in press].

Rodbell, D.T., Subdivision, subsurface stratigraphy, and estimated age of fluvial terraces in northwestern Tennessee: U.S. Geological Survey Bulletin, [submitted].

Swolfs, H.S., 1992, Structural features in the Dow Chemical B.L. Garrigan No. 1, Mississippi County, Arkansas, and their paleotectonic implications: Seismological Research Letters, v. 63, no. 3, [in press].

Earthquake Hazard Investigations in the Pacific Northwest and southern Alaska using network data

14-08-0001-G1803

R.S. Crosson and K.C. Creager
Geophysics Program
University of Washington
Seattle, WA 98195
(206) 543-8020

October 1, 1991 - September 30, 1992

Investigations

This research focuses on earthquake hazards in the Pacific Northwest, including large scale plate interactions, through the study of regional structure and tectonics. Current investigations by our research group include determining source scaling and moment estimation using coda amplitudes, completing work on subduction kinematics of the subducting plate, investigating P-wave multiplets arising from teleseismic arrivals reflected from the subducting plate, and refraction interpretation of earthquake travel times.

Source moment estimation and magnitude determination using S-coda amplitude:

We wish to provide accurate automated estimates of earthquake magnitude using regional or local (mainly vertical component) short-period data. The current technique for determining magnitudes from short-period data is to use S-wave coda duration. However machine algorithms to automatically assign coda durations are far from satisfactory due to variations in noise level and signal frequency.

We have developed a method to base magnitudes on coda amplitude rather than duration. Using standard coda amplitude models based on scattering theory (e.g. Aki and Chouet, 1975), we can relate the amplitudes back to the source spectrum and hence directly to moment. Magnitudes can then be derived directly from the moment estimates.

S-wave coda amplitudes from local earthquakes recorded by the regional network were used with the single-scattering coda model of Aki and Chouet (1975) to estimate source spectra in a narrow frequency band. We found an omega-square, constant stress drop scaling model provided the best fit to the source spectra estimate. Using an event with a known seismic moment, moment estimates for subsequent events can be determined.

We feel this method of moment estimation provides better source size estimates for locally recorded earthquakes than S-wave coda duration. The method is being prepared for routine testing on data from the WRSN (Washington Regional Seismograph Network).

Kinematic Modeling:

Several aspects of the surface geology of the Pacific Northwest, such as volcanism and crustal deformation, are related to mantle flow associated with subduction. Along-arc variations in the geology require a three- dimensional analysis of convection. In order to make a three-dimensional flow calculation both tractable and interpretable, we consider the limiting case that the subducting slab is very thin, and that its viscosity far exceeds that of the surrounding crust and mantle. With these assumptions, we have developed a non-linear finite-element optimization scheme to find the slab configuration with the least amount of membrane (in-plane) deformation rate while satisfying boundary conditions such as the known relative plate convergence rates, and partial geometric constraints obtained from Wadati-Benioff earthquake locations. Because of a concave-oceanward bend in the trench axis located seaward of the Olympic Mountains, the subducted Cascadia slab has a geometric space problem analogous to a table cloth hanging over the corner of a table. This induces along-arc compression within the slab surface which can be relieved by forming an arch or by an along-arc buckling structure. Our numerical experiments suggest that the arch-like structure, revealed from seismic observations, is a natural consequence of the subducted slab responding to the concave-

oceanward bending of the trench. The locus of points where both the observed and theoretical slab dips are less than 10° is offshore everywhere except along the arch, beneath the Olympic Mountains. According to the Critical Taper Theory, the height of an accretionary wedge will grow landward until the slab dip exceeds about 10°. This provides a plausible explanation for the origin and geographic location of the Olympic Mountains accretionary prism. The concentration of seismicity beneath the Puget Sound area appears to be the result of bending the already arched slab. The computed deformation is dominated by N-S compression in the Puget Sound area and the peak compressional strain-rate is around $2\times10^{-16}s^{-1}$ which is comparable to the value estimated from seismic moment release rates of the last century. A manuscript describing the results will be submitted to JGR.

Like Cascadia, the trench off Alaska has concave-oceanward curvature. Given this geometry and the assumption that the slab is continuous, our calculations (Creager and Chiao, 1992) predict that the slab under central Alaska should have a shallow dip relative to the dip under the Aleutian Islands to the west and under the Wrangell Mountains to the east. Our models also predict along-arc compressive strain rates under Alaska and along-arc extensional strain rates under the central Aleutians. The observed subduction geometry and the orientations of seismic moment tensors are in close agreement with our models.

Preliminary Investigation of P multiples from Teleseisms

We are using teleseismic P waves incident on the subducted Juan de Fuca slab to investigate local dipping structure through multiple P reflections. The potential advantage of using this method for regional networks is that:

a) A single component vertical short period station can be used;

b) Vertical structure information can be obtained for a large number of network stations, allowing lateral variations in structure to be mapped; and

c) Signal stacking and other array processing techniques can be applied to leverage the structure information using large numbers of stations.

We first investigated the expected amplitudes of multiple reflections using standard ray tracing techniques. These results indicated that amplitudes were sufficient that stacking techniques could be used to increase the signal-to-noise ratio. However, because earthquakes have individual source-time functions the source signals must be deconvolved prior to stacking.

We found that source signals could be approximately estimated using network averaging, and each source was deconvolved using its average signal. We immediately found strong signal coherence in the deconvolved signals for similar source distances and back azimuths. We are currently working on modeling some particularly strong coherent phases on selected stations using dipping interface models.

Work is continuing on improving our methods of source estimation and deconvolution in order to reduce the "noise" in the deconvolved signals and improve the stacking results. In addition, we are continuing work on modeling identified phases.

Refraction Interpretation of Earthquake Travel Times

In an attempt to gain a better understanding of the crust and upper mantle transition across the Cascade Range, we are using techniques of refraction interpretation with earthquakes as sources. We have constructed a profile from the central Puget Sound region southwest of Seattle to a point near Walla Walla in eastern Washington. There are a number of moderate sized earthquakes along the profile and near each of its ends, which can be well located with network stations. We are using these events as "sources" by assuming their locations are known, but allowing their origin times to float to minimize residuals. The advantage of earthquakes over man-made sources is that sources located at depth provide more information on velocities at depth. This advantage is at least partially offset by the uncertainties of the source locations and origin time.

Our analysis is being done using the forward and inverse modeling program developed by Colin Zelt. Both reflections and refractions can be utilized with this method. Preliminary results suggest that we will be able to produce an improved model of the Cascadia transition structure.

Articles

Chiao, L.-Y., and K. C. Creager (in preparation) Geometry and lateral membrane rate of the subducting Cascadia slab, to be submitted to JGR

Dewberry, S.R. and R.S. Crosson, (in preparation), Source scaling and moment estimation for the Washington Regional Seismograph Network using coda amplitudes, to be submitted to BSSA.

Lees, J.M. and R.S. Crosson, (1991), Bayesian ART versus conjugate gradient methods in tomographic seismic imaging: An application at Mount St. Helens, Washington, in *Spatial Statistics and Imaging*, A. Possolo, editor, Inst. of Math. Statistics, Hayward, CA, V. 20, p. 186-208.

Ma, L., R.S. Crosson, and R.S. Ludwin, 1991, Focal Mechanisms of western Washington earthquakes and their relationship to regional tectonic stress, USGS Open File OF-91-441-D, will also be published in a USGS Professional Paper.

Ma, L., R.S. Crosson, and R.S. Ludwin, (submitted), Focal Mechanisms of western Washington earthquakes and their relationship to regional tectonic stress, in: USGS Professional Paper "Assessing and Reducing Earthquake Hazards in the Pacific Northwest")

Mundal, I., M. Ukawa, and R.S. Crosson, (in press), Normal and anomalous P phases from local earthquakes, and slab structure of the Cascadia Subduction zone, BSSA

VanDecar, J.C., R.S. Crosson and K.C. Creager, (in preparation), Travel-time inversion for subduction zone structure: I. The effect of three-dimensional ray tracing on resolution analysis, to be submitted to JGR.

Abstracts

Carroll, D. C., and K. C. Creager, 1992. Mapping seismic discontinuities under central Alaska by stacking receiver functions, Seismol. Res. Lett.,V. 63, p. 36.

Creager, K. C. and L.-Y. Chiao, 1992, Membrane Deformation Rate and Geometry of Aleutian-Alaska Subduction, Wadati Conference on Great Subduction Earthquakes, Geophysical Institute, University of Alaska, Fairbanks, Alaska.

Creager, K.C. and Chaio, L.Y, 1992, Relationships among surface geology, seismicity, and three-dimensional models of Cascadia Slab Flow, GSA 88th Annual Cordilleran Section, 1992 Abstracts with Programs, V. 24(5), p. 17.

Crosson, R.S. and R.S. Ludwin, 1992 (Invited), Cascadia Subduction Zone: Constraints on slab structure from seismic observations, GSA 88th Annual Cordilleran Section, 1992 Abstracts with Programs, V. 24(5), p. 18.

Crosson, R.S., and J.C. VanDecar, 1992, Cascadia Subduction Zone: Large scale structure from receiver function analysis, seismicity, and teleseismic arrival time tomography, Wadati Conference on Great Subduction Earthquakes, Geophysical Institute, University of Alaska, Fairbanks, Alaska.

Dewberry, S.R. and R.S. Crosson, 1992, Source scaling and moments for the Washington Regional Seismic Network data using coda amplitudes, Seism. Res. Lett., V. 60, p. 71-72.

VanDecar, J.C., R.S. Crosson, and K.C. Creager, (in press), Teleseismic travel-time inversion for Cascadia subduction zone structure employing three-dimensional ray tracing (extended abstract), presented at the XXII General Assembly, European Seismological Commission, Barcelona, Spain, Fall, 1990.

Seismic Potential of Major Offshore Faults in the Santa Monica and San Pedro Basins

Agreement No. 1434-92-G-2167

James K. Crouch
J.K. Crouch & Associates, Inc.
3463 State St., Suite 282
Santa Barbara, CA 93105

(805) 967-2892

Introduction:

During the past 20 years, numerous small (M_L = 2.5-4.9) earthquakes and three moderate-sized (M_L = 5.0-5.9) earthquakes have occurred within or along the margins of the Santa Monica and San Pedro basin, offshore southern California (e.g., Hauksson and Saldivar, 1989; Hauksson, 1990). In addition, the epicenter of the 1930 Santa Monica (M_L = 5.2) earthquake has been relocated to a position along the shelf, several kilometers south of Malibu (Hauksson and Saldivar, 1986), and a 1912 M_L = 5.0 event is inferred to have occurred offshore, about 20 kilometers due west of Point Dume (Davis et al., 1989). The mainshock-aftershock sequences of the three more recent of these moderate-sized events (i.e., the 1973 Pt. Mugu and the 1979, 1989 Malibu earthquakes) are dominated by reverse focal mechanisms. These events, as well as the earlier 1912 and 1930 events, have all been associated with either the Anacapa-Dume or Santa Monica faults that extend offshore along the northern margin of the Santa Monica basin (Yerkes and Lee, 1979; Hauksson and Saldivar, 1986, 1989; Davis et al., 1989). These structures are known to be predominantly reverse faults that generally strike east-west and dip steeply to the north. The offshore location of these faults, however, is based upon a limited number of high-resolution, relatively shallow-penetration, single-channel seismic-reflection profiles (e.g., Junger and Wagner, 1977). Hence, along much of their length, the locations and down-dip directions of these, as well as other major faults within this offshore region are largely inferred and only in limited places, has their surface or near surface trace been imaged. Moreover, because the known mainshock hypocenters of the moderate-sized events occurred at depths of 12.1 to 13.8 km and the aftershocks occurred at depths that generally range from 9 to 16 km (Hauksson and Saldivar, 1989; Hauksson, 1990), significant extrapolation is required in order to correlate these events to offshore faults that have only been mapped at or near the sea-floor.

Investigations:

The primary focus of this investigation is to more precisely determine the location and character of major structures in the offshore Santa Monica and San Pedro basins by augmenting the existing U.S.G.S. high-resolution grid with an 860 km grid of more closely-spaced, deeper penetration (5.0 sec.), migrated, CDP seismic-reflection data shot by industry. This information is, in turn, being used to improve correlations between well-located offshore earthquakes and their causitive faults. Additional investigations include: 1) determinations of the tectonic framework and history of this offshore region, 2) estimates of the nature, timing, and

amount of offset on major faults along with the history of associated folds, and 3) estimates of the length and segmentation (if any) of major faults. The objective of this investigation is to improve our understanding of the seismic potential of major active faults in the offshore Santa Monica and San Pedro basins and thereby, improve estimates of the seismic risk that these structures pose to nearby coastal communities.

Results:

Within the offshore Santa Monica and San Pedro basins there are three mapped faults or fault zones that can be categorized as active, major, and a potential seismic risk to nearby coastal communities. These faults include: 1) the west-trending Dume fault (also referred to as the Anacapa-Dume fault), which chiefly follows the base of the slope along the northern margin of the Santa Monica basin, but crosses the Malibu-Santa Monica shelf where it appears to merge with (or connect to) the offshore extension of the Santa Monica fault zone, 2) the relatively straight, northwest-trending San Pedro basin fault, which bisects the long axis of the basin, and 3) the Palos Verdes fault, which crosses the Palos Verdes Hills onshore and extends offshore, both northwestward across the Santa Monica shelf and southeastward across the San Pedro shelf (e.g., Junger and Wagner, 1977). In addition to these well-kown major faults that extend to or near the sea-floor, more recent interpretations of the geometry and kinematics of the upper crust (0-20 km) using retrodefomable cross sections strongly suggest that a number of concealed (blind), seismogenic thrusts, thrust ramps, backthrusts, and a subhorizontal regional detachment probably exist at depth, beneath the central and marginal parts of the offshore Santa Monica and San Pedro basins (e.g., Davis et al., 1989; Namson and Davis, 1991).

Although the available CDP data in the offshore Santa Monica and San Pedro basins were collected and processed to 5.0 seconds, the relatively deep, low-angle thrust faults are not imaged and the planes of previously mapped major faults are generally only interpretable to depths of <3 km below the seafloor. Large anticlines or anticlinoria associated with (overlying) these faults, however, generally extend to or near the seafloor and these structures are well-imaged to subsea depths as great as 5 km. These are chiefly fault-bend and fault-propagation folds, and detailed mapping of their geometry, axes, and lengths is leading to improved constraints on both mapped reverse faults and concealed low-angle thrust faults. More importantly, this information is providing better control for the correlation of well-located earthquake hypocenters to causitive faults within the offshore Santa Monica and San Pedro basins.

Our work is also leading to proposed revisions in previously reported correlations between earthquakes located offshore and causitive faults, and to new estimates of the seismic activity and potential of specific faults in this offshore region. For example, the 1979 Malibu (M_L = 5.0) mainshock-aftershock sequence has previously been correlated to an inferred eastern extension of the north-dipping Anacapa-Dume fault (Hauksson and Saldivar, 1986), and more recently, to the north-dipping Elysian Park thrust (Davis et al., 1989; Hauksson and Saldivar, 1989). The Elysian Park thrust is interpreted to be responsible for the development and uplift of the Santa Monica Mountains anticlinorium, and it is also interpreted to be the source of the 1987 Whittier Narrows (M_L = 5.9) earthquake, as well as a number of other moderate-sized events that have occurred along the Santa Monica uplift zone (Davis et al., 1989). Detailed mapping of the offshore with CDP data, however, suggest that neither the Elysian Park thrust nor the Anacapa-Dume fault are the causitive source of the 1979 Malibu event. According to our study, the relocated epicenter of the 1979 Malibu mainshock and the tightly clustered

aftershocks epicenters (Hauksson and Saldivar, 1986) are respectively 5 km and 2-7 km south of the surface trace of the north-dipping Anacapa-Dume fault.

Because the 1979 Malibu mainshock occurred at a depth of 12.2 km and the mainshock-aftershock sequence define a west-northwest-trending hypocentral zone at depths ranging chiefly from 10-15 km (Hauksson and Saldivar, 1989), the Elysian Park thrust (Davis et al., 1989) would seem to be a more likey candidate for this event. However, the north-dipping nodal plane for the 1979 Malibu event, favored by Hauksson and Saldivar (1986,1989) and Hauksson (1990), dips 55 to 60 degrees to the north, whereas the geometric constraints of the Elysian Park thrust suggest that, along its entire length, this fault dips to the north at angles that are probably no greater than about 25 degrees (see Davis et al., 1989; Namson and Davis, 1991).

Structural mapping with CDP data in the offshore suggests that the 1979 Malibu earthquake most likely occurred on a blind, south-dipping, backthrust that underlies the northernmost end of the Palos Verdes anticlinorium (i.e., an extension of fault A interpreted and depicted in Davis et al., 1989 and Namson and Davis, 1991). Although the Palos Verdes anticlinorium is deeply incised by several cross cutting submarine canyons, and is mantled by numerous small amplitude and several large amplitude folds, the principal axial trend of this large northwest-trending structure can be tracked with a fair degree of confidence. It extends over a distance of about 80 km, from the southernmost end of the San Pedro shelf (near Lasuen Knoll) across the Palos Verdes Hills and Santa Monica shelf projection and into the Santa Monica Bay where it finally terminates. The epicentral locations of the 1979 Malibu earthquake sequence cluster around the northernmost axial trace of the Palos Verdes anticlinorium, where it plunges and appears to die out beneath the Santa Monica Bay. Moreover, the alternative nodal plane determined for the 1979 Malibu earthquake by Hauksson and Saldivar (1986), which dips between 30 to 38 degrees to the south and strikes between 100 and 120 degrees, corresponds reasonably well with the inferred dip of the backthrust (fault A) and the strike of the overlying Palos Verdes anticlinorium. The 1989 Malibu (M_L=5.0) earthquake, which occurred about 6.5 km to the southeast of the 1979 event and had very similar characteristics (Hauksson, 1990), most likely was a result of rupture on fault A as well. Finally several slightly smaller (M_L = 4.0-4.5) south-dipping thrust earthquakes that occurred in 1982, 1984, and 1988 (Hauksson, 1990) also appear to be associated with fault A. Two of these occurred at the southern terminus of the Palos Verdes anticlinorium and one occurred on the slope seaward of the San Pedro shelf; all occurred at depths that range from 9.3-11.7 km (Hauksson, 1990).

The 1979, 1989 Malibu events, together with these three events and numerous smaller thrust events (see Hauksson, 1990), strongly suggest that fault A may pose a much greater seismic risk than the mapped surficial faults along the northeast flank of the Santa Monica and San Pedro basins (e.g., the Palos Verdes fault). Assuming that fault A is 80 km long (the length of the overlying Palos Verdes anticlinorium) and, as interpreted by Davis et al. (1989), 11 km wide, this thrust ramp could potentially have a rupture area of 880 km^2 and could potentially generate a rather destructive event, on the order of M = 6.8.

References Cited:

Davis, T.L., Namson, J., and Yerkes, R.F., 1989, A cross section of the Los Angeles area: Seismically active fold and thrust belt, the 1987 Whittier Narrows earthquake, and earthquake hazard, J. Geophys. Res., vol.94, p.9644-9664.

Hauksson, E., 1990, Earthquakes, faulting, and stress in the Los Ageles basin. J. Geophys. Res., vol.95, p.15365-15394.

Hauksson, E., and Saldivar, G.V., 1986, The 1930 Santa Monica and 1979 Malibu, California, earthquakes, Bull. Seismol. Soc. Am., vol.76, p.1542-1559.

Hauksson, E., and Saldivar, G.V., 1989, Seismicity and active compressional tectonics in Santa Monica Bay, southern California, J. Geophys. Res. vol.94, p.9591-9606.

Junger, A., and Wagner, H.C., 1977, Geology of the Santa Monica and San Pedro basins, California Continental Borderland, scale 1:250,000, U.S. Geol. Surv. Misc. Field Stud. Map, MF-820, 5 sheets, 1 pamphlet.

Namson, J., and Davis, T.L., 1991, Late Cenozoic thrust ramps of California, Final Report to the Southern California Earthquake Center, 26p., 18 Figs.

Yerkes, R.F., and Lee, W.H.K., 1979, Maps showing faults and fault activity and epicenters, focal depths and focal mechanisms for 1970-1975 earthquakes, western Transverse Ranges, California, U.S. Geol. Surv. Misc. Field Studies Map, MF-1032.

Reports:

Crouch, J.K., and Suppe, J., in press, Neogene tectonic evolution of the Los Angeles basin and inner borderland: a model for core complex-like crustal extension, submitted to the Geol. Soc. Am Bull.

Using High-Accuracy VLBI to Improve Estimates of the Vertical from GPS

Agreement No. 1434-92-G-2170

James L. Davis
Harvard-Smithsonian Center for Astrophysics
60 Garden St., MS 42
Cambridge, Massachusetts 02138
617-496-7640

Arthur E. Niell
Haystack Observatory
Massachusetts Institute of Technology
Westford, Massachusetts 01886
508-692-4764

Investigations

(1) Improvements in the model for the atmospheric propagation delay in order to improve estimates of site position obtained from space geodetic data.
(2) Comparison of a series of estimates of site position obtained independently from Global Positioning System (GPS) data and from very long baseline interferometry (VLBI) data.

Results

We have investigated numerically the effects of stochastic atmospheric refractive index fluctuations on the estimates of gradient parameters obtained from GPS, VLBI, and WVR data. We have found that significant differences in estimated parameters can be obtained, even when no gradient is present, due to the different spatial and temporal sampling of each technique. Since the second investigation involves comparison of data and results from the two geodetic techniques, an algorithm for comparison of the estimated parameters needs to be developed.

We have analyzed GPS and VLBI data obtained at the times of the NASA VLBI "R & D" experiments. The GPS data were all obtained from Rogue receivers and processed at JPL using the GIPSY analysis software. The VLBI data were processed at the CfA using the SOLVK analysis software. As a preliminary step, we have compared all the length estimates from the common baselines for the experiments performed during January–August 1992. (Length estimates are insensitive to differences in the reference frames used by each analysis group.) For these experiments, there were three common baselines: Fairbanks–Kauai (4,728 km), Fairbanks-Wettzell (6,857 km), and Kauai–Wettzell (10,358 km). No effort was made to "tie" the GPS and VLBI reference

points together at each site. For each series of estimates for a given baseline, we formed residuals of the estimated lengths around a best-fit straight line constrained to change at a rate obtained from a VLBI "global solution." The fits were performed independently for the GPS estimates and for the VLBI estimates.

The results are given in Figure 1 for each of the three baselines. The plots are presented as residual length obtained from VLBI vs. residual length obtained from GPS. For each set of estimates, the value of the weighted correlation coefficient is given. The weighted correlation coefficients range (in absolute value) from 0.07 to 0.94. The high correlation was obtained on the Kauai-Wettzell baseline, and it indicates that over 90% of the scatter of the length vs. time results could be explained by scatter which is common to both the VLBI and GPS length estimates. If we use the residuals in the VLBI estimates to "correct" the GPS estimates, we obtain a reduced χ^2 of 0.1. The probability of this occurring due solely to random error is less than 2.5%. This result could indicate that both the VLBI and the GPS results are dominated by a common error, e.g., atmosphere. It will be interesting to see if this correlation continues to hold as more data are obtained. Our goal is to use such correlations to isolate and eliminate errors in both techniques.

Acknowledgements

The analysis of the VLBI data was performed in part by Pan Rongshi at the Harvard-Smithsonian Center for Astrophysics. The analysis of the GPS data was performed by M. Heflin and G. Blewitt at the Jet Propulsion Lab.

Publications and Reports

Davis, J.L., G. Elgered, A.E. Niell, and I.I. Shapiro, Horizontal gradients in the "wet" atmospheric propagation delay, to appear in Proceedings of the Symposium on the Refraction of Transatmospheric Signals in Geodesy, Netherlands Geodetic Commission, The Hague, May 19–22, 1992.

Davis, J.L., The effect of turbulence on atmospheric gradient parameters determined from ground-based radiometric and space geodetic measurements, *Geophys. Res. Lett.*, *19*, 2183–2186, 1992.

Ronghsi, P., J.L. Davis, A.E. Niell, M.B. Heflin, G. Blewitt, A comparison of VLBI and GPS estimates for long baselines, paper delivered at the 1992 Fall AGU Meeting, San Francisco, December 7–11, 1992.

Davis, J.L., G. Elgered, A.E. Niell, C.E. Kuehn, Ground-based measurements of gradients in the "wet" radio refractive index of air, submitted to *Radio Science*, 1992.

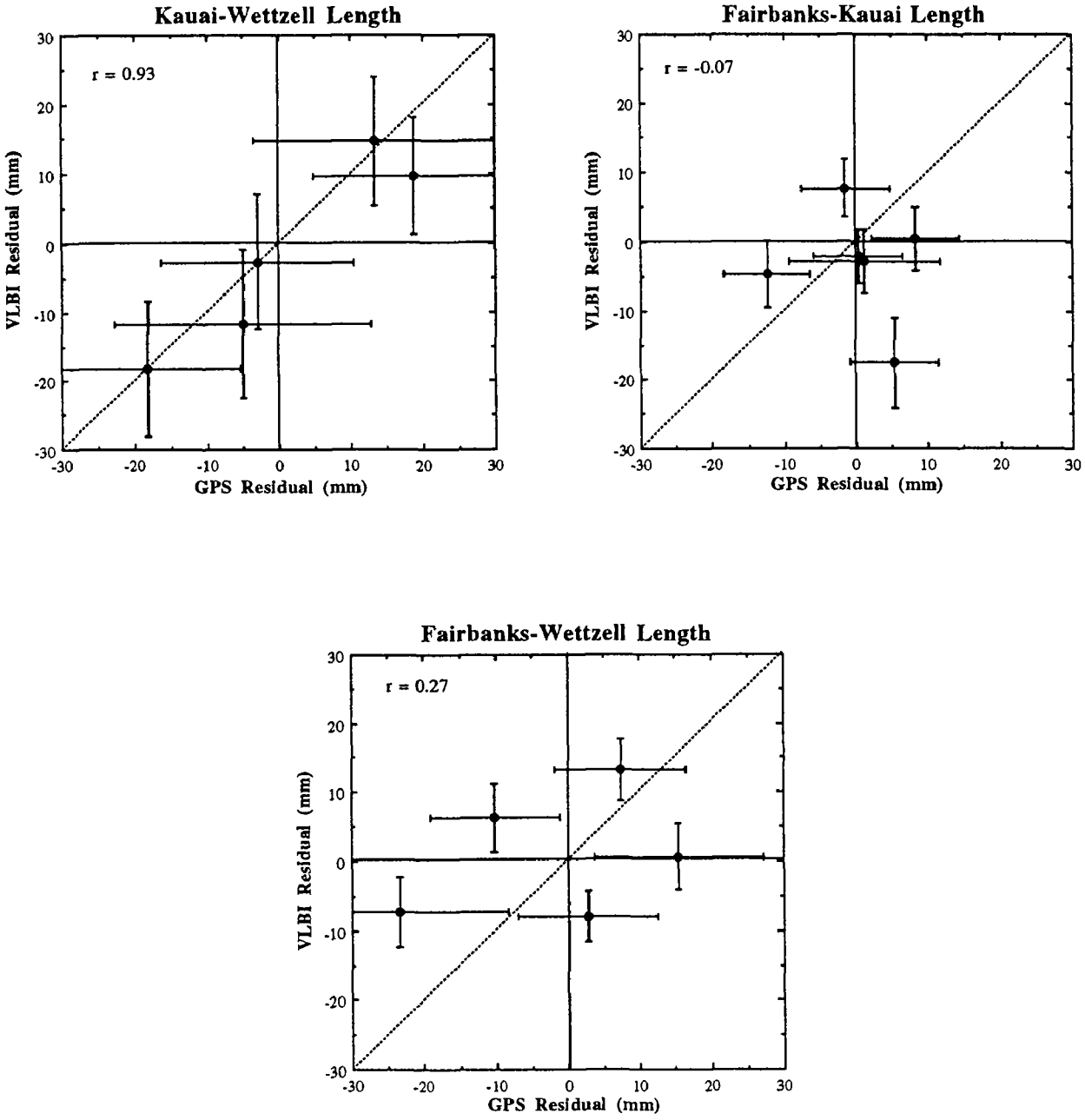

Figure 1. Plots of GPS vs. VLBI residual length (see text). Values of the weighted correlation coefficient are shown.

Reanalysis of Instrumentally Recorded United States Earthquakes

9920–10122

J. W. Dewey
and
William Spence
Branch of Global Seismology and Geomagnetism
U.S. Geological Survey
Denver Federal Center
Box 25046, Mail Stop 967
Denver, CO 80225
(303) 273–8419

Investigations

1. Describe the seismicity before and after the M_W 8.7, 1957 Aleutian arc earthquake to better understand the earthquake cycle in subduction zones. This major undertaking also will answer numerous questions concerning the size and probable rupture characteristics of this important earthquake (William Spence with extra-project colleagues T. Boyd and E. R. Engdahl).

2. Interpret the seismicity before and after the M_S 7.8, 1974 Peru earthquake to clarify the nature of subduction at this complex convergence zone (William Spence with extra-project colleague C. J. Langer).

3. Study the stress-loading process responsible for great thrust earthquakes (i.e., catastrophic slip between subducting and overriding plates at coupled subduction zones), with emphasis on understanding the relationship between seismicity patterns seaward of the trench and regional stress fields associated with the rupture of plate-coupling asperities (Steve Mueller and W. Spence with extra-project colleague G. Choy).

4. Quantify the compressional stress seaward of the asperity that controlled the M_S, 1985 Valparaiso, Chile, earthquake, and quantify the compressional stress seaward of the Shumagin seismic gap in the Aleutian arc (S. Mueller and W. Spence with extra-project colleague G. Choy).

5. Relocate epicenters, recompute magnitudes, and evaluate the tectonic implications of teleseismically recorded earthquakes from Yellowstone Park, Wyoming, and adjacent Montana and Idaho, including shocks associated with the Hebgen Lake earthquake (M_S 7.5) of August 1959 (J. W. Dewey).

Results

1. Magnitudes and relocations have been determined for nearly 7,000 earthquakes in the region of the great 1957 Aleutian arc earthquake for the period 1950–present. The catalog for the 1957 aftershocks is complete above magnitude 5.5.

2. The October 3, 1974, Peru earthquake filled a major seismic gap. Aftershocks were recorded by a temporary seismic network deployed within a week of the main shock. C. Langer and Spence have determined focal mechanisms for aftershock clusters and have relocated all aftershocks using the joint hypocenter determination (JHD) method. Focal mechanisms for aftershocks located at the shallow-dipping interface between the Nazca and overriding plates indicate continued underthrusting of the Nazca plate. Focal mechanisms for earthquakes downdip of the shallow-dipping interface indicate right-lateral, strike-slip motion on planes approximately parallel to the local plate convergence direction. This subsidiary deformation may be due to rebound of the overriding plate, as these earthquakes are associated with the location of greatest displacement during the main shock (as based on recent modeling by S. Hartzell and C. Langer).

3. It has been proposed that compressional seismicity within the outer rise complex indicates the presence of a substantial compressional stress field and, thus, and imminent great thrust earthquake near the trench axis. The modeling of Mueller, Spence, and Choy indicates that such a relationship cannot be universal. Compressional events within the subducting plate may occur in the complete absence of a compressional regional stress field, either during "unbending" of the inelastic lithosphere or the relaxation of a tensional stress field. Such a conclusion is supported by the fact that, worldwide, only 4 out of 30 hitherto identified compressional outer-rise events have actually been followed by great thrust earthquakes. Mueller et al. have developed a simple method that may allow innocuous (i.e., non-precursory) compressional outer-rise events to be distinguished from similar events that are potentially ominous.

4. Yield envelopes, which characterize lithospheric strength as a function of depth and loading history, have been used to infer the stress origin of the 20 km-deep M_S 7.2, 1981 reverse-fault earthquake that occurred at the Chilean outer trench wall. This earthquake is shown to result from stress concentration at the interplate asperity that ruptured in the M_S 7.5 Valparaiso underthrust earthquake, rather than being due to bending of the subducting Nazca plate.

5. J. Dewey completed reanalysis of 250 teleseismically recorded earthquakes that occurred in the Yellowstone/Hebgen Lake area in 1947–1989. The earthquakes were relocated with respect to calibration events recorded in the period 1973–1981 by a local network of stations run by A. M. Pitt (USGS, Menlo Park).

The relocated epicenter of the Hebgen Lake main shock of August 18, 1959 (M = 7.5 is at or near the east edge of the zone of surface faulting associated with the shock, at the margin of the zone of maximum subsidence and near the edge of the geodetically inferred fault plane. The location of the point of nucleation on the margins of, rather than within, the site of maximum moment release is consistent with observations that have recently been made on a number of large earthquakes for which accurate hypocenters and moment-release maps are available.

The zone of early aftershocks to the 1959 earthquake corresponds quite closely to the region of most intense activity in the decades following 1959. Early aftershocks occurred in a broad zone that trends west from the Norris Geyser Basin through the Hebgen Lake region to the southern Gravelly Range, Montana; most later activity has occurred in the same zone, though, with passing years, there has been a tendency for more activity to occur at greater distances outside of the 1959 aftershock zone. Dewey currently favors the hypothesis that the correspondence of later activity with the 1959 aftershock zone is due to the later activity having been part of the transient response of the Earth's crust to the 1959 earthquake.

Reports

Boyd, T.M., Engdahl, E.R., and Spence, W., 1992, Analysis of seismicity associated with a seismic cycle along the Aleutian arc—1957 through 1989 [abs.]: Wadati Conference on Great Subduction Earthquakes, Fairbanks, p. 43–50.

Dewey, J.W., and Suarez, G., 1991, Seismicity of Middle America, in Slemmons, D.B., Engdahl, E.R., Zoback, M.D., and Blackwell, D., eds., Neotectonics of North America: Boulder, Colorado, The Geological Society of America, DMV–1, p. 309–321.

Mueller, S., Choy, G.L., and Spence, W., 1992, Regional stress seaward of subduction zone asperities: Nature (submitted).

Spence, W., Herrmann, R.B., Johnston, A.C., and Reagor, G., 1992, Responses to Iben Browning's prediction of a 1990 New Madrid, Missouri, earthquake: U.S. Geological Survey Circular 1083, approximately 300 p. (in press).

Seismic Studies of Fault Mechanics

9930-02101

William L. Ellsworth
David A. Castillo, Alex Cole, and Lynn Dietz

Branch of Seismology
U.S. Geological Survey
345 Middlefield Road - MS 977
Menlo Park, California 94025
415-329-4784

Investigations

1. Analysis of preshocks, mainshock, and aftershocks of the 1989 Loma Prieta earthquake.
2. Temporal variations in wave propagation associated with the 1989 Loma Prieta earthquake.
3. Seismotectonics of the San Andreas fault system in northern California.
4. Earthquake monitoring along the Hayward fault.
5. Prototype rapid earthquake notification system for the San Francisco Bay Area.

Results

1. The standard approach to the imaging of the earthquake source solves an inverse problem in which far-field velocities (or displacements) are linearly related to the space-time distribution of slip acceleration (or velocity) on the fault through the de Hoop-Knopoff representation theorem. I am developing a complementary procedure for recovering some aspects of the rupture process that relies solely upon forward operations on the data. The basic idea is to stack the observed seismograms, with correction for the source radiation pattern, at each point of interest in the focal region to form a space/time image of the rupture. Stacking the data in this manner is equivalent to pre-multiplying the representation theorem convolution of the source time history and Green's functions with the transpose of the travel time delay operator. The stack adds coherently when the fault is radiating, as each unknown Green's function will be in phase. When no radiation is occurring at the image point, the stacked seismograms will tend to cancel due to incoherence between the Green's functions from station to station. Thus, the method works best at frequencies where the Green's functions may be considered a stochastic process. In this case, the stack will have a Gaussian distribution at times when no seismic radiation is taking place, and signal detection can be based upon their *a priori* probability of occurrence. The method is particularly well suited for use with clipped (sign bit) data. In this case, the phase but not absolute amplitude of slip acceleration (or velocity) can be determined. The computational efficency of the method make both detailed 2-D and 3-D sampling of the source volume practical.

   Application of the method to 256 heavily clipped short-period, vertical component Calnet seismograms ($1 \leq \Delta \leq 500$ km) of the 1989 Lake Elsman (M 5) and Loma Prieta (M 7) earthquakes yields detailed images of rupture nucleation and growth in the 1-10 Hz frequency band. The former is a simple rupture with a duration of about 0.8 s. In contrast,

the Loma Prieta earthquake begins with at least three acceleration pulses in the first 1.6 s ("the foreshock"), before the rupture begins to propagate away from the initial hypocentral region at a velocity of 3 km/s.

2. We use pairs of nearly identical earthquakes (doublets) to search for changes in high frequency wave propagation through the Earth's crust in the vicinity of the 1989 Loma Prieta, California earthquake, with a moving window cross-correlation technique capable of detecting traveltime changes of less than 2 msec. We analyze 36 events from 21 individual source zones, recorded during the interval 1979-1991. We find a strong change in traveltime for time windows containing the early shear wave coda for all doublets that span the Loma Prieta mainshock. The direct shear wave arrival time, however, is stable to within 1-2 msec. In each case, and for all stations that show an anomaly, traveltimes were greater after the Loma Prieta mainshock than they were before it. Time shifts exceed 35 ms at some stations, which amounts to a 0.3% path-averaged velocity change. The region of reduced velocity coincides with the aftershock zone of the earthquake, and has very sharp boundaries, particularly on its northeast side. Doublets occurring after the mainshock indicate that velocity has not recovered in the post-seismic period. Shear wave arrival times measured in the pre-seismic interval, from ten years to 4 days before the mainshock, varied by no more than 0.05%. Seismograms for pre-event doublets recorded at stations near the earthquake weakly display decreasing traveltimes in the coda, suggestive of an increasing shear wave velocity. It remains to be demonstrated, however, that this pre-seismic change has a precursory relationship to the Loma Prieta earthquake.

   We are also examining the hypothesis that temporal changes in shear wave attenuation are related to large earthquakes through the study of pairs of nearly identical earthquakes (doublets) located in the vicinity of the M_w 6.9 1989 Loma Prieta, California earthquake. The high coherency of waveforms for the doublets make them an ideal tool for searching for changes in seismic wave amplitude. By forming the spectral ratio of short windows of seismogram for each station observing the doublet, we can measure amplitudes with a precision of about 10% over a 1 Hz bandwidth from 1-15 Hz. Multiple samples of each pair of seismograms, obtained by moving the analysis window along the trace from the S-wave arrival into the coda, permit us to determine the change in coda Q (δQ_c) in multiple frequency bands and with a precision of about 5%. The measurement of δQ_c obtained in this way differs in some respects from Aki's method for determining Q_c, since our measurements utilize the near-shear wave coda waves out to about twice the shear wave traveltime, in contrast to beginning the measurement at twice the shear wave traveltime.

   Our Results indicate that Q_c is very stable over the time interval from 1978-1991. Doublets which span in time the occurence of the Loma Prieta earthquake display no evidence for systematic temporal or spatial variations in Q_c ($\pm 5\%$). These results are in sharp contrast to the large and systematic reduction in path-averaged shear wave velocity (0.3%) caused by the earthquake we have found using cross-spectral timing of the same doublet seismograms.

3. Focal mechanisms of earthquakes occuring along the northernmost and relatively youthful members of the San Andreas fault system between Point Arena and Cape Mendocino show that strike slip motion predominates both on and off of the major faults. by the San Andreas fault to the west and the Bartlett Springs fault to the east. The San Andreas fault north of Point Arena has been virtually aseismic in recent decades. In contrast, dense clusters of microearthquakes locate along . Seismicity at the northern ends of these faults zones terminates above the southern edge of the subducted Gorda Plate. Mechanisms from the Maacama and Bartlett Springs faults are dominated by right-lateral fault planes that dip 60°-80° to the northeast, rather than along vertical faults which is the norm along more mature faults within the San Andreas fault system. Although the San Andreas is virtually aseismic in this region, there are a few events located near enough to it to be on the fault, given location uncertainties, and these events have vertical nodal planes striking parallel to the fault. Focal mechanisms along and near the Maacama fault, and near the San Andreas were inverted separately to determine the orientation of the stress tensor. Both regions are in a strike slip regieme. The angle between the greates horizontal stress and the strike of the Maacama fault is 35°, suggesting a normal frictional strength for this fault. For the San Andreas fault, this angle is 60°, intermediate between high and low friction.

4. As part of the Bay Area Future Earthquakes Project, a new all-digital seismic network is being installed along the Hayward fault in the eastern San Francisco Bay region. This work is being done in cooperation with Malcolm Johnston and Paul Spudich (U.S.G.S.), and Tom McEvilly and Barbara Romanowicz (U.C. Berkeley). Downhole installation of sensors developed by Tom McEvilly at borehole strainmeter sites along the southern Hayward fault by Malcolm Johnston is now complete. Delivery of our digital field acquisition hardware and central site recording hardware has begun, and we anticipate conducting conducting acceptance tests of the hardware in early 1993.

5. A multi-year partnership has been formed between the U.S. Geological Survey and Pacific Gas and Electric Company for development and improvement of prototype rapid earthquake notification and response capabilities, initially focused on the greater San Francisco Bay region. Experience with recent California earthquakes illustrates the gap between earthquake occurrence and the delivery of accurate, appropriate seismological information to diverse private and public users. The goals of the partnership are to improve the seismological quantification of earthquakes, to speed the broadcast of this information, and to develop an increasing capability for recipients to wisely and rapidly use the notifications for knowledgeable and effective emergency response. The development strategy includes (1) maximizing the use of existing seismic resources (high-gain, short-period networks, real-time processors, broad-band and strong-motion stations); (2) integrating user requirements for information (location and severity) with scientific information (e.g., P-wave arrival times, spatial distribution of ground motion values); and (3) conducting an iterative development to assure balanced growth between user experience and acceptance, and increasingly rapid and sophisticated notification broadcasts.

Reports

Castillo, D.A., and Ellsworth, W.L., in press, Seismotectonics of the San Andreas fault system between Point Arena and Cape Mendocino in Northern California: implications for the development and evolution of a young transform: Journal of Geophysical Research, 45 p.

Ellsworth, W.L., and Heaton, T.H., 1992, Real-time analysis of earthquakes for early-warning and rapid post-event damage assessment: Proceedings Sensors Expo, Helmers Publishing, Inc. Peterborough, NH, p. 255-259.

Ellsworth, W.L., 1992, Imaging fault rupture without inversion (abs): Seismological Research Letters, v. 63, p. 73.

Verwoerd, M.C., Ellsworth, W.L., Cole, A.T., and Beroza, G.C., 1992, Changes in crustal wave propagation properties associated with the 1989 Loma Prieta, California earthquake: implications for coda-Q as and earthquake precursor and for the mechanism of stress-induced velocity changes (abs): Seismological Research Letters, v. 63, p. 71.

White, R.A., and Ellsworth, W.L., in press, Near-source short-to intermediate-period ground motions prior to the October 18, 1989 Loma Prieta M_S 7.1 earthquake: U.S. Geological Professional Paper on the Loma Prieta Earthquake, v. 1, 30 p.

Global Seismology

9920–70212

E. R. Engdahl
and
E. A. Bergman
Branch of Global Seismology and Geomagnetism
U.S. Geological Survey
Denver Federal Center
Box 25046, Mail Stop 967
Denver, CO 80225
(303) 273–8422

Investigations

1. **Travel-Time Tables.** Develop new standard global travel-time tables to locate earthquakes.

2. **Arrival-Time Data.** Coordinate planning for an International Seismological Observing Period (ISOP)—a time interval during which there would be enhanced reporting of arrival-time data.

3. **Earthquake Location in Island Arcs.** Develop practical methods to accurately locate earthquakes in island arcs.

4. **Subduction Zone Structure.** Develop techniques to invert seismic travel times simultaneously for earthquake locations and subduction zone structure.

Results

1. **Travel-Time Tables.** A major international effort within IASPEI over the last three years has led to the construction of two new global travel-time models for earthquake location and phase identification (iasp91, Kennett and Engdahl, 1991; and SP6, Morelli and Dziewonski, 1992). These radially stratified models have been constructed so that the travel times for the major seismic phases are consistent with the observations for events in the ISC Bulletin for 1964–1987. The baseline for the P-wave travel times in the iasp91 model has been adjusted to provide only a small bias in estimated origin time for independently constrained events at the main nuclear testing sites around the world. A set of algorithms has been developed (Buland and Chapman, 1983) that provides rapid calculations of the travel times of an arbitrary set of phases in these models for a specified source depth and epicentral distance.

Generally, differences in predicted travel times between the iasp91 and SP6 models are not significant—a few tenths of seconds. There are, however, certain classes of arrivals where the discrepancies are larger and the phase is important enough that the differences should be better understood. This presents a fundamental problem: exactly how lateral heterogeneity (and anisotropy) in the Earth's mantle and core contributes to the global variance in the teleseismic travel times of individual phases is not well understood. The differences between iasp91 and SP6 could therefore simply reflect the particular choices made in data selection and processing. It is quite possible that for many phases the global variance is large enough so that, for the current global data set, the two models are equally satisfactory.

To clarify these issues, a simple experiment is performed. First, a modified ISOP event-selection algorithm is applied to the ISC Catalog for 1964–1989. The selection algorithm has been designed so that selected earthquakes are not only rich in later phases, but also provide a relatively even global distribution of phase ray paths for the sampling of Earth structure. The selected events are then relocated in both models using P, pP and PKP arrivals to reduce errors in depth determination which are common for locations based solely on P-wave data. The relocation is performed for each model in an interactive manner and includes a re-identification of phases after each iteration. Since the upper and lower mantles in each model are virtually identical, the two models do not produce significantly different hypocentral parameters.

The emphasis in this work is to clarify the effects of lateral heterogeneity on the global travel times. Travel-time data for both P- and S-type phases are plotted globally over selected depth ranges to reveal effects produced by structure in different regions of the Earth. The plots clearly isolate systematics which are related to the lateral heterogeneity of the mantle. The data for direct P and S waves are surprisingly well correlated and illuminate features of the upper and lower mantle which are common to both data sets. Effects of lateral heterogeneity in the core are more problematic, as the travel times of core waves are seriously contaminated by lateral variations in the structure of the overlying mantle. Removal of these effects is a challenging problem that is now overcome only by using differential travel-time data for core phases.

2. **Arrival-Time Data.** Current seismological practice relies heavily on a complex, worldwide infrastructure, based on the efforts of thousands of people in over 100 countries, for the collection, processing, and dissemination of seismic data. Measurements reported by the existing global network of seismic observatories and compiled by agencies such as the National Earthquake Information Center (NEIC) and the International Seismological Center (ISC) have led to scientific discoveries of the first magnitude.

The accumulated observatory data continue to provide new information about earthquakes and Earth structure of fundamental importance to the Earth sciences. Yet progress toward the solution of a number of important problems in seismology is impeded largely by the lack of appropriate, globally distributed data sets. A set of important seismological problems are identified whose solutions require improvements of operational practice in the spirit of the ISOP. These problems include the detailed structure and lateral variations of major internal boundaries (e.g., the 400- and 650-km discontinuities and the core-mantle boundary), the need for improved resolution and wider sampling in tomographic studies of the Earth's three-dimensional structure, and the detection of small-scale structures deep in the Earth. Further progress on many of these problems will require the use of phases other than P. Such data are relatively scarce, not because they are weak phases, but because they are infrequently reported. The ISOP would be particularly effective in extending the sampling of later phases.

The current practice of most seismological agencies is to use the arrival times of short-period P waves to estimate earthquake origin times and hypocenters which are used in turn for such diverse purposes as analyzing seismic risk and studying Earth structure. Accurate locations are vital for many of these applications, yet it is well known that current procedures often lead to inaccurate and biased hypocenters especially in subduction zones. Additional problems may arise when inferences concerning source processes of larger earthquakes are made from the spatial and temporal offsets between the hypocentroid (point of initial rupture) and the source moment centroid, which is estimated independently from long-period waveform data. All of these problems suggest the use of phase information supplementary to P.

The enhanced reporting of times of first- and later-arriving, high-frequency seismic phases will be an important ISOP activity: first, because such data have a clear role to play in resolving important seismological issues, and, second, because the organizational structure planned for this purpose also supports a number of other ISOP initiatives which, in the long run, may have even greater significance to the Earth sciences.

Under the ISOP project, observatory personnel will receive training necessary to take advantage of the rapid spread of digital seismograph systems. The ISOP project can also serve as a stimulus for observatories to upgrade their instrumentation, communications links, and routine operations. The training and assistance which will be provided to participating seismologists and observatories represents a much-needed investment in the infrastructure of seismology, particularly in developing countries. The return on this investment will be counted in the form of a general enhancement of the quantity and quality of data available for global seismological studies of all types, in an increased capacity for seismologists in all countries to effectively monitor local seismic hazards, and in the cultivation of young seismologists of talent and energy.

3. **Earthquake Location in Island Arcs.** During the past 35 years, the central and eastern portions of the Aleutian Arc have been ruptured by two great earthquakes. The first, which occurred in March 1957 (M_W = 8.6), generated aftershocks along a 1200-km long segment of the arc, the largest length extent ever observed for an aftershock sequence. This event nucleated south of Amlia Island and ruptured bilaterally. The second occurred in May 1986. This smaller earthquake (M_W = 8.0) nucleated within a few tens of kilometers of the epicenter of the 1957 earthquake and re-ruptured a 250-km long portion of the arc. The short time span between the 1957 and 1986 earthquakes provides a unique opportunity to study a complete seismic cycle bounded by two instrumentally recorded, great earthquakes. In fact, it represents the only complete seismic cycle instrumentally observed along the Aleutian arc. Published and ongoing research activities have focused mainly on the final two thirds of this rupture cycle. To supplement our picture of the tectonic processes involved during the entire rupture cycle, to test recently proposed seismic hazard estimates, and to shed light on the connection between the seismic moment distributions observed for great earthquakes and the mechanical nature of the plate interface, a more fundamental understanding of the rupture characteristics of the 1957 earthquake and the nature of seismicity between the 1957 and 1986 earthquakes are needed.

   Seismicity recorded from 1957 through 1989 (March) with epicenters lying between 175° and 160° W have been relocated and cataloged. The relocations include epicenter-dependent, P-wave station corrections which account for near-source velocity structure. These corrections are calculated for 686 stations using a slab geometry detailed by a recent, teleseismic, travel-time study and the iasp91 travel-time model. Unless other information is available, source depths are constrained to 35 km. For events deeper than 50 km, stations corrections are not applied, and source depths are determined using both P and pP arrivals. Arrival times for earthquakes occurring between 1957 and 1963 are obtained by optically scanning of the ISS and BCIS bulletins. For this time period, magnitudes are available for only a small percentage of the relocated events. Magnitudes for as many of these events as possible are calculated using body- and surface-wave amplitudes recorded at Pasadena. For events recorded between 1964 and 1989, arrival times and magnitudes are obtained from the ISC phase tapes.

   The completed catalog consists of approximately 7,300 earthquakes. Dividing the geographical distribution of observing stations into four azimuthal zones (Europe and the Arctic, North and South America, Asia, and the South Pacific), the earthquakes are classified into one of four quality groups. Group A consists of events recorded by at least two stations in all four azimuthal zones. Group B consists of events recorded by at least two stations in three of the four azimuthal zones. Group C consists of events recorded by at least one station in three of the four azimuthal zones. Group D consists of all those events not meeting the requirements of groups A, B, or C. All events within groups A and B, 3,200, have 90 percent error vectors of less than 25 km. Catalog entries for earthquakes with groups A and B have been distributed on a CD–ROM.

The minimum magnitude of completeness for this catalog is determined by plotting the number of events per magnitude increment. For this comparison, all of the observed magnitudes are converted to M_S using a regression relationship derived from events for which both m_b and M_S are available. The log of the number of events per 0.2 M_S magnitude unit is plotted. The distribution of the events per incremental magnitude unit should be linear above the magnitude of completeness. Between 1964 and 1989, the catalog is complete above $M_S = 4.6$. From 1957 through 1963, the minimum magnitude of completeness is 5.5. To uniformly sample the seismic record over the entire time period of our catalog, only events larger than or equal to 5.5 can be used. Also, earthquakes whose magnitudes are above the level of completeness for each time period can be expected to be well located.

4. **Subduction Zone Structure.** Compressional body waves from earthquakes in the central part of the Tonga-Kermadec subduction zone arrive very early in New Zealand stations (Ansell and Gubbins, 1986), and the waveforms of these phases are often characterized by an emergent high-frequency precursor. Examples of these slab phases have been collected from short-period seismograms of SRO station SNZO in Wellington, and from Leeds' POMS array of nine 3-component broad-band seismometers in the Tararua Mountains, New Zealand.

   Gubbins and Snieder (1991) explained both the early arrivals and the body-wave dispersion by P-wave propagation through a high-velocity layer in the Tonga-Kermadec subduction zone. The absence, however, of detailed information about the morphology of the Tonga-Kermadec subduction zone prohibited the establishment of the relation between slab structure and observed waveforms.

   With the objective to further investigate the relation between the frequency characteristics of the digital seismograms and propagation through subducted slab, a tomographic study is performed to determine the morphology of the Tonga-Kermadec subduction zone. For the tomographic study, an approach similar to that described by Van der Hilst et al. (1991) is followed. The earthquakes are relocated in the iasp91 model for P- and S-wave velocities (Kennett and Engdahl, 1991) and computed travel-time residuals for P and pP phases relative to the iasp91 travel-time tables computed. In the linear inversion for aspherical Earth's structure, about 1,100,000 P and 35,000 pP data were used. By incorporating data of the pP phase, the sampling of shallow slab structure is improved, in particular below regions where only few seismological stations are located. New tomographic images depicting aspherical variations in P-wave velocity associated with the Tonga-Kermadec subduction zone are constructed.

Reports

Hwang, L.J., and Clayton, R.W., 1991, A station catalog of ISC arrivals—Seismic station histories and station residuals: U.S. Geological Survey Open-File Report 91–295, 3187 p.

Kennett, B.L.N., and Engdahl, E.R., 1991, Travel times for global earthquake location and phase identification: Geophysical Journal International, v. 105, p. 429–465.
Van der Hilst, R.D., and Engdahl, E.R., 1991, On the use of PP and pP data in delay time tomography: Geophysical Journal International, v. 106, p. 169–188.
Van der Hilst, R.D., Engdahl, E.R., Spakman, W., and Nolet, G., 1991, Tomographic imaging of subducted lithosphere below northwest Pacific island arcs: Nature, v. 353, p. 37-42.

Teleseismic Tomography of the Loma Prieta Region

Project 9930-01172

John R. Evans and H. M. Iyer
U.S. Geological Survey
Branch of Seismology
345 Middlefield Road, MS-977
Menlo Park, California 94025
415-329-4753

Investigations Undertaken

This Project is completing a teleseismic tomography study of the Loma Prieta region, using data we recorded late in 1990 in a large field experment. Data from this experiment also have been used by other Projects for local-earthquake tomography. This FY was consumed by extensive software development and the massive data-reduction process.

Early parts of FY 1992 also included an extended operational test of our PC-based trigger for teleseisms. Our aim was to ready the PC for assisting the capture of these events by CUSP. We successfully demonstrated the efficacy of this system for reliably capturing even very small teleseisms and for assisting with network maintenance and the capture of rare low-frequency local earthquakes known to occur beneath several parts of the network.

Results Obtained

Loma Prieta: Understanding the lower crust and upper mantle provides NEHRP with boundary conditions and structural information prerequisite to any master model of this transverse plate-boundary system. Understanding the detailed structure and state of the lower crust and upper mantle below the depths resolvable by local-earthquake tomography is necessary for understanding that fraction of the plate boundary that is responsible for earthquake hazards. Loma Prieta teleseismic tomography targets the source region of the 1989 earthquake to clarify the condition and location of the controlling plate boundary and to delineate the root structure of the imbricate thrust system bounding the Santa Clara Valley. This thrust system is now recognized as both a major, poorly understood structural feature and as a significant seismogenic zone in its own right.

We operated a 31-site portable seismograph network through December, 1990. This network augmented CalNet in the target region around Loma Prieta, forming nested oval shaped networks centered on the seismogenic zone. Three types of seismographs were used in this study, but most of the the data were recorded by the old "5-day" recorders. Digitizing and processing these data is very labor intensive and again consumed most of our efforts in FY92. At this writing, the data are 100% digitized and 50% analysed. Reaching this point has consumed about 2.5 person-years of effort. The USGS currently owns no other equipment suited to this type of work, and must rely on IRIS equipment for which NSF-funded projects take precedence. Three GEOS recorders tested at Loma Prieta recorded fewer than half the requisite events.

CUSP Teleseismic Triggering: In the first half of FY 1992 we performed an extended operational test of a PC-based trigger for teleseisms. CUSP routinely fails to capture most of these events; our aim was to use the PC as a specialized trigger to assist CUSP. We successfully demonstrated the efficacy of this system for reliably capturing even very small events while maintaining acceptable false-alarm rates. It is now clear that network telemetry glitches are a principal contributor of the false alarms that do occur. These glitches generally do not trigger CUSP, hence, the PC can assist technicians with identifying network trouble spots in addition to capturing teleseisms. Our PC teleseism effort was discontinued on Branch Chief orders, in lieu of planned changes directly to CUSP algorithms. No system is now in place for recording teleseisms reliably. Instead, we are investigating the efficacy of this system for capturing rare low-frequency events that occur in several parts of CalNet.

We have captured four of the five low-frequency events in the last six months at Mammoth Mountain, even recording a very small one missed in a scan by the best analyst the USGS has (Figure 1).

Reports Published

No reports were produced in FY92, excepting our contribution to W. H. K. Lee's Open-File Report of PC software. Most resources were applied to processing the largest teleseismic tomography data set yet collected by this Project, to software development, and to testing the PC teleseismic trigger system for CUSP. Data reduction was hampered seriously by Branch reassignment of a principal technician to other Projects.

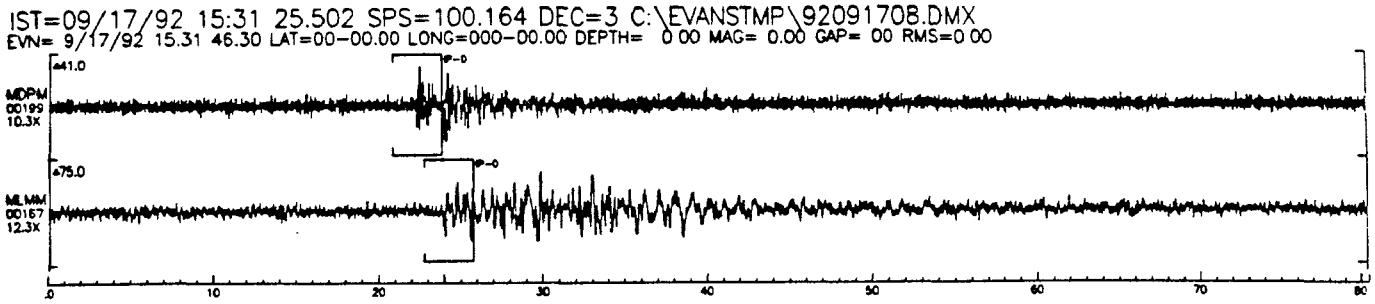

This low-frequency event occurred during a film change but triggered the PC successfully.

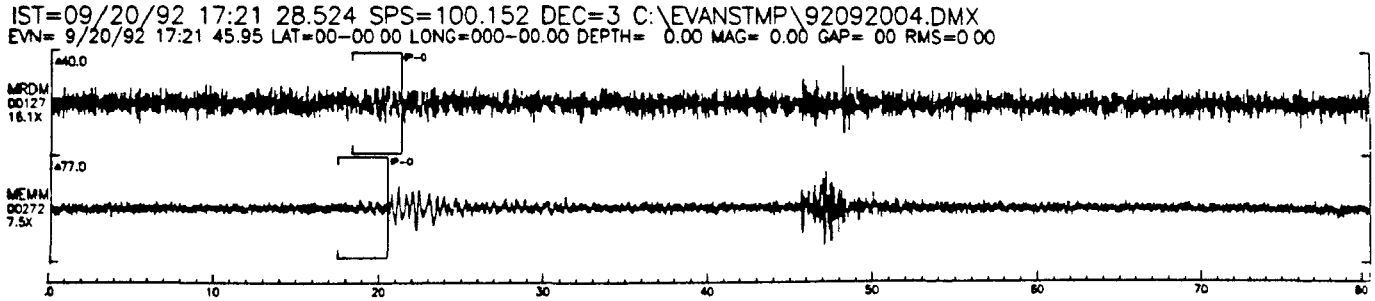

A very small low-frequency event missed by analyst.

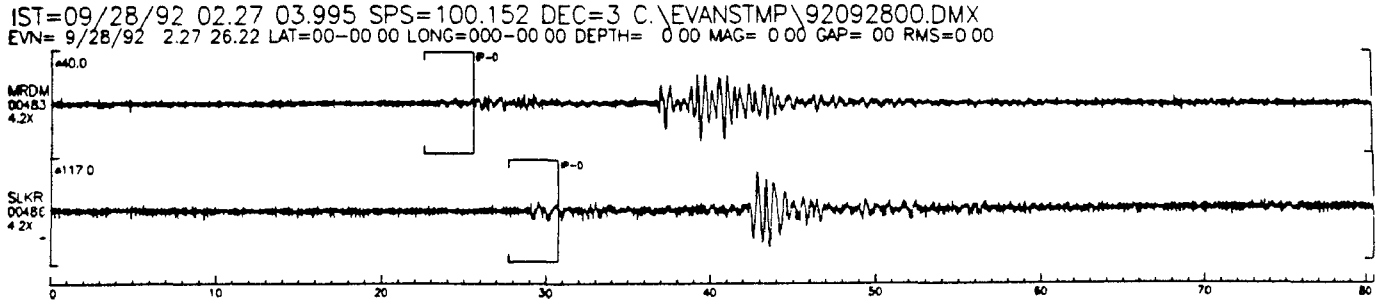

Both the analyst and the PC found this event pair.

PC missed a large low-frequency event at 09/28/92 03:12, probably disregarding it because of its modest high-frequency component. (The trigger attempts to discard high-frequency local earthquakes to avoid swamping the recording system.) The analyst found it easily; trigger parameters have been modified accordingly.

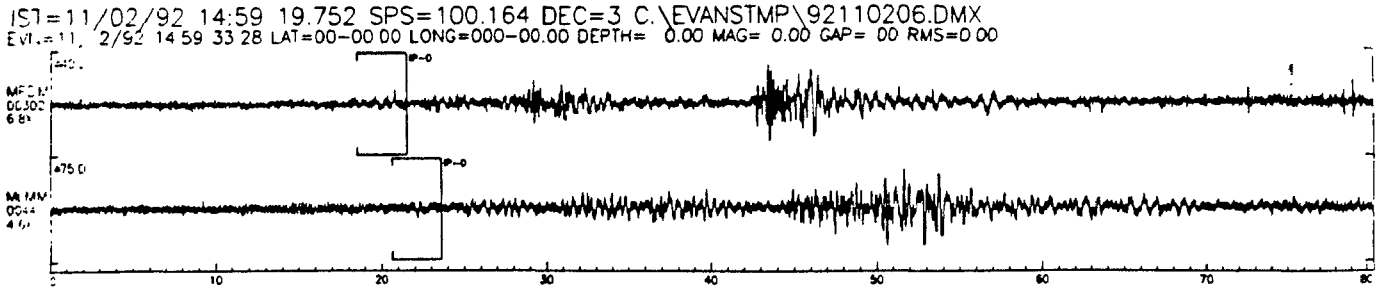

Both the analyst and the PC found this event.

Figure 1: Examples of the small low-frequency earthquakes occurring near Mammoth Mountain, east central California. These mid-crustal events are thought to be associated with the movement of magma.

THEODOLITE MEASUREMENTS OF CREEP RATES ON SAN FRANCISCO BAY REGION FAULTS

Grant Number 14 - 08 - 0001 - G1992

Jon S. Galehouse
Department of Geosciences
San Francisco State University
San Francisco, California 94132

(415) 338-1204

We began to measure creep (aseismic slip) rates on San Francisco Bay region active faults in September 1979. Over the past 13.2 years, we have made nearly 1300 creep measurements, with about 450 of these occurring in the three years following the Loma Prieta earthquake (LPEQ). Amount of slip is determined by noting changes in angles between sets of measurements taken across a fault at different times. This triangulation method uses a theodolite to measure the angle formed by three fixed points to the nearest tenth of a second of arc. Each day that a measurement set is done, the angle is measured 12 times and the average determined. The amount of slip between measurements can be calculated trigonometrically using the change in average angle. The precision of our measurement method is such that we can detect with confidence any movement more than 1-2 mm between successive measurement days.

We presently have measurement sites at 23 localities on active faults in the San Francisco Bay region (see Figure 1). We also have a measurement site on the San Andreas fault in the Point Arena area and one on the Maacama fault in Willits that do not appear on Figure 1. We remeasure most sites about once every two to three months. Most sites span a fault width of about 50-225 m, but a few must span a greater width because of site considerations. These distances are noted on Figures 2 through 5 as the IS (Instrument Station) to ES (End Station) distances. These figures also show the average rate of movement at each site as determined by the slope of the least-squares line which also appears on each of the graphs. The graphs also show the time of the 17 October 1989 LPEQ as a vertical line. The following is a brief fault-by-fault summary of our results through 30 November 1992.

SAN ANDREAS FAULT (see Figure 2) - We have been measuring horizontal slip on the San Andreas fault at Site 14 at the Point Reyes National Seashore Headquarters for 7.7 years and at Site 10 in South San Francisco for 12.7 years. Both sites have shown virtually no net slip and neither was affected by the LPEQ thus far.

In November 1989, we began measuring a USGS site (our Site 22) in Woodside that had not been remeasured for many years. Our results compared to unpublished USGS measurements in 1977 show that virtually no surface slip occurred between 16 February 1977 and 4 November 1989 and very little has occurred since. We also established in November 1989 Site 23 on the San Andreas fault near the

southeastern end of the LPEQ aftershock zone and northwest of San Juan Bautista. Very little slip has occurred at this site.

In July 1990, we established Site 25 on the San Andreas fault just southeast of San Juan Bautista and the aftershock zone. This site is on the central creeping portion of the fault and has been moving at a rate of 14.5 mm/yr for the past 2.2 years. This is considerably faster than the longer-term pre-LPEQ rate of about 7-8 mm/yr as determined by a USGS creepmeter at this site (Schulz, 1989).

Site 18 in the Point Arena area has averaged 1 mm/yr of right slip in the 11.1 years between 9 January 1981 and 31 January 1992.

In summary, the San Andreas fault at our measurement sites (18, 14, 10, 22, 23) along the previously locked portion of the fault both northwest and southeast of the LPEQ aftershock zone does not appear to have been affected by the LPEQ in the three years since October 1989. This portion of the San Andreas fault has remained virtually locked, with 1 mm/yr or less of creep occurring along it. In contrast, the post-LPEQ creep rate on the northern portion of the central creeping segment of the fault near San Juan Bautista is about twice the longer - term creepmeter average.

HAYWARD FAULT (see Figure 3) - We have been measuring horizontal slip at five sites along the Hayward fault for 12.2 to 13.2 years and have determined that the overall right-lateral creep rate is about 4.3 to 4.8 mm/yr. Although the creep characteristics (steady or episodic) differ from site to site, the overall rates are quite similar. A detailed discussion of the pre-LPEQ and post-LPEQ creep rates on the Hayward fault is in Galehouse (1993).

Since we began measuring Site 1 in Fremont in September 1979, the fault has moved rather episodically. Typical surface movement characteristics are relatively rapid right slip of about a cm over a few months time alternating with relatively slower slip over a period of two or more years. The fault at Site 1 was in one of the relatively slower phases of movement prior to the LPEQ and the slower phase has now persisted for about 4.5 years with virtually no net slip during this time. The creep rate before the LPEQ was 5.4 mm/yr but this present slow phase has brought the overall average down to 4.7 mm/yr for the past 13.2 years.

In February 1990 we established Site 24 on the Hayward fault on Camellia Drive in Fremont, about four km southeast of Site 1 (see Figure 1). Although relatively rapid creep had been reported for this site in recent years, we have measured virtually no creep at all. Perhaps the fault at this site moves episodically (similarly to nearby Site 1) and has been in a slower, dormant phase since we began measuring it 2.8 years ago.

Movement along the Hayward fault at Site 2 in Union City has been much more continuous and much less episodic than movement at Site 1. Site 2 has been moving at a fairly uniform rate of about 4.6 mm/yr for the 13.2 years since we began measurements in September 1979.

Extremely uniform movement characterizes Site 12 on D Street in Hayward. Two active traces of the Hayward fault occur here and their combined movement rate has been about 4.6 mm/yr for the 12.4 years since we began measurements in June 1980. Our nearby Site 13 on Rose Street in Hayward has a similar overall average rate of movement (4.8 mm/yr) since June 1980, but the movement is much more episodic than at Site 12.

In the 12.2 years since we began measurements in August 1980 in San Pablo (Site 17) near the northwesterly end of the Hayward fault, the overall average rate of

right slip (about 4.3 mm/yr) has been slightly slower, but similar to the overall rates at the other Hayward fault sites. However, superposed on the overall slip rate in San Pablo are changes between some measurement days of up to nearly a cm in either a right-lateral (more common) or left-lateral (less common) sense. This pattern was more pronounced between mid-1980 to mid-1986 and has been somewhat less pronounced since.

In summary, the creep rates on the Hayward fault from Union City to San Pablo are about the same as they were before the LPEQ. However, the southern portion of the fault in Fremont has shown virtually no post - LPEQ net slip.

CALAVERAS FAULT (see Figure 4) - We have been measuring horizontal slip at two sites on the Calaveras fault in the Hollister area for 13 years. Slip at both sites has been rather episodic with intervals of relatively rapid right slip typically lasting a couple months or less alternating with longer periods of time when little net slip occurs. The LPEQ occurred during an interval of slower movement that had persisted for about a year at Site 4. The earthquake apparently triggered up to 14 mm of right slip at Seventh Street (see Figure 4). Overall the rate of right slip is about 7.1 mm/yr for the past 13.1 years.

Slip at Site 6 along Wright Road just 2.3 km northwest of Site 4 is also episodic. The LPEQ occurred during an interval of slower movement that had persisted for about a year at Wright Road (similar to the situation at Seventh Street). The earthquake apparently triggered up to 12 mm of right slip. The overall rate of slip at Wright Road is about 11.0 mm/yr for the past 13.0 years. Except for our relatively new site (25) on the central creeping portion of the San Andreas fault, this rate is the fastest of any of our sites in the San Francisco Bay region. It is about 4 mm/yr faster than the rate at nearby Seventh Street. Either the creep rate decreases significantly from Wright Road southeast to Seventh Street or undetected surface movement is occurring outside our 89.7 m-long survey line at Seventh Street.

After the rapid slip triggered by the LPEQ, both sites in the Hollister area returned to a slower mode of movement which has now persisted for more than three years. At the present time, there appears to be a "slip deficit" of about 2 cm at Site 6. A more detailed discussion of the effect of the Loma Prieta earthquake on the Calaveras fault in the Hollister area was published in Geophysical Research Letters shortly after the quake (Galehouse ,1990). This paper also discusses the effect of the Morgan Hill earthquake in 1984. No immediate surface displacement had occurred at either of our Hollister area sites when they were measured the day after the Morgan Hill earthquake. However, within the following 2.5 months, both sites showed over a cm of right slip which was followed by a relatively long interval of slower slip (see Figure 4). A more detailed discussion of the longer-term effect of the LPEQ on the Calaveras fault is in Galehouse (1993).

In contrast to our sites in the Hollister area, Site 19 in San Ramon near the northwesterly terminus of the Calaveras fault was not affected by the LPEQ. It has remained virtually locked throughout our 12.0 years of measurements.

CONCORD - GREEN VALLEY FAULT (see Figure 5) - We began our measurements at Site 3 and Site 5 on the Concord fault in the City of Concord in September 1979. It appears that typical movement characteristics at both sites are intervals of relatively rapid right slip of about 7-10 mm over a period of a few months alternating with intervals of relatively slower right slip of about 1-2 mm/yr over a period

of several years. For the past 13 years, the overall average creep rate along the Concord fault in the City of Concord is about 3 mm/yr (3.4 at Site 3 and 2.6 at Site 5).

It appears that the LPEQ and the 1990 swarms of earthquakes near Alamo (between the southeastern end of the Concord fault and the northwestern end of the Calaveras fault) had little or no effect on the Concord fault at our measurement sites in the City of Concord.

We began measuring Site 20 on the Green Valley fault near Cordelia in June 1984. Large variations tend to occur at this site between measurement days, possibly because logistical considerations resulted in our survey line being particularly long (335.8 m). However, our results suggest that the Green Valley fault behaves similarly to the Concord fault i.e., relatively rapid right slip in a short period of time (months) alternating with relatively slower slip over a longer period of time (years). The Green Valley fault was in a period of relatively slower movement for the first 20 months of our measurements, averaging a few mm/yr of right slip. In early 1986, however, the fault slipped right-laterally more than a cm. This was followed by about three years in which the net slip was less than 1 mm/yr. Sometime after 6 August 1989, the Green Valley fault entered into another phase of relatively rapid right slip that totaled about 15 mm by 22 April 1990. For the past 2.5 years, there has been virtually no net slip on the Green Valley fault. The overall average rate of movement has been 5.3 mm/yr for the past 8.4 years.

Regarding the relationship between the Green Valley and Concord faults, the episodes of relatively rapid slip and relatively slower slip do occur at different times and the rate of slip is higher on the Green Valley fault. The episodic nature of the slip and the duration of the faster and slower intervals, however, are similar. Based on these similarities and the small step between their respective trends, we consider the Concord and Green Valley faults to be different names for the southeastern and northwestern segments of the same fault system.

RODGERS CREEK FAULT - We measured a site (16) on the Rodgers Creek fault in Santa Rosa from August 1980 until we had to abandon it for logistical reasons in January 1986. During these 5.4 years of measurements, no significant surface slip occurred and we concluded that the Rodgers Creek fault was not creeping at this site.

In September 1986, we established Site 21 on the Rodgers Creek fault near Penngrove (see Figure 1). The average at Site 21 is about 1-2 mm/yr for the past 6.1 years. Because variations of several mm tend to occur from one measurement day to another, it is difficult to know whether the Rodgers Creek fault is really creeping slowly or whether it is not moving much at all and our average rate at this point in time is due to the "noise" level at this particular measurement site. Perhaps the results will become less ambiguous as we continue our measurements over a longer period of time. The LPEQ does not appear to have had any effect on the Rodgers Creek fault at Site 21.

WEST NAPA FAULT - We began measurements at Site 15 in the City of Napa in July 1980. Similarly to the situation at Site 21 on the Rodgers Creek fault, there tends to be a lot of surface "noise" at this measurement site. However, the average rate of right slip on the West Napa fault over the past 12 years is only 0.4 mm/yr. In other words, the West Napa fault is virtually locked at the surface with no creep occurring. The LPEQ does not appear to have had any effect on our results for the West Napa fault.

SEAL COVE-SAN GREGORIO FAULT - We began measurements at Site 7 on the Seal Cove fault segment in Princeton in November 1979. The least-squares average indicates that virtually no creep has occurred at this site over the past 13 years. We began measuring Site 8 on the San Gregorio fault segment in May 1982. This site shows very large variations from one measurement day to another, probably due in part to the particularly long distance (452 m) between the IS and ES. The least-squares average shows no creep for the past 10.5 years. Therefore, the Seal Cove-San Gregorio fault is not presently creeping and the LPEQ does not appear to have had any noticeable effect on the rate of movement at either of our sites on this fault system.

ANTIOCH FAULT - We began measurements at Site 11 in the City of Antioch in May 1980. The average rate of movement has been virtually zero for the past 12.5 years. Site 9 just south of town showed 1.7 mm/yr for the 7.6 years from 21 November 1982 to 1 July 1990. New construction then destroyed our measurement array at this site. We have noted that much subsidence and mass movement creep occur both inside and outside the Antioch fault zone in the area of our two measurement sites and it is probable that these nontectonic movements are influencing our measurement results. If any tectonic creep is occurring along the Antioch fault, it is probably at a very low rate. The LPEQ does not appear to have had any noticeable effect at either of our sites on the Antioch fault.

MAACAMA FAULT - The Maacama fault extends from northern Sonoma County to north of Laytonville in Mendocino County and is the northwesterly continuation of the Hayward-Rodgers Creek fault trend. We began measurements at Site 26 in Willits in November 1991. Preliminary results over the past year indicate that the Maacama fault is creeping at about 5 mm/yr which is similar to the creep rate on the Hayward fault.

REFERENCES CITED

Galehouse, J.S., 1990, Effect of the Loma Prieta earthquake on surface slip along the Calaveras fault in the Hollister area: Geophysical Research Letters, v. 17, no. 8, p. 1219-1222.

Galehouse, J.S., 1993, Effect of the Loma Prieta earthquake on fault creep rates in the San Francisco Bay region: in U.S. Geological Survey Professional Paper (Postseismic Effects), in review.

Schulz, S.S., 1989, Catalog of creepmeter measurements in California from 1966 through 1988: U.S. Geological Survey Open-File Report 89-650, 193 p.

1992 PUBLICATIONS

Galehouse, J.S., 1992, Creep rates and creep characteristics on certain North and East Bay faults: 1979-1992: Program and Abstracts, Second Conference on Earthquake Hazards in the Eastern San Francisco Bay Area, p. 24.

Galehouse, J.S., 1992, Creep rates and creep characteristics of Eastern San Francisco Bay Area faults: 1979-1992: in Borchardt, G. and others, editors, Proceedings of the Second Conference on Earthquake Hazards in the Eastern San Francisco Bay Area, California Division of Mines and Geology Special Publication 113, in press.

Lienkaemper, J.J., Galehouse, J.S., and Simpson, R. W., 1992, Hayward fault, California: longterm creep rates versus slower creep since 1989 Loma Prieta earthquake: EOS, Transactions, American Geophysical Union, v. 73, no. 43, p. 119.

Galehouse, J.S., Sowma-Bawcom, J.A., and Prentice, C.S., 1992, The Maacama fault: preliminary creep and paleoseismic data, Mendocino County, California: EOS, Transactions, American Geophysical Union, v. 73, no. 43, p. 123.

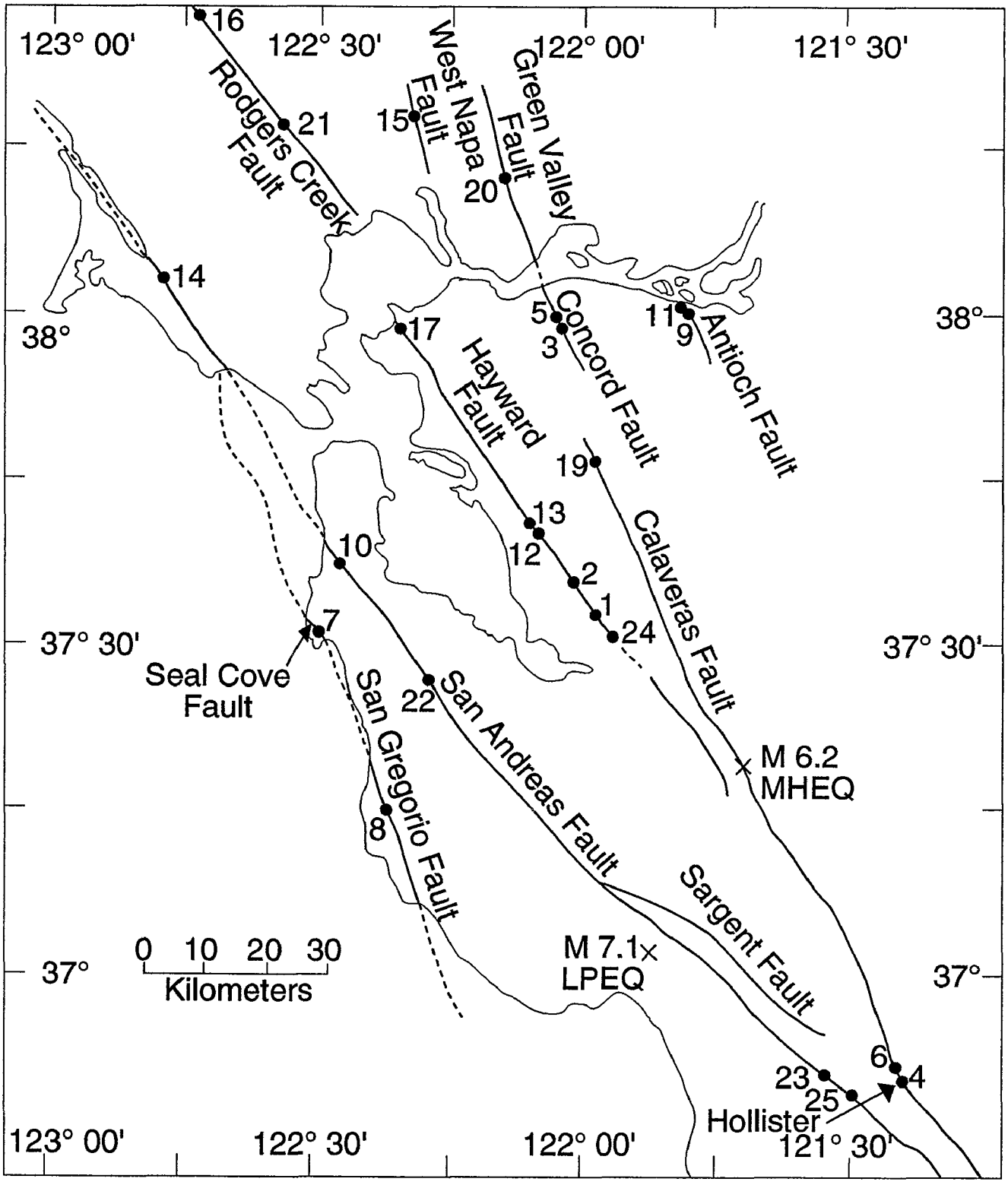

Figure 1. Numbered dots are San Francisco State University theodolite measurement sites. Epicenters and magnitudes are indicated for the 24 April 1984 Morgan Hill earthquake (MHEQ) and the 17 October 1989 Loma Prieta earthquake (LPEQ).

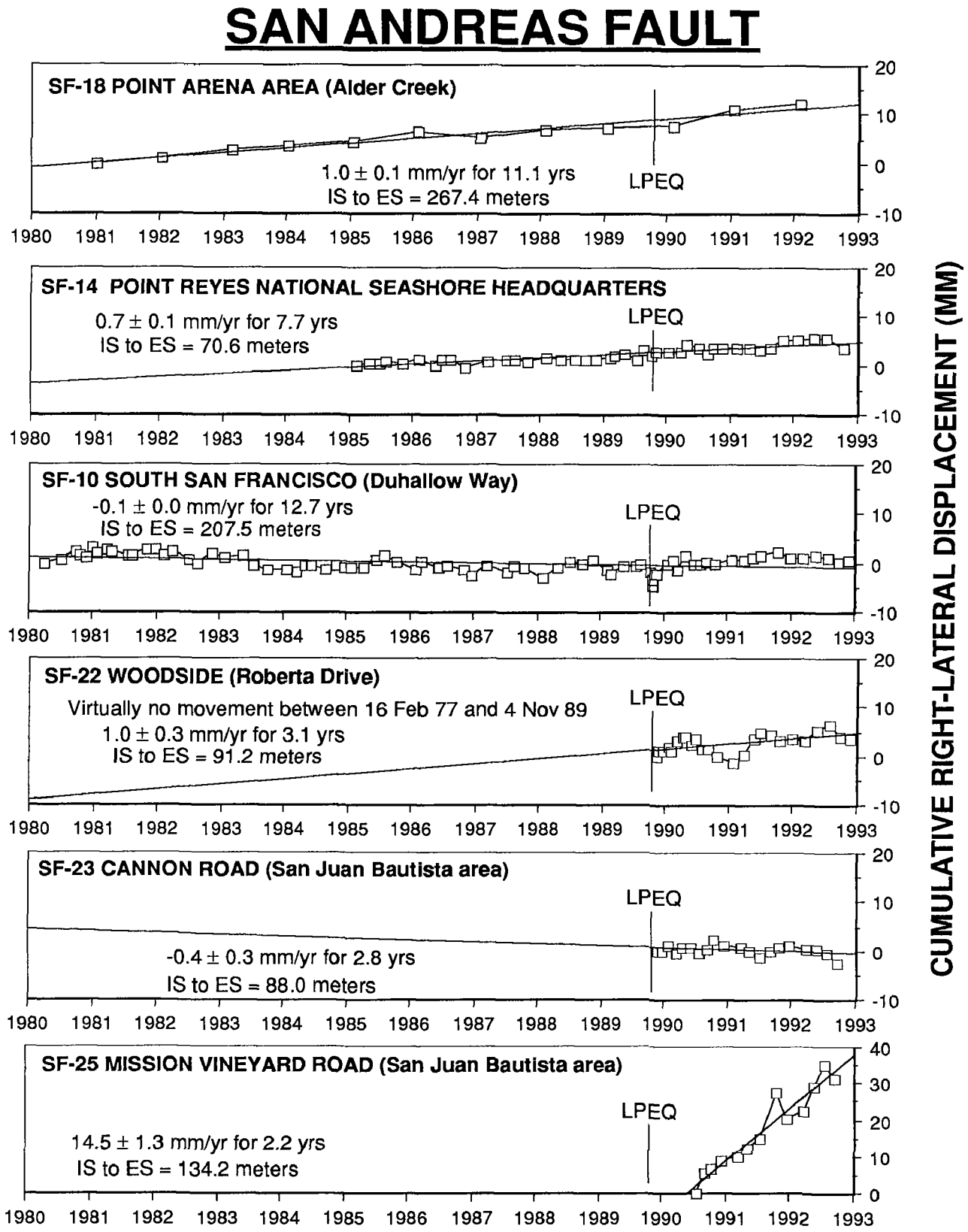

Figure 2. San Andreas Fault Displacement (1980 - 1992)

HAYWARD FAULT

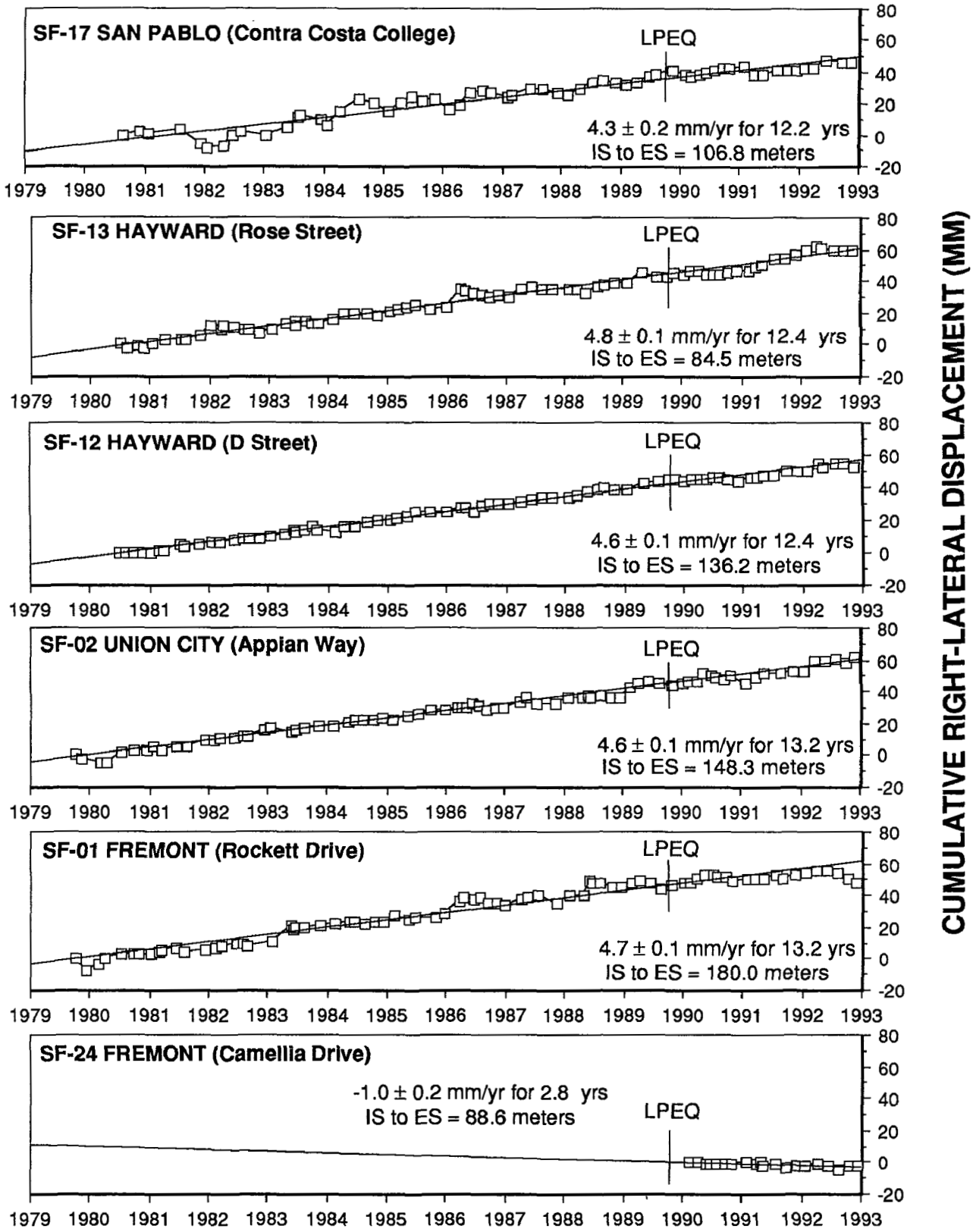

LPEQ = Loma Prieta Earthquake of 17 Oct 89

Figure 3. Hayward Fault Displacement (1979 - 1992)

CALAVERAS FAULT

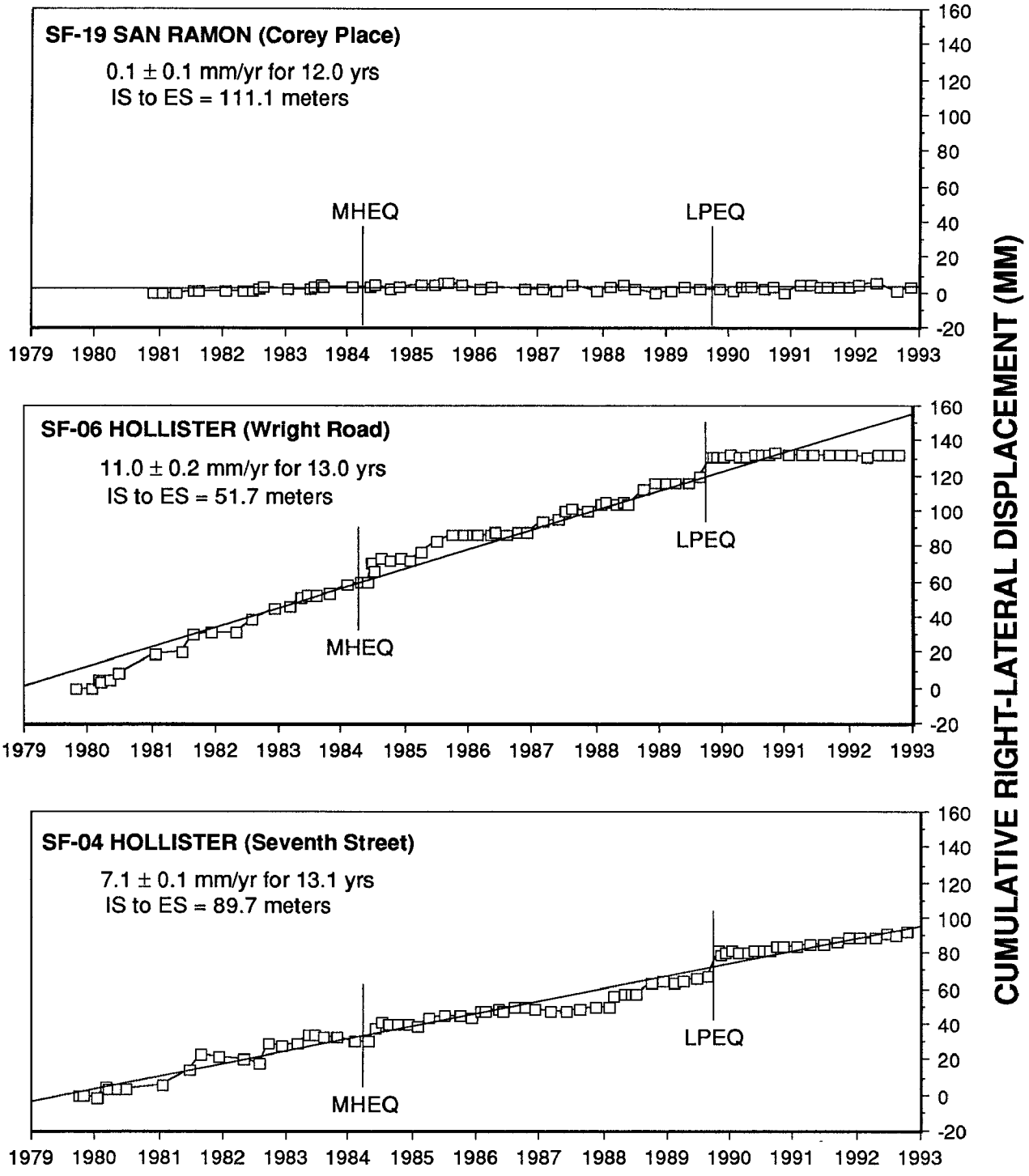

MHEQ = Morgan Hill Earthquake of 24 Apr 84
LPEQ = Loma Prieta Earthquake of 17 Oct 89

Figure 4. Calaveras Fault Displacement (1979 - 1992)

CONCORD - GREEN VALLEY FAULT

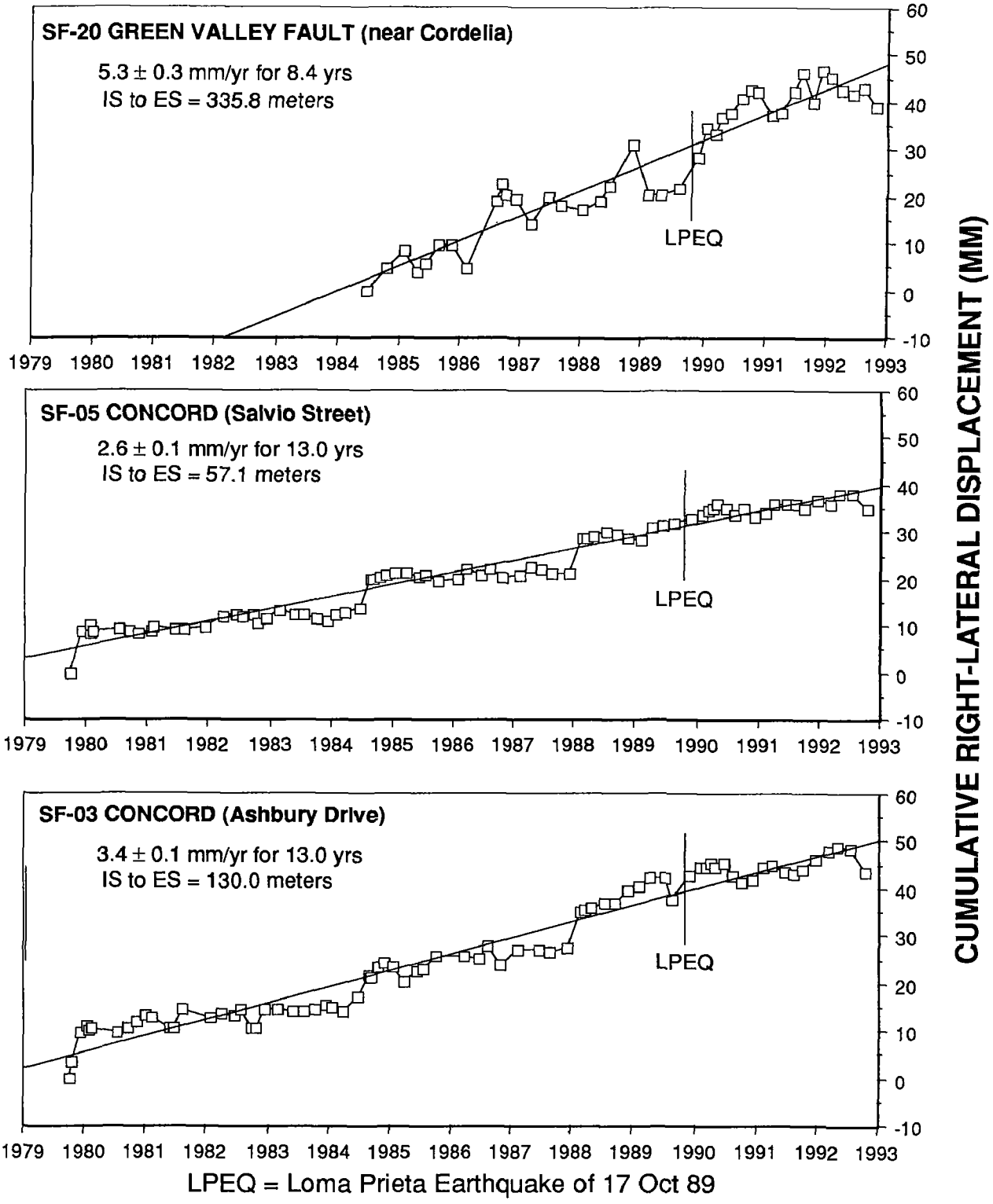

Figure 5. Concord - Green Valley Fault Displacement (1979 - 1992)

DEEP BOREHOLE PLANE STRAIN MONITORING
14-08-0001-G1812

Michael T Gladwin,

Department of Physics
University of Queensland
St.Lucia, 4067
AUSTRALIA.
ph. (+ 617) 3652473

ACTIVITIES

Two data processing procedures were refined further during 1992. Removal of dual exponentials (one of short time constant relating to grout cure effects and a long time constant exponential related to long term hole deformation processes) has been successfully implemented for data from the San Juan instrument. This procedure has been extended to the consideration of long term strain data from other U.S instruments, one at Pinon Flat (PFT) and three at Parkfield (EDT, FLT and DLT). Such a process is generally feasible, and yields residuals which give a much clearer picture of medium term strain anomalies present in the data. The tidal calibration procedure developed for analysis of the San Juan dataset has been extended to data from Parkfield (EDT and DLT), and will be used routinely in data reported from these sites. A paper detailing this calibration procedure is under preparation, in conjunction with D. Agnew and F. Wyatt from U.C.S.D., who are incorporating a comparison of tidal calibration of our Pinon Flat data with data from the laser strainmeter also located at that site.

The Pinon Flat instrument has registered strain steps associated with a number of earthquakes in that region during 1992. In particular strain steps coseismic with the Joshua Tree earthquake M_L 6.1 (April 23) and the Landers M_L 7.4 and Big Bear M_L 6.5 earthquakes (June 28) were inverted to determine most likely source dislocation parameters using seismically determined locations.

A detailed review of strain data from the three Parkfield instruments has been undertaken for inclusion in the special Parkfield review session of the Fall 1992 AGU. In particular coseismic steps associated with the M_L 4.7 Middle Mountain earthquake of 28 October, a series of strain steps correlated with nearby creepmeter events, a significant event common to both Eades and Donalee data during April 1989, and long term strain changes on all three instruments have all been investigated.

During November two further tensor strain instruments were installed as part of a borehole strain array situated in the vicinity of the Hayward fault east of San Francisco Bay. These instruments have been providing data (initially dominated by grout curing effects) since November 1, and data from these is now being processed as part of the routine processing of all U.S. instruments. Calibration of data from these two sites, one near Lake Chabot (CHT) and one in Garin State Park (GAT), will be conducted after some months of settling.

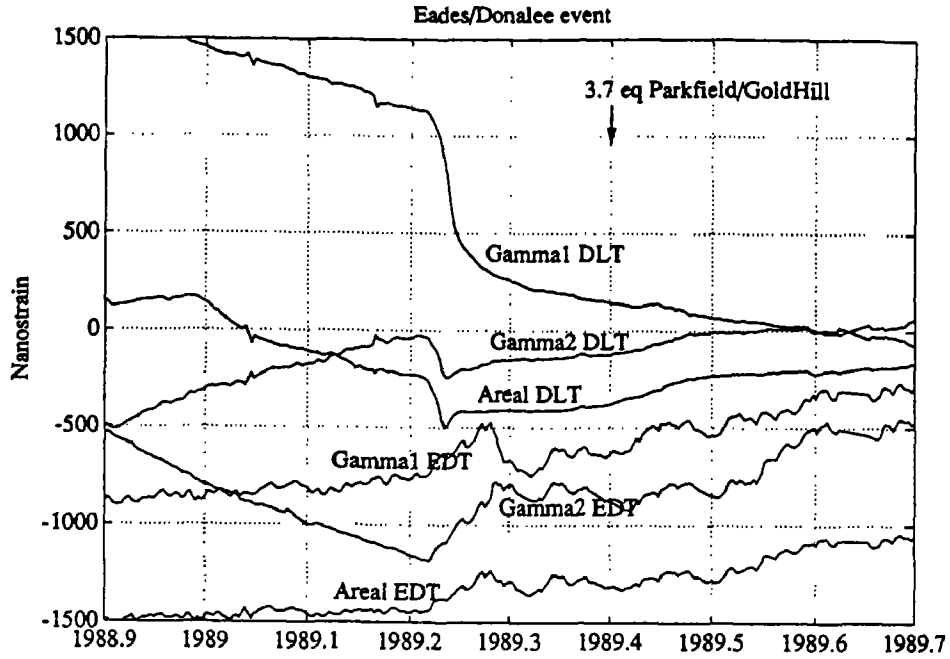

Figure 1. Detrended strain data from Eades and Donalee tensor strain instruments during 1989. The time of the M_L 3.7 earthquake is indicated.

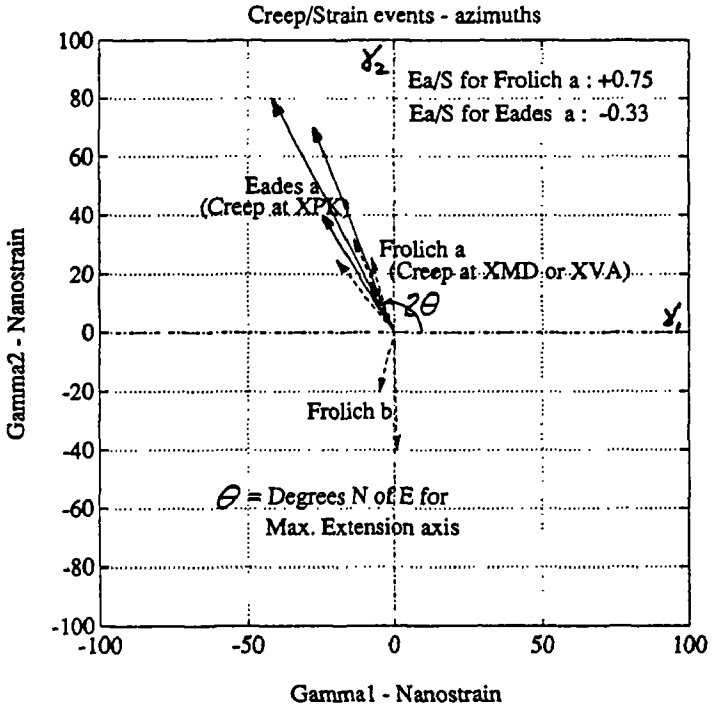

Figure 2. Plot of some representative strain steps during 1991-92 at Eades and Frolich. For each step, shear strain γ_1 is plotted against γ_2. The resulting vector has length corresponding to the size of the maximum shear strain, and orientation 2θ where θ = azimuth of the maximum extension axis north of east. Note the similarity of maximum shear and azimuth for the three groups Eades(a), Frolich(a) and Frolich(b).

RESULTS

Two papers were published during the year. In the first paper we analysed the continued shear strain anomaly in SJT data following the Loma Prieta earthquake, and proposed that the observed strain accumulation results from increased slip around a nearby locked section of the fault, this slip arising from loading by the failed Loma Prieta source region to the north. This model suggests an increased probability of a moderate earthquake near San Juan Bautista, and that interactions between fault regions are critical in earthquake processes. In the second paper, published jointly with A. Linde of D.T.M., Carnegie Inst. of Washington and M. Johnston of U.S.G.S., Menlo Park, we reported the absence of any changes in M_2 and O_1 tidal amplitudes precursory to the Loma Prieta earthquake, and estimated that any large scale changes in Young's modulus must have been less than about 2%. A further paper detailing investigation of episodic creep/strain events in the San Juan strain data over the period 1986-1992 has been completed in conjunction with K. Breckenridge of U.S.G.S, Menlo Park.

Strain steps observed in the Pinon Flat shear strain data were in broad agreement with those predicted from consideration of the seismically determined fault plane solution for the Joshua Tree Earthquake. Strain signals following the Landers earthquake in June indicated a large decay of order some hundreds of Nanostrain over a few days after the event, correlating with similar decays observed on co-located instruments such as the Pinon Flat laser strainmeter.

The anomaly present in the strain data from Eades and Donalee in April/May 1989 is shown in Figure 1. An anomaly in the same period was reported by S. Park (*J.G.R. 96(B9), pp14211-14237*) for resistivity measurements, and by E. Karageorgi (*B.S.S.A. 82(3), pp1388-1415*) in shear wave velocity. Preliminary investigation of a series of correlated creep/strain events during 1991-92 present mainly in the Eades and Frolich data indicates remarkably similar strain fields associated with the steps (see Figure 2), and suggests similar source regions.

Use of seismically determined source parameters for the M_L 4.7 earthquake near Middle Mountain on 28 October predicted strain steps in reasonable agreement with observed steps in all three tensor instruments, as shown below:

	Modelled *(Nanostrain)*			**Measured Dilatometer** *(Nanostrain)*	**Measured)) Tensor BCSM** *(Nanostrain)*		
Station	ε_a	γ_1	γ_2	ε_a	ε_a	γ_1	γ_2
DLT	+12	+15	-5	+9.5	+12 ±1	+12 ±1	-16 ±1
EDT	+10	+18	+2		+5 ±1	+20 ±1	+13 ±1
FLT	-5	+15	-1.5	-18.0	-10 ±5	+10 ±5	+1 ±5

Analysis of long-term data indicates no excursions in shear strain likely to be precursive to the expected M_L 6 earthquake, however the 5 year baseline of data will

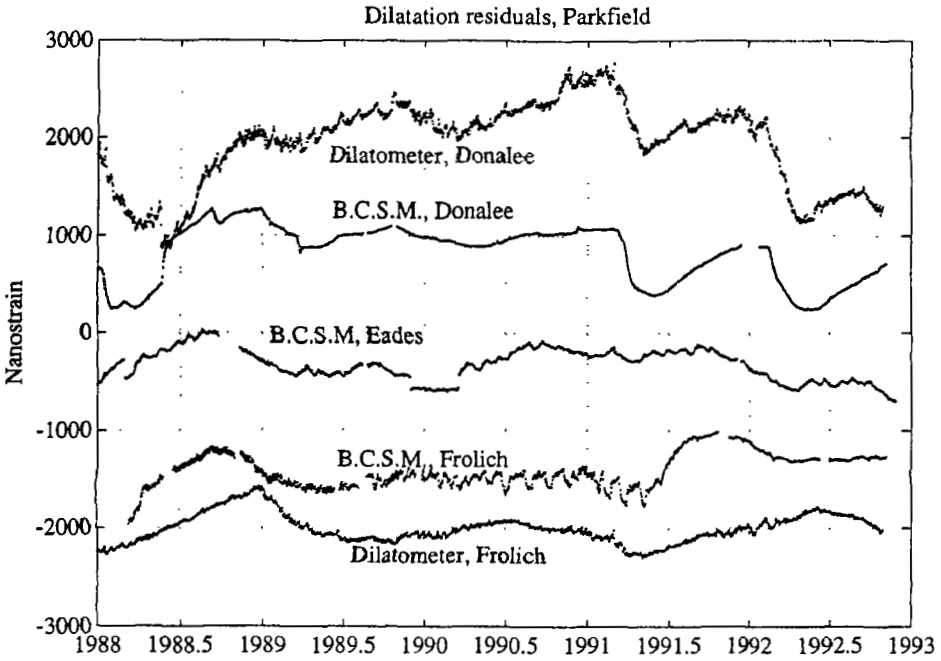

Figure 3. Long term dilatation at Frolich and Donalee and Eades as measured by tensor strain meters and by dilatometers (long term exponentials have removed from data).

provide a reliable determination of strain changes associated with an event of such magnitude. Comparison of long term dilation strains measured by the tensor instruments at Frolich and Donalee with dilatometer data from colocated instruments suggests an overall correspondence in the resulting data (see Figure 3) and provides strong evidence of consistency in the measurement of borehole strain by the two types of instrument.

RELEVANT PUBLICATIONS

Gladwin, M. T., High Precision multi component borehole deformation monitoring. *Rev.Sci.Instrum., 55*, 2011-2016, 1984.

Gladwin, M.T., Gwyther, R., Hart, R., Francis, M., and Johnston, M.J.S., Borehole Tensor Strain Measurements in California. *J. Geophys. Res. 92*. B8 pp7981-7988, 1987.

Gladwin, M. T. and Hart, R. Design Parameters for Borehole Strain Instrumentation. *Pageoph.,123, 59-88, 1985.*

Gladwin, M. T. and Wolfe, J. Linearity of Capacitance Displacement Transducers. *J.Sc.Instr. 46,* 1099-1100, 1975.

Johnston, M.J.S., Gladwin, M.T., and Linde, A.T. Preseismic Failure and Moderate Earthquakes. *I.A.S.P.E.I.* , Tokyo, August 19-30, S7-65, 35 , 1985.

Johnston, M. J. S., Linde, A.T., Gladwin, M.T., and Borcherdt, R.D. Fault Failure with Moderate Earthquakes. *Tectonophysics.* 144, 189-206, 1987.

Gladwin, M. T., Hart, R., and Gwyther, R. L. Continuous Deformation Measurements prior to the Loma Prieta Earthquake. *EOS, (Trans. Am. G. Un.) 71,* p 1461, 1990

Gwyther, R. L., Gladwin, M.T. and Hart, R.H.G., A Shear Strain Anomaly Following the Loma Prieta Earthquake. *Nature 356,* 142-144, 1992.

Linde, A.T., Gladwin, M.T. and Johnston, M.J.S. The loma Prieta Earthquake, 1989 and Earth Strain Tidal Amplitudes: An Unsuccessful search for Associated Changes. *Geo. Res. Lett., 19(3),* 317-320, 1992.

Gladwin, M.T., Gwyther, R.L., Higbie, J.W. and Hart, R.G., A Medium Term Precursor to the Loma Prieta Earthquake? *Geo. Res. Let. 18* #8 pp 1377-1380, 1991.

Gladwin, M. T., Breckenridge, K.S., Hart, R., and Gwyther, R. L. Recent Accelaration of Characteristic Creep-Strain Events at San Juan Bautista. *EOS, (Trans. Am. G. Un.) 72* p 484, 1991.

Gladwin, M.T., Borehole Strain Arrays: Insights from Parkfield, *EOS, (Trans. Am. G. Un.) 73* p 407, 1992.

Gwyther, R. L., Gladwin, M.T. and Hart, R., Interpretation of Continued Shear strain anomalies of the Loma Prieta Earthquake. *EOS, (Trans. Am. G. Un.) 72* p 310, 1991.

Seismicity and Crustal Structure in an Active Collisional Orogen, Central Asia

14-08-0001-G1802

Michael W. Hamburger, Gary L. Pavlis,
Haydar J. Al-Shukri, Emmanuel G. Ramos
Department of Geological Sciences, Indiana University
Bloomington, Indiana 47405
(812) 855-2934

Terry L. Pavlis
Department of Geology and Geophysics
University of New Orleans
New Orleans, Louisiana 70148
(504) 286-6797

Investigations

This program focuses on the highly active seismic zone between the Pamir and Tien Shan mountain belts in Soviet Central Asia. The Garm region is located directly atop the collisional boundary between the Indian and Eurasian plates, and is associated with a dense concentration of both shallow and intermediate-depth earthquakes. The fundamental aims of this collaborative research project with the Russian Academy of Sciences include: (1) elucidation of the structures and processes involved in active deformation of a complex collisional plate boundary, and (2) examination of the temporal variations in seismicity near Garm, in the form of changing spatial, depth, and stress distribution of microearthquakes that precede larger events. The seismological data base for this study includes the combined resources of the global, regional, and local seismic networks. Geological structures in the Garm region have been studied using compilation of published geological information, analysis of satellite imagery, and geological field work in the Peter the First, Gissar, and Darvaz mountain ranges near Garm.

Results

Geological Structure. The outbreak of a civil war in Tadjikistan during the late spring of 1992 led to cancellation of our plans for the 1992 field season. That work is now planned for 1993 if the political conflinct is resolved, but if hostilities continue we anticipate moving our field effort to the neighboring republic of Kyrgyzstan, where structures similar to the Garm region are exposed. In the absence of a field season in 1992 we concentrated our effort on the completion of a 1:100,000 scale geologic map and cross-sections for the Garm region. This effort and an accompanying manuscript are nearing completion and should be submitted for publication by early 1993. The map was produced by a combination of: 1) photo interpretation of two SPOT satellite images acquired in 1991, and 2) a compilation of our field observations together with those of Dr. V. Schevchenko who assisted us in the compilation during a visit to New Orleans in April 1992. Two major conclusions have arisen from this effort.

First, the present day structure of the Peter the First Range (Figure 1) is dominated by dextral transpression. This conclusion is indicated by both seismicity data [Ramos *et al.*, 1991; Ramos, 1992] and surface geology [Pavlis *et al.*, 1992]. The geological manifestations that support this conclusion include: 1) a system of south-vergent thrusts along the axis of the Peter the First Range that are both very young and form an *en echelon* array suggestive of dextral slip; 2) the general structure and topography of the Peter the First Range have all the characteristics of a classic "positive flower structure" with a prominent north and south-vergent thrust system forming an *en echelon* array centered on a topographic high.

Second, the present deformation front appears to be an erosionally controlled system, along which thrust systems are actively overriding a Quaternary surface generated by stream erosion. This conclusion is indicated primarily by the observation that throughout the Garm region, the present deformation front is marked by a major river valley (formed by the Surkhob River) with the Tien Shan Mountains forming a topographic barrier along its northern flank. The coincidence between the river and the deformation front suggests that the deformation front is dynamically maintained by stream erosion. That is, as thrust sheets advance toward the topographic wall of the Tien Shan Mountains, most of the mass delivered by the thrust systems is carried laterally by stream erosion.

The balance between thrust sheet advance and fluvial erosion has important implications for the interpretation of subsurface structure beneath the Peter the First Range, where most of the earthquake activity occurs in the Garm region. Our analysis of structures exposed at the deformation front suggests that the thrust systems have advanced faster than erosion could remove the material laterally. That is, projection of surface geology along the southern margin of the Tien Shan mountains southward (beneath the deformation front of the Peter the First Range) suggests that the complex geologic structure of the Tien Shan has been overridden by thrusts. This observation suggests that these structures were beveled by stream erosion and then overriden by the thrust sheets. One potential implication of this observation is that the dextral transpressional structures found along the axis of the Peter the First Range may represent the surface expression of a strike-slip fault system that originally developed along the southern edge of the Tien Shan mountains, but which has now been overriden by thrust sheets advancing from the south.

Seismicity and Focal Mechanism Studies. In order to study the style of active deformation in the Peter the First Range--the most seismically active portion of the Garm region--we examined the spatial patterns of high-quality hypocentral locations and the orientations of principal stresses determined from earthquake focal mechanisms in Garm. We first recalculated the hypocentral locations for about 60,000 earthquakes using the data collected by the Complex Seismological Expedition (CSE) network for the period 1969 to 1990 (Figure 2). A systematic method for evaluating relative quality of hypocentral locations, based on number and distribution of recording stations, standard error ellipsoid calculations, and RMS residuals was applied to the relocated earthquake catalog [Hamburger *et al.*, 1992*b*]. Earthquake focal mechanisms were determined for over 14,000 well recorded events in the Garm region [Ramos *et al.*, 1991; Ramos, 1992].

One salient feature of the earthquake mechanisms in the Garm region is that the diversity of focal mechanisms prevents the construction of reliable composite focal mechanism solutions, even along a single, well constrained seismogenic structure. This pattern mirrors that observed in the Transverse Ranges of California [Nicholson, 1986; Pechman, 1987; Real, 1987]. Our analysis also suggests that the compressional axes of focal mechanisms in Garm exhibit a more consistent orientation than the extensional axes, as observed in the Transverse Ranges [Pechman, 1987]. We have used this consistent orientation of the P-axes as an aid in delineating the seismically active structural features of the area. The well defined, sub-parallel orientation of the P-axes can be used as a guide in tracing the structures, particularly in areas where the dispersed distribution of the events masked the actual geometry of the faults (Figure 3). The resulting structural map was then correlated with the structures mapped on the surface and with other geological and geophysical observations in the region.

Among the most significant of our results is the delineation of a seismically active, vertical fault in the middle of the Peter the First Range. This structure, the Petrovsky Thrust (Figure 4) is presently the most active seismogenic feature in the Garm region. We have also identified other seismogenic structures in the region (Figure 5), including: a near-horizontal structure, the Nimich Fault, located at about 5 km depth near the boundary of the Peter the First Range and the Tien Shan; the intersecting Yasman and the Obi-Khabut faults near the 1949 Khait earthquake (M=7.4) epicenter; and segments of the Darvaz-Karakul Fault, which appear to be associated with more dispersed, but deeper, seismicity. The surface traces of most of the structures that we have

identified from the seismicity and P-axis distribution coincide with faults previously delineated based on geologic mapping and macroseismic effects of historical earthquakes. We have also used the orientation of the P-axes relative to the mapped structures in order to infer the dominant sense of slip along these faults. The inferred sense of motion along these faults (Figure 6) suggests that the ongoing deformation in Garm is dominated by westward oblique slip of crustal material along the mapped faults. This westward transport of materials appears to be a consequence of the north-south convergence of the Pamir and Tien Shan ranges, resolved along the oblique boundaries that define the margins of these two tectonic features.

Related Seismological Investigations. We are continuing are ongoing work on related studies of seismicity, crustal structure, and earthquake prediction investigations. These include: (1) regional velocity structure of the crust and upper mantle of the Pamir-Tien Shan region, based on teleseismic travel-time inversion [Mellors *et al.*, 1991; Hamburger *et al.*, 1992*c*]; (2) work on 1- and 3-dimensional velocity structure of the Garm region, using local earthquake travel-time inversion [Hamburger *et al.*, 1991; 1992*b,c*]; (3) study of the temporal distribution of earthquakes associated with moderate- and large mainshocks in the Garm region [Zheng *et al.*, 1991; Eneva *et al.*, 1992*a*; Zheng, 1992]; and (4) analysis of magnitude distribution and completeness of the Garm catalog [Eneva *et al*, 1990; 1992*b*].

References

Eneva, M., R. E. Habermann, M. W. Hamburger and G. A. Popandopulo, 1990, Man-made changes in the earthquake catalog of the Garm region, Soviet Central Asia [abs.], *EOS, Trans. Am. Geophys. Un., 71*, 1453.

Eneva, M., M. W. Hamburger and G. A. Popandopulo, 1992*a*, Spatial distribution of earthquakes in the Garm region, Soviet Central Asia, *Geophys. J. Intl., 109*, 38-53.

Eneva, M., R. E. Habermann, and M. W. Hamburger 1992, Man-made changes in the earthquake catalog of the Garm region, Soviet Central Asia, *Geophys. J. Int.*, in review.

Hamburger, M. W., H. J. Al-Shukri, G. L. Pavlis, and G. A. Popandopulo, 1991, P-wave velocity structure of the crust beneath the Garm region, Soviet Central Asia [abs.], *EOS, Trans. Am. Geophys. Un., 72*, 350.

Hamburger, M. W., D. E. Sarewitz, T. L. Pavlis and G. A. Popandopulo, 1992*a*, Structural and seismic evidence for intracontinental subduction in the Peter the First Range, Soviet Central Asia. *Geol. Soc. Amer. Bull., 104*, 397-408.

Hamburger, M. W., W.A. Swanson and G.A. Popandopulo, 1992*b*, Velocity structure and seismicity of the Garm region, Soviet Central Asia, *Geophys. J. Intl.*, in review.

Hamburger, M. W., H. J. Al-Shukri, R. J. Mellors, G. L. Pavlis. A. A. Lukk, and G. A. Popandopulo, 1992*c*, Crustal and upper mantle velocity structure in the Pamir-Tien Shan region, Central Asia [abs.], *Seismol. Res. Lett., 63*, 43.

Nicholson, C., L. Seeber, P. Williams and L. R. Sykes, 1986, Seismicity and fault kinematics through the eastern Transverse Ranges, California: Block rotation, strike-slip faulting, and low anlge thrusts, *J. Geophys. Res., 91*, 4891-4908.

Mellors, R.J., H.J. Al-Shukri, M.W. Hamburger, A.A. Lukk and G.A. Popandopulo, 1991, Velocity structure of the crust and upper mantle in the Pamir-Tien Shan region, Soviet Central Asia [abs.], *EOS, Trans. AGU, 72*, 203.

Pechman, J. C., 1987, Tectonic implications of small earthquakes in the central transverse ranges in recent reverse faulting in the transverse ranges, California, *U.S. Geol. Surv. Prof. Pap. 1339*, 97-112.

Ramos, E. G., 1992, Seismic expression of faults within the Peter the First Range, an active fold-thrust belt in Central Asia, *M.S. Thesis*, Indiana University, Bloomington.

Ramos, E. G., M. W. Hamburger, G. L. Pavlis, S. L. Yunga, and A. A. Lukk, 1992, Seismic expression of faults within the Peter the First Range, an active fold-thrust belt in Central Asia [abs.], *EOS, Trans. AGU, 73*, 213.

Pavlis, T.L., R.D. Myers, G.L. Pavlis, J.H. Holbrook, M.W. Hamburger, A.A. Lukk, and S.L. Yunga, Transpressional tectonics in the Peter the First Range, Soviet Tadjikistan [abstract], *EOS, Trans. Am. Geophys. Un., 72*, 514.

Real, C. R., 1987, Seismicity and tectonics of the Santa Monica-Hollywood-Raymond Hill fault zone and northern Los Angeles Basin in recent reverse faulting in the Transverse Ranges, California, *U.S. Geol. Surv. Prof. Pap. 1339*, 113-124.

Zheng, B., 1992, Temporal Variations in Seismic Activity in the Garm Region, USSR: Evidence for Quiescence Preceding a M = 6.3 Earthquake, *M.S. Thesis*, Indiana University, Bloomington.

Zheng, B., M.W. Hamburger, G.L. Pavlis, and G.A. Popandopulo, 1991, Temporal variations in seismic activity in the Garm region, USSR: Evidence for quiescence preceding a M=6.3 earthquake [abs.], *EOS, Trans. AGU, 72*, 322.

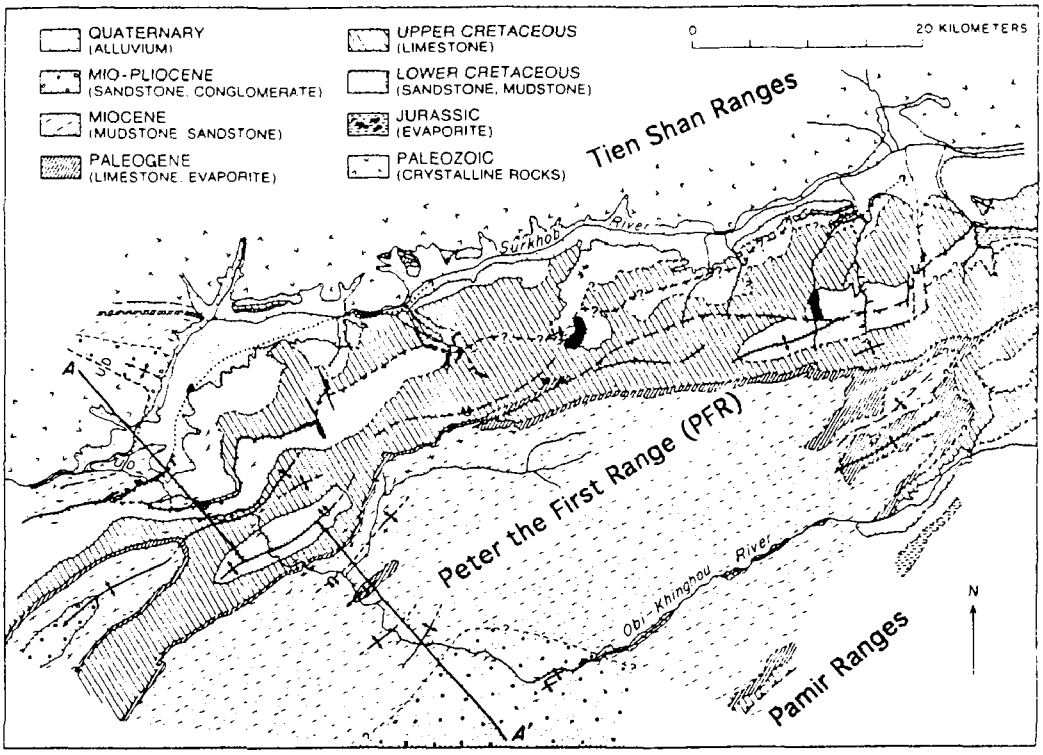

Figure 1. Reconnaissance geologic map of the Garm region based on field mapping, satellite imagery interpretation, and field data collected by V. I. Shevchenko. Contacts and structures are shown as solid where well constrained, dashed where approximate, queried where uncertain, and dotted where inferred. Drainage network is shown as dot-dash line (from Hamburger et al., 1992).

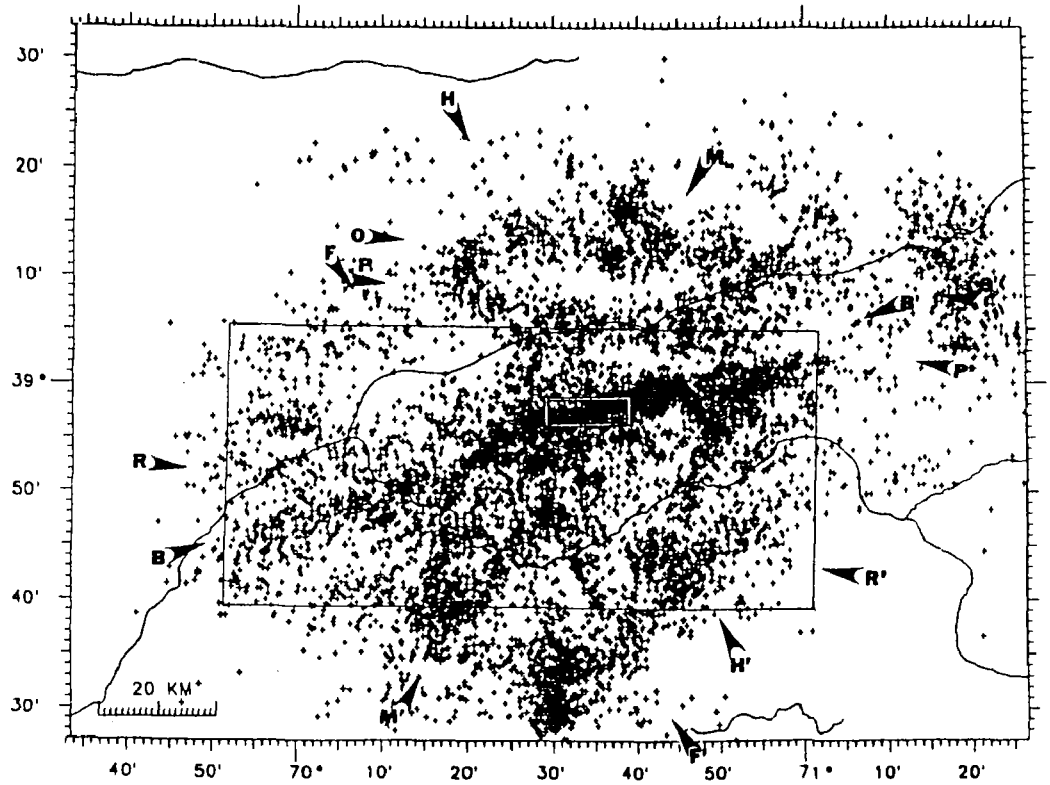

Figure 2. Plot of earthquakes located by the CSE network from 1969-1989, for which focal mechanism solutions have been determined. Note the dense concentration of events along the ridge of the Peter the First Range. Compare distribution of events with the structural map shown in Figure 5. Large rectangle shows area covered by Figure 3 Arrowheads labeled F and F' mark the cross-section line shown in Figure 4.

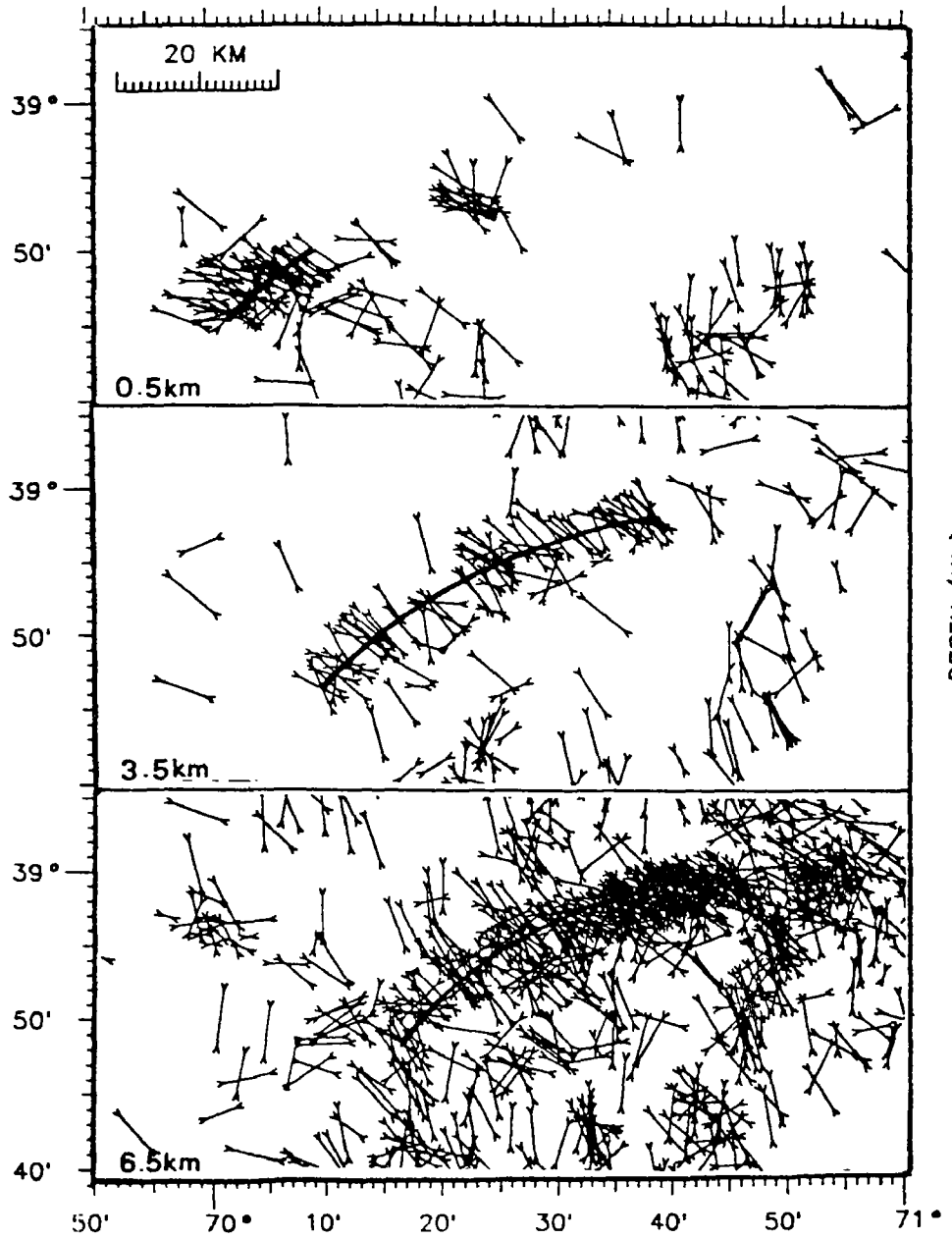

Figure 3. Three horizontal, 1-km thick slices constructed at various depths using the 1969-1989 focal mechanism catalog, showing the sub-parallel orientation of the P-axes under the PFR. The alignment of events with uniformly oriented P-axes is shown by a heavy line for each depth-slice. On the central part of the PFR, this alignment coincides at all depths indicating a vertical structure. In the west, this alignment shifts, indicating a southeast-dipping structure. The location of the slices is shown in Figure 2.

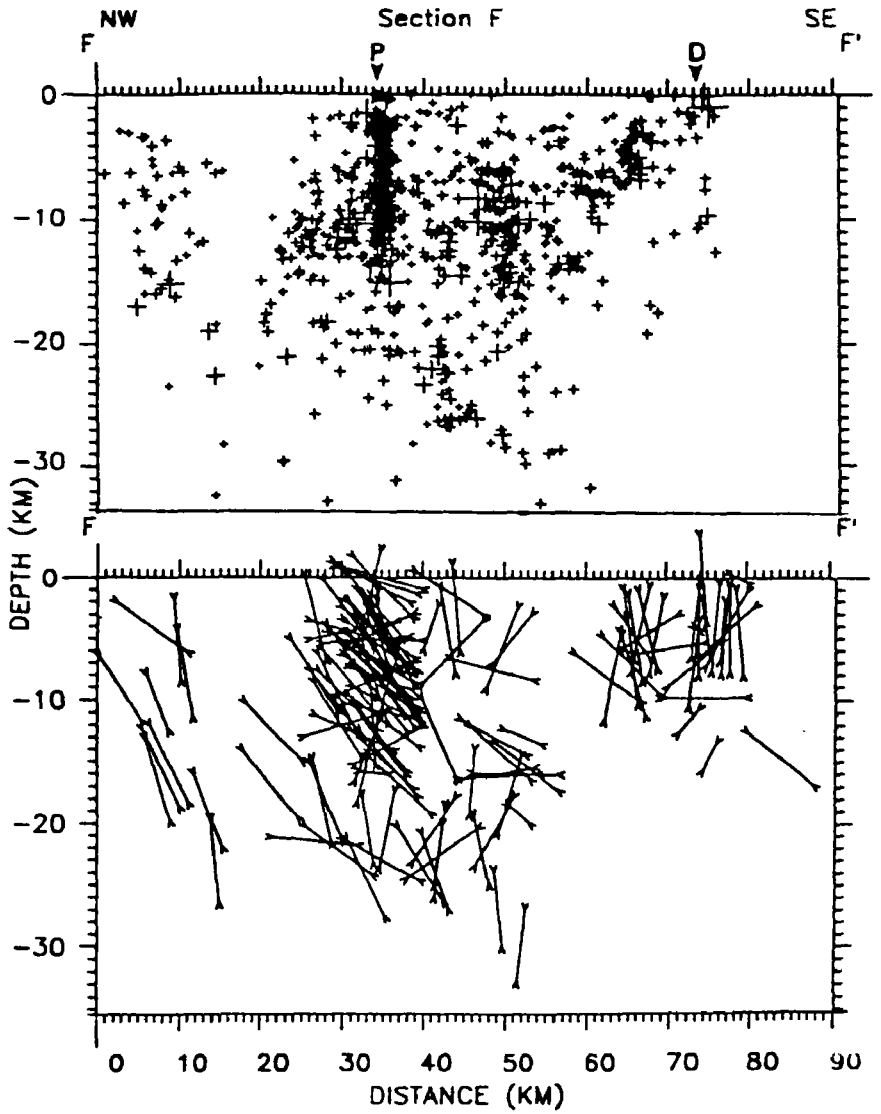

Figure 4. Seismicity (top) and P-axes (bottom) cross sections along line F-F' shown in Figure 2. Note the vertical cluster marking the Petrovsky Fault (marked P) and the dispersed seismicity near the Darvaz-Karakul Fault (D). The sections are 2 km thick. The orientation of the P-axes, here showing an apparent northerly upward thrust for the Petrovsky Fault cluster, was used to infer the relative motion of blocks along the faults.

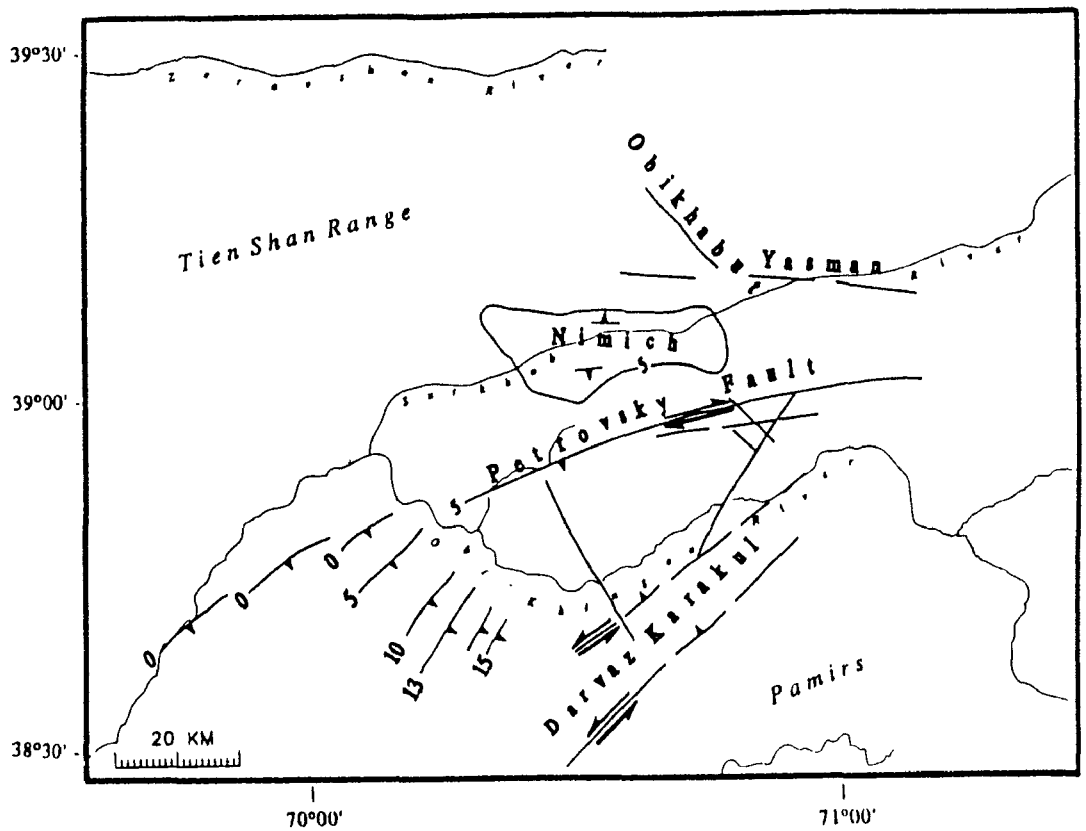

Figure 5. Structural interpretation of the P-axes and hypocenter distribution. The numbers near each structure indicate the depth of the respective segments of the faults. Note that the Petrovsky Fault along the axis of the PFR does not extend above ~5 km depth. The extent of the seismicity marking the horizontal Nimich Fault is shown as an outline at 5 km. The parallel lines along the Darvaz-Karakul Fault mark the outside boundaries of its seismogenic zone.

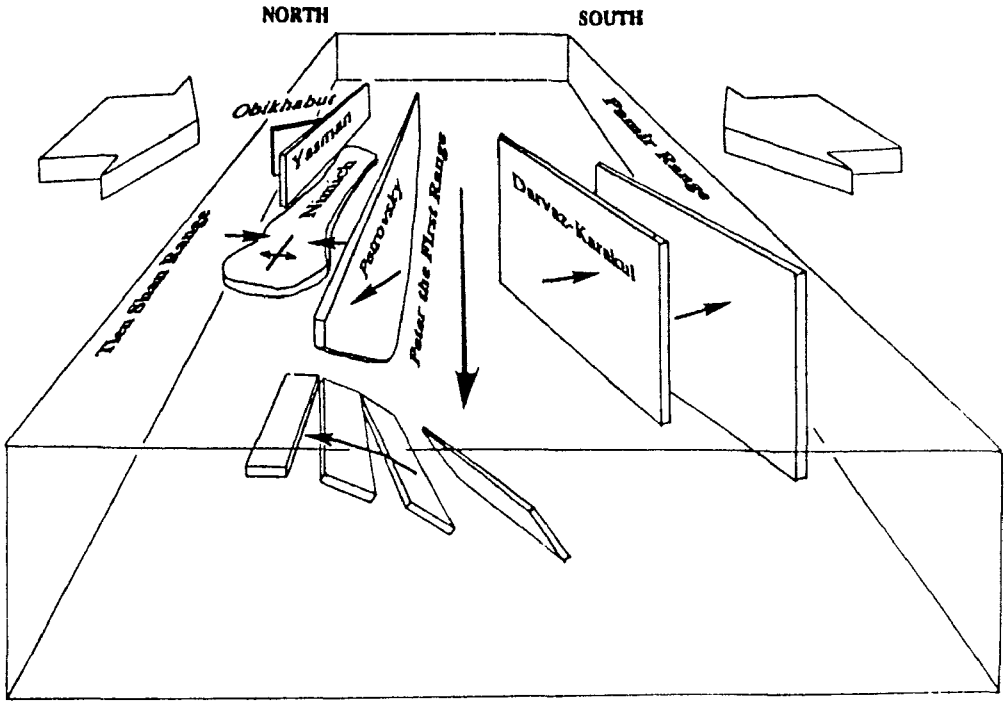

Figure 6. A perspective model of the active deformation in the Garm region. The large horizontal arrows show the north-south compression due to the collision of the Pamirs with the Tien Shan Range. The faults are shown as thin zones of weakness along which motion of crustal blocks (thin arrows) occur. The small discontinuous zones in the foreground are the imbricate, dipping thrusts of the Petrovsky Fault. A net westward motion of the southern PFR is suggested by the overall sense of transport along these faults (long horizontal arrow).

Analysis of Earthquake Data from the Greater Los Angeles Basin and Adjacent Offshore Area, Southern California

#14-08-0001-G1761

Egill Hauksson

Seismological Laboratory,
California Institute of Technology,
Pasadena, CA 91125
818-356 6954

INVESTIGATIONS

Seismotectonic analysis of earthquake data recorded by the CIT/USGS and USC networks during the last 16 years in the greater Los Angeles basin. Improve models of the velocity structure to obtain more accurate earthquake locations including depth and to determine focal mechanisms. Studies of the earthquake potential and the detailed patterns of faulting along major faults in the metropolitan area and adjacent regions.

A comprehensive study of the velocity structure of the Los Angeles basin is in progress. We have also analyzed aftershock data from the 1992 M6.1 Joshua Tree, M7.3 Landers, and M6.2 Big Bear earthquake sequence although it is located outside of the Los Angeles basin. Below we report some of the preliminary results.

RESULTS

Three-Dimensional Velocity Model of the Los Angeles Basin

Preliminary results of our work were presented at the 1992 SSA meeting (Hauksson, 1992). Arrival time data from 530 earthquakes and two blasts have been inverted for the P-wave velocity structure of the Los Angeles basin. An initial one-dimensional velocity model was specified at 648 nodes forming a sparse grid with 21 km horizontal spacing between grid points at depths of 1, 4, 8, 12, and 16 km. The velocity model from the sparse grid was interpolated and used as input for an inversion for a second set of 2048 grid nodes with 6 km horizontal spacing. Both grids are rectangular and centered on the basin proper. The velocities at most of the nodes of the dense grid are well resolved except to the northwest where the resolution is below average.

Because the starting model is one-dimensional the final three-dimensional model can be correlated with the local geologic structures. Preliminary results of the inversion show high velocities in the crystalline rocks beneath the Santa Monica mountains and to the southeast. The flanks of the basin, where thrust faulting and folding is observed, can be recognized in the three-dimensional velocity structure and are characterized by intermediate velocities. The lowest velocities reflect the shape of the basin and form a gently dipping zone extending from Palos Verdes to the center of the basin. The more steeply dipping northeast flank of the basin can also be seen where the northeast trending velocity model cross section is compared to the north-northwest trending geologic cross section from Davis et al. [1989]. In the deepest part of the central basin low velocities extend down to 8-10 km depth. Some shallow basement velocity contrast exists across the Palos Verdes and the Newport-Inglewood faults. The most prominent low velocity zone associated with thrust faulting exists adjacent to the Sierra Madre fault zone.

Wright (1991) provided an excellent summary of the geology of the Los Angeles basin. Figure 1, from Wright (1991), is an index map that shows major structural features and the location of geologic cross section A through F. We have made similar cross sections through our preliminary three-dimensional model and made an overlay with the geologic cross sections from Wright (1991). Figure 2 is an overlay of our velocity model and geologic cross sections A, B, C, and D Wright (1991; Figure 8). These overlays show

remarkable agreement between the geology and the preliminary velocity model. The bottom of the basin is clearly reflected by velocities of 6 km/s or higher. The near-surface sediments correspond to low velocities of 3.0 km/s or less. The west flank of the basin is clearly defined by higher velocities at shallower depth than beneath the center of the basin. The east flank of the basin that consists of metamorphic rocks has lower velocities than the west flank and hence is not as well defined as the west flank.

The next step is to use the final three-dimensional model to improve hypocenters and focal mechanisms. Results from such inversions for the greater Los Angeles basin combined with results from our focal mechanisms studies, will provide a more comprehensive picture of the geological structure and seismotectonics of the Los Angeles basin than available before.

The M7.3 Landers Mainshock Rupture

The 1992 Mw7.3 Landers mainshock ruptured along separate segments of five major surficial faults. The rupture began at the epicenter, approximately 8 km south of the community of Landers (Figure 3). It proceeded along the Johnson Valley fault for a distance of 17 km. It used the newly named Landers fault to step the slip over to the Homestead Valley fault. The rupture continued for a distance of 25 km along the Homestead Valley fault and stepped over a broad shear zone to the Emerson fault. The final step over was from the Emerson fault to the Camp Rock fault.

The spatial distribution of aftershocks along the mainshock rupture is complex and appears to be 5-20 km wide in places. (Figure 3) The distribution is characterized by tight spatial clusters of aftershocks, wide diffuse distributions extending away from the rupture surface, and small areas where no aftershocks occur but where surface slip was reported. This complexity may in part be explained by: 1) the rupturing of subparallel and overlapping fault segments; 2) the large amount of slip causing an aura of large strains around the rupture; 3) the change in strike of the rupture, starting with northerly strike near the epicenter and gradually rotating to north-west; 4) roughness or small steps along individual fault segments; and 5) variations in slip along the mainshock rupture surface. None of these explanations are mutually exclusive and all may contribute simultaneously to the observed distribution of aftershocks.

Near the epicenter of the mainshock the aftershock distribution forms a simple north trending zone. A small cluster 8 km to the north of the mainshock epicenter is associated with a small right-step in the Johnson Valley fault. Some of the largest clusters of aftershocks occur between subparallel fault segments such as the Johnson Valley and Homestead Valley faults. This cluster also crosses the Homestead Valley fault where it coincides with a few kilometer wide slip gap identified independently from TERRAscope data by Kanamori et al., [1992]. A large aftershock cluster between the Emerson and Camp Rock faults may be associated with the change in strike to the north of the Emerson fault and transfer of slip to the Camp Rock fault.

The aftershock distribution extends from the surface to depths of 12-14 km. Four different depth cross sections along the mainshock rupture and five orthogonal cross sections are shown Figure 3. The large or M>4.0 aftershocks occur usually at the edges, bottom or top, of the mainshock rupture. The almost vertical dip and less than 2 km width of the aftershock zone where two strands do not overlap is illustrated in cross sections such as E-E'.

PUBLICATIONS and REPORTS

Hauksson, E. and L. M. Jones, The 1988 and 1990 Upland earthquakes: Left-lateral faulting adjacent to the central Transverse Ranges, *J. Geophys. Res.*, *96*, 8143-8165, 1991.

Hauksson, E., Seismotectonics, US National Report to International Union of Geodesy and Geophysics 1987-1990, *Reviews of Geophysics*, Supplement, 721-733, 1991.

Hutton, L. K., L. M. Jones, E. Hauksson, and D. D. Given, Seismotectonics of southern California, Slemmons, D. B., Engdahl, E. R., Zoback, M D., and Blackwell, D. D., eds., *Neotectonics of North America*, Boulder, Colorado, Geological Society of America, Decade Map Volume 1, 133-152, 1991.

Hauksson, E., K. Hutton, K. Douglass, and L. Jones, Earthquake atlas for southern California, 1978-1990, *Engineering Geology Practice in Southern California,* Belmont, California, Association of Engineering Geologists, B. Pipkin and R. J. Proctor, eds., 181-190, 1992.

Hauksson, E., Seismicity, faults, and earthquake potential in Los Angeles, southern California, *Engineering Geology Practice in Southern California*, Belmont, California, Association of Engineering Geologists, B. Pipkin and R. J. Proctor, eds., 167-179, 1992.

Hauksson, E., Hutton, K., and Jones, L. M., Preliminary Report on the 1992 Landers Earthquake Sequence in Southern California, *Landers Earthquake of June 28, 1992 San Bernardino County, California Field Trip Guidebook,* So. Calif. Section of the Association of Engineering Geologists, Ed. D. Ebersole, 23-32, 1992.

Hauksson, E., The 1991 Sierra Madre earthquake: Seismological and tectonic analysis, submitted to *J. Geophys. Res.,* 1992.

Landers Earthquake Response Team, (E. Hauksson, among 19 authors), Near-field investigations of the Landers earthquake sequence, April-July, 1992, submitted to *Science*, 1992.

Qian, H. X., E. Hauksson, and L. M. Jones, The Effect of the 1992 M7.5 Landers Earthquake on the Seismicity of the Southern San Andreas Fault, (Abstract), submitted to Fall AGU Meeting, 1992.

Hauksson, E., K. Hutton, H. Kanamori, S. Bryant, H. Qian and K. Douglass, L. M.Jones, D. Eberhart-Phillips, J. Mori and T. Heaton, Overview of the 1992 (M6.1,7.5,6.6) Landers Earthquake Sequence in San Bernardino County, California, (Abstract), submitted to Fall AGU Meeting, 1992.

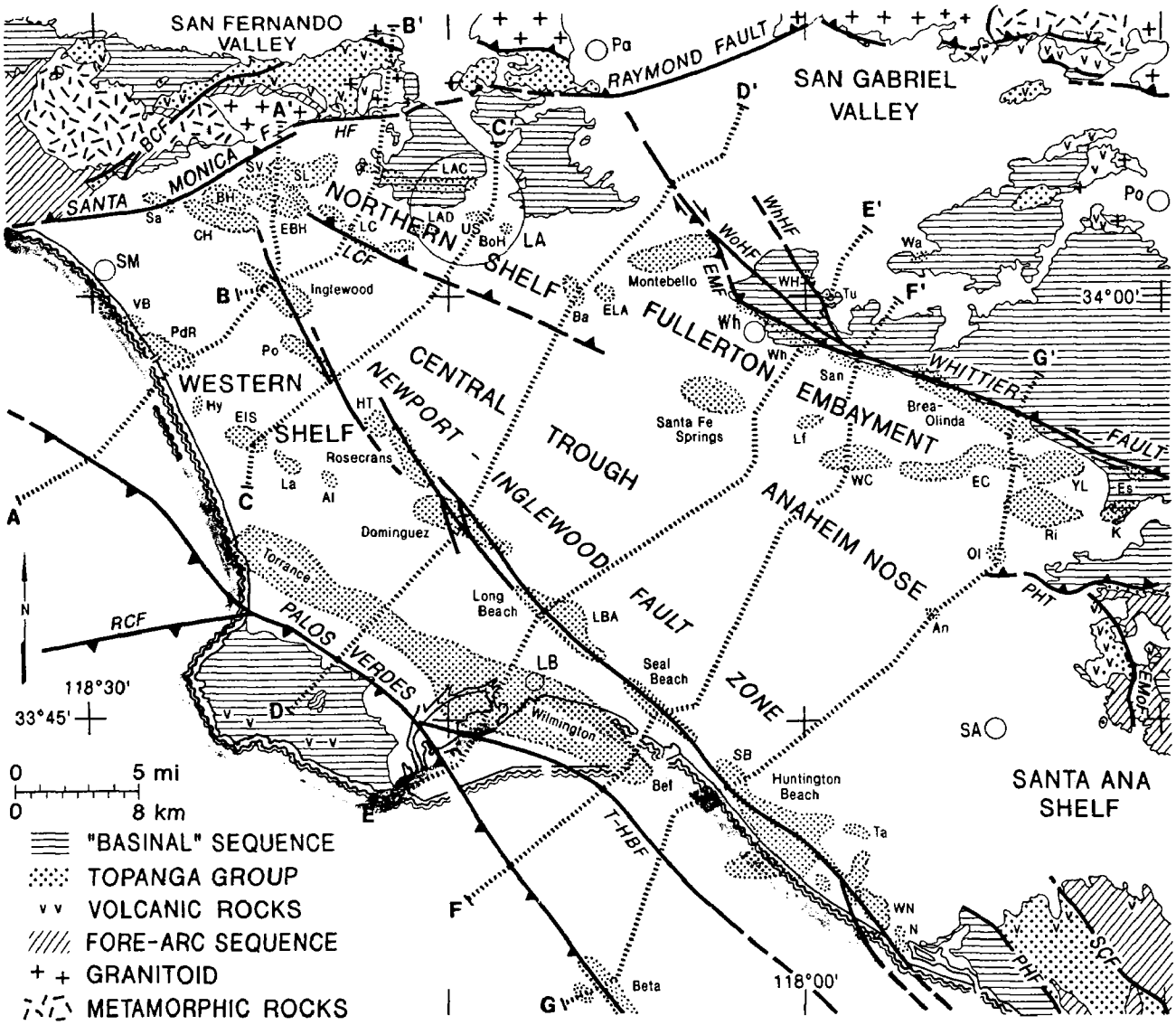

Figure 1. From Wright (1991). An index map that shows major structural features and the location of cross section A through F.

Wright, T. L., Structural geology and tectonic evolution of the Los Angeles basin, in *AAPG- Volume on Active-Margin Basins*, vol. 52, edited by K. T. Biddle, pp. 35-134, 1991.

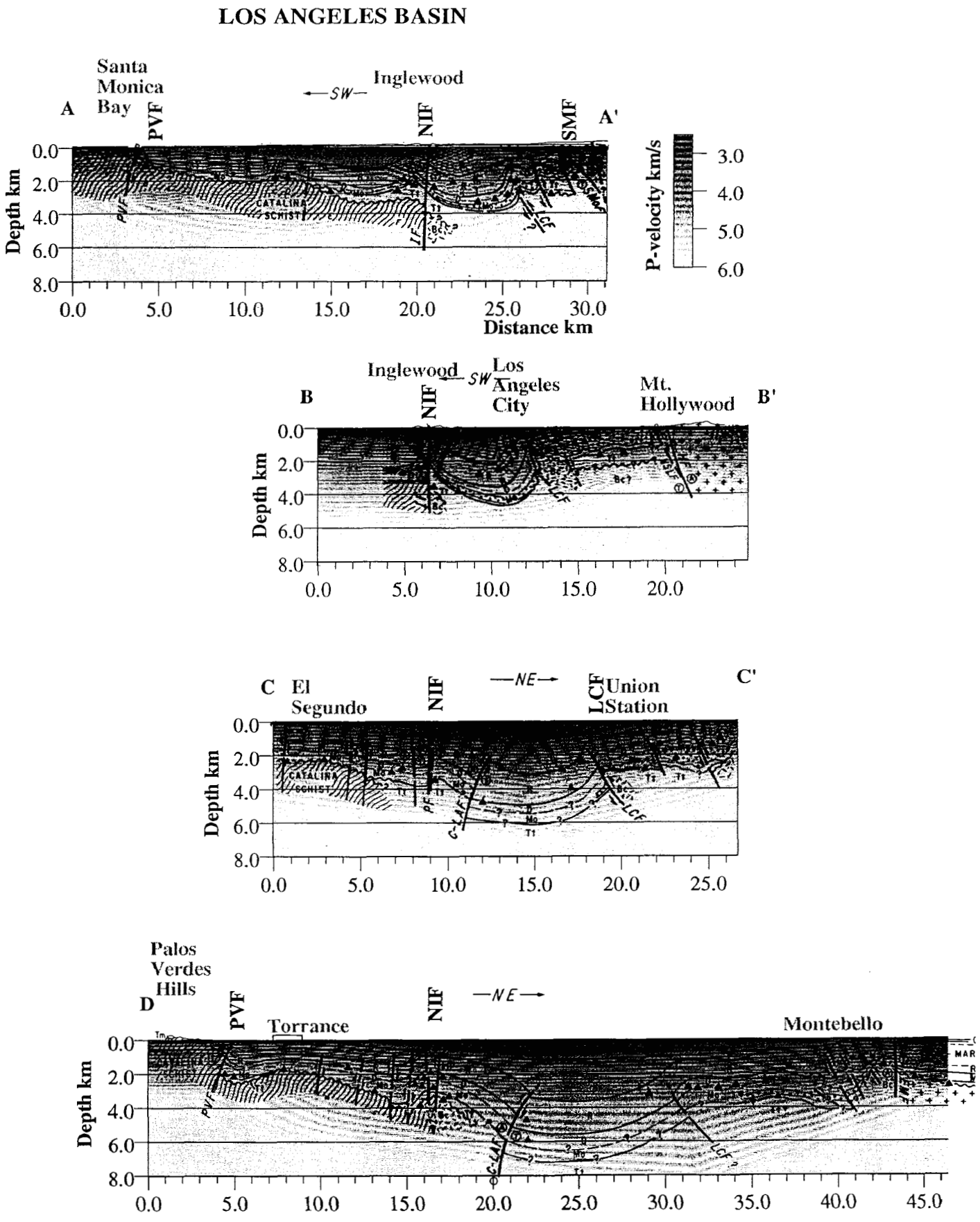

Figure 2. Overlay of our preliminary 3-D velocity model and geologic cross sections A, B, C, and D from Wright (1991; Figure 8).

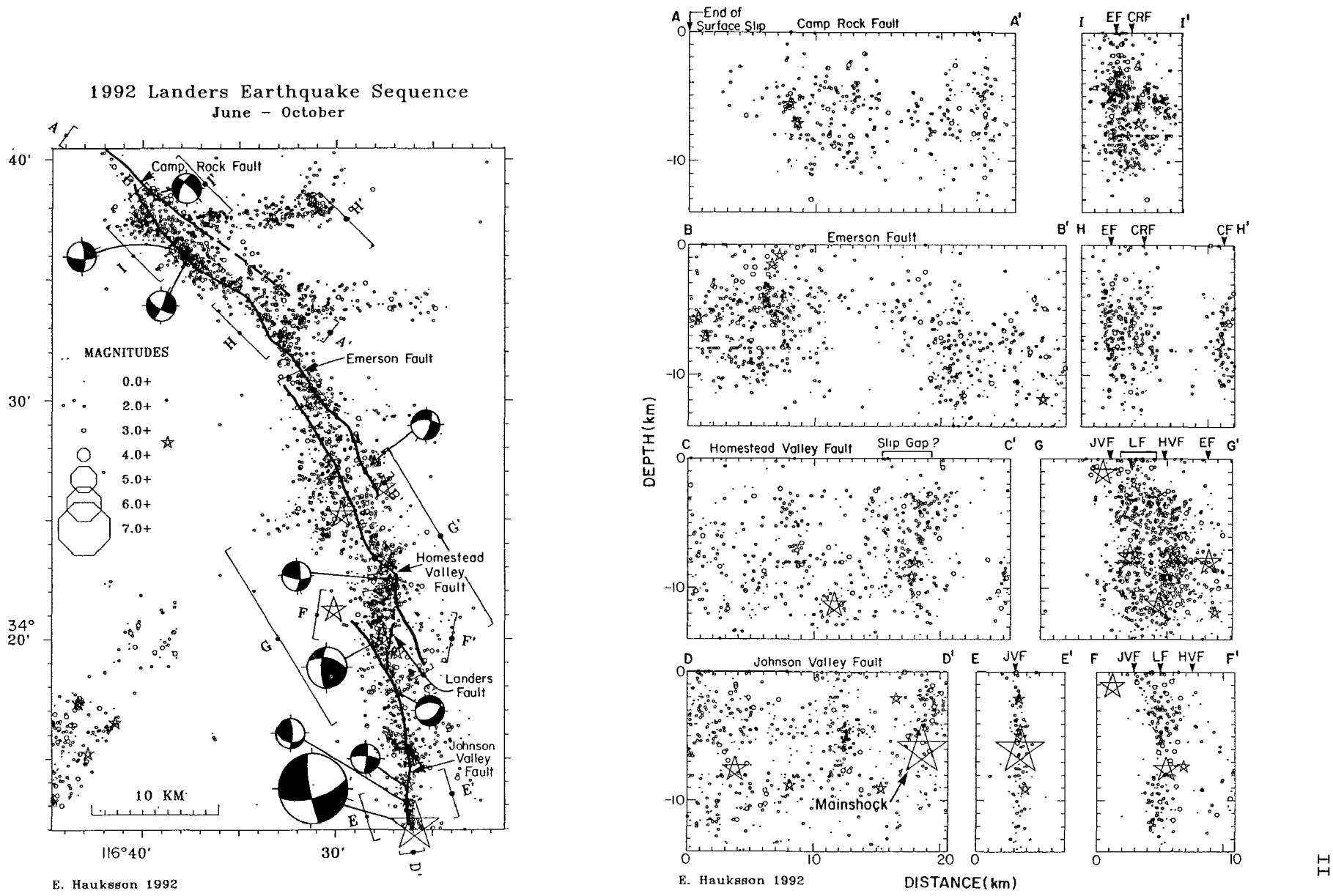

Figure 3. (Left) Map of 1992 M7.3 Landers mainshock and aftershocks and selected focal mechanisms. Surface rupture (provided by K. Sieh) is also shown. (Right) cross sections parallel to the fault strands (A-D) and across the fault strands (E-I). Note how the different fault strands overlap.

Assessment of Quaternary Deformation Between the Hayward and Calaveras Faults, San Francisco Bay Region, California

Award Number: 1434-92-G-2209

Mark A. Hemphill-Haley
Woodward-Clyde Consultants
500 12th Street, Suite 100
Oakland, CA 94607-4014
(510) 874-3269

Keith I. Kelson
William Lettis and Associates, Inc.
1000 Broadway, Suite 612
Oakland, CA 94607-4014
(510) 832-3716

Investigations

We are investigating the distribution and style of deformation within the complex intersection between the Hayward and Calaveras fault zones in the southern East Bay Hills of the San Francisco Bay region. The amount and mode of strain transfer from the central Calaveras fault zone onto the Hayward and northern Calaveras fault zones are poorly understood. The purpose of this investigation is to provide information about the mechanisms of slip transfer between these two major seismogenic faults, and thus to help define potential seismic hazards in the southern San Francisco Bay region.

Our research is designed to address: 1) the distribution and style of Quaternary deformation between the Calaveras fault in Sunol Valley and the Hayward fault in Fremont, where slip is transferred from the central Calaveras fault onto the southern Hayward fault, and 2) the nature and loci of Holocene deformation along a microseismically defined fault splay between the southern Hayward and Mission faults (Wong and Hemphill-Haley, 1992). We anticipate obtaining the following information from this investigation:

- Paleoseismologic data on the northwestern projection of the Mission fault in Fremont
- Structural relations of surficial lineaments along the mapped trace of the Mission fault, its northwestern extension, and a microseismically defined splay of the southern Hayward fault (Wong and Hemphill-Haley, 1992)
- Geologic and geomorphic assessments of the loci and nature of Quaternary deformation between the Calaveras fault in Sunol Valley and the Hayward fault in Fremont

Our data collection consists of two tasks: 1) interpretation of aerial photography, field reconnaissance, and paleoseismologic investigations of the Mission fault and the microseismically defined splay of the Hayward fault, and 2) quantitative geomorphic and geologic analyses of Quaternary deformation between the Hayward and Calaveras faults. These analyses include investigations of deformation of late Quaternary fluvial terraces flanking Niles Canyon and a possible late Tertiary to early Quaternary paleovalley (Mission Pass) through analysis of aerial

photography, field mapping, shallow drilling, and construction of envelope, subenvelope, and residual geomorphic maps.

Results

Paleoseismologic Investigations - Through our analysis of aerial photography and field reconnaissance, we identified a potential trace of the Mission fault along its northwestern projection in the Mission District of Fremont. We selected a trench site for paleoseismologic studies on an alluvial fan within an abandoned orchard on Ohlone College property, based on the presence of a strong tonal lineament, a subtle topographic swale, and a vegetation lineament possibly related to a fault-induced groundwater barrier. Based on our analysis of aerial photographs and field studies, this lineament is the most prominent feature possibly related to Holocene movement on the Mission fault on the alluvial fan complex in Fremont. In addition, the presence of the lineament across Holocene and late Pleistocene alluvial fan deposits suggested that a trench would expose datable surficial deposits. Our intent with the trench was to expose stratigraphic and structural relations associated with the swale and lineament, and determine if the lineament is related to late Quaternary movement on the Mission fault.

In April 1992, we excavated, logged, and backfilled a trench across the margin of the topographic swale that was approximately 18 m long, 1 m wide, and up to 3.5 m deep. Historic, Holocene, and late Pleistocene fluvial overbank and channel deposits were exposed in the trench, based on the presence of cultural remains (i.e., nails, bricks) and a probable late Pleistocene jaw bone of a horse. We observed no evidence of tectonic displacement of the fluvial deposits. The trench was reviewed informally by personnel with the U.S. Geological Survey (USGS) and Lawrence Berkeley Laboratory (LBL).

Based on analysis of aerial photography and field reconnaissance with personnel from the USGS, LBL, and the University of California at Berkeley, we identified another potential trench site in the southern East Bay Hills near Mission Peak. We are currently assessing the site to determine if investigation would be fruitful.

Quantitative Geomorphic Analyses - We have obtained 1:20,000-scale, black-and-white aerial photography taken in 1939 and 1940 of the southern East Bay Hills between the Calaveras fault in Sunol Valley and the Hayward fault in Fremont, and are currently interpreting the distribution of fluvial terrace surfaces flanking Niles Canyon on these photos. In addition, we are using these photographs to assess the presence of possible fluvial deposits or surfaces associated with the Livermore and Santa Clara/Irvington Gravels in the vicinity of Mission Pass. We are testing the hypothesis that the topographically low part of the southern East Bay Hills near Mission Pass is a paleovalley associated with these gravels. If so, this paleovalley may provide a long-term indicator of strain across the range, as may terraces along Niles Canyon.

As part of the quantitative analysis of the range, we have constructed an envelope map of the southern East Bay Hills at a scale of 1:62,500 (Lettis and Kelson, 1992), which is a generalized topographic contour map that ignores present-day valley incision. We are currently constructing a subenvelope map of the same area, which is a contour map drawn on the valley floors of second-order drainages. We anticipate that the quantitative difference between these two maps (a residual map) will yield information on the amount and distribution of erosion in the range, which in turn can be interpreted as a function of tectonic uplift. In addition, we are researching the feasibility of using digital elevation models (DEMs) and appropriate software to digitally construct these maps at a scale of 1:24,000.

Reports

Lettis, W.R., and Kelson, K.I., 1992, Distribution of geologic slip along faults in the San Francisco Bay and Santa Maria Basin Regions: Abstracts for American Geophysical Union Chapman Conference, Tectonics and Topography, Snowbird Utah, p. 37.

Wong, I.G., and Hemphill-Haley, M.A., 1992, Seismicity and faulting near the Hayward and Mission fault: *in* Galehouse, J.S. (ed.), Program and Abstracts, Second Conference on Earthquake Hazards in the Eastern San Francisco Bay Region, California State University, Hayward; also, in press, *in* Borchardt, G. (ed.), Proceedings, Second Conference on Earthquake Hazards in the Eastern San Francisco Bay Region, California Division of Mines and Geology Special Publication 113.

Collaborative Research: Analysis of PANDA data and continuation of PANDA experiment in the Central New Madrid Seismic Zone

14-08-0001-G2138

Robert B. Herrmann
Department of Earth and Atmospheric Sciences
Saint Louis University
3507 Laclede Avenue
St. Louis, MO 63103
(314) 658-3131

Investigations

The purpose of this segment of the collaborative effort is to learn as much as possible about the dynamics of the earthquake process in the New Madrid Seismic Zone by using data from the dense PANDA deployment of three component sensors on top of the seismicity in the central seismicity trend between New Madrid, Missouri, and Dyersburg, Tennessee.

Results

Since Booth *et al* (1991) reported on observable shear-wave splitting in the PANDA data set, and since this splitting could possibly affect the inference of focal mechanism parameters, a program for determining the Zoepritz coefficients for plane waves in a general anisotropic media was developed to determine how the peak amplitude of the shear wave from the source is affected by the anisotropy. This background work was essential prior to modeling the observed waveforms in terms of earth structure.

The other problem affecting analysis is the effect of the Q structure in the thick (600 m) sediments beneath the PANDA stations. Two different analysis techniques were applied. The first was that of Anderson and Hough (1984) whereby an attenuation operator was derived from the acceleration spectra. This was done for the P-wave on the vertical component and for the S-wave on the transverse component. The problem with technique is the effect of the unknown corner frequency upon the inference. The other technique follows Clouser and Langston (1991) to determine a differential attenuation between the P- and S-wave in the sediments. This is possible since an S-wave incident at the base of the sediments is converted into a P-wave which appears on the vertical component and into an SV-wave that appears on the radial component. Since the effect of source spectrum and crustal path drop out in the spectral ratio, the second technique yields stabler numbers than the second.

If the attenuation operator is given by $\exp(-\pi\kappa f)$, then we estimated $\kappa_S = 0.03 \pm 0.01$, $\kappa_P = 0.008 \pm 0.02$ by the Anderson and Hough technique , and $\Delta\kappa = 0.02 - 0.03$ by the Clouser and Langston technique. The individual station estimates showed an excellent correlation with sediment thickness,

this permitting another estimate by looking at the slope with respect to depth. Making reasonable estimates of the mean P- and S- wave velocities in the sediments permits and estimate that $Q_P = Q_S = 25 - 40$.

References

Booth, D. C., H. J. Rowlands, and J.-M. Chiu (1991). observation of shear-wave splitting in the New Madrid seismic zone, eastern USA (abs), *Seism. Res. Letters* **62,** 163.

Clouser, R. H., and C. A. Langston (1991) Q_P and Q_S relations in a sedimentary basin using converted phases, *Bull. Seism. Soc. Am.* **81,** 733-750.

Anderson, J. G, and S. E. Hough (1984). A model for the shape of the Fourier amplitude spectrum of acceleration at high frequencies, *Bull. Seism. Soc. Am.* **74,** 1969-1993.

Publications

Liu, Z., M. Wuenscher and R. B. Herrmann (1993). Attenuation of body waves in the New Madrid seismic zone, *Seism. Res. Letters.* **64,** (in review).

Ground Motion Estimation For The Central U. S.

14-08-0001-G2142

Robert B. Herrmann
Department of Earth and Atmospheric Sciences
Saint Louis University
3507 Laclede Avenue
St. Louis, MO 63103
(314) 658-3131

Investigations

The purpose of this effort is to improve strong ground motion prediction methodology for the central United States. Current techniques rely on early and dated work by Nuttli and Herrmann or random process theory techniques which do not take into account the effects of local structure, especially for sites in the Mississippi Embayment.

Results

Ou and Herrmann (1990a, 1990b) proposed extensions to random process theory to account for the effect of crustal structure on signal duration and level. Their technique included the direct and all supercritical S arrivals, but did not account for the reflection and transmission coefficients as the rays propagated through the crust. They calibrated their simple technique for the actual earth model by using wavenumber integration techniques.

Their work has been upgraded to use asymptotic ray theory for the estimation of individual ray amplitudes. This permits the following:

a) Estimates of peak motion for the vertical, radial, transverse, and vectorial horizontal time histories.

b) Use of a distance - focal mechanism dependent source excitation factor

c) Direct computation high frequency asymptotic seismograms that incorporate crustal complexity.

Other than generating peak motion estimates for realistic plane layered crustal models, the new technique permits sensitivity tests for changes in stress parameter, source depth, and source mechanism. Figure 1 presents the result of a set of simulations for a hard rock site for m_{Lg} = 5.0 and 7.5, for two mid-continent earth models, for four source depths, 5, 10, 15 and 20 km, for two stress parameter values, 100 and 200 bars, and for three mechanisms. One mechanism consisted of predominantly vertical strike slip source, another predominantly 45° dip slip sources, and the last all mechanisms having dip angles between 30° and 90° and which had either the P- or T-axis within 22.5° of the horizontal. The *mLg* values were determined by synthesizing vertical component WWSSN short period peak motions.

The peak motions presented in Figure 1 are peak transverse acceleration, velocity and PSRV at 1 and 10 Hz for 5% damped oscillators. Several features

are noted: first since all simulations had the same target *mLg* values, which is determined at distances greater than 100 km, there is very little dispersion in the estimates at large distances. The effects of different crustal structure are seen at 100 km distance where the first supercritical Moho reflection arrives. The major variation is at short distances, where the focal depth effect is profound.

Another interesting result is that, for fixed seismic moment and corner frequency, when compared to the other two focal mechanism simulations, the predominantly vertical strike slip source has an m_{Lg} 0.15 - 0.20 magnitude units smaller, while the peak transverse motion is about a factor of 1.3 - 1.4 times larger. Thus for a fixed m_{Lg}, the transverse motions of a vertical strike slip source will be about a factor of 2 times larger at large distances than the other mechanisms. At short distances, this difference is overwhelmed by the SH-wave excitation. This implies that specification of expected focal mechanism is important for hazard analysis. This may be difficult for older events where the magnitude is based on intensity, since the magnitude thus derived is probably related more to horizontal motions.

References

Ou, G.-B., and R. B. Herrmann (1990a). Estimation theory of peak ground motion, *Seism. Res. Letters* **61**, 99-107.

Ou, G.-B., and R. B. Herrmann (1990b). A statistical model for ground motion produced by earthquakes at local and regional distances, *Bull. Seism. Soc. Am.* **80**, 1397-1417.

Publications

Herrmann, R. B. and G.-B. Ou (1993). Random process theory and synthetic seismograms, *Bull. Seism. Soc. Am.* (in review).

Boore, D. M., K. W. Campbell, and R. B. Herrmann (1993). Characterization of strong ground shaking, in *Earthquake Hazard Assessment in the Central and Eastern US*, S. T. Algermissen and G. A. Bollinger, eds, EERI.

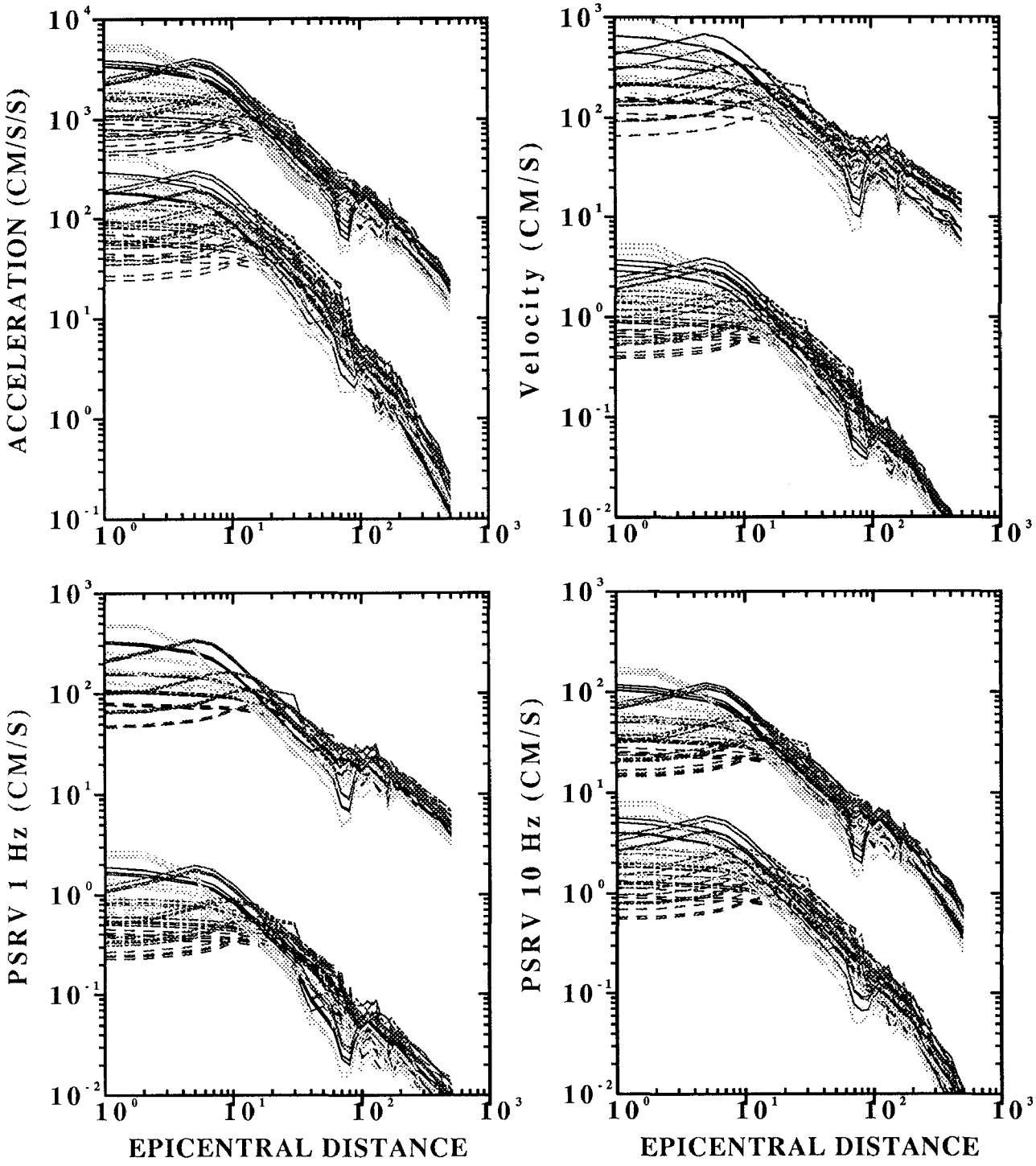

Figure 1. Sensitivity test to depth, model, stress drop and mechanism.

ACTIVE SEISMIC STUDIES OF VOLCANIC SYSTEMS

9930-01496

D.P. Hill, H.M. Benz, J.A. Olson, J.E. Vidale
Branch of Seismology
U.S. Geological Survey
345 Middlefield Road, MS 977
Menlo Park, California 94025
(415) 329-4795

Investigations

Over the last decade, this project has focussed on the activity in Long Valley caldera and coordination of associated monitoring research, and hazard reduction activities. Because project funding has come from the Volcano Hazards Program, the project has not been a regular contributor to the NEHERP semi-annual technical reports. For current reporting period, however, the following efforts funded under NEHERP have been administratively associated with this project in addition to the on-going coordination of Long Valley caldera monitoring and research:

1) Applications using the regional seismograph networks in the western United States for array studies of seismic scattering from upper mantle structures (J.E. Vidale and H.M. Benz).
2) Seismicity patterns associated with the Loma Prieta segment of the San Andreas fault (J. Olson and D.P. Hill).
3) Analysis of the geometry of seismogenic strike-slip and normal faults and its significance for fault strength and stress levels in the brittle crust (W. Thatcher and D.P. Hill).

Results

Long Valley Caldera (D.P. Hill)

Monitoring activities in Long Valley caldera through FY92 showed continued inflation of the resurgent dome at a strain rate of 2 to 3 microstrain per year and an uplift rate of 2 to 3 cm per year based on both two-color geodimeter measurements (see Langbein's report and Langbein et al., in press) and occupation of the leveling network within the caldera and along Highway 395 between Lee Vining and Tom's Place. Earthquake activity within the caldera persists at modest levels with occasional swarms of $M \leq 3$ events in the south moat and in the Sierra Nevada block south of the caldera. A most remarkable development in caldera seismicity occurred on June 28 when earthquake activity increased abruptly following the $M = 7.5$ earthquake at 4:58 AM (PDT) near Landers in southern California over 400 km to the south. This

dramatic increase in activity following the Landers event within the caldera and at multiple other sites in the western United States (as distant as Yellowstone National Park) is the first unambiguous example of a large earthquake triggering remote seismicity. In collaboration with a number of co-authors, Paul Reasenberg and I are preparing a manuscript describing the remote seismicity triggered by the Landers earthquake, which we intend to submit to Science for publication.

Figure 1 illustrates the abrupt increase in seismicity rate within the caldera at the time of the Landers earthquake. By applying a 5- to 30-Hz band-pass filter to the data from caldera seismic stations, Andy Michael was able to show that the onset of this triggered seismic activity began approximately 40 seconds after the S wave from the Landers mainshock passed through the area (or just over 2 minutes after the origin time of the Landers event). The first of the triggered events was located in the swarm area near the southwest margin of the resurgent dome. Seismicity spread to the other common centers of swarm activity in southern half of the caldera and parts of the Sierra Nevada block to the south over the next few hours. Notably, no activity was triggered beneath Mammoth Mountain, which had sustained a six-month-long swarm in 1989.

The triggered activity included over 300 earthquakes within the caldera before it gradually died out five to seven days after the Landers mainshock (Figure 1). Several $M \approx 3$, locally felt earthquakes occurred as part of the triggered activity, the largest of which was a $M = 3.7$ earthquake at 10:37 PM (PDT) on the 28th.

Loma Prieta seismicity patterns (J.A. Olson and D.P. Hill)

We examine the spatial distribution of the well-located earthquakes in the twenty years preceding the Loma Prieta earthquake, and their association with faults, along a 100-km-long extent of the southern Santa Cruz Mountains. Several faults in the area are clearly associated with background seismicity since 1969. Notably, however, the principal southwest-dipping portion of the Loma Prieta rupture below 10-km depth was virtually aseismic. Most of the seismicity in the area was associated with the creeping segment of the San Andreas fault south of Pajaro Gap and adjacent faults to the east. The area near the intersection of the San Andreas and Sargent fault traces, however, also produced persistent seismicity albeit at a much lower rate. This seismicity includes the 1988 (M5.3) and the 1989 (M5.4) Lake Elsman earthquakes, which have fault plane solutions consistent with oblique strike-slip and reverse-slip components on a plane that dips about 65^0 NE. These events stand out because they are a full magnitude unit larger than other events within a 15-km radius for at least 74 years, and because they occurred within 15 months and 2 1/2 months, respectively, of the Loma Prieta earthquake. Aside from these two Lake Elsman events, the seismicity patterns in the twenty years prior to the Loma Prieta earthquake were essentially stable showing no clear precursory changes. In the preceding twenty five years, however, two other $M \geq 5$ events occurred along the Loma Prieta rupture zone, near its southern end:

the 1964 (M5.0) and the 1967 (M5.3) Corralitos earthquakes.

Fault orientation and fault strength (D.P. Hill and W. Thatcher)

In a short note to the Bulletin of the Seismological Society of America (Hill, in press), I extended the definition of apparent friction used in Hill and Thatcher (1992, Bull. Seismol. Soc. Am., v. 82, pp. 883-897) to include ambient pore pressure, P_a, in the rock surrounding a fault zone with a fault-confined pore pressure, P_f. The modified definition is of the form

$$\mu^* = \mu(1 - \lambda'_n) = \mu\frac{(\sigma_n - P_f)}{\sigma_n - P_a)}$$

where

$$\lambda'_n = \frac{\Delta P}{\sigma'_n} = \frac{(P_f - P_a)}{\sigma_n - P_a)}$$

and σ_n is the normal stress across the fault plane. This form of the definition emphasizes that the upper bound on the apparent coefficient of friction, μ^*, for slip on a fault of arbitrary orientation, θ, in the presence of a second fault with the optimum, Coulomb orientation, θ_0 may be accommodated by variations in the intrinsic coefficient of friction, μ, and / or the pressure excess ΔP, of the fault-confined pressure over the ambient pore pressure.

Array Studies of Seismic Scattering (J.E. Vidale and H.M. Benz)

See separate summary by John E. Vidale and Harley M. Benz for project no. 9930-01496.

Publications

Hill, D.P., (in press), A note on ambient pore pressure, fault-confined pore pressure, and apparent friction: Bull. Seismol. Soc. Am.

Langbein, J.O., D.P. Hill, T.N. Parker, and S.K. Wilkinson, (in press), An episode of re-inflation of the Long Valley caldera, eastern California; 1989-1991; Jour. Geophys. Res.

Olson, J.A., and D.P. Hill, (in press), Seismicity in the southern Santa Cruz Mountains in the twenty years preceding the 1989 Loma Prieta, California, earthquake; in M.J.S. Johnston, ed., The Loma Prieta, California, Earthquake of October 17, 1989; Chapter C, Preseismic Observations, U.S. Geol. Survey Prof. Paper I - Earthquake Occurrence.

LONG VALLEY CALDERA — SEISMICITY
June 1 — July 2 1992

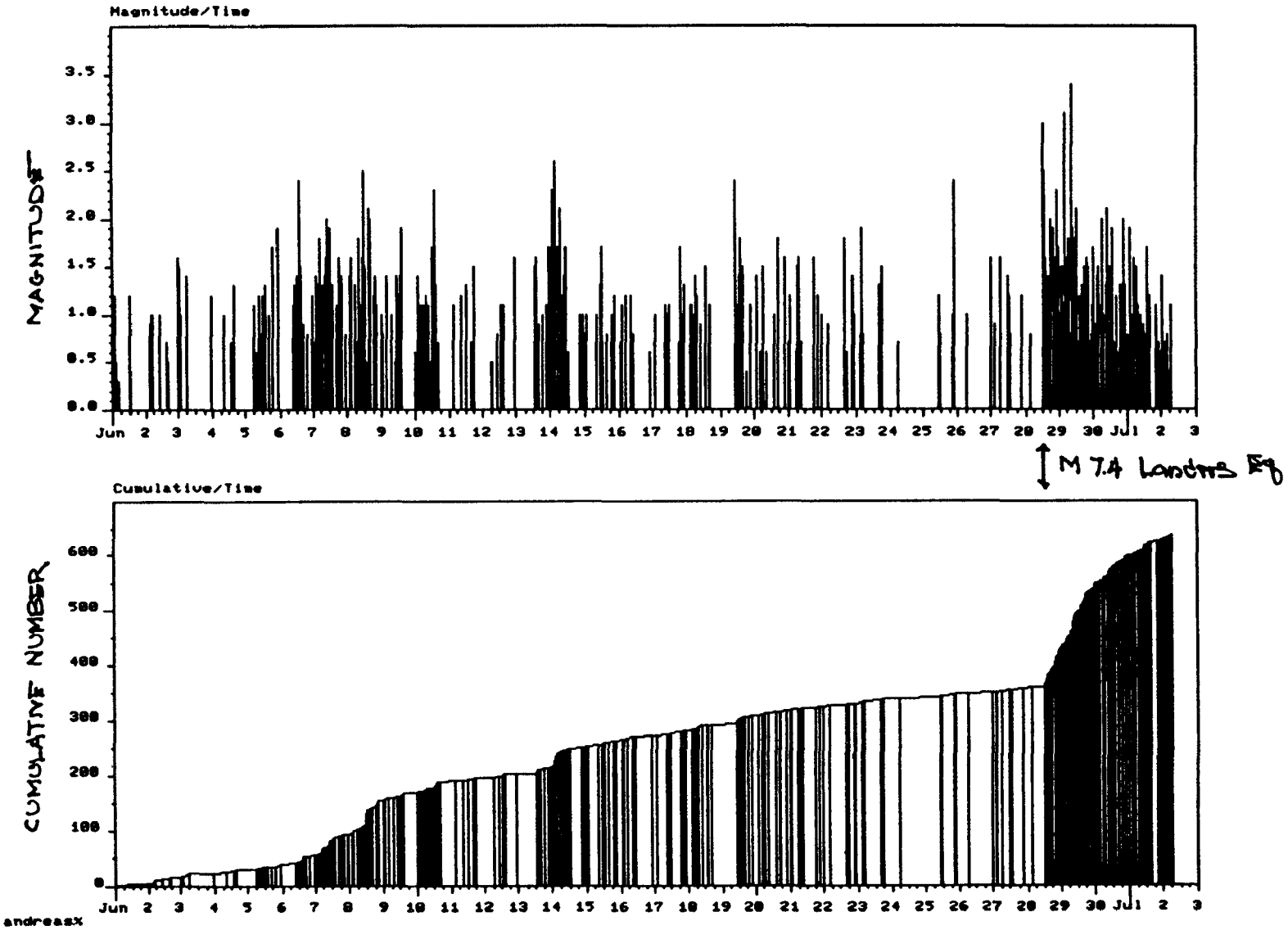

FIGURE 1

Computer Support Project

9920–10262

Roger N. Hunter
Branch of Global Seismology and Geomagnetism
U.S. Geological Survey
Denver Federal Center
Box 25046, Mail Stop 967
Denver, Colorado 80025
(303) 273–8472

Investigations

This project provides assistance to branch personnel in the area of IBM personal computers (hardware and software) and VAX programs. Primary focus has been on hardware procurement and graphics programs. The project also produces programs of its own as described below.

Results

Ethernet cards were procured for all branch PCs and are currently being installed. The net will link all PCs, Macintoshes, SUN workstations, and VAX computers using the TCP/IP network protocol.

The Interactive Mapping Program (IMP) is being sold to the public. IMP will plot the user's data on a Mercator map with a wide range of options. Two or three world outline sets are available (depending on the version). IMP was intended as an adjunct to the EPIC CD–ROM and reads those output files by default.

Two holograms were completed which use computer-generated images to display seismic information. They depict the seismicity in the San Francisco area. The first shows the Loma Prieta aftershock sequence and was featured on the cover of the special edition of the Bulletin of the Seismological Society of America (BSSA) distributed in October 1991. The second is a wider view of the San Francisco Bay area as seen from the northwest. These holograms are the second and third time that seismic information has been holographically displayed. (We also produced the first hologram representing seismic information.)

A PC-based Bulletin Board System (BBS) continues to serve as a focal point for seismic and geomagnetic information to the general public as well as participating scientists. It can be accessed by calling (303) 273–8508. We hope to add an 800 number in the future which will make the call less burdensome to the public. The BBS is used to permit the public to access the Quick Epicenter

Determination files and to leave messages to branch staff. Scientists can use it to leave seismic information or messages. The intent is to take some of the workload off of the VAX and to reduce the danger to the VAX from hackers. In order to promote amateur seismology, we have added an area for such purposes in the BBS and have allowed Mr. Robert Samuelson of New Hope, Minnesota, to post his programs and files there. Mr. Samuelson has built his own seismometer and is recording digital waveforms on his PC. He has also written a program to display the waveforms which can then be enlarged or shifted as needed. While this may have no immediate usefulness to the branch, we feel that amateur interest in seismology should be encouraged.

Global Seismograph Network Evaluation and Development

9920-68152

Charles R. Hutt
Branch of Global Seismology and Geomagnetism
U.S. Geological Survey
Albuquerque, New Mexico 87115-5000
(505) 846-5646

Investigations

Continued work in support of the US/USSR Joint Seismic Program.

Results

Equipment was ordered, assembled, and tested for a new Global Seismograph Network (GSN) station at Yuzhno-Sakhalinsk and two engineers from the station were trained over a two-week period at the Albuquerque Seismological Laboratory. The equipment and installation team were flown to Yuzhno-Sakhalinsk in May on a chartered Aeroflot plane and a successful installation was completed in June. Site visits were made to Petropavolvsk-Kamchatsky and Yakutsk to formulate agreements and to discuss actions needed to prepare these sites for installation of GSN systems in 1993. Both sites will require the construction of new vaults. A visit was also made to Magadan to meet with members of the seismological organization and inspect facilities to assess the feasibility of the future installation of a GSN station. Equipment has been ordered for the stations to be installed in 1993 and plans are being made for a training program.

Geophysical Framework
San Francisco Bay Earthquake Hazards

9380-03074

Robert C. Jachens and Andrew Griscom
U.S. Geological Survey MS 989
345 Middlefield Road
Menlo Park, CA 94025
(415) 329-5300

Investigations Undertaken

1) Gravity surveys were conducted in the Santa Cruz Mountains to fill in regional data gaps and to define the gravity anomalies along profiles critical to understanding the subsurface structure and lithology.

2) A new detailed aeromagnetic survey of northern San Jose and the east San Francisco Bay area was received from the contractor and merged with previous detailed surveys of San Jose, Menlo Park, and the San Francisco Peninsula.

3) A compilation of rock density and magnetic susceptibility was begun on samples from outcrops in the San Francisco Bay Area and surrounding mountains.

4) Most of our effort this past year was devoted to an interpretation of the structure of the upper crust surrounding the focus of the Loma Prieta earthquake. The main goals were to define the geophysical framework of this event and to examine the possible influence of crustal structure on fault movement and the distribution of aftershocks. This interpretation is based primarily on surface geology and modeling of gravity and magnetic anomalies constrained by information from seismic tomography and aftershock distributions. The interpretation is focused on the upper ten kilometers in the region bounded by the San Gregorio Fault to the west, the Gabilan Range to the south, the Calaveras and Silver Creek Faults to the east, and the latitude of the southern tip of San Francisco Bay to the north.

Results Obtained

1) The newly merged aeromagnetic map of the greater San Francisco Bay Area provides a detailed portrayal of the geomagnetic field in an area that extends from south of Santa Cruz to north of San Pablo Bay and from the west edge of the Great Valley nearly to the Pacific Coast. This map contains

detailed information on the subsurface distribution of plutonic rocks of the Salinian block southwest of the San Andreas Fault, mafic and ultramafic rocks of the Franciscan and younger terranes northeast of the San Andreas and Pilarcitos Faults, Cenozoic volcanic rocks throughout the region, and magnetic sedimentary strata mainly in the Diablo Range and the Santa Cruz Mountains. The new map displays prominant anomalies related to the Hayward Fault under San Pablo Bay and the northward continuation of the structures exposed at Mount Diable, anomalies which will provide additional insights into the crustal structure imaged by the BASIX experiment.

The new detailed aeromagnetic map has been merged with less detailed (1 km grid) aeromagnetic data to produce a statewide map of the geomagnetic field at an effective height of 300m above the earth's surface. This map provides a regional perspective for the highly detailed San Francisco Bay area survey and allows local structures to be interpreted within a regional context.

2) Combined interpretation of the geology, gravity, magnetic, and seismic data has resulted in substantial progress toward a model of the geology and structure of the upper 10 km of the crust of the Santa Cruz Mountains and adjacent Santa Clara Valley. The region southwest of the San Andreas Fault is made up of fault-bounded blocks floored by Mesozoic intrusive rocks. The La Honda Basin, wedged between the San Andreas and Zayante-Vergeles Faults, contains up to 6 km of Tertiary sedimentary rocks that overly a gabbroic basement probably related to ophiolitic rocks exposed at the southern end of the Sierra Nevada batholith. The Zayante-Vergeles Fault dips to the southwest, with Salinian block granitic rocks overriding the La Honda Basin block by as much as 10 km in places. In contrast the San Gregorio Fault farther southwest under Monterey Bay dips to the northeast.

Immediately northeast of the San Andreas Fault, the magnetic data have been critical in defining the upper crustal structure of the Franciscan and overlying terranes, and interpretations based on the gravity and magnetic anomalies indicate a tectonic history that includes obduction, uplift, tectonic wedging, dismemberment, and major lateral transport. One implication of this interpretation is that tectonic wedging has played a major role in the development of the Santa Cruz Mountains and that, unlike along the Great Valley-Coast Range boundary where the wedging is mostly confined to the subsurface and only revealed through geophysical and geologic inference, here the tectonic wedges have been tilted and eroded, providing exposed cross sections along which to study the phenomenon.

Still farther to the northeast but southwest of the Silver Creek Fault, the structural style within the Franciscan terranes is characterized by sedimentary blocks interleaved with flatlying sheets of serpentinite and mafic metavolcanic rocks. We infer that the Silver Creek Fault dips to the southwest.

3) A comparison of our crustal model with the distribution of aftershocks of the Loma Prieta earthquake leads us to the following observations and conclusions:

a) Many of the aftershocks that in plan view plot northeast of the San Andreas Fault trace, probably occurred on this fault. Although the distribution of aftershocks defines a major southwest-dipping zone of activity that most likely defines the San Andreas fault in the subsurface, the magnetic interpretation indicates that locally the San Andreas Fault must dip to the northeast in the top few km. The location of the inferred northeast dip coincides with a place where the aftershocks plot northeast of the fault trace.

b) Some isolated clusters of aftershocks southwest of the San Andreas Fault coincide with the inferred southwest subsurface projection of the Zayante-Vergeles Fault and probably reflect minor movement on this fault.

c) Many aftershocks appear to be associated with the Sargent Fault, which according to our crustal model cuts across the major structural boundaries in the Sierra Azule and underlying blocks. None of the inferred major structural boundaries are significantly offset by the Sargent Fault, suggesting that total offset on this fault is no more than a few kilometers

d) Some aftershocks near the northwest end of the aftershock zone probably occurred on a suite of southwest-dipping thrust faults in the vicinity of Cupertino.

e) The La Honda basin is floored by a coherent gabbroic block that is bounded on the northeast by the San Andreas Fault from just south of Logan quarry on the south to Lexington reservoir on the north. This reach coincides closely with the Loma Prieta "kink" in the San Andreas. The gabbroic block, as defined by the magnetic data, is remarkably free of aftershocks.

4) We now have a physical property data base with nearly 1300 elements, containing information on rock type, formation name, age, location, density, and magnetic susceptibility.

Reports Published

Jachens, R.C., and Griscom, Andrew, in press, Geologic and geophysical setting of the 1989 Loma Prieta earthquake, California, inferred from magnetic and gravity anomalies: U.S. Geological Survey Professional paper.

Jachens, Robert C., Griscom, Andrew, and McLaughlin, Robert J., 1992, Anatomy of the San Francisco Bay region: An evolving 3-D crustal model based on surface geology, and gravity and magnetic anomalies (abs.): EOS, Transactions, American Geophysical Union v. 73, p. 401.

Jachens, R.C., and Roberts, C.W., 1992, Aeromagnetic map of the San Francisco Bay area, California: U.S. Geological Survey Geophysical Investigations Map GP-1007, 1 sheet, scale approximately 1:286,500.

Roberts, C.W., and Jachens, R.C., 1992, Isostatic residual gravity map of the San Francisco Bay area, California: U.S. Geological Survey Geophysical Investigations map GP-1006, 1 sheet, scale approximately 1:286,500. (on satellite image, with interpretive text)

U.S. Geological Survey, 1992, Aeromagnetic map of Livermore and vicinity, California: U.S. Geological Survey Open File Report 92-531, 1 sheet, scale 1:250,000.

Wentworth, C.M., Jachens, R.C., Simpson, R.W., and Michael, A.J., 1992, Structure of the Parkfield region, CA, from geology and geophysics compiled in a geographic information system (GIS) (abs.): EOS, Transactions, American Geophysical Union v. 73, p. 396.

Instrument Development and Quality Control

9930-01726

E. Gray Jensen
Branch of Seismology
U.S. Geological Survey
345 Middlefield Road - Mail Stop 977
Menlo Park, California 94025
(415) 329-4729

Investigations

This project supports other projects in the Office of Earthquakes, Volcanoes and Engineering by designing and developing new instrumentation and by evaluating and improving existing equipment in order to maintain high quality in the data acquired by the Office. Tasks undertaken during this period include production of a 20 digital seismic telemetry field stations, support and maintenance of Seismic Group Recorders operations, development of a new Real Time Processor (RTP) for CALNET and supporting the establishment of an instrument center among other things.

Results

Twenty digital seismic telemetry (DST) field station a nearing completion. A prototype unit has been in field operation for some time monitoring a borehole seismic station. All printed circuit boards for the field station have been created. Final assembly and testing of the 20 production units is proceeding. In anticipation of deployment of these and other commercial digital stations, this project has been instrumenting and monitoring new borehole seismometers along the southern Hayward Fault. Use of portable recorders has proved the lower noise capability of the borehole sensors and revealed which sensors are not functioning in the preliminary test holes.

Development of an new RTP has shifted from Rex Allen's design based on transputers to a broader project based on multiple PCs or Suns connected by networks. In addition to picking and locating events on CalNet, we would like to integrate data from other sources such as new digital seismic stations. The goals for system output have been expanded to include rapid notification of event parameters to a variety of users.

The PASSCAL Instrument Center was established at this office late in 1991. The center now has over 100 3-channel, 195 megabyte seismic recorders for refraction and other experiments. This project has supported the establishment and operation of this IRIS center.

The Seismic Group Recorders have been busy during the last year. They were used in projects in the Pacific Northwest, southern California, Mexico, Canada, Montana, Nevada and the California north coast. This project supported most of these operations with instrument maintenance and some field support.

Piñon Flat Observatory: Comparative Studies and Geophysical Investigations

14-08-0001-G1763

Hadley O. Johnson, Frank K. Wyatt,
Duncan C. Agnew, James W. Happer
Institute of Geophysics and Planetary Physics
Scripps Institution of Oceanography
University of California, San Diego
La Jolla, CA 92093-0225
(619) 534-2411

This grant provides support for collaborative studies with several USGS-sponsored investigators conducting research at Piñon Flat Observatory (PFO). We briefly describe here a few of the projects we have been engaged in during the previous year. Each of these turns out to involve, in one way or another, GPS geodesy; while this has not been our primary focus in the past, we have found it very useful to examine this widely-used technique. Much of the work in this field has been, quite reasonably, on applying the technique to solving tectonic problems. Instead, our focus under this grant has been to try to fully understand the capabilities and error sources involved with this technique.

A particularly interesting study we have undertaken is a comparison between GPS and the two-color EDM data of Dr. John Langbein from his networks at Pinyon Flat and Anza—both near the San Jacinto Fault in southern California. Figure 1 shows the relative locations of the two-color and Geodolite (one-color EDM) networks to PFO. Over the span of these networks (1—10 km), the two-color system has been shown to have 1 mm or better precision, something we would like to be able to duplicate with GPS. But in order to understand how to process GPS data over these distances, we need a standard for comparison; the two-color data provide this.

The comparison is not straightforward, however, because of the nature of the 2-color Terrameter measurements.[1] This system does not in fact measure the absolute distance; unlike most EDM's it does not measure the phase of a signal modulated at different frequencies, but instead adjusts the modulation frequency until a null is found, meaning that there are an integer number of modulation wavelengths, N, in the optical path. This is done for two colors, red and blue, giving two frequencies f_i^r and f_i^b for the measurement over the i-th line. If f_i^r and f_i^b are separated by approximately 42 kHz (which is forced by the operator), N will be the same for both (because of the dispersive nature of the atmosphere). The relationship between the line distance d_i and the measurements is then

$$d_i = N_i \frac{c}{2}\left[\frac{1}{f_i^r} - A_i^r\left(\frac{1}{f_i^b} - \frac{1}{f_i^r}\right)\right] + C_\tau \equiv N_i \lambda_i + C_\tau$$

where c is the speed of light, A^r is related to the ratios of the index of refraction of red and

[1] We have received much help on this from Dr. Langbein, and have also found the thesis of Slater (1975) very useful.

blue light (and is found from end-point meteorological data), λ_i is the (defined) modulation wavelength, and C_τ is an instrument (and reflector) constant. If the instrument is used to find only changes in d_i, as it usually is, C_τ drops out and we need only a rough estimate of N, which is calculated using a measurement over a nearby parallel line with an HP3808 EDM. However, if we seek to compare absolute lengths, we need to know both N_i and C_τ—and neither of these is known *a priori*. (Note that for measurements on i lines there will always be $i + 1$ unknowns.)

Now suppose that we have measured GPS distances g_i over M lines; assuming that the 2-color measurement is error-free, we have $d_i = g_i + e_i$, e_i being the error in the GPS distance. Then N is given as a function of C_τ and e_i by

$$N = \frac{g_i + e_i - C_\tau}{\lambda_i}$$

For any value of C_τ we must select a set of e_i to make the N found by this formula an integer. This does not constrain C_τ at all, but we may do so by minimizing the variance of the GPS errors, that is by choosing C_τ to make $S(C_\tau) = \sum_{i=1}^{M} e_i^2$ a minimum. For each survey line, the curve of e_i as a function of C_τ will be periodic with period λ_i (see figure 2). Since for the actual measurements λ_i is always 5 cm to within a few parts per million, S will have this same periodicity. We can uniquely determine the minimum GPS error, and will then find C_τ to "modulo" 5 cm. Of course, our method chooses a distribution of e_i's centered on zero; any length-independent bias in the GPS results will bias our estimate of C_τ.

In April 1992 we conducted a GPS survey of most of the lines in the two-color network across Pinyon Flat, in two eight-hour sessions in the afternoon and evening of the same day. The data were processed using the GAMIT software and orbits provided by Dr. Yehuda Bock at UCSD from the PGGA network.[2] One line (Green to the fixed station PIN2) was common to both surveys. The ionosphere-free observable LC was used for final processing, even though the lines were all less than 5 kilometers long; this gave the most consistent results for the two surveys of this one repeated line. Data from two EDM surveys conducted in January and May 1992 were used for comparison. (The two EDM surveys used different two-color instruments which have different error characteristics and different instrument constants.) Figure 2 shows the process of comparing the GPS and EDM data sets. The left panels show the individual traces of e_i^2 as a function of C_τ for each line (each two-color line is actually shown twice, since the USGS crew routinely makes two measurements on successive nights during each survey, resulting in two independent estimates of the line length.) The right panels show $S^{1/2}$ as a function of C_τ; the minima are well-defined and lead to estimates for the rms error of the GPS measurements of 1.2 mm and 1.5 mm—impressively small misfits. The best estimates for C_τ are 2.052 m and 2.061 m for the two EDM instruments used; these particular values were chosen over the other equally good ones based on Dr. Langbein's previous best estimates for the C_τ.

We have thus determined the precision of these GPS measurements over distances of a few kilometers, as well as the instrument constants of two of the Terrameter instruments. We

[2] The Permanent GPS Geodetic Array (PGGA) is a continuous GPS network covering the southern California region and operated as a joint project between a consortium of universities and the Jet Propulsion Laboratory.

have yet to fully reduce the data for the two-color networks near the town of Anza, but the field work has been completed, and the computer work is progressing nicely. We will examine these additional data to check their consistency with the results from the PFO net. Since some of the Anza lines are up to 12 kilometers long it will be interesting to see what GPS errors appear at these longer distances. In comparing these longer GPS results with the two-color data we can use the instrument constant derived from the shorter network around Piñon to see if any bias appears in the GPS results at longer distances; we can also see if the scatter goes up to the level that we expect from our repeat measurements over a 14-kilometer continuous line (briefly described below).

We are also in a position to help others use the two-color net at PFO for testing precise GPS techniques; in particular, the lack of obstructions at PFO means that a kinematic survey of the two-color marks could be done as easily as a more conventional one. Finally, the determination of C_τ means that the absolute line-lengths of other two-color measurements can be found to a few mm as long as they are known to within 5 cm: an easy task using conventional EDM or GPS. (With more data for our comparisons we should be able to reduce this few mm uncertainty to less than 1 mm.)

The favorable results from our comparison work with the two-color EDM system lead one to the issue of benchmark stability. With the level of precision that is possible with modern geodetic techniques, it is important to be sure that the data are not degraded because the ground mark moves in response to local soil instabilities. The construction of well-stabilized monuments is something that our long-term focus on strain and tilt measurements has caused us to be interested in, and we have tried to apply our knowledge to create several designs of highly-stable marks (Figure 3). These designs have as a basic principle the concept of bracing the mark using several inclined rods cemented into holes; this is an extension of the NGS "rod mark," which uses a single vertical rod. The angled rods form a space frame, making their intersection point very resistant to applied forces, including forces applied by the near-surface material especially as the monument is nearly free-standing over its upper 6 m. This gives deep-ground stability to a near-surface mark in both the horizontal and the vertical directions.

We have constructed three deeply-anchored monuments to be used by the two-color EDM at Pinyon Flat. One, at Green (Green c), is intended to replace the existing central monument; a second one (PF5c) is near PF5, and the third (PIN3c) is adjacent to the existing GPS marks at PFO, with which it can thus be compared. These new marks have already been surveyed twice by the USGS crew (both before and after the Landers earthquake of June 1992) and accurately tied to the previous measurements.

Finally, since May 1991 we have operated a continuously tracking "GPS strainmeter" between two receivers located near PFO as a joint project with Dr. Yehuda Bock and Dr. David Jackson at UCLA (see figure 1 for locations). The receivers are located on an almost directly east-west line of 14 km length—a length scale of particular interest for fault mechanics studies. During the last year this instrument has operated well and is providing an unparalleled understanding of the true spectrum of the errors associated with GPS measurements. From our work with this data, it appears that the day-to-day scatter of the GPS positioning estimates is approximately ±5 mm E-W, ±4 mm N-S, and ±12 mm U-D (over a 14 km line). These uncertainties are comparable to those attained by the USGS single-color Geodolite EDM program. As a comparison of the relative detection capabilities of the GPS strainmeter, figure 4 presents a series of East-West GPS distance estimates (converted to strain) and data from the three

long-baselength laser strainmeters we operate at PFO (the modulation seen on the laser strainmeter data are the earth tides). Clearly, and even with averaging, the strainmeters can detect much smaller signals, by a factor of 100 to 1,000, than the GPS data can over the relatively short time-span of this figure. Last year's report presents more details of this experiment.

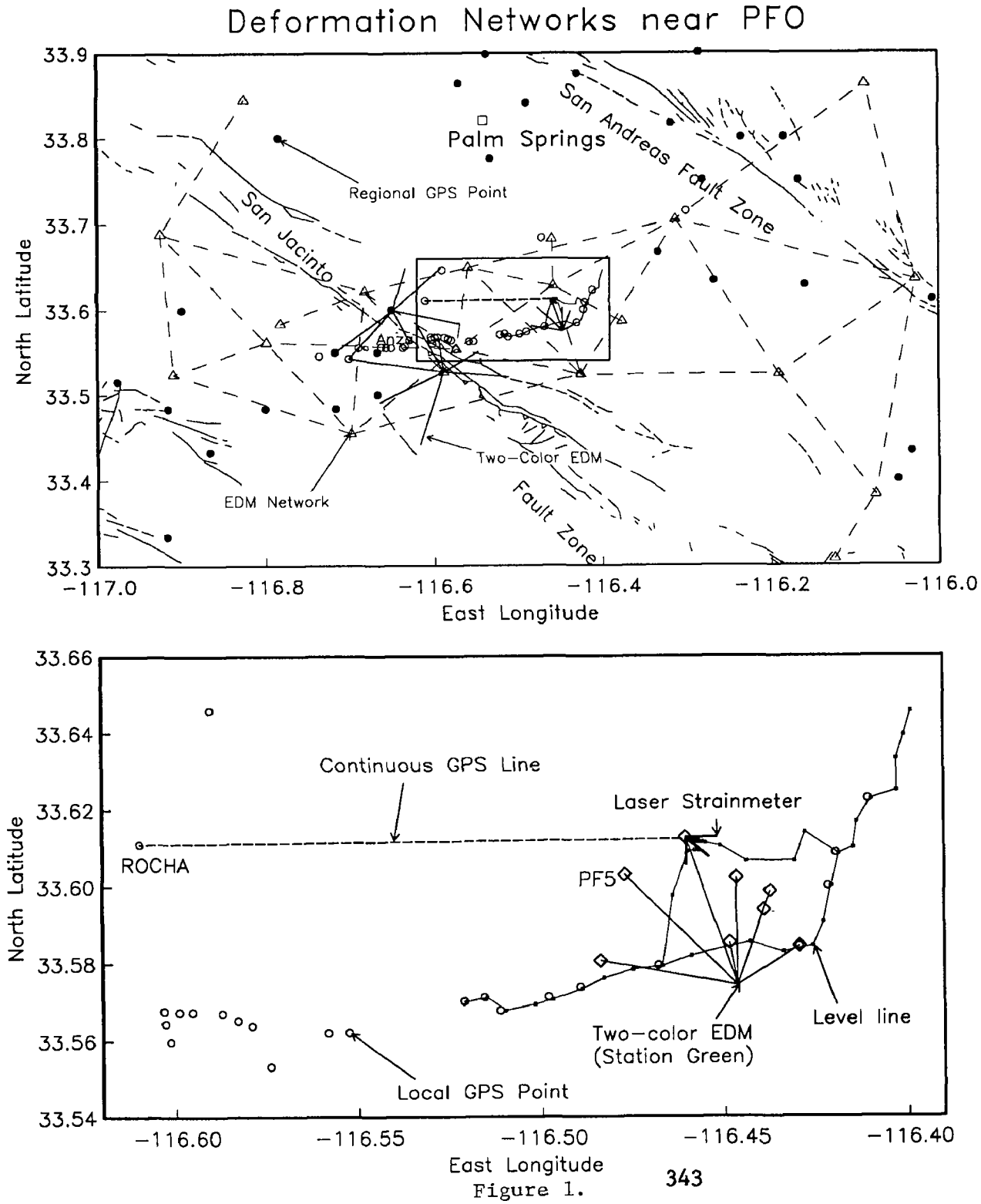

Figure 1.

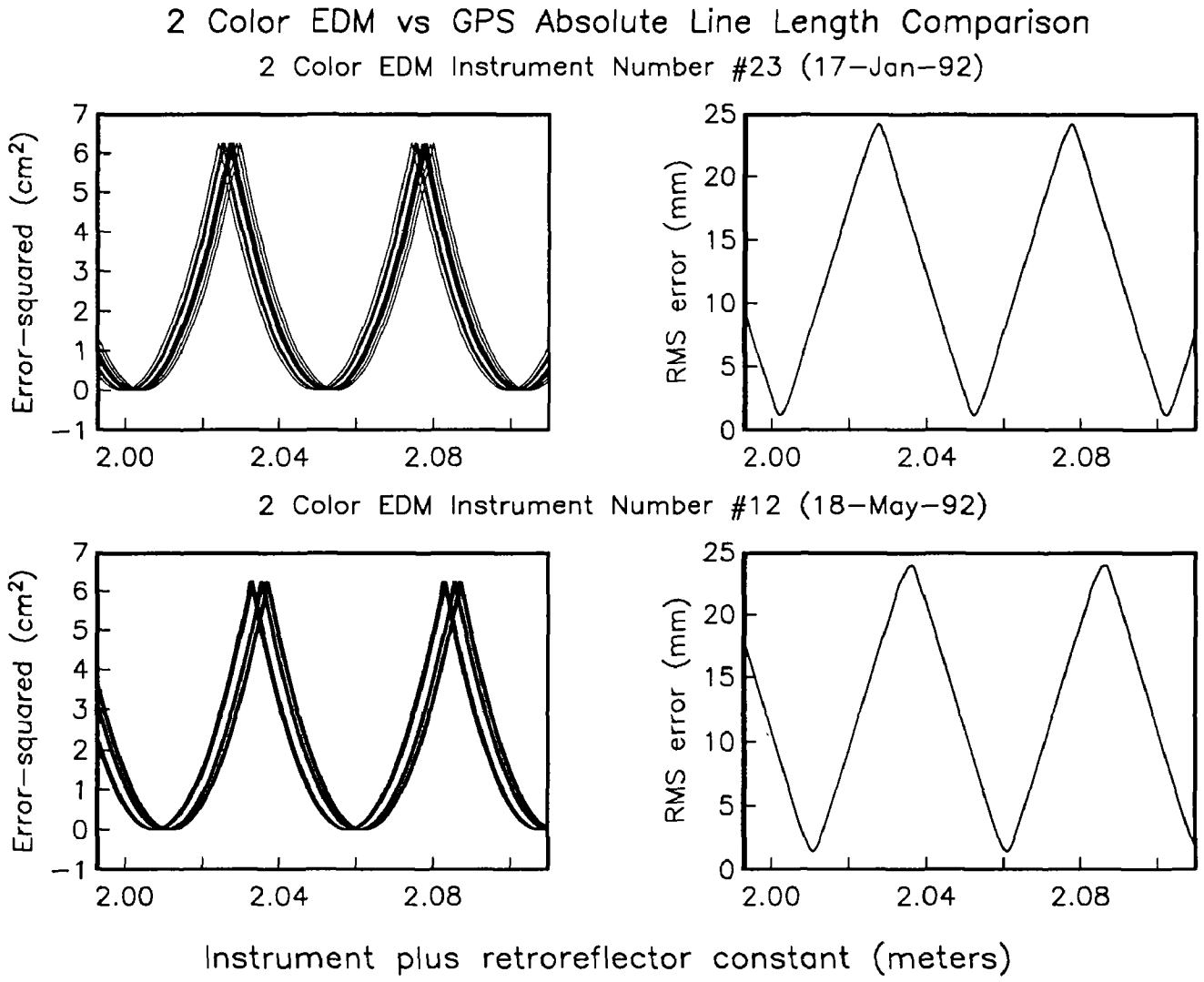
2 Color EDM vs GPS Absolute Line Length Comparison
2 Color EDM Instrument Number #23 (17-Jan-92)
Error-squared (cm²)
RMS error (mm)
2 Color EDM Instrument Number #12 (18-May-92)
Error-squared (cm²)
RMS error (mm)
Instrument plus retroreflector constant (meters)

Figure 2.

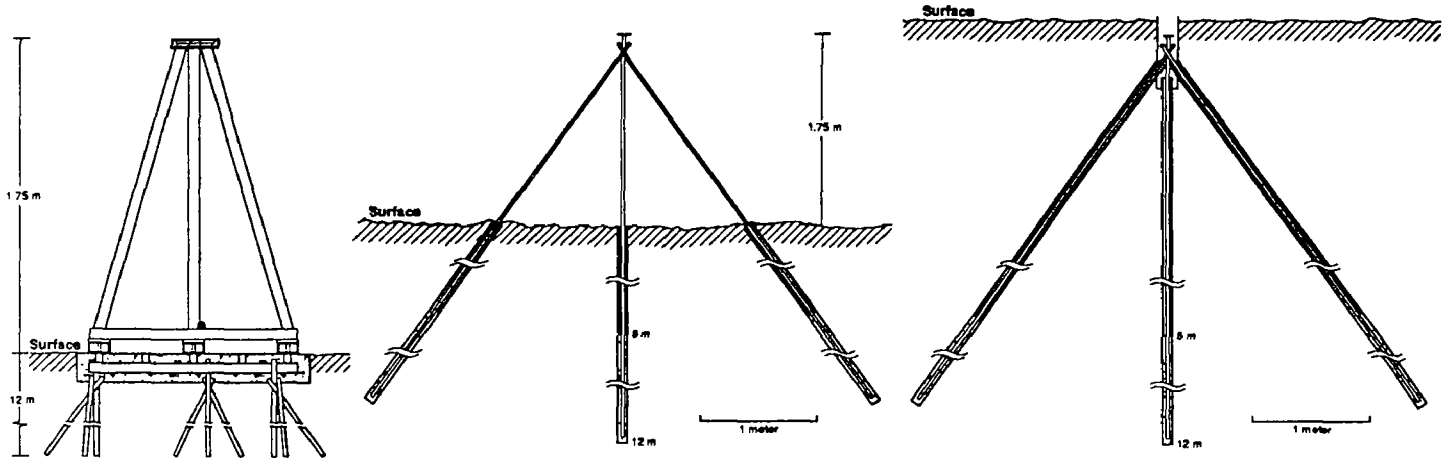

PIN1 PIN2 PIN3, Green c, PF5c

Figure 3.

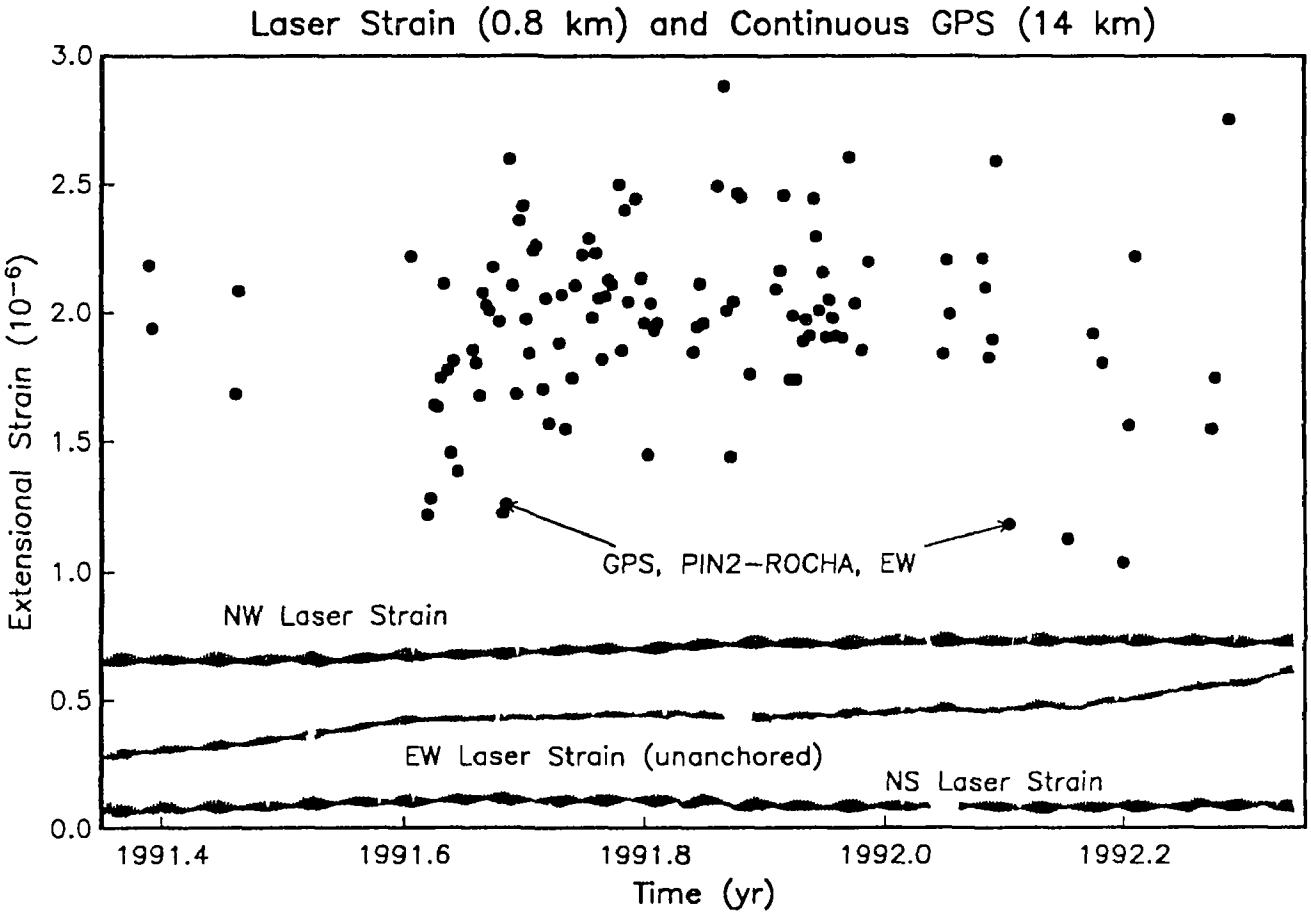

Figure 4.

Source Parameters of the 1957 Aleutian Earthquake from Tsunami Waveforms

Agreement No. 1434-92-G-2187

Jean M. Johnson and Kenji Satake
University of Michigan
1006 C.C. Little Building
Ann Arbor, MI 48109-1063
(313) 763-4069

I. Introduction

On 9 March 1957 a great earthquake (M_S=8.1) occurred in the central Aleutian Islands at 51.63°N, 175.41°W at 14:22 GMT. There are little seismic data available for this earthquake because it occurred before the introduction of the WWSSN stations. Due to this dearth of high quality data, this earthquake has been poorly understood. Elementary source parameters such as rupture area, seismic moment and slip distribution have not been well determined.

The source area of an earthquake is often identified as the region containing the aftershocks, which often delineate the fault rupture plane. The aftershock zone of the 1957 earthquake is the longest of any earthquake ever recorded. It stretches 1200km along the Aleutian Trench from approximately 164°W to 180°W (Figure 1). Both Sykes (1971) and Kanamori (1977) used the 1200km long aftershock zone of the 1957 earthquake in estimating the seismic moment. But these estimates are an order of magnitude different. Sykes' estimate of 30×10^{20}Nm is derived from the length of the aftershock zone and an average slip on the fault of 0.45m. Kanamori estimated the moment as 585×10^{20}Nm based on the relationship between source area and moment release, making the 1957 earthquake the third largest this century. However, House*et al.* (1981) argued that the easternmost area of the aftershock zone near Unalaska Island is anomalous and suggested that this area did not rupture in the 1957 main earthquake. In any case, the aftershock zone is an indirect means of deriving the moment.

The moment of the 1957 earthquake has also been estimated by more direct methods. Abe (1979) used the relationship between maximum tsunami height and earthquake moment to assign a tsunami magnitude of M_t=9.0 to the 1957 earthquake. The equivalent moment is 400×10^{20}Nm. Ruff *et al.* (1985) used the single

available surface wave record from the 1957 earthquake to estimate the slip distribution and determined a moment of 100×10^{20}Nm. However, the response of the instrument in Pietermaritzburg, South Africa where the surface wave was recorded, is poorly known, making results from this seismic data suspect. Lane and Boyd (1990) have studied the surface wave directivity of this surface wave record by a nonlinear inversion (simulated annealing), but they could only determine the rupture length of the earthquake.

From this brief review it is obvious that many questions about the basic source parameters of the 1957 Aleutian earthquake remain. Moment estimates range from $30\text{-}585 \times 10^{20}$Nm. Even the rupture area is not well established. Lack of seismic data has hampered past efforts to determine these parameters precisely. There is, however, a good quality data set available for this earthquake. The tsunami generated by the earthquake was recorded on tide gauges all around the Pacific Ocean. The tsunami waveforms can be used to determine the source parameters of the 1957 earthquake.

2. Computation of Tsunami Propagation

A tsunami which is generated by a large earthquake and propagates across the ocean can be treated as a linear long wave because the wavelength is much larger than the water depth. The wave equation for the small amplitude, linear long wave is

$$\nabla h^2 = \frac{1}{c^2}\frac{\partial^2 h}{\partial t^2}$$

where $c = \sqrt{gd}$, h is the height of water displaced from the equilibrium position, g is the acceleration of gravity, and d is water depth. Equivalently, the equation of motion and the equation of continuity are

$$\frac{\partial Q}{\partial t} = -gd\nabla h$$

$$\frac{\partial h}{\partial t} = -\nabla \cdot Q$$

where Q is the flow rate vector.

Given an initial condition, or water height, the equation of motion and equation of continuity can be solved by finite-difference calculations on a staggered grid system. Using highly accurate, digital bathymetry of the Pacific Ocean, the tsunami velocity and thus tsunami propagation can be calculated very accurately.

The initial condition is specified by the deformation of the ocean floor due to a buried fault as given by a program like Okada's (1985). This provides the initial condition in the source area. The tsunami propagation is calculated and a synthetic waveform is computed at the location of the tide gauges where the tsunami was actually observed.

Obviously, the tsunami velocity depends only on the water depth; therefore, the synthetic waveform is very sensitive to the bathymetry. The more accurate the bathymetry, the more accurate the computation. This suggests that a fine grid system be adopted in which to calculate the tsunami propagation. However, very fine grid-spacing on the entire northern Pacific Basin would be impractical due to the enormous computational effort. For the majority of the deep Pacific Ocean where the bathymetry changes slowly, the grid space need not be any finer than 5' (approximately 10 km). However, near coastal areas, the bathymetry changes much more rapidly. Also, islands and harbors where tide gauges are located cannot be adequately represented by 5' grid spacing. Therefore, in coastal areas, 1' (less than 2 km) grid spacing is used. Bathymetry of 1' accuracy is used for the west coast of North America, the Hawaiian Islands, and around the tide gauges in Alaska. Figure 2 shows the difference between 5' and 1' grid spacing around the island of Unalaska. With 5' bathymetry, Dutch Harbor, where the tide gauge is located, completely disappears.

3. Tsunami Source Area

As stated previously, the aftershock zone of the 1957 earthquake is the longest of any earthquake ever recorded. The eastern end of this aftershock zone has very few aftershocks, and it has been suggested that this area did not rupture in the 1957 main event. An alternative to equating the aftershock area and the source area is to determine the source area by tsunami data.

The tsunami source area can be located by a backward computation of the tsunami travel time from the source to the tide gauge. An initial condition is given at the tide gauge location. The tsunami propagates from the tide gauge for the duration of the observed tsunami travel time to that tide gauge. The location of the leading wavefront, or travel time arc, gives the origin point of the tsunami that reached that tide gauge. When many such travel time arcs from tide gauges distributed around the earthquake are combined, they bound a region that is the source area of the tsunami. Hatori (1981) used this method to determine the source area (Figure

3). Hatori's source area includes the eastern end of the aftershock area. However, this estimate may be unreliable. Few of the available observations were used. Also, the travel time arcs associated with both Unalaska Island and Sitka are questionable. The travel time used by Hatori for Sitka does not agree with any published travel time, nor does it agree with the apparent arrival time on the Sitka tide gauge record. Hatori's travel time arc for Unalaska is not compatible with a backward travel time of 83 minutes from Dutch Harbor where the tide gauge is located. Without these two travel time arcs, there is no constraint on the eastern end. But most significantly, Hatori drew the inverse refraction diagrams for all the travel times manually from large-scale bathymetric maps of the Pacific Ocean.

Our numerical calculation done on a fine grid of the actual Pacific Ocean bathymetry gives more reliable results. We computed travel time arcs from tide gauges in Alaska, N. America, and Hawaii. Figure 4 shows the travel time arcs and source area. Our source area is approximately 850km long, from 180°E to 168°W, and does not include the eastern end of the aftershock zone. Similar results were obtained by Lane and Boyd (1990) using surface wave directivity.

This supports the theory of House *et al.*(1981) that the 1957 earthquake ruptured a smaller section of the arc than can be assumed from the aftershock area.

We further performed forward modeling on two different fault models, with different lengths as shown in Figure 5. The longer fault is 1100km and covers the entire aftershock area, while the shorter is 600km and covers the western half of the aftershock area. The other parameters are the same for both (W=150km, δ=30°, and average slip S=1m). The results for one tide gauges is shown in Figure 6. The observed tsunami waveform from Dutch Harbor, Unalaska Is. is shown with synthetic waveforms from the short and long fault models. Clearly, the arrival time for the long fault model synthetic waveform is inconsistent with the observed tsunami arrival time. This again supports the hypothesis that the eastern end of the aftershock zone was not involved in the 1957 event.

5. Tsunami Waveform Inversion

Method

The best way to determine the source area and moment distribution of the 1957 earthquake is to directly invert the waveforms. We can obtain the slip distribution on the 1957 rupture zone, which will give an estimate of the moment and source area.

The method for inverting tsunami waveforms has been used previously by Satake (1989) for determining the slip distribution of the 1968 Tokachi-Oki and the 1983 Japan Sea earthquakes. Those studies used local and regional tsunami data, while this study is the first to determine slip distribution from far-field tsunami waveforms. However, the method is the same.

The fault area is divided up into subfaults. The latitude, longitude, strike, dip, depth, and area of each subfault is specified. The vertical deformation of the seafloor from unit displacement on each subfault is calculated. This bottom deformation is then used as the initial condition, and a waveform is calculated at each tide gauge from each subfault. This results in Green's functions for each tide gauge. The observed waveform is a linear superposition of the Green's functions, so the displacement on each subfault can be determined by solving the linear equation

$$A_{ij} \cdot x_j = b_i$$

where A_{ij} is the computed Green's function at tide gauge i for unit slip on subfault j, b_i is the observation at tide gauge i, and x_j is the unknown slip on subfault j. This equation can be solved by least-squares method by minimizing the misfit between the observed and synthetic waveforms.

Results

We divided the aftershock zone of the 1957 earthquake into eleven subfaults. The fault parameters were the same for each subfault. The parameters were L=100km, W=150km, δ=15°, and depth to the top of the subfault 1km. Figure 9 shows the location of the subfaults in relation to the Aleutian Arc. Each subfault has unit displacement in the direction of Pacific Plate motion relative to N. America. The displacement direction was determined for each subfault individually from the Euler pole at 48.7°N, -78.2°E with rotation rate of 0.78 deg-m.y.$^{-1}$ (DeMets *et al*, 1990). This means that the slip changes from pure dip-slip in the eastern end of the rupture zone to nearly equal components of dip-slip and strike-slip in the west. The tsunami waveform was then computed for each subfault. Figure 7 shows an example of the resulting Green's functions for the tide gauge at Massacre Bay, Attu Island.

Next we inverted the waveforms from 12 tide gauges from Alaska, the Aleutians, Hawaii, and N. America. These tide gauges are Attu, Unalaska, and Yakutat, AK; Neah Bay, WA; San Francisco, Alameda, San Pedro, Los Angeles Harbor, Newport Bay, and San Diego, CA; and Hilo, HI. The waveform data at each tide gauge station

consists of an average of 110 time points (dt=1 min) and the total number of data points is 1312. Figure 8 shows the observed and computed waveforms from some of these tide gauges. We performed both a free inversion (least-squares with no constraints on the solution), and an inversion with a positivity constraint. The slip distribution from the solution with a positivity constraint can be seen in Figure 9. It shows that the greatest slip occurred in the western half of the aftershock zone between 174°W and 180°E. The greatest slip occurred on subfault 4 (7m) and subfault 5 (5m) between 174° and 177°W. There is very little slip in the eastern half of the aftershock zone, with subfault eight having the only appreciable slip. There is no slip in the easternmost subfaults (aside from negligible slip on subfault 11) from 164° to 169°W, which corresponds to the results from determination of the tsunami source area. The results for both free and constrained solutions are compared in Table 1. The slip distributions in the western half of the rupture zone for both inversions are fairly compatible. In the eastern half the negative values in the free inversion are almost all zero under the positivity constraint. The RMS values for both inversions are almost the same. However, the synthetic and observed waveforms match more closely in the constrained solution, particularly for Dutch Harbor, as shown in Figure 10. The positivity constraint forces the slip in subfaults 10 and 11 to zero to match the Dutch Harbor waveform.

It is obvious from Figures 9 and 10 that the solutions from both the free and constrained inversion are unable to match the first positive pulse at Unalaska and San Francisco. A large displacement on subfault 8 can explain the pulse at Unalaska, and a large displacement on subfault 9 can explain the first pulse at San Francisco. However, large displacements in either of these subfaults is incompatible with the large amplitude wave at Hilo. We hypothesized from an examination of first arrival times at the three tide gauges in question that a large displacement on a subfault of smaller area and at the down-dip edge of subfault 8 or 9 might be compatible with all three waveforms. Accordingly, we divided subfaults 8 and 9 into smaller faults. Figure 11 shows the position of the additional subfaults 12 and 13. These subfaults have parameters L=50km, W=75km, δ=15°, and depth to the top of fault 20.4km. Green's functions were computed for these additional faults, and the inversion was performed again. The results are listed in Table 2. Figure 10 shows that a displacement of 3.3m on subfault 12 matches the first pulse on the Unalaska waveform and is still compatible with the Hilo waveform. However, the first pulse on the San Francisco waveform is still poorly matched. The solution for 13 subfaults is

compatible with our hypothesis of concentration of slip on a smaller subfault in the eastern half of the rupture zone. It is also compatible with the total average slip for the entire rupture zone, as the slip on subfault 12 is approximately four times the slip on subfault 8 from the solution for eleven subfaults.

Error Estimates

The formal statistical errors for a standard least-squares inversion are not considered a good estimate of the actual errors (Tichelaar and Ruff, 1989). Further no formal errors can be estimated for a non-negative least-squares inversion. Therefore, we applied a resampling technique to determine the errors. We reinverted the tsunami waveforms twelve times, each time dropping one waveform from each of the tide gauge stations from the data. This gives twelve estimates of the slip distribution, and a mean and standard deviation for the slip on each subfault can be determined. The results are listed in Tables 1 and 2 for each of the four inversions described in the previous section. The error estimates are almost all less than a meter. The errors show that the data is well-resolved, except for subfault 11. Therefore, the concentration of slip in the western half of the rupture zone and the small slip in the eastern half are real.

This technique for determining the errors is similar to the jackknifing technique described by Tichelaar and Ruff (1989). In jackknifing, a fixed number of random data points are deleted to produce a resample that is then inverted for the model parameters. Our technique is a pseudo-jackknife because we treat each waveform as a single data point. The resulting standard deviations of this pseudo-jackknifing technique are the same as the standard deviations derived above. If we treat each waveform as 110 data points out of a total of 1312 data points, then we must consider our resample as a delete-110 jackknife with corresponding errors. These errors are simply the standard errors derived above multiplied by a scale factor. In our case, that scale factor is approximately 3. This increases the errors we have determined enormously. However, since we delete an entire waveform at a time, rather than 110 random data points, the errors determined can be strongly influenced by the presence or absence of certain waveforms. Hence, we cannot compare directly the errors from the pseudo-jackknife to the true jackknife errors.

6. Discussion

As stated in the introduction, estimates of the seismic moment release in the 1957 earthquake vary by as much as an order of magnitude. With slip distribution as determined by tsunami waveforms, the seismic moment can now be accurately estimated. Table 1 summarizes the moment as determined by the four inversions. The highest of these estimates is 88×10^{20}Nm and the lowest is 67×10^{20}Nm. These estimates give a moment magnitude of M_W=8.5-8.6. This is much smaller than the estimate of Mw=9.1 originally assigned by Kanamori (1977). However, this estimate is in good agreement with the later estimate of 100×10^{20}Nm by Ruff *et al.* (1985), which was determined from the surface wave record. Although the magnification of the Pietermaritzburg instrument is only poorly known, the results from surface wave studies are more reliable than determining the moment purely from the aftershock area which has already been shown to be smaller than the actual rupture area. Ruff *et al.* also determined the moment distribution as shown in Figure 12. It shows that the greatest moment release occurred in the western half of the aftershock zone and that little moment was released in the eastern half. Again this is similar to results from the tsunami waveform inversion. Therefore, the estimates from the surface wave record and the tide gauge records confirm each other. It should be noted, however, that Boyd *et al* (1992) have speculated from the aftershock sequence that moment release was concentrated in the eastern section of the aftershock zone from 167° to 175°W rather than in the western section.

7. Conclusions

We studied the source parameters of the 1957 Aleutian earthquake using the tsunami waveform data recorded on tide gauges around the Pacific Ocean. Using a finite-difference computation, this tsunami can be numerically simulated. The tsunami source area was estimated by backward computation of the tsunami. The tsunami records were inverted for the slip distribution on the rupture area. Results show that slip was concentrated in the western half of the aftershock zone with a maximum displacement of 7m. The moment computed from the slip distribution is 88×10^{20}Nm, giving the 1957 earthquake a moment magnitude of M_W=8.6. Both the backward computation and the waveform inversion confirm that no slip occurred in the Unalaska Island area, making this area a possible

seismic gap with a potential to rupture in a great earthquake and generate a Pacific-wide tsunami.

8. References

Abe, K., Size of great earthquakes of 1873-1974 inferred from tsunami data , *J. Geophys. Res., 84*, 1561-1568, 1979.

Boyd, T.M., E.R. Engdahl, and W. Spence, Analysis of Seismicity Associated with a Complete Seismic Cycle Along the Aleutian Arc: 1957-1989, in Wadati Conference on Great Subduction Earthquakes, Sept. 16-19, University of Alaska (43-50 in extended abstracts).

DeMets, C., R.G. Gordon, D.F. Argus, and S. Stein, Current plate motions, *Geophys. J. Int., 101*, 425-478, 1990.

Hatori, T., Tsunami magnitude and source area of the Aleutian-Alaska tsunamis, *Bull. Earthq. Res. Inst., Univ. of Tokyo, 56*, 97-110, 1981.

House, L.S., L.R. Sykes, J.N. Davies, and K.H. Jacob, Identification of a possible seismic gap near Unalaska island, eastern Aleutians, Alaska, in *Earthquake Prediction - An International Review*, edited by D. W. Simpson and P. G. Richards, 81-92, American Geophysical Union, 1981.

Kanamori, H., The energy release in great earthquakes, *J. Geophys. Res., 82*, 2981-2987, 1977.

Lane, F.D., and T.M. Boyd, A simulated annealing approach to the inversion of surface wave directivities, *EOS, 71*, 1468, 1990.

Okada, Y., Surface deformation due to shear and tensile faults in a half-space, *Bull. Seism. Soc. Am., 75*, 1135-1154, 1985.

Ruff, L., H. Kanamori, and L.R. Sykes, The 1957 great Aleutian earthquake, *EOS, 66*, 298, 1985.

Satake, K., Inversion of tsunami waveforms for the estimation of heterogeneous fault motion of large submarine earthquakes: the 1968 Tokachi-oki and the 1983 Japan Sea earthquakes, *J. Geophys. Res., 94*, 5627-5636, 1989.

Sykes, L., Aftershock zones of great earthquakes, seismicity gaps, and earthquake predicion for Alaska and the Aleutians, *J. Geophys. Res., 76*, 8021-8041, 1971.

Tichelaar, B. W., and L. J. Ruff, How Good are Our Best Models? Jackknifing, Bootstrapping, and Earthquake Depth, *EOS, 70*, 593,605-606, 1989.

Table 1 Inversion results for 11 subfaults

	non-negative LS		standard LS	
subfault #	slip	error	slip	error
1	1.1	0.66	1.3	1.93
2	1.5	0.51	1.3	1.17
3	3.7	1.00	3.6	1.31
4	7.0	1.07	6.1	1.15
5	5.2	0.59	4.5	0.74
6	0.0	0.00	-1.4	0.37
7	0.0	0.16	-0.25	0.44
8	0.76	0.32	0.81	0.27
9	0.0	0.35	-0.45	0.47
10	0.0	0.00	-2.5	0.54
11	0.08	0.27	2.5	0.53

RMS error, cm	10.02	9.67
average slip, m	1.77	1.42
Mo, 10^{20} Nm	87.6	70.3

Table 2 Inversion results for 13 subfaults

	non-negative LS		standard LS	
subfault #	slip	error	slip	error
1	1.5	0.74	1.7	1.77
2	1.3	0.46	0.99	1.30
3	4.0	1.04	4.0	0.53
4	6.9	1.10	6.0	1.01
5	4.8	0.56	3.6	0.65
6	0.0	0.00	-1.4	0.43
7	0.0	0.01	-0.12	0.37
8	0.0	0.13	-0.30	0.75
9	0.0	0.32	-0.55	0.46
10	0.0	0.00	-2.8	1.76
11	0.32	0.27	3.0	1.67
12	3.3	0.26	5.1	0.64
13	0.0	0.03	-1.6	1.49

RMS error, cm	9.75	9.25
average slip, m	1.70	1.36
Mo, 10^{20} Nm	84.2	67.3

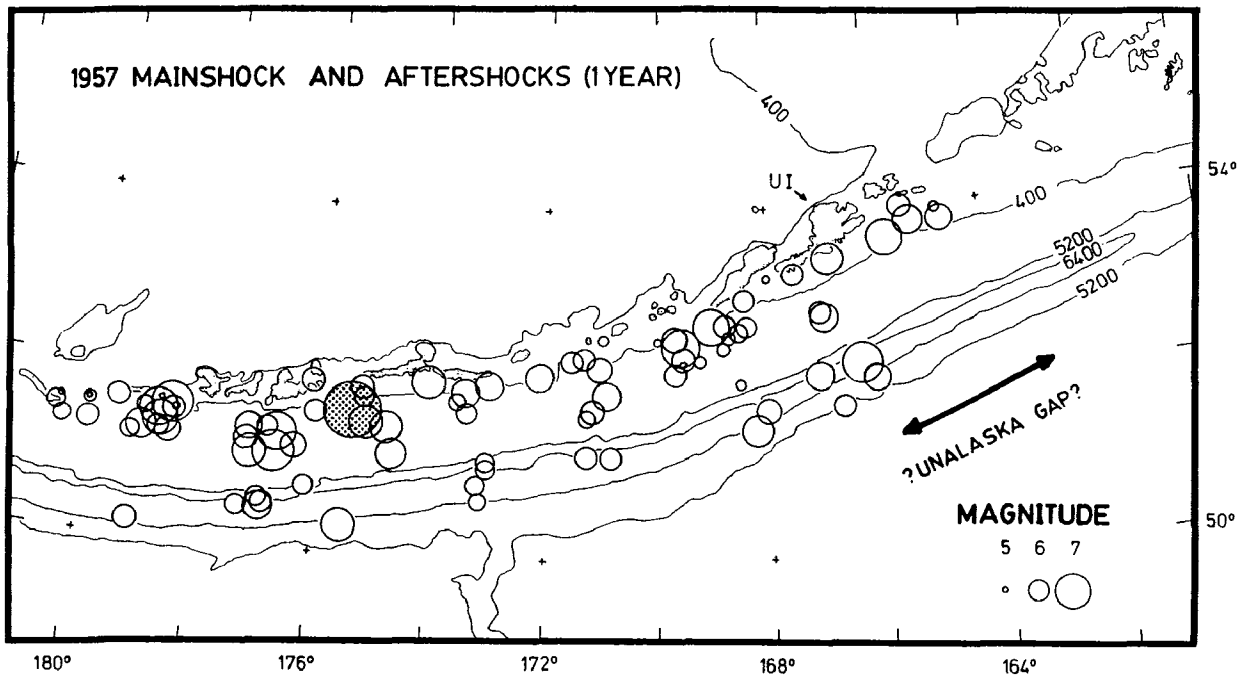

Figure 1: Detailed plot of the 1957 main shock and aftershocks over a period of 1 year. Aftershocks of March 1957 relocated by Sykes [1971] are supplemented by aftershocks located by the International Seismological Summary and the U.S. Coast and Geodetic Survey. Size of symbols is scaled to magnitude; only events assigned a magnitude of 5 or larger are plotted. The 1957 main shock is shaded and is plotted with a symbol appropriate for its surface wave magnitude (M_S) of 8.1 rather than its M_W of 9.1. UI indicates the location of Unalaska Island. Bathymetry is in meters. (from House *et al*, 1981)

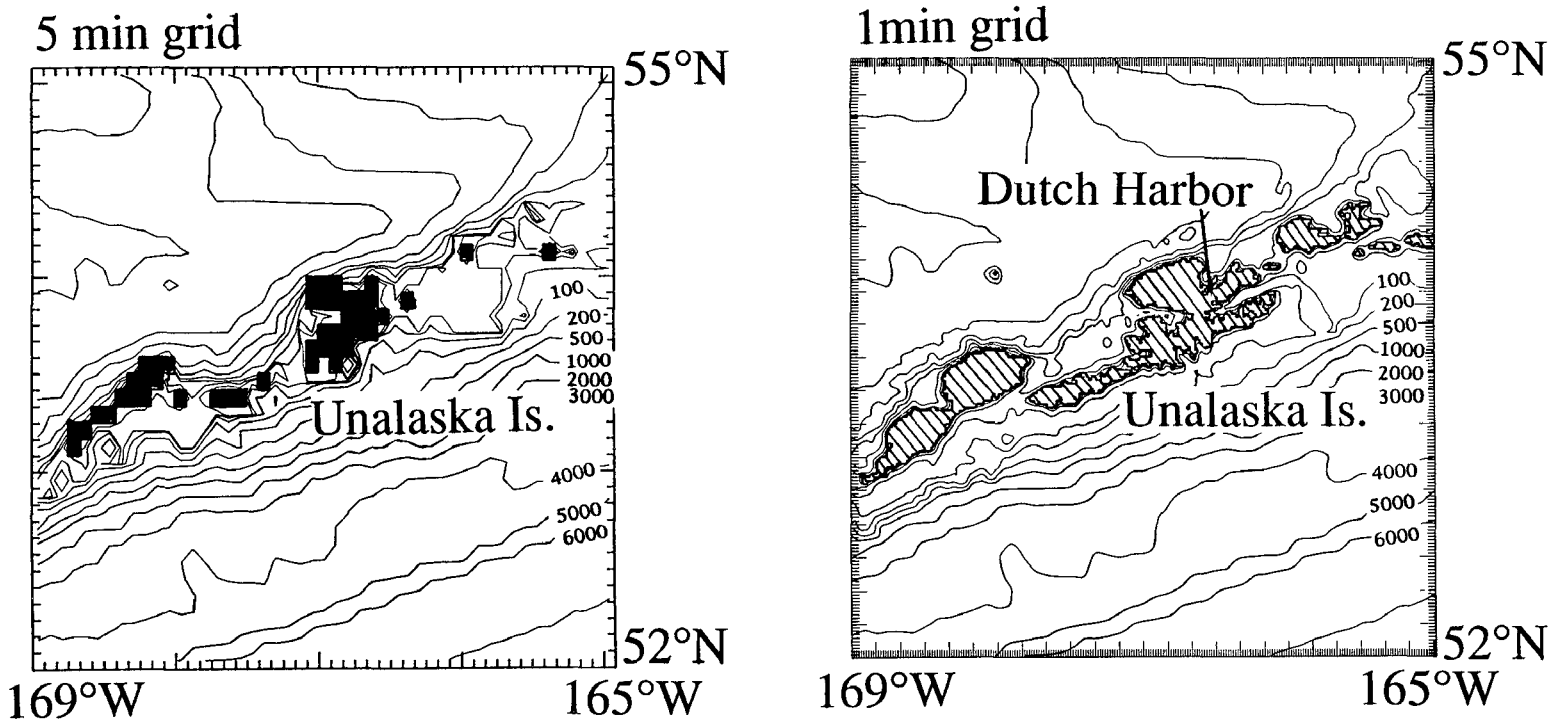

Figure 2: Comparison of detailed bathymetry near Unalaska Island using 5 minute grid size and 1 minute grid size. Bathymetry of the deep ocean is identical at 1 min or 5 min, but the islands cannot be well-represented at 5 min. The location of Dutch Harbor is indicated in the figure with 1 min grid size; at 5 min it disappears entirely. Bathymetry is in meters.

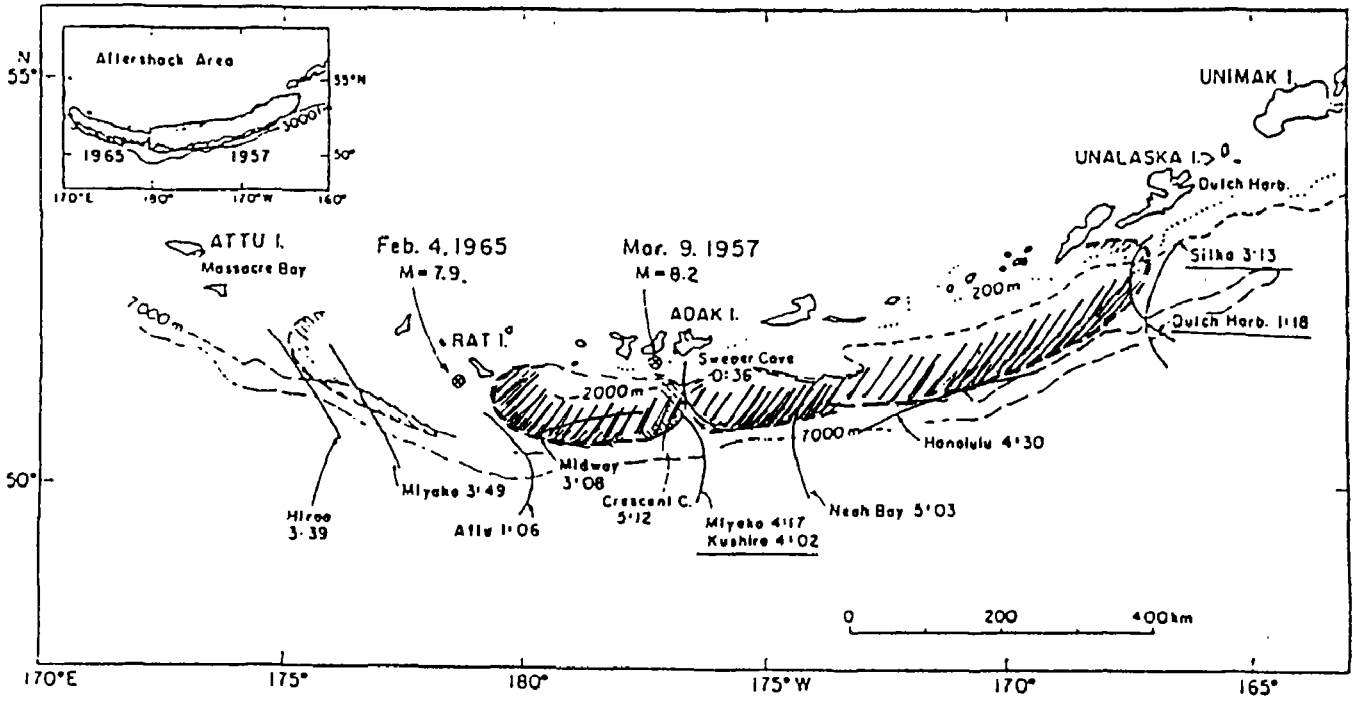

Figure 3: The tsunami source area of the 1957 and 1965 Aleutian earthquakes estimated by Hatori (1981).

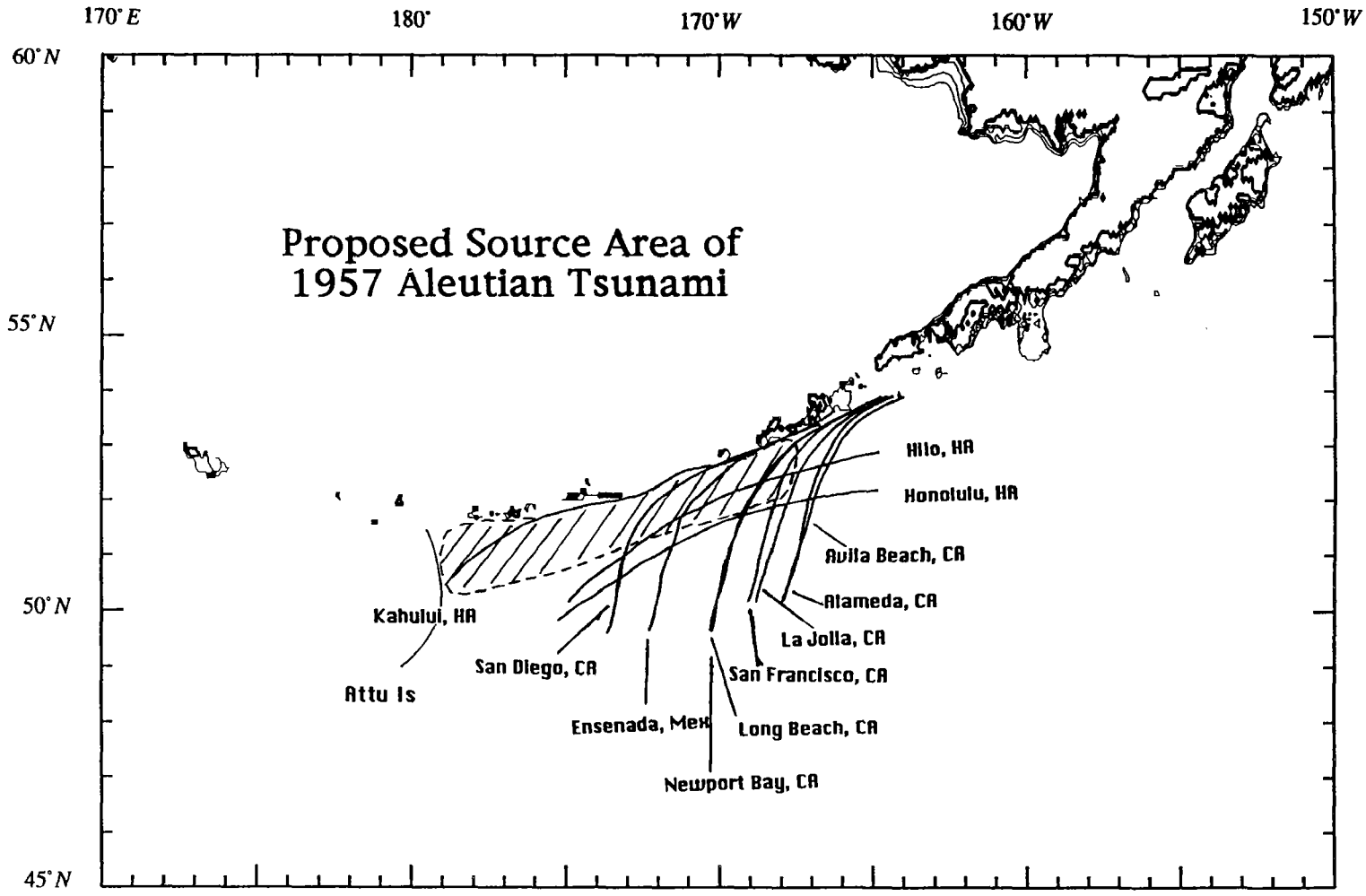

Figure 4: The source area of the 1957 Aleutian earthquake estimated by backward computation (finite-difference) of the tsunami.

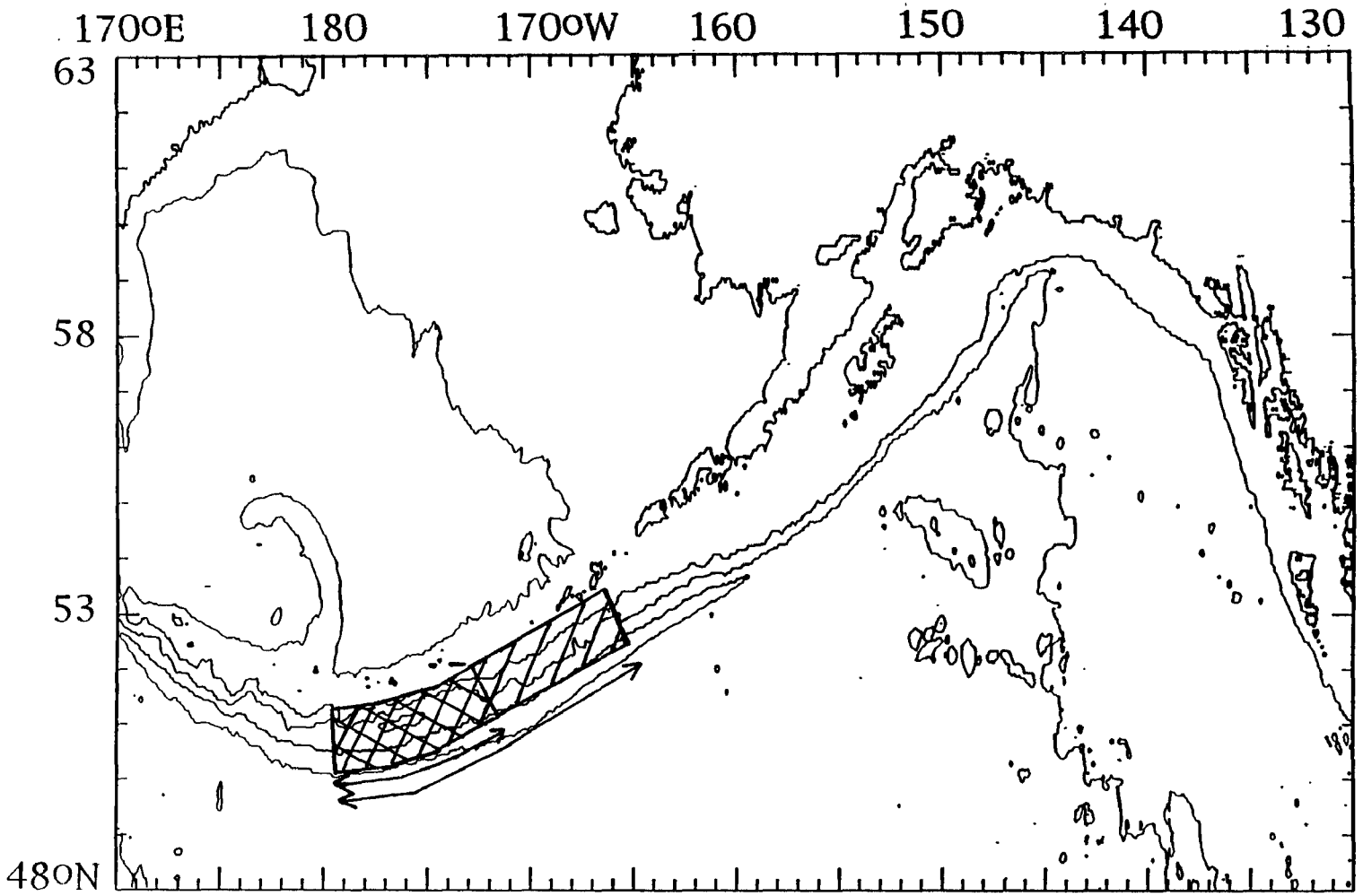

Figure 5: Long and short fault models for forward modeling of tsunami. The short fault is 600km long, the long fault is 1100km long. Both models have width 150km, and dip 30°.

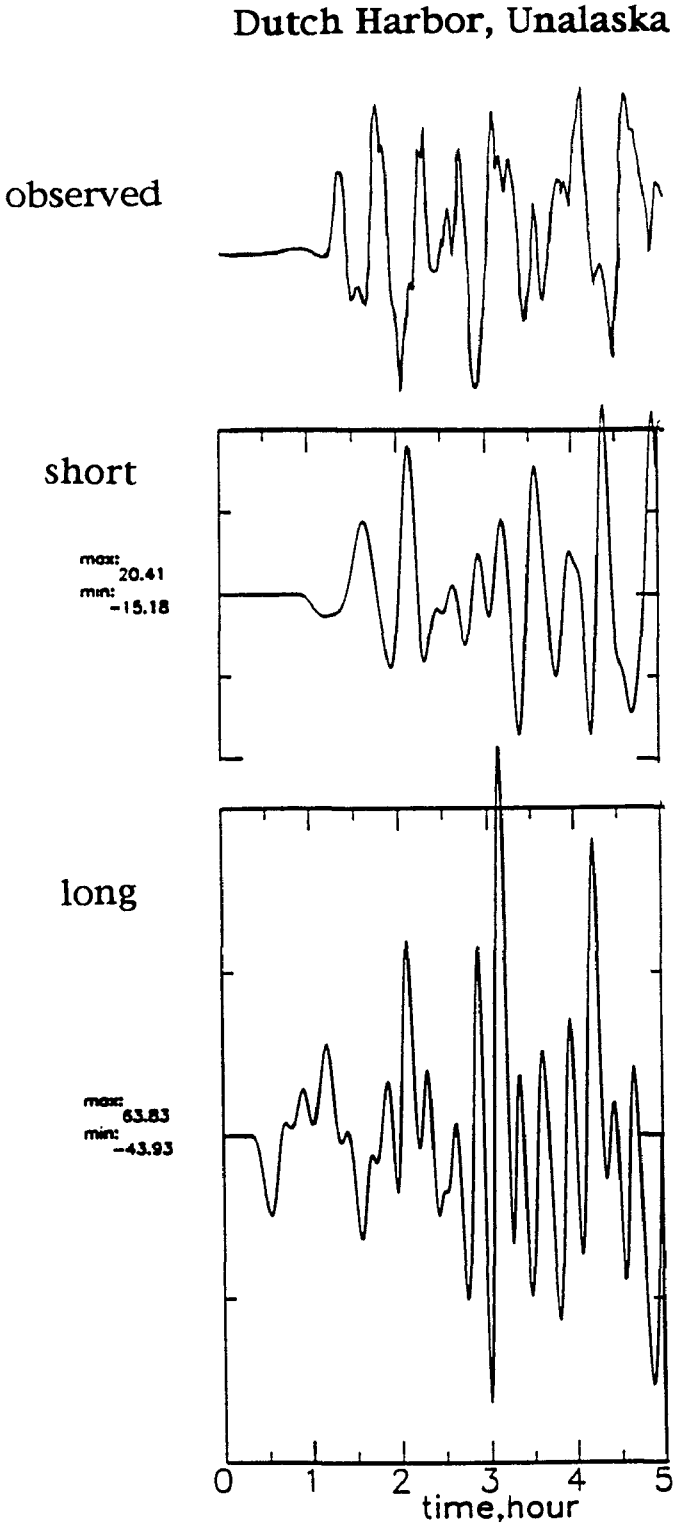

Figure 6: Results of forward modeling. The upper figure is the observed tsunami waveform recorded at Dutch Harbor, Unalaska. The middle figure is the synthetic waveform from the short fault model, the lower figure is the waveform from the long fault model. The amplitude is given in centimeters.

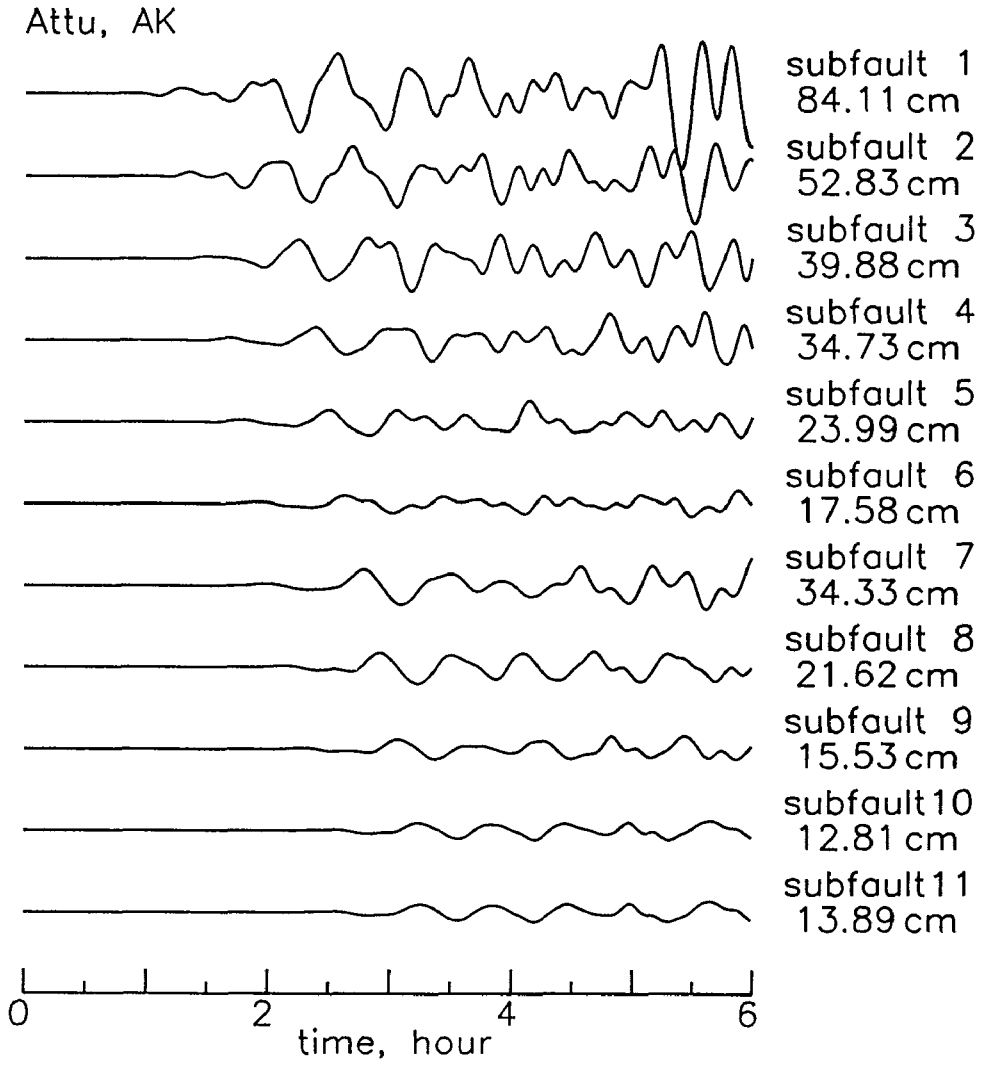

Figure 7: Computed waveforms from each subfault for Attu Island, AK. Amplitude is maximum peak-to-peak amplitude in centimeters.

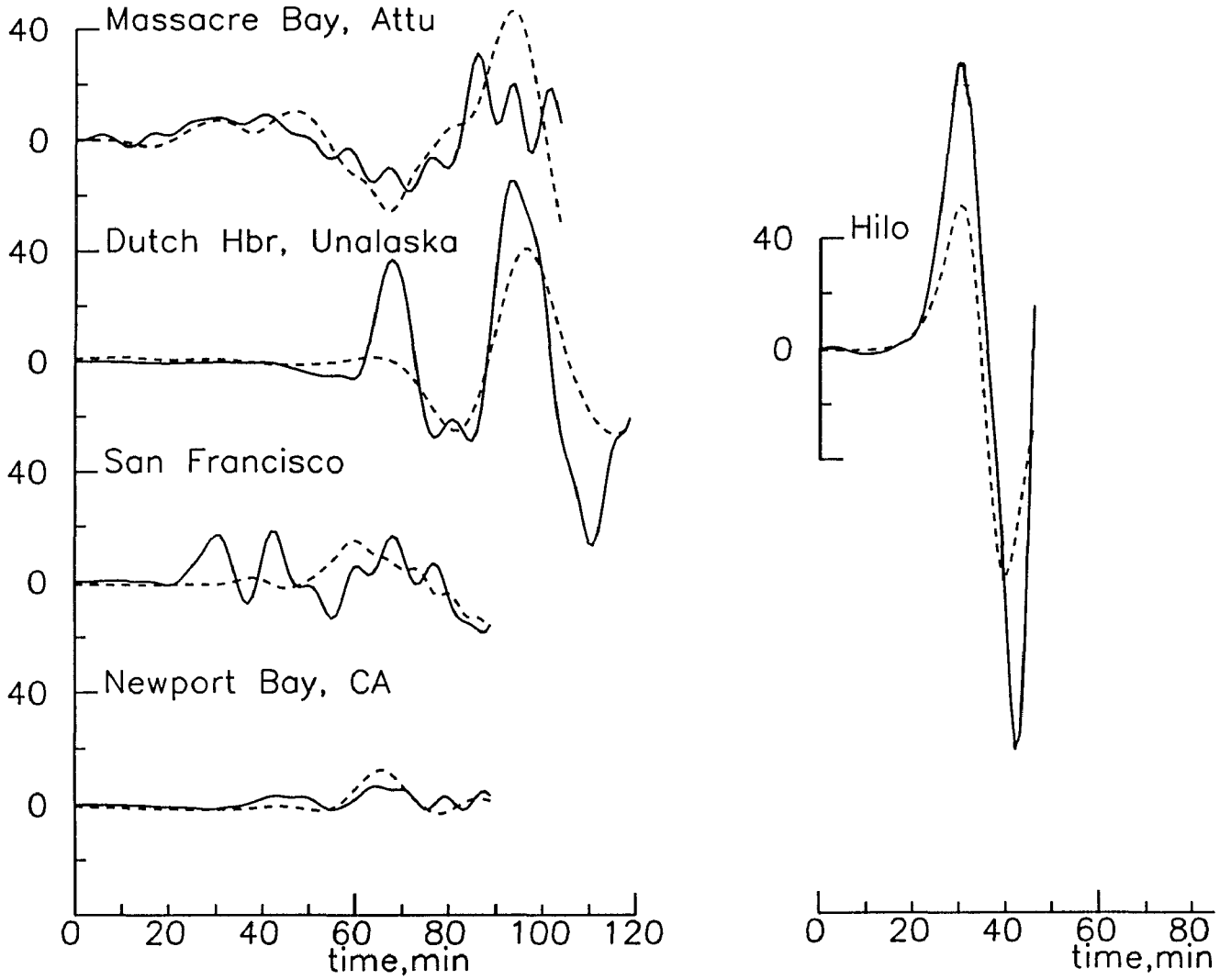

Figure 8: Observed and synthetic waveforms from non-negative least squares inversion for eleven subfaults. The solid line is observed and dashed is synthetic. Amplitude is in centimeters. Start time of each waveform is different.

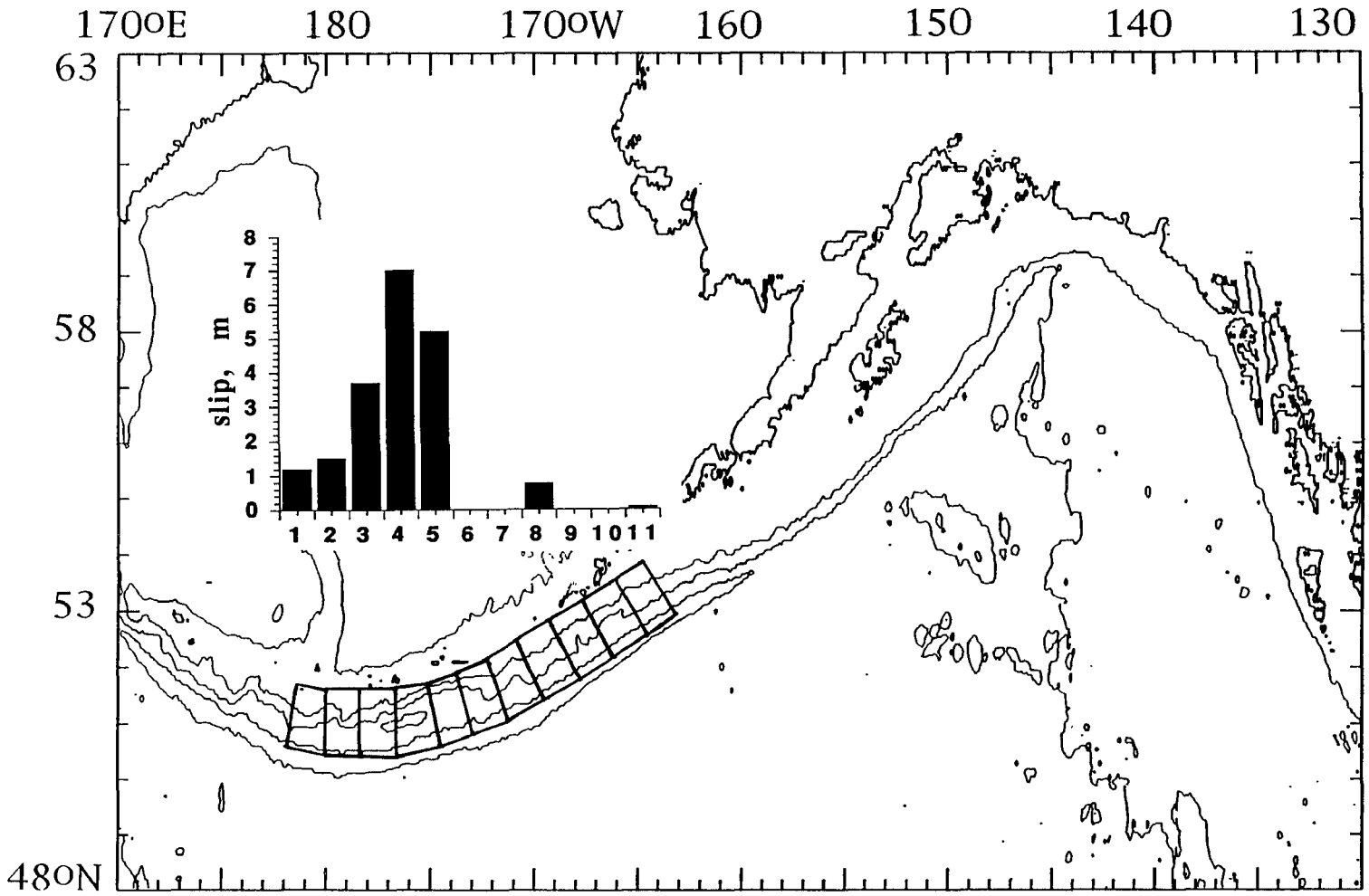

Figure 9: Slip distribution on rupture zone of 1957 earthquake from non-negative least-squares inversion on eleven subfaults. The numbered segments correspond to the subfault immediately below.

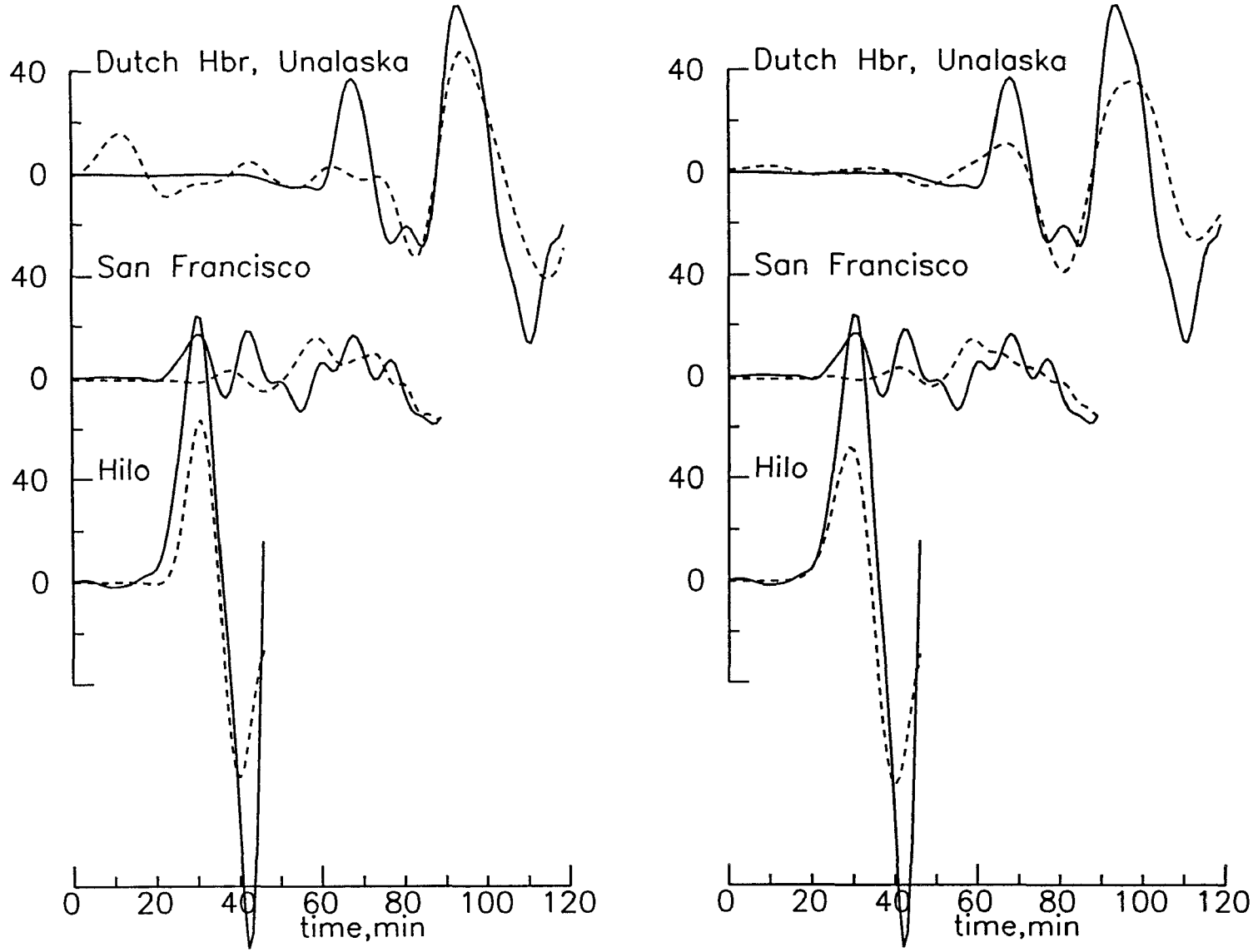

Figure 10. Observed and synthetic waveforms from (left) standard least squares inversion for eleven subfaults and (right) nonnegative least squares inversion for 13 subfaults. Solid line is observed and dashed is synthetic.

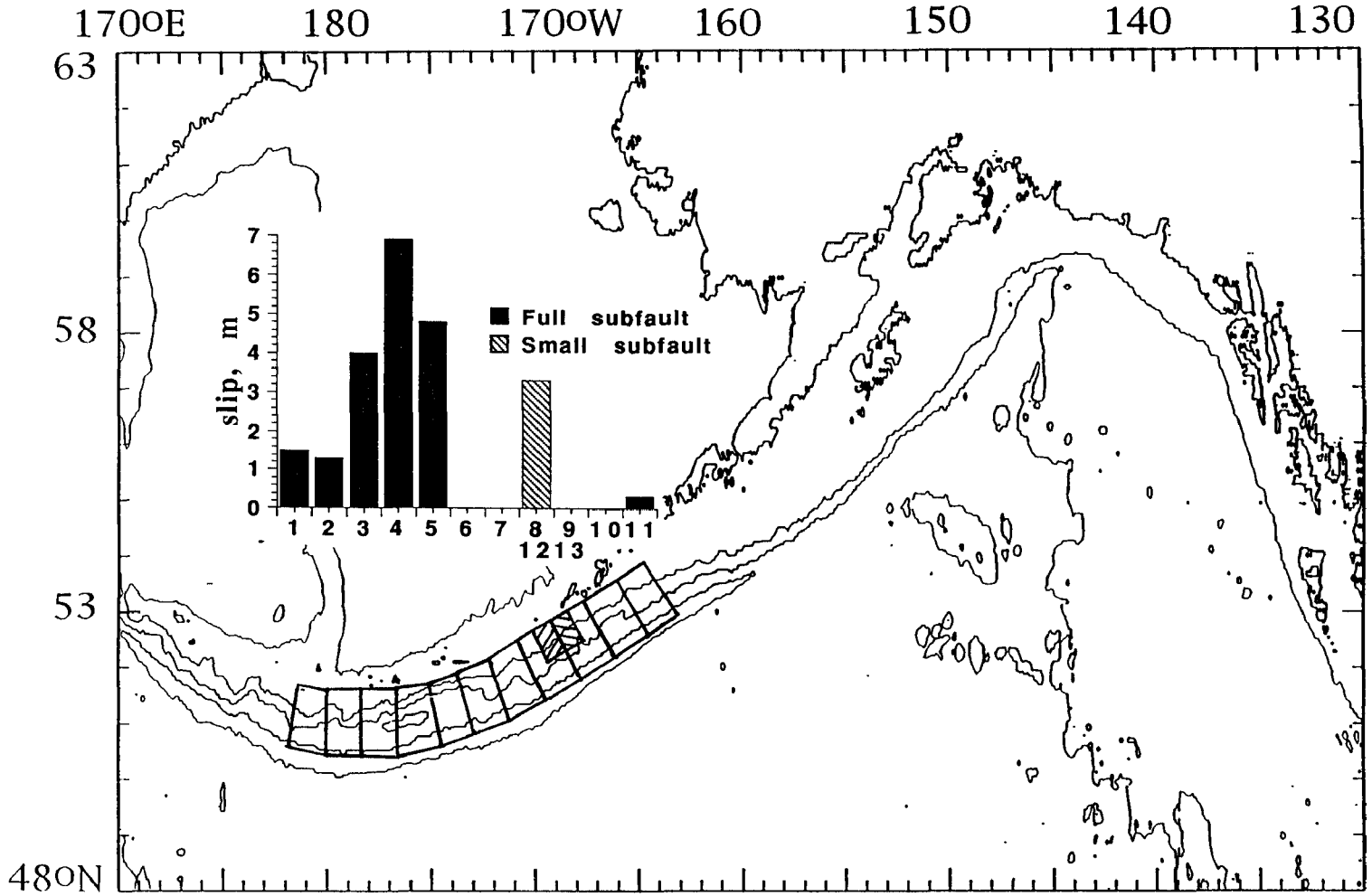

Figure 11: Slip distribution on rupture zone of 1957 earthquake. The numbered segments correspond to the subfault immediately below. The subfaults corresponding to 12 and 13 are shaded.

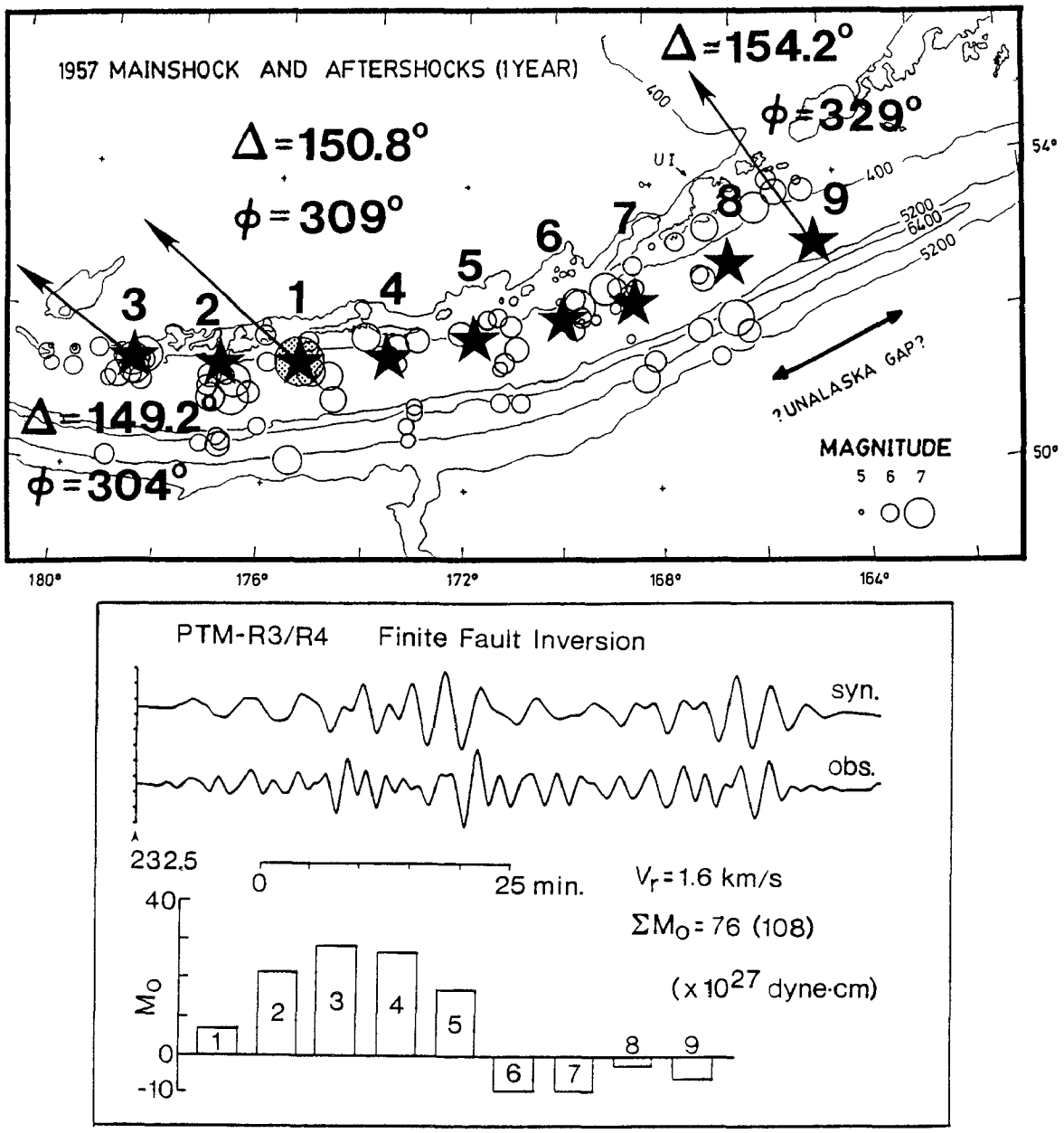

Figure 12: Slip distribution for the 1957 Aleutian earthquake by Ruff *et al.*, (1985) based on PTM record. The grid points in the lower figure corresponds to those in the upper map.

CENOZOIC TECTONIC AND PALEOGEOGRAPHIC EVOLUTION OF THE PUGET LOWLAND SEISMIC ZONE

9450-50551

Samuel Y. Johnson
Branch of Sedimentary Processes
U.S. Geological Survey
MS 939, Box 25046, DFC,
Denver, Colorado 80225
(303) 236-1545

Investigations

This research is designed to describe and interpret the stratigraphy, sedimentology, petrology, and age of Cenozoic units within and bounding the Puget Lowland seismic zone (fig. 1), with the goal of reconstructing the Cenozoic paleogeography of the region. Questions posed include the following: What sedimentary basins formed, what was their geometries, what were the tectonic controls on their origins, and at what rates did they subside? What is the petrology of Cenozoic sediments and in what environments were they deposited? How deeply were sediments buried as determined by thermal maturity and diagenetic studies? Where, when and how were Cenozoic strata deformed?

When these data are collected and analyzed, other important questions can be posed. Are there juxtaposed, mismatched, sedimentary facies, petrofacies, or burial-history trends across the Puget Lowland seismic zone that indicate significant lateral offset or horizontal shortening? If so, what units or features can be used as piercing points or markers in constraining amounts, rates, and timing of offset? Is there evidence for large throughgoing fault systems that have displaced units and(or) influenced depositional patterns? Are offsets distributed across wide zones? Do identified structures coincide with known zones of recent seismicity? If not, should identified structures be considered zones of potential seismicity?

Continuing project investigations in FY92 consisted of analyzing data collected in FY91, collecting additional field and borehole core data from Eocene sedimentary rocks, soliciting relevant seismic reflection data from industry, and studying/modeling Cenozoic subsidence in several areas within the Puget Lowland. These investigations are also sponsored by the USGS Evolution of Sedimentary Basins Program.

A significant amount of the field sedimentologic and stratigraphic data collected in FY91 has been plotted on vertical profiles; these data are being used to document and reconstruct depositional environments and systems. In FY92, additional detailed stratigraphic and sedimentologic studies were undertaken in the Morton anticline area, the Tiger Mountain area, the Black Diamond area, the northeastern Olympic Peninsula, and in the Centralia coal mine (fig. 1). Reconnaissance field studies were undertaken in the Vader-Ryderwood area. Five cores from the Jackson Prairie area in the Chehalis Basin were also described and cuttings were collected from the Mobil Kingston and So-Cal Whidbey wells (fig. 1). Cumulatively, stratigraphic sections totalling more than about 5,000 m were measured and sampled in FY92.

Petrologic data needed to provide constraints on paleogeography and sediment dispersal patterns were collected from thin sections of 63 samples collected in FY91, and 36 thin sections were point counted. Thin sections are now being made on an additional

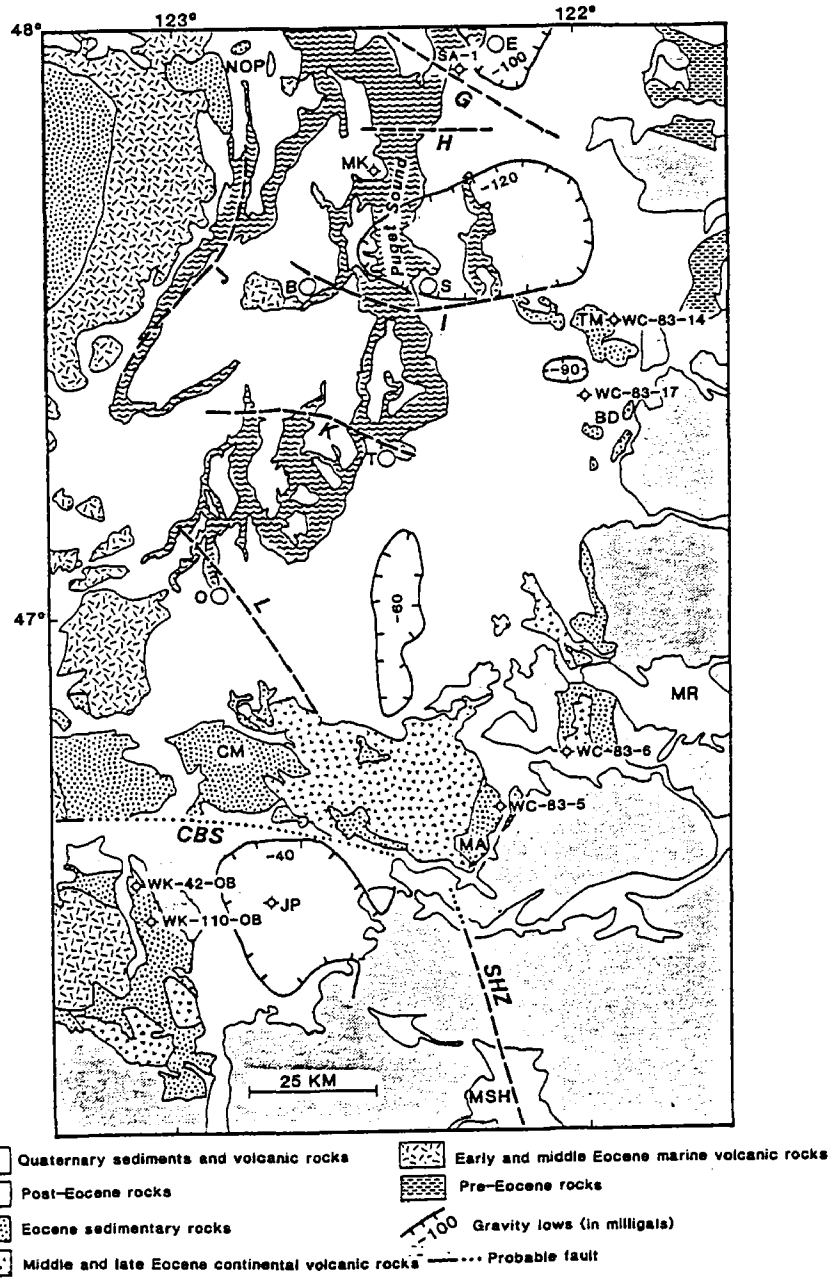

Figure 1. Schematic geologic map of the Puget Lowland seismic zone, showing locations of concentrated FY91 and FY92 field work (TM, MA, CM, BD, NOP) and borehole cores described and sampled (for example, WC-83-14). Probable faults include structures *G, H, I, J, K,* and *L* of Gower and Yount (1985), the Saint Helens seismic zone *(SHZ)* of Weaver and Smith (1983), and an inferred structure on the northern margin of the Chehalis sub-basin *(CBS)*. Other abbreviations as follows: B, Bremerton; BD, Black Diamond; CM, Centralia Mine; JP - Jackson Prairie; MA, Morton anticline area; MK - Mobil Kingston well; MR, Mount Rainier; MSH, Mount Saint Helens; NOP - northeastern Olympic Peninsula; O, Olympia; S, Seattle; T, Tacoma; TM, Tiger Mountain. Gravity data from Bonini and others (1974).

105 samples collected in FY 92. About 15 samples have been given to a colleague for analysis of heavy mineral content, which should further aid provenance and correlation studies. Geochronologic studies continue. Fifteen FY91 samples were submitted for mineral separation; five of these samples yielded sufficient zircons for dating and are in the hands of a colleague for fission-track dating. An additional six samples collected in FY92 have been submitted for mineral separation. Tephra correlation studies of Eocene strata also continue. Working with Paul Hammond of Portland State University, 141 samples have been submitted for XRF and INAA geochemical analyses; partial results have been obtained for 93 of these samples. Finally, the burial and thermal histories of these strata are being examined by vitrinite reflectance analysis (44 samples submitted, results back for twenty samples) and organic geochemical analysis (twelve samples submitted, results obtained for six samples).

In order to integrate and correlate the outcrop and well data and develop a coherent paleogeographic/paleotectonic model, a major effort was made to solicit regional seismic reflection data from industry. This effort has resulted in significant contributions (with some publication rights) from Mobil, Chevron, and L.B. Industries in late FY92. Chris Potter and I have also laid the groundwork for a multi-USGS Program (NEHRP, Evolution of Sedimentary Basins, and Deep Continental Studies) purchase of commercial seismic reflection data from the southern Puget Lowland in FY93.

Results

Published results of FY92 investigations are in Johnson (1992) and Johnson and Yount (1992). Johnson (1992) describes the stratigraphy and sedimentology of the lower? and middle Eocene Raging River Formation in the east-central Puget Lowland, and provides key information for understanding regional paleographic and tectonic evolution. The Raging River Formation is especially significant because (among other things) it provides the only surface analog for the conductive rocks (the SWCC) that underlie a large part of the southern Washington Cascade foothills and occur in other deep Eocene basins of the Puget Lowland area. Stanley and others (1987, 1991, 1992) have inferred the SWCC has significant control on regional seismicity and volcanism. Three informal stratigraphic units (designated 1 to 3 from base to top) are here recognized in the Raging River Formation based on distinctive sedimentary facies and lithologies. Unit 1, approximately 230 m thick, consists of interbedded sandstone, mudstone, and conglomerate of inferred nonmarine (lower part) and transgressive shallow-marine (upper part) origin. Unit 2, approximately 185 m thick, consists of interbedded conglomerate, sandstone, and mudstone, and is inferred to be of mainly alluvial origin. A significant transgression is recorded by Unit 3 (about 300 m thick), which consists of gray silty mudstone and lesser sandstone, and was deposited in a marine shelf (lower part) and bathyal slope (upper part) setting. This transgression reflects local tectonism and not fluctuating eustasy. The Raging River Formation is overlain by prodelta(?) marine shelf deposits in the lower part of the Tiger Mountain Formation. Three sandstone petrofacies were identified in the Raging River Formation and lower part of the Tiger Mountain Formation. These petrofacies reveal an upward evolution in sediment source from Mesozoic basement rocks of oceanic affinity (petrofacies 1), to lower Tertiary volcanic rocks (petrofacies 2), to a mixed provenance including Mesozoic oceanic rocks, lower Tertiary volcanic rocks, and more distal plutonic or crystalline rocks (petrofacies 3). This report will be formally published when colleagues provide additional heavy mineral analyses and isotopic dates.

Johnson and Yount (1992) discuss constraints on the Cenozoic paleogeography of the Puget Lowland based largely on new geologic data and subsidence models (fig. 2). Following up on Johnson (1984, 1985), they suggest the Puget Lowland was the site of Eocene dextral strike-slip faulting along the Puget fault zone, a structure inferred from

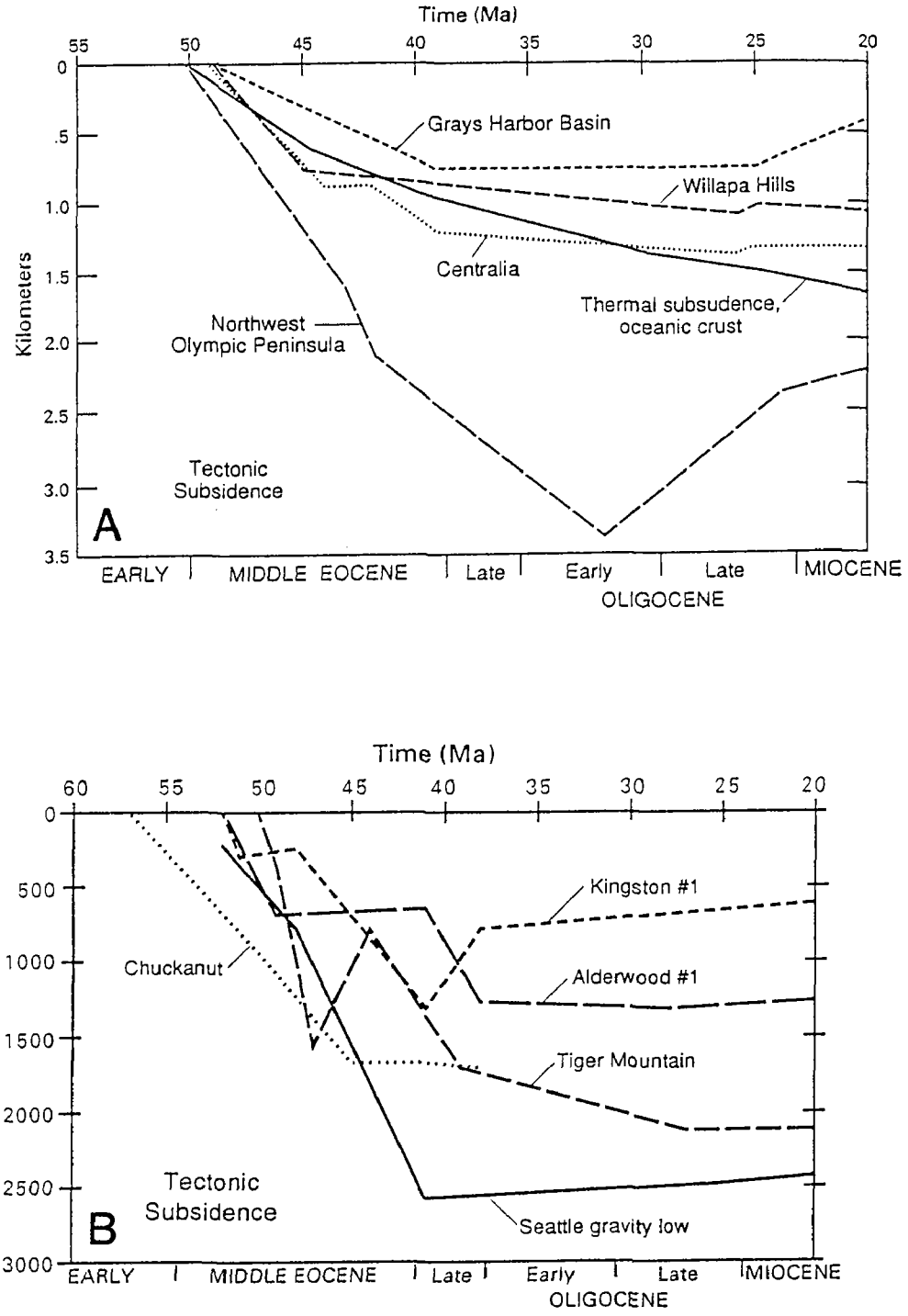

Figure 2. Diagrams showing subsidence histories of (A) three sites in the southwest Washington Coast Range, one site on the northern Olympic Peninsula, and the idealized thermal subsidence curve for oceanic crust; and (B) four sites in the central Puget Lowland and one site in the Bellingham area, northern Puget Lowland. Subsidence curves are corrected for the load induced by the weight of sediment and water through time. Paleobathymetry is approximate and based on foraminiferal data provided by Weldon Rau.

patterns and contrasts in basin evolution, and from facies and petrographic mismatches. This inferred fault zone forms the boundary between pre-Tertiary basement rock of the Cascades to the east and early and middle Eocene marine basaltic basement rock (Crescent Formation) of the Coast Range to the west. The inferred fault zone extends northward from Mt. St. Helens through the Puget Lowland and Puget Sound and bends northwestward into a zone of transpressive, south-directed thrust faults on southern Vancouver Island. The fault zone was initiated about 55 Ma when the Crescent Formation was erupted in a marginal rift basin (Wells and others, 1984; Snavely, 1987; Babcock and others, 1992). Northward movement of the Coast Range probably continued into the Neogene. Eocene-Oligocene subsidence of Crescent basement in southwest Washington is inferred to be mainly of thermal origin; much higher subsidence rates for Crescent basement on the northern Olympic Peninsula (fig. 2A) require an additional driving force, inferred to be loading from southern Vancouver Island thrust sheets. Some offset on the Puget fault zone was transferred eastward to the Straight Creek fault, leading to development of a broad, rapidly subsiding, pull-apart basin in the eastern Puget Lowland and Cascade foothills. Local sub-basins, such as the prominent gravity low near Seattle, formed within or adjacent to the Puget fault zone. Intrabasinal tectonics is reflected in local unconformities, abrupt facies change, and highly variable subsidence histories within limited geographic areas (fig. 2B). Much of the modern crustal seismicity in the Puget Lowland appears to be concentrated along the structural boundary described above between the Crescent Formation and pre-Tertiary basement. Documentation of the geometry and kinematics of this zone will enhance understanding of the modern seismic hazard.

Field studies conducted in FY92 have yielded several preliminary observations and interpretations relevant to understanding the regional geologic framework. Two problems addressed by these field studies are discussed below:

Morton anticline: FY91 studies indicate that Eocene sedimentary strata in the Morton anticline area consist of thick, alternating intervals of nonmarine and less common marine strata. FY92 studies provide further documentation of these facies and the presence of numerous tuffs that will be dated isotopically and correlated geochemically. Cross sections across the anticline indicate that far more section is present on the west flank than on the east flank, requiring the presence of an east-dipping normal fault or a west-dipping reverse fault in the anticline core. A steep east-dipping fault would project very close to the focus of the magnitude 5.5 (1987) earthquake below Storm King Mountain. Continuing analysis of field and seismic reflection data collected from the Morton anticline will provide documentation of its structure and stratigraphy and enhance understanding of the connection between surface faults and modern seismicity.

Comparison of Eocene stratigraphy in the Tiger Mountain--Black Diamond area (eastern Puget Lowland) and the Northeastern Olympic Peninsula: (western Puget Lowland) In FY92, I examined in detail the Eocene Puget Group in the Tiger Mountain-Black Diamond area and the correlative Lyre and Twin River Formations on the northeastern Olympic Peninsula. Puget Group strata consist of nonmarine to minor marginal marine sandstone, mudstone, and coal. Sandstone is mainly arkose and lithic arkose. In contrast, the Lyre and Twin River Formations consist of coarse-grained conglomerate, sandstone, and mudstone deposited in deep marine settings. Conglomerates contain abundant chert and basalt clasts and sandstones are rich in lithic detritus. These rocks are correlative with mainly nonmarine and marginal marine strata exposed in the Tiger Mountain-Green River Gorge area in the eastern Puget Lowland but have very different petrologies and represent very different sedimentary facies. The present geographic positions of these disparate correlative rocks and their variable subsidence histories (fig. 2B)suggests significant Eocene tectonism in the central Puget Lowland. Ongoing analysis of outcrops, wells, and seismic reflection data will lead to understanding Eocene structural features. These

prominent features have likely been reactivated repeatedly through time, and their documentation is essential to an understanding the modern structure and seismic hazard.

Publications

Johnson, S.Y., 1992, Stratigraphy and sedimentology of the Raging River Formation (Early? and Middle Eocene), King County, Washington: U.S. Geological Survey Open File Report 92-581, 38 p.

Johnson, S.Y., and Yount, J.C., 1992, Toward a better understanding of the Eocene paleogeography of the Puget Lowland, western Washington: Geological Society of America Abstracts with Programs, v. 24, p. 36.

References

Babcock, R.S., Burmester, R.F., Engebretson, D.C., and Warnock, A., 1992, A rifted margin origin for the Crescent basalts and related rocks in the northern Coast Range volcanic province, Washington and British Columbia: Journal of Geophysical Research, v. 97, p. 6799-6821.

Bonini, W.E., Hughes, D.W., and Danes, Z.F., 1974, Complete Bouguer gravity anomaly map of Washington: Washington Division of Geology and Earth Resources, Geologic Map GM-11.

Gower, H.D., and Yount, J.C., 1985, Seismotectonic map of the Puget Sound region, Washington: U.S. Geological Survey Map I-1613.

Johnson, S.Y., 1984, Evidence for a margin-truncating transcurrent fault (pre-late Eocene) in western Washington: Geology, v. 12, p. 538-541.

Johnson, S.Y., 1985, Eocene strike-slip faulting and basin formation in Washington, *in* Biddle, K.T., and Christie-Blick, N., Strike-slip deformation, basin formation, and sedimentation: Society of Economic Paleontologists and Mineralogists Special Publication 37, p.283-302.

Snavely, P.D., Jr., 1987, Tertiary geologic framework, neotectonics, and petroleum potential of the Oregon-Washington continental margin, *in* Scholl, E.W., Grantz, A., and Vedder, J.G., eds., Geology and resource potential of the continental margin of western North America and adjacent ocean basins, Beaufort Sea to Baja California: Circum-Pacific Council for Energy and Mineral Resources, Earth Science Series, v. 6, p. 305-335.

Stanley, W.D., Finn, C., and Plesha, J.L., 1987, Tectonics and conductivity structures in the southern Washington Cascades: Journal of Geophysical Research, v. 81, p. 810-820.

Stanley, W.D., Gwilliam, W.J., Latham, F., and Westhusing, K., 1992, The southern Washington Cascade conductor -- A previously unrecognized thick sedimentary sequence? American Association of Petroleum Geologists Bulletin, v. 76, p. 1569-1585.

Stanley, W.D., Finn, C.A., Williams, J.L., and Weaver, C.S., 1992, Tectonics and seismicity of the Mount Rainier region: EOS, Transactions, American Geophysical Union Fall Meeting, p. 526.

Weaver, C.S., and Smith, S.W., 1983, Regional tectonic and earthquake hazard implications of a crustal fault zone in southwestern Washington: Journal of Geophysical Research, v. 88, p. 10,371-10,383.

Wells, R.E., Engebretson, D.C., Snavely, P.D., and Coe, R.S., 1984, Cenozoic plate motions and the volcano-tectonic evolution of western Oregon and Washington: Tectonics, v. 3, p. 274-294.

TILT, STRAIN, AND MAGNETIC FIELD MEASUREMENTS

9960-70146
M. J. S. Johnston, R. J. Mueller, G. D. Myren
Branch of Tectonophysics
U. S. Geological Survey
Menlo Park, California 94025
415/329-4812

Investigations

[1] To investigate the mechanics of failure of crustal materials using data from both deep borehole tensor and dilational strainmeters and near surface strainmeters, tiltmeters, and arrays of absolute magnetometers.

[2] To develop physical models of incipient failure of the earth's crust by analysis of real-time records from these instruments and other available data.

Results

[1] A FOCUSED FAULT MONITORING EXPERIMENT ON THE HAYWARD FAULT

The identification of reliable short- and intermediate-term precursors to damaging earthquakes remains an critical challenge to the earthquake hazard reduction program. To this end, a focused fault monitoring experiment has been installed on the southern segment of the Hayward fault. Instruments used in this experiment include, dilational strainmeters, tensor strainmeters, water well monitors, creepmeters, continuous GPS displacement monitors, seismic velocity and acceleration transducers. The strainmeters and seismometers are installed in boreholes at about a 200 m depth. At this depth, measurement precision about 20 dB below that of surface instruments can be attained. Short-term strain changes less than one ppb can easily be identified. The borehole array of eight strainmeters has been installed along the segment of the Hayward fault between San Leandro and Milpitas with most sites at distances from 2 km to 7 km from the Hayward Fault. These sites are shown in Figure 1. Data are being transmitted using digital satellite and radio telemetry to Menlo Park, Ca. for analysis and display. Various other geophysical and geological data were also collected during the borehole drilling program. The overall array design was influenced by the form and amplitude of strain and displacement fields calculated from simple models of various possible damaging earthquakes that might occur on either the southern segment of the Hayward fault, or on the Calaveras fault.

[2] RECENT SEISMOMAGNETIC AND VOLCANOMAGNETIC EVENTS: IMPLICATIONS FOR PHYSICAL MECHANISMS

Recent seismic and volcanic events for which focussed magnetic and electromagnetic monitoring data have been obtained occurred on the Izu Peninsula in Japan, the Long Valley volcanic region in California, on the San Andreas fault, and on Mt. Unzen, in Japan. An example from Long Valley, California is shown in Figure 2.

For volcanic events (ie eruptions, intrusions, etc), contributions from different physical processes with different time durations can be identified. These processes include slow, near-surface thermal demagnetism effects, piezomagnetic effects, and effects from rotation/displacement of magnetized material. Second-order effects such as electrokinetic effects and changes in the telluric current system that result from

modification of the electrical conductivity structure, may also occur but critical parameters such as pore pressure gradients, zeta potentials, etc, are rarely measured and are poorly constrained. Well level measurements were obtained during the current deformational episode shown in Figure 1 but have remained essentially unchanged during this time. This suggests that the simplest expectation from electrokinetic processes are not a major contributor to the observed magnetic field changes for this event.

For seismic events, zero-frequency or coseismic contributions are instantaneous with no indication of short-term response effects with a decay time constant as expected for fluid driven electrokinetic processes. An example from the North Palm Springs earthquake is shown in Figure 2.

Simple piezomagnetic dislocation models using parameters determined geodetically or seismically generally match the observed zero-frequency signals in size and sign but other possibilities can not be completely discounted. Transient, higher frequency signals might be driven by localized dynamic changes in electrical conductivity, localized charge generation mechanisms, and electrokinetic effects. However, signals that appear to occur prior to a significant local earthquake but do not occur coincident in time with the earthquake, should generally be considered suspicious since many other data indicate that moment release prior to and earthquake is minor compared with that during the rupture. In other words, calibration with coseismic moment release is an important test of the reality of observed coseismic signals.

Unusual ULF signals were recorded predominately in the frequency band 1 Hz to 0.01 Hz at three different times during the month prior to the October 18, 1989, Loma Prieta M_s7.1 earthquake (Fraser-Smith et al., 1990). Three physical mechanisms are considered relevant if these signals are assumed to be generated in the hypocentral region. These are: 1) dynamic changes in electrical conductivity due to strain driven crack opening and closure, 2) dynamic charge generation due to strain, hydrodynamic, and gasdynamic processes, and 3) electrokinetic effects due to dynamic pore pressure variations.

Since the electrical conductivity varies between 1 S/m and 0.01 S/m and the seismic attenuation factor (1/Q) is about 0.03 in this region, dynamic magnetic, seismic and strain signals are attenuated comparably in the 1 Hz to 0.01 Hz frequency band. The absence of detectable seismic or strain signals on nearby seismometers and borehole strainmeters at the 10 micron/sec and 10^{-11}/sec level, respectively, strongly limits the size (i.e. the moment) of the source region driving the mechanisms above.

Models of these processes suggest dynamic stress gradients and pore pressure gradients exceeding 1 Kbar/km and 1 bar/km, are required to generate crack oscillation and electrokinetic effects, respectively, but associated strain oscillations from these gradients should be readily detectable unless the region effected is quite small. These problems, together with the inherent difficulty in maintaining charge separation continuously within this conducting region for long enough and over a large enough area, suggest that these ULF electromagnetic signals were generated relatively close to the receiver.

[3] MAGNETIC FIELD OBSERVATIONS IN THE NEAR-FIELD OF THE JUNE 28, 1992 M_L 7.5 LANDERS, CALIFORNIA, EARTHQUAKE.

Recent reports suggest that large magnetic field changes occur prior to, and during, large earthquakes. Two continuously operating proton magnetometers, LSBM and OCHM, at distances of 13.3 km and 21 km, respectively, from the epicenter of the June 28, 1992, M_L 7.5 Landers earthquake, recorded data through the earthquake and its aftershocks. These two stations are part of a differentially connected array of proton magnetometers that has been operated along the San Andreas fault since 1976. The instruments operate at a sensitivity of 0.25 nT of better and transmit data every 10 minutes through the GEOS satellite to the USGS headquaters in Menlo Park, CA.

Seismomagnetic offsets of -0.5 nT and -0.2 nT were observed at these sites. In contrast, offsets of 1.2 nT and 0.3 nT were observed during the July 8, 1986 M_L 5.9 North Palm Springs earthquake although this earthquake occurred right beneath the magnetometer sites.. The observations are generally consistent with a seismomagnetic model of the earthquake in which right-lateral rupture is assumed on four connected fault segments that roughly match the location of the surface rupture. The length of the segments from south to north are 15 km, 23 km, 22 km, and 23 km, the widths are 13 km, 17 km, 17 km, 17 km, and the assumed slip is 3 m, 4m, 4m, 5m, respectively. The average magnetization is assumed to be 1 A/m in general agreement with observations of surface magnetization at the two sites that range between 1.0 A/m and 0.1 A/m. An alternate explanation in terms of electokinetic effects seems unlikely since the changes are complete within a 10 minute period.

[4] ON THE DECTECTION OF SHORT-TERM STRAIN EVENTS - A COMPARISON OF THE SENSITIVITIES OF GPS AND BOREHOLE STRAIN MEASUREMENTS

For detection of short term deformation events which take place at or below seismogenic depths along the San Andreas Fault system we compare the capability of a network of GPS receivers with that of an array of Sacks-Evertson borehole strainmeters. We have compared the two techniques using different assumptions for the station distribution with respect to the location of the event, including cases where the sites have the most favorable geometry for detection. We also use the locations (now partially occupied) for the planned array of borehole sites along the Southern Hayward Fault. Since Earth strain noise level increases with period, we also allow the duration of the slip event to vary. We have concentrated on strike slip sources of deformation, but have also considered dip slip dislocations.

While many may be aware that for short duration signals (less than months) strain monitoring provides greater sensitivity than does GPS, the quantitative difference in threshold level is not widely perceived. For example consider how much right lateral slip, over a duration of 1 day, must occur on 1 km^2 of fault at a depth of 10 km for detection by an ideally located instrument array. The borehole strain array will provide a clear signal for a displacement of about 2 cm; the position monitoring will require about 10 m (assuming a detection threshold of a few mm) -- a ratio of 500. The strain threshold increases with period and the crossover period is about several months, depending on the characteristics of individual sites. At shorter periods the threshold ratio increases in favor of strain monitoring (5000 at 1 hour). This explains the apparent inability of the GPS net in southern California to detect the coseismic change due to the Sierra Madre (1991) earthquake (Hudnut *et al* & Zumberge *et al*, 1991 Fall AGU) which produced a very large offset on the nearest borehole instrument. Continuous strain monitoring should be an integral component of any program to detect possible short term earthquake precursors.

[5] BOREHOLE STRAIN ARRAY IN CALIFORNIA

A network of 15 borehole strainmeters along the San Andreas fault zone and in the Long Valley Caldera continues to be monitored and maintained. All instruments are installed at depths between 117-m and 324-m and all are between 1-km and 5-km from the the surface trace of the fault. High frequency dilatometer data in the frequency range 0.005 Hz to 100 Hz are recorded on 16-bit digital recorders with least count noise less than 10^{-11}. Low frequency data from zero frequency to 0.002 Hz are transmitted through the GOES satellite to Menlo Park, CA, using a 16-bit digital telemetry system. At the USGS in Menlo Park the data are displayed in "almost real time" and are continuously monitored with detection algorithms for unusual behavior. Least-count noise is about $5*10^{-12}$ for the on-site digital recordings, and about $2*20^{-11}$ for the satellite telemetry channels. Earth strain tides, strain transients related to fault creep and numerous strain

seismograms from local and teleseismic earthquakes with magnitudes between -1 and 6 have been recorded on these instruments. Static moments and total earthquake moments are determined from the co-seismic strains and total strain changes observed with the larger events.

[6] **REVIEW OF CONTINUOUS NEAR-FAULT AND NEAR-CONTINUOUS 2-COLOR DEFORMATION DATA AT PARKFIELD, CALIFORNIA: 1986-1992.**

Continuous strain along a 36-km segment of the San Andreas fault zone near Parkfield California is monitored with a network of 8 borehole dilatometers and 3 borehole tensor strainmeters (precision $<10^{-9}$). Near-continuous strain and fault displacement is also monitored with a 2-color laser geodimeter (precision $<10^{-7}$) using a 17-line array of 1-km to 9-km lines emanating from Carr Hill. The most remarkable features of these data during the last six years (1986-1992) are:

[1] The relative absence of short term strain transients greater than 10^{-7} that are coherent across the networks and can thus be clearly related to fault activity. Some coherent strain transients are observed on a limited scale, particularly on the more northern borehole instruments though these do not appear directly related to patterns of microseismicity during this time. The largest earthquake that occurred was a magnitude 4 just southeast of Parkfield on August 29, 1986. This generated coseismic strainsteps of a few nanostrain on the nearest instruments in agreement with expectations from dislocation theory.

[2] The smooth gradient in fault slip from about 20 mm/a in the north to 3 mm/a in the south and the overall linear nature of the slip time-history at each location.

[3] A broad scale geodetically determined strain rate of about 0.2 ppm/a that is significantly lower than the near-fault shear strain accumulation rate of about 1 ppm/a although the near-fault measurements may be contaminated by the effects of fault slip beneath Carr Hill..

[4] The relative absence of strain transients on the borehole strainmeters greater than 10–9, or on the 2-color lines greater than a millimeter or so, at the times of nearby creep events. Exceptions occur at two sites; one where a strainmeter is within 0.75 km of a creepmeter and the second where coupling appears to occur between a secondary fault near the strainmeter and the San Andreas fault.

The apparent invariance of the slip geometry and slip distribution during this time period is curious. Modeling of the expected nucleation region of the next Parkfield earthquake indicates that changes in fault slip of only a few millimeters over a square kilometer at depths of 5 km to 8 km would be readily detected by this array. The absence of short period transients (duration less than 1 day) on both geodetic and borehole strain at the times of surface creep observations indicates a complicated and spatially variable near-surface response to relatively uniform deep slip.

[7] **DIFFERENTIAL MAGNETOMETER ARRAY IN CALIFORNIA**

We continue investigations of local magnetic fields and relationships to crustal strain and seismicity in the Parkfield region and in southern California. The network consists of 9 stations which are all sampled synchronously every 10 minutes and transmitted with 16-bit digital telemetry to Menlo Park, CA through the GOES satellite. Data are monitored daily with particular attention to the seven stations operating in the Parkfield region of central California and the three stations operating in the Long Valley caldera. At these latter sites a magnetic field anomaly first became obvious in late 1989 and in continuing to the present in concert with anomalous 2-color geodetic strain measurements and spasmodic swarms of minor earthquakes.

Reports

Fenoglio, M. A., A. C. Fraser-Smith, G. Beroza, M. J. S. Johnston, 1992, Comparison of Ultra-Low Frequency Electromagnetic Signals with Aftershock Activity During the 1989 Loma Prieta Earthquake Sequence. Bull. Seis. Soc. Am. (in press)

Valdes-Gonzalez, C. M., B. Armstrong, J. D. Leaird, and M. J. S. Johnston, 1992, Low Strain Level Acoustic Emission Due to Seismic Waves and Tidal/Thermoelastic Strains Observed at the San Francisco Presidio, IBM PASC Report G320-3572, 28pp.

Johnston, M. J. S., R. J. Mueller, and J. O. Langbein, 1992, Ongoing Volcanomagnetic, Geodetic, and Seismicity Anomalies Observed from Mid-1989 in Long Valley Caldera, California, *Trans. Am. Geop. Un.*, **73**, 60.

Park, S. K., M. J. S. Johnston, T. R. Madden, F. D. Morgan, and H. F. Morrison, 1992, Electromagnetic Precursors to Earthquakes in the ULF Band: A Review of Observations and Mechanisms, Report to NSF, IGPP 92-15.

Johnston, M. J. S., G. D. Myren, R. J. Mueller, A. T. Linde, and M. T. Gladwin, 1992, A Focused Earthquake Prediction Experiment on the Southern Hayward Fault: Detection Array and Expected Strains and Displacements during Fault Rupture. . Proc. Second Conference, Earthquake Hazards in the Eastern San Francisco Bay Area, March 25-29, 1992, Cal. Div. Mines Geol. (in press).

Johnston, M. J. S., and A. T. Linde, 1992. Near-Field High Precision Strain Prior to the October 18, 1989 Loma Prieta M_L 7.1 Earthquake. USGS Prof. Paper on Loma Prieta Earthquake (in press).

Mueller, R. J. and M. J. S. Johnston, 1992. Seismomagnetic Effect generated by the October 18, M_L 7.1 Loma Prieta, California, Earthquake. USGS Prof. Paper on Loma Prieta Earthquake (in press).

Linde, A. T., M. T. Gladwin, and M. J. S. Johnston, 1992 Tidal Strain Response Before the 1989 Loma Prieta Earthquake: An Unsuccessful Search For Variations in Mechanical Properties. USGS Prof. Paper on Loma Prieta Earthquake (in press).

Mueller, R. J., M. J. S. Johnston, J. O. Langbein, and K. S. Breckenridge, 1992, Local Differential Magnetic Fields at Parkfield, California: July, 1985 to January, 1992, Proc. U.S.-China Conf. San Juan Bautista, (in Press).

Johnston, M. J. S., and J. Langbein, 1992, Review of Continuous Near-fault Strain and Near-Continuous 2-Color Deformation Data at Parkfield, California: 1986-1992, *Trans. Am. Geophys. Un.* (in press)

Johnston, M. J. S., R. J. Mueller and Y. Sasai, 1992, Magnetic Field Observations in the Near- Field of the June 28, 1992, M_L7.5 Landers, California, Earthquake, 1992, *Trans. Am. Geophys. Un.* (in press)

P. A. Reasenberg, D. P. Hill, A. J. Michael, W. L. Ellsworth, R. W. Simpson, S.

Walter, M. J. S. Johnston, R. Smith, S. J. Nava, W. J. Arabasz, J. C. Pechmann, J. Gomberg, J. N. Brune, D. DePolo, G. Beroza, S. D. Davis, and J. Zollweg, 1992, Remote Seismicity Triggered by the M7.5 Landers, California, Earthquake of June 28, 1992, *Trans. Am. Geophys. Un.* (in press)

Linde, A. T., I. S. Sacks, and M. J. S. Johnston, 1992, On the Detection of Short Term Strain Events - A Comparison of the Sensitivities of GPS and Borehole Strain Measurements, *Trans. Am. Geophys. Un.* (in press)

Park, S. K., M. J. S. Johnston, T. R. Madden, F. D. Morgan, and H. F. Morrison, 1992, Electromagnetic Precursors to Earthquakes in the ULF Band: A Review of Observations and Mechanisms, *Rev. Geophysics*, (submitted).

B. H. Armstrong, C. M. Valdes-Gonzalez, M. J. S. Johnston, and J. D. Leaird, 1992, Low Strain Level Acoustic Emission Due to Seismic Waves and Tidal/Thermoelastic Strains Observed at the San Francisco Presidio, Phys. Earth. Planet. Int. (Submitted).

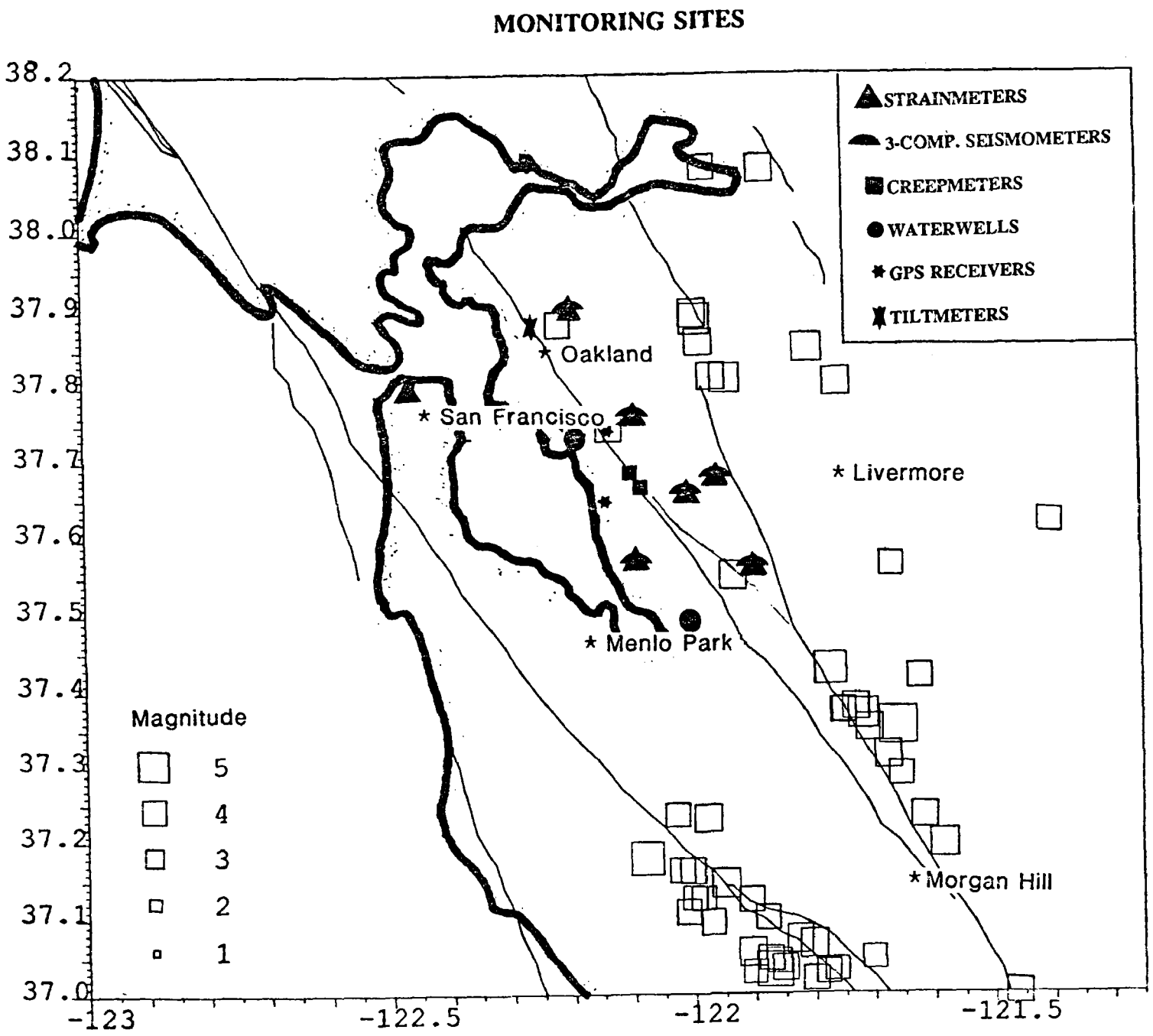

Figure 1. Monitoring instruments in the San Francisco Bay Area.

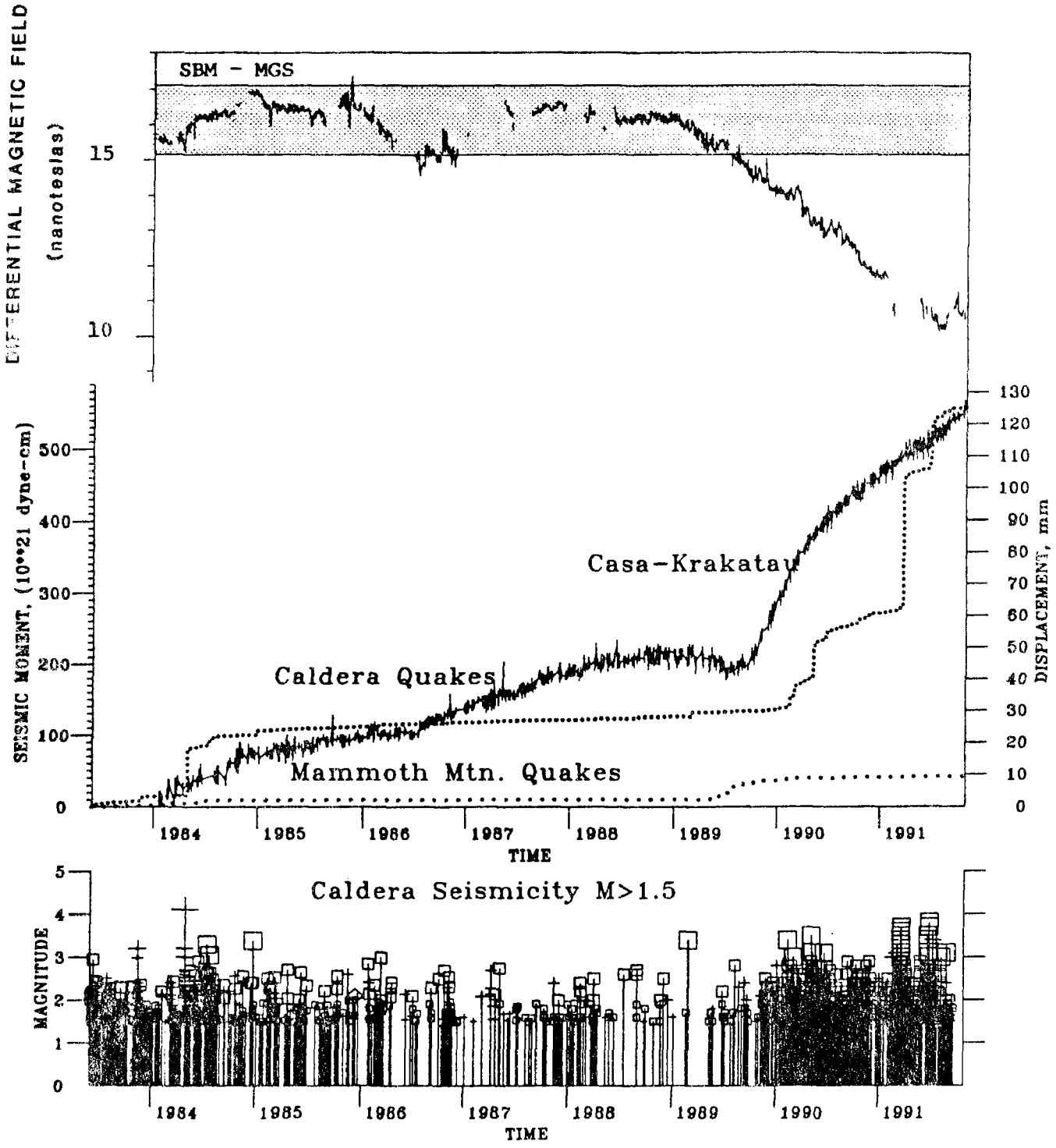

Figure 2. Magnetic, geodetic and seismic data from the Long Valley Caldera preceding and following the start of volcanic activity in 1989.

Earthquake and Seismicity Research Using SCARLET and CEDAR

Agreement No. 14-08-0001-G1774

Hiroo Kanamori , Robert W. Clayton, and Leon T. Silver
California Institute of Technology
Pasadena, California

(818) 356-6914

Investigation

Determination of Earthquake Energy Release and M_L Using TERRAscope

We estimated the energy radiated by earthquakes in southern California using on-scale very broadband recordings from TERRAscope. The method we used involves time integration of the squared ground-motion velocity and empirical determination of the distance attenuation function and the station corrections. The time integral is typically taken over a duration of 2 min after the *P*-wave arrival. The attenuation curve for the energy integral we obtained is given by $q(r) = cr^{-n}\exp(-kr)$ $(r^2 = \Delta^2+h_{ref}^2)$ with c=0.49710, n=1.589, k=0.0089 km^{-1}, and h_{ref}=8 km, where Δ is the epicentral distance. A similar method was used to determine M_L using TERRAscope data. The station corrections for M_L are determined such that the M_L values determined from TERRAscope agree with those from the traditional optical Wood-Anderson seismographs. For $1.5<M_L<6.0$, a linear relationship $\log E_S = 1.96M_L+9.05$ (E_S in ergs.) was obtained. However, for events with $M_L>6.5$, M_L saturates. The ratio E_S/M_0 (M_0: seismic moment), a measure of the average stress drop, for six earthquakes, the 1989 Montebello earthquake (M_L=4.6), the 1989 Pasadena earthquake (M_L=4.9), the 1990 Upland earthquake (M_L=5.2), the 1991 Sierra Madre earthquake (M_L=5.8), the 1992 Joshua Tree earthquake (M_L=6.1) and the 1992 Landers earthquake (M_W=7.3) are about 10 times larger than those of the others that include the aftershocks of the 1987 Whittier Narrows, the Sierra Madre earthquake, and the Joshua Tree earthquake and the two earthquakes on the San Jacinto fault. The difference in the stress drop between the mainshock and their large aftershocks may be similar to that between earthquakes on a fault with long and short repeat times. The aftershocks, which occurred on the fault plane where the mainshock slippage occurred, had a very short time to heal, hence a low stress drop. The repeat time of the major earthquakes on the frontal fault systems in the Transverse Ranges in southern California is believed to be very long, a few thousand years. Hence, the events in the Transverse Ranges may have higher stress drops than those of the events occurring on faults with shorter repeat times, such as the San Andreas fault and the San Jacinto fault. The observation that very high stress-drop events occur in the Transverse Ranges and the Los Angeles Basin has important implications for the regional seismic potential. The occurrence of these high stress drop events near the bottom of the seismogenic zone strongly suggests that these fault systems are capable of supporting high stress that will eventually be released in major seismic events. Characterization of earthquakes in terms of the E_S/M_0 ratio using broadband data will help delineate the spatial distribution of seismogenic stresses in the Los Angeles basin and the Transverse Ranges.

Publications

Kanamori, H., 1992, Locating Earthquakes with Amplitude--Application to Real-Time Seismology--, Bull. Seismol. Soc. Am., *in press*.

Kanamori, H., and E. Hauksson, 1992, A Slow Earthquake in the Santa Maria Basin, California, Bull. Seismol. Soc. Am., 82, 2087-2096.

Kanamori, H., E. Hauksson, T. H. Heaton, L. K. Hutton and L. M. Jones, 1992, Determination of Earthquake Energy Release and M_L Using TERRAscope, Bull. Seismol. Soc. Am., in press.

Jones, C., H. Kanamori and S. W. Roecker, Missing Roots and Mantle "Drips": Regional P_n and Teleseismic Arrival Times in the Southern Sierra Nevada and Vicinity, California, J.G.R., submitted 1991

Magistrale, H., Kanamori, H., Jones, C., Forward and inverse three-dimensional P-wave velocity models of the southern California crust, Geophys. Res. Lett., submitted August 1991.

Paleoseismicity in the Puget Sound Area as Recorded in Sediments from Lake Washington

Agreement No. 1434-92-G-2188

Robert Karlin
Mackay School of Mines/168
University of Nevada, Reno
Reno, NV 89557

(702) 784-1770

Brief Description of Project

This study was undertaken to evaluate the sediments of Lake Washington as a possible recorder of earthquake activity during the Holocene. Initial analyses show that a series of terrigenous silt layers have been episodically deposited throughout the lake. The objectives of this research have been to ascertain the timing, sources, and causes of the quasi-periodic disruptions in sedimentation. The work involves textural analysis, compositional characterization, and paleo/rock magnetism on gravity and piston cores. Radiocarbon dating supplemented by tephrachronology was used to establish an absolute time scale for several of the cores. If the layers are confirmed to be of seismogenic origin, the results from this study could provide an estimate of earthquake recurrence intervals for western Washington for the last 11,000 years.

Results

The first year's work concentrated on characterizing and dating eleven 3-m gravity cores which span the last 3,000 years. Magnetic susceptibility profiles, X-radiography, petrography, chemistry, and grain size analyses show that turbidites have been deposited episodically and can be readily correlated throughout the lake. These layers are characterized by highs in magnetic susceptibility, relatively coarse grain sizes, increases in aluminosilicate content and relative decreases in organic matter and biogenic silica. The sedimentary disturbances are most easily explained as the result of slumping of the steep-sided basin walls and increased detrital flux from landslides in the drainage basin as a result of large earthquakes. Because of the drainage configuration and analyses of modern major flood events, it is unlikely that these layers are caused by floods or other climatic phenomena.

One prominent turbidite layer was deposited in response to a major seismic event at about 1100-1200 yrs BP. Downcore patterns in susceptibility for this event can be readily correlated throughout the lake and suggest that near-simultaneous slumping occurred in at least three separate locations, two of which now contain submerged forests. The age of this event agrees with high

resolution radiocarbon dating and tree ring correlations of submerged trees (Jacoby et al., 1992). The event also coincides with >7 m of uplift at Alki and Restoration Points in south Seattle, submergence at Winslow Harbor and West Point (Bucknam et al., 1992), rock avalanches in the Olympic Mountains, (Schuster et al., 1992) and tsunami deposits at West Point and Whidbey Island (Atwater et al., 1992). All of these lines of evidence suggest a large magnitude 7 earthquake due to movement on the nearby Seattle Fault.

The susceptibility records from throughout the lake are suggestive of a correlation of Lake Washington disturbances with events observed elsewhere. In addition to the 1100 year event, sedimentary disturbances are found in the gravity cores 300 to 400, 1600 to 1700, 2200 to 2400, and 2800 to 3100 years ago. The latter three intervals correspond with periods of landsliding deduced from the dating of drowned trees in the lake (Jacoby et al., 1992). Major seismic events of the same age have also been reported from coastal marshes along the Washington coast (Atwater, 1987, 1992; Darienzo and Peterson, 1990). The event about 300 years ago is synchronous with probable coseismic submergence of marsh grass and trees along the Washington coast (Atwater, 1992; Atwater and Yamaguchi, 1991). Our results have been published in a report in *Science* (Karlin and Abella, 1992a) and were presented at the 1992 Fall meeting of the American Geophysical Union in San Francisco, California (Karlin and Abella, 1992b).

Piston cores provide a longer record of sedimentation extending to about 13.4 ka. Magnetic susceptibility profiles show remarkably consistent downcore patterns which can be readily correlated throughout the lake. A characteristic series of magnetic peaks is observed that correspond exactly with ash horizons and X-ray opaque intervals containing terrigenous layer which appear to be turbidites. From the size and lithologies of the turbidites and their areal distribution, these deposits are not due to flooding or local slides, but must represent basinwide disruptions such as associated with seismic activity. In 11 piston cores, more than fourteen sedimentary disturbances have occurred since deposition of the Mazama Ash at 6850 BP. If these events are all of seismic origin, the sediment record from Lake Washington suggests that large earthquakes occur on average about every 500 years in the Puget Sound region.

References

B. F. Atwater, *Science* **236**, 942 (1987).
B. F. Atwater and D. K. Yamaguchi, *Geology* **19**, 706-709 (1991).
B. F. Atwater, *J. Geophys. Res.* **97**, 1901 (1992a).
B.F. Atwater and A.L. Moore, *Science*, **258**, 5088, 1614 (1992).
R.C. Bucknam, E. Hemphill-Haley, E.B. Leopold, *Science*, **258**, 5088, 1621 (1992).
M. E. Darienzo and C. D. Peterson, *Tectonics* **9**, 1 (1990).
G. Jacoby, P. Williams, and B. M. Buckley, *Science*, **258**, 5088, 1621 (1992).
R.E. Karlin and S.E. Abella, *Science*, **258**, 5088, 1617 (1992).
R.E. Karlin and S.E. Abella, EOS **73**, 43, 527 (1992b)
R.L. Schuster, R. L. Logan, and P. Pringle, *Science*, **258**, 5088, 1620 (1992).

Proposal to Collaborate with the USGS Deep Continental Studies Group on the North Deployment of the Pacific Northwest Refraction Experiment

14-08-0001-G2073

G. R. Keller, K. C. Miller, J. M. Gridley
Department of Geological Sciences
University of Texas at El Paso
El Paso, Texas 79968
(915) 747-5501
e-mail address: keller@garrett.geo.ep.utexas.edu

Investigations

This research focuses on delineating the crustal structure of western Washington state and studying its implications for seismicity patterns in the Pacific Northwest. Key objectives addressed by this work are:

- Shallow crustal structure of the Pacific Northwest - What is the geometry of the sedimentary basins of the Puget Sound Basin? What is the nature and structure of terrane boundaries?

- Definition of the deep crustal structure - What is the along-strike geometry of the continental and oceanic Mohos? How is the crustal structure related to the subduction zone?

- Relationship of crustal structure to seismicity patterns - Are there north-south changes in crustal structure that correlate with seismicity patterns? Are there additional structural boundaries which have not yet been inferred from seismicity patterns?

Current investigations by our research group include determining seismic velocity structure by forward and inverse modeling of refraction/wide-angle reflection seismic data, constrained by analyses of gravity and magnetic data.

Seismic data were collected as part of the Pacific Northwest Seismic Experiment of 1991. The data set consists of two 300 km long

north-south deployments in the Willamette Lowlands of Oregon and the Puget Basin of Washington. Seismic data were acquired in collaboration with the U.S. Geological Survey Deep Continental Studies Group, Canadian Geological Survey, Oregon State University and several other academic contributors. This report addresses the north deployment in the Puget Basin of Washington (Figure 1). Approximately 485 instruments were deployed at intervals of 600 meters. Nine borehole shots were successfully detonated as the sources (~30 km intervals) over the length of this transect.

Results

The field program was successfully completed in September, 1991. In spite of some noisy recording conditions due to the high population density in the area, first arrival energy was seen to distances exceeding 280 km. In general, the data contain clearly identifiable first arrivals. Later phases such as PmP and Pn have less energy and are more difficult to identify.

To enhance arrivals, deconvolution, bandpass filtering, and three different gain corrections have been applied to the data, using a conventional reflection seismic data processing package. This processing effort has significantly enhanced PmP and Pn arrivals as well as some later phases. True amplitude records, records with automatic gain control applied, and trace normalized records, have been generated for each shot. Figures 2 to 4 show examples of this processing for the northernmost shot. Each type of record has been used in the phase identification process.

To date, preliminary crustal velocity models have been produced using first-arrival, PmP, and Pn picks. The velocity field has been interpreted using the seismic velocity inversion outlined by Zelt and Smith (1992). This analysis has resulted in a multilayered velocity model for the crust (Figure 5). The model shows upper crustal velocities to range from 2.50 km/s to 6.30 km/s and middle crustal velocities to range from 6.10 km/s to 6.80 km/s. Upper crustal velocities in the model are comparable to upper crustal velocities found by Taber et al. (1986) in an area southwest of this study area. Middle crustal velocities are within a +/- 0.2 km/s range of velocities found by Crosson (1976). The middle crust shows a significant lateral velocity gradient. Velocities from north to south increase from 6.20 km/s to 6.30 km/s at ~10 km depth and 6.50

km/s to 6.80 km/s at ~20 km/s. Lower crustal velocities range from 7.15 km/s to 7.40 km/s. Lower crustal velocities show a lateral velocity change from 7.40 km/s to 7.25 km/s north to south, respectively. Significant topography on the Moho has also been detected. Depth to Moho varies from ~36 km to ~48 km along the transect.

The inversion results have been used as a basis for forward modeling more subtle features in the data. The method of forward ray trace modeling is from Luetgert (1992). This model (Figures 6 & 7) uses the generalized seismic velocity structure from the inversion results and adds the constraints from known geology, gravity and magnetic data. Figures 6 & 7 show an example of the ray trace model from the northernmost shot. These results (Figures 6 & 7) better define the velocity structure of the surface structure and particularly the Puget Basin. Velocities in the Puget Basin range from 2.00 km/s to 5.50 km/s. Along this transect, the basin has a maximum depth of 8 km. Velocities used to define the basin range from 2.00 km/s to ~4.80 km/s. Velocities of the upper crust beneath the Cascades ranges are significantly faster at 4.50 km/s at the surface to 6.00 km/s at ~10 km depth. The mid-crustal lateral velocity gradient remains unchanged from the inversion model. Forward modeling of the Moho results in a more smoothly varying interface than that produced by the inversion model.

Study of true amplitude records (e.g. Figure 2) indicate significantly lower amplitudes in the southern part of the profile. This pattern of lower amplitudes to the south is seen on every shot in the experiment. Reflectivity analysis is being used to study the origin of these diminished amplitudes.

At present, phases later than PmP are being interpreted. This includes a wide-angle reflection that may represent the top the subducted Juan de Fuca plate. 2 1/2 - D gravity modeling is being done in concert with the seismic velocity modeling. Reflectivity analysis has also begun in an effort to resolve the origin of amplitude changes along the profile.

References

Crosson, R. S., 1976, Crustal modeling of earthquake data; 2, Velocity structure of the Puget Sound Region, Washington: Journal of Geophysical Research, v. 81, p. 3047-3054.

Luetgert, J. H., 1992, MacRay Interactive Two-Dimensional Seismic Ray Tracing for the Macintosh®, U. S. Geo. Survey Open-File Report 92-356, 43 p.

Taber, J. J., Jr., Lewis, B. T. R., 1986, Crustal structure of the Washington continental margin from refraction data: Bulletin of the Seismological Society of America, v. 76, p. 1011-1024.

Zelt, C. A., and Smith, R. B. 1992. Traveltime Inversion for 2-D Crustal Velocity Structure, Geophysical Journal International, vol. 108(1), p. 16-34.

Reports

Luetgert, J. H., Mooney, W.D., E. Criley, G. R. Keller, J. Gridley, K. Miller, A. Trehu, J. Nablek, S. B. Smithson, C. Humphreys, N. I. Christensen, R. Clowes, and I. Asudeh, 1991. Crustal Architecture of the Pacific NW: The 1991 Seismic Field Experiment, EOS, 72(44), p.323.

Mooney, W.D., Luetgert, J. H., E. Criley, G. R. Keller, J. Gridley, K. Miller, A. Trehu, J. Nablek, S. B. Smithson, C. Humphreys, N. I. Christensen, R. Clowes, and I. Asudeh, 1991. Crustal Architecture of the Pacific NW: The 1991 Seismic Field Experiment, EOS, 72(44), p.326.

Luetgert, J. H., Mooney, W.D., E. Criley, G. R. Keller, J. Gridley, K. Miller, A. Trehu, J. Nablek, S. B. Smithson, C. Humphreys, N. I. Christensen, R. Clowes, and I. Asudeh, 1992. Crustal Velocity Structure of the Pacific NW: The 1991 Seismic Refraction/Wide-Angle Reflection Experiment, 1992 Abstracts with Programs, Geological Society of America, Cordilleran Section, May 11-13, 1992, Eugene, Oregon, p.66.

Trehu, A. M., Nabelek, S., Azevedo, T. M., Brocher, J., Luetgert, J. H., Mooney, Asudeh, I., Clowes, R., Keller, G. R., Miller, K., Nakamura, Y., 1992, Crustal Structure of the Cascadia Subduction Zone Beneath Western Oregon, 1992 Abstracts with Programs, Geological Society of America, Cordilleran Section, May 11-13, 1992, Eugene, Oregon, p.87.

Gridley, J. M., Keller, G. R., and Miller, K. C., 1992, Crustal Structure of Western Washington State: Results of the Pacific Northwest Seismic Experiment 1991, (In Press), EOS, 1992 AGU Fall Meeting.

Miller, K. C., Roberts, D. G., Gridley, J. M., and Keller, G. R., 1992, Upper Crustal Structure of Northwestern Washington State: Integration of 3-Component Reflection Spread with Wide-angle Results, (In Press), EOS, 1992 Fall AGU Meeting.

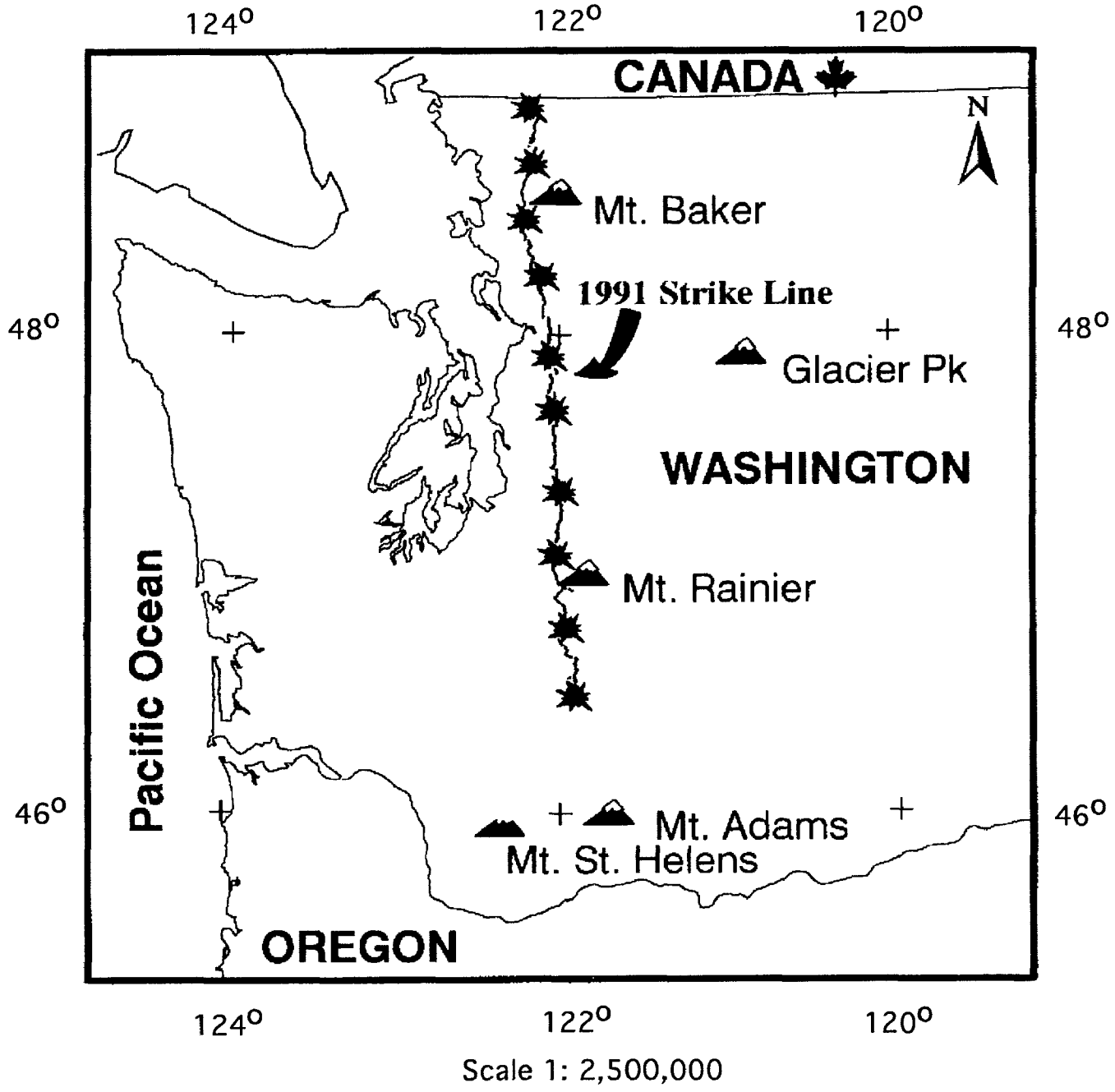

Figure 1. Location map of the profile recorded in 1991.

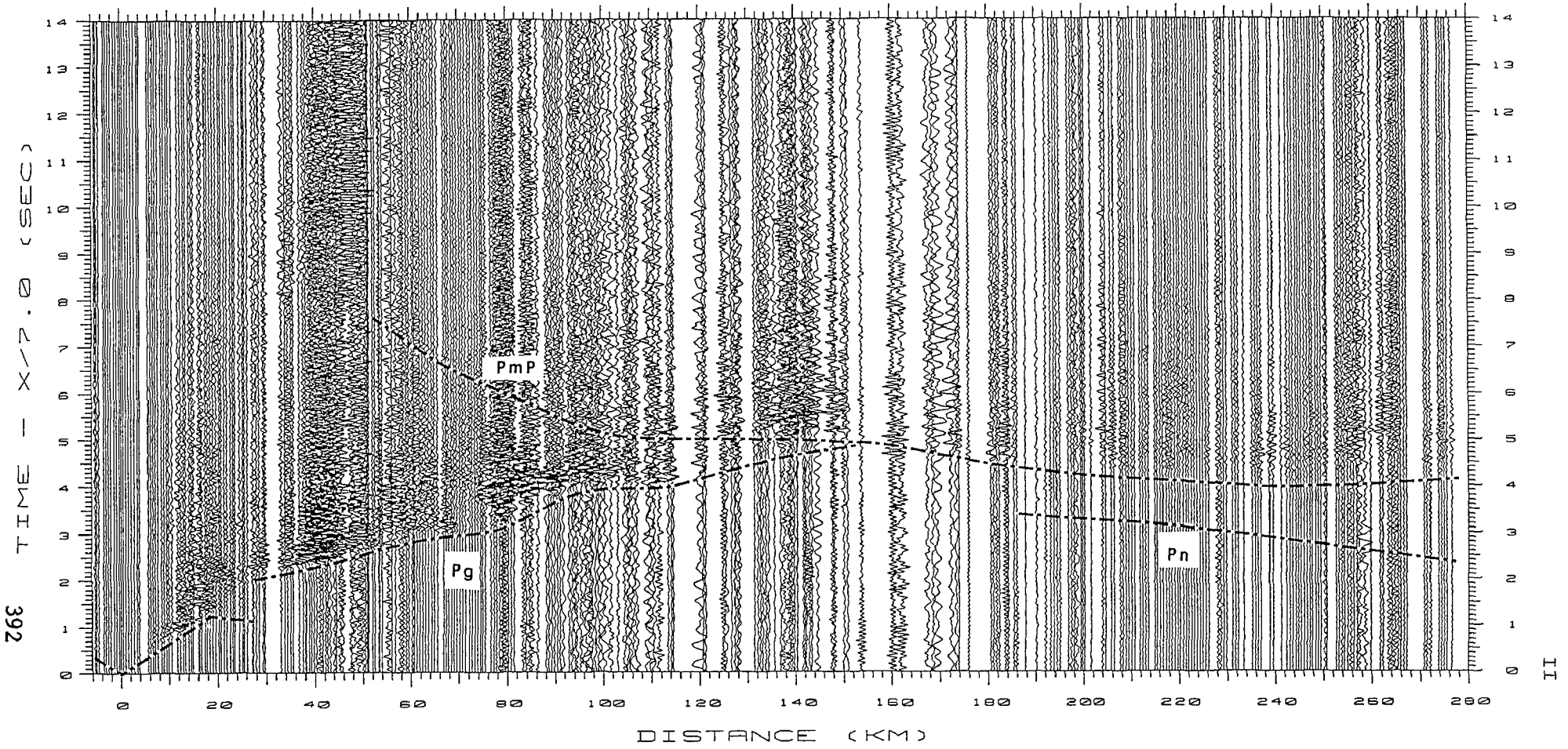

Figure 2. Seismic record of shot 1 with Pg, Pn and PmP arrivals denoted by the dashed line. This has been bandpass filtered, deconvolved and corrected for spherical spreading and plotted as true amplitude.

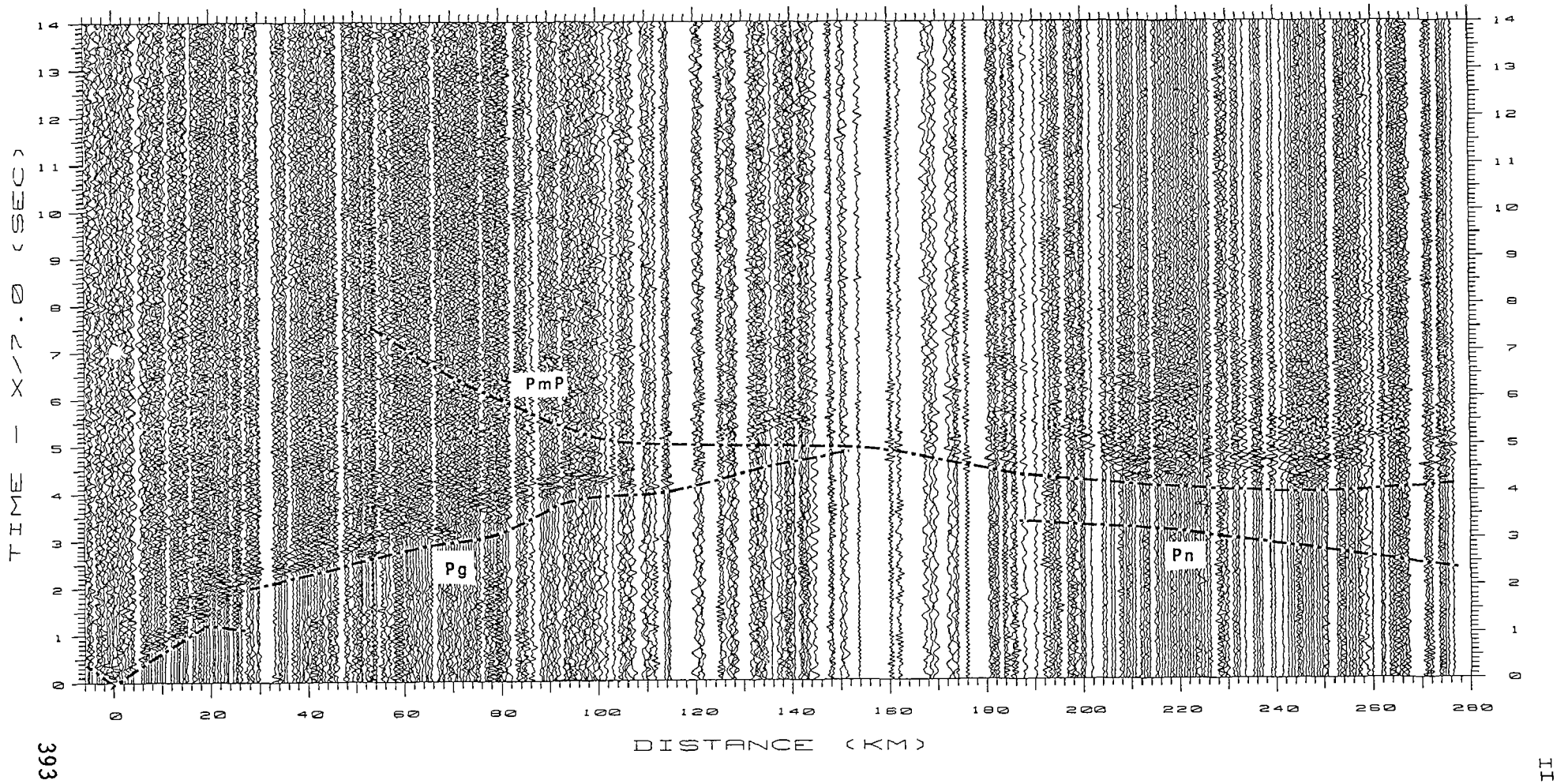

Figure 3. Seismic record of shot 1 with Pg, Pn and PmP arrivals denoted by the dashed line. This has been bandpass filtered, deconvolved and an automatic gain control has be applied.

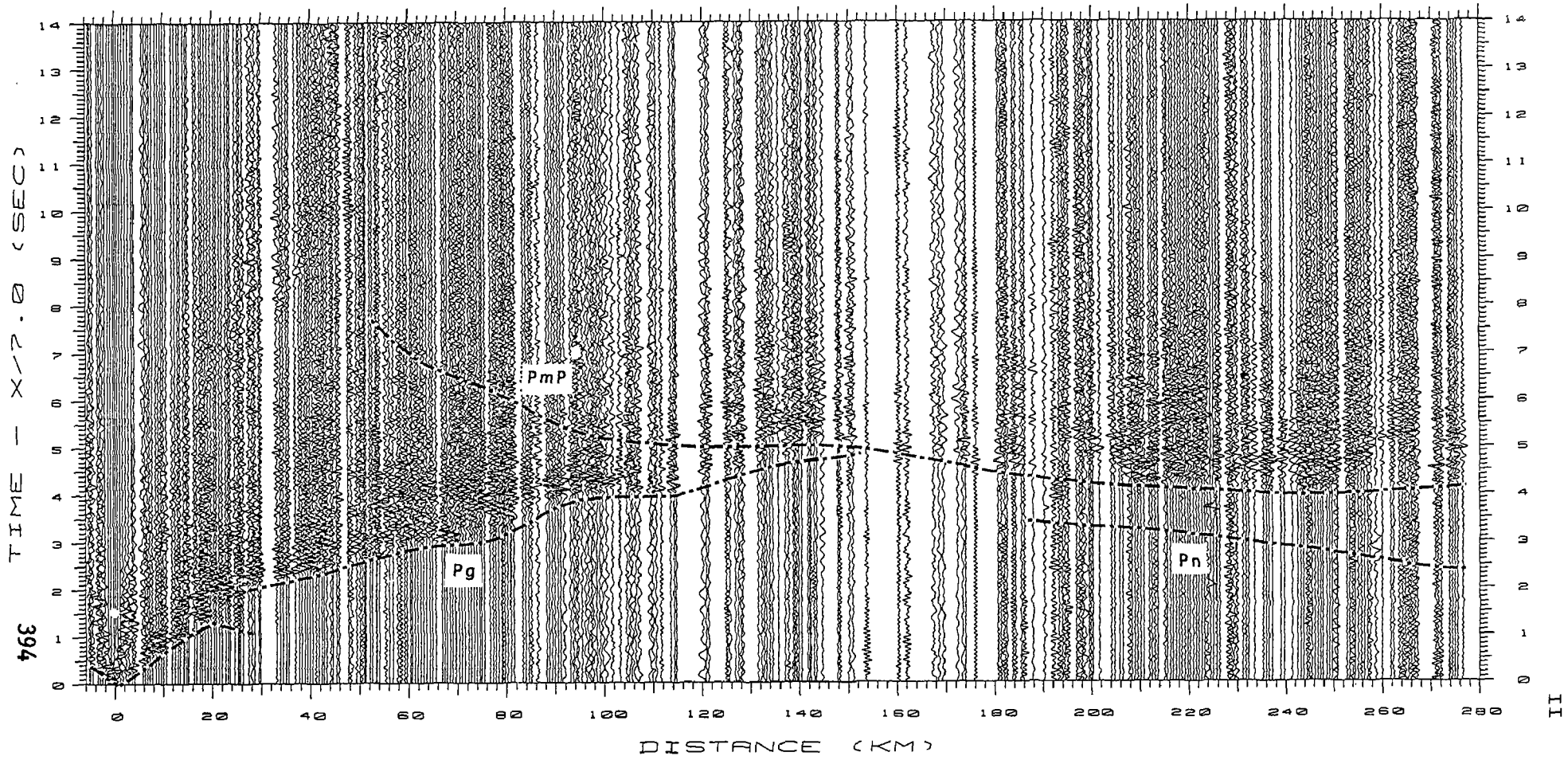

Figure 4. Seismic record of shot 1 with Pg, Pn and PmP arrivals denoted by the dashed line. This has been bandpass filtered, deconvolved and plotted with trace normallization.

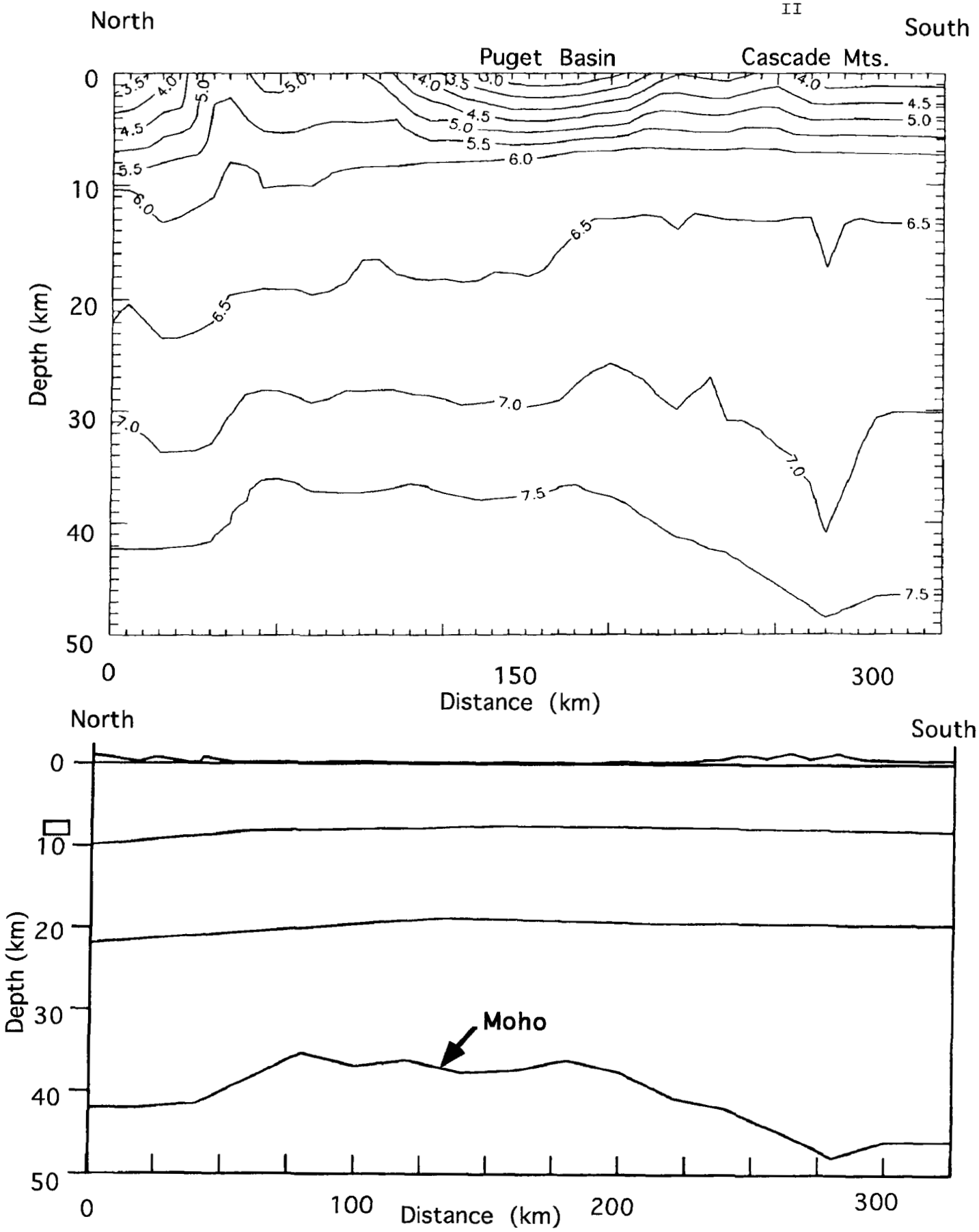

Figure 5. Seismic velocity model produced from inversion results of Pg, PmP and Pn arrivals. Upper figure shows the velocity field and the lower figure shows structure. Velocities are in km/s.

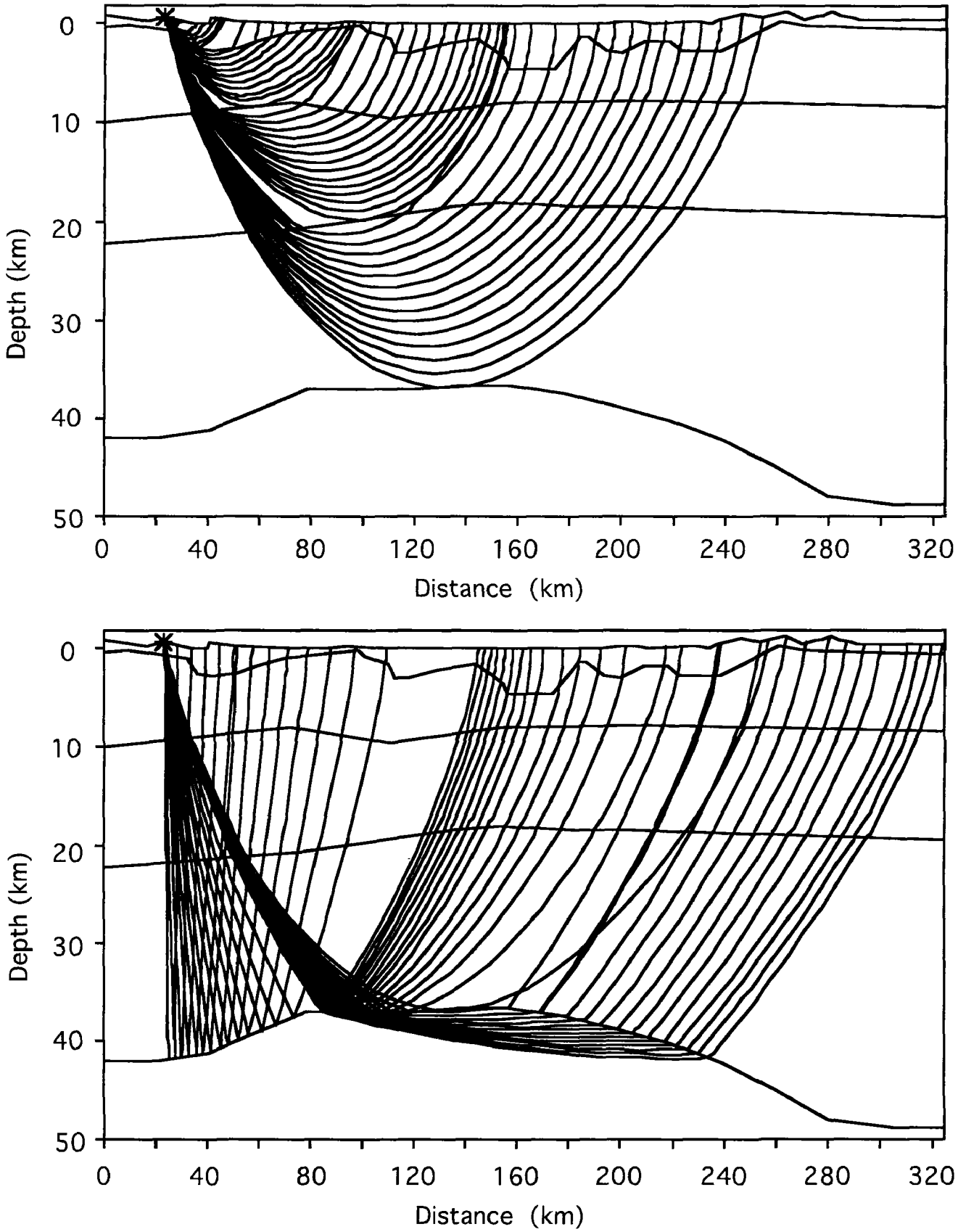

Figure 6. Forward ray trace model of the northern most shot. Upper figure is Pg arrivals and the lower figure is PmP and Pn arrivals.

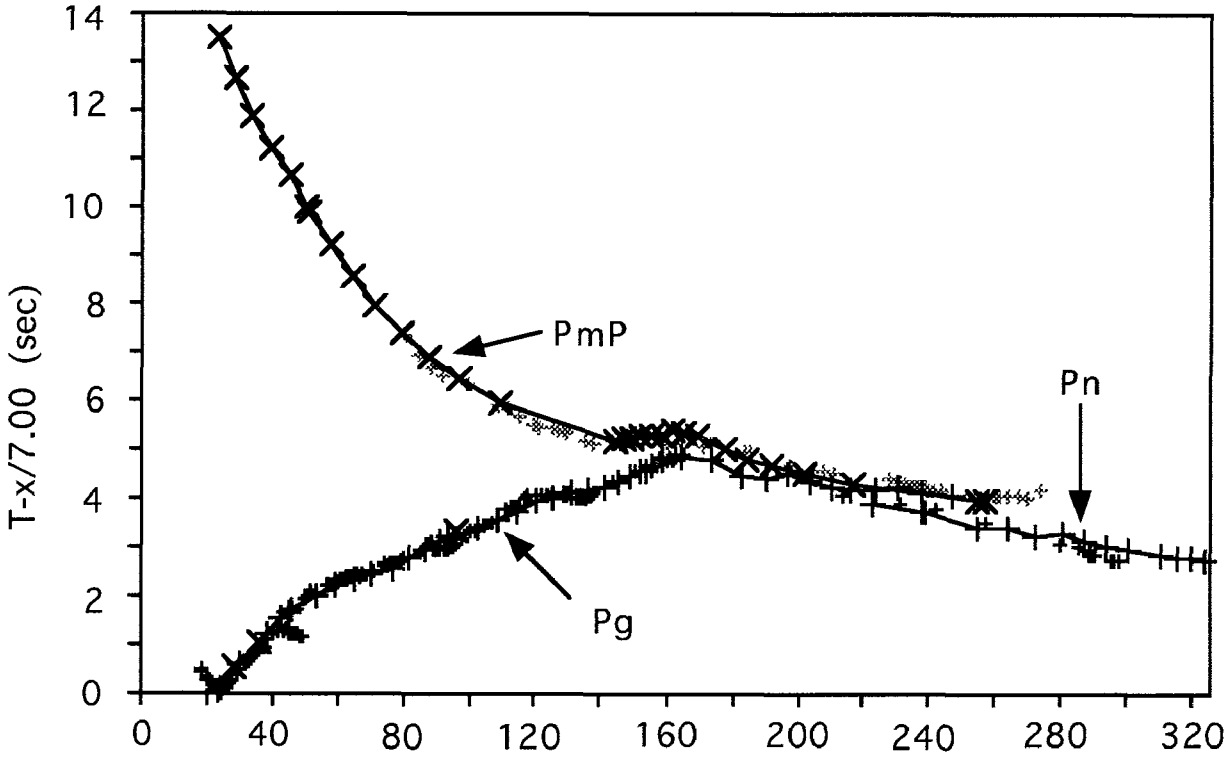

Figure 7. Forward ray trace model arrival fit for arrivals in Figure 6.

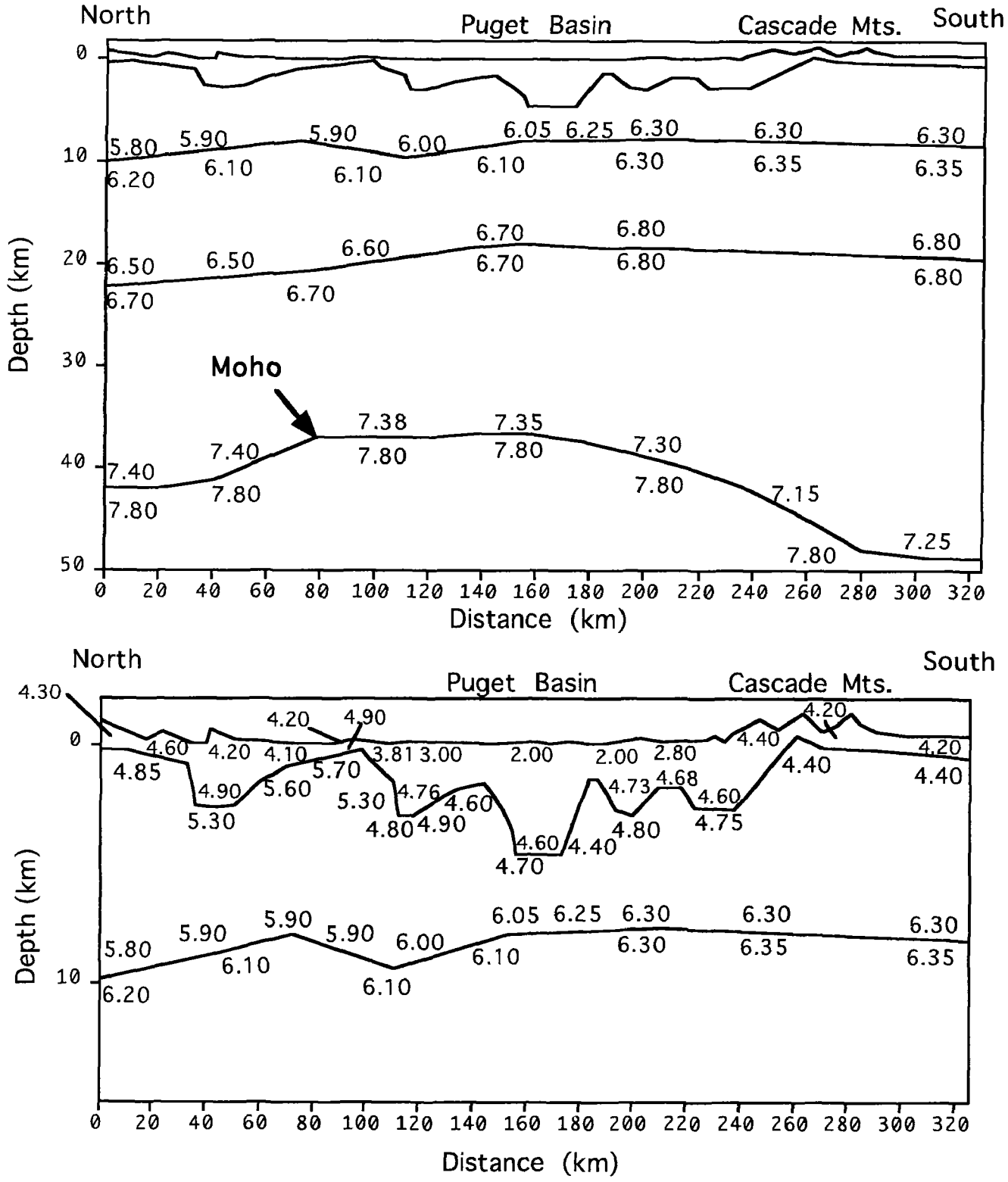

Figure 8. Top portion of the figure is the middle and lower crustal velocity structure from the forward ray trace model in Figures 6 & 7. Lower portion of the figure an is an elargement of the upper crustal velocity structure. Velocities are in km/s.

FAULT MECHANICS AND CHEMISTRY

9960-01485

C.-Y. KING
Branch of Tectonophysics
U.S. Geological Survey
345 Middlefield Road
Menlo Park, CA 94025
(415) 329-4838

Investigations

[1] Water temperature and radon content were continuously monitored at two water wells in Parkfield, California.

[2] Water level was continuously recorded at six other wells in central California.

[3] Water temperature and electrical conductivity were periodically measured, and water samples were taken from most of these wells and two springs in San Jose for Chemical analysis.

[4] Radon content of soil gas was surveyed across several faults.

Radon Surveys across Active Faults in California

Radon emanation is known to be anomalously high along active faults in many parts of the world. To check whether this is so for various faults in California, in late July and early August of 1992 we conducted soil-gas radon surveys with a portable radon meter (FD-3017, Shanghai Electronic Instruments, Inc.) across two creeping segments and one locked segment that was coseismically offset nearly three meters in the epicentral area of the magnitude 7.5 Landers earthquake on June 28, 1992.

Across the two creeping segments (Calaveras fault at Seventh Street in Hollister and San Andreas at Nyland Ranch in San Juan Bautista), the emanation was not anomalously high in the fault zones themselves, which are several meters wide, but was so on both sides of the fault. The survey lines were about 400 meters long and the maximum values, which are 5 to 8 times the background values, were measured at 10 to 55 meters from the center of the fault zones. This feature may indicate a relatively low permeability of the fault-gouge zone and high permeability of fractured rocks on both sides for terrestrial gases under pressure to escape into the atmosphere.

Along a 144-m survey line cross the currently locked segment of the San Andreas fault at the Earthquake Trail near Olema, the emanation was indeed anomalously high in the fault zone, by a factor of two above background values. However the maximum values (3 to 6 times background) were still recorded on the sides, about 10 meters away.

Alongside two roads (Encantado and Reche) that were offset by the Landers earthquake, the emanation at the two main breaks of the fault zone was an order of magnitude higher than background values measured over a distance of 300 and 420 meters, respectively.

Reports

King, C.-Y., (Group Chairman), 1991, Statements and recommendations (5 pages), in *Advisory Group Meeting Report on Isotopic and Geochemical Precursors of Earthquakes and Volcanic Eruptions,* reported by V. Dubinchuk, International Atomic Energy Agency, 1991.

King, C.-Y.,1991, Hydrological land geochemical approaches to earthquake prediction in *Proceedings of Symposium on Geology and Seismology of the Taiwan Strait and its Coasts,* China Ocean Press, 243-246.

King, C.-Y., Earthquake mechanism and predictability shown by a laboratory fault: *Journal of Geophysical Research,* (submitted), 40 Pages. (Branch Chief Approval, December 1991).

King, C.-Y., 1992, Earthquake-Prediction techniques: Encyclopedia of Earth system *Science, 2,* 111-118, *Academic Press Inc.*

King, C.-Y., 1992, Advances in Geophysical Research Vol. (Book review): Earthquake Spectra, v. 8, p. 637-639.

King, C.-Y., 1992, Earthquake-prediction techniques, *Proceedings of International School Symposium on Earthquake Prediction and Earthquake Engineering,* Plovdiv, Bulgaria, 16-23 April 1990.

King, C.-Y., 1992, Gas-geochemical approaches to earthquake prediction, *Proceedings of International School Symposium on Earthquake Prediction and Earthquake Engineering*, Plovdiv, Bulgaria 16-23 April 1990, p. 236-266.

King, C.-Y., Thermal stress in meteoroids by aerodynamic heating. *Journal of Geophysical Research,* (submitted), 23 pages. (Branch Chief approval, December 1991).

King, C.-Y.,Comment on "^{222}Rn premonitory signals for earthquakes" by R.L. Fleischer and A. Mogro-Campers: *Eos, American Geophysical Union Transactions,* (in press), 9 pages.

King, C.-Y., Basler, D., Minissale, A., Presser, T.s., Evans, W.C., and White, L.D., 1992, Hydrogeochemical measurements on Hayward fault (under review).

King, C.-Y., 1992, Thermal stress in meteoroids by aerodynamic heating, presented at *29th International Geological Congress*, Kyoto, Japan 24 August - 3 September, 1992, (abstract), v. 3, p. 641.

King, C.-Y., and Zhang W., 1992, Radon surveys across active faults in California, (abstract) *Supplement to Eos, American Geophysical Union Transactions,* 1992 Fall Meeting pl 362.

Minissale, A., and King, C.-Y., 1992, Seasonal variability of radon concentration in soil gas in central California (under review).

CASCADIA SUBDUCTION ZONE: NEOTECTONICS OF THE ACCRETIONARY WEDGE AND ADJACENT ABYSSAL PLAIN OFF OREGON AND WASHINGTON

CONTRACT 14-08-0001-G1800

Principal Investigator: LaVerne D. Kulm*
Co-Principal Investigator: Robert S. Yeats**
Graduate Research Assistant: Chris Goldfinger**

*College of Oceanography
**Department of Geosciences
Oregon State University
Corvallis, OR 97331
(503) 737-5211

Investigations

The overall objective of this project is to characterize and determine the timing of deformational events in the subducting Juan de Fuca plate (abyssal plain), deformation front (accretionary prism), and forearc basins (continental shelf) of the Cascadia convergence zone off Oregon and Washington. Field studies in 1992 were concentrated on potential active deformational zones identified in the recently completed neotectonic map of the Oregon margin. New sidescan sonar images and submersible dives discovered several active fault zones on the Oregon continental shelf and upper slope. We are continuing to identify and characterize discrete strike-slip fault and flexural-slip zones and relate them to potential fault and fold zones in the adjacent coastal region where co-seismic subsidence events in coastal bays are believed to be associated with large earthquakes in the Cascadia subduction zone. Alternatively, these co-seismic events may be related to local structures, rather than, or in addition to the unflexing of the plate margin.

Results

1. New Data Acquisition

Approximately 15,000 km of pre-existing oil industry multi-channel and single-channel seismic reflection records were acquired for the Oregon and Washington margins in 1992. In addition, biostratigraphic data were made available for surface outcrops cored on the shelf and slope. The Oregon records were used to construct the Oregon neotectonic map described below. We also obtained unprocessed BS^3 swath bathymetry from NOAA's National Ocean Service (NOS) for the submarine banks on the central and northern Oregon continental shelf and uppermost slope which allows the three-dimensional modeling of these features. SeaBeam swath bathymetry is now available in digital form for the Oregon continental slope and adjacent abyssal plain from NOAA/NOS.

In March 1992 we acquired a modest amount of funding from NOAA's National Undersea Research Program (NURP) to conduct a sidescan sonar and submersible dive project on the Oregon continental shelf and uppermost slope. Primary emphasis was placed on potential active fault zones. The NURP program provides funding chiefly for marine data acquisition, which was completed July 27 to August 4, 1992. The USGS's National Earthquake Reduction Program (NEHRP) provided the funding for data analyses and interpretation in this joint research program.

2. Neotectonic Map of Oregon Margin

We have completed the neotectonic map of the Oregon continental shelf, slope and adjacent abyssal plain that is the fundamental framework of our Oregon research program (Fig. 1, modified version of colored map; Goldfinger et al., 1992). The interpretation and correlation of the marine features on the map draws upon a combination of SeaBeam swath bathymetry, GLORIA long-range sidescan sonar, high-resolution SeaMARC-IA sidescan sonar, multi-channel and single-channel seismic reflection records, and DELTA and ALVIN submersible dives. This map will be published by the Oregon Department of Geology and Mineral Industries (DOGAMI) late in 1992. Several papers, which provided information to and utilized information from this map, were published during 1992 (Appelgate et al., 1992; Goldfinger et al., 1992a, 1992b; MacKay et al., 1992).

3. Active Faults of the Oregon Continental Shelf

In July-August 1992, we began a new and detailed study of selected active fault and fold structures of the Oregon continental shelf and upper slope which were previously identified in the Oregon neotectonic map (Goldfinger et al., in press). The objective of this program is to investigate active structures on the Oregon shelf and to determine their relationship to previously studied accretionary wedge active structures to the west and the active deformation of the Oregon coastal region to the east. The oil industry multi-channel seismic reflection profiles were combined with the field data from high-resolution 50 kHz Klein sidescan sonar surveys and DELTA submersible dives to locate, ground truth and map in detail the active structures. Three distinct styles of active deformation occur on the Oregon continental shelf: (1) active folding and associated flexural-slip faulting; (2) active strike-slip faulting; and (3) broad vertical deformation that may or may not be associated with individual faults. Each of these styles plays a role in the vertical and horizontal deformation of the Oregon shelf, and we infer, the adjacent coastal region. These structures also may be a seismic hazard to coastal communities in addition to or independent of the Cascadia plate interface.

Flexural-slip thrust faults are a common feature of active folding on the Oregon shelf. We made several DELTA dives on this type of fault off the Tillamook Bay area and southeast of Daisy Bank. These dives confirmed the active nature of these faults as previously postulated (Goldfinger et al., 1992) on the central shelf in water depths of 180-150 m. We documented several active flexural slip thrust faults with overhanging scarp morphology developed in poorly consolidated material. These scarps offset the Holocene transgressive sediments (i.e., post-20 Ka features). It is unlikely they survived the inner shelf erosive wave action during the last low stand of sea level. We have previously linked some of these folds and associated faults to Oregon's coastal bays, and suggested that these active folds may be partly or solely responsible for documented co-seismic subsidence and salt marsh burial (Goldfinger et al., 1992). Confirmation of the active nature of these folds by direct observation, along with onshore mapping by other investigators, supports the premise that upper plate folding and faulting plays a significant role in the vertical tectonics of a number of Oregon's coastal bays.

Several strike-slip faults in different localities were studied in detail in the field program. We recorded sidescan images and made submersible dives on two active strike-slip faults: (1) fault B on the uppermost continental slope-outer shelf off the central Oregon coast (Goldfinger et al., 1992); and (2) Coquille fault on the continental shelf off Bandon, OR along the southern Oregon coast. Fault B truncates the southern flank of a structural uplift named Daisy Bank on the uppermost continental slope. The fault zone was observed as a WNW-trending vertical shear zone with vertical scarps locally 10 m in height. Submersible observations confirmed the trend, dip, and slip-sense of this fault as hypothesized by Goldfinger et al. (1992a,b). A second similar fault bounds the northern slope of the bank. The orientation of secondary shear fractures on both fault segments suggests left-lateral motion, thus the uplift of Daisy Bank may be due to the

compressional zone between these two faults. Gentle deformation of unconsolidated Holocene transgressive sand and mud deposits (Kulm et al., 1975) indicates both these faults are currently active.

We mapped a series of WNW trending left-lateral strike-slip faults on the inner shelf off the mouth of the Umpqua River. These faults cut probable Elkton Formation rocks of Eocene age, and also displace the surficial trangressive sands (Figure 2a). The Coquille fault is a similarly active, NNW-trending strike-slip fault, with open fractures and scarps observed from the submersible in 85 m water depth (Figure 2b). Preliminary analysis of the main fault and secondary structures confirm the Coquille fault as a right-lateral strike-slip fault. Nearby reflection profiles suggest 3-5 km of right lateral separation of NNE trending fold axes.

4. Vertical Tectonics of the Oregon Continental Shelf

SeaBeam swath bathymetry and sidescan sonar images of Heceta Bank off central Oregon identified two Pleistocene shorelines (i.e., wave cut platforms and sea cliffs) in water depths of 115-130 m, and 190-210 m. The shorelines are about 25 km in length, and the latter is better defined than the former. The shallower shoreline approximates the latest Pleistocene eustatic sea level lowstand at about 20 Ka. The deeper shoreline lies some 65-85 m below this lowstand and is tilted down to the south. Sediment samples were collected on the platform with the aid of the submersible for dating. Paleo-water depths of sedimentary rocks indicate that Heceta Bank has undergone an average of 900-1000 m of post-Miocene uplift (Kulm and Fowler, 1974). The largest amount of uplift on the Oregon shelf occurs in late Miocene and early Pliocene strata from Heceta Bank. However, the deepest shoreline suggests subsidence has occurred along the seaward flank, possibly sometime during middle to late Pleistocene time. Likewise, paleo-water depths of sedimentary strata comprising Nehalem Bank to the north and Coquille Bank to the south indicate several hundred meters of uplift along the outer shelf during the Pliocene, but 100 and 200 m of subsidence on their seaward flanks, respectively, is documented during the Pleistocene (Kulm and Fowler, 1974). The vertical movements of these three outer shelf banks are complex but consistent over a distance of 325 km.

Reports (also cited in text)

Appelgate, B., Goldfinger, C., MacKay, M., Kulm, L.D., Fox, C.G., Embley, R.W., and Meis, P.J., 1992, A left lateral strike slip fault seaward of the central Oregon convergent margin: Tectonics, v. 11, p. 465-477.

Goldfinger, C., Kulm, L.D., Yeats, R.S., et al., 1992, Neotectonic map of the Oregon continental margin and adjacent abyssal plain, Oregon Department of Geology and Mineral Industries, Open File Report O-92-4.

Goldfinger, C., Kulm, L.D., Yeats, R.S., Appelgate, B., MacKay, M.E., and Moore, G.F., 1992a, Transverse structural trends along the Oregon convergent margin: Implications for Cascadia earthquake potential and crustal rotations, Geology, v. 20, p. 141-144.

Goldfinger, C., Kulm, L.D., Yeats, R.S., Appelgate, B., MacKay, M.E., and Cochrane, G.R., 1992b, Active strike-slip faulting and folding of the Cascadia plate boundary and forearc in central and northern Oregon, U.S.G.S. Professional Paper 1560, Earthquake Hazards in the Pacific Northwest, in press.

MacKay, M.E., Moore, G.F., Cochrane, G.R., Moore, J.C., and Kulm, L.D., 1992. Landward vergence and oblique structural trends in the Oregon margin accretionary prism: Implications and effect on fluid flow, Earth and Planetary Science Letters, v. 109, p. 477-491.

References

Kulm, L.D., Roush, R.C., Harlett, J.C., Neudeck, R.H., Chambers, D.M., and Runge, E.J., 1975, Oregon continental shelf sedimentation: Interrelationships of facies distribution and sedimentary processes, Journal of Geology, v. 83, p. 145-175.

Kulm, L.D. and Fowler, G.A., 1974, Oregon continental margin structure and stratigraphy: a test of the imbricate thrust model, in Burke, C.A., and Drake, C.L., eds., The geology of continental margins: New York, Springer-Verlag, p. 261-284.

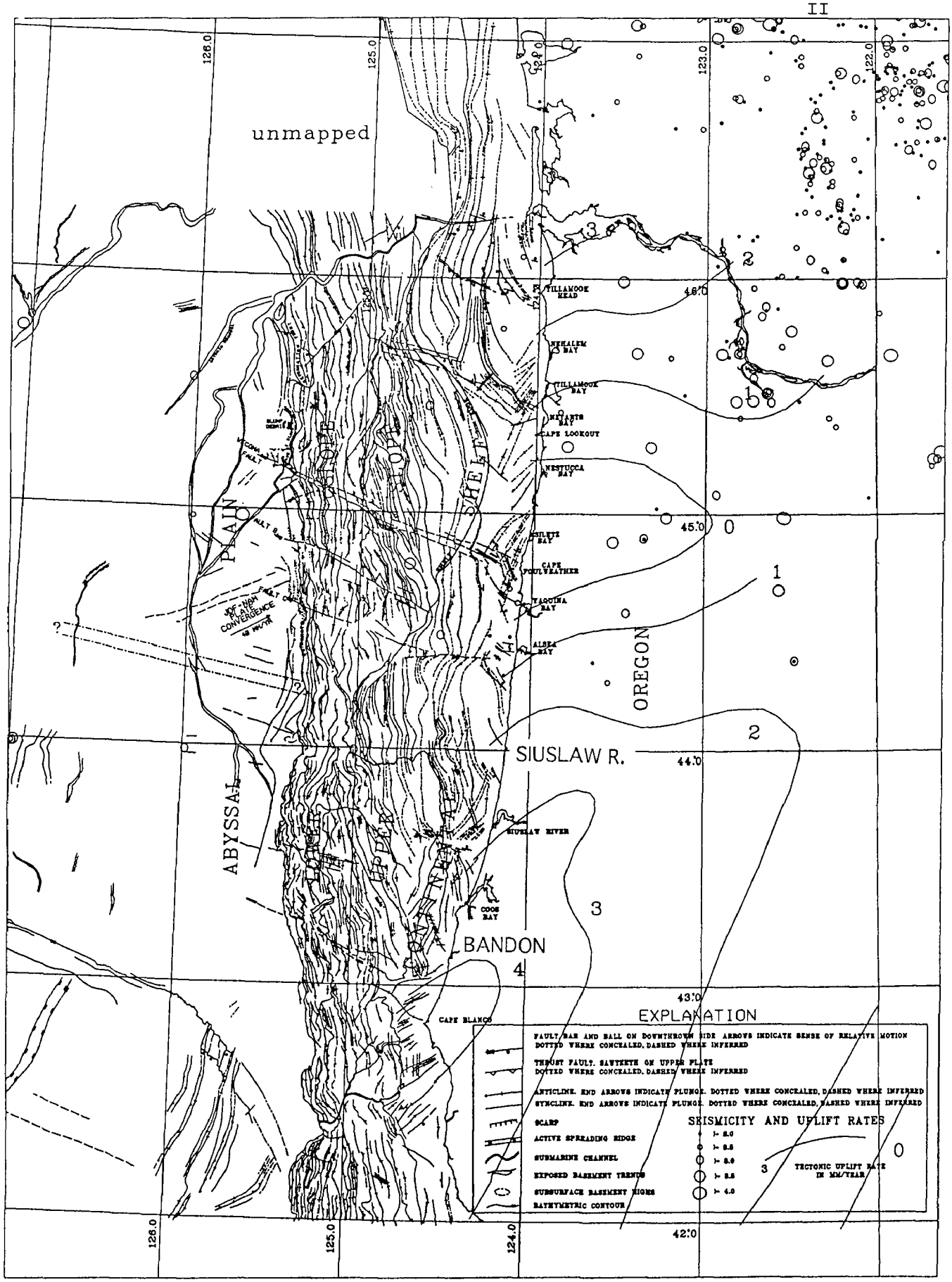

Figure 1. Neotectonic map of the Oregon continental margin showing structure, geodetic uplift rate contours, and seismicity. After *Goldfinger et al.*, 1992b, seismicity from *Kulm et al.*, 1984.

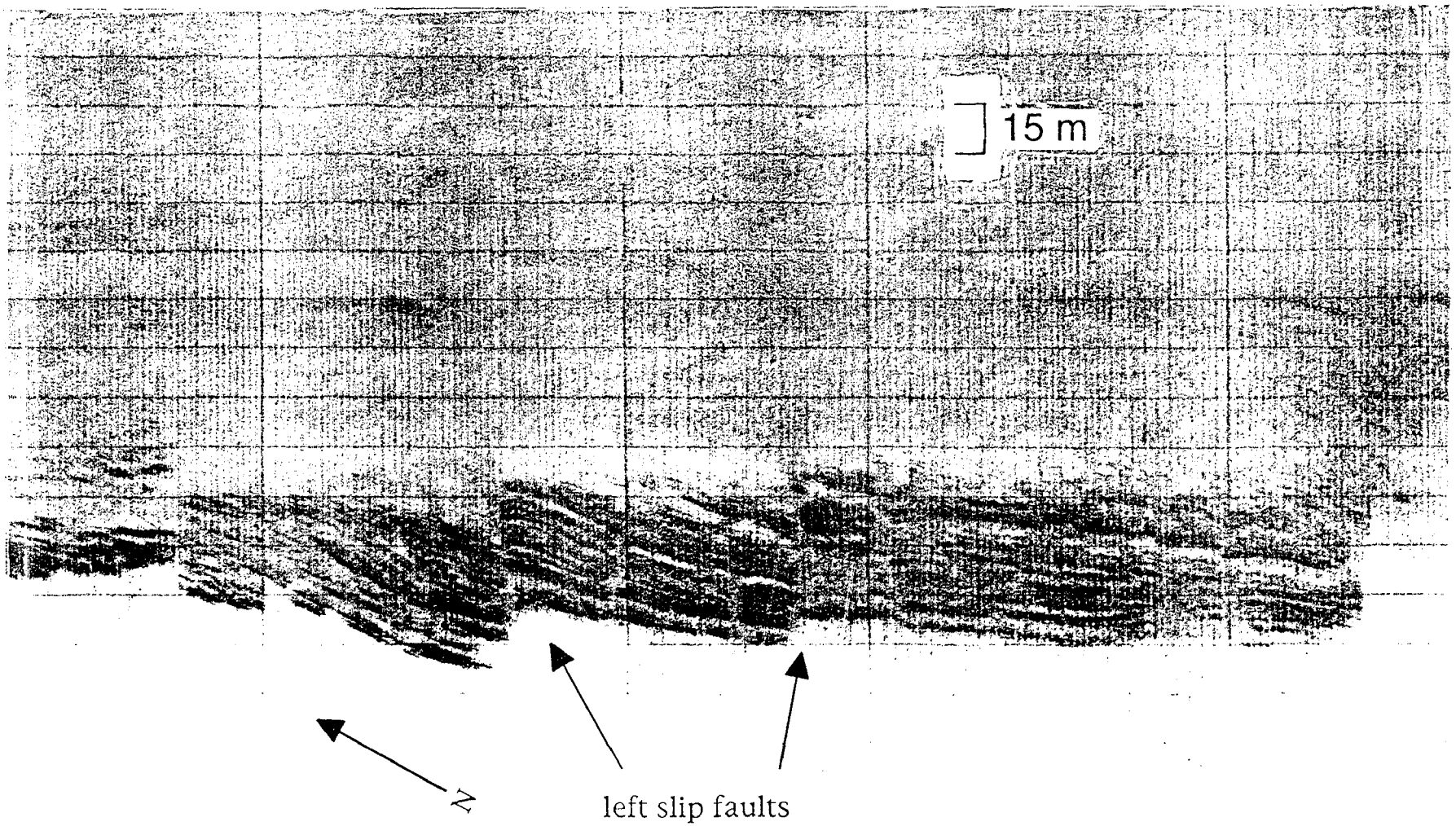

Figure 2a. 50 kHz sidescan record showing closely spaced left lateral strike-slip faults offsetting bedrock ridges of probable Elkton Formation off the Siuslaw River, southern Oregon. Strike-slip motion confirmed by mapping the same sense of offset on both limbs of a syncline. Water depth 90 m.

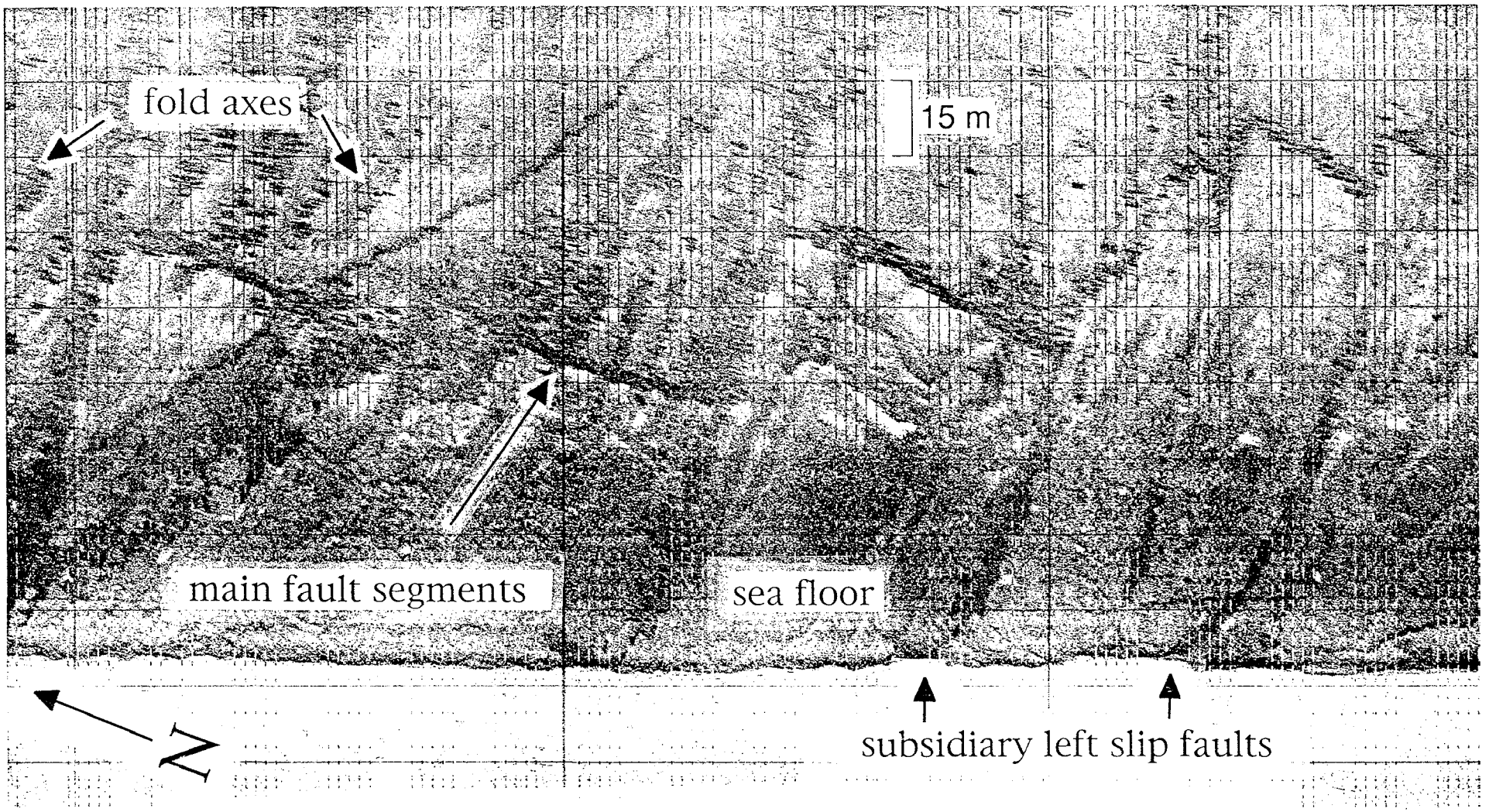

Figure 2b. 50 kHz sidescan record of the Coquille fault off Bandon, Oregon. En echelon main rupture segments trend north, while trend of the zone is NNW. Subsidiary WNW trending left-lateral faults are also clearly visible, as are active folds, establishing the direction of maximum compressive stress. Water depth 85 m.

Alaska Seismic Studies

9930-70023

John C. Lahr, Christopher D. Stephens,
Robert A. Page, and Kent A. Fogleman
Branch of Seismology
U. S. Geological Survey
345 Middlefield Road
Menlo Park, California 94025
(415) 329-4744

Investigations

1. Cooperated with the Geophysical Institute of the University of Alaska (UAGI) and the USGS National Earthquake Information Center (NEIC) in the operation of the Alaska Earthquake Information Center (AEIC) in Fairbanks. The AEIC is responsible for recording and analyzing Alaskan earthquake data and disseminating earthquake information and advisories to government agencies and to the public. As part of AEIC, continued lead role in collection and analysis of data from the high-gain short-period seismograph network extending across southern Alaska from the volcanic arc west of Cook Inlet to Yakutat Bay, and inland across the Chugach Mountains.

2. Cooperated with the Branch of Igneous and Geothermal Processed, UAGI, and the Alaska Division of Geological and Geophysical Surveys in operating the Alaska Volcano Observatory (AVO). Under this program, we have principal responsibility for monitoring the seismicity of Redoubt and Spurr, the recently active northern Cook Inlet volcanoes.

3. Cooperated with the Branch of Engineering Seismology and Geology and the UAGI in operating 13 strong-motion accelerographs in southern Alaska, including 11 between Icy Bay and Cordova in the area of the Yakataga seismic gap.

Results

1. For the time interval July 1991-June 1992, AEIC processed more than 7200 event triggers, of which 5187 were caused by earthquakes in southern and central Alaska (Figures 1 and 2). Seventeen of the earthquakes had magnitudes of 4.5 or greater, with the largest of these being a 5.9 ML shock on May 5 located 139 km deep beneath Iliamna volcano in a zone where earthquakes of similar size commonly occur. The largest shallow (depth above 30 km) earthquake was a 5.0 m_b (NEIS) shock on March 8 located along the Fairweather fault system northwest of Glacier Bay in southeastern Alaska. Of note is the persistence of aftershock activity in the northern Gulf of Alaska where two magnitude 7-class earthquakes occurred in 1987-88 (Lahr and others, 1988), a cluster of small earthquakes along the Transition fault zone near 58.75°N, 141.5°W, and the pesistence of shallow crustal activity beneath northern Cook Inlet about 75 km west-southwest of Anchorage. No unusual seismicity patterns were noted in and around the Yakataga seismic gap.

2. Focal mechanisms were compiled for nearly 1000 earthquakes that occurred between January 1987 and April 1992 in the area 60°-62.5°N latitude, 146°-153°W longitude. The more reliable solutions show a remarkably consistent pattern of stress orientation in the subducted plate beneath southern Alaska (Figure 3). Beneath Prince William Sound and the Chugach Mountains to the north, where the shallow subducted plate plunges northwestward at a low angle, the axes of least-compressive-stress (T-axes) tend to be subhorizontal and oriented west-east to northwest-southeast, with the general trend of the axes becoming more northerly to the north, roughly paralleling the change in the downdip direction of the subducted plate. The focal mechanisms of these events vary and range from normal to oblique-normal to strike-slip faulting. As both the depth and dip of the subducted plate increase, the dips of the T-axes also tend to systematically increase, so that the axes remain approximately aligned in the downdip direction of the Wadati-Benioff seismic zone within the descending plate to depths of at least 150 km. These observations are consistent with a model of the subducted plate acting as a stress guide transmitting upward the pull from deeper parts of the sinking slab. Evidence that this stress field may extend seaward of the trench is found in the northwestward orientation of T-axes determined for the sequence of two magnitude 7-class earthquakes in the northern Gulf of Alaska in 1987-88 (Lahr and others, 1988). The orientations of the axes of maximum-compressive-stress (P-axes) tend to be more variable. At depths less than about 65 km the axes tend to orient normal to the plane of the seismic zone; below 65 km the axes systematically rotate into the plane of the seismic zone and parallel the strike direction of the zone, and this tendency increases with depth (Kissling and Lahr, 1991). Many of the focal mechanisms for earthquakes in the overthrust North American plate have P-axes that are compatible with maximum subhorizontal compression aligned approximately in the direction of plate convergence.

3. Increasing seismic unrest at Spurr Volcano alerted AVO seismologists to magmatic activity beneath the volcano that culminated on June 27, 1992 in an explosive eruption at the historically active Crater Peak vent, which was the site of the last eruption in 1953. AVO issued a formal warning of a potential eruption one day before it occurred. The earliest indication of unrest was a swarm of shallow, high-frequency volcano-tectonic earthquakes (VT's) that occurred beneath Crater Peak in August 1991, the first swarm recorded at this location in ten years of monitoring. In the ensuing months levels of seismicity increased throughout the caldera, and notices of the increased activity were disseminated by AVO. In early June 1992, discontinuous episodes of tremor began following a brief swarm of VT's beneath Crater Peak. About 19 h before the June 27 eruption, continuous tremor started and persisted until about 4.5 hours before the eruption when a vigorous swarm comprising VT's and a few long-period events (LP's) began. The explosion blew away a seismic station located on the crater rim. Within several days after the eruption the level of seismic activity gradually declined to slightly elevated levels. A second explosive eruption occurred on August 18, but unlike the first event it was not preceded by significant seismic activity energetic enough to be recognized on the closest stations operating at that time (at distances greater than 4 km). The plume from this eruption was carried over Anchorage where as much as 3 mm of ash was deposited, disrupting aviation and commerce. After the August eruption, the seismic activity declined again but not to the level preceding August 18. In fact, at depths below 20 km the activity increased and suggested that magma was being replenished in the system. The crater rim station recorded the onset of continuous tremor starting a few hours before a third explosive eruption on September 17 and enabled AVO to issue an advance warning of the eruption. This explosion was followed by days of vigorous tremor

and in mid-November by an intense swarm of shallow events that led to an eruption alert but did not result in an eruption.

4. Earthquakes within a zone of seismicity beneath the Copper River delta area are being relocated using a model based on velocity structures determined for nearby TACT seismic profiles. Most of the well-recorded seismicity is concentrated near the top of a mid-crustal high-velocity (6.9 km/sec) layer that, in adjacent areas to the south and west, has been inferred to correlate with subducted lower crustal rocks of the Yakutat terrane. Typical focal mechanisms for these earthquakes are compatible with oblique reverse faulting controlled by compressive stress aligned approximately with the northwestward direction of plate convergence. However, the dips of the most northerly dipping nodal planes are probably too steep for these events to be associated with slip on the interplate thrust. Below about 20 km depth the rate of seismicity is much lower and the focal mechanisms generally have T-axes aligned in a northwest-southeast direction, which is characteristic of earthquakes in the Wadati-Benioff seismic zone in adjacent areas to the west. Relatively few earthquakes are located in the upper crust, but among them is the largest (by one magnitude unit) earthquake recorded by the regional network in this area since 1972, a magnitude 4.3 ML shock on September 15, 1989 that was followed by a significant aftershock sequence.

5. A patch of earthquake epicenters near Waxell Ridge marks the approximate center of the Yakataga seismic gap (see Figure 1). For many years the nature of this seismicity has remained uncertain due to poor local station coverage. However, with new data available since two additional seismographs were installed north of the Waxell Ridge, and with some velocity control available from nearby TACT seismic profiling, both the distribution and focal mechanisms of this seismicity can now be studied in more detail. In the southern part of this patch, many of the better constrained hypocenters tend to be concentrated in a diffuse zone between about 20 and 30 km depth that may lie at or near the top of the subducted plate. Offset from this zone by about 30 km to the northeast is a cluster of hypocenters centered at a depth of about 27 km. Focal mechanisms for earthquakes in this cluster are highly consistent and compatible with almost pure thrusting on a northward-dipping plane. Thus, this seismicity may be occurring at a weak spot on the interplate thrust. Near the hypocenter of the 1979 St. Elias earthquake (7.4 M_w; Estabrook and others, 1992), which is located about 50 km to the east, a similarly isolated cluster of seismicity was active for at least several years prior to the mainshock (Stephens and others, 1980). By analogy, the earthquake cluster at the northeast corner of the seismicity patch in the Waxell Ridge area may indicate a possible location for rupture initiation during a future large earthquake in the Yakataga gap.

6. Among the more significant computer software developments are: a new program (SPLAY) to display and interactively scroll through SSAM spectral data using a color VGA or super VGA monitor; a new version of the online event detection program XDETECT (version 3.0) that allows coeval triggers on multiple subnets which may have some stations in common; implementation of an automatic calibration analysis program to monitor and record station operational status; and changes to the event triggering algorithm in XDETECT to correct computational errors that tended to desensitize the algorithm.

7. Only one of the SMA units that were serviced had a trigger (Middleton Island), but the record has not yet been processed to check for an earthquake signal.

References

Estabrook, C.H., J.L. Nábělek, and A.L. Lerner-Lam, 1992, Tectonic model of the Pacific-North American Plate Boundary in the Gulf of Alaska from broadband analysis of the 1979 St. Elias, Alaska, earthquake and its aftershocks, J. Geophys. Res., v. 97, p. 6587-6612.

Lahr, J.C., R.A. Page, C.D. Stephens, and D.H. Christensen, 1988,Unusual earthquakes in the Gulf of Alaska and fragmentation of the Pacific plate, Geophys. Res. Lett., v. 15, p. 1483-1486.

Plafker, G., and K. Jacob, 1986, Seismic sources in Alaska, *in* Hayes, W.W., and P.L. Gori, eds., A workshop on evaluation of regional and urban earthquake hazards and risk in Alaska, U.S. Geol. Surv. Open-File Report 86-79, p. 76-82.

Reasenberg, P. and D. Oppenheimer, 1985, FPFIT, FPPLOT, and FPPAGE: Fortran computer programs for calculating and displaying earthquake fault-plane solutions, U.S. Geol. Surv. Open-File Report 85-739, 109 p.

Stephens, C.D., J.C. Lahr, K.A. Fogleman, and R.B. Horner, 1980, The St. Elias, Alaska, earthquake of February 28, 1979: Regional recording of aftershocks and short-term pre-earthquake seismicity, Bull. Seismol. Soc. Amer., v.70, p. 1607-1633.

Reports

Brocher, T. M., M. J. Moses, M. A. Fisher, C. D. Stephens, and E. L. Geist, 1991, Images of the plate boundary beneath southern Alaska, in Continental Lithosphere: Deep seismic reflections, AGU Monograph, Geodynamic Series, v. 22, p. 241-246.

Chouet, B.A., R.A. Page, C.D. Stephens, J.C. Lahr, and J.A. Power, Precursory swarms of long-period events at Redoubt Volcano, Alaska (1989-1990), Alaska: Their origin and use as a forecasting tool, submitted to J. Volcanol. Geotherm. Res.

Dawson, P.B., B.A. Chouet, R.A. Page and J.C. Lahr, 1992, A post-eruptive seismic survey of Redoubt Volcano, Alaska (abs.), Seismol. Res. Lett., v. 63, p. 67.

Jolly, A.D., R.A. Page, C.D. Stephens, J.C. Lahr, J.A. Power, and G.R. Cruse, 1991, Seismicity in the vicinity of Mt. Spurr Volcano, south-central Alaska, based on a revised velocity model (abs.), EOS (Trans. Am. Geophys. Un.), v. 72 (44 supplement), p. 567.

Kissling, E., and J.C. Lahr, 1991, Tomographic image of the Pacific Slab under southern Alaska, Eclogae geol. Helv., v. 84, p. 297-315.

Lahr, J.C., B.A. Chouet, C.D. Stephens, J.A. Power, and R.A. Page, Earthquake classification,

location and error analysis in a volcanic environment: Implications for the magmatic system of the 1989-1990 eruptions of Redoubt Volcano, Alaska, submitted to J. Volcanol. Geotherm. Res.

Moore, J. C., John Diebold, M. A. Fisher, J. Sample. T. Brocher, M. Talwani, John Ewing, R. von Huene, C. Rowe, D. Stone, Chris Stephens, and Dale Sawyer, 1991, EDGE deep seismic reflection transect of the eastern Aleutian arc-trench layered lower crust reveals underplating and continental growth, Geology, v. 19, p. 420-424.

Page, R.A., N.N. Biswas, J.C. Lahr, and Hans Pulpan, 1991, Seismicity of continental Alaska, in, Slemmons, D.B., E.R. Engdahl, M.D. Zoback, and D.D. Blackwell, eds., Neotectonics of North America, The Geological Society of America, Boulder, CO, CSM V-1, p. 47-68.

Page, R.A., J.C. Lahr, B.A. Chouet, J.A. Power, and C.D. Stephens, Statistical forecasting of repetitious dome failures during the waning eruption of Redoubt Volcano, Alaska, February-April 1990, submitted to J. Volcanol. Geotherm. Res.

Page, R.A., J.C. Lahr, C.D. Stephens, K.A. Fogleman, T.M. Brocher, and M.A. Fisher, 1992, Seismicity and stress orientation in the Alaska subduction zone after the great 1964 earthquake and speculation on the origin of a giant asperity [abs], in Wadati Conference on Great Subduction Zone Earthquakes, September 16-19, 1992, Fairbanks, Alaska, p. 31-32.

Power, J.A., J.C. Lahr, R.A. Page, B.A. Chouet, C.D. Stephens, D.A. Harlow, T.L. Murray, and J.N. Davies, Seismic evolution of the 1989-90 eruption sequence of Redoubt Volcano, Alaska, submitted to J. Volcanol. Geotherm. Res.

Rogers, J.A, and W.M. Kohler, 1992, XDETECT Version 2.01 Technical Reference, U.S. Geol. Surv. Open-File Report 92-364, 28 p.

Stephens, C.D., B.A. Chouet, R.A. Page, J.C. Lahr, and J.A. Power, Seismological aspects of the 1989-1990 eruptions at Redoubt Volcano, Alaska: The SSAM perspective, submitted to J. Volcanol. Geotherm. Res.

Stephens, C.D., J.C. Lahr, R.A. Page, and K.A. Fogleman, 1992, Recent seismicity in and near the Yakataga seismic gap, southern Alaska [abs], in Wadati Conference on Great Subduction Zone Earthquakes, September 16-19, 1992, Fairbanks, Alaska, p. 30.

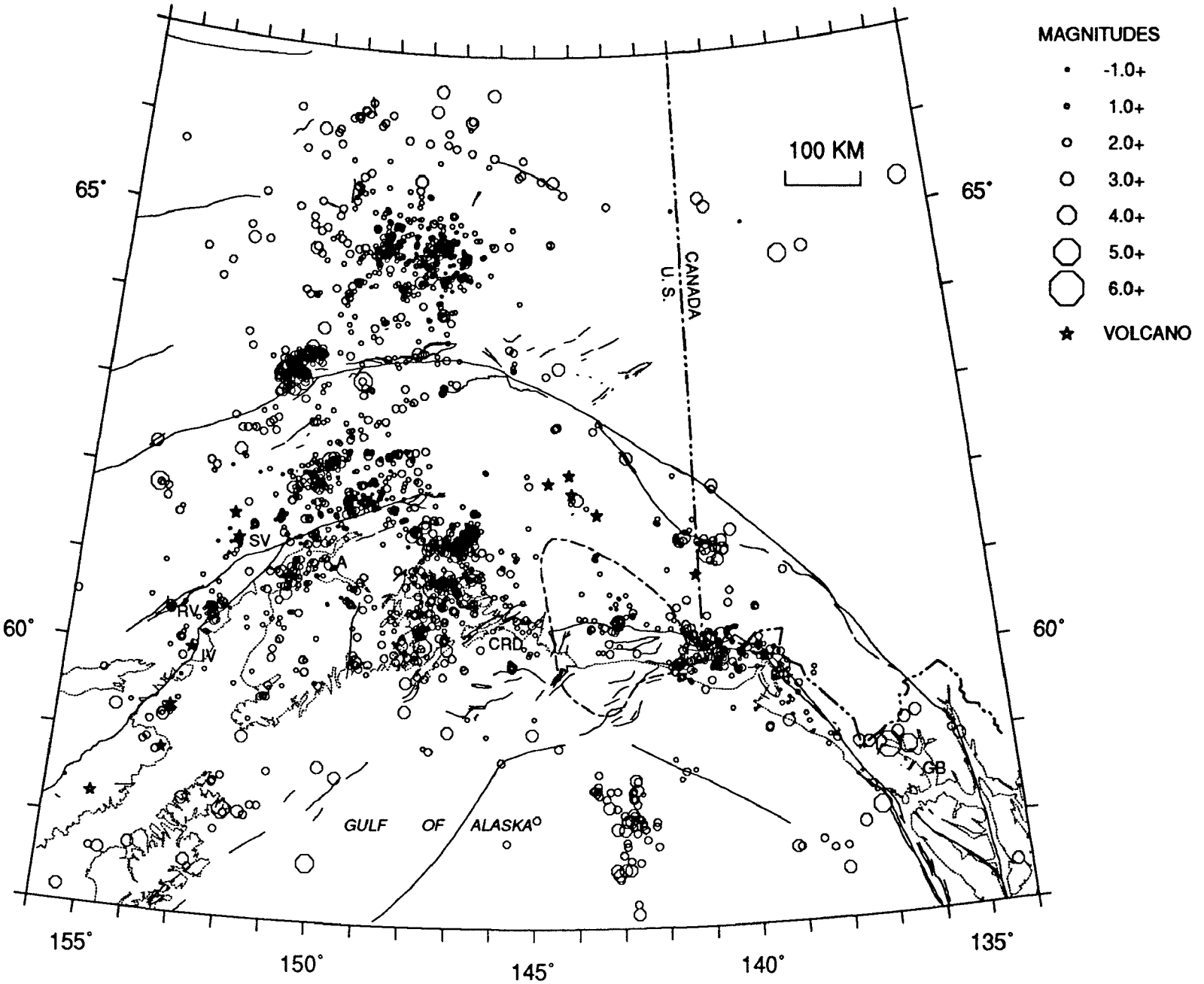

Figure 1. Preliminary hypocenters for 2488 earthquakes that occurred between July 1991 and June 1992 and were located above 30 km depth. Magnitudes are determined from amplitudes of seismic signals; the magnitude threshold for completeness varies across the region. Contour with alternating long and short dashes outlines inferred extent of Yakataga seismic gap. Neogene and younger faults (Plafker and Jacob, 1986) are shown as solid lines. A - Anchorage; CRD - Copper River delta; GB - Glacier Bay; IV, RV, SV - Iliamna, Redoubt and Spurr volcanoes.

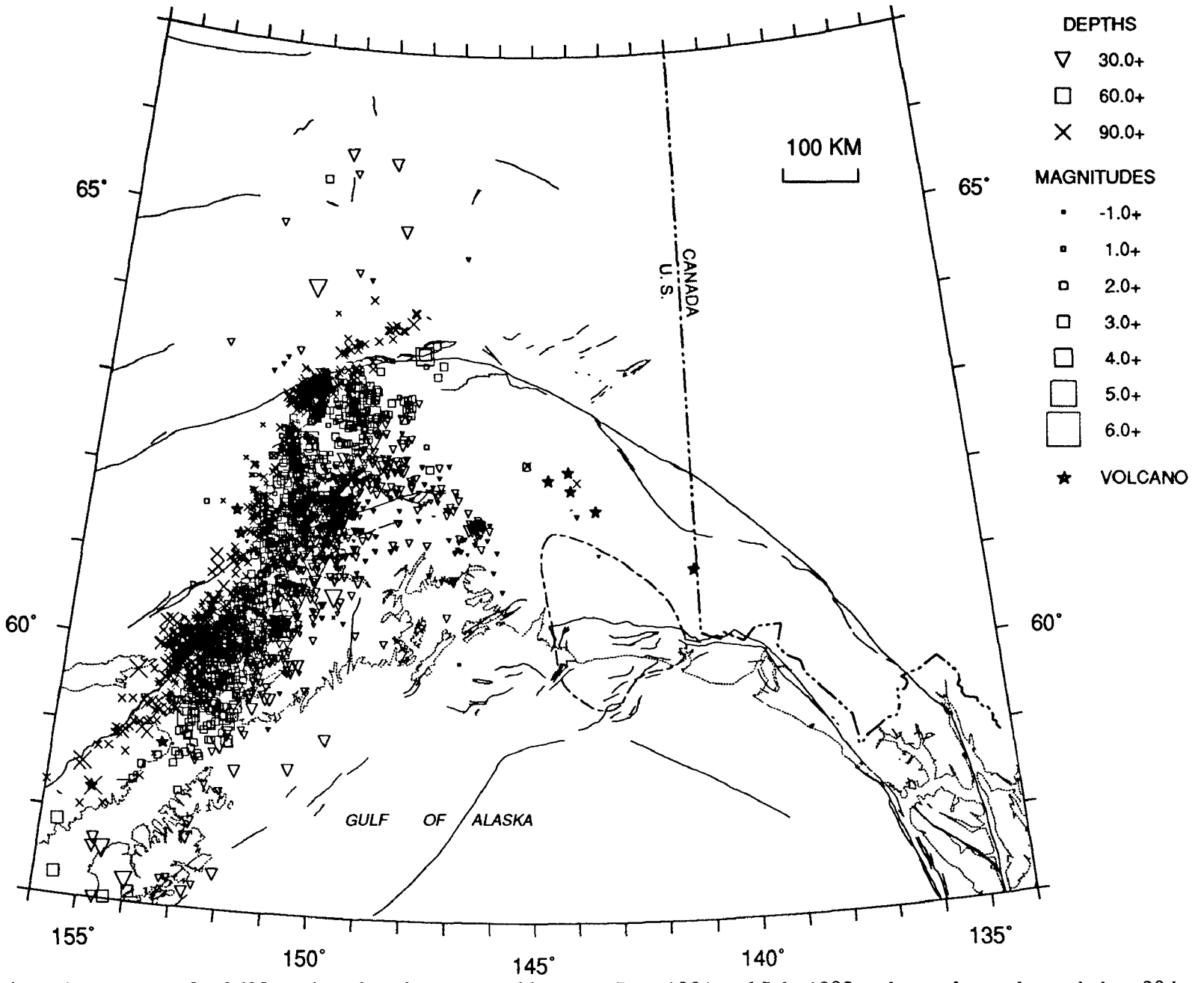

Figure 2. Preliminary hypocenters for 2699 earthquakes that occurred between June 1991 and July 1992 and were located at or below 30 km depth. See Figure 1 for details about magnitudes and identification of map features.

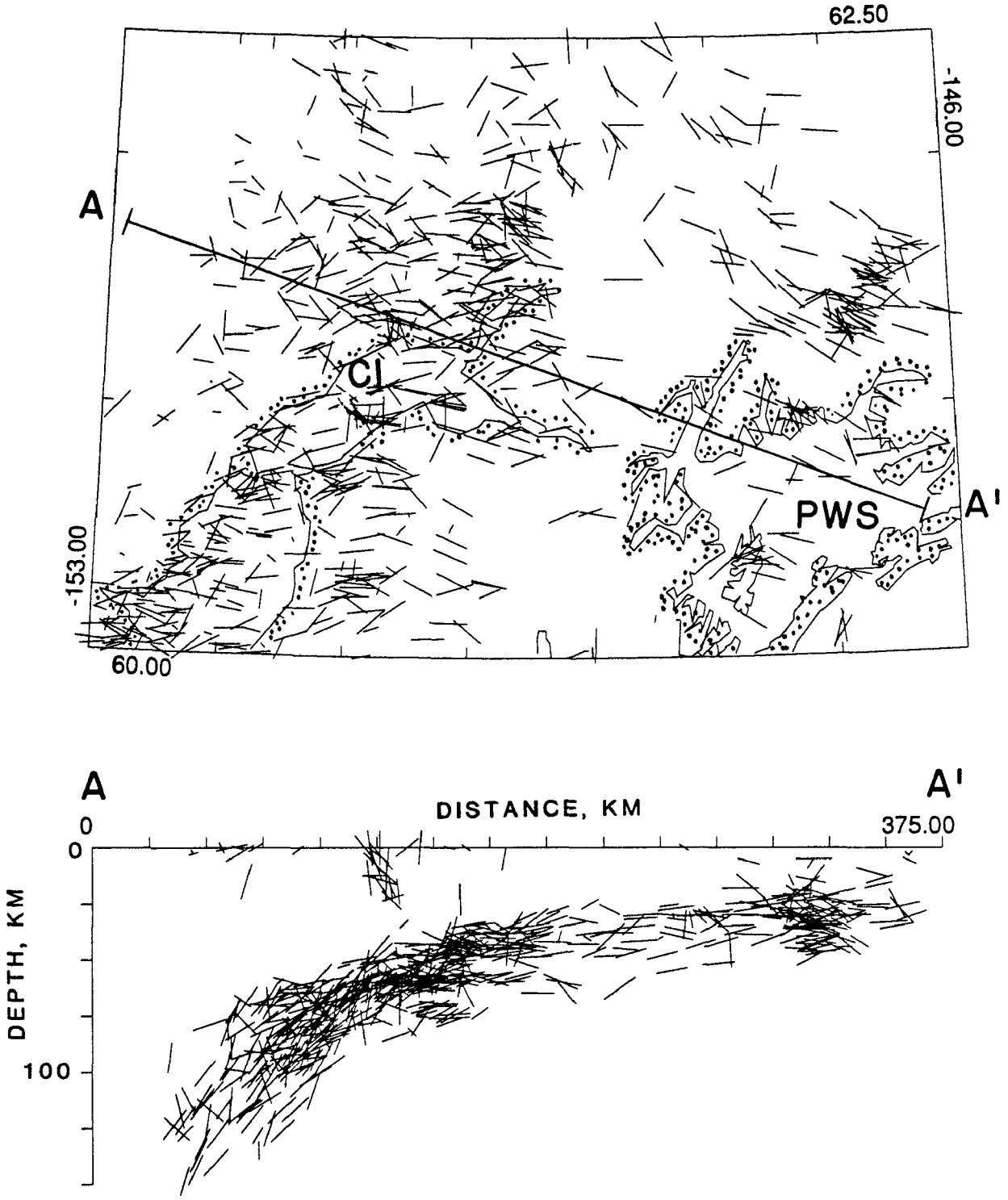

Figure 3. Orientation of T-axes for higher-quality focal mechanisms of 779 earthquakes. Unit-length axes are projected onto horizontal (*top*) and vertical (*bottom*) planes, so that shorter line segments correspond to nearly perpendicular axes. Focal mechanisms were determined using initial P-wave polarites and a modified version of the computer program FPFIT (Reasenberg and Oppenheimer, 1985), and were selected on the basis of having the 90% confidence regions for both the P- and T- axes cover less than 20% of the focal sphere. Line A-A' (*top*) shows the orientation of cross section (*bottom*), which is approximately perpendicular to the downdip direction of the Wadati-Benioff seismic zone in the subducting plate. CI - Cook Inlet, PWS - Prince William Sound.

POST-EARTHQUAKE STUDIES OF THE JUNE 28, 1992 LANDERS, CALIFORNIA, EARTHQUAKE

9910-01623

KENNETH R. LAJOIE
BRANCH OF ENGINEERING, SEISMOLOGY, AND GEOLOGY
U.S. GEOLOGICAL SURVEY
345 MIDDLEFIELD ROAD, MS/977
MENLO PARK, CALIFORNIA 94025
(415) 329-5641

Investigations

Post earthquake studies of June 28,1992 Landers earthquake. As part of joint USGS/CDMG effort mapped and analyzed surface fault rupture in Landers area.

Results

Surface fault rupture associated with the June 28, 1992 M_s 7.5 Landers earthquake extends 85 km from the Little San Bernardino Mountains in the south to the Rodman Mountains in the north. The rupture occurs along parts of several previously mapped north- to northwest-trending, subparallel faults (Eureka Peak, Johnson Valley, Homestead Valley, Emerson and Camp Rock), and along several unmapped north-trending faults connecting them. A 5-km gap in this otherwise continuous zone separates the northern end of the Eureka Peak fault and the southern end of the Johnson Valley fault. No surface rupture occurs on the east-trending Pinto Mountain fault, which runs through this gap. Southwest of the main rupture zone minor surface rupture occurs on the Lenwood fault and on the newly mapped Upper Johnson Valley fault. Northeast of the main zone rupture occurs on the Pisgah and Calico faults. Minor surface rupture also occurs on small faults northeast of Barstow. Surface rupture on the Eureka Peak, Lenwood, Upper Johnson Valley, Pisgah and Calico faults might reflect triggered, not primary, slip. Triggered slip did occur along the Indio segment of the San Andreas fault (40 km south of Landers) and along the entire length of the Superstition Hills fault (160 km southeast of Landers).

Displacement along the main faults is entirely right-lateral. Displacement along the connecting faults, with minor exceptions, is also right lateral. Thus, the connecting faults are not conjugate to the main faults, but are extensions of them. Horizontal displacement along the main faults is typically 2 to 3 m, but along the Emerson fault it reaches 5.5 m. Vertical displacement along the main faults is typically less than 0.3 m, but reaches about 2.0 m on the Emerson fault. In many places the sense of vertical displacement changes over short distances, and in some places it opposes general topographic relief.

Surface ruptures along the major faults generally follow topographic lineations and pre-existing fault scarps. However, at two places on the Emerson fault surface ruptures lie

up to 20 m from clearly expressed Quaternary scarps, possibly indicating local changes in stress. Most minor ruptures branching from the main faults follow no pre-existing geomorphic features, but along the Kickapoo fault there is clear geomorphic evidence of prior fault activity. In most places and on a wide range of scales surface ruptures are discontinuous, consisting of simple to complex patterns of en-echelon fractures and mole tracks. In some places, the rupture zone is over 100-m wide. Because of these complexities, few slip vectors could be measured precisely.

Surface rupture occurs along only on parts of the major faults. For example, it occurs only on the southern third of the Johnson Valley fault, and only on the northern halves of the Emerson and Camp Rock faults. Apparently, the numerous north-trending connecting faults transferred slip from part of one major fault to part of another. It is doubtful that this complex rupture pattern could have been predicted prior to the Landers event. Also, it is uncertain whether the same pattern occurred in the past or will occur again in the future. The pattern suggests that rupture started on the Johnson Valley fault and propagated northwestward. The pattern also suggests that the driving mechanism was a deep, northwest trending right-lateral couple that integrated parts of pre-existing faults at the brittle crustal surface. If correct, this model supports the conclusion of others that a major shear zone carries significant right-lateral motion between the North American and Pacific plates from the southern San Andreas fault across the Mojave desert into the western Great Basin. In effect, the Landers earthquake might reflect the northwestward propagation of the right-stepping transform system in the Gulf of California into the western Great Basin.

Reports

Staff (U.S. Geological Survey Menlo Park, CA 94025; California Division of Mines and Geology, Sacramento, CA 94518),1992, Pattern of Surface rupture associated with the June 28,1992 Landers Earthquake, EOS, v. 73, no. 43, p. 357. (Abs.)

Lajoie, K. R., 1992, Holocene Coastal Uplift in the Region of the 1992 Petrolia Earthquake, Northern California, EOS, v. 73, no. 43, p. 497. (Abs.)

McLaughlin, R.J., Lajoie, K. R., Castle, R. O. and Beutner, E. C., 1992, Tectonic Framework of the Mendocino Triple Junction of Northern California, EOS, v. 73, no. 43, p. 496. (Abs.)

Sebrier, M., McLaughlin, R. J., Lajoie, K.R. and Oppenheimer, D., 1992, Fault Kinemetics in the San Francisco Peninsula Area: is the 1989 Loma Prieta Earthquake Anomalous?, EOS, v. 73, no. 43, p. 4589. (Abs.)

Geodetic Strain Monitoring

9960-02156

John Langbein

Branch of Tectonophysics
U.S. Geological Survey
345 Middlefield Road MS/977
Menlo Park, California 94025
(415) 329-4853
langbein@shasta.wr.usgs.gov

Investigations

Two-color geodimeters are used to survey, repeatedly, geodetic networks within selected regions of California that are tectonically active. This distance measuring instrument has a precision of 0.1 to 0.2 ppm of the baseline length. Currently, crustal deformation is being monitored within the south moat of the Long Valley caldera in eastern California, across the San Andreas fault at Parkfield, California, at three locations near Palmdale, California on a section of the San Andreas fault that is within its Big Bend region, and at two locations near Pinon Flat, California. Periodic comparisons with other other two-color geodimeters are conducted both at Parkfield and at Mammoth Lakes. These intercomparisons measurements serve as a calibration to monitor the relative stabilities of these instruments.

Results

1. Long Valley Caldera

The line length changes measured using a two-color geodimeter still show high extension rates within the Long Valley Caldera. Figure 1 shows the line-length changes measured from mid 1983 to 27 monuments using our centrally located monument at CASA. The location of these baselines along with other baselines that are infrequently measured is shown in Figure 2.

The results from our measurements have been submitted for publication in *JGR*:

Abstract: Following the episodes of inflation of the resurgent dome associated with the May 1980 earthquake sequence (four M6 earthquakes) and the January 1983 earthquake swarm (two M5.2 events), seven years of frequently repeated two-color geodimeter measurements spanning the Long Valley Caldera document gradually decreasing extensional strain rates from 5 ppm/a in mid-1983, when the measurements began, to near zero in mid-1989. The corresponding seismic activity within the caldera persisted at a low rate of fewer than 10 M≥1.2 earthquakes per week from 1985 through November 1989 with no events exceeding M3.0. Early October 1989 marked a change in activity when measurements of the two-color geodimeter network showed a significant increase in extensional strain rate (9 ppm/a) across the caldera. The seismic activity began exceeding 10 M≥1.2

per week in early December 1989 and rapidly increased to a sustained level of tens of M≥1.2 per week with bursts having hundreds of events per day. Many events exceeded M3.0 and the largest event was M≈4. The 1989-91 inflation episode is the firs' have sufficient geodetic measurements in Long Valley to define the temporal relation between onset of an inflation episode and onset of brittle failure (earthquake swarm within the caldera). Here, the onset of events per day. Many events exceeded M3.0 and the largest event was M≈4. The 1989-91 inflation episode is the first time that we have sufficient geodetic measurements in Long Valley to define the temporal relation between onset of an inflation episode and onset of brittle failure (earthquake swarm within the caldera). Here, the onset of deformation preceded the onset of increased earthquake activity by more than two months. The seismicity rate began to decrease in mid-July 1990, consistent with a gradually slowing of extension across the caldera as measured by the two-color geodimeter. The recent episode of inflation can be modeled by a single Mogi point source located about 7 km beneath the center of the resurgent dome. In contrast, the deformation pattern observed between mid-1983 and mid-1989 is best reproduced by fault slip in the south moat, inflation at 6.5 km-depth near Casa Diablo Hot Springs and inflation beneath the resurgent dome. It appears that the source beneath the resurgent dome that was active for the earlier episodes is the primary source for the more recent episode. The model used to satisfy the line-length observations predicts 7.5 cm of uplift along leveling route along highway 395 from mid-1983 to mid-1989 and an additional 11 cm through the end of 1991. Thus the recent inflation episode represents a significant portion of the observed geodetic deformation with only little seismic energy release

During the summer of 1992, Dzurisin and co-workers of CVO releveled many of the routes within and near the Long Valley Caldera. Their observations show 11 cm of uplift during the interval between 1988 and 1992 which support the model of inflation derived from the two-color measurements.

2. Parkfield

Frequent measurements of a 17 baseline networks are made for a geodetic network near Parkfield, California. Approximately one-half of these baselines straddle the San Andreas Fault along the segment that last ruptured in 1966. The data from these baselines are shown in Figures 3a and 3b.

3. Southern California

Following the 1992 Landers earthquake, we used the two-color geodimeter to remeasure 3 out of our 5 networks in southern California. Below, is a compilation of the co-seismic strain changes inferred from the line-length changes. These networks were measured in the two-week interval following the 4 July holiday. To compute the co-seismic strain changes, the parameters of secular strain accumulation and a co-seismic strain change were simultaneously determined. The table below shows the results of this calculation. The error bars represent the one-standard deviation level and are computed on the basis of propagating the a-priori estimates of the data error through the inversion and the error bars are re-scaled by a factor representing the RMS misfit of the predicted to the observed length changes. The RMS misfit ratio of the misfits to the a-priori data error ranges between 1.34 and 1.82 mm/mm. The estimated error on the co-seismic strain changes could by considered "optimistic" since they represent offsets from extrapolating a linear trend. Had we differenced the lengths between the survey preceding and following the time of the Landers earthquake, the

standard errors would be larger.

The center of mass given for each network is a rough estimate. In reality, one should use the actual line-length change data to model the slip distribution of the Landers events. From the estimates of the strain changes for Pinon and Anza, which are located within 20 km of each other, the gradient in strain is significant because these networks are located near a node of the strain field.

Network period	Center of mass		Secular strain rate ppm/yr			Co-seismic strain ppm		
	longitude	latitude	$\dot{E}_{ee}$	$\dot{E}_{en}$	$\dot{E}_{nn}$	E_{ee}	E_{en}	E_{nn}
Pearblossom 1980-1992	-117° 51.7′	34° 27.7′	0.158±0.005	0.151±0.003	-0.200±0.005	-0.34±0.08	-0.18±0.06	0.14±0.08
Pinon 1986-1992	-116° 27.1′	33° 35.6′	0.142±0.020	0.127±0.013	-0.054±0.010	-0.46±0.28	-1.27±0.20	0.80±0.15
Anza 1988-1992	-116° 37.1′	33° 35.2′	0.189±0.027	0.071±0.021	-0.232±0.025	-0.22±0.13	0.19±0.09	1.85±0.12

4. Northern California

During the summers of 1991 and 1992, we measured the baseline lengths of 2 networks established in North California (Figure 4) to measure strain accumulation due to subduction of the Gorda Plate near Crescent City, California. From these line-length changes, a model of uniform strain is fit to the data from each of these networks:

Network	Secular strain ppm/yr			Principal strain Axis; Max. Compr. Degrees	ppm/yr Max. Compr.	Min Compr.
	$\dot{E}_{ee}$	$\dot{E}_{en}$	$\dot{E}_{nn}$			
Gorda	0.04±0.06	-0.01±0.06	-0.08±0.12	N5°E±28	0.08±0.12	-0.04±0.09
Scott	-0.30±0.08	-0.25±0.06	0.18±0.08	N67°W±5	0.41±0.09	-0.29±0.09

These estimates of strain rate are very preliminary since there was an instrument mal-function during the survey in 1992 which resulted in a length dependent offset. We have now enough test measurements which simulate the mal-function and we have incorporated a calibration curve into the adjustments of the line length data. Further testing and refinements of the calibration curve are necessary before the above results should be referenced.

We expect to remeasure these networks infrequently over the next few years in order to refine our estimates of secular strain. With two accurate measures of the strain rate provided by these networks, we can test the hypothesis of whether the Gorda Plate is locked beneath the North American Plate.

5. Publications

Langbein, J.O., D.P. Hill, T.N. Parker, and S.K. Wilkinson, An episode of re-inflation of the Long Valley caldera, eastern California; 1989-1991, *J. Geophys. Res.*, submitted

FIGURE 1. A plot of changes in line length for the baselines that use CASA as a common station. The line-length changes have been normalized to the nominal baselines length therefore transforming the displacements from units of mm to parts per million (ppm). The error bars represent plus or minus one standard deviation.

FIGURE 2. The location of the baselines that are measured using a two-color geodimeter are shown along with the location of the boundaries of the Long Valley caldera (solid line) and the resurgent dome (dashed line).

FIGURE 3a. Plot of the two-color geodimeter data for measurements of line-length changes since mid 1984 for those baselines that cross the San Andreas fault near Parkfield. The error bars represent one standard deviation of each observation. The data as plotted has had a linear trend removed and the computed secular rate is next to the plot of the residuals. Data are particularly noisy between April 1989 and May 1990 because of an intermittent, systematic error within the two-color geodimeter. See previous technical reports for a discussion of this problem.

FIGURE 3b. Same as Figure 3a except that these baselines do not cross the San Andreas fault.

FIGURE 4. Map showing the location of the two geodetic networks used to measure strain accumulation in northern California. The Gorda network consists of 13 baselines while the Scott network consists of 10 baselines.

LONG VALLEY NETWORK

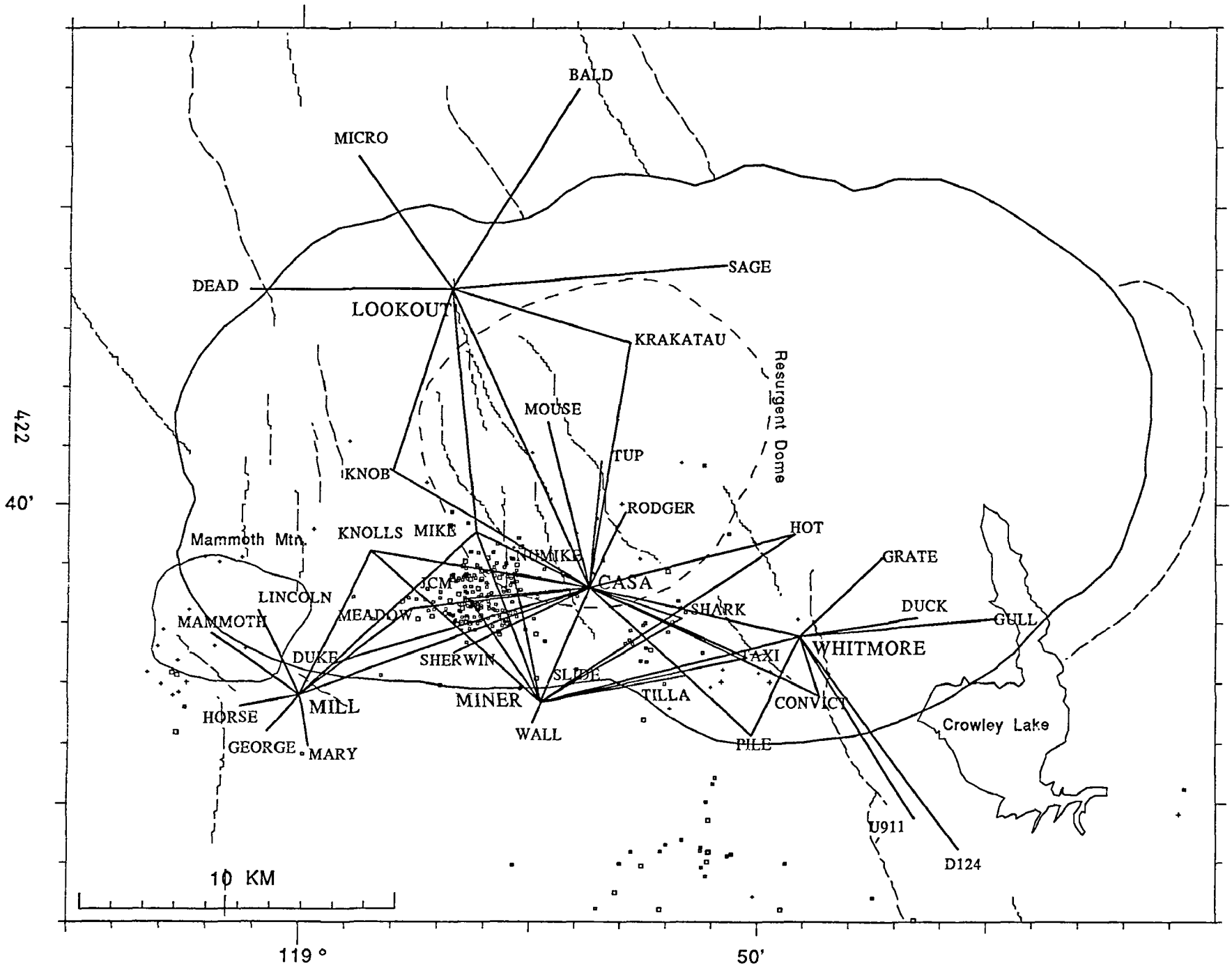

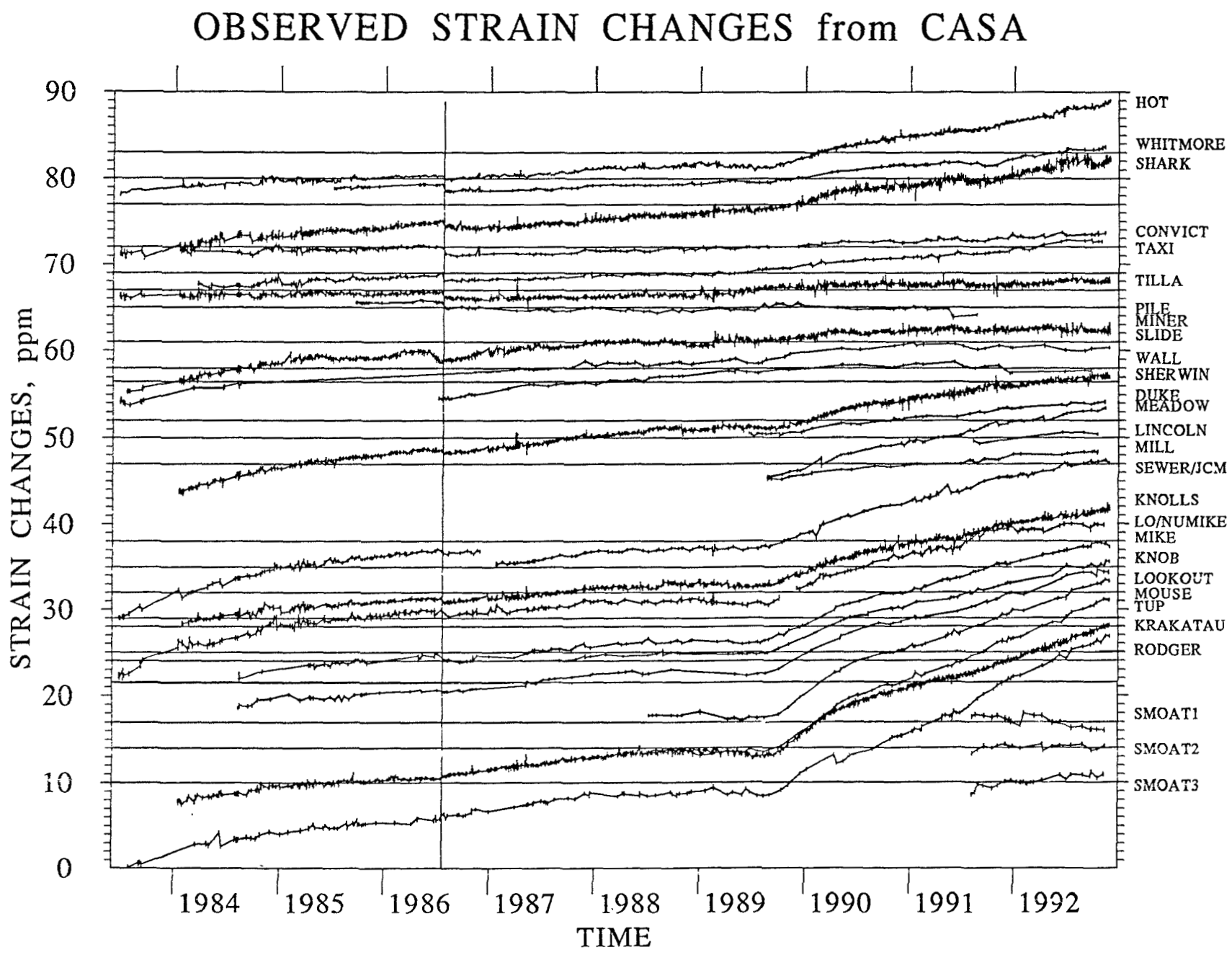
OBSERVED STRAIN CHANGES from CASA
STRAIN CHANGES, ppm
TIME
0
10
20
30
40
50
60
70
80
90
1984
1985
1986
1987
1988
1989
1990
1991
1992
HOT
WHITMORE
SHARK
CONVICT
TAXI
TILLA
PILE
MINER
SLIDE
WALL
SHERWIN
DUKE
MEADOW
LINCOLN
MILL
SEWER/JCM
KNOLLS
LO/NUMIKE
MIKE
KNOB
LOOKOUT
MOUSE
TUP
KRAKATAU
RODGER
SMOAT1
SMOAT2
SMOAT3

Parkfield; Fault crossing lines

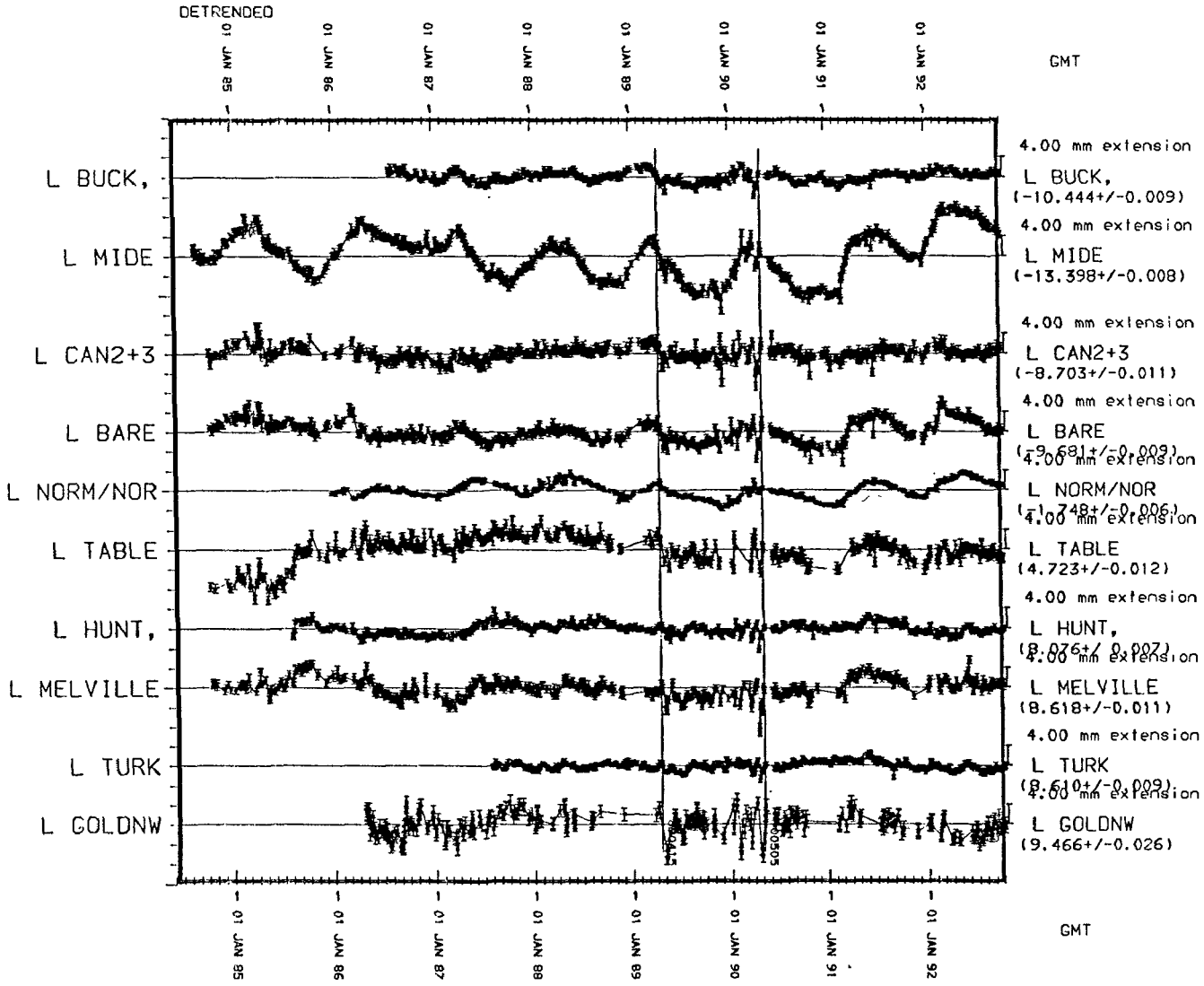

Parkfield; Fault crossing lines

Parkfield; non-fault crossing lines

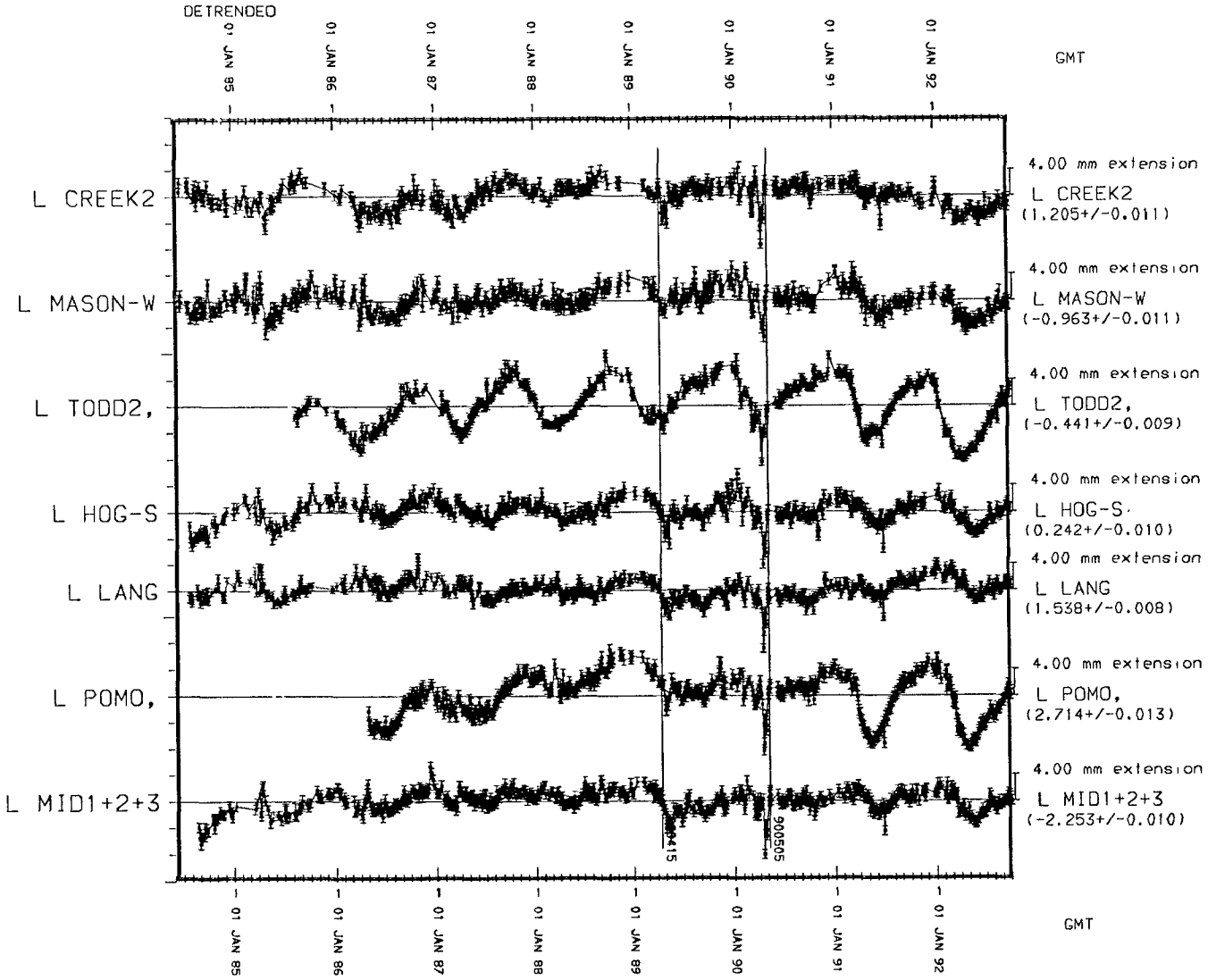

Parkfield; non-fault crossing lines

NORTHERN CALIFORNIA 2-COLOR NETWORKS

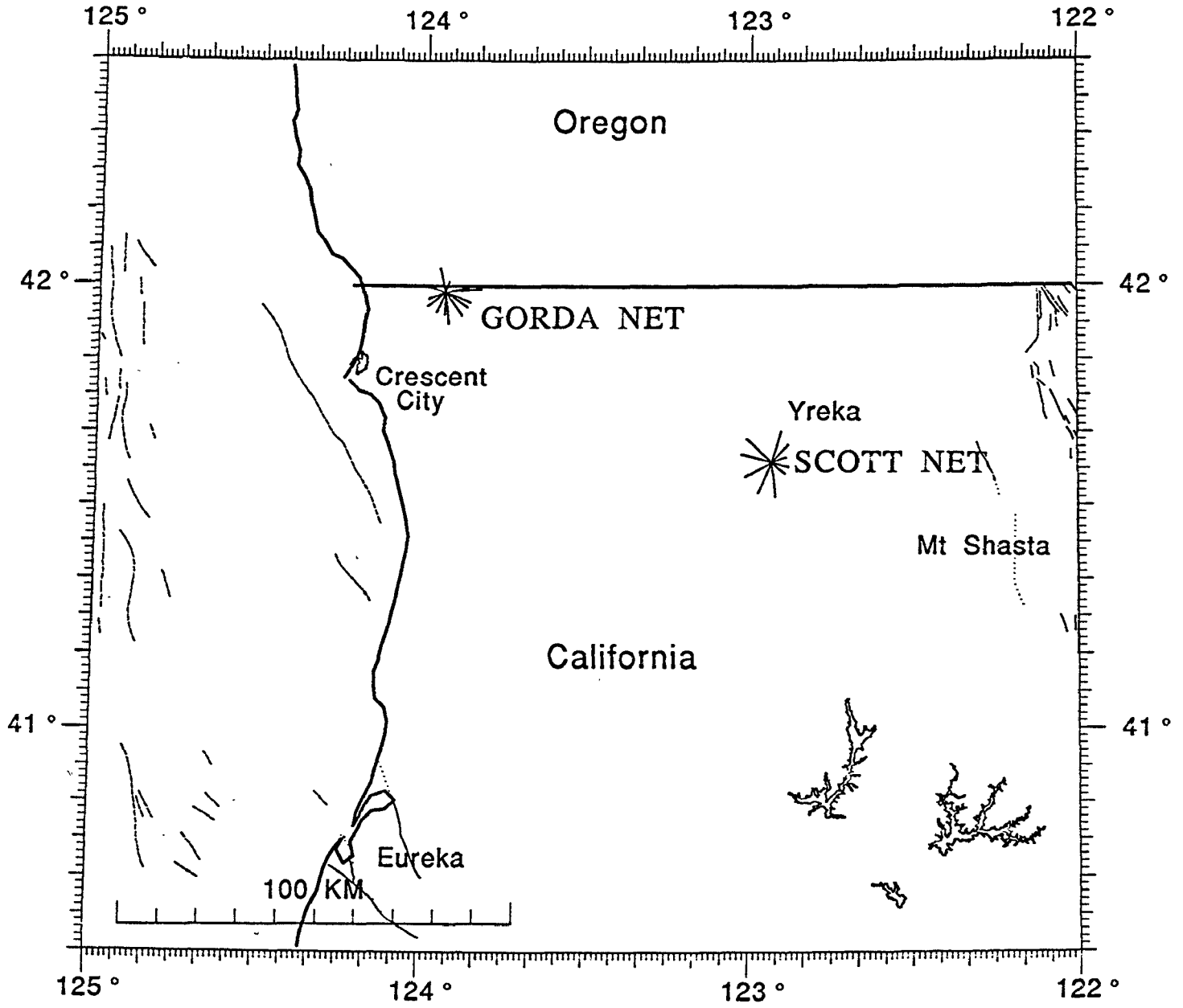

Parkfield Prediction Experiment

9960-04561

John Langbein

Branch of Tectonophysics
U.S. Geological Survey
345 Middlefield Road MS/977
Menlo Park, California 94025
(415) 329-4853

Investigations

This project coordinates the different experiments at Parkfield run by both USGS and non-USGS investigators. Some of the experiments are focused on the prediction in the short-term of the next Parkfield earthquake. Other experiments will document pre-seismic, the co-seismic, and post-seismic events. Both data from seismicity and from deformation are examined for significant events. This project has been examining the formal rules used in either calling an "alert" or "status-level".

Results

1. Significant Signals

The table summarizes the events in the past 1.75 years that meet established criteria to be called either an "alert" or "x-level status". For purposes of semantics, low-level signals which meet the "C" and "D" levels are called "status-levels", and the larger signals which meet the "A" and "B" levels remain as "alerts".

2. Parkfield in review workshop

From June 28 to 30, 1992 the Parkfield Working Group met at UC Santa Cruz to consider the future of the Parkfield Earthquake Prediction Experiment in light of the fact that the Parkfield mainshock has not yet occurred and that the 95% confidence window approved by the National Earthquake Prediction Evaluation Council would close at the end of the year. Despite this circumstance the working group reaffirmed its commitment to the Parkfield experiment as a critical part of the nations earthquake prediction program and reaffirmed their willingness to continue devoting time to it. The primary evidence of success of the Parkfield experiment was seen in the transfer of lessons learned at Parkfield over the broad range of monitoring techniques, scientific advances, and the alert scheme to other areas. As such the experiment has fulfilled part of its role as a prototype monitoring and short-term prediction experiment. However, much remains to be learned and, despite the debate over which is the correct model, all of the proposed statistical models conclude that Parkfield is the most likely place for a M6 earthquake in a region small enough to monitor in this way. And even if another area had similar mainshock probability, no other area has as much baseline data collected. The dense monitoring of varied networks was considered a critical aspect of

understanding anomalies on the various instruments and the group felt that Parkfield should be considered to be a National Earthquake Prediction Observatory and that future instruments should be tested there in order to allow comparison with the existing data. The major changes envisioned were expansion of the geodetic and strain networks in the northern part of the area in order to better image aseismic slip at depth near the expected hypocenter, expansion of real-time data transmission to Menlo Park to more of the monitoring networks in order to ease comparison between the various data sets, an online data repository to allow better access to the data by both the working group and the larger research community, and an expansion of shared technical support at Parkfield in order to save money.

3. Sensitivity of crustal deformation instruments to changes in secular rate

A paper was written examining the sensitivity of three of the Parkfield networks for determining the amount of changes in rate that would be significant.

Abstract. A variety of instruments (including borehole strainmeters, water wells, creepmeters, laser ranging and differential magnetometers) are used to monitor crustal deformation in areas that are prone to geologic hazards such as earthquakes and volcanic eruptions. In monitoring the deformation, one typically examines the data for either a change in rate, or a simple offset in the record. However, one needs to place a statistical confidence level that the detected signal differs from the background "noise". Calculation of the statistical confidence level may be done using the formalism of the *matched filter*. The output from a matched filter is the signal-to-noise ratio, ρ. Two ingredients are needed to form a matched filter: 1) The power density spectrum of the instrument and 2) the functional form of the signal that we desire to detect. Using the available crustal deformation data from the Parkfield, California earthquake prediction experiment, the background noise for individual instruments as a function of frequency, f, is estimated using the traditional method of the power density spectra. Except for two-color laser distance-ranging data, the power spectra for most of the instruments have a frequency dependence of f^{-n} where $2 \le n \le 3$. The power spectrum from laser ranging has a slight frequency dependence with $0 \le n \le 1$. The confidence level with which a hypothesized signal can be within the measurements is determined directly from the signal-to-noise ratio, with the numerator being a function of the signal and the denominator being a function of the power spectrum. Using a creepmeter as an example, a 0.04-mm change occurring over 1 hour, a 0.06-mm occurring over 10 hours, or 0.20-mm over 100 hours are all signals for which $\rho=2$ and therefore have only a 5% confidence that these signals could be background noise. The use of a single technique to determine the confidence for anomalous signals from all types of strain instruments might be suited to the Parkfield experiment where we can explicitly express a statistical confidence that a detected signal exceeds its background noise.

4. Publications

Langbein, J., E. Quilty, and K. Breckenridge, Sensitivity of crustal deformation instruments to changes in secular rate, *GRL*, in press, 1993.

Parkfield Working Group, The October 1992, Parkfield, California Earthquake prediction, *Science*, submitted, 1993.

Michael, A.J., and J. Langbein, Learning while waiting; Summary of the 1992 Santa Cruz Review Meeting, *EOS*, submitted, 1993.

Table. 1991 Parkfield alerts.

Date	Location	Description	Size	Level	Comments
910109	Parkfield	Earthquake	M 3.1	D	
910121	Cholame Valley	Earthquake	M 2.9	D	
910201	Middle Ridge	Creep	1.3 mm	D	
910204	Cholame Valley	Earthquake	M 2.8	D	Combine to C
910205	Middle Mtn	Earthquake	M 2.1	D	
910210	Middle Mtn	Earthquake	M 2.0	D	
910307	SW Trace (Hearst)	Creep	-5.4 mm	D	rain related
910311	Middle Mtn	Earthquake	M 1.8	D	
910319	XPK1 and XVA1	Creep	5 mm in 16 hours	B	raining
910319	XMM1	Creep	Surge 3.3mm in 7 days	D	Rain in past week
910322	Middle Mtn	Earthquake	M 2.2	D	
910327	X461	Creep	1.9mm in 7 days	D	rain in past week
910330	X461	Creep	2.9mm	D	Surge over past 10 days
910331	XMM1	Creep	0.8 mm in 30 minutes	D	
910331	Middle Mountain	Water well	9 cm	D	familiar combination, no C
910409	Middle Mountain	Earthquake	M 2.7	D	
910410	Middle Mountain	Earthquake	M 2.1	C	2 earthquakes M>1.5 in 72 Hrs
910412	Middle Mountain	Earthquake	M1.8 and M2	C	
910426	Middle Mountain	Earthquake	M 1.6	D	
910506	Middle Mountain	Earthquake	M 1.9	D	
910508	Middle Mountain	Earthquake	M 1.9	D	
910521	XMM1	Creep	0.7 mm in 30 min.	D	
910521	Middle Mountain	Water Well	4 cm	D	familiar combination
910711	Middle Mountain	Earthquake	M 2.0	D	
910722	Middle Mountain	Earthquake	M 1.6	D	
910726	Middle Mountain	Water Well	-12 cm	D	
910806	Slack Canyon	Earthquake	M 2.7	D	
910903	Middle Mountain	Earthquake	M 2.2	D	
910925	Middle Mountain	Earthquake	M 2.2	D	
911018	Parkfield	Earthquake	M 2.6	D	South end of M. Mtn.
911020	XMD1 & XMM1	Creep	2 events of 0.6mm in 1 hr	C	
911020	Middle Mountain	Water well	6 cm drop	D	
911108	Slack Canyon	Earthquakes	M 2.8?	D	
911201	Middle Mountain	Earthquakes	2 M>1	D	2 M1.0 in 72hrs
911218	Middle Mountain	Earthquake	M 2.3	D	

Note. Right lateral creep, water level rises, and compressive strain are positive.

1991 Combined Alert Totals: 1 B alert, 3 C alert, 29 D alerts.

Total alerts since beginning experiment: 1 B alert, 30 C alerts, 85 D alerts.

Table. 1992 Parkfield alerts.

Date	Location	Description	Size	Level	Comments
920127	Middle Ridge	Creep Event	0.9 mm	D	
	Middle Mountain	Water well		D	familiar combo
920224	Gold Hill	Earthquake	M 2.5	D	
920404	Middle Mountain	Earthquake	2 M >1.1	D	originally missed
920420	Middle Ridge	Creep Event	1 mm RL	D	Strain changes at Frolich
920420	Middle Mountain	Water well	13.7 cm drop	D	familiar combo
920529	Gold Hill	Earthquake	M 3.2	D	Strain change at GH dilatometer and water well
920603	Middle Mountain	Earthquake	M 1.5	D	
920916	Gold Hill	Earthquake	M 2.5	D	

Note. Right lateral creep, water level rises, and compressive strain are positive.

1992 Combined Alert Totals: 1 C alert, 9 D alerts.

Total alerts since beginning experiment: 1 B alert, 33 C alerts, 94 D alerts.

Microearthquake Data Analysis

3-9930-10053

W.H.K. Lee
U.S. Geological Survey
Branch of Seismology
345 Middlefield Road, MS 977
Menlo Park, California 94025
(415) 329-4781

Investigations

The primary focus of this project is the development of state-of-the-art computation for analysis of data from microearthquake networks. For the past twelve months I have been involved in:

(1) Implementing Seismic Instrumentation for Topical Volcano Studies

In collaboration with Gray Jensen and Sam Rodriquez, I am designing and implementing seismic instrumentation for topical volcanic studies. Two portable arrays (one telemetered and one hardwired) are being implemented to meet the scientific objectives of volcano research. These two portable arrays are based on PC-technology, and are designed to have a dynamic range of about 90 db. The hardwired array has 64 channels, and the digital telemetered array has up to 48 channels.

A shallow refraction experiment was carried out using the hardwired array in August, 1992 at the Zayante Vineyard (located in the epicentral area of the 1989 Loma Prieta earthquake) in collaboration with UC Santa Cruz. Excellent data were recorded using a sledge hammer as a source of compressional waves and an air-powered shear-wave generator as a source of shear waves. A data report of this experiment was released as Zayante Seismic Experiment Team (1992), and a paper will be presented at the Fall AGU National Meeting (Bonamassa, et al. 1992).

The hardwired array was also deployed in the Landers earthquake fault zone in October, 1992 in collaboration with the Southern California Earthquake Center. Up to 31 three-component geophones were recorded by two PC-based systems across and along the rupture zone of the 1992 Landers earthquake using about 12 km of cables. Several hundreds earthquakes were recorded. A detailed shallow refraction experiment using a sledge hammer and an air-powered chear-wave generator was also conducted. Excellent records of trapped waves in the fault zone were obtained. Because of the large amount of data

(about 2 gigabytes), it will take some time for us to process and analyze the data.

Descriptions of these two portable seismic arrays are being released in a series of Open-File Report; so far three have been released (Lee, 1992 a, b, c). The telemetered portable array is scheduled for field tests in the spring of 1993.

(2) Lecture Notes on PC-based Seismic Networks

A course on PC-based seismic networks was given to about 20 students in Menlo Park, CA from September 9 through 20, 1991. The purpose of this course was to show students how to operate a PC-based seismic network, carry out routine data processing, and perform basic data analysis. Twenty-one lectures were given and the lectue notes were edited by W.H.K. Lee and D.A. Dodge. These lecture notes were released as USGS Open-File Report 92-441, and contain the following separate lectures:

1. Regional seismic networks in California by J. P. Eaton.
2. PC-based seismic systems by W.H.K. Lee.
3. Seismometers theory and practice by J.P. Eaton.
4. Basic techniques for telemetry by J.C. VanSchaack.
5. Realtime seismic data acquisition by W.H.K. Lee.
6. The XDETECT program by W.H.K. Lee.
7. The TDETECT program by J.R. Evans.
8. Routine seismic network data processing by W.H.K. Lee.
9. Plotting seismograms and maps by R. Banfill.
10. Mathematics for earthquake location by W.H.K. Lee.
11. Local earthquake location programs by J.C. Lahr.
12. Computing travel time and derivatives by W.H.K. Lee.
13. Development of earthquake magnitude scales by J. P. Eaton.
14. Coda waves for magnitude and Q by W.H.K. Lee.
15. PCEQ and QCODA by C.M. Valdes.
16. Mathematics for waveform analysis by A. Lomax.
17. The SEISGRAM program by A. Lomax.
18. Focal mechanism: theory and history by P.A. Reasenberg.
19. The FPFIT program by D.H. Oppenheimer.
20. Mathematics for seismic tomography by W.H.K. Lee.
21. Applications of seismic tomography by H.M. Iyer.

Reports

Lee, W.H.K., and D.A. Dodge, (editors), 1992. "A course on: PC-based seismic networks", USGS Open-File Report 92-441, 535 pp.

Lee, W.H.K., (compiler), 1992a. Descriptions of seismic array components: Part 1. DIGGER, DIGIREC, and MULTIPLEXER, USGS Open-File Report 92-430 A and B, 276 pp. and 1 diskette.

Zayante, Seismic Experiment Team, 1992. Zayante seismic experiment: data report, USGS Open-File Report 92-561, A and B, 268 pp. and 4 diskettes.

Lee, W.H.K., (compiler), 1992b. Descriptions of seismic array components: part 2. software modules for data acquisition/processing, USGS Open-File Report 92-597, A and B, 313 pp, and 1 diskette.

Lee, W.H.K. (compiler), 1992c. Descriptions of seismic array components: Part 3. Software modules for data conversion, USGS Open-File Report 92-598, A and B, 106 pp. and 1 diskette.

Lee, W.H.K., 1992. PC-based seismic networks for monitoring earthquakes and volcanoes, (abstract), EOS, v. 73, p. 68-69.

Bonamassa, O., J.E. Vidale, W.H.K. Lee, and H.P. Liu, 1992, The relation between ground motions and near-surface geology, (abstract), EOS, v. 73, p. 338.

Northern and Central California Seismic Network Processing

9930-70013

Fredrick W. Lester
Branch of Seismology
U.S. Geological Survey
345 Middlefield, MS 977
Menlo Park, CA 94025
(415) 329-4747

Investigations

1. In 1966 a seismographic network (CALNET) was established by the USGS to monitor earthquakes in central California. In the following years the network was expanded to monitor earthquakes in most of northern and central California, particularly along the San Andreas Fault, from the Oregon border to Santa Maria. In its present configuration there are over 300 stations in the network, and more than 60 of those consist of more than one component. Also recorded are signals from more than 60 stations operated by other agencies or institutions, including the University of California, Berkeley, the University of Nevada, Reno, the California Institute of Technology, the California Department of Water Resources, and the Lawrence Livermore National Laboratory. The primary responsibility of this project is to monitor, process, analyze, and publish seismic data recorded from this network.

2. This project maintains a seismic data base of CALNET data for the years 1969 to the present on both computers and magnetic tapes for those office staff who are doing research using the network data.

3. Project staff often act as the primary spokesperson or authority when inquires are received from the press, the public, or scientists from both inside and outside the Geological Survey regarding earthquakes that have been recorded by the network. Inquires include simple questions about recent earthquakes in the region, such as the date and time of occurrence, the location, and the magnitude of the earthquake. Or they may be somewhat complex and require expert opinion or interpretation, such as the relationship of recent swarms of earthquakes to historical seismicity, and how each relates to the seismogenic potential of a region or fault.

4. As time permits research projects are undertaken by project personnel on some of the more interesting or unusual events or sequences of earthquakes that have occurred within the network, or related topics.

Results

1. Figure 1 illustrates most of the 20198 earthquakes located in northern and central California and vicinity during the time period October 1991 through September 1992.

   There were several significant earthquakes and their aftershocks that affected the network during this this time period. On April 25, 1992 a M7.1 earthquake occurred in the Cape Mendocino region of northern California. It was followed by two large aftershocks on April 26 that were magnitude 6.6 and 6.7. In the month following these large earthquakes more than 3300 aftershocks occurred and were located by this office, mostly by project staff. These were mostly within 50 to 60 kilometers of the larger events, forming an football-shaped aftershock zone centered on Cape Mendocino (Fig. 1).

On June 28 a magnitude 7.5 earthquake struck the region near Landers, in southern California. It was followed by a few hours later by a M6.6 quake in the region near Big Bear Lake, just north of the Landers epicenter. These two earthquakes were followed by thousands of smaller aftershocks, which are still occurring. While those earthquakes are beyond the region monitored by this office, they are still recorded by our automatic detection systems and must be processed, in at least a minimal way. Our detection system is triggered by most earthquakes in that sequence that are larger than magnitude 3.0. Since there have been several hundred of those the impact on our data processing has been significant.

On April 23, 1992 a magnitude 6.3 earthquake struck the Joshua Tree region of southern California. As with the Landers-Big Bear earthquakes those are outside of our monitoring region, but the magnitude 3.0 or larger events still trigger our network stations and therefore are recorded and must be processed. A few hundred of those recorded throughout the CALNET, and therefore impacted data processing in the project.

Work is currently underway on the publication of a catalog of earthquakes for northern and central California for 1991. The format is patterned after the format of the USGS-Caltech catalogs of southern California earthquakes that have been published in the last few years. Work on this publication is a joint effort between several projects and more than a dozen people. The catalog should be published by early 1993. It is our intention, after that time, to publish a yearly catalog on a regular basis within a few months of the end of each year. Data prior to 1991 will be published in yearly catalogs, as soon as time permits, in 1993. These catalogs will supersede previous catalogs for the years 1967 - 1978.

2. The 1992 catalog is relatively complete and correct through September 1992. We are currently adding events from the Cape Mednocino swarm in April and May that were missed in the routine detection and processing. These are earthquakes that are mostly smaller than magnitude 3.0. Quarry blasts still need to be identified for April through September.

3. More than 55 requests were received for seismic data which required computer searches of the data base. Most of the searches were for specific regions and time periods. Some were more complex requiring multiple searches and some interpretation. Data from these searches were most often distributed as printed listings, but but some were also sent as data files over electronic mail or files on magnetic tape.

   Telephone inquires were handled at a rate of 3 to 5 per day. Most of these required verbal responses that were of short duration, 10 minutes or less. The majority of these were simple requests for information about recent earthquakes, ongoing or past USGS research, maps and publications, and some interpretation of geologic information. During periods of higher than normal seismic activity the project may receive as many as 20 to 30 requests of this type per hour.

   Recognition of earthquake risk and related hazards has increased dramatically since the Loma Prieta earthquake of October 1989. A consequence of this has been an increase in insurance claims related to earthquakes that has resulted in an increase in insurance company requests for data searches for recent earthquake activity. Another consequence of that earthquake is the increasingly common request from homeowners or potential homeowners for information about all types of geologic hazards, particularly earthquake hazards, in the area around their homes or where they plan to purchase a home.

4. Due to the large number of earthquakes that occurred during this time period no staff members had time to pursue any research.

Reports

None

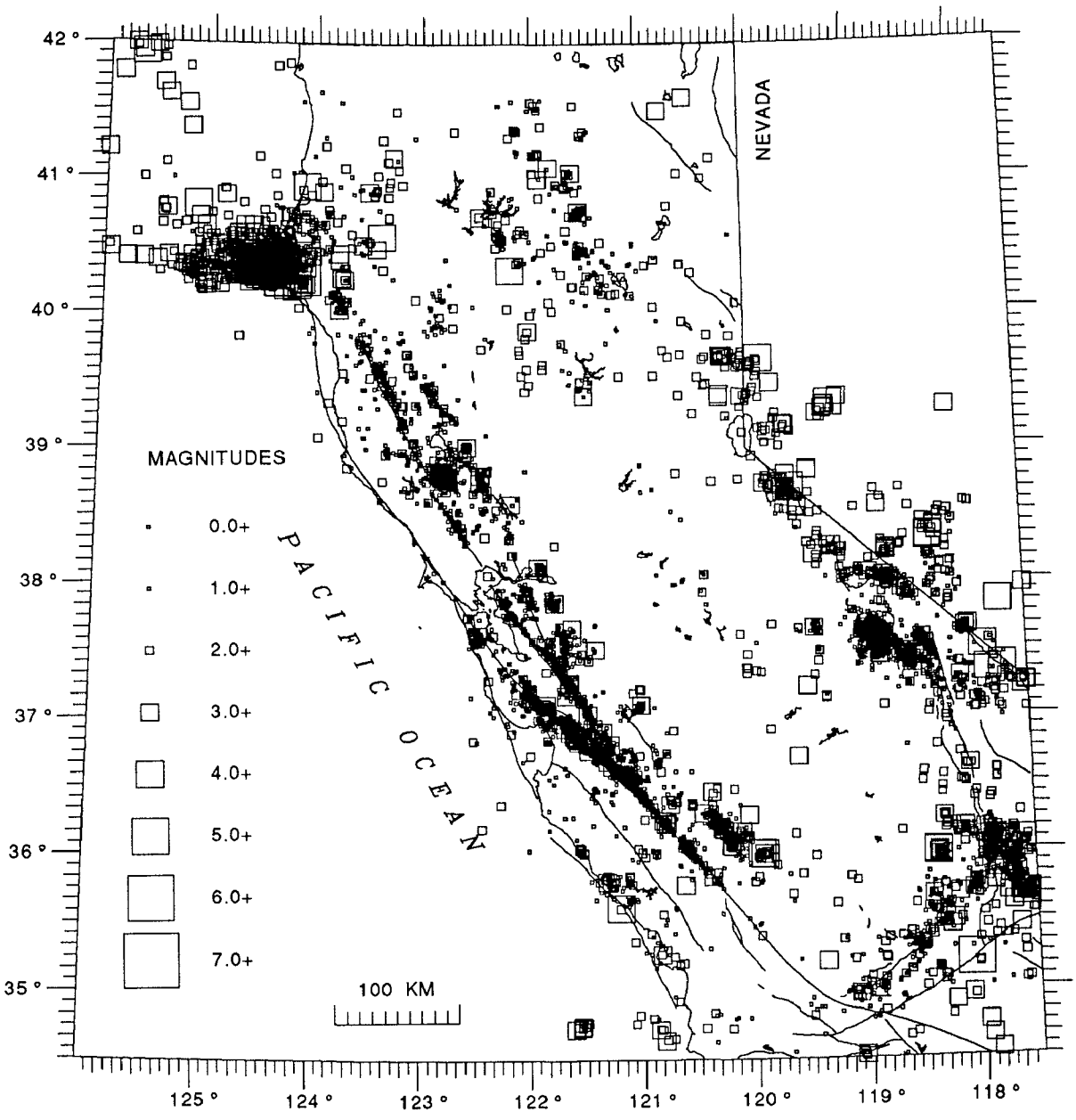

FIGURE 1. Seismicity for October 1991 - September 1992

Characterization of Range Front Deformation, Northeastern Margin of Santa Cruz Mountains, Southern San Francisco Bay Region, California

Award Number: 1434-92-G-2220

William R. Lettis, Gary D. Simpson, and Keith I. Kelson
William Lettis & Associates, Inc.
1000 Broadway, Suite 612
Oakland, CA 94607
(510) 832-3716

Investigations

Apparent coseismic ground deformation during the 1989 Loma Prieta earthquake is coincident with and/or subparallel to the system of faults along the northeastern margin of the Santa Cruz Mountains, indicating possible coseismic movement along the Sargent-Berrocal, Shannon, and Monte Vista faults. These faults displace the Pliocene and Pleistocene Santa Clara Formation, and locally deform overlying Quaternary surficial deposits and associated geomorphic surfaces adjacent to and in the communities of Los Gatos, Saratoga, Cupertino, and Los Altos Hills. Because the amount and timing of this deformation is poorly known, these faults pose a significant, heretofore undocumented, earthquake hazard to the southern San Francisco Bay region. We believe that a critical issue for evaluating the earthquake hazards along the range front is whether the Sargent-Berrocal, Shannon, and Monte Vista faults are a result of secondary coseismic deformation related to the San Andreas fault, or whether they are independent seismic sources. We anticipate that the results of this study will contribute to a better understanding of the structural and kinematic association of the range-front deformation with the San Andreas fault, and thus help estimate potential seismic hazards in the southern Bay region.

We are using two distinct, yet complementary, approaches to investigate the nature of deformation and seismogenic potential of faults along the range front between the towns of Los Gatos and Los Altos Hills. Our approach to assessing the style and pattern of deformation associated with the Sargent-Berrocal, Shannon, and Monte Vista faults is to conduct a quantitative geomorphic analysis of the range front and adjacent areas, and to delineate late Quaternary deposits and geomorphic surfaces. Age-estimates of these surfaces and deposits will yield data on the long-term rates of range-front deformation. Our approach to assessing the timing of deformation and fault-specific physical and behavioral characteristics is to conduct detailed paleoseismologic investigations at selected sites along one or more of these faults. The goal of this task is to obtain quantitative data that can be used to assess potential rupture lengths, fault segmentation, displacement per event, slip rate, sense of slip, and recurrence intervals for faults along the range front. We anticipate that this information will be used to evaulate whether the range-front structures are independent seismic sources or are solely related to deformation along the San Andreas fault.

Results

We are using three quantitative geologic and geomorphic analyses to define the style and patterns of Quaternary deformation along the range front. First, we are mapping late Quaternary fluvial

terraces along Los Gatos, Saratoga, and Stevens creeks, at a scale of 1:20,000, based on field reconnaissance and analysis of black-and-white aerial photographs taken in 1939. At this time, we identify a well-developed sequence of four major fluvial terraces along Los Gatos Creek, of which the oldest two are displaced by thrust faults at the base of the range. Second, we are utilizing the 1939 air photos and recent mapping by Wesling and Helley[1] to delineate alluvial fan surfaces along the range front. This mapping shows that an older fan surface at the range front is separated from younger fans to the northeast by a linear topographic scarp that is coincident with the mapped trace of the Shannon fault (Wesling and Helley, *ibid.*). This scarp extends across business and residential areas of Los Gatos, Saratoga, and Cupertino. Third, we are initiating construction of envelope, sub-envelope, and residual maps of the northeastern Santa Cruz Mountains that will help assess the locations and spatial variations of tectonic uplift. We are obtaining digital elevation models (DEMs) and appropriate software to construct these maps.

Based on preliminary field reconnaissance and analysis of existing reports, we have selected a preliminary site for paleoseismologic investigation of the Monte Vista fault in Cupertino. Through our ongoing analysis of aerial photography and field mapping, we are currently assessing whether this site is the most promising location for obtaining paleoseismologic information.

[1]Wesling, J.R., and Helley, E.J., 1989, Quaternary geologic map of the San Jose West quadrangle, California: U.S. Geological Survey Open-file Report 89-672, scale 1:24,000

Operation of Borehole Tiltmeters at Pinon Flat Observatory, California and Analysis of Secular and Tidal Tilt

14-08-0001-G1765

Judah Levine
Joint Institute for Laboratory Astrophysics
Campus Box 440
University of Colorado
Boulder, Colorado 80309
(303) 492 - 7785

Objectives: To install borehole tiltmeters at Pinon Flat Observatory in Southern California; to compare the performance our instruments installed at three different depths; to analyze the data at secular and tidal periods; and to compare our results with those obtained from other instruments at the same site.

Results: We currently have three instruments installed at Pinon Flat Observatory and all three have been operating during this report period. Our previous reports discussed our finite-element studies of the effects on the measured tilt resulting from a borehole that is not perfectly vertical and from the variation in the topography of the weathering layer boundary. Our calculations predicted that both of these effects would result in appreciable strain-tilt coupling. During this reporting period, we tested the predictions of these models by performing several different experiments in boreholes BOA (24 m deep) and BOB (36 m deep).

In the first series of experiments, we modified the instrument installed in BOB so that it could be operated at different depths within the borehole. In particular, we operated the instrument both below the weathering layer boundary and just above it. Our calculations predicted that this change in depth would change the sign of the difference between the signals recorded at BOA and BOB, and the observation was almost exactly what we had predicted.

In the second series of experiments, we studied the effect of different installation methods on the tilt signal. Our previous design used the side of the borehole as the reference for the tiltmeter; we changed the mounting brackets so that the reference for the instrument became the center of the bottom of the borehole and three points spaced symmetrically around the side of the casing near the top of the instrument compartment. (This is essentially the method used in the Askania instrument, and we implemented the change using retractable pins that are quite similar to the Askania design.) This latter coupling method is theoretically more sensitive to tilt-strain coupling than our initial design, but the theoretical advantage of our design can not be realized in practice if the borehole is tipped (as it almost always is). The results of this set of experiments also agreed very well with our models, and we are now

in the process of confirming this agreement with additional measurements along different azimuths in the same borehole.

Using the results of these measurements it is possible to install an instrument in borehole BOB so that the tilt-strain couplings due to the weathering layer and due to the mounting of the capsule very nearly cancel. We are testing this possibility with a third set of experiments that are currently underway. These experiments have been interrupted by a serious failure due to a recent lightning strike at PFO very close to our instruments. (Other instruments, including the Askania were also damaged by that strike.) We have just returned from a repair trip to PFO, and an additional repair trip will probably be necessary in the near future.

In addition to providing insight into methods of improving tilt measurements, our results suggest that it may be possible to construct a combined strainmeter-tiltmeter using two tiltmeters installed in the same borehole at different depths and along different azimuths. An installation of this kind could provide simultaneous measurements of both tilt and strain -- the sensitivity to local strain arises from the difference between the tilt-strain coupling coefficients of the two instruments and this difference allows us to both estimate the strain and remove it from the tilt records. Such a device would have certain technical advantages over borehole strainmeters: the instruments need not be installed permanently, for example, and the instrumental calibration is easier to perform and is likely to be more stable in time. We hope to make some preliminary tests of this idea early in 1993.

Summary of Data Collected: We acquire the data from our three instruments at PFO (2 channels/instrument) every 6 minutes. These same values are also transmitted to the PFO central recording trailer and are digitized and recorded there 12 times/hour.

Slip History of San Andreas and Hayward Faults

9910-04192

J. J. Lienkaemper
Branch of Engineering Seismology and Geology
U.S. Geological Survey
345 Middlefield Road, MS 977
Menlo Park, California 94025
(415) 329-5642

Investigations

Determine slip rates and earthquake recurrence times on San Andreas and Hayward Faults. Compare rates of geologically determined surface slip to rates of historic creep and geodetically determined deep slip. Analyze effects of structural complexity and fault segmentation upon inferring recurrence from slip rate. Participant in 1992 Landers Earthquake Investigation.

Results

1. Creep Rates, Hayward Fault. We report interesting results on creep rate for the initial 3 years (1989-1992) of precision monitoring of about 20 arrays established for observing afterslip expected in the next major earthquake on the Hayward Fault [*Lienkaemper, Galehouse, and Simpson,* 1992]. Creep rate along most of the fault since the 1989 Loma Prieta Earthquake (LPE) has averaged only half the long-term rate. At the southeast end where long-term rates have been about 9 mm/yr right-lateral, the post-LPE creep rate has been 2 mm/yr left-lateral. This reversal in the direction of creep rate is a predictable effect of modelled static stress changes and can be expected to continue for at least another 3 years at our southernmost array. North of central Fremont, creep is now returning to normal at some sites (where long-term rate is 5-6 mm/yr and creep is steady), but at many sites creep is still strongly retarded (where long-term rate is 3.5-5 mm/yr and behavior is episodic).

2. Holocene Slip Rates, Masonic Site. We submitted 8 more radiocarbon samples to refine the ages of the basal contacts of the early Holocene (unit G) and mid-Holocene (unit E) fan deposits. A serious problem at the NSF AMS facility delayed completion of this project. Age dating is still incomplete. Some new dates suggest that greater accuracy in unit-E slip rate is possible. Preliminary reports: *Lienkaemper and Borchardt* [1992a&b].

3. Map of Holocene traces of the Hayward Fault. USGS printed the new map of the Hayward fault [*Lienkaemper,* 1992] with financial support from the Second Conference on Earthquake Hazards in the Eastern San Francisco Bay Area. This map was introduced to the public for sale as a poster exhibit at the Conference. For the Conference I served on several committees and authored/co-authored/edited various volumes, papers, abstracts (omitted below, replaced by Proceedings) and field guide articles listed below.

Reports *(referenced using the abbreviated volume names below:)*

East Bay '92-Proceedings: Proceedings of the Second Conference on Earthquake Hazards, Eastern San Francisco Bay Area, March 25-29, 1992, California State University, Hayward; G. Borchardt, S.E. Hirschfeld, J.J. Lienkaemper, P. McClellan, P.L. Williams, and I.G. Wong, eds.: *California Division of Mines and Geology Special Publication 113.*

East Bay '92-Field Guide: Field Trip Guidebook of the Second Conference on Earthquake Hazards, Eastern San Francisco Bay Area, March 25-29, 1992, California State University, Hayward; Taylor, C.L., compiler, and Hall, N. T. and Melody, M., eds., 225 p.

East Bay '92-Program and Abstracts: Program and Abstracts of the Second Conference on Earthquake Hazards, Eastern San Francisco Bay Area, March 25-29, 1992, California State University, Hayward; Galehouse, J.S., ed., 91 p.

Borchardt, G., J. J. Lienkaemper, and K. Budding, in press, Holocene slip rate of the Hayward Fault at Fremont, California: *East Bay '92-Proceedings*.

Lienkaemper, J.J., 1992, Map of recently active traces of the Hayward Fault, Alameda and Contra Costa Counties, California: U.S. Geological Survey Miscellaneous Field Studies Map MF-2196, scale 1:24,000, 13 p. text.

Lienkaemper, J.J., 1992, Stop B-2, Contra Costa College and El Portal School: *East Bay '92-Field Guide*, p. 25-27.

Lienkaemper, J. J., 1992, Optional Stop A-4, Masonic Home slip rates: *East Bay '92-Field Guide*, p.173.

Lienkaemper, J. J., and G. Borchardt, in press, Holocene slip rate of the Hayward Fault at Union City: *East Bay '92-Proceedings*.

Lienkaemper, J. J., and G. Borchardt, in press, Hayward Fault: Large earthquakes versus surface creep: *East Bay '92-Proceedings*.

Lienkaemper, J.J. and J.C. Hamilton, 1992, Stop A-3, Holy Sepulchre fault scarp: *East Bay '92-Field Guide*, p. 151-156.

Taylor, C.L, and J.J. Lienkaemper, 1992, Contribution 6-2: Location of Hayward Fault traces in the Montclair Village area, Oakland, California; and Stop B-4, Montclair Park and Village: *East Bay '92-Field Guide*, p. 83-93.

CRUSTAL STRAIN

9960-70076

M. Lisowski, J.C. Savage, N.E. King, J.L. Svarc, M. Murray
Branch of Tectonophysics
U.S. Geological Survey
345 Middlefield Road, MS/977
Menlo Park, California 94025
(415) 329-4855

Investigations

The principal subject of investigation was the measurement and analysis of deformation in a number of tectonically active areas in the United States.

We list the networks surveyed during FY 92 along with some information about the surveys in Table 1. Many of the surveys were in response to magnitude 6 and 7 earthquakes in northern and southern California.

We used Geodolite (trilateration) and Global Positioning System (GPS) to survey the San Gabriel, Loma Monitor (three times), Fairweather, and Joshua (twice) networks. We surveyed the San Gabriel network several months after the Sierra Madre earthquake and the Joshua network two months before and one month after the Landers earthquake. The Lake San Andreas, Calaveras, and Black Mountain small aperture fault crossing trilateration networks were surveyed with the Geodolite. The Calaveras network was also surveyed with GPS.

We used GPS to survey the following networks: Juan de Fuca, Southern Oregon, Eureka, Southern California Monitor (twice), Parkfield Monitor (twice), Parkfield Regional, Parkfield Quad (three times), Farallon-Sierra, Long Valley-Mono Chain, Landers Profile, and five profiles in the San Francisco Bay Area. The Southern Oregon network and Landers Profile are new networks. Surveys of the Eureka network were in response to the Honeydew and Cape Mendocino earthquakes. As part of our response to the Landers earthquake we used GPS to measure part of the Mojave and all of the Landers trilateration networks. The Landers Profile was established to monitor post-seismic strain diffusion. We experimented with rapid static GPS surveys after the Cape Mendocino and Landers earthquakes. The Hayward fault crossing Richmond, East Bay, and Hayward short range trilateration networks were measured with GPS. We monitored deformation across the Hayward fault with two continuously recording GPS receivers. The sites also provide a reference for other measurements in the area.

The Juan de Fuca network survey was a cooperative effort with the Geologic Survey of Canada. We list only the part of the project in the U.S.A. in Table 1. The southern Oregon GPS survey was in cooperation with the University of Oregon. Not listed in the table is the rapid static survey of a 110-station network in Parkfield conducted by NASA's Jet Propulsion Laboratory in cooperation with the Crustal Strain Project.

Table 1. Field Surveys FY 1992

Project	Region/ Program	Survey Dates	Field Days	Tra-vel Days	Geod-olite Lines	GPS Station Days	Local Ties	GPS Sta-tions	Local Sta-tions	Rapid Static
Hayward Continuous	BAFEP	Continuous								
Juan de Fuca	PACNW	91/10/04-09	6	3		43	18	21	5	
Eureka-Honeydew Eq.	PACNW	91/10/11	2	1		6	1	6	1	
L. San Andreas	BAFEP	91/10/21&29	2		9					
Calaveras	BAFEP	91/10/22-23	2		17					
Black Mt.	BAFEP	91/10/24	1		14					
San Gabriel	SCAL	91/10/31-11/05	6	2	47	11	3	10	3	
S. Cal Monitor	SCAL	91/11/19-11/21	3	2		13	9	13	9	
S. Cal Monitor	SCAL	91/12/04-12/05	2	1		13	9	13	9	
Parkfield Monitor	CORE	91/12/06	1	1		5		5		
Calaveras	BAFEP	91/12/12	1			7		7		
Loma Monitor	CORE	91/12/17	1			7		7		
Richmond	BAFEP	91/12/18	1			4		4		
Hayward	BAFEP	91/12/20	1			5	1	6	1	
NBay Profile	BAFEP	92/02/11-02/13	3			18		14		
GG Profile	BAFEP	92/02/14	1			7		7		
CBay Profile	BAFEP	92/02/19-02/20	2			14		12		
Coso	VHAZ	92/02/25-02/27	3	2		12	1	7	1	
SBay Profile	BAFEP	92/03/04-03/06	4			22	1	19	1	
Farallon-Sierra	BAFEP	92/03/11-03/14	5	1		35	5	13	5	
Loma Profile+Monitor	BAFEP	92/03/17-03/19	3			20	1	16	1	
Loma Monitor	CORE	92/3/24	1		3					
Ricmond	BAFEP	92/03/25	1			2	1	1	1	
Parkfield Regional	CORE	92/04/11-04/14	1			24	4	20	2	
Joshua & Coach Monit	SCAL	92/04/24-04/27	7	2	45	17	2	9	2	
Eureka-Mendocino Eq.	PACNW	92/05/06-05/09	4	2		39	4	21	1	
S. Cal Monitor	SCAL	92/05/27-05/31	5	2		20	6	20	7	
Mendo Post-Seismic	PACNW	92/06/10-06/13	3	2		22	3	15	1	11
Fairweather	CORE	92/06/17-06/28	11	2	12	40		14		
Landers Eq. Resp 1	SCAL	92/06/30-07/02	9	2		42				
Landers Eq. Resp 2	SCAL	92/07/08-07/16	8	2	44	17				
Landers Eq. Resp 3	SCAL	92/07/29-08/06	8	2		20	3	52		39
Long Valley-Mono Chain	VHAZ	92/07/11-07/16	6	2		43		35		
Southern Oregon	PACNW	92/08/26-09/03	9	3		86	3	75	4	
Loma Monitor	CORE	92/09/22	1			8	2	5	2	
Parkfield Monitor	CORE	92/09/23	1	1		6		6		
Loma Monitor	CORE	92/09/22	1			6	2	5	2	
		Totals	126	35	191	634	79	458	58	50

We have established an internal data archive using a 10 gigabyte capacity rewriteable magneto-optical jukebox for easy access and permanent storage. We plan to archive all native format and RINEX format GPS data collected by the Crustal Strain project along with data from some of the global tracking sites. The archive currently includes only data collected since October 1992. The project data archive will simplify processing the data as well as collecting and transmitting the RINEX files to the Southern California Earthquake Center and to the USGS-Berkeley data archives.

Results

1. *Coseismic Displacement Associated with the 1992 Landers Earthquake* ($M_s = 7.5$)

The rupture associated with the 1992 Landers earthquake ($M_s = 7.5$) extended along the west edge of a 60 × 50 km trilateration network that had been surveyed two months before the earthquake and was resurveyed a month after it. The coseismic displacement field within the network was calculated from the changes observed in the trilateration network supplemented by the absolute displacements measured at four GPS stations and other less timely trilateration measurements. Stations near the rupture were displaced by as much as 3 m. The observed changes are reproduced reasonably well by dislocation modeling in which the Landers rupture is represented by 8 vertical fault segments, each extending from the surface to 9 km depth. A slightly better fit is obtained if we allow the depth of the model faults to vary. Two additional segments represent the Big Bear and Eureka Peak faults. The average modeled right-lateral slip on the Landers rupture is about 5 m. However, the residuals for the best-fit slip distribution are about four times greater than expected from measurement error. Given that uncertainty, a broad range of slip models furnish acceptable fits to the data (one model is shown in Figure 1). The large residuals are attributed to inelastic deformation (principally sympathetic slip on numerous unmodeled faults) within the fault blocks assumed to be elastic in the model.

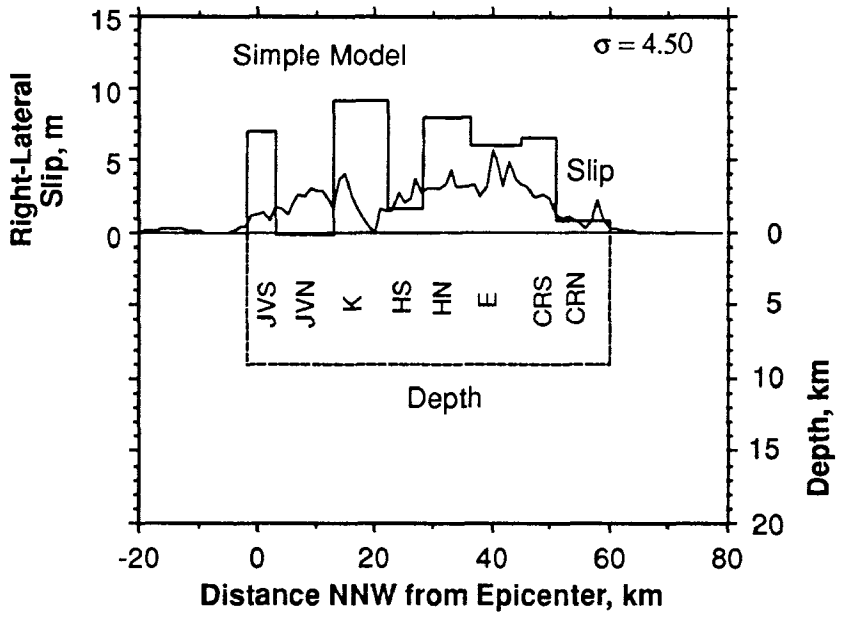

Fig. 1. Distribution of slip along the Landers rupture inferred from the fit to trilateration data. Fault segments are identified as follows: Johnson Valley South (JVS) Johnson Valley North (JVN), Kickapo (K), Homestead South (HS), Emerson (E), Camp Rock South (CRS), and Camp Rock North (CRN).

2. *Deformation in the Epicentral Area of the Landers, California, Earthquake in the Decade Prior to the Earthquake*

A 55-km-aperture trilateration network that spans the epicenters of the 1992 Joshua Tree ($M_s = 6.1$) and Landers ($M_s = 7.5$) earthquakes was surveyed in 1974, 1975, 1977, 1979, 1980, 1981, 1988, and in 1992 after the Joshua Tree earthquake but before the Landers earthquake. No premonitory anomaly is obvious in these data. The velocity field determined from these measurements shows a northwest-southeast extension north of the San Andreas fault in addition to the right-lateral shear across the fault. That velocity field suggests a pull-apart basin connecting the San Andreas fault south of Indio and the Camp Rock-Emerson fault farther north. The Landers earthquake ruptured northward diagonally across this basin before turning northwest along the Camp Rock-Emerson fault. A 6-line monitor net located 15 km from the epicenter of the Joshua Tree earthquake and 35 km from the epicenter of the Landers earthquake was surveyed several times each year between 1982 and 1990 and surveyed again in 1992 after the Joshua Tree earthquake but before the Landers earthquake. After allowance was made for coseismic offsets associated with the North Palm Springs and Joshua Tree earthquakes, no significant change in strain rate before the Landers earthquake was identified.

3. *Inferred Depth of Creep on the Hayward Fault, Central California*

A relation between creep rate at the surface trace of a fault, the depth to the bottom of the creeping zone, and the rate of stress accumulation on the fault is derived from Weertman's 1964 friction model of slip on a fault. A 5 ± 1 km depth for the creeping zone on the Hayward fault is estimated from the measured creep rate (5 mm/yr) at the fault trace and the rate of stress increase on the upper segment of the fault trace inferred from geodetic measurements across the San Francisco Bay area. Although fault creep partially accommodates the secular slip rate on the Hayward fault, a slip deficit is accumulating equivalent to a magnitude 6.6 earthquake on each 40 km segment of the fault each century. Thus, the current behavior of the fault is consistent with its seismic history, which includes two moderate earthquakes in the mid-1800's.

4. *The Parkfield Prediction Fallacy*

The Parkfield earthquake prediction is generally stated as a 95% probability that the next moderate earthquake there should occur before January 1993. That time limit is based on a two-sided 95% confidence interval. Because at the time of the prediction (1985) it was already clear that the earthquake had not occurred prior to 1985, a one-sided 95% confidence interval would have been more appropriate. That confidence interval ended in October 1991. The Parkfield prediction was based on an extrapolation of 5 of the 6 events in the 1857–1966 earthquake sequence; the 1934 event was omitted because it did not fit the regularity exhibited by the other data. The fallacy in the prediction is that it did not take account of other less-contrived explanations of the Parkfield seismicity (*e.g.*, not excluding the 1934 event). Even if the Parkfield earthquake should occur in the near future, it would be better explained by less-contrived hypotheses.

5. *Coulomb Plasticity Within the Fault Zone*

A well-developed fault zone is represented by as layer of granular material (fault gouge) confined between two competent fault blocks. Slip on such a fault involves plastic shearing of the fault gouge. That is, the fault gouge behaves as a Coulomb material, and the plastic flow is accomplished by slip on the two sets of Coulomb shears appropriate to the stress state and the frictional properties of the gouge. Neither set of Coulomb shears is coplanar with the fault zone. This explains the observation of Mandl that slip in such a fault model occurs when the plane of maximum shear in the gouge is parallel to the fault plane. The fault appears to slip as if friction on the plane of the fault were less than on planes of other orientations, whereas, in fact, the apparent slip is simply a consequence of Coulomb plasticity in the gouge (*i.e.,* cooperative slip on the two sets of Coulomb shears). The explanation requires that the apparent coefficient of friction on the fault μ_a is related to the coefficient of internal friction μ by $\mu_a = \sin(\tan^{-1}\mu)$. *Lockner et al., Eos,73,* 511, 1992] show that values of μ_a and μ measured at various normal stresses do indeed satisfy this relation.

6. *Coseismic Displacement Models for the 1992 Cape Mendocino, California, Earthquake from GPS and Coastal Uplift Observations*

Horizontal and vertical displacements due to the Cape Mendocino earthquake ($M_s = 7.1$) was recorded by Global Positioning System (GPS) surveys. Observed changes between pre-earthquake surveys in 1989 and 1991 and a survey one month after the earthquake are corrected for secular motions as derived from 1981–1989 trilateration surveys. The 1991 survey included the subset of the network near the 1991 Honeydew earthquake ($M_b = 6.0$). The observed coseismic displacements relative to the northernmost site are shown in Figure 2. The maximum displacements were measured at a site 5 km NE of the epicenter, which moved 400 ± 20 mm to the WSW and subsided by 160 ± 80 mm. Die-off of intertidal marine organisms provide an independent measure of coastal uplift.

Our preferred coseismic displacement model, estimated from both the coseismic geodetic and uplift data, indicates that 2.7 m of nearly pure thrust motion occurred on a shallow dipping (12°) fault plane that is consistent with the location of the mainshock hypocenter (10.5 km depth), focal mechanism, and distribution of aftershocks. We assume uniform slip on a rectangular, planar fault embedded in an elastic half-space. To determine the best-fitting model, we performed a Monte Carlo search for the parameters describing the location and geometry of the fault plane and estimated the magnitude and rake of the slip. The scatter of the residuals for the best-fitting model was 2.2 times observational errors. The range of other acceptable models suggest that our estimates of the dip and depth of the fault are well constrained and that the geodetic moment was $3.0 \pm 0.5 \times 10^{26}$ dyne-cm, which is about 60% of the moment estimated from seismic data. The preferred model predicts a maximum coastal uplift of about 800 mm, which is consistent with but somewhat less than the observed uplift of marine organisms; non-uniform slip models that concentrate moment release offshore are likely to provide a better fit to the uplift and seismic moment observations.

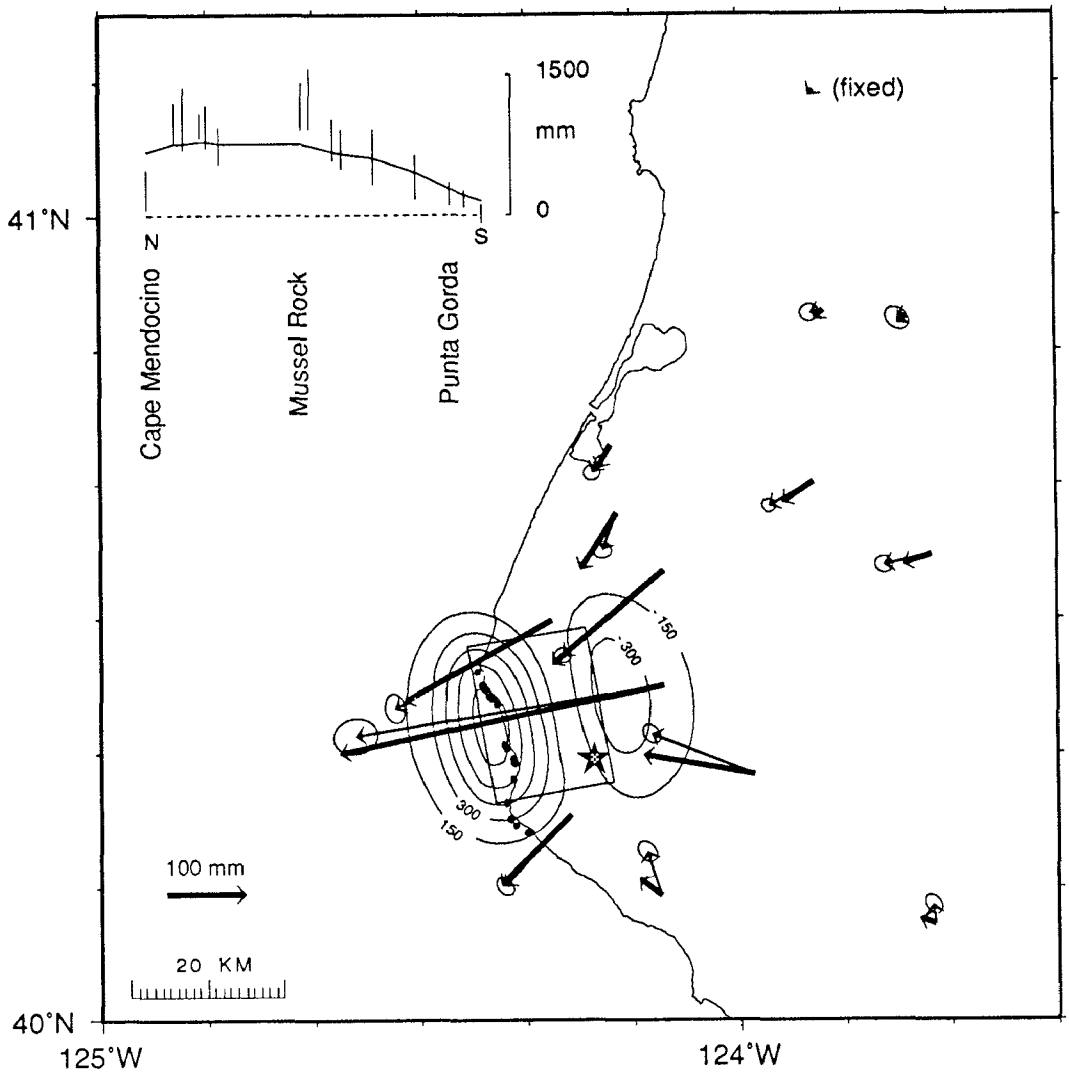

Figure 2. Horizontal and vertical displacements for the Cape Mendocino earthquake (epicenter shown with a star). The light vectors with 95% confidence region ellipses are the GPS measured displacements relative to the northernmost site. The dark vectors are the modeled displacements. The surface projection of the model fault is outlined with a rectangular box. The contours show the modeled uplift. The graph compares the uplift deduced from the die-off of marine organisms along the coast at the positions marked by black dots with that from the dislocation model.

7. *Continuous GPS Across the Hayward Fault*

In September 1991 the U. S. Geological Survey began continuous GPS monitoring of a north-south trending 8.1 km baseline that crosses the Hayward fault. This segment of the fault last ruptured in a major earthquake in 1868, and is now a zone of high seismicity and creep. We operate codeless dual-frequency Ashtech LM-XII receivers at 30 second sampling, archive daily files, and process seven-hour sessions with the Bernese version 3.2 software. Figure 3 shows the results through November 22, 1992. For this

short baseline, the broadcast orbit yields satisfactory results (Fig. 3). The rms scatter about the best linear fit is 2.2 mm in the north, 2.9 mm in the east, 10.4 mm in the vertical, and 2.1 mm in baseline length. The vertical rate of change is implausibly high.

We made several equipment changes, some of which introduced offsets in the time series. The offsets are removed by solving simultaneously for average slope and offsets at given times in a least squares adjustment. The largest offset is associated with the conversion to a forced center antenna mount. We experimented with borrowed P-code receivers for one month in the summer of 1992. A major firmware upgrade (1992.6) for the codeless receivers significantly reduced the L2 cycle slips and noise.

We made significant progress toward automating the data reduction. Data are downloaded automatically. We use PhasEdit, adapted by Jeff Freymuller of Stanford, to remove most of the low elevation angle noise. The Bernese automatic cycle slip detector fixes most of the remaining problems. As a result, our manual data cleanup time has gone from 2 hours to about 30 minutes.

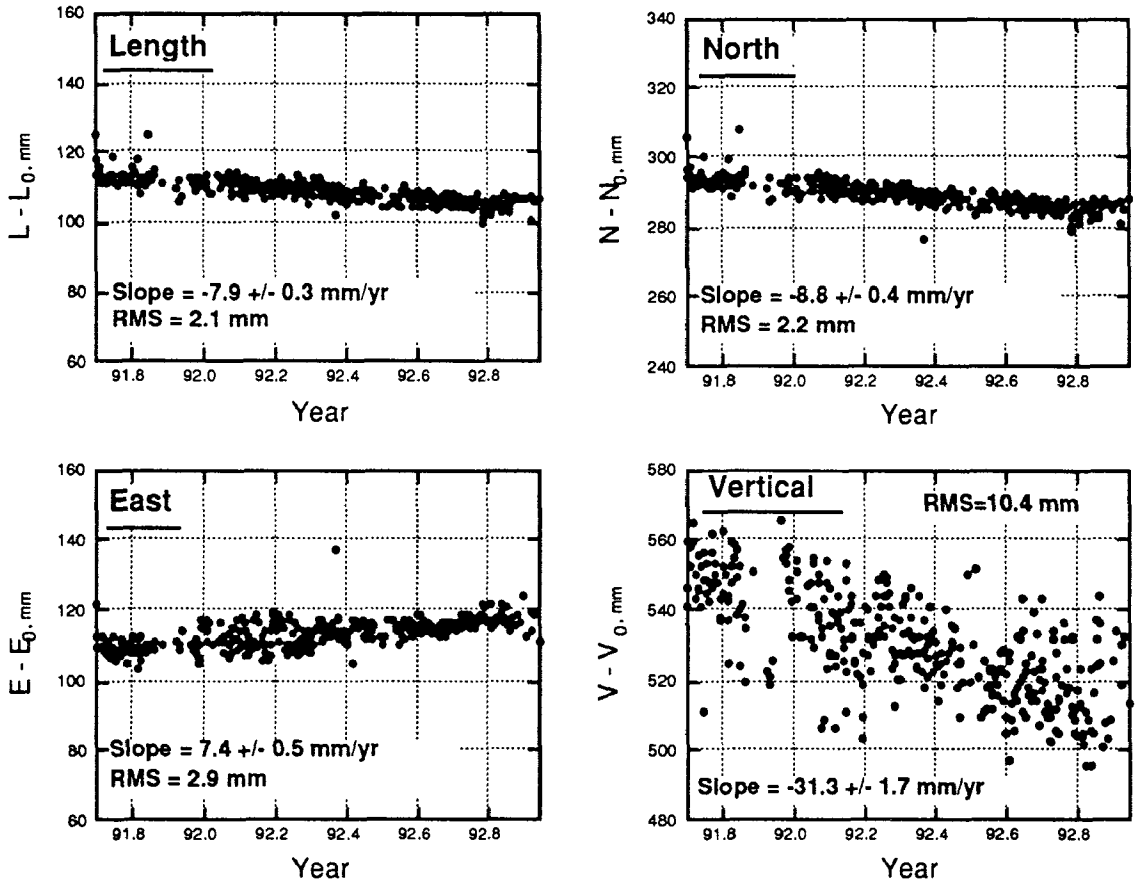

Figure 3. Length and vector components as a function of time for the 8.1 km baseline between the continuously recording GPS receivers near the Hayward fault. Uncertainties are one standard deviation as derived from the rms scatter about a weighted linear fit.

Reports

Savage, J.C., and W.Thatcher, Interseismic deformation at the Nankai Trough, Japan, subduction zone, *J. Geophys. Res. 97*, 11,117–11,135, 1992.

Savage, J.C., The uncertainty in earthquake conditional probabilities, *Geophys. Res. Lett.*, *19*, 709–712, 1992.

Savage, J.C., M. Lisowski, and W.H. Prescott, Strain accumulation across the Wasatch fault near Ogden, Utah, *J. Geophys. Res.*, *97*, 2071–2083.

Nonlinear velocity inversion for subsurface imaging of the Hosgri fault, offshore California

Agreement No. 14-08-0001-G-N2210

John N. Louie
Seismological Laboratory
The University of Nevada
Reno, NV 89557-0141
(702) 784-4219 louie@seismo.unr.edu

30 November 1992

Annual Technical Report

Motivation

The geometry and tectonics of the Hosgri fault have been the subject of intense debate. Opposing models have been developed that characterize the Hosgri as being dominated by either compressional (Crouch et al., 1978; Namson and Davis, 1990) or trans-tensional tectonics (DiSilvestro et al., 1990; Hanson and Lettis, 1990) over its history. These theories conflict on the nature of the neotectonic motion of the Hosgri, leaving the seismic potential of this major fault in doubt. Other points of contention have centered on the validity of structural models and/or interpretations of geologic features.

Our Investigations

Performing post- and pre-stack migration of data obtained from the NE-oriented seismic reflection line RU-3 (McIntosh et al., 1991) helps determine the character of the Hosgri Fault. A suite of post-stack images calculated at different migration velocities were produced for analysis. The stacked data show the best images of the stratigraphy within the Santa Maria basin near the Hosgri (figure 1). Our pre-stack migration utilized the Kirchhoff summation method (Louie and Qin, 1991). This method takes into account strong lateral variations in seismic velocity across the fault, for which any stacking process gives incorrect results. We derive the velocity model used in performing the Kirchhoff migration from a simulated-annealing (Rothman, 1985) Monte-Carlo inversion of RU-3 first-arrival picks, developed by Pullammanappallil and Louie (1992). Previous attempts to image structure within the fault zone (Shih and Levander, 1989) suffered from lack of constraint on velocities. Our model (figure 1) constrains lateral velocity variations to 2 km depths with 0.2 km/s accuracy, and is a consistent superset of the stacking velocities.

Results to Date

Results from the post-stack migration indicate thinning of Miocene-Pliocene sedimentary deposits northeastward, as they lap onto the south-west limb of the Point San Luis anticline (figure 1). The sediments, characterized by prominent reflections, are terminated and displaced upward on the north-east side of the Hosgri Fault Zone (HFZ). On the post-stack images, the HFZ is primarily characterized by columns of diffractions and truncations of reflectors. The pre-stack migration (figure 1) images the fault plane and characterizes it as dipping from 50-60 degrees to the NE.

Our images (figure 1) indicate upward-thrust pre-Miocene rocks on the NE side of the Hosgri Fault truncating Miocene to post-Miocene sedimentary reflectors underthrust on the SW side of the fault. The combination of the post-stack and pre-stack migrations

gives good control on both sedimentary and fault-plane structures. Further work will concentrate on eliminating the arcing artifacts in the pre-stack migrations with coherency criteria similar to those used by Louie and Qin (1991), and on enhancing fault-plane reflection strength with additional pre-processing of the unstacked data.

Reports submitted for publication:

Honjas, B., J. Louie, and S. Pullammanappallil, 1992, Results of post and pre-stack migrations imaging the Hosgri fault, offshore Santa Maria basin, CA: presented at the Amer. Geophys. Union Fall Meeting, San Francisco, Dec. 7-11.

Pullammanappallil, S. K., and J. N. Louie, 1992, Inversion of seismic reflection travel times using a nonlinear optimization scheme: submitted to *Geophysics*, 30 August.

References

Crouch, J. K., Bachman, S. B., and Shay, J. T., 1984, Post-Miocene compressional tectonics along the central California margin: *in* Crouch, J. K., and Bachman, S. B., Eds., Tectonics and Sedimentation Along the California Margin, Pacific Section, Soc. Economic Paleontologists and Mineralogists, **38**, 37-54.

DiSilvestro, L. A., Hanson, K. H., Lettis, W. R., and Shiller, G. I., 1990, The San Simeon/Hosgri pull-apart basin, south-central coastal California (abstract): EOS Trans. Am. Geophys. Union, **71**, 1632.

Hanson, K. L., and Lettis, W. R., 1990, Use of ratios of horizontal to vertical components of slip to asses style of faulting — Hosgri fault zone, California (abstract): EOS Trans. Am. Geophys. Union, **71**, 1632.

Louie, J. N., and Qin, J., 1991, Subsurface Imaging of the Garlock Fault, Cantil Valley, California, J. Geophys. Res., **96**, 14461-14480.

McIntosh, K. D., Reed, D. L., Silver, E. A., and Meltzer, A. S., 1991, Deep structure and structural inversion along the central California continental margin from EDGE seismic profile RU-3: J. Geophys. Res., **96**, 6459-6474.

Namson, J., and Davis, T. L., 1990, Late Cenozoic fold and thrust belt of the southern Coast Ranges and Santa Maria Basin, California: Am. Assoc. Petrol. Geologists Bull., **74**, 467-492.

Rothman, D. H., 1985, Non-linear inversion, statistical mechanics, and residual statics estimation: Geophysics, **50**, 2784-2796.

Shih, R.-C., and Levander, A. R., 1989, Pre-stack layer-stripping reverse-time migration (abstract): EOS Trans. Am. Geophys. Union, **70**, 1222.

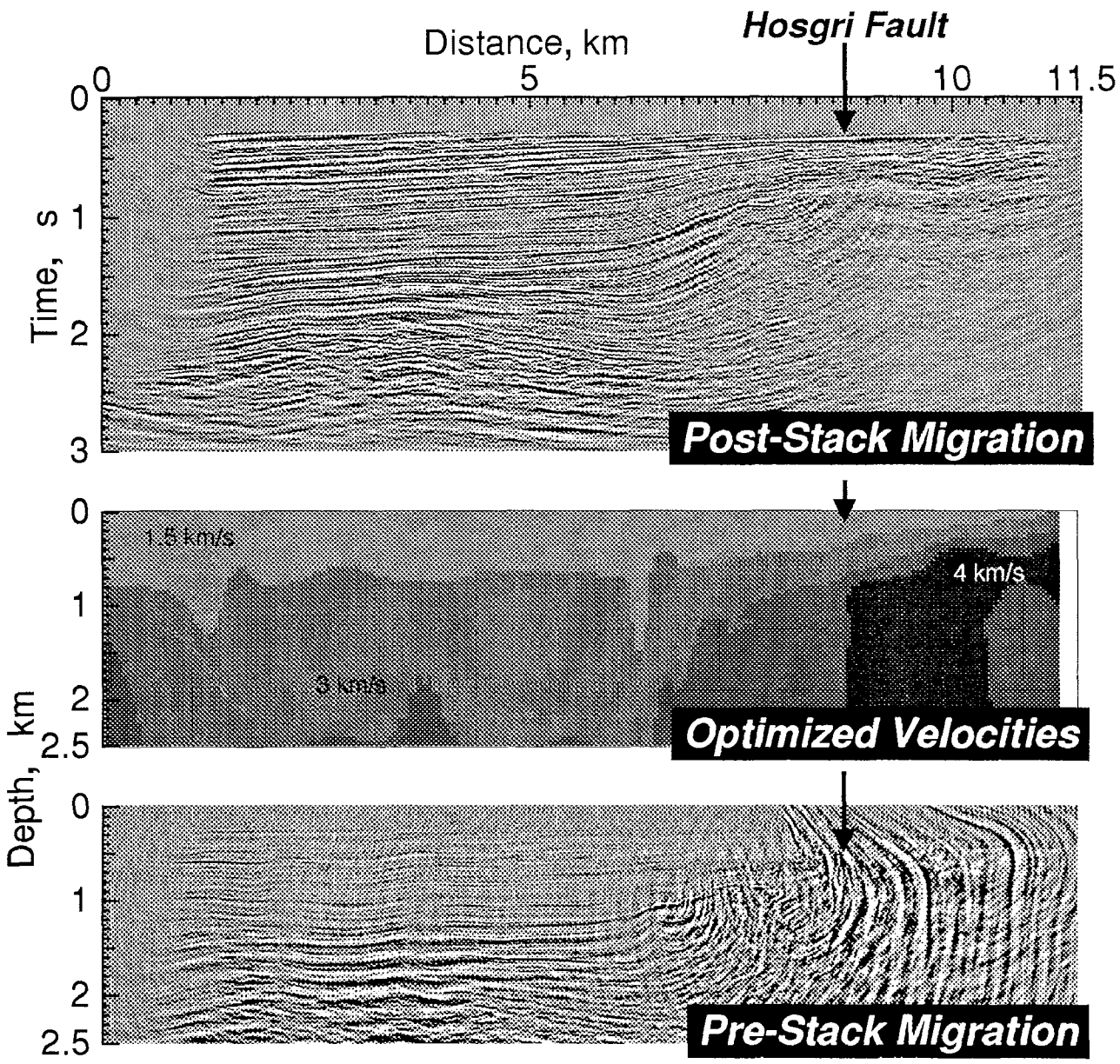

FIGURE 1: Analysis of seismic reflection data previously acquired by the EDGE Consortium and Rice University crossing the offshore Hosgri fault near San Luis Obispo, California. The top image is a common-midpoint stacked section, after F-K migration. It is similar to the stacks published by McIntosh et al. (1991) and shows the details of basin stratigraphy. However, strong lateral velocity variations near the Hosgri fault (arrows) disrupt the stacked image nearby. The middle image shows the result of a non-linear, curved-ray velocity inversion using picked first arrival times and a simulated-annealing optimization method. Having found estimates of the lateral velocity contrasts, we can then compute a pre-stack migration of the reflection data that accounts for these contrasts. The resulting lower image has almost as much detail on the basin sediments, but is much more accurate near the Hosgri fault. The arrow points to steep, east-dipping fault-plane relfections, with truncated basin stratigraphy below.

CRUSTAL VELOCITY STRUCTURE AND GROUND RESPONSE IN THE PACIFIC NORTHWEST - COAST RANGES THROUGH CASCADES

Project Number: 9930-03791
Project Co-P.I.'s: James Luetgert, Walter D. Mooney
Institution : U.S. Geological Survey, Branch of Seismology
Address: 345 Middlefield Road / MS 977
Menlo Park, CA 94025
Telephone: 415-329-4763/4764

This project is a continuation of the investigation of lithospheric velocity structure and ground response in the Pacific Northwest begun in 1991 with collection of seismic refraction/wide angle reflection data in the Puget Sound/Willamette lowland region funded by NEHRP and DCS.

Despite the importance of the Pacific Northwest as a region of seismic and volcano hazard, and as a laboratory of active tectonic processes, limited deep seismic profiling has been conducted in the region. Our present knowledge of the structural framework of the Pacific Northwest is largely based upon projections of surface geology to depth, inferences from gravity, aeromagnetic and magnetotelluric data, limited seismic reflection data and observed patterns of seismicity. Seismic characterization of a portion of the Pacific Northwest, the Puget Sound/Willamette lowland region, has begun as a result of field work completed in September, 1991.

We have continued to investigate the geophysical framework of this region by proceeding with the analysis and interpretation of the data collected in 1991 (Figure 1). The 1991 field program consisted of three seismic refraction/wide angle reflection profiles: a 300-km-long N-S profile on the eastern flank of the Puget Sound Basin of Washington; a second 330-km-long N-S profile on the west flank of the Willamette Lowland of Oregon; and a 140-km-long cross-strike (E-W) profile across the central Oregon Coast Ranges and Willamette Lowland. A total of 24 large bore-hole shots were fired, and recording was accomplished with more than 500 portable seismographs from the USGS, Stanford, IRIS/PASSCAL, and the GSC, Ottawa. In addition, two 96-channel seismic reflection spreads were deployed by the University of Wyoming. These data, in consort with other geological and geophysical data, will provide a model of the velocity and structure of both the upper crust and the lower crust/upper mantle through this region.

During FY92, the data collected in September, 1991, have been collated, distributed to University collaborators, and an Open-File Report is in final preparation. Preliminary modeling of crustal velocity structure has begun and has already yielded intriguing results. P-wave velocities in the upper crust from the north-south profile along the eastern side of the Puget Basin (Figure 2) show that the basin is deepest toward the center of the profile and is relatively shallow at the north and south ends. Upper crustal velocities greater than 6 km/s underlie the basin and are found as shallow as 5 km in depth. Velocities rise from 6.3 to 6.7 km/s to 7.1 km/s across a mid-crustal gradient zone near 25 km depth. Crustal thickness is approximately 45 km along the length of the profile.

The Coast Ranges of western Oregon constitute a large portion of the Cascades forearc. In central Oregon, the Coast Ranges consist of a thick accumulation of basalt and associated marine sediments; pre-Tertiary crust is apparently missing. The

seismic refraction/wide angle reflection profile was recorded along the west flank of the Willamette Lowland of Oregon. These profiles provide more than 330 km of deep seismic data, which define the crustal and upper mantle structure in unprecedented detail. The N-S seismic profile in Oregon indicates a substantially thicker crust (more than 30 km) than appears in many previous geophysical interpretations (Figure 3). The average crustal velocity is high (6.8 km/s or greater), and is indicative of substantial amounts of mafic rocks in the deep crust, in agreement with the positive Bouguer gravity anomaly. Strong wide-angle reflections from depths of 40+ km may be from the subducting Juan de Fuca plate.

More than forty rock samples have been collected along the 1991 profiles and laboratory velocity measurements have begun (N. Christensen) The crustal seismic velocities determined from the 1991 Oregon seismic refraction data are in excellent agreement with laboratory velocity measurements made at high pressure on rock samples collected in the Coast Ranges. The following presentations of early results have been made.

Luetgert, J.H., Mooney, W.D., E. Criley, G.R. Keller, J. Gridley, K. Miller, A. Tréhu, J. Nabelek, S.B. Smithson, C. Humphreys, N.I. Christensen, R. Clowes, and I. Asudeh, 1991. Crustal Architecture of the Pacific NW: The 1991 Seismic Field Experiment, EOS, 72:44:323.

Luetgert, J.H., Mooney, W.D., E. Criley, G.R. Keller, J. Gridley, K. Miller, A. Tréhu, J. Nabelek, S.B. Smithson, C. Humphreys, N.I. Christensen, R. Clowes, and I. Asudeh, 1992. Crustal velocity structure of the Pacific NW: The 1991 Seismic refraction/wide-angle reflection experiment, GSA Abst. with Programs, 24:5:66.

Mooney, W.D., J.Luetgert, E. Criley, G.R. Keller, J. Gridley, K. Miller, A. Tréhu, J. Nabelek, S.B. Smithson, C. Humphreys, N.I. Christensen, R. Clowes, and I. Asudeh, 1991. The 1991 Pacific Northwest Seismic Field Experiment, EOS, 72:44:326.

Trehu, A. M., J.N. Nabelek, S. Azevedo, T.M. Brocher, J. Luetgert, W.D. Mooney, I. Asudeh, R. Clowes, G.R. Keller, K. Miller, and Y. Nakamura, 1992. Crustal Structure of the Cascadia Subduction Zone Beneath Western Oregon, GSA Abst. with Programs, 24:5:66.

Luetgert, J.H., Mooney, W.D., A. Tréhu, N.I. Christensen, and I. Asudeh, 1992. Crustal Structure of the Oregon Coast Ranges from 1991 Seismic Refraction Data, EOS, 73:43:526.

Trehu, A. M., J.N. Nabelek, S. Azevedo, T.M. Brocher, J. Luetgert, W.D. Mooney, I. Asudeh, R. Clowes, Y. Nakamura, S.B. Smithson, and K. Miller, 1992. A Crustal Cross-section across the Cascadia Subduction Zone in Central Oregon, EOS, 73:43:391.

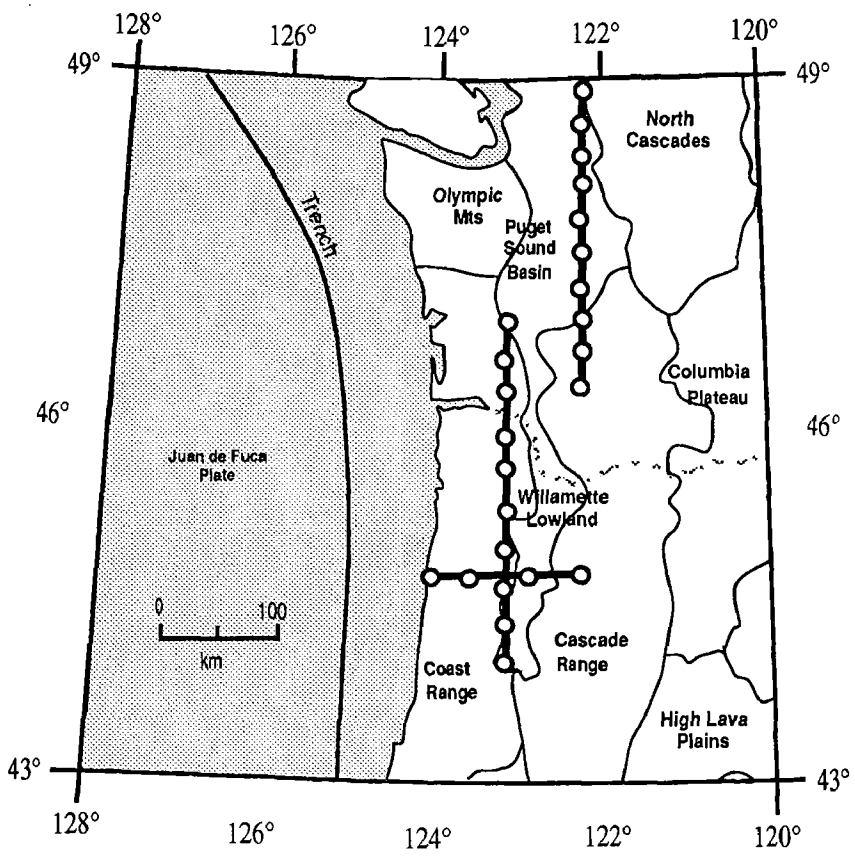

Figure 1: Locations of shotpoints and recording arrays used for the 1991 Pacific NW seismic refraction/wide-angle reflection experiment.

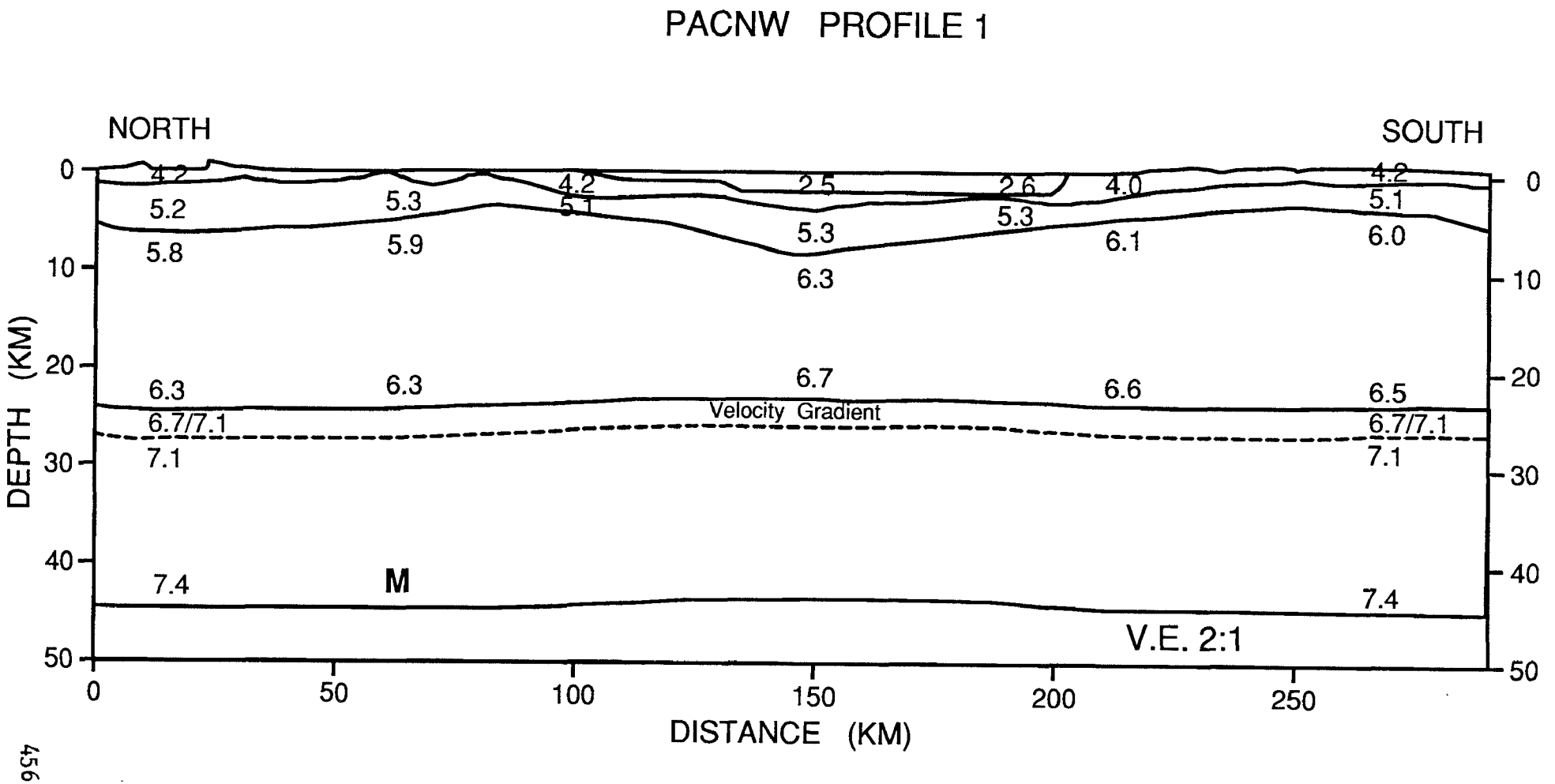

Figure 2: Preliminary velocity model for PACNW profile 1; located at the eastern edge of the Puget Basin in Washington State.

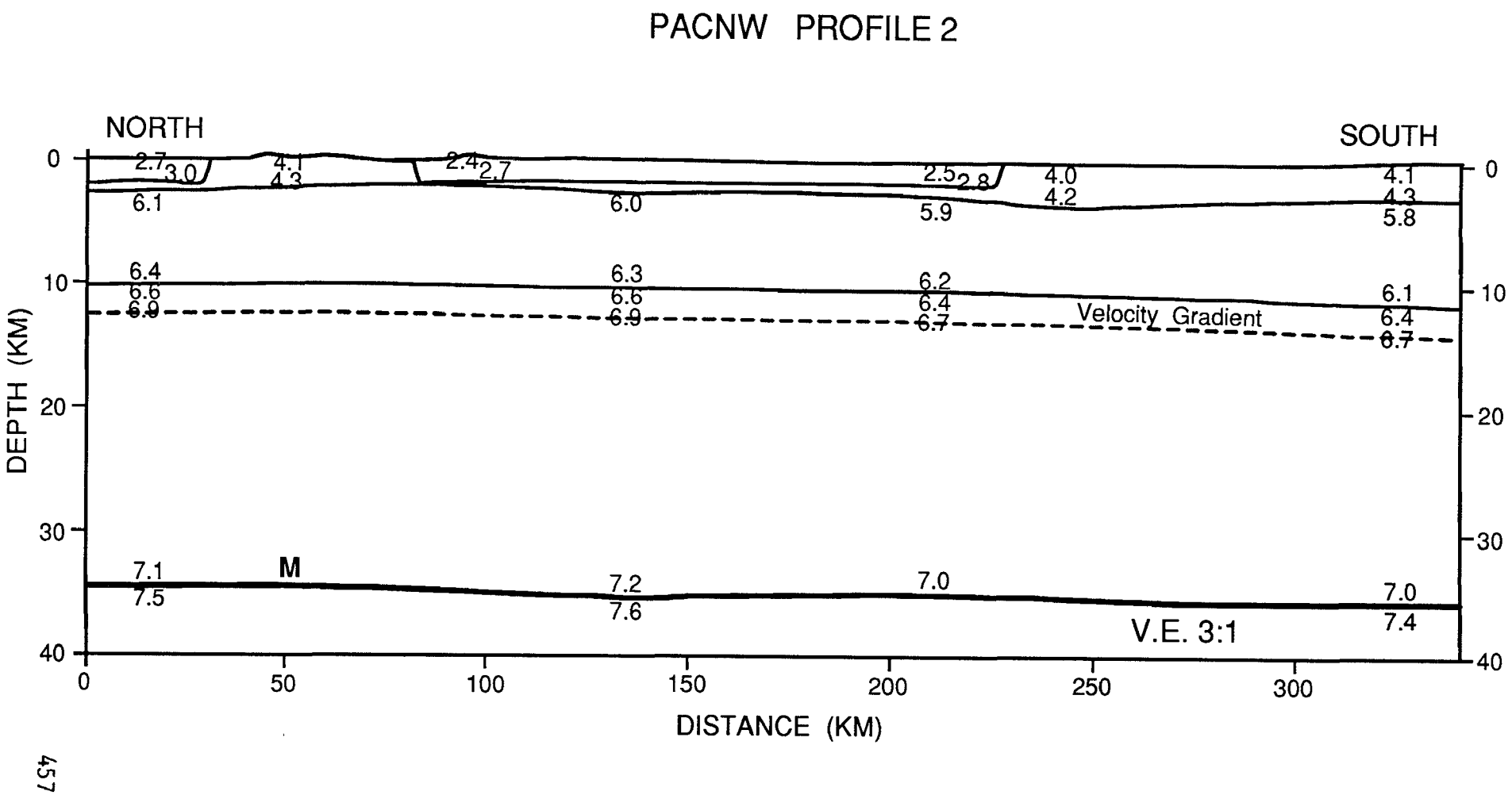

Figure 3: Preliminary velocity model for PACNW profile 2; located at the western edge of the Willamette Valley in Oregon State.

TEMPORAL AND SPATIAL BEHAVIOR OF LATE QUATERNARY FAULTING, WESTERN UNITED STATES

9950-04540

Michael N. Machette
Branch of Geologic Risk Assessment
U.S. Geological Survey, Box 25046, MS 966
Denver, CO 80225-0046
(303) 273-8612

PURPOSE OF PROJECT

To define regional variations in the time-space distribution of late Quaternary paleoseismic activity as a guide to understanding the accumulation and release of strain on extensional faults in the Western United States. Our main objective is to study selected historic faults to interpret the paleoseismic and neotectonic history in regions of active faulting, especially in the Central Nevada seismic belt (CNSB). In addition, at least one-half of FY 92 was spent on a new International Lithosphere Program (ILP) project entitled "World Map of Major Active Faults, Western Hemisphere." Project members are Michael N. Machette, Richard L. Dart, and Kathleen M. Haller.

INVESTIGATIONS

1. This summer, Machette, Haller, and Kelvin Berryman (visiting scientist from New Zealand Geological Survey) completed describing and sampling six large exploratory trenches that were excavated in Pleasant Valley, south of Winnemucca, Nev. Four of the trenches cross surface ruptures of the 1915 Pleasant Valley earthquake (estimated Richter magnitude $7^3/_4$) in order to investigate the timing of prehistoric faulting. Two additional trenches were located on nearby pre-1915 fault scarps; one on a valleyward strand of the Tobin Scarp and a second that is to the north along the frontal fault of the Sonoma Range in Grass Valley. Detailed topographic/geologic maps were made of the trench sites using an EDM Total Station on loan from S.G. Wesnousky of the University of Nevada-Reno. Samples were taken for TL and ^{14}C dating and tephrochronologic studies.

2. In January 1992, we were asked by ILP to help compile the World, North American, and United States maps of major active faults in support of a new Global Seismic Hazards Assessment Program (GSHAP). This work began in earnest in mid-1992 with a carefully chosen list of participants for the Western Hemisphere. We are enlisting technical experts from Canada, the United States, and Mexico/Central America that are known to be both productive and knowledgeable, and to have strong national contacts. For the United States, the compilation will be done by the USGS in Denver, under the direction of this project. Given the limited time to produce the North American map (two to three years at the most), the project must be limited to just those elements needed for the GSHAP. The number of features to be included on the map were reduced at an initial GSHAP planning meeting in San Francisco (Dec. 1991) and further modified at the 1992 meeting in Rome.

Assembling the fault map and database for the United States (and North America) will involve:

1) General supervision and interpretation of geologic/tectonic information (M.N. Machette),
2) Data compilation and entry for the fault catalog (all personnel) and the design and management of the database (K.M. Haller), and
3) Digitization and manipulation of data (file transfer, transform projections) using ARCINFO software on a Sun-workstation (R.L. Dart).

By the end of FY 92, we had obtained digital files for California, Nevada, Utah, Montana, Colorado, and parts of New Mexico. The California faults were scanned on the Menlo Park Scitex using a specially prepared version of Jennings' 1992 fault map. The files for the other states come from sources within the USGS or state geological surveys.

Our strategy is to assemble a large body of data on the Quaternary faults in the U.S. portion of North America. Although many authors have compiled maps, few have taken the time to fully document their maps with databases, particularly in computer form; thus, fault data in catalog form is relatively sparse. However, the state of Utah will soon publish an excellent catalog and Malcolm Clark (USGS) continues to compile a catalog of slip-rate data for California. Overall, we suspect that there are catalog data for about 20% of the faults on the U.S. map.

The customers for these products include internal (USGS) to external NEHRP scientists, as well as scientists, engineers, planners with state and local governments, universities, and consulting firms. We are using ARC Info on a SUN-platform for the map preparation and are compiling fault data on a relational database (FoxBase, MicroSoft Corp.) on the Macintosh. However, because most of the intended users do not have Macintosh computers, we intend to supply the data in a DOS and/or Windows version of the database. We hope to write the database, a run-time version of the program, and the digital map files to CD-ROM for easy access at low user cost.

3. Crone and Machette completed two comprehensive manuscripts that describe the results of their 1991 Gilbert Fellowship field studies of the 1988 earthquakes at Tennant Creek, Australia (Crone and others, 1992) and Marryat Creek, Australia (Machette and others, 1993). These manuscripts discuss the implications of long-recurrence intervals for intraplate faulting. They will be published as USGS Bulletins that contain lithologic/structural logs of six exploratory trenches, detailed site maps, plots of scarp profiles, and preliminary results of TL and ESR dating.

RESULTS

1. Last summer we spent about 5 weeks logging trenches across surface ruptures of the 1915 Pleasant Valley earthquake, south of Winnemucca, Nev., and nearby prehistoric scarps. These trenches revealed evidence of 2-3 faulting events during late Pleistocene time (10-130 ka). The first and most important conclusion of our study is that earthquakes of similar magnitude to the 1915 Pleasant Valley earthquake must have long recurrence intervals (*i.e.*, many tens of thousands of years). The two trenches along the Pearce scarp (at Miller Basin and just south of Siard Canyon) crossed large (>6- to 13-m-high) scarps on alluvium believed to be of pre-late Pleistocene age (>130 ka). The two trenches along the Tobin scarp, which is a right-stepping, northward extension of the Pearce scarp, crossed a 8-m-high scarp on pre-late(?) Pleistocene alluvium and colluvium at Sheep Creek and a small (0.5-m-high) scarp on pre-late(?) Pleistocene alluvium just south of Jim Creek near the northern end of the Tobin scarp. At all of these sites, we found no evidence of pre-1915 faulting events on surfaces of Holocene or latest Pleistocene (<15 ka) age. No trenches were excavated along the China Mountain and Sou Hills scarps (the distal sections of the 1915 ruptures) because evidence of prior faulting is sparse and discontinuous, recorded on bedrock or steep hillslopes, or is restricted to small (<1-m high) scarps on old alluvium.

Two additional trenches were excavated to investigate the history of subjacent faults that were not activated during the 1915 Pleasant Valley earthquake. A long, deep trench was placed across a 9-m-high scarp that is about 1 km valleyward of the Tobin scarp in the northern part of Pleasant Valley. The other trench was across a 4.4-m-high scarp of the range-front fault of the Sonoma Range near Elbow Canyon about 12 km south of Winnemucca in Grass Valley. The history of faulting along the Sonoma Range is particularly interesting in that it may show if late Quaternary faults in the Grass Valley near Winnemucca were part of an integrated prehistoric analog of of the CNSB, or whether the seismic belt has included the China Mountain, Tobin, Pearce, and Sou Hills fault blocks in late Quaternary time. We are suspucious that the recent rupturing along China Mountain is defining a relatively new NE-oriented rupture path.

The tectonic stratigraphy in these trenches is dominated by loess (eolian silt) and fine sand derived from Quaternary lake deposits and local debris flows that postdate and commonly lie on middle(?) Pleistocene alluvium; as a result, these trenches presented a special challenge to map and decipher previous faulting events owing to a lack of distinguishing lithologies, sedimentary features, and organic matter. The following discussion briefly summarizes results of our trenching.

Miller Basin Trench

Three colluvial wedges and a fourth unit of colluvium were found in this trench. The wedges become progressively more lenticular with time as a result of increasing scarp height, such that the post-1915 wedge extends across most of the 13-m-high scarp. The oldest colluvium lies on alluvium of probable pre-late Pleistocene age (>130 ka) age. The second and third wedges are separated by a moderately well developed soil (Av, Btk horizons) that probably required tens of thousands of years to form. The fault zone is at least 9 m wide and consists of a main shear zone (70° W dip) that was active in 1915 (and earlier), and associated minor faults, the most basinward of which is a high-angle reverse fault. The bulk of sediment on the downthrown side of the fault is derived from debris-flows and loess and have no correlative on the upthrown block. No organic material or tephra were found in this trench.

South of Siard Canyon Trench.

The 1915 scarp at this site is large (ca. 2-3 m) and comprises about 1/2 of the total scarp height (5.8 m) at the site. However, the upper surface is steep (10° slope) and may represent earlier faulting events. The total surface offset here is probably about 10 m. Three colluvial wedges and a fourth tectonically derived unit were found in the trench, however these material are concentrated in a healed graben that was exposed in the midslope position of the scarp. The oldest tectonic material fills a portion of the graben. The third wedge fills a meter-wide fissure and is characterized by abundant organic matter and/or basaltic ash (see also Sheep Creek trench). The two younger wedges are lenticular and contain many sedimentary packages. The main shear zone is about 1.5 m wide, dips 53-66° W., and daylights high on the scarp. The entire fault zone is about 18 m wide and forms a deep graben, which was entirely filled by debris flows and loess prior to reactivation in 1915. Pods of Mazama ash (6,845±50 ^{14}C yr B.P.; Bacon, 1983) are concentrated within the graben and except for one problematic exposure, the Mazama seems to be deformed by only one faulting event (1915). All of the material in the 3.5-m-deep trench across the graben is either debris flows or loess. A buried soil at 1.4 m depth (valleyward of the graben) probably correlates with the upthrown surface above the scarp and is covered by loess. This soil has a strong accumulation of clay in gravel, suggesting considerable antiquity. The abundant organic material in the fissure fill and the tephras were sampled for dating/correlation.

Sheep Creek Trench

R.E. Wallace found Mazama ash exposed in the fault scarp at Sheep Creek along of the Tobin scarp and argued that the ash is faulted by only the 1915 earthquake. On this basis, the minimum recurrence interval for surface faulting along the Tobin scarp is at least 6,800 yr; however, we suspect that it may be substantially longer (several tens of thousands of years?). To evaluate the fault's recurrence interval, a trench was placed across a large composite fault scarp that is superposed on a 10-15° west-facing hillslope, about 50 m south of Sheep Creek.

The main faulting is concentrated in a 1-2-m wide zone and an adjacent back tilted half graben. The 1915 and prior faulting event (2nd) resulted in a colluvial wedge comprised of slump blocks and finely laminated wash-slope sediment. The next older events (3rd and 4th) are characterized by large slump blocks comprised of well developed Bt and Btk horizon material. Interspersed within the blocks is a prominent clean mafic ash(?) that was probably emplaced after the 4th faulting event and prior to the 3rd event. Considering that there are three faulting events recorded after deposition of the ash and that the faulted land surface appears old based on soil development, the ash may be correlative with the pre-late Pleistocene Wadsworth ash bed(A.M. Sarna-Wojcicki, oral commun., 1992). The Wadsworth is a mafic ash in the upper part of the pluvial in the Eetza Alloformation of Lake Lahontan in west-central Nevada (Davis, 1978). The Eetza was deposited during oxygen isotope stages 6 and 10, and thus could be as young as 130 ka (end of stage 6), although Sarna-Wojcicki and others (1991) estimated an age of 155 ka for a correlative ash from Tule Lake in northern California. If the correlation of the Sheep Creek ash and the Wadsworth ash bed is substantiated, then the recurrence interval for faulting at the Sheep Creek site is about 65-75 ky.

Upper Jim Creek Trench

This trench crossed a small scarp (total height of about 0.5 m) that had been nearly healed prior to the 1915 event. However, if one walks along the scarp you can detect the presence of a pre-1915 scarp, however subtle. A shallow graben that extends almost 20 m west of the main fault was found to be at least 2 m deep and filled mainly with loess. The well developed soil on the upthrown surface (Av/Bt/Cox profile) was not found in the graben, but is evident valleyward of the antithetic fault beneath about 1.5 m of loess. These relations suggest about 2-2.25 m of net thrown across the fault zone. The number of faulting events recorded in this trench is problematic owing to the thick fill of loess and the absence of easily recognizable colluvial wedges that were probably the result of individual <1-m displacements. If prior faulting events had displacements similar to the 1915 event (0.7 m from trench log), then only 3 events are needed to form the scarp and graben found at this site. If the surface is a of pre-late Pleistocene age, which seems to be the case for most surfaces that have large scarps and well developed soils, then recurrence intervals are on the order of 50 ky or longer. However, the site is near the northern end of the Tobin scarp and thus may not record all of the events that occurred at the Sheep Creek site or along the Pearce scarp to the south. The downdropped surface can be traced west to the Lower Jim Creek site (see next description), where the surface also has a well developed soil profile.

Lower Jim Creek Trench

This trench crossed a 9-m-high scarp having a maximum slope angle of about 17°. No faulting occurred along this fault in 1915, although the scarp joins the Tobin scarp just north of Sheep Creek. The trench revealed evidence for 3 or 4 events in the late(?) Pleistocene, the youngest of which occurred before the most recent episode of loess deposition (latest Pleistocene to Holocene time). There is about 3 m of fill on the downdropped side of the fault, and another 2 m of disturbed fluvial gravels are preserved within a narrow graben. The fill averages about 25 percent gravel, whereas the source material on the upthrown block is almost entirely sandy gravel. Therefore, about 3/4 of the fill is probably derived from eolian deposits and 1/4 is derived from erosion of the fault scarp.

Elbow Canyon Trench

This trench is along a prehistoric fault scarp that parallels the western front of the Sonoma Range. Wallace (1979) considered this scarp to be of latest Pleistocene age (ca. 12 ka) on the basis of its morphology. The trench crossed a 4.4-m high scarp having a maximum slope angle of about 14.5° and revealed evidence for 3 events in the late(?) Quaternary (past 130 ka); however, the most recent event probably predates the desiccation of Lake Lahontan at about 12 ka. The lake's highest shoreline is about 5 km to the west of the trench site, and the lake undoubtedly supplied the bulk of the eolian material found in the trench. At the base of the trench, we found a large block of soil that had collapsed from the fault's free face during the oldest event; the preservation of this delicate block indicates that it was soon buried by colluvium. Samples from the intact Av horizon at the former top of this block will provide a TL date for the third (oldest) event, and thus allow us to calculate a minimum recurrence interval and slip rate at this site.

Summary of Trenching Investigations

Our preliminary interpretations from the trenching lead us to believe that large-magnitude surface-rupturing events occur on long time intervals (many tens of thousands of years) along the eastern side of Pleasant and Grass Valleys. This conclusion contrasts markedly with the historic pattern of surface-rupturing in the northern part of the CNSB. Careful dating of paleoseismic events will be required to document whether or not ancient episodes of temporal earthquake clustering occured in the CNSB. In addition, regional fault studies may show that seismic belts (such as the CNSB) may move back and forth through regions, allowing temporal clustering on long time frames.

From the materials exposed in our trenches, it seems obvious that the use of fault scarp morphology for discriminating times of faulting in the western Basin and Range province is handicapped by two problems. First, many fault scarps are probably not eroded in a closed system (as often modeled) but instead are buried by eolian materials derived from distant sources (tens to hundreds of km away). Second, most scarps more than 3-4 m high are probably the result of multiple faulting events and thus scarp height will be a compound value, whereas scarp slope will be related to the most recent faulting event. One must be careful in applying morphometric analysis to multiple-event scarps; chances are good that young scarps will seem too old (Holocene will look like late Pleistocene) and old scarps will seem too young (owing to the compound nature of the scarps). We are optimistic that our trench mapping and sampling for dating and tephrochronologic correlation will allow us to decipher the approximate timing of prehistoric faulting events along the Pleasant Valley scarps and nearby faults. The results of this study will be compared to paleoseismic histories being developed by Bell and dePolo on the 1934 Cedar Mountain scarps, by Bell on the 1954 Dixie Valley scarps, and with work planned by Wesnousky on the 1954 Fairview Peak scarps, in order to better understand the temporal and spatial patterns of prehistoric seismicity along the northern part of the CNSB.

2. No modern map of active faults exists for the entire United States, either in paper or digital form. The proposed map of the United States (and probably North America) will be compiled and digitized at 1:250,000 scale (AMS quadrangles). This scale will allow eventual output at state map scales (commonly 1:500,000 to 1:750,000) without serious loss of information. We favor the AMS quadrangles because they are uniformly available, are near the maximum size of personal-computer digitizer tables, and have been used as a base for many of the state compilations of Quaternary faults in the Western United States (*e.g.*, Utah and Nevada).

In addition to fault location and style, our maps will depict times of most recent movement and slip rate as a proxy for fault activity. Our age scheme allows some flexibility owing to differing levels of understanding and the fact that the age of some faults can only be inferred from stratigraphic relations. Five ages of movement can be shown on the U.S. map using colors (colors tentative):

Red	Historic (date, generally <200± years),
Orange	Holocene (<10 ka) to post-latest Pleistocene (<15 ka),
Green	Late Quaternary (<130 ka),
Blue	Late and middle Quaternary (<730 ka), or
Black	Quaternary (<1.6 Ma).

TABLE 1. Status of Quaternary fault data for different regions of the United States
[Quality: ***A***, good; ***B***, adequate; ***C***, poor or nonexistent]

State/region	Regional Map	Database Type	Main Contacts
Alaska	***A***. Digital, 1992	***A***. Text, unpublished	Plafker
Washington	***B***. Compiled, 1991	***C***. Uncompiled	Walsh
Oregon	***B***. Part digital, 1992	***B***. Partial; text, 1992	Weldon, Pezzopane
California	***A***. Recompiled, 1992	***B***. Partial; text, 1984	CDMG, USGS
Nevada	***A***. Digital, 1991	***C***. Uncompiled	Dohrenwend
Idaho	***C***. Uncompiled	***C***. Uncompiled	Haller
Montana	***B***. Part digital, 1992	***C***. Uncompiled	Stickney
Utah	***A***. Digital, 1992	***A***. R-base, 1992	Hecker
Arizona	***B***. Nondigital, ca. 1987	***B***. Partial; text, ca. 1987	Pearthree
New Mexico	***B***. Part digital, ca. 1987	***B***. Partial; text, ca. 1987	Machette
Colorado	***B***. Digital, ca. 1987	***B***. Partial; text, ca. 1987	Colman, Kirkham
Texas	***B***. Nondigital, 1992	***C***. Uncompiled	Collins
Mid-Continent	***C***. Uncompiled	***C***. Uncompiled	Crone, Obermeier
Eastern U.S.	***C***. Uncompiled	***C***. Uncompiled	Prowell, Talwani

Three ranges of slip rates (mm/yr or m/ky), depicted by fault-line thickness, will be used on the map to differentiate rates of activity:

>5	Faults at plate boundaries and along subduction zones (San Andreas fault, Cascadia subduction zone),
1-5	Lesser strike-slip and major extensional faults (Garlock and Wasatch faults), or
<1	Most extensional and intraplate faults.

3. The results from our Gilbert Fellowship research on intraplate faulting in Australia (1986 Marryat Creek, Machette and others, in press; 1988 Tennant Creek earthquakes Crone and others, 1992) show that these historic intraplate earthquakes reactivated ancient faults. However, there was no clear evidence of fault-scarp derived colluvium in the Quaternary deposits in any of the six trenches, nor is there any compelling geomorphic evidence of prehistorical faults scarps at any of the sites. TL age estimates from eolian sand at Tennant Creek are as old as 61±5 ka (John Prescott, University of Adelaide, Australia). These relations indicate that the historical earthquakes were associated with faults that had ruptured in the past, but that the recurrence interval for surface-rupturing earthquakes on these faults is probably measured in time increments of tens of thousands of years and possibly hundreds of thousands of years or more. These investigations of historical intraplate faulting and our brief observations of a trench across the 1968 Meckering (Western Australia) fault scarp suggest that Australian intraplate faults have long repeat times; with this in mind, the concept of recurrence intervals may not be appropriate for earthquakes that occur in the 'stable' interiors of continents. Perhaps hazard assessments in Australia and other continental interiors should be based on models where moderate- to large-magnitude earthquakes occur at any time on suitably oriented faults, rather than only on faults having Quaternary movement.

REFERENCES CITED

Bacon, C.R., 1983, Eruptive history of Mount Mazama and Crater Lake caldera, Cascade Range, U.S.A.: Journal of Volcanology and Geothermal Research, v. 18, p. 57-115.

Davis, J.O., 1978, Quaternary tephrochronology of the Lake Lahontan area, Nevada and California: Nevada Survey Archeological Research Paper 7, 137 p.

Jennings, C.W., 1992, Fault activity map of California: California Division of Mines and Geology Open-File Report 92-03, scale 1:750,000 (preliminary version of second edition).

Sarna-Wojcicki, A.M., Lajoie, K.R., Meyer, C.E., and Adam, D.P., 1991, Tephrochronologic correlation of upper Neogene sediments along the Pacific margin, conterminous United States, *in* Morrison, R.B., ed., Quaternary nonglacial geology; Conterminous U.S.: Geological Society of America, The Decade of North American Geology, v. K-2, p. 117-140.

Wallace, R.E., 1979, Map of young fault scarps related to earthquakes in north central Nevada: U.S. Geological Survey Open-File Report 79-1554, 2 plates, 1:125,000 scale.

REPORTS

Crone, A.J., Machette, M.N., Bowman, J.R., 1992, Geologic investigations of the 1988 Tennant Creek, Australia, earthquakes—Implications for paleoseismicity in stable continental regions: U.S. Geological Survey Bulletin 2032-A, 51 p., 2 plates.

Machette, M.N., and Haller, K.M., 1992, Late Quaternary faulting in the Western United States—Evidence of geologically recent extension of the northern Basin and Range province: Kyoto, Japan, 29th International Geological Congress Abstracts with Programs, p. 398.

Machette, M.N., Personius, S.F., and Nelson, A.R., 1992, The Wasatch fault zone, USA: Accepted for Special Issue of Annales Tectonicae, 58 ms. p., 22 figs., in press.

Machette, M.N., Crone, A.J., Bowman, J.R., 1993, Geologic investigations of the 1986 Marryat Creek, Australia, earthquake—Implications for paleoseismicity in stable continental regions: U.S. Geological Survey Bulletin 2032-B, 54 ms. p., 19 figs., 8 tables, 1 plate, in press.

Trifonov, V.G., and Machette, M.N., 1993, The World Map of Major Active Faults Project (14 p.), *in* P.W. Basham and D. Giardini, eds., The Global Seismic Hazards Assessment Program (GSHAP): Proceedings of the GSHAP Planning Meeting, Rome, Italy, June 1-3, 1992.

Analysis of Seismic Data from the Rose Canyon and Elsinore Fault Zones

Project Number 1434-92-G2173

Harold Magistrale
San Diego State University
Department of Geological Sciences
San Diego, California 92182
(619) 594-6741

The purpose of this work was to analyze existing phase data of earthquakes along the Elsinore and the Rose Canyon fault zones, as recorded on the USGS-Caltech southern California seismic network, in order to relate seismicity patterns to geologic structures. Arrival times were inverted for hypocenters and one- and three-dimensional P and S wave velocity structures.

Rose Canyon fault zone.

Earthquakes from the period of 1983 to 1990 are examined. Most happened in the three distinct time-space clusters of 6/85, 8-10/86, and 9/87 under the San Diego Bay. The 6/85 swarm contained three $M_L \approx 4$ earthquakes and many smaller events. It forms a southwest dipping hypocenter blob 2 to 11 km deep under the central San Diego Bay that is elongate in a northeast direction. First motion focal mechanisms indicate oblique slip (reverse plus left lateral) on northeast striking planes. The 1986 events include an 15 km deep M_L 4.6 strike slip earthquake under the south San Diego Bay. Prior to that event was a three month long swarm of M_L 2.0-3.5 events further west whose epicenters form a northeast trend on strike with the 1985 and 1987 swarms. The 9/87 events were all $M_L<3$. The epicenters form a short, northeast trending, southwest plunging, 5 to 14 km deep lineation just abutting the south edge of the 1985 blob. Focal mechanisms again show oblique slip on northeast striking planes. The 1985 and 1987 earthquakes were in clusters that dip to the southwest yet many of the earthquakes occurred on northeast striking faults. These earthquakes appear to be located on northeast striking faults, similar to those mapped at nearby Point Loma, where those faults intersect the northwest striking, southwest dipping Rose Canyon fault zone. The dip of the earthquake clusters thus reflects the dip of the Rose Canyon fault zone. The 1985 and 1987 clusters occurred at places where no earthquakes had previously been located (within the limits of location accuracy and detection threshold) since at least 1934. The maximum earthquake depths found here (up to 15 km) are much deeper than those found previously, implying a greater fault width and correspondingly larger potential earthquakes.

Elsinore fault zone.

Relocations of several thousand earthquakes between 1981 and 1991 along the Elsinore fault zone identify a fault east of, and parallel to, the Elsinore fault defined by an alignment of hypocenter clusters (Fig. 1). The fault defined by the microseismicity coincides in part with the Earthquake Valley and Agua Tibia faults (EQVAT) as mapped on the state geologic sheets. The hypocenter clusters represent activity

concentrated near fault steps and conjugate fault intersections. Where the EQVAT fault ends to the south and north seismicity shallows and becomes diffuse. These areas mark steps where slip is transferred to and from the EQVAT fault from the Elsinore fault; the steps have prominent topographic expressions. A prominent northeast striking seismicity lineation defines the left lateral Sawtooth Ridge fault near the south end of the EQVAT fault. An M 5.1 event in June 1940 occurred near the intersection of the Sawtooth Ridge feature and the Elsinore fault, the largest event in the Elsinore fault zone since 1910. Aftershocks paralleled the Sawtooth Ridge fault. Currently, both the Elsinore and the Earthquake Valley-Agua Tibia faults are active. The three-dimensional velocity model images relatively slow velocities between the Elsinore and EQVAT faults, interpreted as a component of down to the east motion across the primarily strike slip Elsinore fault.

Report published:

Magistrale, H. (1992). Relocation of 1983-1990 earthquakes near San Diego, California (abstr.), *Seismol. Res. Lett.*, **63**, p.68.

Figure 1. Relocated earthquakes along the Elsinore fault zone. Newly defined EQVAT fault shown by heavy line. Symbol size scaled to earthquake magnitude.

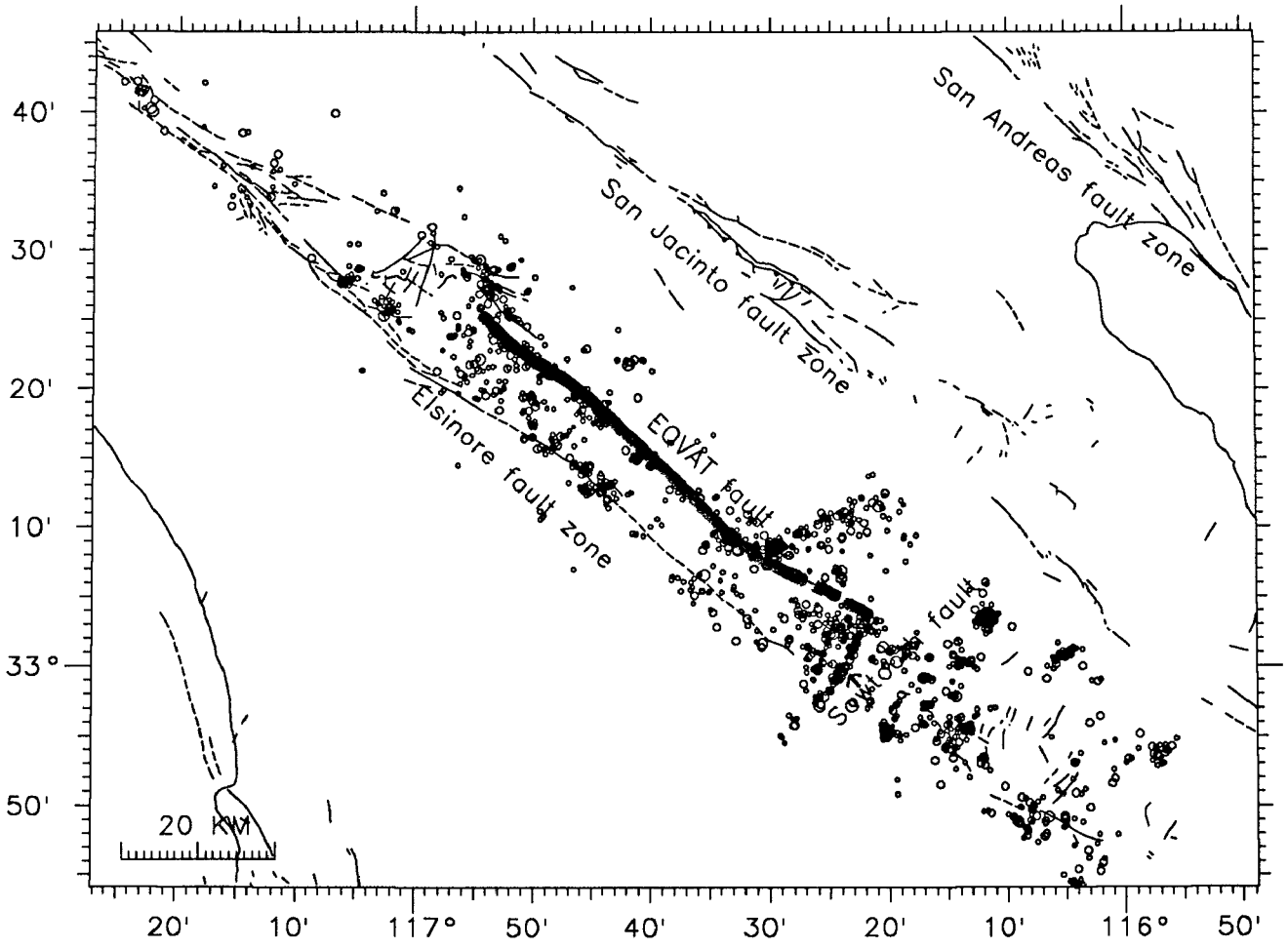

Instrumentation to Improve the Washington Regional Seismograph Network
1434-92-G-2195 S.D. Malone and R.S. Crosson, P.I.s

Geophysics Program
University of Washington
Seattle, WA 98195
(206) 543-8020
March 1, 1992 - Sept. 30, 1992

Introduction

This contract is for the purchase and installation of four new, high quality broad-band digital seismograph stations as an addition to the Washington Regional Seismograph Network. It also includes funding for the development of the data acquisition process and integration of these data into the routine data collection and analysis procedures. In addition to the four stations funded under this contract we have a prototype station already in hand, and will also incorporate data from the USNSN station at Newport, WA. On completion 18 months from now, there will be 7 high quality seismograph stations operating in the Pacific Northwest (5- operated by us, one by USNSN, NEW and one by the GSN, COR).

Progress

Development efforts have proceded on schedule. Funding for this project was received on March 1, 1992 and equipment was ordered as soon as possible. Three of the four new data loggers were received in October; the seismometers have not yet been delivered.

Our prototype broad-band station was operated in a test configuration in Seattle for several months and then moved to Longmire (LON) near Mount Rainier in May, where it has been operating on the same pier as the DWWSSN station. Sites for three of the four new stations have been selected and permits obtained (Liberty- LIB, Tolt Resevoir- TOT, Satsop- SAT). Selection of the final site is still to be done; it will be near Port Townsend, WA. Site construction, including power and telephone service, has been completed for the site near Liberty, WA. Figure 1 shows the current analog telemetry network configuration as well as the existing and planned new broad-band station locations.

We adapted the *GOPHER* dial-up system from IRIS to access our new broad-band stations and have now recovered data from 68 events recorded on our prototype station at LON. In other software development, we are developing the capability to archive our trace data in SEED format so that it can be all be stored at the IRIS Data Management Center and be easily available to anyone, along with the rest of the global data. We have developed a SEED writer for trace data from our analog telemetry network, and tested it at the IRIS DMC.

We have completed all conduit, antenna mounting hardware, and power access requirements for installation of the VSAT communications link from Seattle to the USNSN; through which we plan to receive data from the USNSN station at Newport, WA (NEW), and also possibly other stations they will install later. We await installation of satellite communications by the USGS, initially planned for June, 1991.

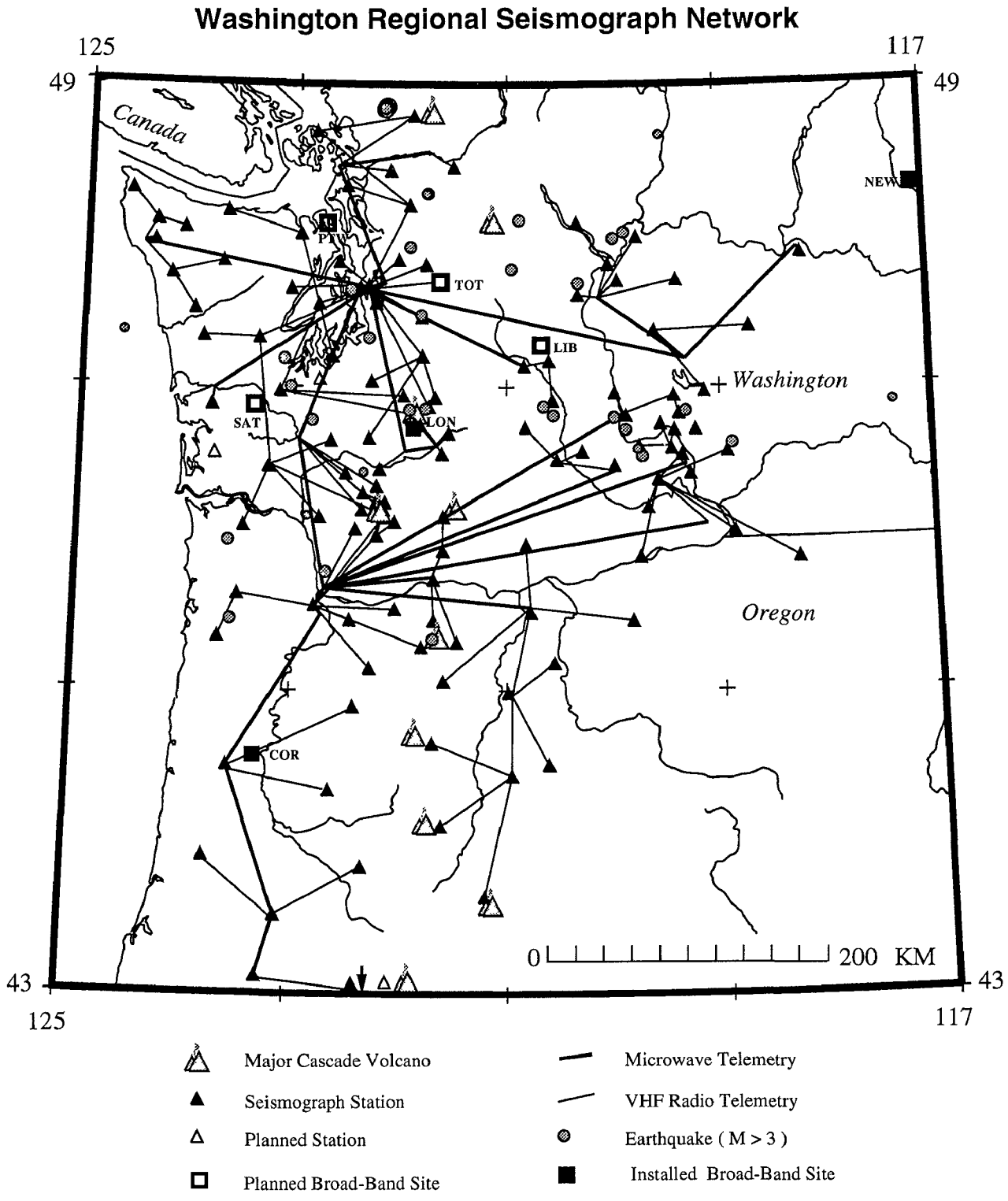

Figure 1. Map showing WRSN stations, telemetry and state of new broad-band stations

QUANTITATIVE ANALYSIS OF LANDFORMS: A WAY TO DELINEATE ACTIVE TECTONIC STRUCTURES

Agreement No. 1493-92-G-2229

Larry Mayer
Department of Geology
Miami University
Oxford, Ohio 45056

(513) 529-3241

ABSTRACT

Analysis of landforms in the New Madrid seismic zone using digital elevation data at 30 degree-, 3 degree-resolutions, and digitized planforms, indicates that several topographic features exist, with different wavelengths, that may be related to processes other than simple fluvial erosion. Landform analysis is based on image processing of digital elevation data within the context of geomorphological hypothesis testing, and the study of river planforms. These studies indicate that surface deformation of the scale and style of the Tiptonville dome may exist in several places in the region. Larger wavelength features are inferred to exist as well. Although theses larger features, are at present, defined only by their apparent effects on river pattern, they do coincide with a significant topographic blocking boundary that extends from Newport southeastward past the southern tip of Crowley's Ridge and across the embayment.

INTRODUCTION

Quantitative studies of topography are being carried out using digital elevation data, digitized representations of fluvial features such as river planforms, slope breaks, and valley morphometry, and SAR and SPOT images. The primary purpose of these studies is the delineation of tectonic features with topographic expression in the New Madrid area. By means of quantitative analysis of landforms we hope to

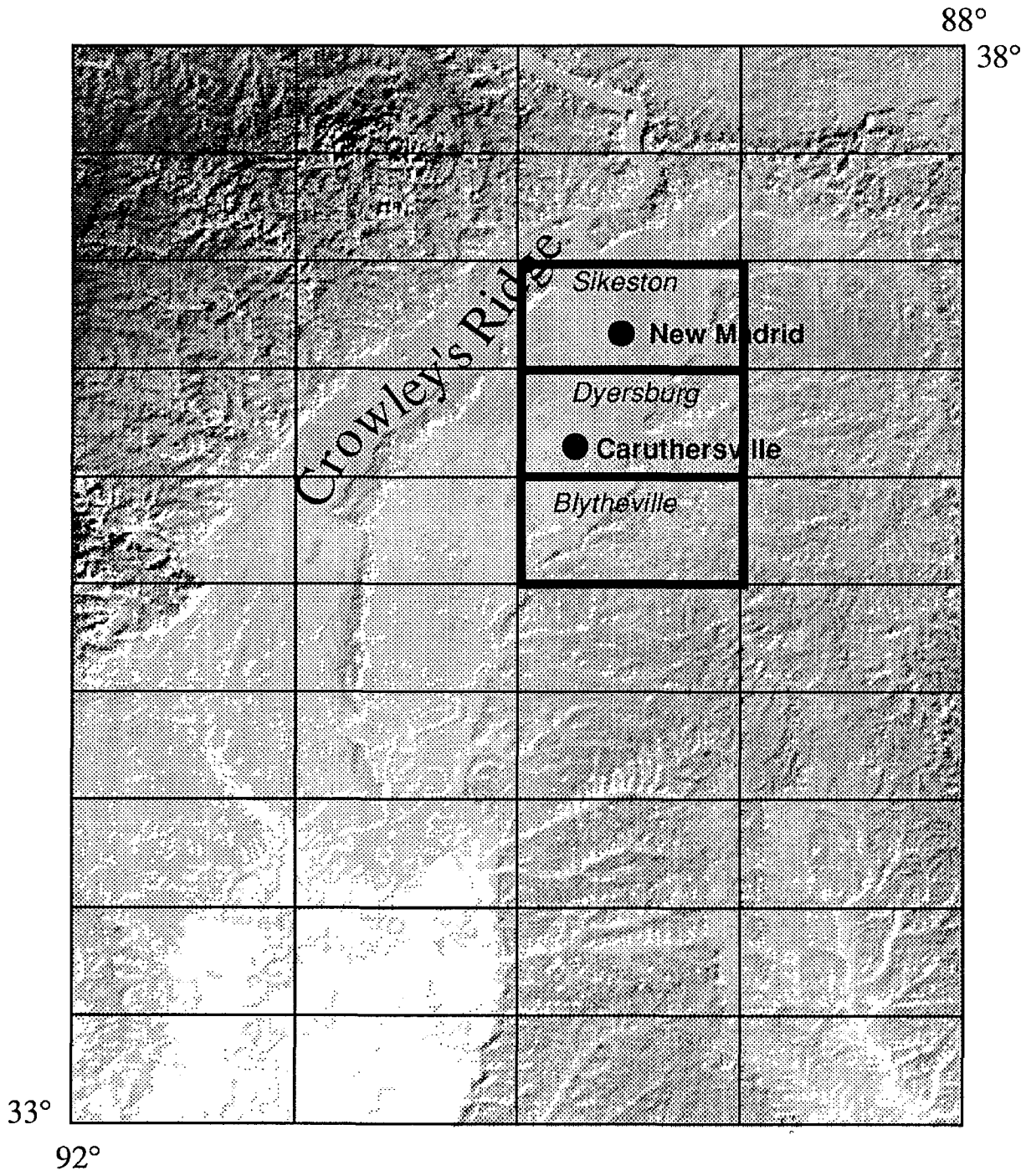

Figure 1. Digital topographic map image from 30 arc-second data showing features cited in text and location of individual 3 arc-second quadrangles. This image was produced with a simple spatial convolution.

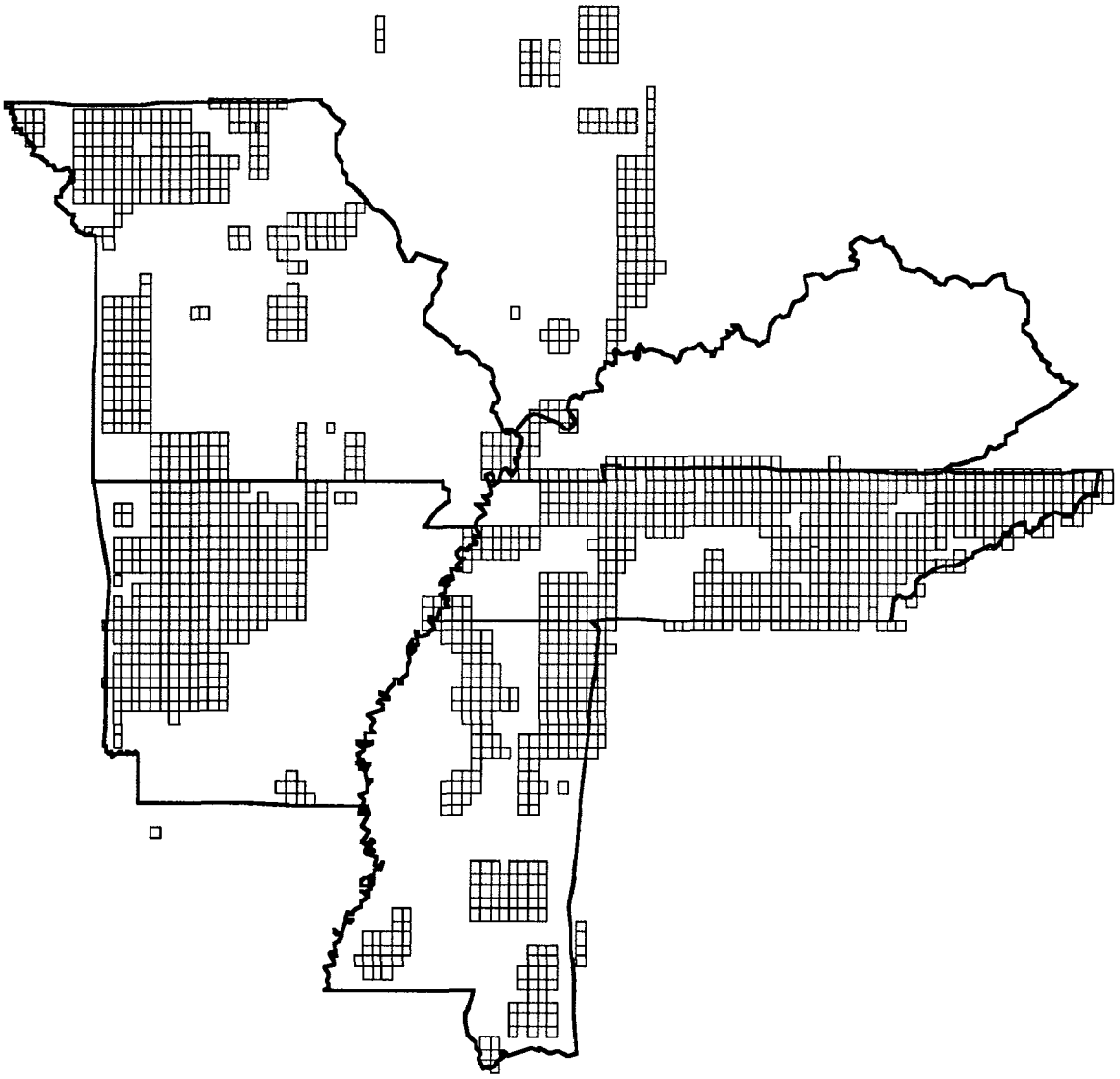

Figure 2. Index map to 7.5 DEMs for the region.

better document the history and geometry of strain and to identify potential seismic sources.

The main assumption of topographic studies is that tectonic strain deforms the surface. Surface deformation may or may not be associated with earthquakes. The challenge to the geomorphologist is the recognition of a deformed landform despite its presence in a dynamic surface environment. Another assumption is that the expression of topographic deformation has a finite survival time, which is dependent on the particular surface environment. For example, a fault scarp can be reasonably easy to recognize on a hillslope or piedmont, but it is rapidly altered by the action of a river. On the other hand a dynamic environment, one where new geomorphic surfaces are frequently generated, also provides morphostratigraphic data that can be helpful in identifying surface deformation.

Surface deformation occurs at different wavelengths. At one end of the spectrum are short wavelength features such as fault scarps that distribute vertical or horizontal strain over a very short distance measured perpendicular to strike. At the other end of the spectrum are long wavelength features such as uplifts or depressions that have vertical displacements distributed along great distances. The detection of both short and long wavelength surface deformation is sometimes directly observable and sometimes can only be inferred. The definition of surface deformation as a phenomenon with a specific wavelength or amplitude permits quantitative treatment of topographic data using digital image processing in the spatial domain.

DIGITAL ELEVATION DATA AND DIGITIZED PLANFORMS

Digital data were obtained for the study area to maximize geographic coverage and spatial resolution. The raw data tapes are downloaded onto a DEC Vax minicomputer and then transferred to the Geomorphology Computer Laboratory's Macintosh LAN using the file-transfer protocol. Locally, the data are stored on either a Ricoh optical (250M) or Bernoulli (90M) drive. Computer programs were written to convert the USGS digital elevation data sets into ASCII numeric files that could be analyzed using statistical and imaging software. The data coverage consists of both 30 arc-second and 3 arc second coverage (Fig. 1). Forty separate 1 degree by 30 minute quadrangles have been processed. The geographic coverage for 7.5 minute DEMs is very spotty (Figure 2).

The planforms of streams and the loess bluffs were obtained by digitizing these features from 1:250,000 scale and

Figure 3. Digital line map of hydrography of the Memphis and Helena 2° Sheets. Maps digitized by Kimberly Johnson, Miami University.

1:24,000 scale topographic maps respectively using a digitizing board with a 1000 lines/inch resolution. Digitized stream networks taken from the Memphis and Helena 1:250,000 scale maps are shown on Figure 3. We are now in the process of downloading and converting hydrological features from the USGS in Golden and converting them to a locally compatible format.

IMAGING OF DIGITAL ELEVATION DATA

Imaging of digital elevation data is based on standard processing techniques within the contexts of geomorphological hypothesis testing. For example, to identify areas that are anomalously high in elevation, a density slice is used. In the present context, the elevation of the Mississippi river floodplain and meander belt are morphostratigraphic data. The lower part of the density slice is set to river floodplain level. The upper part of the density slice is set at progressively higher elevations in order to identify maximum local departure from river level. This technique clearly identifies known tectonic uplifts such as the Tiptonville Dome. The usefulness of using density slicing and thresholding of digital elevation data is that it addresses a simple geomorphic hypothesis. Russ (1982; especially Figs. 4,7) used essentially the same hypothesis when he documented the relationships between the Lake County uplift, including the Tiptonville dome, to the channel levees of the Mississippi. For the same area as Russ (1982) discussed, the digital image shows Tiptonville dome and Reelfoot Lake clearly (Fig. 4).

Density slicing reveals interesting dome-like features in many places within the region shown on Figure 1. Low features are also identified. Within the area corresponding to the Dyersburg 1:100,000 scale quadrangle are two pertinent features (Fig. 5). The first informally referred to as the Caruthersville anomaly appears to be a high area that has been trimmed by the Mississippi. On the other side of the river, towards the bluffs is a low area which is informally referred to as the Dyersburg low. Both of these anomalies are, like the Tiptonville Dome, difficult to explain with fluvial processes alone.

Farther south, within the area defined as the Blytheville 1:100,000 scale quadrangle are a pair of anomalies adjacent to one another and with opposite sense of vertical strain (Fig. 5). These topographic features, like the ones to the north, are comparable in size to the Tiptonville Dome. They also are all loosely paired in the sense that a positive anomaly (higher than expected) is closely associated geographically with a negative anomaly (lower than expected).

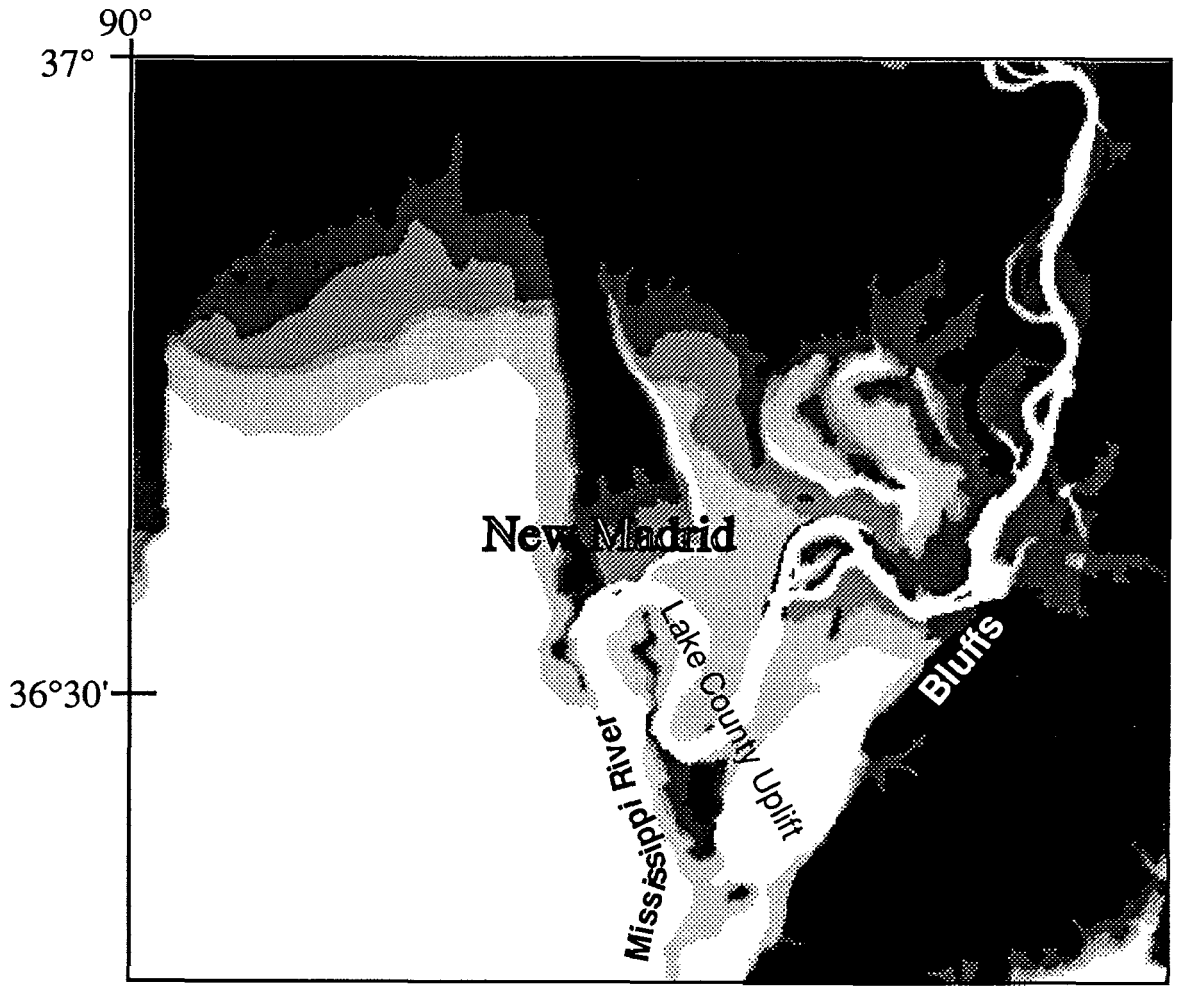

Figure 4. Digital topographic map image from 3 arc-second data showing the areas corresponding to the Sikeston 1:100,000 scale map and portion of Blytheville map. The Tiptonville dome is easiliy recognized and the broader boundary of the Lake County Uplift identifyable as a higher area relative to the that on the west of Sikeston Ridge.

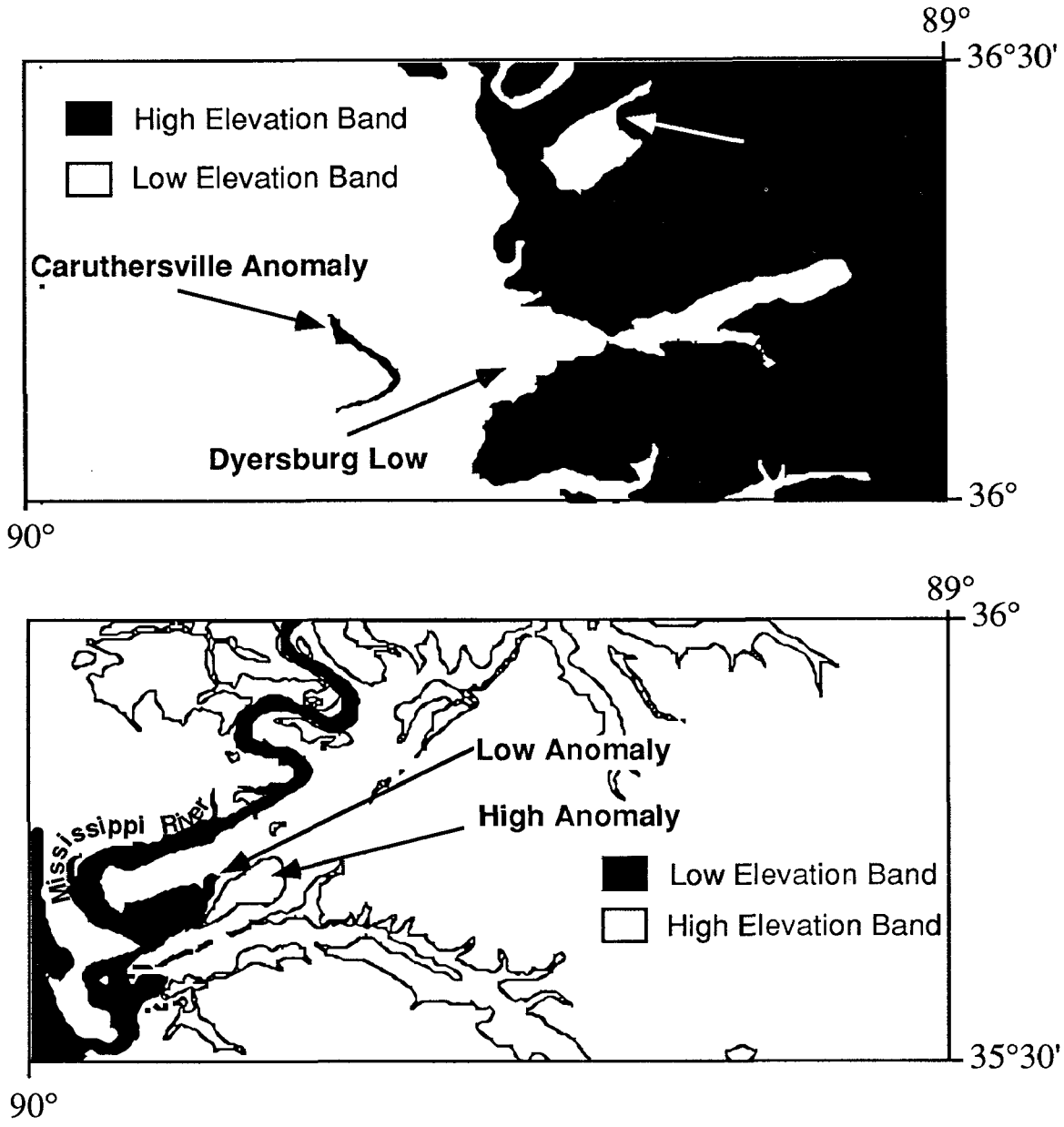

Figure 5. Digital topographic map images from 3 arc-second data showing the areas corresponding to the Dyersburg 1:100,000 scale map (TOP) and Blytheville 1:100,000 scale map (BOTTOM). Anomalous topographic features analogous to the Tiptonville dome are found in each area.

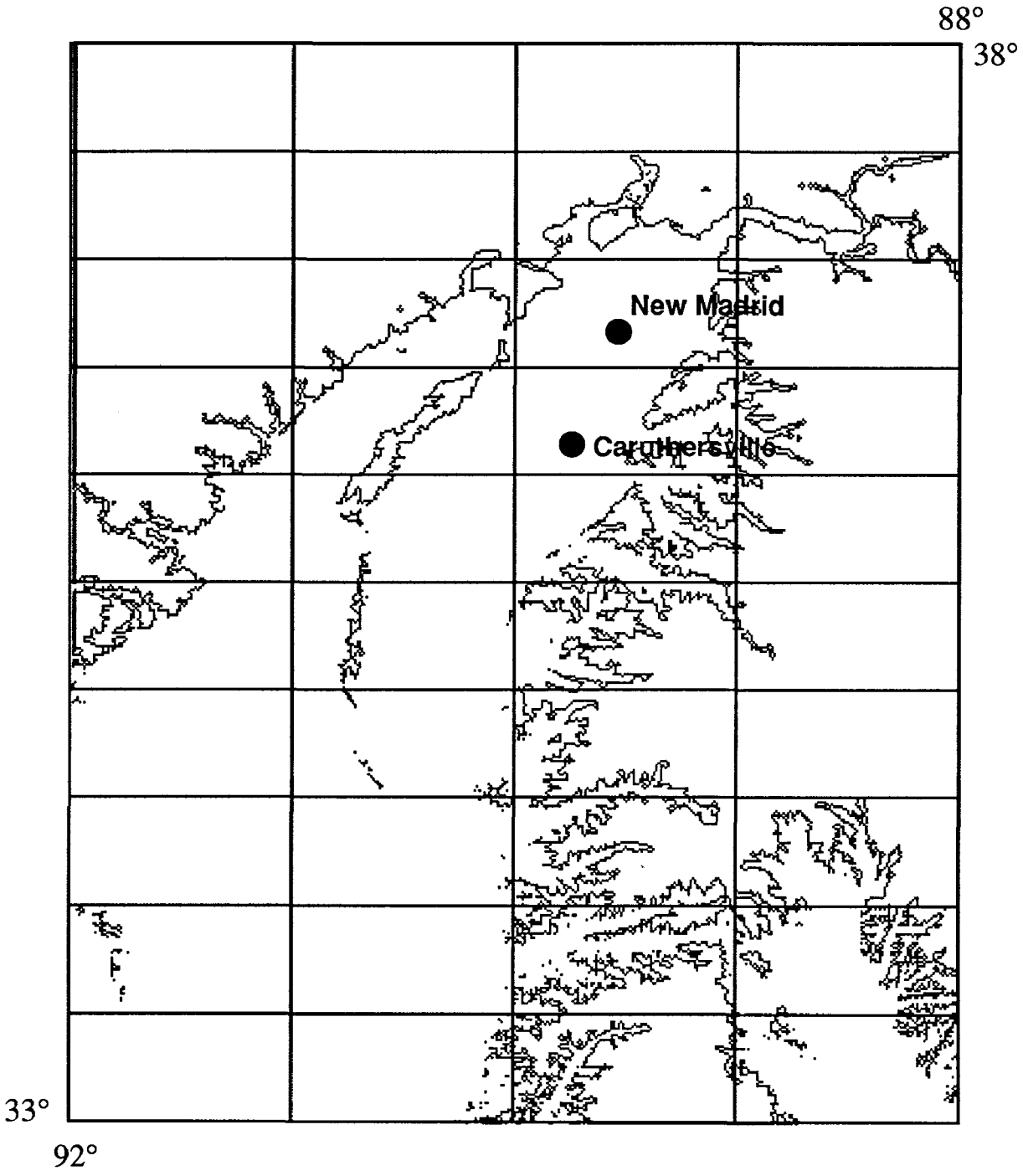

Figure 6. Digital topographic map image from 30 arc-second data showing high western boundary of the Mississippi embayment relative to the eastern boundary. This image was produced by thresholding and boundary tracing.

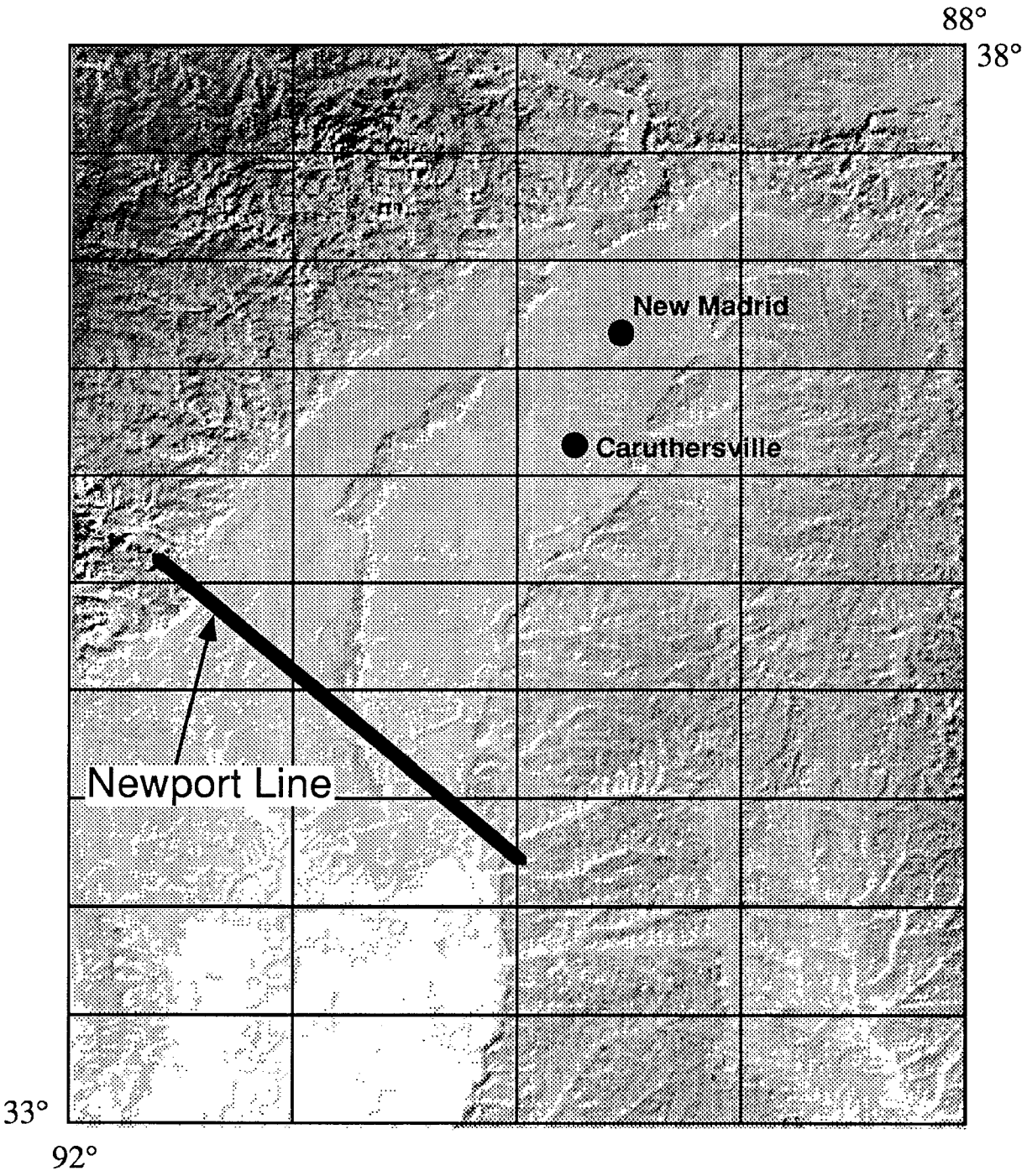

Figure 7. Digital topographic map image from 30 arc-second data showing location of the Newport line. On this image it appears as a topographic lineament.

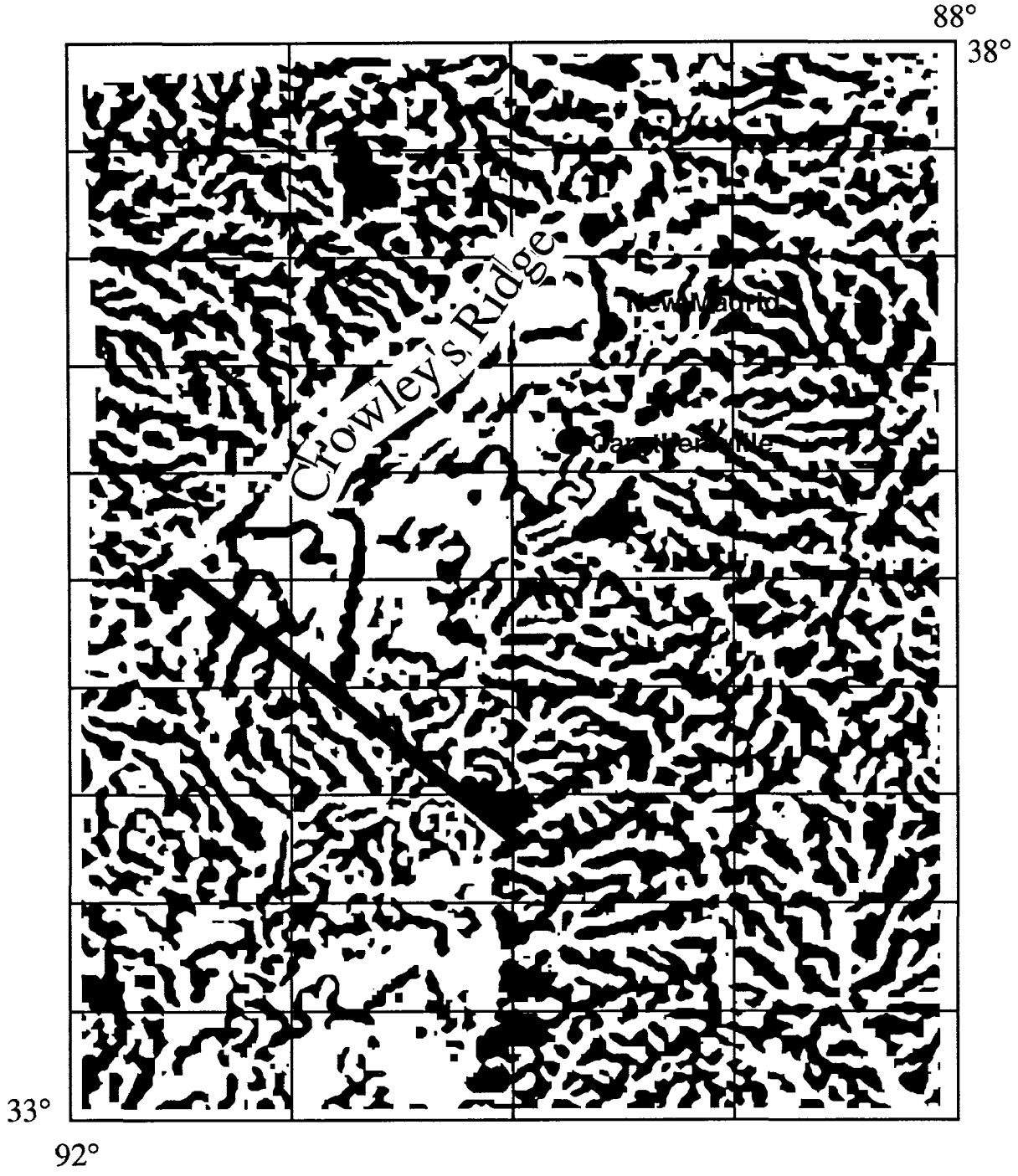

Figure 8. Digital elevation data processed from 30 arc-second files showing topographic blocking, or regionalized patterns of relief. Here the Newport line appears as a boundary separating distinct block textures.

Thresholding and edge detection is a convenient method to identify contours on a digital elevation image. A regional perspective using this view clearly shows that the western side of the embayment is much higher that the eastern side and that a horizontal slice through both regions traces a highly dissected eastern embayment boundary relative to the west (Fig. 6). The significance of the topographic difference is not yet clear, however, it becomes particularly intriguing towards the north where the Mississippi river itself skirts the boundary between these two distinct physiographic regions.

Even farther to the south and within the embayment there several topographic lines of evidence suggesting active control of surface patterns. In particular is a linear feature, here informally referred to as the Newport line, is a boundary between the narrower upper and wider lower Mississippi embayments. The Newport line appears to be a lineament on the digital images that emphasize short wavelength topography (Fig. 7).

Topographic blocking refers to the notion that the texture of topography and the relative scaling of topographic elements is related to the scale and perhaps depth of the forces generating topography. Rigorous methods to delineate blocking have not been proposed, however blocks can be described in ways that are reproducible. For example, since blocks represent regionalizations of topography, image smoothing at larger and larger scales could delineate a pattern related to blocking. A box filter whose dimensions represent the spatial extent of the smoothing function was used. The digital elevation data were first passed through an 18 by 18 pixel smoothing box filter and then thresholded until a stable block pattern appeared. That block pattern is shown on Figure 8. The Newport line appears to be a line separating distinct topographic textures.

Imaging of the loess bluffs on the eastern side of the Mississippi river also indicates that dome-like topographic features may exist there as well. These features are recorded as bluff edges where the drainage flows eastward away from the Mississippi river. Delineation of these features is ongoing.

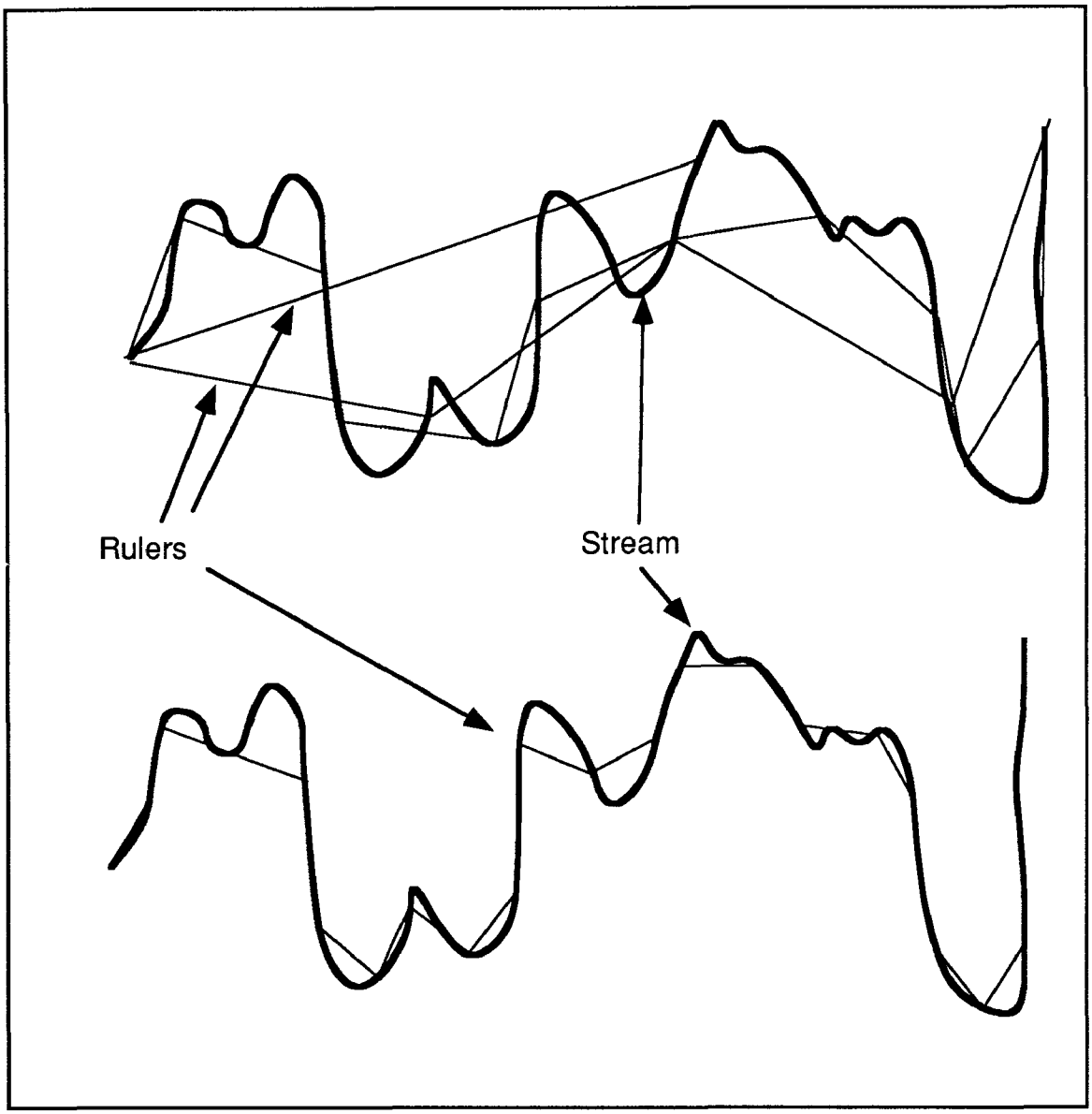

Figure 9. Cartoon illustrating "Richardson Analysis". The rulers used to measure stream length are systematically shortened to determine the rate of apparent increase in length as a function of scale. This technique can be used to identify the changes in the scale of wavelength patterns and to quantify river sinusosity.

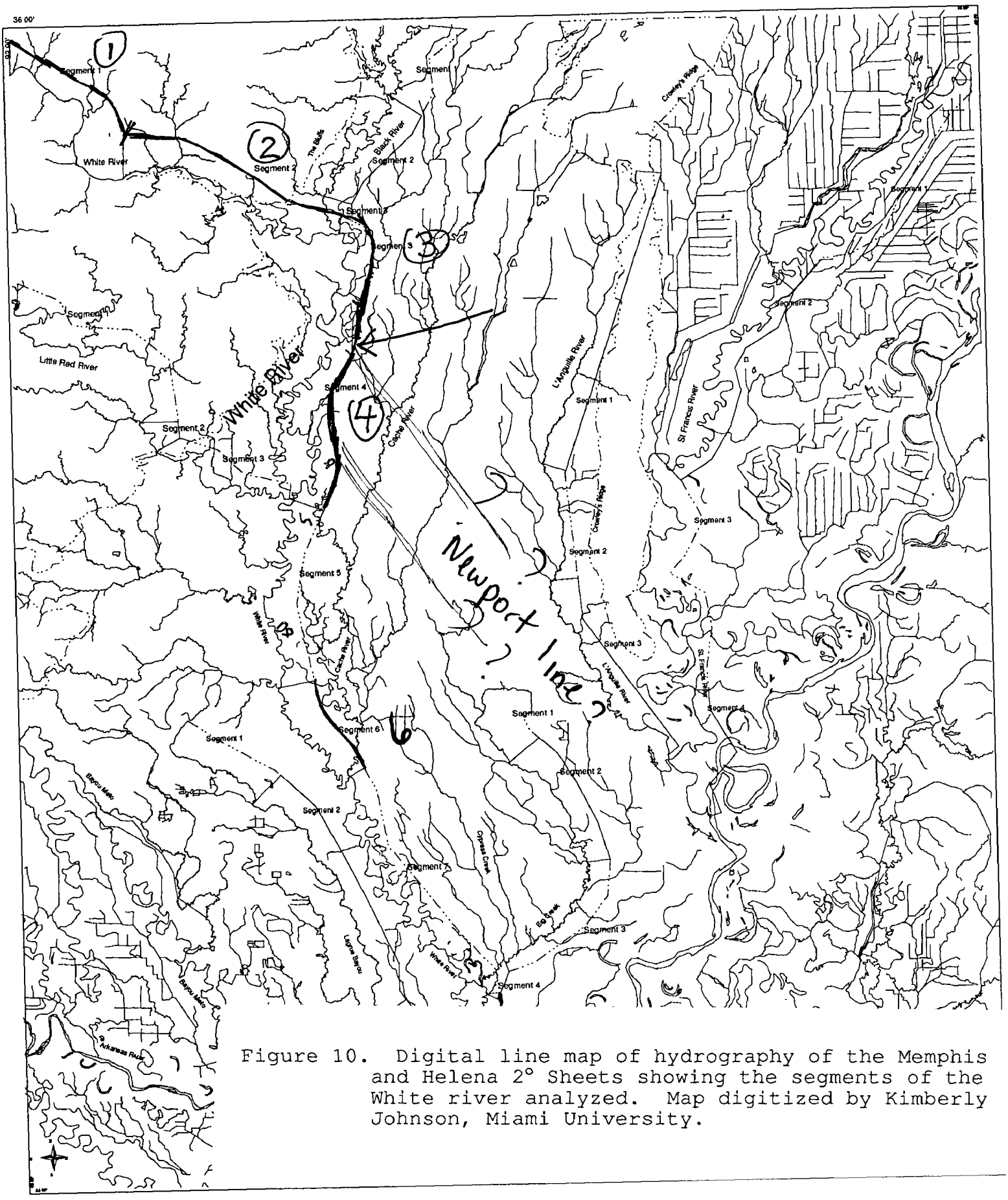

Figure 10. Digital line map of hydrography of the Memphis and Helena 2° Sheets showing the segments of the White river analyzed. Map digitized by Kimberly Johnson, Miami University.

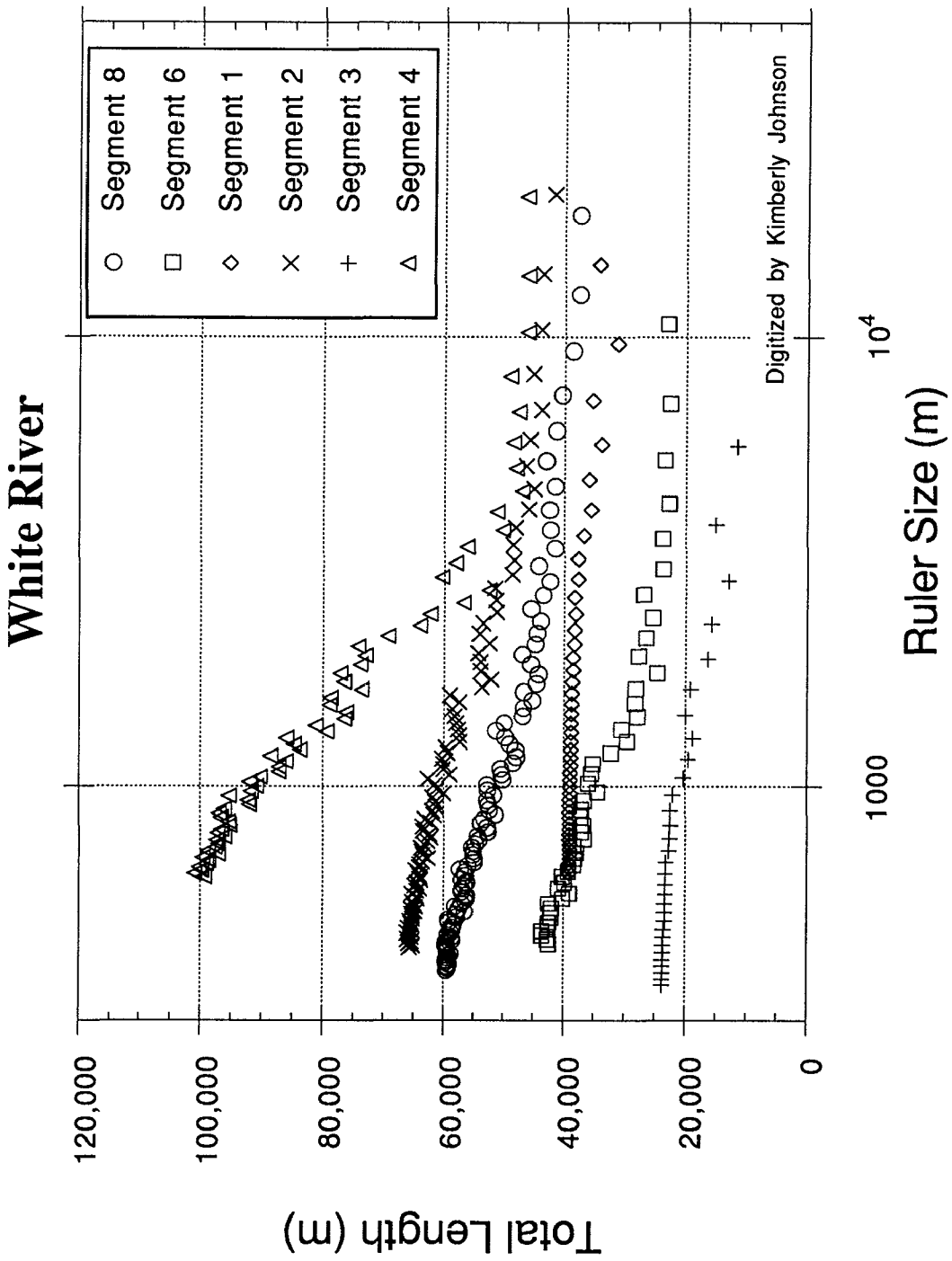

Figure 11. Richardson analysis of the meandering characteristics of the White River. Data that have little change with ruler size are relatively straight features. Steeply sloping patterns indicate rapid increase in sinuosity at that particular scale. Stream reach 4 has the steepest slope and also crosses the Newport line.

ANALYSIS OF PLANFORMS

River planforms that meander can adjust to active deformation of their channels by altering the sinuosity of the channel. Changes in sinuosity compensate for changes in channel slope. However a single river may have a variable sinuosity due to non-tectonic factors such as dominant sediment load. The wavelength and scale of their meander bends may provide a deeper insight to distinguishing between tectonic and non-tectonic changes in sinuosity. In any event, the coincidence of river pattern changes with other topographic features should be sought in order to further confirm the nature of the feature.

Richardson analysis is a technique based on the notion of statistical self-similarity which allows one to quantify how a planform is changing in a way more meaningful than simple sinousity. Basically the technique uses a systematically changed scale to calculate a length of an object thereby measuring the scale at which variation occurs (Fig. 9). It essentially describes the scale dependent sinuosity if a river. A useful demonstration is given using the White River, which drains into the Mississippi embayment from the west (Fig. 10). The White River also crosses the Newport line. Figure 11 is a summary of its scale dependent sinuosity. Note how one reach of the White River in particular is very different from the rest in that the rate of its increase in sinousity with decreasing scale is very rapid (Fig. 11). This reach is the reach which crosses the Newport line. Similar analyses are underway for numerous other meandering streams in the area.

REFERENCE

Russ, D.P., 1982, Style and significance of surface deformation in the vicinity of New Madrid, Missouri: in Makeown, F.A. and Pakiser, L.C., editors, Investigations of the New Madrid, Missouri, earthquake region, U. S. Geological Survey, Professional Paper 1236, p. 95-114.

REPORTS

Mayer, Larry, Tectonic geomorphology of the New Madrid seismic zone based on imaging of digital topographic data: Geological Society of America Abstracts with Programs, submitted for publication in 1993.

Mayer, Larry, Topographic Analysis for tectonic geomorphology using digital image processing of elevation data from the Mississippi Embayment and adjacent areas: Geological Society of America Abstracts with Programs, submitted for publication in 1993.

Mayer, Larry, Rates and scales of topographic change in response to tectonic perturbations as suggested from computer simulation using DEMs: Third International Conference on Geomorphology, submitted for publication in 1993.

Johnson, K.A., and Mayer, Larry, Analysis of river planforms in the New Madrid region and possible relations to tectonic warping across the loess bluffs and within the meander belt of the Mississippi river: Geological Society of America Abstracts with Programs, submitted for publication in 1993.

Church, Amy, and Mayer, Larry, Morphologic characteristics of upland bluffs east and west of Crowley's ridge in the New Madrid area: Geological Society of America Abstracts with Programs, submitted for publication in 1993.

Assessing the Paleoseismic Activity of the Brigham City Segment, Wasatch Fault Zone, Utah; Probable Site of the Next Major Earthquake on the Wasatch Front?

Award No. 1434-92-G-2205

James P. McCalpin
Department of Geology
Utah State University
Logan, UT 84322-4505
303-586-3217

Steven L. Forman
Byrd Polar Research Institute
The University of Ohio
1090 Carmack Rd.
Columbus, OH 43210-1002
614-292-6085

Investigations

During August, 1992, we excavated 9 backhoe trenches across multiple fault scarps of the Wasatch fault zone (WFZ) at Brigham City, Utah. These seven parallel scarps (Fig. 1) displace the surface of a delta built into Lake Bonneville during the occupation of the Provo Shoreline (ca. 13-14 ka). The scarps potentially record all paleoseismic events of the WFZ in the last 13-14 ka, a time span which is twice as long as that covered by current paleoseismic evidence (Personius, 1991). The Brigham City segment is thought to be unique for two reasons: 1) it has the longest elapsed time since surface rupture of any of the 5 Holocene segments of the WFZ, and 2) paleoseismic events may have occurred in closely-spaced pairs separated by longer time intervals (Nishenko and Schwartz, 1990). The objective of trenching is to date at least 6-10 paleoearthquakes in the last 13-14 ka, refine recurrence intervals, and confirm if paired clustering has occurred more than once.

Methods

Four trenches (1-4 in Fig. 1) were excavated on July 1, 1992. These trenches were logged between July 1 and July 15, but little datable material was found. Accordingly, a second round of trenching occurred on July 16, when trenches 5 through 9 (Fig. 1) were excavated. Total trench length is now about 900 feet. Four radiocarbon samples were collected during logging of the second set of trenches from July 29-Aug. 7, 1992. These numerical ages help to constrain the ages of faulting events on several of the seven scarps (Fig. 2).

Because organic material was scarce, but dating events is critical to project goals, we are using two other dating methods to control event timing. First, detailed soil profile sampling was performed by Dr. Margaret Berry, Southern Illinois University, to

characterize the soil catena relationships on fault scarps and fluvial scarps. Comparison of soil development on fault scarps with soils on dated stable geomorphic surfaces may yield a first approximation of the ages of latest faulting. Second, eight samples for luminescence dating were collected from four trenches on Sept. 25-26, 1992. Some of these samples may be subjected to optically-stimulated luminescence (OSL) dating if thermoluminescence (TL) dating reveals a large component of relict signal.

Results

1) Scarps C and H are not underlain by faults. Trenches 1 and 8 on scarp C both reveal unfaulted deltaic topset beds extending across the scarp, overlain by a thick, monolithic colluvial wedge. The soil developed on this wedge is somewhat better developed than the soil on the Provo delta surface, indicating that the scarp was formed at about the same time as the delta. Personius (pers. comm., 1992) suggests that this scarp may be a fluvial scarp, which formed by lateral ersoion when the delta surface was active. A similar fluvial scarp exists on the delta about 1 km south (Personius, 1990).

Scarp H, at least at the location of trench 6, was formed about 13,010$\pm$460 yr B.P. Immediately afterward it was buried by a landslide (cls on Fig. 1) that fell onto the delta surface. The landslide is clearly not faulted in the trench, nor do the underlying lacustrine sediments appear faulted. Personius (Pers. comm., 1992) speculates that scarp H is a fluvial scarp cut by a small tributary to the NE of trench 6, back when the delta surface was active.

2) The latest event dated in trench 5 (ca. 3420$\pm$60 yr B.P.) is probably the same (latest) event dated by Personius (1991) at 3600$\pm$500 yr B.P. at a site several km to the north. The penultimate event dated by Personius (at 4700$\pm$500 yr B.P.) has not been identified in our trenches.

3) Gravelly delta surfaces are sterile environments in regard to datable carbon. So far, datable carbon has been found only in trenches where a younger unit (such as landslide or alluvial fan) overlies the deltaic gravels. In addition, thick loesses amenable to luminescence dating are absent, even in grabens. Several trenches expose thin (5-10 cm) buried Av soil horizons that are somewhat enriched in silt. These soils are the best targets found so far for luminescence dating (see F numbers on Fig. 2).

Future Work

We anticipate that a third round of trenching may be necessary in spring, 1993. Three target sites have already been identified. The existing trenches will be left open (winter, 1993) until the first round of luminescence samples have been dated.

References

Personius, S.F., 1990, Surficial geologic map of the Brigham City segment and adjacent parts of the Weber and Collinston segments, Wasatch fault zone, Box Elder and Weber Counties, Utah: U.S. Geological Survey Miscellaneous Investigations Map I-1979, scale 1:50,000, with inset at 1:10,000.

Personius, S.F., 1991, Paleoseismic analysis of the Wasatch fault zone at the Brigham City trench site, Brigham City, Utah and Pole Patch trench site, Pleasant View, Utah: Paleoseismology of Utah, vol. 2, Utah Geological and Mineral Survey, Special Studies 76, Salt Lake City, Utah, 39 p.

Nishenko, S.P. and Schwartz, D.P., 1990, Preliminary estimates of large earthquake probabilities along the Wasatch fault zone, Utah: EOS, AGU Transactions, v.71, no 43, p.1448.

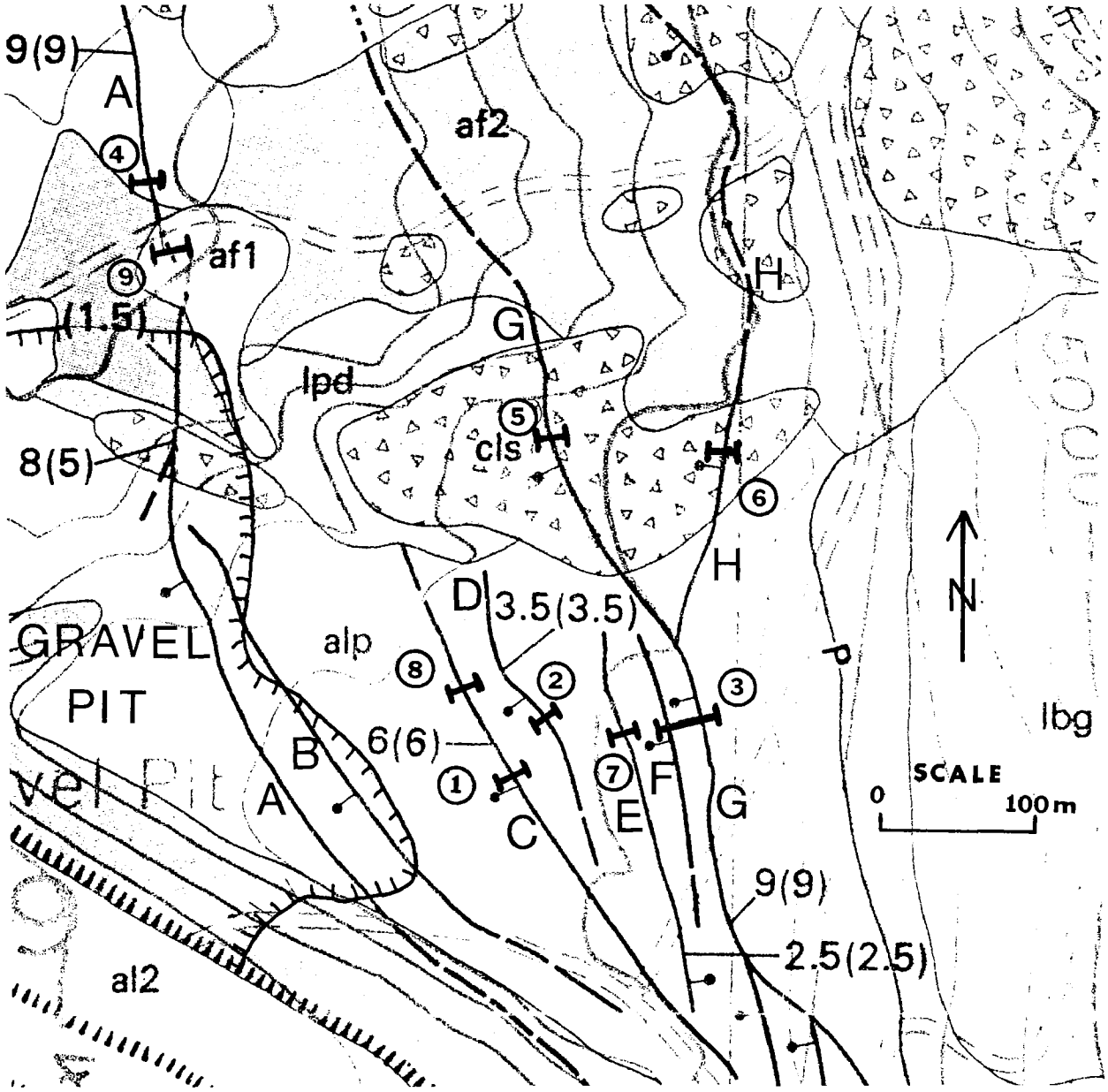

Fig. 1. Surficial geologic map of the Brigham City trench site (from Personius, 1990). Fault scarps are shown by heavy lines, with ball on downthrown side. Map units: alp, Provo topset deltaic beds;lpd, Provo foreset deltaic beds; cls, landslide; af2, older alluvial fan; af1, younger alluvial fan; al2, Holocene alluvium. Large numbers show scarp height, with surface offset in parentheses (both in m). Scarps are lettered from W to E. Trenches are shown by heavy bars, labelled by circled numbers.

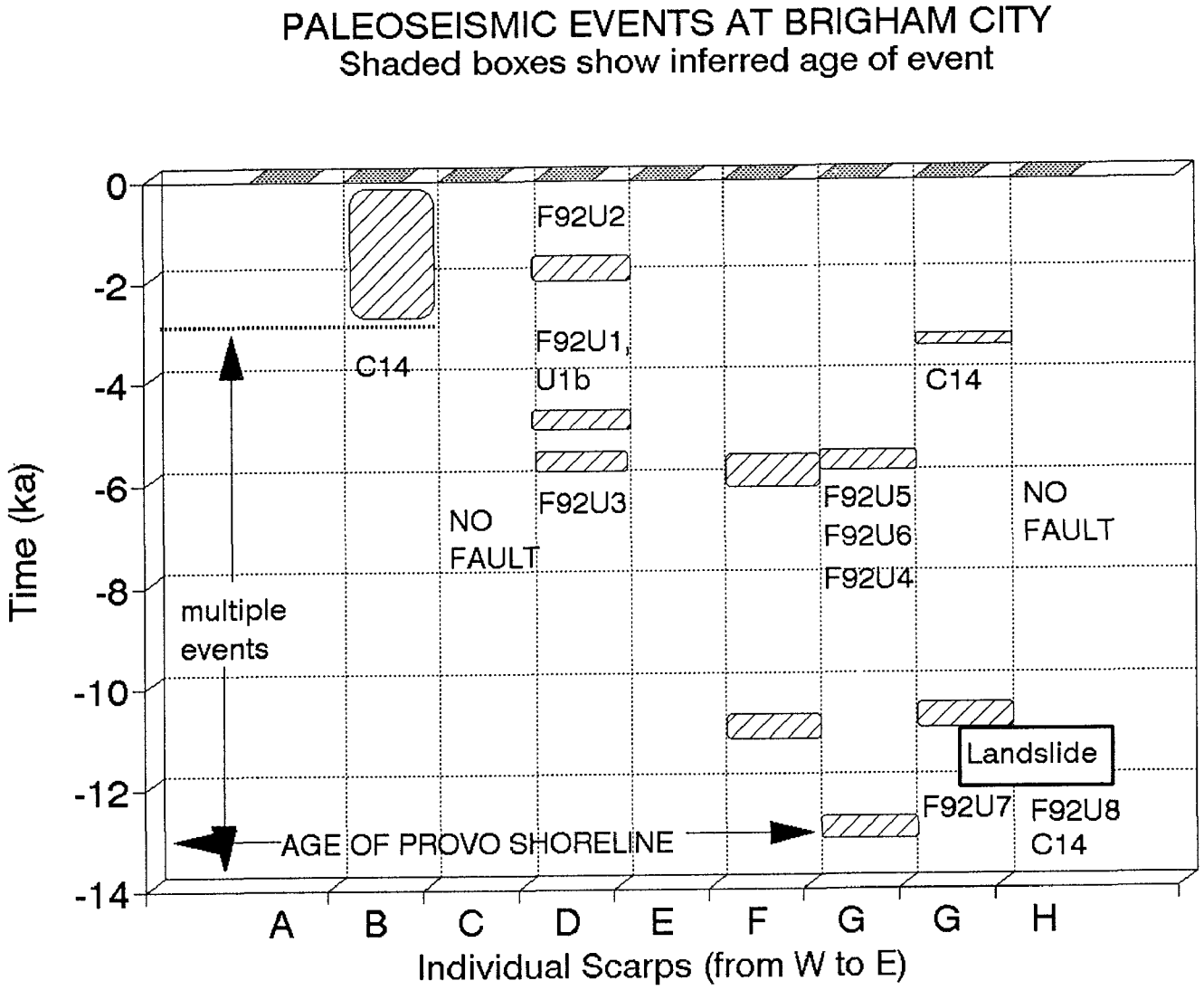

Fig. 2. Time/space diagram showing inferred paleoseismic events at the Brigham City trench site. C14 indicates position of dated radiocarbon sample. The overall time position of events is mainly inferred from degree of soil development, assuming: 1) a Bt horizon takes roughly 5 ka to form, and 2) a Bw horizon takes at least 2 ka to form. Numbers such as F92U2 show inferred age range of thermoluminescence samples that have not yet been dated. This diagram will be updated as TL samples are analyzed during winter, 1993.

ACTIVE MARGIN TECTONICS, PACIFIC NORTHWEST REGION

9910-04492

P. A. McCrory

Branch of Engineering Seismology and Geology
U. S. Geological Survey
345 Middlefield Road, MS 977
Menlo Park, California 94025
(415) 329-5677

Investigations

This research project addresses the problem of how the Cascadia subduction margin of the Pacific Northwest responds tectonically to varying rates of convergence with the objective of understanding whether a history of convergence, if coupled with a history of regional tectonism, can partially explain the timing, style, and rates of regional deformation. This problem can be approached both spatially and temporally in the Pacific Northwest as active convergence rates vary along the margin. Current research utilizes the technique of geohistory modeling to discern the record of tectonism in late Cenozoic rocks and sediments along the southern Washington margin, along with more traditional geologic techniques to quantify fault movement and tilting of strata.

Although current seismic activity is low along the Cascadia margin, geodetic data indicates interseismic strain accumulation reflecting compression between the Juan de Fuca and North American plates and the Holocene paleoseismic record in the Pacific Northwest reveals cycles of episodic large earthquakes and coseismic downwarping of coastal marshes. Upper Cenozoic rocks and sediments in this region also record a history of intense and episodic tectonism that reflects convergence between the Juan de Fuca and North American plates. Field investigations in coastal Washington have identified several sites with geomorphic and stratigraphic evidence of youthful folding, faulting, uplift or subsidence. Strata at these sites are being examined in detail to quantify recent tectonic deformation.

Field investigations during FY 92 included completion of stratigraphic description and sampling of the Cape Elizabeth section of the Quinault Formation; sampling and description of Quaternary deposits adjacent to the Raft River; reconnaissance of Quaternary deposits exposed in the seacliffs from Iron Springs to Pacific Beach and from Queets River to Kalaloch.

Lab investigations during FY 92 included microscope analysis of microfossils collected from Quinault Formation and tephra analysis of tuffaceous clasts from faulted Quaternary deposit near Raft River.

Results

1. The sedimentary sequence exposed at Cape Elizabeth displays evidence of syndepositional deformation such as slumping, liquifaction, and sand venting which may be related to paleoseismic shaking. Contacts between the Quinault Formation and the underlying and intruding accretionary prism rocks (Hoh Formation) indicate diapirism post-dated deposition of the Quinault Formation, continued into the late Quaternary and may be ongoing.

2. Investigated an exposure of severely tilted Quaternary strata that may be related to paleoliquifaction features documented along the Copalis River.

3. Continued analyses of sedimentary rock samples collected in southern Washington in FY89 for age and uplift data.

4. Rock samples collected in FY 91 have been processed for microfossil analyses.

Reports

McCrory, P. A., 1992, Quaternary deformation along the Washington margin of the Cascadia subduction zone: Evidence from the Raft River area: GSA Abstracts with Programs, Cordilleran Section, v. 24, p. 69.

McCrory, P. A., 1992 , Isopach map of upper Quaternary deposits in the Gulf of Catalina area, California: U. S. Geological Survey MF-2212 Map Series, scale 1:250,000.

SEISMIC WAVE MONITORING AT PARKFIELD, CALIFORNIA

14-08-0001-G1703

T.V. McEvilly, R. Clymer, E. Karageorgi, M. Antolik, R. Nadeau, P. Johnson
Seismographic Station, University of California, Berkeley, CA 94720
and
Earth Science Div, Lawrence Berkeley Lab, Berkeley, CA 94720

INTRODUCTION

Two programs of seismic wave analysis continue: Earthquake recording with the high-resolution seismic network (HRSN), begun in December, 1986, and controlled-source monitoring with HRSN begun in June, 1987.

The HRSN (Figure 1) consists of ten, 3-component, borehole seismometers surrounding the 1966 Parkfield epicenter. Data-acquisition features digital telemetry with 125-Hz bandwidth and 16-bit resolution, and can operate in external-trigger (i.e., controlled-source) or event-trigger (earthquake) modes. Five low-gain recorders with similar parameters, on loan from the IRIS PASSCAL instrument pool, are also installed. Network characteristics are summarized in Karageorgi *et al.*, 1992.

INVESTIGATIONS

1) Earthquakes.

Local microearthquakes of magnitude about -0.5 to about +1.8 are routinely recorded on scale by the high-gain, telemetered system, extended to near M5 at the five low-gain sites. (The M4.7 event on October 20, 1992 within the nucleation zone recorded on-scale at three of the five low-gain sites, and clipped only the S-wave at the other two.) A 3-D velocity model (Michelini and McEvilly, 1991) and a high-precision relative hypocenter location procedure for clustered events with similar waveforms have been developed for use in high-resolution analyses of local earthquakes. Clustered events are being studied for evidence of temporal changes in fault zone processes and properties, including anisotropy. Studies are underway in source scaling, failure processes, fault zone structure, and material properties within the Parkfield nucleation zone. All of these parameters plus the vibrator-generated wavefields are subject to analyses for temporal changes that may be premonitory to the expected M6 event.

With the October, 1992 A-level alert, we increased the coverage of the HRSN with installation of seven temporary surface sites using 3-component recorders. Five of the sites are to the north of the present array, and two between the EAD and GHI sites at the south end. These recorders were obtained under the IRIS RAMP program, and will operate into January, 1993.

2) Controlled-source monitoring with HRSN.

From June, 1987 through October, 1992, the HRSN has been illuminated 42 times with S-waves of three polarizations at (presently) seven source positions throughout the study zone, using a shear-wave Vibroseis source, in an on-going monitoring program (Figure 1). The resulting data are searched for temporal variations of wave propagation characteristics throughout the nucleation zone. Data reduction is accomplished at the Center for Computational Seismology (CCS) in the Earth Sciences Division of the Lawrence Berkeley Laboratory (LBL). This work was reported by Karageorgi, *et al.*, 1992.

DATA COLLECTED

Earthquake data are archived as IEEE-format binary files on magnetic tape with simple headers. These will soon be converted to a standard SEGY format. We have archived some 1500 local events.

Six vibrator data sets have been collected and the data reduced

in this project year. Data after routine processing (edit, stack, correlation, gather by source site) are archived in SEGY format on magnetic tape.

RESULTS

Earthquake Studies:

Event analysis: Local Parkfield events are now picked and located with the 3-D model within a month of occurrence.

Clustering analysis: When located with high-resolution methods, more than half of the 1500 local microearthquakes recorded to date are seen to have occurred as members of some 80 clusters of 1-12 highly similar sources on small patches typically about 100m in extent throughout the 30-km Parkfield zone, in both creeping and locked sections. The total area of all the clusters constitutes only a small fraction of the fault zone approaching failure at Parkfield. Many clusters span the five years of data collection. Waveforms are remarkably coherent to frequencies of 50-100 Hz. This coherency provides the opportunity for precise relative timing of P and S arrivals among the cluster members, based on the slope of the cross-spectral phase. Timing precision to better than 0.5 msec yields relative hypocenter locations of cluster members uncertain apparently to about 10m. The archived clusters are presently the basis for various on-going studies of fault zone processes. A paper on the clustering analysis has been submitted (Nadeau, *et al.*, 1992).

Characteristics of seismicity: To first order, the pattern of earthquake locations has remained constant throughout network operation, although the rates of activity change, apparently in concert throughout the region. Parkfield earthquakes yield a b-value of about 0.9 that has not changed significantly during operation of the network.

Magnitude scaling and source parameter variations: The distinct clusters or 'nests' of microearthquakes, typically 100 m or less in dimensions, recorded with high bandwidth, provide a natural laboratory for investigating the scaling of source parameters with magnitude, and the details of the slip process within the fault zone. We are reviewing earthquake mechanisms at Parkfield for evidence of a non-double-couple (tensional or reverse-slip) component. A study earlier this year of S-to-P spectral ratios below the corner frequency gave evidence for non-shear rupture in some (but not all) events, which we interpret to be indicative of a significant component of tensional failure. We have begun to map the source mechanism character and its variation throughout the fault zone.

The October, 1992 sequence of some 100 events larger than about M=-0.5 involved much of the fault zone at Parkfield (Figures 2 and 6), but the energy release was mainly concentrated along a 3 km long segment of the fault surface stretching southeastward at 8 km depth from the 1966 hypocenter into the expected M6 rupture zone. This segment had been inactive throughout the 5 years of monitoring with the HRSN. The SE end of the 3 km segment was particularly energetic, containing a nest of 12 events that included the M4.7 shock ($0.5<M<4.7$). Two other large events (M3.9 and 3.3) fell on the same trend halfway between the SE nest and the 1966 hypocenter. The sequence clearly appears to represent a failed attempt to rupture the M6 asperity SE of the nucleation point at the 1966 focus.

The SE nest of events provides an excellent data set for source scaling studies and for close scrutiny of the waveforms for possible effects of changes in material properties or source mechanisms associated with the M4.7 occurrence, since there are small events in the nest before and after it. The tight clustering of the events eliminates the problem of differing path effects among the cluster members. Preliminary results show:

SCALING: The M4.7 event is clearly and substantially different in source dimension and time function from all the others, which are very similar over the magnitude range -0.5 to 4.0i (Figure 3). Corner frequency increases with decreasing magnitude (around 40Hz and 100Hz for M~1.8 and M~0.5-1.0, respectively (Figure 4).

TEMPORAL CHANGES: There are no obvious differences between foreshocks and aftershocks of the M4.7 event at the M1.5 - 1.9 range.

MECHANISM: An initial computation of low-frequency S/P spectral ratios suggests that the foreshock selected (M1.5) shows no evidence of non-shear source.

Assessment of temporal changes in wafeform polarizations: The clusters, each with nearly identical repeating waveforms and locations, distributed throughout the fault zone, are being used to monitor the nucleation zone for precursory changes in material properties. Most effort to date has gone into study of the stability of waveform polarization applying a vector linearity trace formalism to a cluster about 2 km NW of the 1966 hypocenter at about 10 km depth. It was found that a suite of small events within the cluster (M 0.5) produced apparent temporal variability of polarization on certain paths due to higher attenuation (and therefore lower S/N) on the NE side of the fault. Choice of window lengths and consideration of nodal plane geometry did not explain the variations. However, choice of more energetic events (M 1.5) produces apparent stability of waveforms over time on the several paths analyzed. Preliminary results also indicate that travel times are stable.

There appears to be evidence of anisotropy (S-wave splitting) in the trace polarization displays, with the fast direction parallel to the fault zone, in agreement with results obtained in vibrator studies using HRSN (Karageorgi, *et al.*, 1992) and the Varian Well Vertical Array (Daley and McEvilly, 1991). Further studies will attempt to characterize the spacial extent and consistency of the anisotropy with clustered and unclustered events, and search for temporal variations.

Controlled-Source Studies.

The final working data sets for analysis are "time gathers": one source into one receiver gathered across calendar time, producing 720 files, each containing, at present, up to 42 similar traces. The time gathers are then examined for variations in waveform parameters.

Most displays show only seasonal variations in various properties (travel time, amplitude, spectral properties). Seasonal variations are due to very near-surface moisture changes under the vibrator (Clymer and McEvilly, 1981).

Karageorgi, *et al.*, 1992 describes the analysis techniques and their application to a subset of paths through the expected nucleation zone, and illustrates the types of anomalies found. In the past year, we have extended the analysis to the entire dataset in order to better characterize the prominent travel-time anomaly in the vicinity of source site 2, south-west of the 1966 epicenter, that began in mid 1988, and continues through October, 1992 (Figure 5 and 6). No significant change was found in the anomaly with special surveys run during the October, 1992 M4.7 sequence.

References

Clymer, R.W., and T.V. McEvilly, 1981. Travel time monitoring with VIBROSEIS, *Bull. Seism. Soc. Amer*, 71, 1902-1927.

Publications

Daley, T.M. and T.V. McEvilly, Shear wave anisotropy in the Parkfield Varian Well VSP, *Bull. Seism. Soc. Am.*, **80**, 857-869, 1990.

Michelini, A. and T.V. McEvilly, Seismological studies at Parkfield: I. Simultaneous inversion for velocity structure and hypocenters using B-splines parameterization, *Bull. Seism. Soc. Am.*, **81**, 524-552, 1991.

Karageorgi, E., R. Clymer and T.V. McEvilly, Seismological studies at Parkfield. II. Search for temporal variations in wave propagation using Vibroseis, *Bull. Seism. Soc. Am.*, **82**, 1388-1415, 1992.

Foxall, W., A. Michelini and T.V. McEvilly, Three-dimensional velocity structure and rupture characteristics of the Santa Cruz mountain zone, in *The Loma Prieta, California, Earthquake of October 17, 1989*, USGS Open-file Rept. (submitted), 1992.

Submitted:
Nadeau, R., M. Antolik, P. Johnson, W. Foxall and T.V. McEvilly, Seismological studies at Parkfield. III. Microearthquake clusters in the study of fault-zone dynamics

Ph. D. Theses

Michelini, A., Fault Zone Structure Determined Through the Analysis of Earthquake Arrival Times, 1991.

Foxall, W., Fault-Zone Heterogene Slip and Rupture Models of the San Andreas Fault Zone Based upon Three-Dimensional Earthquake Tomography, 1992

Papers Presented on Parkfield Research - 1992

Seismological Society of America 1992 Annual Meeting, Santa Fe, New Mexico, April 13-15, 1992.

T.V. McEvilly, High-frequency observations of microearthquakes in active fault zones

T. M. Daley and T. V. McEvilly, Joint VSP and microearthquake tomography for fault zone structure

R. M. Nadeau, M. Antolik and T. V. McEvilly, A search for temporal changes in travel times and polarization at Parkfield using earthquake sources

P. A. Johnson, M. Antolik, W. A. Peppin, W. Foxall and T. V. McEvilly, Structure and rupture processes of the fault zone at Parkfield from the spectra of microearthquakes

E. D. Karageorgi, R. W. Clymer and T. V. McEvilly, Shear-Wave propagation in the San Andreas fault zone Monitored with Vibroseis.

1992 Fall AGU, San Francisco, 07-11 Dec.

R. Nadeau and T.V. McEvilly, An Assessment of Temporal Changes in P- and S-Coda Polarizations at Parkfield Using Microearthquake Sources.

M. Antolik and T.V. McEvilly, An Analysis of the 1987-92 Parkfield Seismicity Based on Data From the High-Resolution Borehole Network.

P.A. Johnson and T.V. McEvilly, Magnitude Scaling and Source Parameter Variations of Microearthquakes at Parkfield.

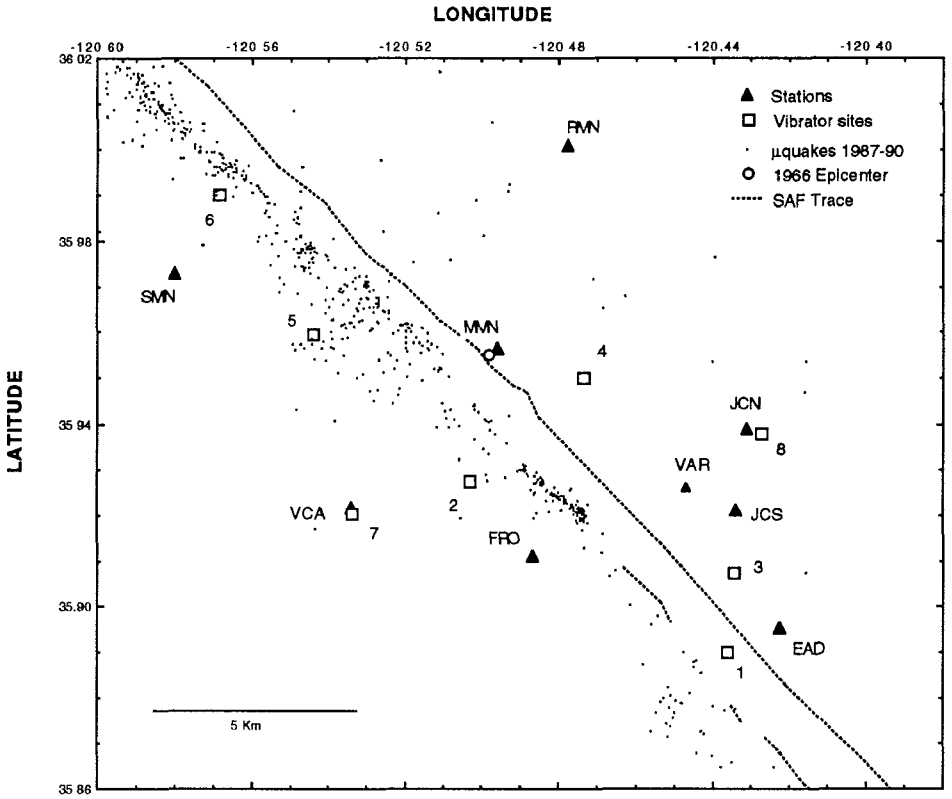

Figure 1. Location map showing the borehole seismometer network, vibrator positions (VPs) and microearthquake seismicity for 1987-1990.

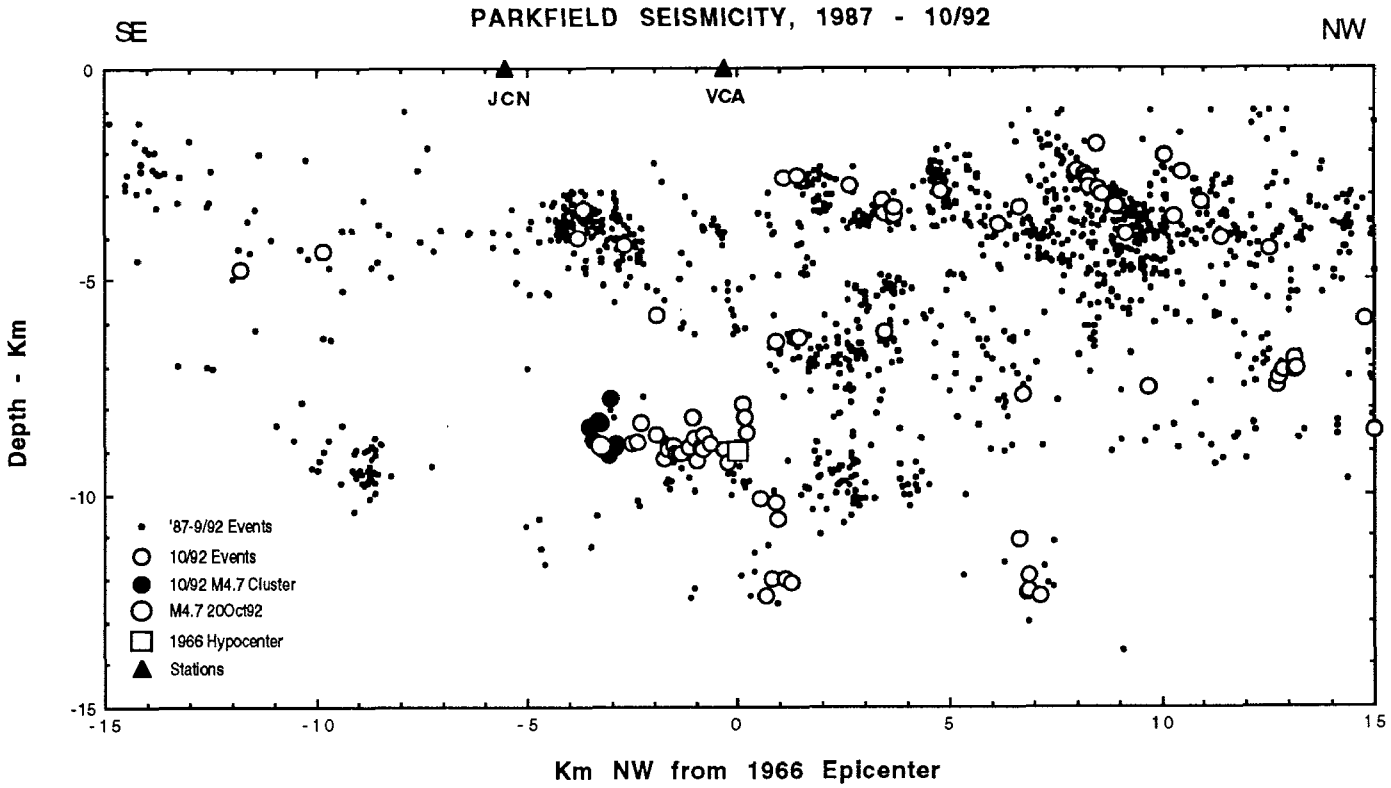

Figure 2. Cross section with seismicity along the San Andreas Fault, showing the October, 1992 earthquake sequence.

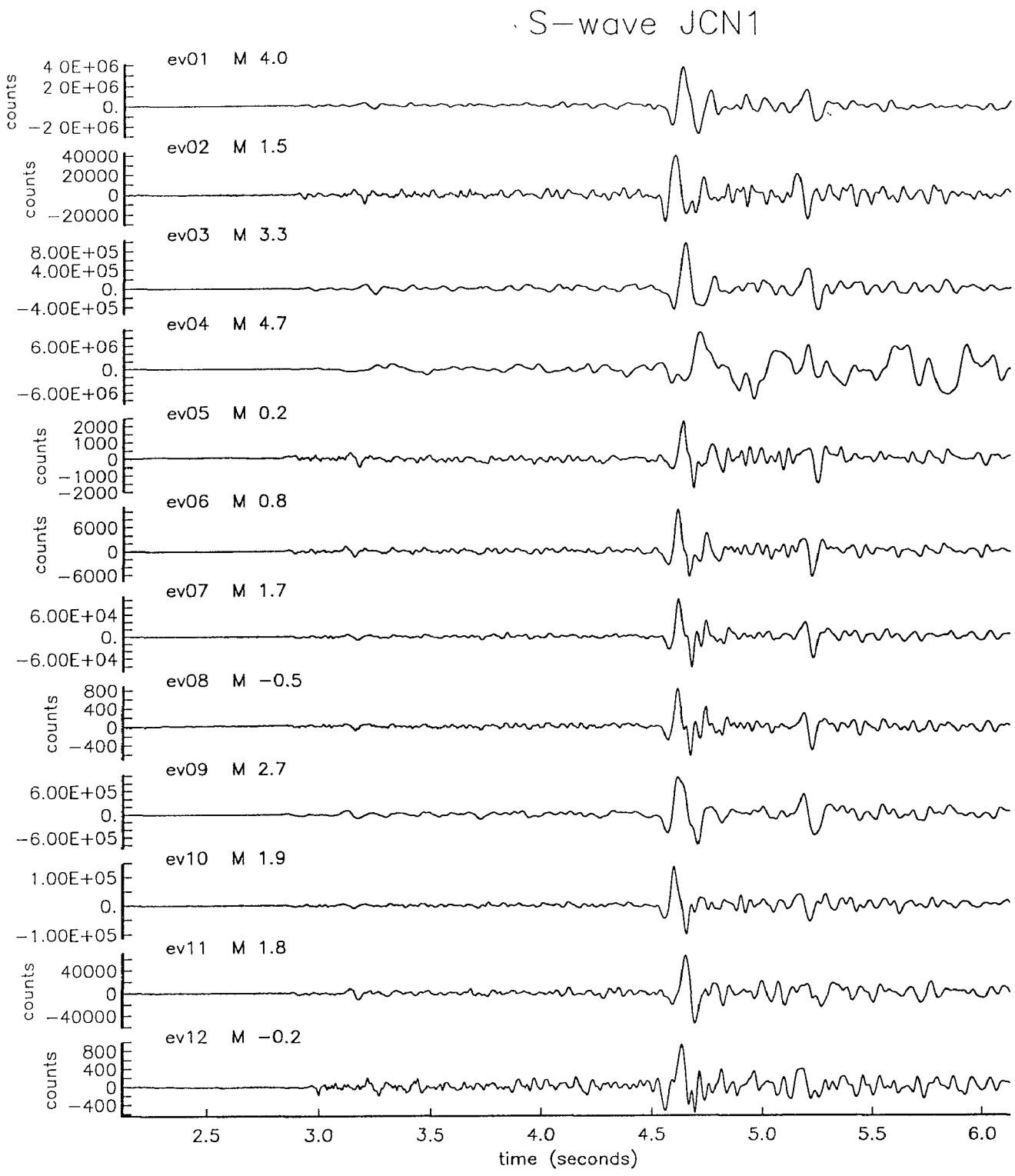

Figure 3. Set of nested events at the M4.7 focus in the October 1992 sequence, shown in chronological order.

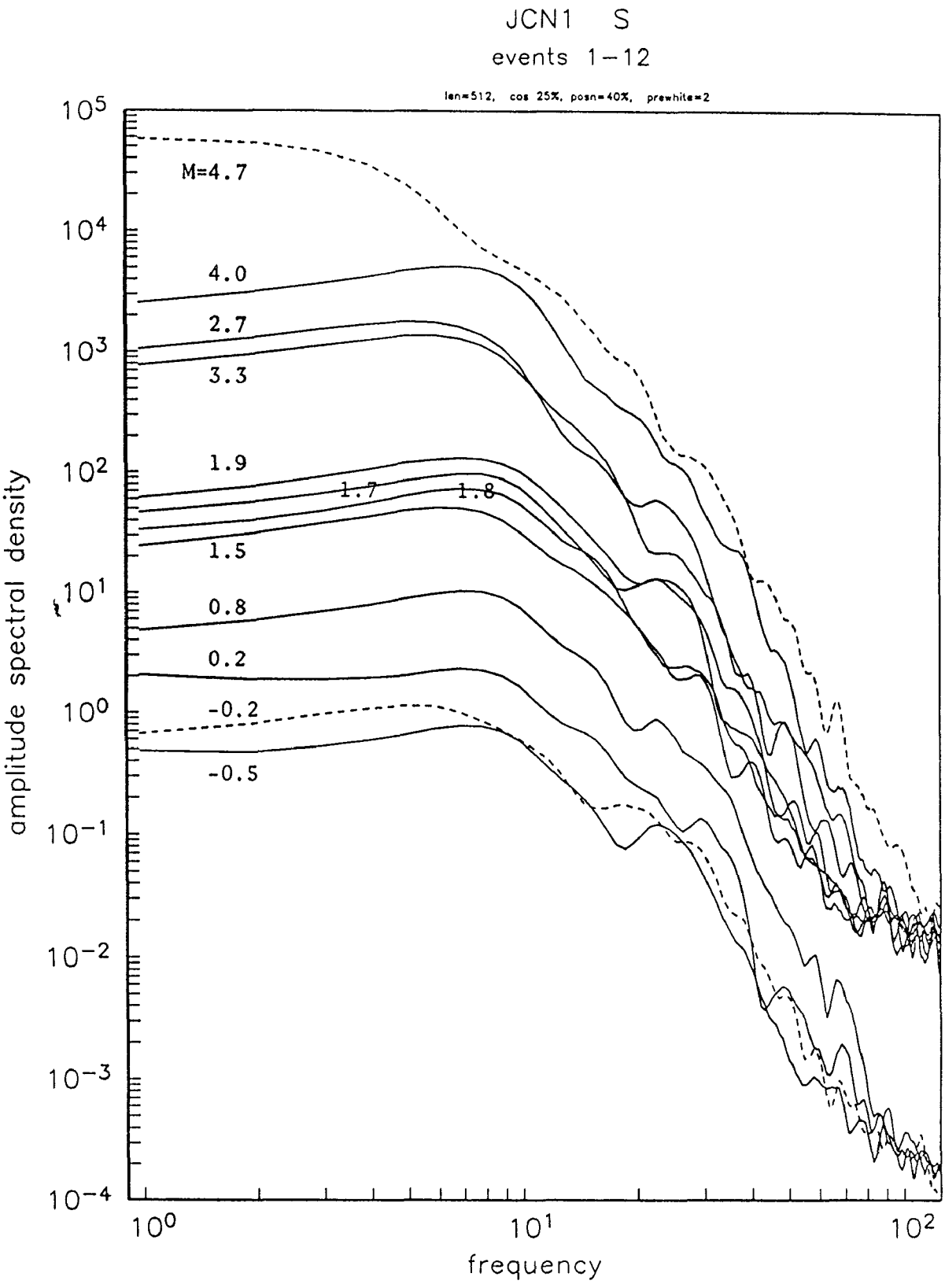

Figure 4. S-wave spectra for suite of events in the October 1992 M4.7 sequence.

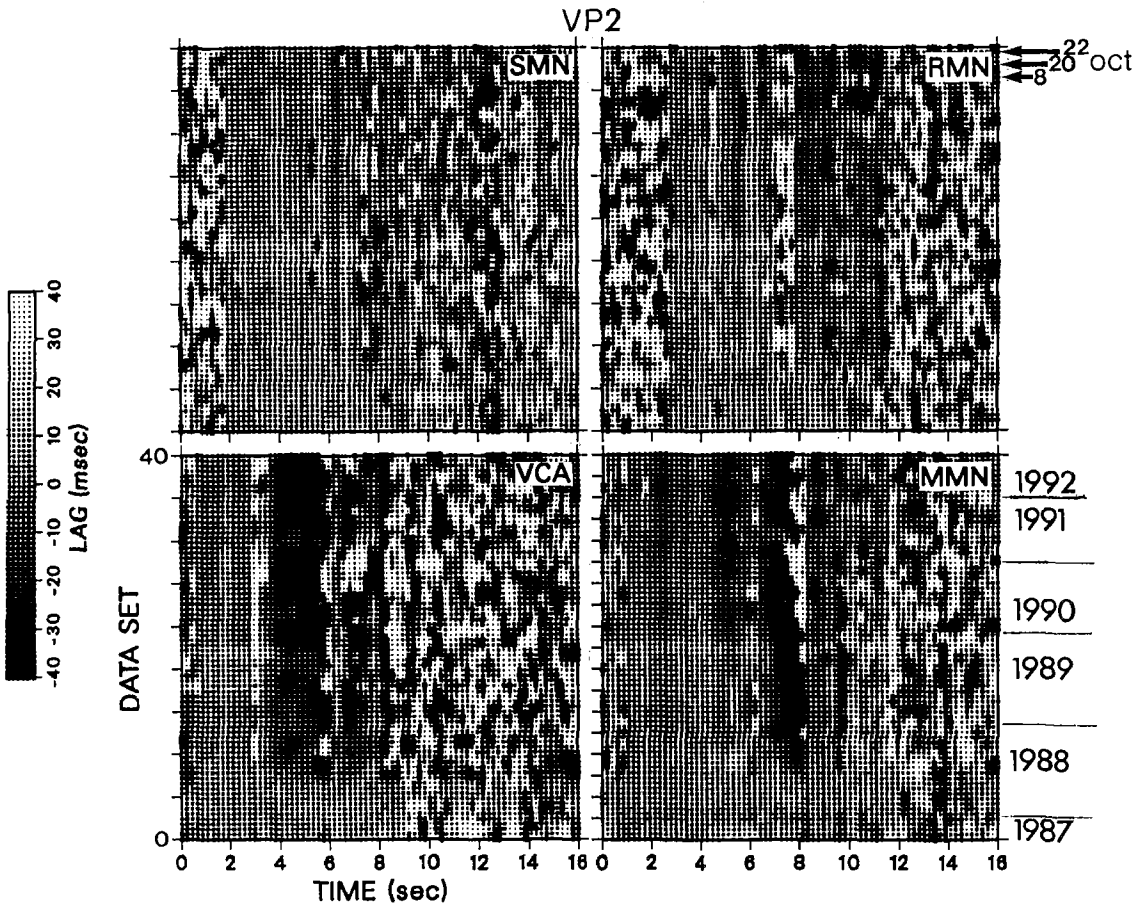

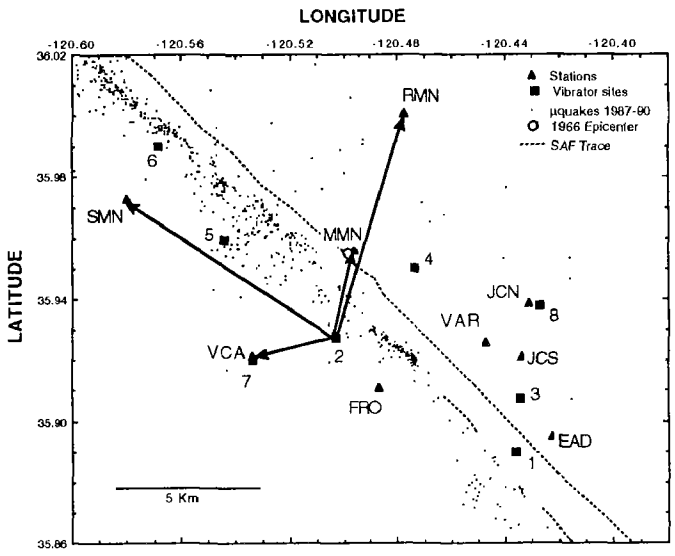

Figure 5. Travel-time variations relative to a reference trace (arbitrarily chosen, here in mid 1988) measured across the repeated 16-sec seismograms in a moving window for several paths from vibrator site two.

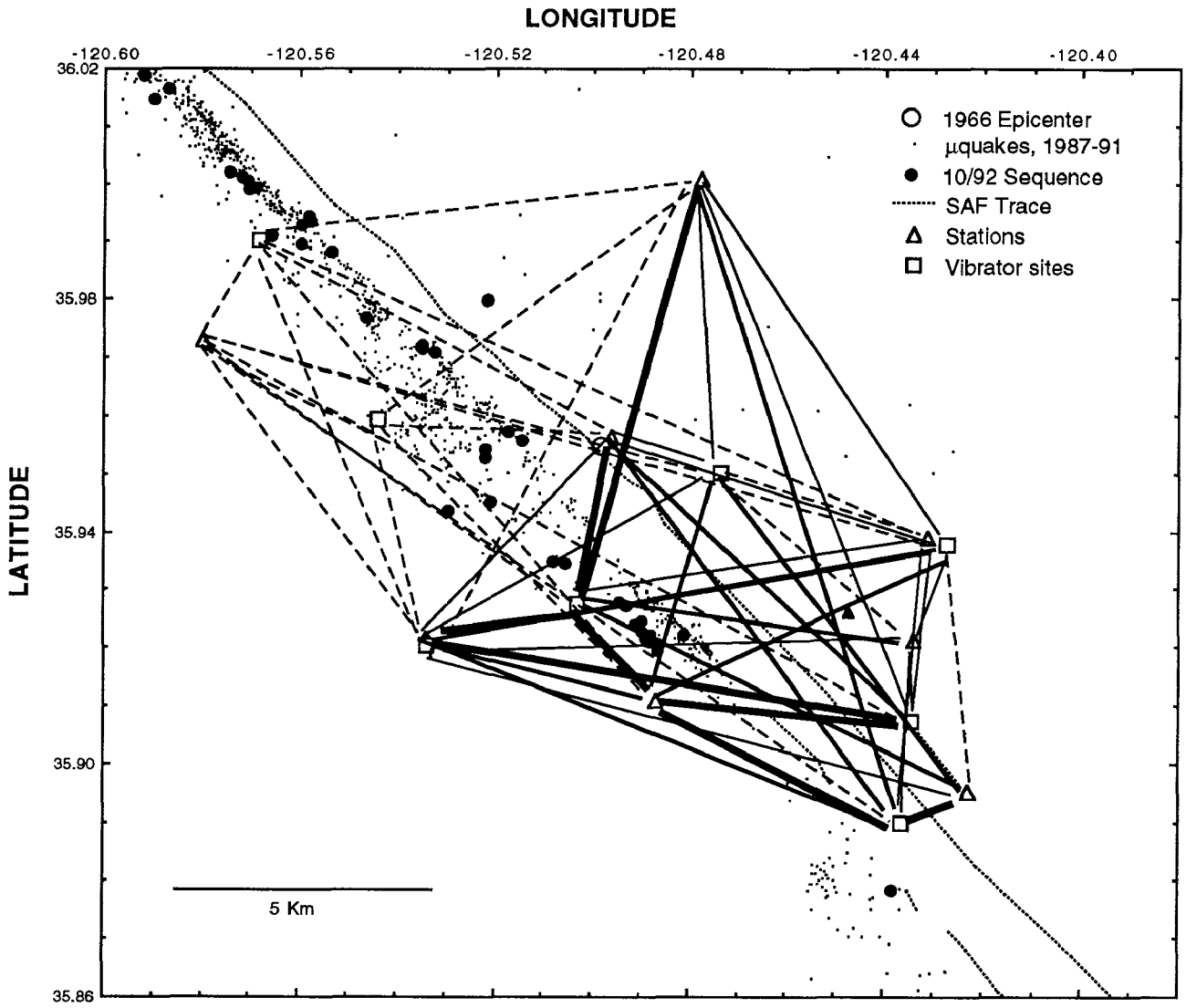

Figure 6. Paths showing velocity anomaly. Heavy solid lines show paths with strong travel-time advance of later phases (concentrated primarily SE of Middle Mountain); dashed paths are stable, light solid paths show marginal indication of anomaly.

INDEX 1

INDEX ALPHABETIZED BY PRINCIPAL INVESTIGATOR

INDEX 2

INDEX ALPHABETIZED BY INSTITUTION

U.S. Geological Survey	Machette, M. N.	458
U.S. Geological Survey	McCrory, P. A.	490
U.S. Geological Survey	McGarr, A.	880
U.S. Geological Survey	Michael, A.	518
U.S. Geological Survey	Mooney, W. D.	528
U.S. Geological Survey	Mori, J.	534
U.S. Geological Survey	Mortensen, C. E.	544
U.S. Geological Survey	Mueller, C. S.	882
U.S. Geological Survey	Mueller, C. S.	951
U.S. Geological Survey	Nelson, A. R.	554
U.S. Geological Survey	Nishenko, S. P.	952
U.S. Geological Survey	Obermeier, S. F.	562
U.S. Geological Survey	Oppenheimer, D. H.	571
U.S. Geological Survey	Park, R. B.	955
U.S. Geological Survey	Person, W. J.	899
U.S. Geological Survey	Plafker, G.	584
U.S. Geological Survey	Ponti, D. J.	588
U.S. Geological Survey	Pratt, T. L.	593
U.S. Geological Survey	Prentice, C.	597
U.S. Geological Survey	Reagor, G.	956
U.S. Geological Survey	Reasenberg, P. A.	599
U.S. Geological Survey	Repetski, J. E.	607
U.S. Geological Survey	Roeloffs, E.	614
U.S. Geological Survey	Rymer, M. J.	959
U.S. Geological Survey	Safak, E.	904
U.S. Geological Survey	Sarna-Wojcicki,A. M.	633
U.S. Geological Survey	Sass, J. H.	906
U.S. Geological Survey	Sato, M.	637
U.S. Geological Survey	Schultz, A.	645
U.S. Geological Survey	Schwartz, D. P.	961
U.S. Geological Survey	Sharp, R. V.	661
U.S. Geological Survey	Shaw, H. R.	663
U.S. Geological Survey	Silverman, S.	671
U.S. Geological Survey	Simpson, R. W.	917
U.S. Geological Survey	Sims, J. D.	682
U.S. Geological Survey	Sipkin, S. A.	686
U.S. Geological Survey	Spudich, P.	920
U.S. Geological Survey	Spudich, P.	922
U.S. Geological Survey	Stein, R. S.	697
U.S. Geological Survey	Stewart, S. W.	700
U.S. Geological Survey	Stuart, W. D.	120
U.S. Geological Survey	Swanson, D. A.	703
U.S. Geological Survey	Tarr, A. L.	967
U.S. Geological Survey	Tinsley, J. C.	711
U.S. Geological Survey	Van Schaack, J.	728
U.S. Geological Survey	Weaver, C. S.	734
U.S. Geological Survey	Wells, R. E.	738
U.S. Geological Survey	Wentworth, C. M.	740
U.S. Geological Survey	Yerkes, R. F.	935
U.S. Geological Survey	Zoback, M.L.	759
Utah Geological Survey	Harty, K. M.	839
Utah Geological Survey	Olig, S. S.	568
Utah State University	McCalpin, J. P.	485

NO REPORTS RECEIVED

Investigators	Institutions
Beck, S.	University of Arizona
Bilham, R.	University of Colorado
Blackwell, R.	U. S. Geological Survey
Bogarert, B.	U. S. Geological Survey
Booker, J.	University of Washington
Carver, G.	Humboldt State University
Christensen, D.	University of Alaska, Fairbanks
Clark, S.	U. S. Geological Survey
Davies, J.	University of Alaska, Fairbanks
Day, S.	San Diego State University
Dieterich, J.	U. S. Geological Survey
Evan, B.	Massachusetts Institute of Technology
Fletcher, J.	U. S. Geological Survey
Gillespie, A.	University of Washington
Goldhaber/Potter	U. S. Geological Survey
Hager, B.	Massachusetts Institute of Technology
Hanks, T.	U. S. Geological Survey
Healy, J.	U. S. Geological Survey
Helliwell, R.	Stanford University
Irwin, P.	U. S. Geological Survey
Jacoby, G.	Lamont-Doherty Geological Observatory
Johnson, D.	Lamont-Doherty Geological Observatory
Julian, B.	U. S. Geological Survey
Keller, E.	University of California, Santa Barbara
Kirby, S.	U. S. Geological Survey
Lasmanis, R.	State of Washington
Lajoie, K.	U. S. Geological Survey
Lerner-Lam, A.	Lamont-Doherty Geological Observatory
Malin, P.	Duke University
Malnar, P.	Massachusetts Institute of Technology
Martin, J.	VA Technology
McGuire,	Risk Engineering, Inc.
Merritts, D.	Franklin/Marshall College
Moses, T.	U. S. Geological Survey
Nye	ADGGS
Pavlis, T.	University of New Orleans
Potter, C.	U. S. Geological Survey
Schuster, G.	University of Utah
Scott, R.	California Institute of Technology
Seeber, L.	Lamont-Doherty Geological Observatory
Segall, P.	U. S. Geological Survey
Sieh, K.	California Institute of Technology
Snavely/Wells	U. S. Geological Survey
Spudich, P.	U. S. Geological Survey
Su, W.	University of Illinois
Sykes, L.	Lamont-Doherty Geological Observatory
Weldon, R.	University of Oregon
Wyss, M	University of Alaska

☆U.S GOVERNMENT PRINTING OFFICE: 1993-785-291/99064